Statistical Thermodynamics

Fundamentals and Applications

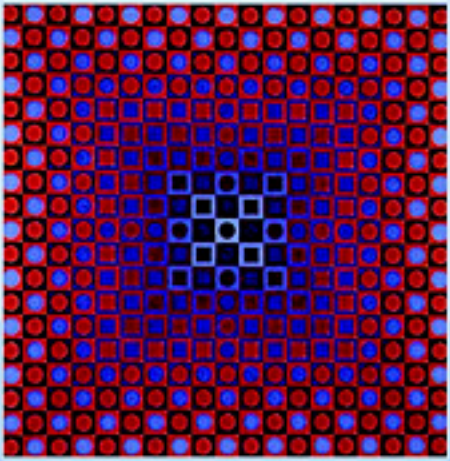

Normand M. Laurendeau

Cambridge

Cambridge www.cambridge.org/9780521846356

This page intentionally left blank

STATISTICAL THERMODYNAMICS: FUNDAMENTALS AND APPLICATIONS

Statistical Thermodynamics: Fundamentals and Applications discusses the fundamentals and applications of statistical thermodynamics for beginning graduate students in the engineering sciences. Building on the prototypical Maxwell–Boltzmann method and maintaining a step-by-step development of the subject, this book makes few presumptions concerning students' previous exposure to statistics, quantum mechanics, or spectroscopy. The book begins with the essentials of statistical thermodynamics, pauses to recover needed knowledge from quantum mechanics and spectroscopy, and then moves on to applications involving ideal gases, the solid state, and radiation. A full introduction to kinetic theory is provided, including its applications to transport phenomena and chemical kinetics. A highlight of the textbook is its discussion of modern applications, such as laser-based diagnostics. The book concludes with a thorough presentation of the ensemble method, featuring its use for real gases. Each chapter is carefully written to address student difficulties in learning this challenging subject, which is fundamental to combustion, propulsion, transport phenomena, spectroscopic measurements, and nanotechnology. Students are made comfortable with their new knowledge by the inclusion of both example and prompted homework problems.

Normand M. Laurendeau is the Ralph and Bettye Bailey Professor of Combustion at Purdue University. He teaches at both the undergraduate and graduate levels in the areas of thermodynamics, combustion, and engineering ethics. He conducts research in the combustion sciences, with particular emphasis on laser diagnostics, pollutant formation, and flame structure. Dr. Laurendeau is well known for his pioneering research on the development and application of both nanosecond and picosecond laser-induced fluorescence strategies to quantitative species concentration measurements in laminar and turbulent flames. He has authored or coauthored over 150 publications in the archival scientific and engineering literature. Professor Laurendeau is a Fellow of the American Society of Mechanical Engineers and a member of the Editorial Advisory Board for the peer-reviewed journal *Combustion Science and Technology.*

Statistical Thermodynamics

Fundamentals and Applications

NORMAND M. LAURENDEAU
Purdue University

CAMBRIDGE
UNIVERSITY PRESS

CAMBRIDGE UNIVERSITY PRESS
Cambridge, New York, Melbourne, Madrid, Cape Town, Singapore, São Paulo

Cambridge University Press
The Edinburgh Building, Cambridge CB2 2RU, UK

Published in the United States of America by Cambridge University Press, New York

www.cambridge.org
Information on this title: www.cambridge.org/9780521846356

First published in print format 2005

ISBN-13 978-0-511-14062-4 eBook (NetLibrary)
ISBN-10 0-511-14062-2 eBook (NetLibrary)

ISBN-13 978-0-521-84635-6 hardback
ISBN-10 0-521-84635-8 hardback

I dedicate this book to my parents,
Maurice and Lydia Roy Laurendeau.

Their gift of bountiful love and support . . .
Continues to fill me with the joy of discovery.

Contents

Preface

My intention in this textbook is to provide a self-contained exposition of the fundamentals and applications of statistical thermodynamics for beginning graduate students in the engineering sciences. Especially within engineering, most students enter a course in statistical thermodynamics with limited exposure to statistics, quantum mechanics, and spectroscopy. Hence, I have found it necessary over the years to "start from the beginning," not leaving out intermediary steps and presuming little knowledge in the discrete, as compared to the continuum, domain of physics. Once these things are done carefully, I find that good graduate students can follow the ideas, and that they leave the course excited and satisfied with their newfound understanding of both statistical and classical thermodynamics.

Nevertheless, a first course in statistical thermodynamics remains challenging and sometimes threatening to many graduate students. Typically, all their previous experience is with the equations of continuum mechanics, whether applied to thermodynamics, fluid mechanics, or heat transfer. For most students, therefore, the mathematics of probability theory, the novelty of quantum mechanics, the confrontation with entropy, and indeed the whole new way of thinking that surrounds statistical thermodynamics are all built-in hills that must be climbed to develop competence and confidence in the subject. For this reason, although I introduce the ensemble method at the beginning of the book, I have found it preferable to build on the related Maxwell–Boltzmann method so that novices are not confronted immediately with the conceptual difficulties of ensemble theory. In this way, students tend to become more comfortable with their new knowledge earlier in the course. Moreover, they are prepared relatively quickly for applications, which is very important to maintaining an active interest in the subject for most engineering students. Using this pedagogy, I find that the ensemble approach then becomes very easy to teach later in the semester, thus effectively preparing the students for more advanced courses that apply statistical mechanics to liquids, polymers, and semiconductors.

To hold the students' attention, I begin the book with the fundamentals of statistical thermodynamics, pause to recover needed knowledge from quantum mechanics and spectroscopy, and then move on to applications involving ideal gases, the solid state, and radiation. An important distinction between this book and previous textbooks is the inclusion of an entire chapter devoted to laser-based diagnostics, as applied to the thermal sciences. Here, I cover the essentials of absorption, emission, and laser-induced fluorescence techniques for the measurement of species concentrations and temperature. A full

introduction to kinetic theory is also provided, including its applications to transport phenomena and chemical kinetics.

During the past two decades, I have developed many problems for this textbook that are quite different from the typical assignments found in other textbooks, which are often either too facile or too ambiguous. Typically, the students at Purdue complete eight problem sets during a semester, with 4–6 problems per set. Hence, there are enough problems included in the book for approximately three such course presentations. My approach has been to construct problems using integrally related subcomponents so that students can learn the subject in a more prompted fashion. Even so, I find that many students need helpful hints at times, and the instructor should indeed be prepared to do so. In fact, I trust that the instructor will find, as I have, that these interactions with students, showing you what they have done and where they are stuck, invariably end up being one of the most rewarding parts of conducting the course. The reason is obvious. One-on-one discussions give the instructor the opportunity to get to know a person and to impart to each student his or her enthusiasm for the drama and subtleties of statistical thermodynamics.

As a guide to the instructor, the following table indicates the number of 50-minute lectures devoted to each chapter in a 42-lecture semester at Purdue University.

Chapter	Number of Lectures	Chapter	Number of Lectures
1	1	11	2
2	1	12	1
3	4	13	2
4	2	14	1
5	3	15	2
6	3	16	3
7	2	17	1
8	2	18	2
9	4	19	2
10	3	20	1

In conclusion, I would be remiss if I did not thank my spouse, Marlene, for her forbearance and support during the writing of this book. Only she and I know firsthand the trials and tribulations confronting a partnership wedded to the long-distance writer. Professor Lawrence Caretto deserves my gratitude for graciously permitting the importation of embellished portions of his course notes to the text. I thank Professor Michael Renfro for his reading of the drafts and for his helpful suggestions. Many useful comments were also submitted by graduate students who put up with preliminary versions of the book at Purdue University and at the University of Connecticut. I appreciate Professor Robert Lucht, who aided me in maintaining several active research projects during the writing of the book. Finally, I thank the School of Mechanical Engineering at Purdue for providing me with the opportunity and the resources over these many years to blend my enthusiasm for statistical thermodynamics with that for my various research programs in combustion and optical diagnostics.

1 Introduction

To this point in your career, you have probably dealt almost exclusively with the behavior of *macroscopic systems*, either from a scientific or engineering viewpoint. Examples of such systems might include a piston–cylinder assembly, a heat exchanger, or a battery. Typically, the analysis of macroscopic systems uses conservation or field equations related to classical mechanics, thermodynamics, or electromagnetics. In this book, our focus is on thermal devices, as usually described by thermodynamics, fluid mechanics, and heat transfer. For such devices, first-order calculations often employ a series of simple thermodynamic analyses. Nevertheless, you should understand that classical thermodynamics is inherently limited in its ability to explain the behavior of even the simplest thermodynamic system. The reason for this deficiency rests with its inadequate treatment of the atomic behavior underlying the gaseous, liquid, or solid states of matter. Without proper consideration of constituent *microscopic systems*, such as a single atom or molecule, it is impossible for the practitioner to understand fully the evaluation of thermodynamic properties, the meaning of thermodynamic equilibrium, or the influence of temperature on transport properties such as the thermal conductivity or viscosity. Developing this elementary viewpoint is the purpose of a course in statistical thermodynamics. As you will see, such fundamental understanding is also the basis for creative applications of classical thermodynamics to macroscopic devices.

1.1 The Statistical Foundation of Classical Thermodynamics

Since a typical thermodynamic system is composed of an *assembly* of atoms or molecules, we can surely presume that its macroscopic behavior can be expressed in terms of the microscopic properties of its constituent particles. This basic tenet provides the foundation for the subject of statistical thermodynamics. Clearly, statistical methods are mandatory as even one cm^3 of a perfect gas contains some 10^{19} atoms or molecules. In other words, the huge number of particles forces us to eschew any approach based on having an exact knowledge of the position and momentum of each particle within a macroscopic thermodynamic system.

The properties of individual particles can be obtained only through the methods of *quantum mechanics*. One of the most important results of quantum mechanics is that the energy of a single atom or molecule is not continuous, but *discrete*. Discreteness arises

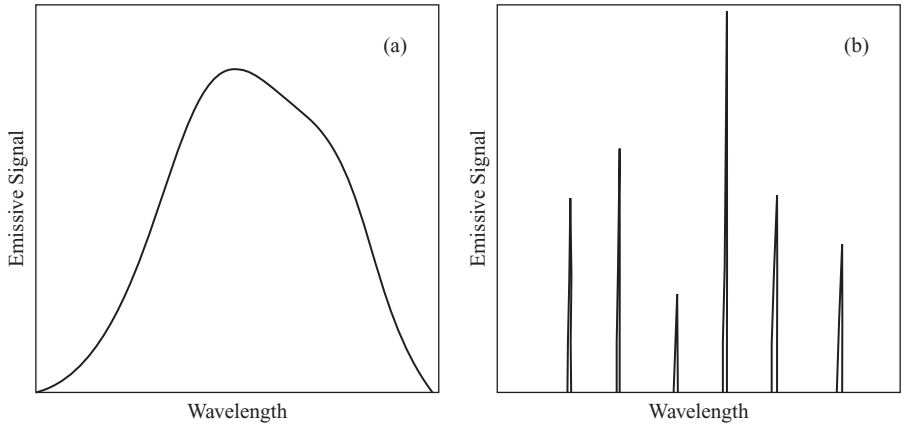

Figure 1.1 Schematic of simplified (a) continuous spectrum and (b) discrete spectrum.

from the distinct energy values permitted for either an atom or molecule. The best evidence for this quantized behavior comes from the field of spectroscopy. Consider, for example, the simplified emission spectra shown in Fig. 1.1. Spectrum (a) displays a continuous variation of emissive signal versus wavelength, while spectrum (b) displays individual "lines" at specific wavelengths. Spectrum (a) is typical of the radiation given off by a hot solid while spectrum (b) is typical of that from a hot gas. As we will see in Chapter 7, the individual lines of spectrum (b) reflect discrete changes in the energy stored by an atom or molecule. Moreover, the height of each line is related to the number of particles causing the emissive signal. From the point of view of statistical thermodynamics, the number of relevant *particles* (atoms or molecules) can only be determined by using probability theory, as introduced in Chapter 2.

The total energy of a single molecule can be taken, for simplicity, as the sum of individual contributions from its translational, rotational, vibrational, and electronic energy modes. The external or *translational mode* specifies the kinetic energy of the molecule's center of mass. In comparison, the internal energy modes reflect any molecular motion with respect to the center of mass. Hence, the *rotational mode* describes energy stored by molecular rotation, the *vibrational mode* energy stored by vibrating bonds, and the *electronic mode* energy stored by the motion of electrons within the molecule. By combining predictions from quantum mechanics with experimental data obtained via spectroscopy, it turns out that we can evaluate the contributions from each mode and thus determine the microscopic properties of individual molecules. Such properties include bond distances, rotational or vibrational frequencies, and translational or electronic energies. Employing statistical methods, we can then average over all particles to calculate the macroscopic properties associated with classical thermodynamics. Typical phenomenological properties include the temperature, the internal energy, and the entropy.

Figure 1.2 summarizes the above discussion and also provides a convenient road map for our upcoming study of statistical thermodynamics. Notice that the primary subject of this book plays a central role in linking the microscopic and macroscopic worlds. Moreover, while statistical thermodynamics undoubtedly constitutes an impressive application of probability theory, we observe that the entire subject can be founded on only two major postulates. As for all scientific adventures, our acceptance of these basic postulates as

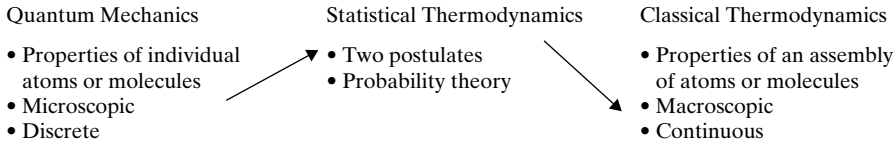

Figure 1.2 Flow chart for statistical thermodynamics.

objective truths rests solely on their predictive power; fortunately, the plethora of resulting predictions invariably comports well with experimental observations in classical thermodynamics. Therefore, despite its analytical nature, the study of statistical thermodynamics is well worth the effort as the final results are indeed quite practical. In fact, as we will see, much of classical thermodynamics ultimately rests on the conceptual bridge provided by statistical thermodynamics, a bridge linking the real world of compressors and gas turbines to the quantized world of ultimate uncertainty and molecular behavior.

1.2 A Classification Scheme for Statistical Thermodynamics

The framework of statistical thermodynamics can be divided into three conceptual themes. The first is *equilibrium statistical thermodynamics* with a focus on *independent particles*. Here, we assume no intermolecular interactions among the particles of interest; the resulting simplicity permits excellent *a priori* calculations of macroscopic behavior. Examples include the ideal gas, the pure crystalline metal, and blackbody radiation. The second theme is again equilibrium statistical thermodynamics, but now with a focus on *dependent particles*. In this case, intermolecular interactions dominate as, for example, with real gases, liquids, and polymers. Typically, such intermolecular interactions become important only at higher densities; because of the resulting mathematical difficulties, calculations of macroscopic properties often require semi-empirical procedures, as discussed in Chapters 19 and 20.

The third conceptual theme might be labeled *nonequilibrium statistical thermodynamics*. Here, we are concerned with the dynamic behavior that arises when shifting between different equilibrium states of a macroscopic system. Although time-correlation methods presently constitute an active research program within nonequilibrium statistical thermodynamics, we focus in this book on those dynamic processes that can be linked to basic kinetic theory. As such, we will explore the molecular behavior underlying macroscopic transport of momentum, energy, and mass. In this way, kinetic theory can provide a deeper understanding of the principles of fluid mechanics, heat transfer, and molecular diffusion. As we will see in Part Five, nonequilibrium statistical thermodynamics also provides an important path for the understanding and modeling of chemical kinetics, specifically, the rates of elementary chemical reactions.

1.3 Why Statistical Thermodynamics?

While the above classification scheme might please the engineering mind, it does little to acquaint you with the drama and excitement of both learning and applying statistical thermodynamics. Yes, you will eventually be able to calculate from atomic and molecular properties the thermodynamic properties of ideal gases, real gases, and metals. Examples

might include equations of state, measurable properties such as specific heats and the internal energy, and also ephemeral properties such as the entropy and free energies. And yes, you will learn how to calculate various transport properties, such as the thermal conductivity and the diffusion coefficient. Furthermore, with respect to chemical reactions, you will eventually be able to determine equilibrium constants and estimate elementary rate coefficients.

While these pragmatic aspects of statistical thermodynamics are important, the real drama of the subject lies instead in its revelations about our natural world. As you work through this book, you will slowly appreciate the limitations of classical thermodynamics. In particular, the first, second, and third laws of thermodynamics should take on a whole new meaning for you. You will understand that volumetric work occurs because of microscopic energy transfers and that heat flow occurs because of redistributions in molecular population. You will realize that entropy rises in isolated systems because of a fundamental enhancement in molecular probabilities. You will also appreciate in a new way the important underlying link between absolute property values and crystalline behavior near absolute zero.

Perhaps more importantly, you will come to understand in a whole new light the real meaning of thermodynamic equilibrium and the crucial role that temperature plays in defining both thermal and chemical equilibrium. This new understanding of equilibrium will pave the path for laser-based applications of statistical thermodynamics to measurements of both temperature and species concentrations, as discussed in Chapter 11. Such optical measurements are extremely important to current research in all of the thermal sciences, including fluid mechanics, heat transfer, combustion, plasmas, and various aspects of nanotechnology and manufacturing.

In summary, the goal of this book is to help you master classical thermodynamics from a molecular viewpoint. Given information from quantum mechanics and spectroscopy, statistical thermodynamics provides the analytical framework needed to determine important thermodynamic and transport properties associated with practical systems and processes. A significant feature of such calculations is that they can bypass difficult experimental conditions, such as those involving very high or low temperatures, or chemically unstable materials. More fundamentally, however, a study of statistical thermodynamics can provide you with a whole new understanding of thermodynamic equilibrium and of the crucial role that entropy plays in the operation of our universe. That universe surely encompasses both the physical and biological aspects of both humankind and the surrounding cosmos. As such, you should realize that statistical thermodynamics is of prime importance to all students of science and engineering as we enter the postmodern world.

PART ONE

FUNDAMENTALS OF STATISTICAL THERMODYNAMICS

2 Probability and Statistics

In preparation for our study of statistical thermodynamics, we first review some fundamental notions of probability theory, with a special focus on those statistical concepts relevant to atomic and molecular systems. Depending on your background, you might be able to scan quickly Sections 2.1–2.3, but you should pay careful attention to Sections 2.4–2.7.

2.1 Probability: Definitions and Basic Concepts

Probability theory is concerned with predicting statistical outcomes. Simple examples of such outcomes include observing a head or tail when tossing a coin, or obtaining the numbers 1, 2, 3, 4, 5, or 6 when throwing a die. For a fairly-weighted coin, we would, of course, expect to see a head for $1/2$ of a large number of tosses; similarly, using a fairly-weighted die, we would expect to get a four for $1/6$ of all throws. We can then say that the probability of observing a head on one toss of a fairly-weighted coin is $1/2$ and that for obtaining a four on one throw of a fairly-weighted die is $1/6$. This heuristic notion of probability can be given mathematical formality via the following definition:

> Given N_s *mutually exclusive*, equally likely points in *sample space*, with N_e of these points corresponding to the *random event* A, then the probability $P(A) = N_e / N_s$.

Here, *sample space* designates the available N_s occurrences while *random event* A denotes the subset of sample space given by $N_e \leq N_s$. The phrase *mutually exclusive* indicates that no two outcomes can occur simultaneously in a single sample space; this criterion is obviously required if we are to convert our heuristic understanding of chance to a well-defined mathematical probability.

As a further example, for a standard deck of playing cards, we have 52 points in sample space, of which four represent aces. Hence, the probability of drawing a single ace from a well-mixed deck is $P(A) = 4/52 = 1/13$, where the event A designates the random drawing of an ace. Visually, the relation between event A and sample space can be described by a so-called Venn diagram, as shown in Fig. 2.1. Here, sample points resulting in event A fall within the area A, while those not resulting in event A fall elsewhere in the surrounding box, whose total area represents the entire sample space. Hence, assuming a uniform point density, we find that the ratio of the cross-hatched area to the total area in Fig. 2.1 provides a visual representation of $P(A)$. Similarly, from the viewpoint of set theory, we observe

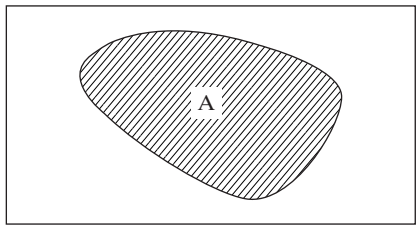

Figure 2.1 Venn diagram representing that portion of sample space which corresponds to random event A.

that for a fairly-weighted die the random event of obtaining an even number $E = \{2, 4, 6\}$ from within the entire sample space $S = \{1, 2, 3, 4, 5, 6\}$ clearly occurs with probability $P(A) = 1/2$.

Our notion of probability becomes more complicated if we consider two different random events, A and B, which can both occur within a given sample space. On this basis, we may define the *compound probability*, $P(AB)$, which represents events A *and* B, and also the *total probability*, $P(A+B)$, which represents events A *or* B (including both). From the viewpoint of set theory, $P(AB)$ is called the *intersection* of A and B ($A \cap B$), while $P(A+B)$ is labeled the *union* of A and B ($A \cup B$). Pictorial displays of the (a) intersection and (b) union of A and B are given by the two Venn diagrams shown in Fig. 2.2.

If the events A and B are mutually exclusive, a single trial by definition permits no overlap in sample space. Therefore, $P(AB) = 0$ so that

$$P(A+B) = P(A) + P(B), \tag{2.1}$$

as displayed by the Venn diagram of Fig. 2.3(a). As an example, the probability of picking a king (K) or a queen (Q) from a single deck of playing cards is given by the total probability $P(K + Q) = P(K) + P(Q) = 2/13$. In comparison, the probability of picking a king from one deck and a queen from a different deck is $P(KQ) = (1/13)^2$. In the latter case, we have two different sample spaces, as indicated by the Venn diagram of Fig. 2.3(b), so that the events are now *mutually independent*. Hence, in general, the compound probability becomes

$$P(AB) = P(A) \cdot P(B). \tag{2.2}$$

In summary, Eq. (2.1) defines two mutually exclusive events within a single sample space, while Eq. (2.2) defines two mutually independent events within two different sample

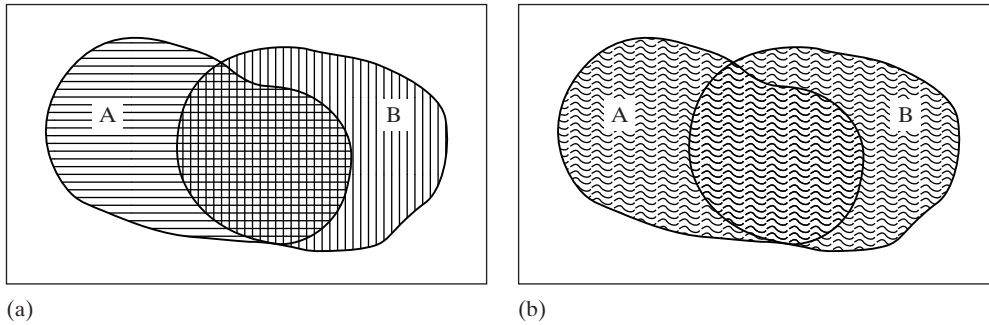

(a) (b)

Figure 2.2 Venn diagrams representing (a) $P(AB)$ and (b) $P(A + B)$.

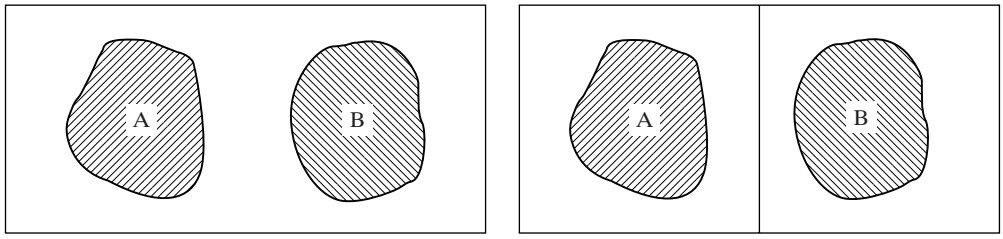

(a) (b)

Figure 2.3 Venn diagrams describing (a) mutually exclusive and (b) mutually independent events.

spaces. Equations (2.1) and (2.2) can, of course, be extended to more than two events, e.g.,

$$P(A+B+C) = P(A) + P(B) + P(C) \qquad \text{Mutual Exclusivity} \tag{2.3}$$

$$P(ABC) = P(A) \cdot P(B) \cdot P(C) \qquad \text{Mutual Independence.} \tag{2.4}$$

EXAMPLE 2.1

Five people are arranged in a row at random. What are the probabilities that two particular people will be (a) next to each other and (b) separated by one person between them?

Solution

We first recognize that randomly arranging two previously chosen people with three other people in a row is no different than randomly choosing these same two people after the arrangement. Because choosing two people at random from among five available people represents two mutually independent events, the compound probability with no further information is (1/5)(1/4). However, if we now specify that these two people are either next to each other or one person apart, we must account for the fact that there are many ways of achieving either specification, each of which will enhance the previously unconstrained compound probability. As for many probability analyses, a combination of visual and conceptual approaches often constitutes the most fruitful tactic for solving the problem.

(a) Visualization indicates that for five people in a row, four possible pairs of people can exist next to each other. Conceptually, the persons comprising each pair can also be switched, thus giving eight independent ways of obtaining two people next to each other among five people in a row. Hence, the final probability that two people will be next to each other when five people are arranged in a row at random must be $(1/5)(1/4)(8) = 2/5$.

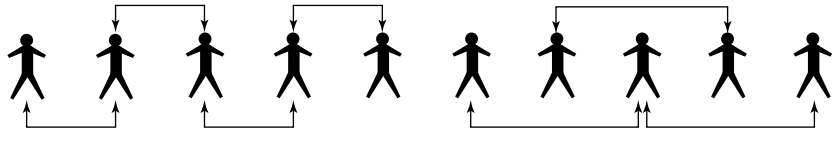

(a) (b)

Possible pairs of people for (a) two people next to each other and (b) two people one person apart.

(b) Similarly, for two people separated by another person, a combined visual and conceptual analysis gives a final probability of $(1/5)(1/4)(3)(2) = 3/10$. Here, three pairs of people are possible one person apart and the individuals comprising each pair can again be switched.

Suppose instead that the five people are arranged in a circle. You should be able to convince yourself that the probability for two people to be either next to each other or separated by another person is now always 1/2.

2.2 Permutations and Combinations

We now apply probability theory to a sequence of distinguishable objects. Consider, for example, an urn containing four marbles labeled A, B, C, and D, respectively. Our aim is to randomly select marbles from the urn without replacement. The first marble chosen can be any of four possibilities, the second can be any of the three remaining possibilities, the third chosen must be one of the two remaining possibilities, and the fourth can only be one possibility. Hence, the number of ways that the four sequential but independent choices can be made must be $4 \cdot 3 \cdot 2 \cdot 1 = 24$. These 24 possible ways of randomly selecting the four original marbles can be taken as the number of possible arrangements or *permutations* of any single sequence of the four marbles, e.g., $ACDB$. If, on the other hand, the marbles were not labeled, then the 24 possible rearrangements would be irrelevant as the marbles would be indistinguishable. In this case, the 24 permutations would become only one *combination*. Moreover, only a single collection or combination of the four marbles would exist, even if labeled, if we simply chose to disregard any ordering of the random objects.

This distinction between permutations and combinations can be pursued further by considering the number of ways by which we can choose M items from a sample of N available objects without replacement, in one case including and in the other case excluding the effect of labeling or ordering. The objects, for example, could be M marbles chosen from an urn containing N marbles, or M cards chosen from a deck of N cards. Following the procedure outlined in the previous paragraph, the number of permutations is $P(N, M) = N(N-1)\cdots(N-M+1)$ or

$$P(N, M) = \frac{N!}{(N-M)!}, \tag{2.5}$$

which is defined as the number of permutations of N objects taken M at a time. We note, by the way, that $P(N, M) = N!$ when $M = N$, so that Eq. (2.5) requires that we define $0! = 1$.

In comparison, the number of combinations represents all the different subsets containing M items that can be sampled from N distinct objects. Here, the particular arrangement of M objects within a subset is irrelevant; thus, the number of combinations can be obtained from the number of permutations of Eq. (2.5) via division by the number of permutations, $M!$, for the subset of M distinct objects. Hence, $C(N, M) = P(N, M)/M!$ or

$$C(N, M) = \frac{N!}{(N-M)!\, M!}, \tag{2.6}$$

which is defined as the number of combinations of N objects taken M at a time. We note that $C(N, M)$ can also be interpreted as the number of different arrangements of N objects when M of these objects are of one distinct type and $(N - M)$ are of a second type. This interpretation of $C(N, M)$ will be employed in Section 2.4, when we consider the binomial distribution.

EXAMPLE 2.2

You wish to choose three marbles at random from an urn containing four marbles labeled A, B, C, and D.

(a) Determine the number of permutations and combinations for the above scenario.
(b) Identify explicitly each combination and permutation for the three chosen marbles.

Solution

(a) The number of permutations when letting $N = 4$ and $M = 3$ is

$$P(N, M) = \frac{N!}{(N - M)!} = \frac{4!}{1!} = 24.$$

Similarly, the number of combinations is

$$C(N, M) = \frac{N!}{(N - M)!\ M!} = \frac{4!}{1!\ 3!} = 4.$$

(b) The four combinations are ABC, ABD, ACD, and BCD. Each of the four combinations can be permuted $3! = 6$ ways, for a total of 24 permutations. Consider, for example, the ABC combination, which offers the following six permutations: ABC, ACB, BAC, BCA, CAB, and CBA.

2.3 Probability Distributions: Discrete and Continuous

You are no doubt familiar with the concept of a grade distribution as a way of reporting results for a course examination. Consider, for example, the simplified distribution of test scores shown for a class of 20 students in Table 2.1. If we convert the number of students associated with each test score to an appropriate fraction of students, we obtain

Table 2.1. *Simplified grade distribution*

Number of students	Fraction of students	Test scores
1	0.05	100
2	0.10	90
4	0.20	80
6	0.30	70
4	0.20	60
2	0.10	50
1	0.05	40

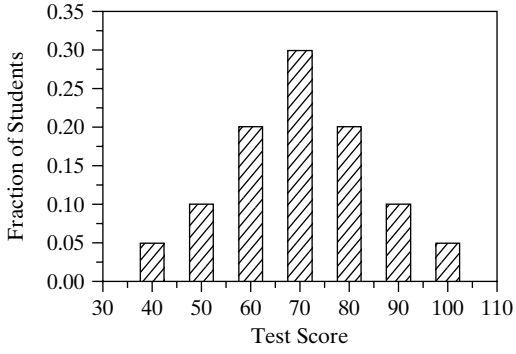

Figure 2.4 Histogram representing Table 2.1.

the *histogram* shown in Fig. 2.4. This histogram is an example of a *discrete probability distribution*, for which

$$\sum_i P(x_i) = 1. \tag{2.7}$$

In other words, the number of students obtaining each grade, x_i, has been *normalized* so that the sum over all probabilities or fractional numbers of students, $P(x_i)$, is unity.

For any discrete distribution, the *mean* may be defined as

$$\bar{x} = \langle x_i \rangle \equiv \sum_i P(x_i)\, x_i \tag{2.8}$$

while the *variance* or mean-square deviation is

$$\sigma^2 = \langle (x_i - \bar{x})^2 \rangle, \tag{2.9}$$

where both the overbar and the brackets denote an average or expected value. The square root of the variance, σ, is commonly called the standard deviation; it provides a measure of the width for the probability distribution. Expanding Eq. (2.9) leads to

$$\sigma^2 = \left\langle x_i^2 - 2\bar{x}\, x_i + \bar{x}^2 \right\rangle = \left\langle x_i^2 \right\rangle - \bar{x}^2,$$

so that the variance can be expressed as the mean of the square minus the square of the mean. Hence, the standard deviation can be written as

$$\sigma = \sqrt{\overline{x^2} - \bar{x}^2} \tag{2.10}$$

where

$$\overline{x^2} = \left\langle x_i^2 \right\rangle = \sum_i P_i(x_i)\, x_i^2. \tag{2.11}$$

We now consider a more realistic distribution of test scores for a group of 400 students rather than 20 students. In this case, we might expect Table 2.1 to contain all possible integer grades between 40 and 100. Hence, the histogram of Fig. 2.4 would approach a more continuous distribution, as displayed by the *probability density function*, $f(x)$, in Fig. 2.5. Normalization would now be given by

$$\int f(x)\, dx = 1$$

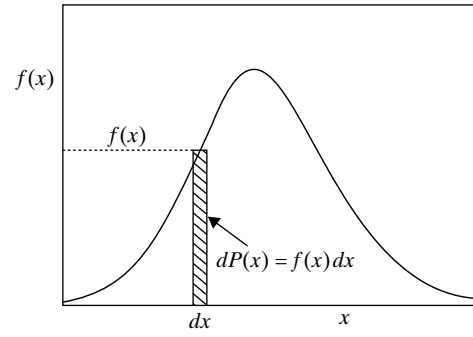

Figure 2.5 Continuous distribution function.

when integrated over all possible values of x. Therefore, the probability density function itself does *not* represent a probability; rather, the probability must be evaluated from knowledge of $f(x)$ via integration. As an example, the probability of achieving values of x between a and b would be obtained from

$$P(a \leq x \leq b) = \int_a^b f(x)\,dx. \tag{2.12}$$

Similarly, the *cumulative distribution function* is

$$F(X) = \int_0^X f(t)\,dt$$

so that Eq. (2.12) can be expressed as

$$P(a \leq x \leq b) = F(b) - F(a).$$

Finally, for any function of x, $H(x)$, the expected value becomes

$$\langle H(x) \rangle = \int H(x)\,f(x)\,dx \tag{2.13}$$

so that $f(x)$ represents a statistical weighting function for $H(x)$. Hence, for $H(x) = x$, $\langle H(x) \rangle$ represents the mean, in analogy with Eq. (2.8). Similarly, for $H(x) = (x - \bar{x})^2$, $\langle H(x) \rangle$ represents the variance, in accord with this same statistical parameter for a discrete distribution.

2.4 The Binomial Distribution

The binomial distribution is of fundamental importance in probability theory, as it describes quite simply any sequence of experiments having two possible outcomes. As an example, consider the tossing of an unfairly-weighted coin, for which the two outcomes are either a head or tail. Suppose that the probability of obtaining a head is p, while that for a tail is $q = 1 - p$. Now, for a sequence of N tosses, the probability of M heads and $(N - M)$ tails in a particular sequence is $p^M q^{N-M}$, as each toss is an independent event in a new sample space. However, because M heads and $(N - M)$ tails can be achieved in more than one way, we must determine the number of possible sequences of heads and tails if we wish to determine the final probability. But the number of possible sequences is just the number

of ways N total objects can be arranged into M identical objects of one type and $(N - M)$ identical objects of a second type. This description defines the number of combinations of N objects taken M at a time, $C(N, M)$, as specified by Eq. (2.6). Hence, the probability of tossing M heads and $(N - M)$ tails regardless of order becomes

$$B(M) = C(N, M)p^M q^{N-M}$$

or

$$B(M) = \frac{N!}{M!\,(N-M)!}p^M(1-p)^{N-M}, \tag{2.14}$$

where $B(M)$ represents the well-known binomial probability distribution. This discrete distribution can be interpreted in many different ways. For example, the probabilities p and $(1 - p)$ can indicate the chances of success and failure or right and left steps of a random walk, as well as of heads and tails in the tossing of a coin. Therefore, in general, N always represents the total number of repeated trials in any binary sequence.

EXAMPLE 2.3

Determine the probability that, in six throws of a fairly-weighted die, the side with four pips will land upright at least twice.

Solution

The probability of landing a four on any throw is 1/6 (success) and thus the probability of not landing a four on any throw is 5/6 (failure). Consequently, the probability that four pips will not appear ($M = 0$) in six throws ($N = 6$) must be

$$B(0) = \frac{6!}{0!\,(6-0)!}\left(\frac{1}{6}\right)^0\left(\frac{5}{6}\right)^6 \simeq 0.335.$$

Similarly, the probability that four pips will appear once ($M = 1$) in six throws is

$$B(1) = \frac{6!}{1!\,(6-1)!}\left(\frac{1}{6}\right)\left(\frac{5}{6}\right)^5 \simeq 0.402.$$

As $B(0)$ and $B(1)$ represent mutually exclusive events, the probability from Eq. (2.3) that four pips will appear at least twice in a sequence of six throws must be

$$P(M \geq 2) = 1 - P(M < 2) = 1 - [B(0) + B(1)]$$

or

$$P(M \geq 2) = 1 - [0.335 + 0.402] = 1 - 0.737 = 0.263.$$

Employing Eqs. (2.8) and (2.10), we may show that the mean and standard deviation for the binomial distribution are given by (Problem 1.3)

$$\overline{M} = Np \tag{2.15}$$

and

$$\sigma = \sqrt{Np(1-p)}. \tag{2.16}$$

Hence, for a fairly-weighted coin ($p = \frac{1}{2}$), the mean number of heads is $\overline{M} = N/2$, as expected. The standard deviation is $\sigma = \sqrt{N}/2$, so that $\sigma/\overline{M} = 1/\sqrt{N}$ and thus the relative width of the binomial distribution always narrows with an increasing number of trials.

2.5 The Poisson Distribution

While the binomial distribution holds for any finite number of repeated trials, physical processes involving large numbers of particles, such as in statistical thermodynamics, imply $N \to \infty$. For such circumstances, the binomial distribution can be simplified to two more familiar distributions, one discrete and the other continuous. We now proceed with these simplifications by first assuming $p \to 0$, which we will find leads to the Poisson distribution. This distribution is particularly applicable to photon-counting processes, for which the total number of photons counted, $N \to \infty$, while the possibility of observing any single photon, $p \to 0$.

We begin by expressing the binomial distribution, Eq. (2.14), as

$$B(M) = \frac{N(N-1)\cdots(N-M+1)}{M!} \left(\frac{\mu}{N}\right)^M (1-p)^{N-M},$$

where the mean $\mu \equiv \overline{M} = Np$ from Eq. (2.15). We then have

$$\lim_{N\to\infty} B(M) = \frac{N^M}{M!}\left(\frac{\mu}{N}\right)^M (1-p)^N = \frac{\mu^M}{M!}(1-p)^{\mu/p}.$$

From the fundamental mathematical definition of the quantity, $e = 2.71828$, it can be shown that

$$\lim_{p\to 0} (1-p)^{1/p} = e^{-1}.$$

Hence, for $N \to \infty$ and $p \to 0$, the binomial distribution becomes the discrete Poisson distribution,

$$P(M) = \frac{e^{-\mu}\mu^M}{M!}. \tag{2.17}$$

Because $P(M)$ is based on $B(M)$, the standard deviation for the Poisson distribution can be obtained from Eq. (2.16) by invoking $p \to 0$, thus giving

$$\sigma = \sqrt{Np} = \sqrt{\mu}, \tag{2.18}$$

as can also be demonstrated (Prob. 1.4) from direct application of Eq. (2.10). We thus find, from Eq. (2.18), that a greater mean value implies a broader range of expected outcomes

when the physical system of interest follows Poisson statistics. Employing Eq. (2.17), we also note that

$$\frac{P(M+1)}{P(M)} = \frac{\mu}{M+1},$$

which indicates a rapid drop in probability for the Poisson distribution as $M \to \infty$. Nevertheless, the Poisson distribution generally remains a good approximation to the binomial distribution for $\mu = Np \ll \sqrt{N}$.

2.6 The Gaussian Distribution

When the number of trials $N \to \infty$, but p is not small, the binomial distribution becomes the continuous Gaussian distribution rather than the discrete Poisson distribution ($p \to 0$). The Gaussian distribution is particularly applicable to various diffusive processes, for which the total number of molecules $N \to \infty$.

We begin by applying the natural logarithm to the binomial distribution, Eq. (2.14), thus obtaining

$$\ln B(M) = \ln\left\{\frac{N!}{M!\ (N-M)!}\right\} + \ln\left\{p^M q^{N-M}\right\},$$

where $q = 1 - p$. Employing Stirling's approximation (Appendix D.2),

$$\ln N! = N \ln N - N + \frac{1}{2}\ln(2\pi N),$$

we may eventually show that

$$\ln B(M) = -\frac{1}{2}\ln\left\{\frac{2\pi M}{N}(N-M)\right\} + \ln\left[\frac{Np}{M}\right]^M + \ln\left[\frac{Nq}{N-M}\right]^{N-M}. \tag{2.19}$$

We now define

$$y \equiv M - \overline{M} = M - Np \tag{2.20}$$

so that

$$\frac{M}{N} = \frac{y}{N} + p$$

and

$$\frac{N-M}{N} = q - \frac{y}{N}.$$

Substitution then gives for the first term of Eq. (2.19),

$$\lim_{N\to\infty} \frac{M}{N}(N-M) = \lim_{N\to\infty} N\left(\frac{y}{N} + p\right)\left(q - \frac{y}{N}\right) = Npq, \tag{2.21}$$

as y/N scales with the relative width of the binomial distribution, which we previously found to display a $1/\sqrt{N}$ dependence. For the remaining two terms,

$$\ln\left[\frac{Np}{M}\right]^M = -M\ln\left[\frac{M}{Np}\right] = -(y+Np)\ln\left[1+\frac{y}{Np}\right]$$

$$\ln\left[\frac{Nq}{N-M}\right]^{N-M} = -(N-M)\ln\left[\frac{N-M}{Nq}\right] = -(Nq-y)\ln\left[1-\frac{y}{Nq}\right].$$

Employing the logarithmic series, $\ln(1\pm z) \simeq \pm z - z^2/2$ for $|z| < 1$ at moderate values of p, we subsequently find to second order in y,

$$\lim_{N\to\infty} \ln\left[\frac{Np}{M}\right]^M \simeq -\frac{1}{2}\frac{y^2}{Np} - y \tag{2.22}$$

$$\lim_{N\to\infty} \ln\left[\frac{Nq}{N-M}\right]^{N-M} \simeq y - \frac{1}{2}\frac{y^2}{Nq}. \tag{2.23}$$

Substituting Eqs. (2.21), (2.22), and (2.23) for each of the three terms of Eq. (2.19), we obtain

$$\lim_{N\to\infty} \ln B(y) = -\frac{1}{2}\ln(2\pi Npq) - \frac{y^2}{2N}\left(\frac{1}{p}+\frac{1}{q}\right),$$

which results in the Gaussian distribution,

$$G(y) = \frac{1}{\sqrt{2\pi Npq}}\exp\left(-\frac{y^2}{2Npq}\right). \tag{2.24}$$

From Eq. (2.16),

$$\sigma^2 = Npq,$$

so that, defining $z \equiv y/\sigma$, we obtain finally the familiar form of the continuous Gaussian distribution,

$$G(z) = \frac{1}{\sqrt{2\pi}\sigma}\exp\left(-\frac{z^2}{2}\right). \tag{2.25}$$

For a continuous distribution, the discrete variable M must be replaced by its continuous analog x so that, from Eq. (2.20), $z = (x-\mu)/\sigma$ where again $\mu \equiv Np$. Note that $G(z)$ is symmetrical about z because of its dependence on z^2, unlike many cases for the discrete binomial or Poisson distributions. Equation (2.25) also indicates that the peak value for $G(z)$ is always $1/\sqrt{2\pi}\sigma$.

In general, the Gaussian distribution can be shown to be a satisfactory approximation to the binomial distribution if both $Np \geq 5$ and $Nq \geq 5$. If the Gaussian distribution holds, the probability for a specified range of the independent variable x can be determined from

$$P(x_1 \leq x \leq x_2) = \int_{x_1}^{x_2} G(x)\,dx,$$

or since $z = (x-\mu)/\sigma$, we have by substitution,

$$P(z_1 \leq z \leq z_2) = \frac{1}{\sqrt{2\pi}}\int_{z_1}^{z_2}\exp\left(-\frac{z^2}{2}\right)dz. \tag{2.26}$$

Equation (2.26) represents the most convenient method for calculating probabilities when the physical system of interest follows Gaussian statistics.

EXAMPLE 2.4

Verify by direct calculation that the mean and variance of the Gaussian distribution are equivalent to μ and σ^2, respectively.

Solution

The Gaussian distribution is given by Eq. (2.25) where $z = (x - \mu)/\sigma$. Direct calculation of the mean and variance requires application of Eq. (2.13).

(a) For the mean,

$$\bar{x} = \int xG(x)\,dx = \frac{1}{\sqrt{2\pi}} \int_{-\infty}^{\infty} (\mu + \sigma z) \exp\left(-\frac{z^2}{2}\right) dz = \frac{1}{\sqrt{2\pi}} \int_{-\infty}^{\infty} \mu \exp\left(-\frac{z^2}{2}\right) dz$$

$$\bar{x} = \frac{2\mu}{\sqrt{2\pi}} \int_0^{\infty} \exp\left(-\frac{z^2}{2}\right) dz = \frac{2\mu}{\sqrt{2\pi}} \left[\frac{(2\pi)^{1/2}}{2}\right] = \mu,$$

where the final Gaussian integration has been performed by using Appendix B.

(b) For the variance,

$$\overline{(x - \bar{x})^2} = \int (x - \mu)^2 G(x)\,dx = \frac{\sigma^2}{\sqrt{2\pi}} \int_{-\infty}^{\infty} z^2 G(z)\,dz$$

$$\overline{(x - \bar{x})^2} = \frac{2\sigma^2}{\sqrt{2\pi}} \int_0^{\infty} z^2 \exp\left(-\frac{z^2}{2}\right) dz = \frac{2\sigma^2}{\sqrt{2\pi}} \left[\frac{1}{4}(8\pi)^{1/2}\right] = \sigma^2,$$

where the Gaussian integration has been evaluated by using Appendix B.

2.7 Combinatorial Analysis for Statistical Thermodynamics

We have previously indicated that quantum mechanics ultimately predicts discrete *energy levels* for molecular systems. As we will see later, each such level is actually composed of a finite number of allowed *energy states*. The number of energy states per energy level is called the *degeneracy*. For our purposes, we can model each energy level of energy, ε_j, as an independent bookshelf holding a specified number of baskets equal to the value of the degeneracy, g_j, as shown in Fig. 2.6. The height of each individual shelf represents its energy. The equivalent containers denote potential storage locations for the molecules of the thermodynamic system at each energy level.

For statistical purposes, we will eventually need to know the distribution of molecules among these energy states, as discussed further in Chapter 3. We now move toward this goal by considering the number of ways that N objects (molecules) can be placed in M containers (energy states) on a single shelf (energy level). Before we can make such combinatorial calculations, however, we must introduce two other important features of quantum mechanics, the details of which we again defer to later discussion (Chapter 5).

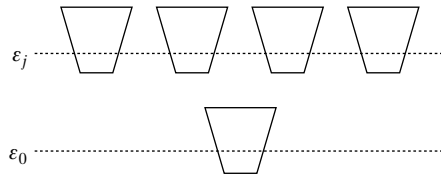

Figure 2.6 Bookshelf model for energy level ε_j, with degeneracy $g_j = 4$.

First, because of the so-called uncertainty principle, we can never determine the exact position *and* momentum of atomic or molecular particles. You may recall from your undergraduate chemistry that the motion of electrons within atoms or molecules is often described in terms of an electron cloud. This cloud analogy reflects the probabilistic nature of fundamental atomic particles; for this reason, such particles are labeled *indistinguishable*. In contrast, the motion of larger bodies such as billiard balls or planets can be determined precisely by solving the equations of classical mechanics. Such bodies can obviously be tracked by observation; hence, in comparison to atomic particles, classical objects are labeled *distinguishable*.

The second important feature of quantum mechanics required for statistical calculations concerns the existence of potential limitations on the population within each energy state. We will show in Chapter 5 that some atomic or molecular particles are inherently limited to one particle per energy state. Other particles, in comparison, have no limit on their occupancy. For proper statistical calculations, we must account for both of these cases, as well as for objects that can be either distinguishable or indistinguishable.

2.7.1 Distinguishable Objects

Combinatorial analyses for distinguishable objects encompass three significant cases. Each case can be considered by posing and answering a different fundamental query.

1. In how many ways may N identical, distinguishable objects be placed in M different containers with a limit of one object per container?

   The limitation of one object per container requires $N \leq M$. The first object may be placed in any of M available containers, the second in $(M-1)$ available containers, and so on. Hence the number of ways for this case becomes

   $$W_1 = M(M-1)(M-2)\cdots(M-N+1)$$

   or

   $$W_1 = \frac{M!}{(M-N)!}. \tag{2.27}$$

2. In how many ways may N identical, distinguishable objects be placed in M different containers such that the ith container holds exactly N_i objects?

   The total number of permutations for N objects is $N!$ However, within each container, permutations are irrelevant as we are concerned only with their number rather than their identity. Hence, the number of permutations, $N!$, overcounts the number of ways

by the number of permutations, $N_i!$, for each container. Therefore, the number of ways is

$$W_2 = \frac{N!}{\prod_{i=1}^{M} N_i!}. \tag{2.28}$$

3. In how many ways may N identical, distinguishable objects be placed in M different containers with no limitation on the number per container?

   Because no limit exists, each object can be placed in any of the M containers. Therefore,

$$W_3 = M^N. \tag{2.29}$$

2.7.2 Indistinguishable Objects

Combinatorial analyses for indistinguishable objects encompass two rather than three cases of significance. Each case can again be considered by posing and answering a fundamental query.

4. In how many ways may N identical, indistinguishable objects be placed in M different containers with a limit of one object per container?

   A similar query for distinguishable objects previously led to Eq. (2.27). For indistinguishable objects, however, any rearrangement among the N objects is unrecognizable. Hence, W_1 overcounts the number of ways for indistinguishable objects by a factor of $N!$ Therefore,

$$W_4 = \frac{M!}{N!\,(M-N)!}. \tag{2.30}$$

5. In how many ways may N identical, indistinguishable objects be placed in M different containers with no limitation on the number per container?

   This fully unconstrained case (indistinguishable objects, no limitation) mandates a totally different approach from that used for W_4. We begin by initially assuming distinguishable objects labeled $1, 2, 3, \ldots, N$. Let us now arrange these N objects in a row, with the M containers identified and separated by partitions. As an example,

$$1, 2, 3 \;|\, 4, 5 \,|\; 6 \;|\ldots|\; N-1, N$$

   specifies that objects 1, 2, and 3 are in the first container, objects 4 and 5 are in the second container, object 6 is in the third container, and so on. Now, regardless of their actual arrangement, the maximum number of rearrangements among the N objects and $M-1$ partitions is $(N+M-1)!$ However, interchanging the partitions produces no new arrangements; thus, we have overcounted by a factor of $(M-1)!$ Similarly, because the N objects are actually indistinguishable, we have again overcounted by a factor of $N!$, as in query 4. Therefore, the number of ways for this case becomes

$$W_5 = \frac{(N+M-1)!}{N!\,(M-1)!}. \tag{2.31}$$

The combinatorial analyses conducted for Cases 3–5 will prove to be of most interest to us for practical calculations. As we will see in the following chapter, Eq. (2.29) corresponds to Boltzmann statistics, Eq. (2.30) corresponds to Fermi–Dirac statistics, and Eq. (2.31) corresponds to Bose–Einstein statistics.

EXAMPLE 2.5

Determine the number of ways of placing two balls in three numbered containers for (a) Boltzmann statistics, (b) Fermi–Dirac statistics, and (c) Bose–Einstein statistics. Construct a table that identifies each of the ways for all three cases.

Solution

(a) For Boltzmann statistics, the balls are distinguishable with no limit on the number per container. Hence, from Eq. (2.29),

$$W_3 = M^N = 3^2 = 9.$$

Employing closed and open circles to identify the two distinguishable balls, these nine distributions can be identified as follows:

Way	Container 1	Container 2	Container 3
1	●○		
2		●○	
3			●○
4	●	○	
5	○	●	
6	●		○
7	○		●
8		●	○
9		○	●

(b) For Fermi–Dirac statistics, the balls are indistinguishable, but with a limit of one ball per container. Therefore, Eq. (2.30) yields

$$W_4 = \frac{M!}{N!\,(M-N)!} = \frac{3!}{2!\,1!} = 3.$$

If only closed circles are used to enumerate the indistinguishable balls, these three distributions are as follows:

Way	Container 1	Container 2	Container 3
1	●	●	
2	●		●
3		●	●

(c) For Bose–Einstein statistics, the balls are indistinguishable, with no limit on the number of balls per container. Hence, using Eq. (2.32), we have

$$W_5 = \frac{(N+M-1)!}{N!\,(M-1)!} = \frac{4!}{2!\,2!} = 6.$$

These six distributions are as follows:

Way	Container 1	Container 2	Container 3
1	••		
2		••	
3			••
4	•	•	
5	•		•
6		•	•

PROBLEM SET I

Probability Theory and Statistical Mathematics (Chapter 2)

1.1 Ignoring leap years, calculate the probability that, among 25 randomly chosen people, at least two have the same birthday.

Hint: Consider the probability that everyone has a unique birthday.

1.2 Assuming that the inherent ratio of male to female children is unity, determine the following probabilities for a family of six children.

a. The four oldest children will be boys and the two youngest will be girls.

b. Exactly half the children will be boys.

c. All six children will be of the same sex.

d. A second girl is born last.

1.3 Consider the probability function for the binomial distribution,

$$B(M) = \frac{N!}{M!\,(N-M)!}\,p^M q^{N-M},$$

where N and p are specified, and the probability $q = 1 - p$.

a. Show that the distribution is properly normalized.

b. Verify that the mean $\overline{M} = Np$.

c. Show that the standard deviation $\sigma = \sqrt{Np(1-p)}$.

d. The fluctuation is defined as the ratio of the standard deviation to the mean. Determine the fluctuation of the binomial distribution for $p = 0.5$. What happens to the fluctuation for large values of N? What are the physical implications of this result when considering the thermodynamic properties of an ideal gas?

Hint: Recall that, for arbitrary values of p and q, the binomial theorem gives

$$\sum_{M=0}^{N} B(M) = (p+q)^N$$

so that, for any value of s,

$$\sum_{M=0}^{N} s^M B(M) = (sp+q)^N.$$

The trick now is to differentiate with respect to s.

1.4 The binomial distribution

$$B(M) = \frac{N!}{M!\,(N-M)!}\,p^M(1-p)^{N-M}$$

describes the probability of placing M identical particles into N equivalent physical sites, with a limit of one particle/site if the probability of a specific site being occupied is p.

a. Using Stirling's formula, show that for $N \gg M$ so that $p \ll 1$, the binomial distribution becomes the Poisson distribution

$$P(M) = \frac{\mu^M}{M!}e^{-\mu},$$

where $\mu = Np$.

Hint: See Appendix B.

b. Verify (i) that the Poisson distribution is properly normalized, (ii) that its mean $\overline{M} = \mu$, and (iii) that its root-mean-square deviation $\sigma = \sqrt{\mu}$.

c. The number of ideal-gas molecules expected in a given volume is described by the Poisson distribution since a finite number of molecules can be distributed in a spatial region offering an infinite continuum of positions. Calculate the mean and root-mean-square deviation for the number of molecules in a volume of 1 cm^3 at a pressure of 1 bar and a temperature of 273 K. What are the implications of your result?

1.5 Consider the probability function for the binomial distribution

$$B(M) = C(N, M)\,p^M q^{N-M},$$

where $C(N, M) = N!\,/\,M!(N-M)!$ is the number of combinations of N objects taken M at a time, and the probability $q = 1 - p$.

a. Verify the recursive relation,

$$B(M+1) = \frac{(N-M)}{(M+1)}\left(\frac{p}{q}\right)B(M).$$

b. Prove that the probability of obtaining a specific number of heads when tossing a fairly-weighted coin is given by the binomial distribution.

c. Using the recursive relation developed in part (a), determine the probabilities of obtaining 0 to 12 heads in 12 tosses of a fairly-weighted coin.

d. Evaluate the probability of obtaining 6 heads in 12 tosses by applying Stirling's formula to $B(M)$.

1.6 The Gaussian and Poisson distributions are both related to the fundamental binomial distribution,

$$B(M) = \frac{N!}{M!\,(N-M)!}\,p^M(1-p)^{N-M},$$

which represents the probability of achieving M successes out of N trials given a probability p of success for any single trial.

a. Develop an expression for a Gaussian distribution with the same mean and standard deviation as the binomial distribution.

b. If the mean $\mu = Np = 15$, where $p = 0.5$, calculate the probabilities $P(M)$ given by the Poisson distribution for $0 \leq M \leq 30$.

c. Recalculate the probabilities of part (b) by utilizing the Gaussian distribution. Display your results for both the Poisson and Gaussian distributions on a single plot.

d. Repeat parts (b) and (c) for $p = 0.1$.

e. Discuss the implications of your comparative plots.

1.7 A fairly-weighted coin is tossed 20 times.

a. Prove that the probability for a specific number of heads is given by the binomial distribution.

b. Calculate the probabilities for each of the possible numbers of heads.

c. Recalculate the probabilities in part (b) by invoking a Gaussian distribution.

d. Display your results from parts (b) and (c) on a single plot. Discuss the implications of your comparison.

1.8 The binomial distribution for a very large number of trials, N, in which the probability of success p, does not become small can be represented by a Gaussian distribution having the same mean and standard deviation as the binomial distribution.

a. Provide an expression for the probability of achieving M successes in N trials for such a Gaussian distribution. Check the suitability of your Gaussian approximation to the binomial distribution by evaluating the probability of obtaining 23 heads in 36 tosses of a coin by both methods.

b. Develop an expression in terms of the error function (Appendix B) for the probability of finding any Gaussian variable to within $\pm k\sigma$ of its mean value. Evaluate this probability for $k = 1, 2$, and 3. Finally, demonstrate the utility of the Gaussian approximation by calculating the probability of obtaining 23 *or more* heads in 36 tosses. Note how tedious this calculation would have been if you had used the binomial distribution!

1.9 The probability density function for the Rayleigh distribution is given by

$$f(x) = Cxe^{-x^2/2a^2},$$

where $a > 0$ and $x \geq 0$.

a. Evaluate the constant C.

b. Determine the mean value $\bar{x}$.

c. Evaluate the standard deviation σ.

Hint: See Appendix B.

1.10 The probability density function for the Laplace distribution is given by

$$f(x) = Ce^{-a|x|},$$

where $a > 0$ and $-\infty < x < \infty$.

a. Evaluate the constant C.

b. Calculate the probability that $x \geq 1/2$.

c. Determine the standard deviation (σ).

1.11 The probability that a monatomic particle will travel a distance x or more between collisions is given by $Ce^{-x/\lambda}$ where C and λ are constants.

a. Show that the probability distribution function $f(x) = \lambda^{-1}e^{-x/\lambda}$.

b. Determine $\bar{x}$ and σ.

c. What fraction of the molecules has $x > 2\lambda$?

1.12 Determine the number of ways of placing three balls in three numbered boxes for each of the following cases.

a. The balls are distinguishable with a limit of one ball per box.

b. The balls are distinguishable with no limit on the number per box.

c. The balls are indistinguishable with a limit of one ball per box.

d. The balls are indistinguishable with no limit on the number per box.

Construct four tables showing all possible distributions for each case.

1.13 A sum we will deal with often is

$$\sum_{J=0}^{\infty} (2J+1)\, e^{-BJ(J+1)},$$

where B is a positive constant.

a. Approximate this sum by assuming that J is a continuous variable.

Hint: Define a new variable $K = J(J+1)$.

b. Using the Euler–MacLaurin summation formula (Appendix D.3), derive Mulholland's expansion

$$\sum_{J=0}^{\infty} (2J+1)e^{-BJ(J+1)} = \frac{1}{B}\left[1 + \frac{B}{3} + \frac{B^2}{15} + \cdots\right].$$

1.14 A rifleman's shots on a target are distributed with a probability density $f(x, y) = Ce^{-r^2}$, where $r = (x^2 + y^2)^{1/2}$ is the distance from the center of the bulls-eye, measured in centimeters. Given that a particular shot is at least 1 cm high, determine the probability that it is also at least 1 cm to the right.

Hint: See Appendix B.

1.15 Let $f(x, y)$ be a joint probability density function, i.e., $f(x, y)\, dx\, dy$ is the probability that X lies between x and $x + dx$ and Y lies between y and $y + dy$. If X and Y are independent, then

$$f(x, y)\, dx\, dy = f_1(x)\, f_2(y)\, dx\, dy.$$

Therefore, if $W = X + Y$, show that

$$\overline{W} = \overline{X} + \overline{Y}$$

and that

$$\overline{(W-\overline{W})^2} \quad = \quad \overline{(X-\overline{X})^2} + \overline{(Y-\overline{Y})^2}.$$

In other words, if X and Y are independent, the mean and variance of their sum is equal to the sum of their means and variances.

1.16 Gaussian integrals appear often in statistical thermodynamics and particularly in kinetic theory. Consider the zeroth order Gaussian integral $I_0(\alpha)$ and the gamma function $\Gamma(x)$:

$$I_0(\alpha) = \int_0^\infty e^{-\alpha x^2}\, dx \qquad \Gamma(x) = \int_0^\infty t^{x-1} e^{-t}\, dt.$$

a. Evaluate $I_0(\alpha)$ by squaring it, i.e.,

$$I_0^2 = \int_0^\infty \int_0^\infty e^{-\alpha x^2} e^{-\alpha y^2}\, dx\, dy,$$

and transforming to polar coordinates.

b. Demonstrate the following results for the gamma function:
(1) $\Gamma(1) = 1$
(2) $\Gamma(x+1) = x\Gamma(x)$
(3) $\Gamma(n+1) = n!$ for n an integer.

c. Show that $\Gamma(1/2) = \sqrt{\pi}$.

d. Verify the following standard expression for the nth order Gaussian integral:

$$I_n(\alpha) = \int_0^\infty x^n e^{-\alpha x^2}\, dx = \frac{1}{2\alpha^{(n+1)/2}} \Gamma\left(\frac{n+1}{2}\right).$$

Use this expression to evaluate the Gaussian integrals for $n = 0 - 5$. Compare your results to those tabulated in Appendix B.

3 The Statistics of Independent Particles

Now that we have reviewed the essentials of probability and statistics, we are mathematically prepared to pursue our primary goal, which is to understand at a basic statistical level the fundamental laws and relations of classical thermodynamics. To avoid unnecessary complications, we will begin by evaluating the macroscopic properties of simple compressible systems composed of *independent particles*. The most important thermodynamic systems of this type are those describing the behavior of ideal gases. Recall that all gases behave as independent particles at sufficiently low density because of their weak intermolecular interactions combined with their extremely short-range intermolecular potentials. Such gaseous systems constitute a propitious place to begin our study of statistical thermodynamics because by invoking the assumption of independent particles, our upcoming statistical analyses can be based rather straightforwardly on probability theory describing independent events, as summarized in Chapter 2.

While considering assemblies of independent particles, we will pursue new insight with respect to three basic concepts important to classical thermodynamics. First, we will seek a whole new statistical understanding of entropy. Second, we will develop a related statistical definition of thermodynamic equilibrium. Third, in so doing, we will gain new perspective concerning the significance of temperature in properly defining thermal equilibrium. Once we understand these three major concepts, we will be in a position to develop statistical expressions allowing us to evaluate the thermodynamic properties of an assembly from the quantum mechanical properties of its individual particles. In essence, by statistically averaging over a sufficient number of particles, perhaps 10^{10}–10^{25}, we will be able to calculate typical thermodynamic properties such as the specific heat at constant pressure, the internal energy or enthalpy, the entropy, and the Gibbs free energy. Such calculated properties are tabulated for selected gaseous species in Appendix E. These compilations should prove helpful as you will be able to compare your calculations to those listed in the tables, thus eventually developing full confidence in your understanding of statistical thermodynamics.

Before proceeding, however, you should carefully examine whether or not our preliminary discussion in this chapter might have already stirred uncertainty regarding your knowledge of undergraduate thermodynamics. While such hesitancy would be unsurprising, nevertheless now is the best time to evaluate honestly your understanding of the important concepts and relations of classical thermodynamics. To guide you in this endeavor, a

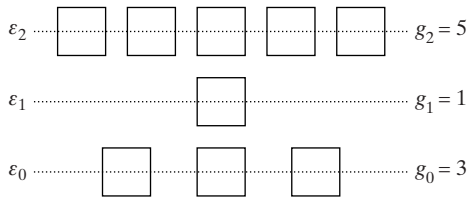

Figure 3.1 Example energy-level diagram.

summary of the most important results from classical thermodynamics that you will need for your study of statistical thermodynamics is provided in Appendix F. You should review this material immediately to make sure that you have the required background for this textbook. If necessary, you should also refresh your knowledge of classical thermodynamics by selectively re-reading your undergraduate textbook on the subject.

3.1 Essential Concepts from Quantum Mechanics

In preparation for our study of elementary statistical thermodynamics, we recapitulate and expand somewhat on those essential notions from quantum mechanics required for our upcoming statistical analyses. To avoid unnecessary complications, the background needed to derive or fully understand the following four conceptual presumptions is deferred for now to Chapter 5.

The first concept is that energy for a single atom or molecule is always *quantized*, as implied by the three discrete energy levels designated ε_0, ε_1, and ε_2 in the energy-level diagram of Fig. 3.1. As discussed previously in Chapter 1, quantization is suggested by the discrete lines appearing in both atomic and molecular spectra. The second essential concept is that the available energy levels are not necessarily equally probable. This statement is in accord with the different number of energy states associated with each energy level, as described by the degeneracies, g_0, g_1, and g_2, in Fig. 3.1. We will find in Chapter 5 that each energy or *quantum* state is defined by its own unique set of so-called *quantum numbers*. This unique specification at either the atomic or molecular level suggests that each energy state, rather than each energy level, can be considered equally likely, as discussed more fully in Section 3.3.

Returning to our discussion in Chapter 2, the third essential concept is that most particles are indistinguishable rather than distinguishable owing to the probabilistic nature of matter at atomic dimensions. From a different perspective, the uncertainty principle suggests that molecules can be counted but not discerned because their momentum and position cannot be specified simultaneously. If, however, atoms are aligned structurally either within or on the surface of a crystalline material, for example, then discernment of particular atoms becomes possible, thus making the particles distinguishable. The fourth and final concept concerns the possible number of particles permitted per energy state. For some particles, such as protons and electrons, only one particle is allowed per energy state. Other particles, such as photons, display no limit on the number allowed per energy state. For simplicity, the former particles are called *fermions* while the latter are called *bosons*.

In summary, then, the crucial information needed from quantum mechanics to make statistical thermodynamic calculations is the energy, ε_j, and the degeneracy, g_j, corresponding to the jth energy level of the relevant atom or molecule. In addition, for statistical purposes, we must know whether the particle of interest is (1) distinguishable or

indistinguishable and (2) fermion or boson. The procedures for determining ε_j, g_j, and the particle type will be discussed at length in Chapters 5–7.

3.2 The Ensemble Method of Statistical Thermodynamics

The most general statistical procedure for calculating thermodynamic properties is called the ensemble method, as developed by the American engineer and scientist J. Willard Gibbs (1839–1903). The Gibbs approach works for both dependent and independent particles, thus making it very powerful for realistic thermodynamic systems. Unfortunately, the ensemble method, while powerful, is quite abstract and often obfuscates the learning process for novices. Indeed, the ensemble method is typically more appreciated by those who already understand statistical thermodynamics!

Accordingly, while certainly exploiting the Gibbs method, our main focus in this book will be on the more restrictive Maxwell–Boltzmann (M–B) method, which presumes an *isolated system of independent particles*. Fortunately, despite the inherent lack of breadth of the M–B approach, many practical systems can, in fact, be modeled as if they were composed of independent particles. Examples include not only the ideal gas, but also electrons, radiation, and the crystalline solid. In addition, pedagogically, the M–B method is more intuitive and thus it furnishes a necessary foundation for fully appreciating the rigorous beauty of the Gibbs method.

Nevertheless, despite the intrinsic utility of the M–B method, conceptual clarity testifies that the basic postulates of statistical thermodynamics are best expressed in terms of the ensemble method. For this reason, we begin our study with the *rudiments* of the ensemble approach, thus developing a solid theoretical foundation for our exploration of statistical thermodynamics. We then shift to the M–B approach in preparation for model development and actual computations of thermodynamic properties. By introducing the ensemble method at this juncture, we proffer an additional advantage – a contextual understanding of the inherent presumptions underlying the M–B approach to statistical thermodynamics. From a practical viewpoint, the resulting insights also build a stronger framework for our eventual exploitation of the ensemble method, as pursued more fully in Chapters 18 and 19.

With this strategy in mind, we begin by defining an ensemble as follows.

> An *ensemble* is a theoretical collection of a very large number η of systems, each of which replicates the *macroscopic* thermodynamic system under investigation.

As we will see in Chapter 18, there are three main types of ensembles, depending on what type of macroscopic system is being replicated to create the ensemble. The *microcanonical* ensemble is composed of η *isolated* systems (N, V, U), for which the total number of particles, N, the volume, V, and the internal energy, U, are the replicated thermodynamic properties. The *canonical* ensemble is composed of η *closed, isothermal* systems (N, V, T), for which the total number of particles, the volume, and the temperature, T, are the independent thermodynamic parameters. Finally, the *grand canonical* ensemble is composed of η *open, isothermal* systems (μ, V, T), for which the chemical potential, μ, the volume, and the temperature are the constant independent variables.

In general, an ensemble is really a supersystem composed of η replicated thermodynamic systems, such as a room, a piston–cylinder assembly, or a nozzle. To ensure proper replication, no mass or energy can be permitted to cross the overall boundary of the

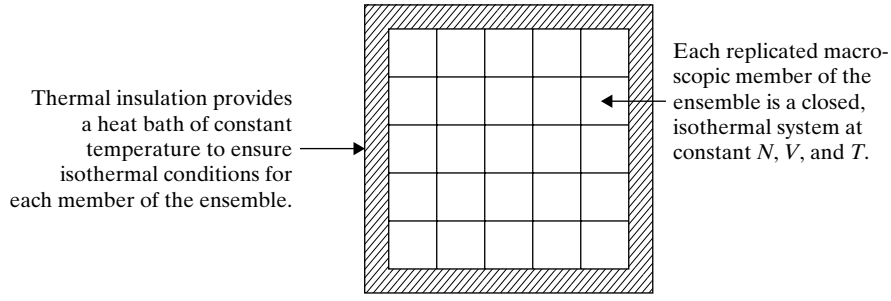

Figure 3.2 Diagram for the canonical ensemble; the entire ensemble is an isolated supersystem.

constructed supersystem. Hence, the entire ensemble, no matter what type, must always be isolated. As an example, Fig. 3.2 demonstrates the construction of an *isolated supersystem* for the canonical ensemble.

We may now link the M–B and Gibbs approaches by first recalling that the M–B method requires an isolated system containing N independent particles. If we consider the canonical ensemble of Fig. 3.2, this condition can be assured by artificially restricting each member of the ensemble to a single particle. In this way, the supersystem of the ensemble method becomes the thermodynamic system of the M–B method. The particles are guaranteed to be independent because each particle is associated with an independent member of the ensemble. The M–B system is guaranteed to be isolated because the constructed supersystem is isolated by definition. The result is that the number of independent particles, N, becomes equal to the number of replicated macroscopic systems, η.

3.3 The Two Basic Postulates of Statistical Thermodynamics

Now that we have linked the M–B and Gibbs approaches, we are ready to introduce the two basic postulates of statistical thermodynamics. These basic postulates are formally expressed in terms of ensemble theory. Hence, after presenting and discussing the postulates, we will convert them to an equivalent form suitable for application when using the M–B method. You should understand from the outset that these two postulates *cannot* be proved; their truth lies solely in the efficacy with which they can eventually provide both a deeper understanding of classical thermodynamics and correct calculations of thermodynamic properties.

The two basic postulates of statistical thermodynamics can be stated as follows:

1. The time average of a system thermodynamic variable is equal to its ensemble average, which is the average over the instantaneous values of the variable in each member of the ensemble as $\eta \to \infty$.
2. For an isolated thermodynamic system, the members of the ensemble are distributed with equal probability over the possible system quantum states defined by specification of N, V, and U.

The first postulate claims that for any thermodynamic variable the average determined by sampling each member of the ensemble at a single moment in time is equivalent to that found by statistically analyzing a time series of that variable when obtained from

one member of the ensemble. Stated more succinctly, this so-called *ergodic hypothesis* simply posits an equivalency between temporal and ensemble averages. The condition, $\eta \to \infty$, ensures that all possible system quantum states are accounted for by the members of the ensemble. On this basis, the second postulate claims that each member of the ensemble becomes equally likely for an isolated thermodynamic system. The system must, of course, be isolated to avoid any interactions with the environment that would perturb the number or identity of system quantum states. Notice that the second postulate, dubbed the *principle of equal a priori probability*, inherently comports with the microcanonical ensemble. As we will see in Chapter 18, the microcanonical and canonical ensembles generally provide the most useful connections between the M–B and Gibbs methods of statistical thermodynamics.

3.3.1 The M–B Method: System Constraints and Particle Distribution

Recall that the M–B method presumes an isolated system of independent particles. For an isolated system, the total mass and energy of the system must remain constant. Hence, we have two system constraints that can be expressed as

$$N = \sum_j N_j = \text{constant}$$
$$E = \sum_j N_j \varepsilon_j = \text{constant},$$

where N_j is the number of particles occupying the jth energy level with energy, ε_j. Expressing the total number of particles, N, and the total energy, E, in terms of summations over all possible energy levels inherently implies independent particles. We also note that the total system energy, E, must, of course, be equivalent to the macroscopic internal energy, U.

The specification of the number of particles, N_j, within each energy level, with its respective energy, ε_j, is called the *particle distribution*. The ratio, N_j/N, indicates either (1) the fraction of total particles in the jth energy level or (2) the probability that a single particle will be in the jth energy level. Many distributions are, of course, possible, and these distributions vary continuously with time because of particle collisions. However, considering the vast number of possible distributions, temporally averaging over all of them would be an overwhelming task. Fortunately, however, we know from classical thermodynamics that properties such as the internal energy have a well-defined value for an isolated system, thus suggesting that a most probable distribution might define the equilibrium state for a system containing a large number of atoms or molecules. We will pursue this strategic point further in Section 3.4.

3.3.2 The M–B Method: Microstates and Macrostates

We have seen in the previous section that a particle distribution is ordinarily specified by the number of particles in each *energy level*, $N_j(\varepsilon_j)$. Because of its importance for the M–B method, this particle distribution is called a *macrostate*. We could, of course, consider more directly the influence of degeneracy and specify instead the number of distinct particles in each *energy state*, $N_i(\varepsilon_i)$. This more refined distribution is called a *microstate*. Clearly, for each separate macrostate, there are many possible microstates owing to the potentially high values of the degeneracy, g_j. Hence, the most probable distribution of

particles over energy levels should correspond to that macrostate associated with the greatest number of microstates.

Based on the above notions of microstate and macrostate, we may recast the two basic postulates of statistical thermodynamics in forms suitable for application to the M–B method. Therefore, for an isolated system of independent particles, we now have the following:

1. The time average for a thermodynamic variable is equivalent to its average over all possible microstates.
2. All microstates are equally probable; hence, the relative probability of each macrostate is given by its number of microstates.

In making the above transformations, we have associated the microstate of the M–B method with the system quantum state of the Gibbs method, as both reflect a distribution over energy states. Hence, for the ergodic hypothesis, the ensemble average over all possible system quantum states is replaced by the analogous average over all possible microstates. Similarly, if each system quantum state is equally likely, then every microstate must also be equally likely. As a result, the most probable macrostate must be that having the largest number of microstates.

EXAMPLE 3.1

Consider an isolated system of independent particles with the following allowed energy levels and associated degeneracies: $\varepsilon_0 = 0$, $g_0 = 1$; $\varepsilon_1 = 1$, $g_1 = 2$; $\varepsilon_2 = 2$, $g_2 = 3$. If the system holds only two particles and the total energy is two units, determine (a) the number of macrostates, (b) the number of microstates for distinguishable particles, and (c) the number of microstates for indistinguishable particles. For simplicity, assume no limit on the number of particles per energy state.

Solution

(a) If only two independent particles are available, they must be distributed among the three allowed energy levels either with one particle at $\varepsilon_0 = 0$ and the other at $\varepsilon_2 = 2$ or with both at $\varepsilon_1 = 1$. Indeed, given two particles, these two particle distributions represent the only ways by which the total energy can be two units. Therefore, this isolated system contains only two macrostates.

(b) The following table identifies the possible microstates for each macrostate when the particles are distinguishable. Macrostate #1 has six microstates and macrostate #2 has four microstates. Hence, the total number of microstates is 10. In this case, macrostate #1 is the most probable macrostate.

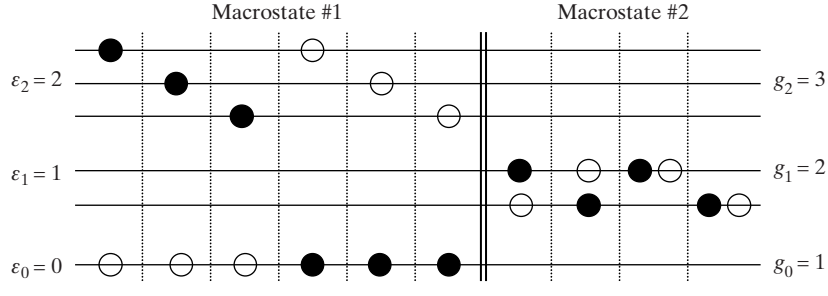

(c) For indistinguishable particles, the distinguishable open and closed circles are irrelevant. Hence, the number of microstates in both macrostate #1 and macrostate #2 is three, for a total of six microstates.

3.4 The Most Probable Macrostate

We have previously hypothesized that thermodynamic properties can be evaluated by considering only the most probable macrostate, i.e., the most probable distribution of particles over energy levels. Surprisingly enough, we can actually demonstrate that a large majority of all possible microstates is affiliated with the most probable macrostate. This remarkable inference is conveniently validated by example in the remainder of this section. More generally, ensemble theory will be employed in Chapter 18 to show rigorously that this conclusion stems from the large number of particles in a typical macroscopic system. On this basis, thermodynamic properties such as the temperature are always well defined, with little or no observable fluctuations in any measurable time series.

To demonstrate the statistical power of the most probable macrostate, we shall formulate a sufficiently generic case, identifying each possible macrostate and then determining the associated number of microstates per macrostate. To ensure realistic magnitudes for the statistical calculations, we assume distinguishable particles with no limit on the number of particles per energy state. For clarity of presentation, we initially choose $N = 6$ particles distributed into $M = 2$ nondegenerate energy levels. To investigate the influence of large numbers, we subsequently consider $N = 10^{23}$ particles so as to model a macroscopic thermodynamic system.

We begin by determining the number of possible particle distributions or macrostates, W_m, which is equivalent to the number of ways that N indistinguishable objects can be placed in M different containers with no limitation on the number of objects per container. Indistinguishability is temporarily presumed here because we are only concerned with the number of objects in each container and not their order of placement. We thus have, from Eq. (2.31),

$$W_m = \frac{(N + M - 1)!}{N!\,(M - 1)!},$$

so that, for $M = 2$,

$$W_m = N + 1. \tag{3.1}$$

Hence, given $N = 6$, we find that $W_m = 7$; these seven macrostates identify six particles distributed between two energy levels as follows: $\{0, 6\}$, $\{1, 5\}$, $\{2, 4\}$, $\{3, 3\}$, $\{4, 2\}$, $\{5, 1\}$, and $\{6, 0\}$.

Next, we determine the number of possible arrangements for a given particle distribution, or the number of microstates per macrostate, W_d, which is equivalent to the number of ways that N distinguishable objects can be placed in M different containers such that N_i objects occupy the ith container. Employing Eq. (2.28), we have

$$W_d = \frac{N!}{\prod_{i=1}^{M} N_i!},$$

so that, for each of the above macrostates, we obtain $W_d\{0, 6\} = W_d\{6, 0\} = 1$, $W_d\{1, 5\} = W_d\{5, 1\} = 6$, $W_d\{2, 4\} = W_d\{4, 2\} = 15$, and $W_d\{3, 3\} = 20$. Hence, we find that the number of microstates associated with the most probable macrostate, W_{mp}, is 20. Similarly, the total number of microstates, W, is given by $2(1 + 6 + 15) + 20 = 64$.

We can independently determine the total number of possible arrangements or microstates because this tally is equivalent to the number of ways N distinguishable objects can be placed in M different containers with no limitation on the number per container. Hence, from Eq. (2.29), the total number of microstates is

$$W = M^N \tag{3.2}$$

so that $W = 2^6 = 64$, in agreement with our previous calculation. In summary, then, we find that $W = 64$, $W_{mp} = 20$, and thus that the mean number of microstates $\overline{W} = W/W_m \simeq 9$. Consequently, comparing these three statistics, we may write the expected result for any $N > M$; i.e.,

$$W > W_{mp} > \overline{W}. \tag{3.3}$$

Let us now consider a very large number of particles, say $N = 10^{23}$. For $M = 2$, the total number of microstates and the mean number of microstates can be expressed as

$$W = 2^N \qquad \overline{W} = \frac{2^N}{N+1},$$

where we have employed Eqs. (3.1) and (3.2). Therefore,

$$\ln W = N \ln 2 \simeq 7.0 \times 10^{22}$$
$$\ln \overline{W} = N \ln 2 - \ln(N+1) \simeq 7.0 \times 10^{22} - 53.$$

Remarkably, almost no difference arises between $\ln W$ and $\ln \overline{W}$ for large N. Consequently, using Eq. (3.3), we have for a very large number of particles

$$\ln W \simeq \ln W_{mp} \simeq \ln \overline{W}, \tag{3.4}$$

so that

$$\lim_{N\to\infty} \frac{\ln W_{mp}}{\ln W} = 1. \tag{3.5}$$

Equation (3.5) indicates that for macroscopic thermodynamic systems almost all microstates are associated with the most probable macrostate. Hence, the only significant particle distribution is that which is most probable. As indicated previously, this result can be validated in a rigorous fashion via ensemble theory, although the statistical proof from ensemble theory is also suggested by the binomial distribution. In particular, from Eqs. (2.15) and (2.16),

$$\frac{\sigma}{\mu} = \frac{\sqrt{Np(1-p)}}{Np} = \frac{1}{\sqrt{N}} \tag{3.6}$$

for a fairly-weighted coin, and thus

$$\lim_{N\to\infty} \frac{\sigma}{\mu} = 0. \tag{3.7}$$

The significant conclusion from both Eqs. (3.5) and (3.7) is that utilizing the most probable distribution of particles over energy levels is essentially equivalent to averaging over

all microstates because those microstates associated with the most probable macrostate invariably account for nearly all possible microstates. Therefore, from the perspective of classical thermodynamics, *the most probable particle distribution must represent the equilibrium particle distribution*!

3.5 Bose–Einstein and Fermi–Dirac Statistics

We now proceed to identify mathematically the most probable macrostate for an isolated system of independent particles by investigating thoroughly both Bose–Einstein and Fermi–Dirac statistics. Bose–Einstein statistics describe the behavior of indistinguishable particles with no limit on the number of particles per energy state. Such particles are called *bosons*. In comparison, Fermi–Dirac statistics describe the behavior of indistinguishable particles with a limit of one particle per energy state. These particles are called *fermions*. For each particle type, we derive a general expression for the number of microstates per macrostate. We then determine the extremum for this expression, including constraints imposed by an isolated system, so as to identify the most probable particle distribution. The mathematical procedure that we will employ is called the method of Lagrange multipliers, which is discussed in detail in Appendix D.1.

3.5.1 Bose–Einstein Statistics

For each case, we begin by deriving an expression for the number of microstates per macrostate, which represents the total number of ways an arbitrary particle distribution can arise when accounting for all possible energy levels. Let us first consider one energy level. The number of ways in which N_j bosons in a single energy level, ε_j, may be distributed among g_j energy states is equivalent to the number of ways in which N_j identical, indistinguishable objects may be arranged in g_j different containers, with no limitation on the number of objects per container. Hence, employing Eq. (2.31), we have

$$W_j = \frac{(N_j + g_j - 1)!}{N_j!\,(g_j - 1)!}.$$

Because each energy level represents an independent event, the total number of ways of obtaining an arbitrary particle distribution becomes

$$W_{BE} = \prod_j W_j = \prod_j \frac{(N_j + g_j - 1)!}{N_j!\,(g_j - 1)!}. \tag{3.8}$$

In other words, W_{BE} identifies the generic number of microstates per macrostate for Bose–Einstein statistics.

Taking the natural logarithm of Eq. (3.8), we obtain

$$\ln W_{BE} = \sum_j \{\ln(N_j + g_j)! \; - \; \ln N_j! \; - \ln g_j!\},$$

where we have neglected the unity terms since $g_j \gg 1$. Applying Stirling's approximation, i.e., $\ln N! = N \ln N - N$ (Appendix D.2), we find that

$$\ln W_{BE} = \sum_j \{(N_j + g_j)\ln(N_j + g_j) - N_j \ln N_j - g_j \ln g_j\}$$

or

$$\ln W_{BE} = \sum_j \left\{ N_j \ln \frac{g_j + N_j}{N_j} + g_j \ln \frac{g_j + N_j}{g_j} \right\}. \tag{3.9}$$

3.5.2 Fermi–Dirac Statistics

We again develop an expression for the number of microstates per macrostate, but this time for fermions. The number of ways in which N_j fermions in a single energy level, ε_j, may be distributed among g_j energy states is equivalent to the number of ways in which N_j identical, indistinguishable objects may be arranged in g_j different containers, with no more than one object per container. Hence, employing Eq. (2.30), we have

$$W_j = \frac{g_j!}{N_j!\,(g_j - N_j)!},$$

where the $N_j!$ term in the denominator accounts for particle indistinguishability. The total number of ways of obtaining an arbitrary particle distribution then becomes

$$W_{FD} = \prod_j W_j = \prod_j \frac{g_j!}{N_j!\,(g_j - N_j)!}, \tag{3.10}$$

so that W_{FD} denotes the generic number of microstates per macrostate for Fermi–Dirac statistics.

Taking the natural logarithm of Eq. (3.10), we obtain

$$\ln W_{FD} = \sum_j \{\ln g_j! \; - \ln N_j! \; - \ln(g_j \; - N_j)!\}.$$

Applying Stirling's approximation (Appendix D.2), we find that

$$\ln W_{FD} = \sum_j \{g_j \ln g_j - N_j \ln N_j - \; (g_j \; - N_j) \ln(g_j \; - N_j)\}$$

or

$$\ln W_{FD} = \sum_j \left\{ N_j \ln \frac{g_j - N_j}{N_j} - g_j \ln \frac{g_j - N_j}{g_j} \right\}. \tag{3.11}$$

EXAMPLE 3.2

A thermodynamic assembly consists of five independent particles having access to two energy levels. A particular particle distribution for this system and the associated degeneracies for each energy level are as follows: (1) $N_1 = 2,\ g_1 = 4;$ (2) $N_2 = 3,\ g_2 = 6$. Determine the number of microstates for this macrostate if the particles are (a) bosons and (b) fermions.

Solution

(a) For bosons, the number of ways that a single energy level can be constructed is

$$W_j = \frac{(N_j + g_j - 1)!}{N_j!\,(g_j - 1)!}.$$

Thus, for each energy level, $W_1 = 5!/(2!3!) = 10$ and $W_2 = 8!/(3!5!) = 56$. As a result, the number of microstates for this macrostate is $W = W_1 \times W_2 = 560$.

(b) For fermions, the number of ways that a single energy level can be constructed is

$$W_j = \frac{g_j!}{N_j!\,(g_j - N_j)!}.$$

Hence, for each energy level, $W_1 = 4!/(2!2!) = 6$ and $W_2 = 6!/(3!3!) = 20$. Consequently, the number of microstates for this macrostate is $W = W_1 \times W_2 = 120$.

3.5.3 The Most Probable Particle Distribution

Equations (3.9) and (3.11) can easily be combined into one expression for both Bose–Einstein and Fermi–Dirac statistics:

$$\ln W_{\left\{\substack{BE\\FD}\right\}} = \sum_j \left\{ N_j \ln \frac{g_j \pm N_j}{N_j} \pm g_j \ln \frac{g_j \pm N_j}{g_j} \right\}, \tag{3.12}$$

where the upper sign (+) refers to Bose–Einstein statistics and the lower sign (−) refers to Fermi–Dirac statistics. For simplicity of nomenclature, from here on we will omit the combined BE-FD subscript; our convention will be that the *upper sign always applies to Bose–Einstein statistics* and the *lower sign always applies to Fermi–Dirac statistics*.

The most probable particle distributions for Bose–Einstein and Fermi–Dirac statistics can now be determined by maximizing Eq. (3.12) subject to the two constraints

$$\sum_j N_j = N \tag{3.13}$$

$$\sum_j N_j \varepsilon_j = E. \tag{3.14}$$

Equations (3.13) and (3.14) reflect the constant (E, V, N) conditions for an isolated system, as required by the M–B method of statistical thermodynamics. Employing the Lagrange method of undetermined multipliers (Appendix D.1), we first expand Eq. (3.12) and then differentiate the result with respect to N_j to find the most probable distribution of N_j among its allowed energy levels. The step-by-step outcome is

$$\ln W = \sum_j \{N_j \ln(g_j \pm N_j) - N_j \ln N_j \pm g_j \ln(g_j \pm N_j) \mp g_j \ln g_j\}$$

$$d \ln W = \sum_j \left\{ \ln(g_j \pm N_j) \pm \frac{N_j}{g_j \pm N_j} - \ln N_j - 1 + \frac{g_j}{g_j \pm N_j} \right\} dN_j$$

$$d \ln W = \sum_j \{\ln(g_j \pm N_j) - \ln N_j\}\, dN_j, \tag{3.15}$$

where g_j and ε_j are taken as constants during the differentiation. From quantum mechanics, it turns out that the degeneracy, g_j, is simply an integer and the level energy, ε_j, is a function only of the total volume, V, which is, of course, constant for an isolated system. These two strategic points will be dealt with more thoroughly when we consider quantum mechanics in Chapter 5.

Equations (3.13) and (3.14) are now differentiated to account for the imposed constraints during the optimization process. The results are

$$\sum_j dN_j = 0 \qquad \sum_j \varepsilon_j \, dN_j = 0. \tag{3.16}$$

Introducing multiplied unknowns into Eqs. (3.16), we then subtract both expressions from Eq. (3.15) to guarantee independent values of N_j. We thus obtain

$$\sum_j \{\ln(g_j \pm N_j) - \ln N_j - \alpha - \beta\varepsilon_j\} \, dN_j = 0, \tag{3.17}$$

where the unknowns α and β are the so-called Lagrange multipliers, and the entire expression is set equal to zero to identify the most probable macrostate.

As discussed in Appendix D.1, the requirement specified by Eq. (3.17) can be achieved for all j only if

$$\ln \frac{g_j \pm N_j}{N_j} = \alpha + \beta\varepsilon_j.$$

Hence, the most probable distribution among energy levels becomes

$$N_j = \frac{g_j}{\exp(\alpha + \beta\varepsilon_j) \mp 1}. \tag{3.18}$$

Equation (3.18) thus defines from a molecular viewpoint the specific condition ensuring thermodynamic equilibrium for a macroscopic system of independent particles.

3.6 Entropy and the Equilibrium Particle Distribution

The most probable particle distribution of Eq. (3.18) is still incomplete as we need expressions for the Lagrange multipliers, α and β. To proceed further, we must now develop a primal correspondence between statistical and classical thermodynamics. This correspondence requires that we relate the macroscopic definition of entropy to a probabilistic description of microscopic particle behavior.

3.6.1 The Boltzmann Relation for Entropy

Our strategy involves seeking a relation between the entropy and the total number of available microstates describing an isolated thermodynamic system. Because each microstate is equally likely, a macrostate becomes more probable upon being affiliated with a greater number of microstates. For this reason, the total number of microstates, W, is often called the *thermodynamic probability*.

The relation between entropy and thermodynamic probability was discovered by the Austrian physicist Ludwig Boltzmann (1844–1906) through a simple thought experiment involving the concept of an irreversible process. Consider the expansion of a gas within a partitioned chamber that is isolated from its environment, as shown in Fig. 3.3. Suppose that chamber A originally contains a gas while chamber B is under vacuum. When the valve is opened and the gas expands into the vacuum, the entropy, S, must increase owing to the irreversibility of the process. On the other hand, from a microscopic perspective, the thermodynamic probability must also increase as the final state of the system must be more probable than its initial state. Hence, we can hypothesize that $S = f(W)$.

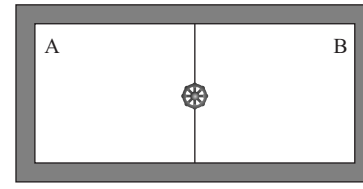

Figure 3.3 Isolated system containing two chambers A and B with valve in separating partition.

The functional form involved in the proposed relation can be discerned by considering two independent subsystems, A and B, again as in Fig. 3.3. Because entropy is additive and probability is multiplicative for independent entities, we may assert that

$$S_{AB} = S_A + S_B \qquad W_{AB} = W_A \cdot W_B.$$

Only one function can convert a multiplicative operation to an additive operation. Hence, we postulate that the entropy is related to the total number of microstates through the *Boltzmann relation*,

$$S = k \ln W, \tag{3.19}$$

where the constant of proportionality, k, is called *Boltzmann's constant*. As we will discover, Eq. (3.19) has received extensive confirmation in the scientific literature; in fact, the resulting statistical calculations, as performed later in this book, comport beautifully with both experimental behavior and thermodynamic measurements.

3.6.2 Identification of Lagrange Multipliers

Equation (3.5) implies that Eq. (3.19) can be represented by

$$S = k \ln W_{mp}, \tag{3.20}$$

so that a general expression for the entropy can be derived from Eq. (3.20) by employing Eq. (3.12) with the most probable distribution, as given by Eq. (3.18). We begin by rewriting Eq. (3.12) as

$$\ln W = \sum_j \left\{ N_j \ln \frac{g_j \pm N_j}{N_j} \pm g_j \ln \frac{g_j \pm N_j}{g_j} \right\}. \tag{3.21}$$

Now, invoking the most probable distribution, from Eq. (3.18) we obtain

$$\frac{g_j \pm N_j}{N_j} = \exp(\alpha + \beta \varepsilon_j). \tag{3.22}$$

Manipulation of Eq. (3.22) gives

$$\frac{N_j}{g_j} = [\exp(\alpha + \beta \varepsilon_j) \mp 1]^{-1},$$

which upon re-multiplication with Eq. (3.22) produces

$$\frac{g_j \pm N_j}{g_j} = [1 \mp \exp(-\alpha - \beta \varepsilon_j)]^{-1}. \tag{3.23}$$

Substitution of Eqs. (3.22) and (3.23) into Eq. (3.21) leads to

$$\ln W_{mp} = \sum_j \{ N_j(\alpha + \beta \varepsilon_j) \mp g_j \ln [1 \mp \exp(-\alpha - \beta \varepsilon_j)] \}, \tag{3.24}$$

whereupon Eqs. (3.20) and (3.24) give, after substitution from Eqs. (3.13) and (3.14),

$$S = k(\beta E + \alpha N) \mp k \sum_j g_j \ln [1 \mp \exp(-\alpha - \beta \varepsilon_j)]. \tag{3.25}$$

We can now evaluate the Lagrange multipliers, α and β, by comparing Eq. (3.25) to its classical analog from Appendix F, i.e.,

$$dS(E, V, N) = \frac{1}{T} dE + \frac{P}{T} dV - \frac{\mu}{T} dN, \tag{3.26}$$

where $U = E$ and P is the pressure for this single-component, isolated system. Applying partial differentiation to Eqs. (3.25) and (3.26), we find that (Problem 2.1)

$$\left(\frac{\partial S}{\partial E}\right)_{V,N} = \frac{1}{T} = k\beta$$

$$\left(\frac{\partial S}{\partial N}\right)_{E,V} = -\frac{\mu}{T} = k\alpha.$$

Therefore, the Lagrange multipliers, α and β, become

$$\beta = \frac{1}{kT} \tag{3.27}$$

$$\alpha = -\frac{\mu}{kT}. \tag{3.28}$$

Hence, while β is related solely to the temperature, α is also influenced by the chemical potential. Substituting Eqs. (3.27) and (3.28) back into Eq. (3.25), the entropy can now be expressed as

$$S = \frac{E - \mu N}{T} \mp k \sum_j g_j \ln \left\{1 \mp \exp\left[-\left(\frac{\varepsilon_j - \mu}{kT}\right)\right]\right\}. \tag{3.29}$$

From Eq. (3.26), a final partial differentiation with respect to the volume, V, ultimately gives the pressure,

$$P = -\sum_j N_j \left(\frac{\partial \varepsilon_j}{\partial V}\right)_{E,N}. \tag{3.30}$$

3.6.3 The Equilibrium Particle Distribution

Having obtained equations for the Lagrange multipliers, α and β, we may now obtain a final expression for the equilibrium particle distribution. Substituting Eqs. (3.27) and (3.28) into Eq. (3.18), we find that, for either Bose–Einstein or Fermi–Dirac statistics,

$$N_j = \frac{g_j}{\exp[(\varepsilon_j - \mu)/kT] \mp 1}. \tag{3.31}$$

Notice that the macroscopic variables, μ and T, entered into the equilibrium particle distribution only after the Lagrange multipliers were evaluated by relating microscopic to macroscopic thermodynamics through the Boltzmann relation. Hence, parameters such as the temperature are in actuality statistical concepts that can be defined only for an assembly of particles. In other words, for independent particles, temperature is a macroscopic property that arises only after a statistical averaging process that occurs through application of the M–B method of statistical thermodynamics.

EXAMPLE 3.3

A well-known professor at Purdue University has discovered a new fundamental particle labeled the boileron. The number of ways by which N_j boilerons in energy level, ε_j, can be distributed among its g_j energy states is found to be

$$W_j = \frac{1}{N_j!}\left[\frac{g_j!}{(g_j - N_j)!}\right]^2.$$

The energy of an isolated assembly of boilerons is fixed, but the total number of these strange particles is not conserved because of mysterious interactions with the walls of the enclosure. Using the methods of statistical thermodynamics, develop an expression for the equilibrium particle distribution for Purdue boilerons if $g_j \gg N_j$ and if β can be assumed, as usual, to be $1/kT$.

Solution

The number of microstates per macrostate for Purdue boilerons is obviously

$$W_B = \prod_j \frac{1}{N_j!}\left[\frac{g_j!}{(g_j - N_j)!}\right]^2.$$

We now use the method of Lagrange multipliers. We first take the logarithm of the above expression to obtain

$$\ln W_B = \sum_j \{2\ln g_j! - 2\ln(g_j - N_j)! - \ln N_j!\}.$$

Applying Stirling's approximation, we find that

$$\ln W_B = \sum_j \{2g_j \ln g_j - 2(g_j - N_j)\ln(g_j - N_j) - N_j \ln N_j - N_j\}.$$

We now take the derivative of the above expression, thus obtaining

$$d\ln W_B = \sum_j \{2\ln(g_j - N_j) - \ln N_j\}\, dN_j.$$

Introducing the Lagrange multiplier, β, and a differentiated form of the energy constraint from Eq. (3.16), we have

$$d\ln W_B = \sum_j \{2\ln(g_j - N_j) - \ln N_j - \beta\varepsilon_j\}\, dN_j = 0$$

at the extremum condition. Hence, we require

$$\ln\frac{(g_j - N_j)^2}{N_j} = \beta\varepsilon_j.$$

Applying the condition $g_j \gg N_j$, we obtain the equilibrium particle distribution,

$$N_j = g_j^2 \exp(-\varepsilon_j/kT).$$

Problems enhancing your understanding of this chapter are combined with those for Chapter 4 in Problem Set II.

4 Thermodynamic Properties in the Dilute Limit

In the previous chapter, we employed the Maxwell–Boltzmann method of statistical thermodynamics to investigate Bose–Einstein (B–E) and Fermi–Dirac (F–D) statistics for an isolated system of independent particles. The result for the number of microstates per macrostate was found to be

$$\ln W = \sum_j \left\{ N_j \ln \frac{g_j \pm N_j}{N_j} \pm g_j \ln \frac{g_j \pm N_j}{g_j} \right\}, \tag{4.1}$$

where the upper sign refers to B–E statistics and the lower sign to F–D statistics. Subsequently, application of the method of Lagrange multipliers to Eq. (4.1) led to an associated expression for the equilibrium particle distribution, i.e.,

$$N_j = \frac{g_j}{\exp[(\varepsilon_j - \mu)/kT] \mp 1}, \tag{4.2}$$

where again the upper sign refers to bosons and the lower sign to fermions. In this chapter, we develop simplified expressions based on Eqs. (4.1) and (4.2) that hold for both B–E and F–D statistics in the so-called dilute limit. The resulting equilibrium particle distribution provides the statistical foundation for the definition of the molecular partition function and consequently for the development of general thermodynamic expressions governing the properties of the ideal gas.

4.1 The Dilute Limit

The only difference between B–E and F–D statistics is the limitation on the number of particles per energy state, i.e., no limit for bosons and a limit of one particle per state for fermions. If, however, few particles were actually available as compared to energy states, then the B–E and F–D distributions should collapse to the same result as it would be rare to have an energy state occupied by more than one particle. This condition, given by $g_j \gg N_j$, is called the *dilute limit*. At this limit, the first and second terms of

Eq. (4.1) become, respectively,

$$\ln\left(\frac{g_j}{N_j} \pm 1\right) \simeq \ln\left(\frac{g_j}{N_j}\right)$$

$$\ln\left(1 \pm \frac{N_j}{g_j}\right) \simeq \pm\frac{N_j}{g_j},$$

where the logarithmic expansion $\ln(1 + x) \simeq x$ has been used to linearize the second term (Appendix B). Therefore, in the dilute limit, Eq. (4.1) becomes, uniquely,

$$\ln W_{DL} = \sum_j N_j \left\{\ln \frac{g_j}{N_j} + 1\right\}. \tag{4.3}$$

Consequently, for $g_j \gg N_j$, we find that the number of microstates per macrostate is

$$W_{DL} = \prod_j \frac{g_j^{N_j}}{N_j!}, \tag{4.4}$$

as could be proven by taking the logarithm of Eq. (4.4) and employing Stirling's approximation (Appendix D.2) so as to recapture Eq. (4.3).

4.2 Corrected Maxwell–Boltzmann Statistics

For comparative purposes, it is instructive at this point to consider the evolution of statistical thermodynamics from the perspective of classical rather than quantum mechanics. From this viewpoint, classical particles were assumed to be distinguishable rather than indistinguishable, with no limit on the number of particles per energy state. Historically, their statistics were independently investigated by James Clerk Maxwell (1831–1879) and Ludwig Boltzmann (1844–1906) before the advent of quantum mechanics. For this reason, such particles are said to follow Maxwell–Boltzmann (M–B) statistics, and may be called *boltzons*.

We begin as usual by developing an expression for the number of microstates per macrostate. Specifically, for classical particles, the number of ways in which N_j boltzons in a single energy level, ε_j, may be distributed among g_j energy states is equivalent to the number of ways in which N_j identical, distinguishable objects may be arranged in g_j different containers, with no limitation on the number of objects per container. Hence, employing Eq. (2.29), we have

$$W_j = g_j^{N_j},$$

so that the total number of ways of obtaining an arbitrary particle distribution for distinguishable particles, when considering all possible energy levels, appears to be

$$W_{\mathrm{a}} = \prod_j W_j = \prod_j g_j^{N_j}. \tag{4.5}$$

In comparison to our previous analyses for bosons and fermions, however, we recognize that, for distinguishable particles, a new microstate is formed when particles are exchanged among energy levels. To account for this classical complication, we must determine the number of possible particle distributions for distinguishable particles. This quantity is equivalent to the number of ways that N identical, distinguishable objects may be arranged

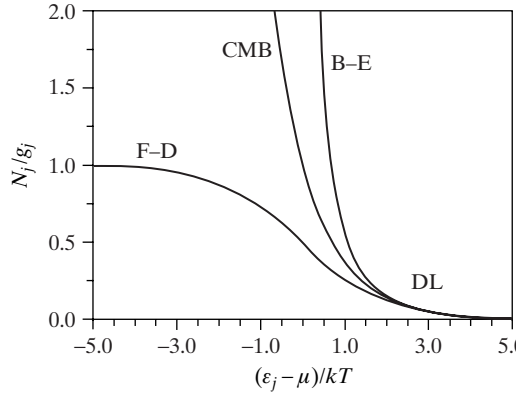

Figure 4.1 The dilute limit (DL) for Fermi–Dirac (F–D) and Bose–Einstein (B–E) statistics as compared to corrected M–B (CMB) statistics.

among available shelves (energy levels) such that N_j objects occupy the jth shelf, i.e., from Eq. (2.28),

$$W_{\mathrm{b}} = \frac{N!}{\prod_j N_j!}. \tag{4.6}$$

Therefore, multiplying Eqs. (4.5) and (4.6), we obtain the number of microstates per macrostate for M–B statistics,

$$W_{MB} = N! \prod_j \frac{g_j^{N_j}}{N_j!}. \tag{4.7}$$

If we now compare Eq. (4.7), based on classical M–B statistics for distinguishable particles, with Eq. (4.4), based on the dilute limit for indistinguishable particles, we note that

$$W_{DL} = \frac{W_{MB}}{N!}. \tag{4.8}$$

Owing to the transparency of Eq. (4.8), the dilute limit is often referred to as *corrected Maxwell–Boltzmann statistics*. In hindsight, we note that division by $N!$ in Eq. (4.8) accounts quite simply and directly for the reduced number of available permutations when distinguishable particles are replaced by indistinguishable particles. Unfortunately, the excess factor of $N!$ in Eq. (4.7) produced great confusion in the nineteenth century because this oversight led to an incorrect expression for the entropy of an ideal gas, as discussed further in Section 4.4.

4.3 The Molecular Partition Function

As might be expected from the previous section, corrected M–B statistics also leads to a unified expression for the most probable particle distribution. Indeed, if we invoke $g_j \gg N_j$, Eq. (4.2) becomes

$$N_j = g_j \exp\left(\frac{\mu - \varepsilon_j}{kT}\right). \tag{4.9}$$

Equation (4.9) represents the equilibrium distribution in the dilute limit, as portrayed by Fig. 4.1 through comparisons with Eq. (4.2) for both B–E and F–D statistics. Notice that the B–E and F–D cases are equivalent and thus $g_j \gg N_j$ only when $\varepsilon_j \gg \mu$. Because ε_j is

always positive, the dilute condition clearly applies when $\mu < 0$. Such negative chemical potentials are characteristic of ideal gases.

Given Eq. (4.9), we next explore some important features of the equilibrium particle distribution for corrected M–B statistics. In particular, we may write

$$N_j \exp\left(-\frac{\mu}{kT}\right) = g_j \exp\left(-\frac{\varepsilon_j}{kT}\right). \tag{4.10}$$

Now, summing over all j, from Eq. (4.10) we obtain

$$Ne^{-\mu/kT} = Z, \tag{4.11}$$

where we have defined the dimensionless *molecular partition function*,

$$Z = \sum_j g_j e^{-\varepsilon_j/kT}. \tag{4.12}$$

The partition function is the most important quantity in statistical thermodynamics. As we will discuss shortly, it indicates how particles in an assembly are partitioned among the various energy levels of an atom or molecule. The partition function can also, of course, be calculated by summing over energy states rather than energy levels, i.e.,

$$Z = \sum_i \exp(-\varepsilon_i/kT), \tag{4.13}$$

where each energy level is now represented by g_j terms of the same energy, ε_j. As Eqs. (4.12) and (4.13) are equivalent, the use of one rather than the other is solely a matter of convenience for a particular application. Although introduced here for indistinguishable particles in the dilute limit, the molecular partition function defined by Eq. (4.12) also works for distinguishable particles, as shown by Problems 2.3 and 2.5. More robust forms of the partition function can also be developed using ensemble theory, as discussed in Chapter 18.

The physical significance of the partition function can be understood by dividing Eq. (4.10) by Eq. (4.11) to obtain

$$\frac{N_j}{N} = \frac{g_j e^{-\varepsilon_j/kT}}{Z}, \tag{4.14}$$

so that for two energy levels, identified as j and k, we have

$$\frac{N_j}{N_k} = \frac{g_j}{g_k} \exp[-(\varepsilon_j - \varepsilon_k)/kT]. \tag{4.15}$$

Equation (4.14) represents the fractional population or the probability that a single atom or molecule resides in a particular energy level for either corrected or uncorrected M–B statistics. For this reason, Eq. (4.14) is often called the *Maxwell–Boltzmann distribution*. Similarly, Eq. (4.15) represents the ratio of particle populations between two different energy levels for bosons or fermions in the dilute limit.

A significant observation from Eq. (4.14) is that the population fraction for the jth energy level is given by the jth term in the molecular partition function divided by the partition function itself. Hence, for a given Z, the jth term in the molecular partition

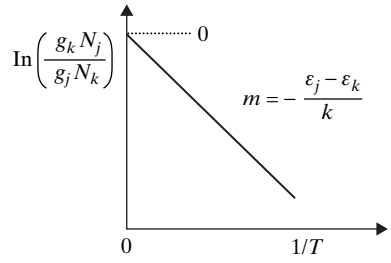

Figure 4.2 Maxwell–Boltzmann equilibrium particle distribution.

function represents the relative probability that a single particle will actually be in the *j*th energy level. From another perspective, at infinite temperature, Eq. (4.12) becomes

$$\lim_{T\to\infty} Z = \sum_j g_j,$$

which signifies the total number of energy states available to the particle assembly. Hence, the exponential factor for each term in the partition function represents a weighting multiplicand that accounts for the influence of temperature on the accessibility of each energy level. In this sense, the partition function indicates not only the effective number of energy states available to the particle assembly but also the partitioning of population among the available energy levels, as determined by both the number of energy states and their accessibility through the temperature of the thermodynamic system.

4.3.1 The Influence of Temperature

The importance of temperature to the equilibrium particle distribution can be further explored for two energy levels by casting Eq. (4.15) in the form

$$\ln\left(\frac{g_k N_j}{g_j N_k}\right) = -\frac{\varepsilon_j - \varepsilon_k}{kT}, \tag{4.16}$$

where $(\varepsilon_j - \varepsilon_k) \geq 0$. Hence, at thermal equilibrium,

$$\lim_{T\to 0}\left(\frac{g_k N_j}{g_j N_k}\right) = 0 \qquad \lim_{T\to\infty}\left(\frac{g_k N_j}{g_j N_k}\right) = 1,$$

so that, as temperature rises, the population shifts dramatically from predominance within lower energy levels to randomization among all energy levels. In other words, a greater temperature means enhanced particle energy and thus, from Eq. (4.16), more access to higher energy levels, as shown schematically in Fig. 4.2.

Continuing our thermal analysis, consider next the application of Eq. (4.15) to two energy levels, each containing a single energy state. If the energy of the ground state is $\varepsilon_\circ$, the population in the *i*th energy state, when fractionally compared to that in the ground state, is

$$\frac{N_i}{N_\circ} = \exp\left(-\frac{\varepsilon_i - \varepsilon_\circ}{kT}\right), \tag{4.17}$$

where $(\varepsilon_i - \varepsilon_\circ) \geq 0$. Hence, at thermodynamic equilibrium, the population of any upper or *excited* energy state can never exceed that of the ground state. Consequently, a so-called *population inversion* is always indicative of a nonequilibrium process. Subsequent

relaxation to the equilibrium distribution predicted by Eq. (4.14) invariably occurs through removal of excess energy from higher energy states via collisions or radiation, as discussed further in Chapter 11.

Presuming thermal equilibrium, we observe from Eqs. (3.14) and (4.17) that, as $T \to 0$, $E \to N\varepsilon_\circ$ because all particles following corrected M–B statistics are required to be in their ground state at absolute zero. Hence, a value of $\varepsilon_\circ$ must be specified to evaluate any properties involving the internal energy. Most often, we stipulate $\varepsilon_\circ = 0$, which is equivalent to making all energy calculations relative to a zero of energy at absolute zero. This methodology ensures consistency with measured values of energy, which must also be taken relative to some arbitrary zero of energy. A similar procedure can, in fact, be used for bosons, fermions, or boltzons so that, in general, $U = 0$ at $T = 0$. In Chapter 13, we will show that the thermodynamic probability of a *perfect* crystalline solid is unity at absolute zero. Hence, from Eq. (3.19), we may also assume that $S = 0$ at $T = 0$. On this basis, all thermodynamic properties should vanish at absolute zero.

4.3.2 Criterion for Dilute Limit

Recall that the dilute limit is defined by $g_j \gg N_j$; hence, from Eq. (4.9), we have

$$\exp[(\varepsilon_j - \mu)/kT] \gg 1.$$

However, $\exp(\varepsilon_j/kT) \geq 1$ so that the dilute limit is absolutely ensured if $\exp(-\mu/kT) \gg 1$. Consequently, Eq. (4.11) indicates that

$$\frac{Z}{N} = \exp(-\mu/kT) \gg 1. \tag{4.18}$$

Because of the ease with which the partition function can be calculated, Eq. (4.18) constitutes a very general and convenient criterion for establishing the dilute limit. In particular, for the ideal gas, this inequality is nearly always satisfied as $\mu \ll 0$.

EXAMPLE 4.1

A dilute system at thermodynamic equilibrium consists of 50 independent, indistinguishable particles. Each particle has three energy levels of energy $0, \varepsilon$, and 2ε, with degeneracies of 300, 600, and 1200, respectively. The system is at a constant temperature $T = \varepsilon/k$, where k is Boltzmann's constant.

(a) Calculate the molecular partition function for this thermodynamic system.

(b) How many particles are in each energy level?

(c) Using Boltzmann's relation, determine the entropy of this system.

Solution

(a) The molecular partition function for this dilute thermodynamic system is

$$Z = \sum_j g_j \exp(-\varepsilon_j/kT)$$

$$= 300 + 600\exp(-\varepsilon/kT) + 1200\exp(-2\varepsilon/kT).$$

Given that $T = \varepsilon/k$, we obtain

$$Z = 300 + 600e^{-1} + 1200e^{-2} = 300 + 221 + 162 = 683.$$

(b) The number of particles in each energy level is given by Eq. (4.14). Hence, $N_0 = (300/683)N \simeq 22$, where $N = 50$. Similarly, $N_1 = (221/683)N \simeq 16$ and $N_2 = (162/683)N \simeq 12$.

(c) For particles in the dilute limit, Boltzmann's relation when using Eq. (4.3) becomes

$$S = k \ln W_{DL} = k \sum_j N_j \left\{ \ln \frac{g_j}{N_j} + 1 \right\}.$$

Thus, we obtain for the entropy,

$$S = k\{22\,[\ln(300/22) + 1] + 16\,[\ln(600/16) + 1] + 12\,[\ln(1200/12) + 1]\}.$$

Evaluation then gives $S = 221k$, where $k = 1.38 \times 10^{-23}$ J/K.

4.4 Internal Energy and Entropy in the Dilute Limit

In general, we know from classical thermodynamics that once we have two independent properties for a single-phase thermodynamic system, we can calculate all of the remaining properties. In this section, we develop general expressions for two such properties in the dilute limit, the internal energy and the entropy. In the following section, we then derive in a more straightforward fashion expressions for all of the remaining thermodynamic properties.

The important result from this upcoming development is that properties such as the internal energy and entropy can always be expressed in terms of the molecular partition function. Hence, knowledge of Z will inevitably permit calculation of all thermodynamic properties. More specifically, we recall from quantum mechanics that ε_j is a function of only the volume of a particle assembly. Therefore, from Eq. (4.12), the natural independent variables for the partition function must be temperature and volume. On this basis, we expect that the temperature and volume will likewise be primary independent variables for all thermodynamic properties in the dilute limit.

Recall from Chapter 3 that

$$U = E = \sum_j N_j \varepsilon_j \tag{4.19}$$

$$S = k(\beta U + \alpha N) \mp k \sum_j g_j \ln \left\{1 \mp \exp[-\alpha - \beta \varepsilon_j]\right\}, \tag{4.20}$$

where the Lagrange multipliers $\alpha = -\mu/kT$ and $\beta = 1/kT$. We may now develop an expression for the internal energy by substituting Eq. (4.14) for the equilibrium particle distribution into Eq. (4.19). The result is

$$U = \frac{N}{Z} \sum_j g_j \varepsilon_j e^{-\varepsilon_j/kT}.$$

But from Eq. (4.12),

$$\left(\frac{\partial Z}{\partial T}\right)_V = \frac{1}{kT^2} \sum_j g_j \varepsilon_j e^{-\varepsilon_j/kT};$$

hence, the previous expression becomes

$$U = \frac{NkT^2}{Z}\left(\frac{\partial Z}{\partial T}\right)_V$$

or

$$U = NkT^2\left(\frac{\partial \ln Z}{\partial T}\right)_V. \tag{4.21}$$

Equation (4.21) is our desired expression for the internal energy, both for corrected and uncorrected M–B statistics (Problem 2.3). Because the molecular partition function depends solely on temperature and volume, we immediately recognize that the natural independent variables for the internal energy are N, T, and V, i.e., $U(N, T, V)$.

Turning now to the entropy, we have from Eq. (4.20) when substituting for α and β,

$$S = \frac{U}{T} - \frac{\mu N}{T} \mp k\sum_j g_j \ln\{1 \mp \exp[(\mu - \varepsilon_j)/kT]\}.$$

In the dilute limit, we note from Eq. (4.9),

$$\exp[(\mu - \varepsilon_j)/kT)] \ll 1,$$

so that by linearly approximating the logarithmic expansion (Appendix B), we obtain

$$\begin{aligned}\mp k\sum_j g_j \ln\{1 \mp \exp[(\mu - \varepsilon_j)/kT]\} &\simeq k\sum_j g_j \exp[(\mu - \varepsilon_j)/kT] \\ &= ke^{\mu/kT}Z = kN,\end{aligned}$$

where we have invoked the partition function via Eqs. (4.11) and (4.12) to get the amazingly simple result, kN. On this basis, the entropy in the dilute limit can be written as

$$S = \frac{U}{T} + kN\left(1 - \frac{\mu}{kT}\right),$$

which can be converted to

$$S = \frac{U}{T} + kN\left[\ln\left(\frac{Z}{N}\right) + 1\right] \tag{4.22}$$

after eliminating the chemical potential using Eq. (4.11). Alternatively, substituting Eq. (4.21) into Eq. (4.22), we produce our desired expression for the entropy,

$$S = Nk\left[T\left(\frac{\partial \ln Z}{\partial T}\right)_V + \ln\left(\frac{Z}{N}\right) + 1\right]. \tag{4.23}$$

As might be expected, Eq. (4.22) can also be derived through a direct statistical analysis of corrected M–B statistics (Problem 2.4). The significant implication is that, for indistinguishable particles in the dilute limit, the natural independent variables for the entropy, as for the internal energy, are N, T, and V. Hence, given these parameters, Eq. (4.23) confirms our prior supposition that the molecular partition function is the key quantity when calculating U and S, and thus all thermodynamic properties.

Finally, from Eq. (4.8), we find, after using Stirling's approximation (Appendix D.2),

$$\ln W_{DL} = \ln W_{MB} - (N\ln N - N),$$

so that, from the Boltzmann relation,

$$S_{MB} = S_{DL} + kN(\ln N - 1). \tag{4.24}$$

Therefore, substituting Eq. (4.22) into Eq. (4.24), we find that the entropy for an assembly of *distinguishable particles* can be represented by the simpler expression,

$$S = \frac{U}{T} + kN \ln Z, \tag{4.25}$$

which explains the persistent miscalculation of entropy for the ideal gas before the development of quantum mechanics (Problem 2.5). Equations (4.22) and (4.25) differ solely because of the factor of $N!$ in Eq. (4.8); this factor, you recall, accounts for the enhanced permutations when determining the thermodynamic probability for distinguishable as compared to indistinguishable particles in the dilute limit.

4.5 Additional Thermodynamic Properties in the Dilute Limit

Having established Eqs. (4.21) and (4.23) for the internal energy and entropy, respectively, we may now derive additional expressions in terms of $Z(T, V)$ for all other thermodynamic properties by invoking standard relations from classical thermodynamics (Appendix F). Beginning with Eq. (4.11), we can express the chemical potential in the dilute limit as

$$\mu = -kT \ln\left(\frac{Z}{N}\right). \tag{4.26}$$

From classical thermodynamics, $G = \mu N$, so that the Gibbs free energy becomes

$$G = -NkT \ln\left(\frac{Z}{N}\right). \tag{4.27}$$

Recall that the Helmholtz free energy is defined as $A = U - TS$; thus, from Eq. (4.22),

$$A = -NkT\left[\ln\left(\frac{Z}{N}\right) + 1\right]. \tag{4.28}$$

From classical thermodynamics, $G = H - TS$; hence, from Eqs. (4.22) and (4.27),

$$H = U + NkT. \tag{4.29}$$

Substituting Eq. (4.21) into Eq. (4.29), the enthalpy can then be expressed as

$$H = NkT\left[T\left(\frac{\partial \ln Z}{\partial T}\right)_V + 1\right]. \tag{4.30}$$

We, of course, also recall that $H = U + PV$, and thus, from Eq. (4.29),

$$PV = NkT, \tag{4.31}$$

which is just a molecular version of the ideal gas equation of state! We obtained this remarkable result because the ideal gas is the prototype for independent but indistinguishable particles in the dilute limit. Furthermore, we anticipated this outcome when we previously commented that ideal gases typically bear large negative chemical potentials, thus automatically satisfying our criterion for the dilute limit, i.e., Eq. (4.18). We conclude, therefore, that all expressions derived for thermodynamic properties in the dilute limit must apply to ideal gases.

Now, for such gases, the macroscopic equation of state is $PV = nRT$, where n is the number of moles and R is the universal gas constant. Comparing this classic equation of state to Eq. (4.31), we immediately recognize that

$$k = \frac{nR}{N} = \frac{R}{N_A}, \tag{4.32}$$

where N_A is Avagadro's number. Hence, we have shown that Boltzmann's constant, which was initially introduced to link quantitatively thermodynamic probability to the entropy, can also be interpreted as simply the universal gas constant divided by Avagadro's number. In other words, Avagadro's number represents a kind of universal scaling factor relating microscopic and macroscopic thermodynamics!

Because the dilute limit automatically implies ideal gases, we are finally in a position to complete our development of statistical expressions for the various thermodynamic properties in the dilute limit. In particular, we recall from classical thermodynamics that the specific heats, at constant volume and constant pressure, respectively, can be expressed as

$$C_V = \left(\frac{\partial U}{\partial T}\right)_V \qquad C_P = \left(\frac{\partial H}{\partial T}\right)_P = \left(\frac{\partial H}{\partial T}\right)_V,$$

where the C_P identity holds because enthalpy is a function only of temperature for ideal gases. Employing the indicated partial derivatives, plus Eqs. (4.21) and (4.30), we thus obtain

$$C_V = Nk\left[\frac{\partial}{\partial T}T^2\left(\frac{\partial \ln Z}{\partial T}\right)\right]_V \tag{4.33}$$

$$C_P = Nk\left\{\left[\frac{\partial}{\partial T}T^2\left(\frac{\partial \ln Z}{\partial T}\right)\right]_V + 1\right\}. \tag{4.34}$$

EXAMPLE 4.2

A dilute system at thermodynamic equilibrium consists of 50 independent, indistinguishable particles. Each particle has three energy levels of energy $0, \varepsilon$, and 2ε, with degeneracies of 300, 600, and 1200, respectively. The system is at a constant temperature $T = \varepsilon/k$, where k is Boltzmann's constant.

(d) Determine the internal energy for this thermodynamic system.

(e) Calculate the entropy directly from the partition function.

(f) Evaluate the Helmholtz free energy of the system.

Solution

This problem is a continuation of Example 4.1, for which we have already calculated the partition function and the number of particles in each energy level.

(d) The internal energy can be obtained from Eq. (4.19), i.e.,

$$U = \sum_j N_j \varepsilon_j = \frac{N}{Z}\sum_j g_j \varepsilon_j \exp(-\varepsilon_j/kT).$$

Therefore, $U = 22 \cdot 0 + 16 \cdot \varepsilon + 12 \cdot 2\varepsilon = 40\varepsilon$.

(e) The entropy can be calculated from the partition function by using Eq. (4.22). Hence, for $T = \varepsilon/k$,

$$S = \frac{U}{T} + kN\left[\ln\left(\frac{Z}{N}\right) + 1\right] = 40k + 50k\left[\ln\left(\frac{683}{50}\right) + 1\right].$$

Consequently, $S = 40k + 181k = 221k$, in agreement with part (c).

(f) The Helmholtz free energy is defined by $A = U - TS$. Hence, we have

$$A = 40\varepsilon - (\varepsilon/k)(221k) = -181\varepsilon.$$

4.6 The Zero of Energy and Thermodynamic Properties

We have previously indicated that thermodynamic properties are normally calculated by presuming that the energy of the ground state $\varepsilon_\circ = 0$. However, it is of interest to ascertain if any of our property expressions are in actuality independent of this arbitrary choice for $\varepsilon_\circ$. Such properties would then become a robust test of the predictive value of statistical thermodynamics.

As we will learn in Chapter 7, we can always measure via spectroscopy the difference in energy between two energy levels; thus, we invariably know

$$\varepsilon'_j = \varepsilon_j - \varepsilon_\circ.$$

Therefore, employing Eq. (4.12), we may now define an alternative partition function,

$$Z' = \sum_j g_j \exp(-\varepsilon'_j/kT) = Z\exp(\varepsilon_\circ/kT). \tag{4.35}$$

Using Eqs. (4.19) and (4.31), we find that for the internal energy,

$$U = NkT^2\left[\left(\frac{\partial \ln Z'}{\partial T}\right)_V + \frac{\varepsilon_\circ}{kT^2}\right]$$

or

$$U - N\varepsilon_\circ = NkT^2\left(\frac{\partial \ln Z'}{\partial T}\right)_V.$$

Hence, we have shown that any calculation of the internal energy produces a ground-state energy, $N\varepsilon_\circ$, which we must arbitrarily set to zero to generate thermodynamic property tables.

In comparison to the internal energy, some special properties might exist that are not affected by our arbitrary choice of a zero of energy. Consider, for example, the specific heat at constant volume, which we may investigate by substituting Eq. (4.35) into Eq. (4.23). In this case, we obtain

$$C_V = Nk\frac{\partial}{\partial T}\left[T^2\left(\frac{\partial \ln Z'}{\partial T}\right) + \frac{\varepsilon_\circ}{k}\right]_V$$

$$C_V = Nk\left[\frac{\partial}{\partial T}T^2\left(\frac{\partial \ln Z'}{\partial T}\right)\right]_V.$$

Similarly, for the entropy, we have from Eq. (4.23),

$$S = Nk\left[T\left(\frac{\partial \ln Z'}{\partial T}\right)_V + \frac{\varepsilon_\circ}{kT} + \ln\left(\frac{Z' e^{-\varepsilon_\circ/kT}}{N}\right) + 1\right]$$

$$S = Nk\left[T\left(\frac{\partial \ln Z'}{\partial T}\right)_V + \ln\left(\frac{Z'}{N}\right) + 1\right].$$

We note that for both of these cases, the ground state energy has no influence on the calculation of thermodynamic properties. Indeed, the derived expressions for the specific heat at constant volume and the entropy are the same whether the partition function is Z or Z'. More generally, we find that the ground-state energy affects calculations of U, H, A, and G, while it does not affect calculations of C_V, C_P, and S. This important result provides the rationale for focusing on specific heats and the entropy when experimentally assessing the validity of statistical calculations for thermodynamic properties (Lewis and Randall, 1961).

4.7 Intensive Thermodynamic Properties for the Ideal Gas

We showed in Section 4.5 that independent, indistinguishable particles in the dilute limit ultimately prescribe ideal gas behavior. Hence, when calculating ideal gas properties, we need only apply the various thermodynamic expressions derived in Sections 4.4 and 4.5. These inherently microscopic properties can be converted to more useful macroscopic properties by employing Eq. (4.32). The resulting classical thermodynamic expressions for the intensive molar properties of the ideal gas can then be cast in dimensionless form as follows:

$$\frac{u}{RT} = T\left(\frac{\partial \ln Z}{\partial T}\right)_V \tag{4.36}$$

$$\frac{h}{RT} = T\left(\frac{\partial \ln Z}{\partial T}\right)_V + 1 \tag{4.37}$$

$$\frac{a}{RT} = -\left[\ln\left(\frac{Z}{N}\right) + 1\right] \tag{4.38}$$

$$\frac{g}{RT} = -\ln\left(\frac{Z}{N}\right) \tag{4.39}$$

$$\frac{s}{R} = T\left(\frac{\partial \ln Z}{\partial T}\right)_V + \ln\left(\frac{Z}{N}\right) + 1 \tag{4.40}$$

$$\frac{c_v}{R} = \left[\frac{\partial}{\partial T} T^2 \left(\frac{\partial \ln Z}{\partial T}\right)\right]_V \tag{4.41}$$

$$\frac{c_p}{R} = \left[\frac{\partial}{\partial T} T^2 \left(\frac{\partial \ln Z}{\partial T}\right)\right]_V + 1. \tag{4.42}$$

We note that all of the above thermodynamic properties are functions of the molecular partition function through $\ln Z$ rather than through Z directly. This feature will play a very important role in our future calculations of ideal gas properties. We also note that any such calculations will require only three functional forms of $\ln Z$, namely,

$$\ln\left(\frac{Z}{N}\right) \qquad \left(\frac{\partial \ln Z}{\partial T}\right)_V \qquad \left(\frac{\partial^2 \ln Z}{\partial T^2}\right)_V.$$

Finally, evaluation of these functional forms requires that we know the degeneracies, g_j, and the energy levels, ε_j, for the atom or molecule of interest. For this purpose, we now turn to quantum mechanics and spectroscopy (Chapters 5–7). Once we have learned how to determine both g_j and ε_j, we will come back to Eqs. (4.36)–(4.42), as these expressions can eventually be used to calculate the thermodynamic properties of ideal gases and their mixtures (Chapters 8–10).

PROBLEM SET II

Statistical Modeling for Thermodynamics (Chapters 3–4)

2.1 We have shown that the entropy for Bose–Einstein and Fermi–Dirac statistics is given by

$$S(E, V, N) = k(\beta E + \alpha N) \mp k \sum_j g_j \ln(1 \mp e^{-\alpha} e^{-\beta \varepsilon_j}),$$

where $N = \sum_j N_j$ and $E = \sum_j N_j \varepsilon_j$. Similarly, from classical thermodynamics,

$$dS(E, V, N) = \frac{1}{T} dE + \frac{P}{T} dV - \frac{\mu}{T} dN$$

for a single-component system.

a. Prove that $\beta = 1/kT$.

b. Prove that $\alpha = -\mu/kT$.

c. Show that the pressure is given by

$$P = -\sum_j N_j \left(\partial \varepsilon_j / \partial V\right)_{E,N}.$$

d. We will soon demonstrate that the internal energy is independent of volume whereas the translational energy $\varepsilon_{j,tr} = C_j V^{-2/3}$, where C_j is a constant for each translational energy level. Utilizing this information, show that

$$PV = \frac{2}{3} E_{tr},$$

where E_{tr} is the translational portion of the total energy (external plus internal) for the particle assembly.

e. Is this result limited to the dilute limit? Does it assume independent particles? Why should the pressure be related only to the translational energy? Explain.

2.2 We have shown that the entropy for Bose–Einstein and Fermi–Dirac statistics is given by

$$S(E, V, N) = k(\beta E + \alpha N) \mp k \sum_j g_j \ln(1 \mp e^{-\alpha} e^{-\beta \varepsilon_j}),$$

where $N = \sum_j N_j$ and $E = \sum_j N_j \varepsilon_j$.

a. Assuming that $\beta = 1/kT$, show that

$$A(T, V, N) = -\alpha NkT \pm kT \sum_j g_j \ln(1 \mp e^{-\alpha} e^{-\varepsilon_j/kT}).$$

b. Confirm that $\beta = 1/kT$ by showing that $S = -(\partial A/\partial T)_{V,N}$.

c. Employing $A(T, V, N)$, prove that $\alpha = -\mu/kT$.

d. Using $A(T, V, N)$, show that the pressure is given by

$$P = -\sum_j N_j (\partial \varepsilon_j/\partial V)_{T,N}.$$

e. We will soon demonstrate that the internal energy is independent of volume whereas the translational energy $\varepsilon_{j,tr} = C_j V^{-2/3}$, where C_j is a constant for each translational energy level. Utilizing this information, show that

$$PV = \frac{2}{3} E_{tr},$$

where E_{tr} is the translational portion of the total energy (external plus internal) for the particle assembly.

f. Is this result limited to the dilute limit? Does it assume independent particles? Why should the pressure be related only to the translational energy? Explain.

2.3 Classical Maxwell–Boltzmann statistics considers particles to be distinguishable with no limit on the number of particles in each energy state. A physical example is a solid composed of localized atoms at distinguishable lattice sites. The thermodynamic probability in this case is given by

$$W_{MB} = N! \prod_j \frac{g_j^{N_j}}{N_j!},$$

where N_j is the number of particles and g_j is the degeneracy of the jth energy level.

a. Using the methods of statistical thermodynamics, show that the equilibrium particle distribution is

$$N_j = g_j e^{-\alpha} e^{-\beta \varepsilon_j}.$$

b. Defining the molecular partition function $Z = \sum_j g_j e^{-\beta \varepsilon_j}$, show that

$$S = k(\beta E + N \ln Z).$$

c. Using classical thermodynamics, verify that $\beta = 1/kT$. Hence, show that the Helmholtz free energy for classical Maxwell–Boltzmann statistics becomes

$$A = -NkT \ln Z.$$

Compare this expression with that for corrected Maxwell–Boltzmann statistics. Explain the difference.

d. Beginning with the equation for Helmholtz free energy derived in part (c), show that the chemical potential and pressure for a classical gas can be expressed as

$$\mu = -kT \ln Z \qquad P = NkT \left(\frac{\partial \ln Z}{\partial V} \right)_T.$$

e. Write comparable expressions for μ and P for a gas following corrected Maxwell–Boltzmann statistics. Explain any agreement or disagreement with the expressions of part (d).

2.4 The thermodynamic probability for corrected Maxwell–Boltzmann statistics is given by

$$W_{CMB} = \prod_j \frac{g_j^{N_j}}{N_j!}$$

where N_j is the number of particles and g_j is the degeneracy of the jth energy level.

a. Using the methods of statistical thermodynamics, show that the equilibrium particle distribution is

$$N_j = g_j\, e^{-\alpha}\, e^{-\beta\varepsilon_j}.$$

b. Defining the molecular partition function $Z = \sum_j g_j\, e^{-\beta\varepsilon_j}$, show that

$$S = k\beta E + kN\left[\ln\left(\frac{Z}{N}\right) + 1\right].$$

c. Employing the Helmholtz free energy and presuming that $\beta = 1/kT$, verify that

$$P = NkT\left(\frac{\partial \ln Z}{\partial V}\right)_T.$$

2.5 Classical Maxwell–Boltzmann statistics considers particles to be distinguishable with no limit on the number of particles in each energy state. A physical example is a solid composed of localized atoms at distinguishable lattice sites. The thermodynamic probability in this case is given by

$$W_{MB} = N!\, \prod_j \frac{g_j^{N_j}}{N_j!}$$

where N_j is the number of particles and g_j is the degeneracy of the jth energy level.

a. Using the methods of statistical thermodynamics, show that the equilibrium particle distribution is

$$N_j = g_j e^{-\alpha} e^{-\beta\varepsilon_j}.$$

b. Defining the molecular partition function $Z = \sum_j g_j\, e^{-\beta\varepsilon_j}$, show that

$$S = k(\beta E + N \ln Z).$$

c. Using classical thermodynamics, verify that $\beta = 1/kT$. Hence, the entropy for classical Maxwell–Boltzmann statistics becomes

$$S = \frac{U}{T} + kN \ln Z.$$

Compare this expression with that for corrected Maxwell–Boltzmann statistics. Explain the difference.

d. Show that the probability of a particle being in the *i*th energy *state* is given by

$$P_i = \frac{N_i}{N} = \frac{e^{-\varepsilon_i/kT}}{Z},$$

where the partition function $Z = \sum_i e^{-\varepsilon_i/kT}$.

e. Demonstrate that the entropy can be directly related to the probabilities P_i of the various energy states accessible to the system, i.e.,

$$S = -kN \sum_i P_i \ln P_i.$$

Discuss the significance of this result.

2.6 Consider a simplified system having four energy levels of relative energy 0, 1, 2, and 3. The system contains eight particles and has a total relative energy of six. Determine the thermodynamic probability for every distribution consistent with the above constraints given the following system characteristics.

a. The energy levels are nondegenerate and the particles obey Maxwell–Boltzmann statistics.

b. Each energy level has a degeneracy of six and the particles obey either (i) Maxwell–Boltzmann or (ii) corrected Maxwell–Boltzmann statistics.

c. Each energy level has a degeneracy of six and the particles obey either Bose–Einstein or Fermi–Dirac statistics.

d. Comment on your calculations for parts (b) and (c).

2.7 The translational partition function for a monatomic ideal gas can be shown to be

$$Z = \left(\frac{2\pi\, mkT}{h^2}\right)^{3/2} V$$

so that the criterion for the dilute limit becomes

$$\left(\frac{2\pi\, mkT}{h^2}\right)^{3/2} \left(\frac{V}{N}\right) \gg 1,$$

where m is the molecular mass, k is Boltzmann's constant, h is Planck's constant, T is the temperature, V is the volume, and N is the number of particles in the gas assembly.

a. Consider helium gas at room temperature (300 K) and pressure (1 atm). Show that the dilute limit is satisfied.

b. Consider the conduction electrons in metallic sodium at room temperature. As a first approximation, interactions between these electrons can be neglected so that they can be treated as an ideal gas. By assuming one conduction electron per sodium atom, show that the dilute limit is *not* satisfied. What are the major differences between the electron case and the helium case that preclude the dilute limit for the former?

c. The criterion for the dilute limit can also be expressed as

$$\frac{V}{N} \gg \Lambda^3,$$

where $\Lambda = (h^2/2\pi mkT)^{1/2}$. Demonstrate that Λ is essentially equivalent to a thermal de Broglie wavelength for the particle. Discuss in a succinct paragraph the physical implications of the above inequality.

2.8 The translational partition function for a monatomic ideal gas can be shown to be

$$Z = \left(\frac{2\pi mkT}{h^2}\right)^{3/2} V$$

so that a suitable criterion for the dilute limit becomes

$$\left(\frac{2\pi mkT}{h^2}\right)^{3/2} \left(\frac{V}{N}\right) \geq 10.$$

a. Consider neon at a pressure of 1 atm. Determine the temperature above which the above criterion holds.

b. Similarly, for argon at 300 K, determine the pressure below which the criterion for the dilute limit is satisfied.

c. The criterion for the dilute limit can also be expressed as

$$\frac{V}{N} \geq 10\Lambda^3,$$

where $\Lambda = (h^2/2\pi mkT)^{1/2}$. Demonstrate that Λ is essentially equivalent to a thermal de Broglie wavelength for the particle. Discuss in a succinct paragraph the physical implications of the above inequality.

2.9 We have shown that, for Bose–Einstein and Fermi–Dirac statistics,

$$\ln W_{\left\{\substack{BE\\FD}\right\}} = \sum_j \left\{ N_j \ln\left[\frac{g_j}{N_j} \pm 1\right] \pm g_j \ln\left[1 \pm \frac{N_j}{g_j}\right]\right\}.$$

a. Prove that, for any given macrostate,

$$\ln W_{BE} > \ln W_{CMB} > \ln W_{FD}.$$

b. What are the implications of part (a)?

2.10 To illustrate the order of magnitude of the fluctuations in a macroscopic system, consider N distinguishable particles, each of which can be with equal probability in either of two available states; e.g., an "up" and a "down" state.

a. Determine the total number of microstates and the entropy of this N-particle system.

b. What is the number of microstates for which M particles are in the "up" state?

Hint: Recall the binomial distribution.

c. The fluctuation in the number of particles M is given by $\sigma/\overline{M}$, where σ is the standard deviation and $\overline{M}$ is the mean number of particles in the "up" state. Develop an expression for $\sigma/\overline{M}$.

d. Consider a macroscopic system for which $N = 6.4 \times 10^{23}$ spatially separated particles. Calculate the fluctuation for this system. What are the implications of your result?

2.11 A thermodynamic system consists of N independent, distinguishable particles. Each particle has four energy levels at 0, ε, 2ε, and 3ε, respectively. The system is in thermal equilibrium with a heat reservoir of absolute temperature $T = \varepsilon/k$, where k is Boltzmann's constant.

a. If the energy levels are nondegenerate, calculate the partition function, the internal energy, the entropy, and the Helmholtz free energy of the system.

b. Repeat part (a) if the energy levels at 0, ε, 2ε, and 3ε have degeneracies of 1, 2, 4, and 4, respectively.

2.12 a. Demonstrate that the average energy per particle, $\bar{\varepsilon}$, in the dilute limit is given by

$$\bar{\varepsilon} = \frac{1}{Z}\sum_j g_j\, \varepsilon_j e^{-\varepsilon_j/kT}.$$

b. By differentiating the above equation with respect to temperature, show that the root-mean-square deviation, σ_ε, for the particle energy is

$$\sigma_\varepsilon = [kT^2 \bar{c}_v]^{1/2}$$

where $\bar{c}_v = (\partial\bar{\varepsilon}/\partial T)_V$ is the mean specific heat per particle at constant volume (J/K).

c. Evaluate the fractional root-mean-square deviation, $\sigma_\varepsilon/\bar{\varepsilon}$, for a monatomic gas. What are the physical implications of your evaluation?

2.13 An insulated vessel contains a partition that separates one volumetric region filled with a monatomic gas from another region at vacuum. The partition is broken and the gas is permitted to fill the entire volume of the vessel. If the translational partition function of a monatomic gas can be taken as

$$Z = \left(\frac{2\pi\, mkT}{h^2}\right)^{3/2} V,$$

show that the microscopic expression derived for the net entropy change during this expansion process is the same as that expected from classical macroscopic thermodynamics.

2.14 The most probable distribution for a thermodynamic assembly is usually taken to be much more likely than any other distribution differing from it by even a small amount. Given an isolated system containing N particles, consider a distribution d for which $N_j = N_{jmp} + \delta N_j$, where the variation $|\delta N_j| \ll N_{jmp}$.

a. Demonstrate that the entropy in the dilute limit for any such distribution must be less than that corresponding to the most probable distribution. *Hint: Start your analysis with Eq.* (*4.3*).

b. Consider one mole of gas having a distribution d in which $|\delta N_j|/N_{jmp} = 10^{-5}$ for every level j. Calculate the ratio of thermodynamic probabilities, W_d/W_{mp}, and also the corresponding difference in entropies. What physical implications can be deduced from these particular calculations?

2.15 A thermodynamic system consists of N independent, distinguishable particles. Each particle has three energy levels at 0, ε, and 2ε, with degeneracies of 1, 3, and 5,

respectively. The system is in thermal equilibrium with a heat reservoir of absolute temperature $T = \varepsilon/k$, where k is Boltzmann's constant.

a. Calculate the partition function for this system.

b. What fraction of the particles resides in each energy level?

c. Determine the average particle energy and the associated mean particle entropy.

d. At what temperature would the population of the energy level having 2ε be equal to that at ε?

2.16 Paramagnetism can occur when some atoms in a crystalline solid possess a magnetic dipole moment owing to an unpaired electron with its associated orbital angular momentum. For simplicity, assume that (1) each paramagnetic atom has a magnetic dipole moment μ and (2) magnetic interactions between unpaired electrons can be neglected. When a magnetic field is applied, the magnetic dipoles will align themselves either parallel or antiparallel to the direction of the magnetic field. If the magnetic moment is parallel to a magnetic field of induction $\vec{B}$, the potential energy is $-\mu B$; when the magnetic moment is antiparallel to $\vec{B}$, the potential energy is $+\mu B$.

a. Prove that the probability for an atomic magnetic dipole moment to point parallel to the magnetic field is given at temperature T by

$$P_{\circ} = (1 + e^{-2x})^{-1}$$

where $x = \mu B/kT$. Give a physical explanation for the value of $P_{\circ}$ as $T \to 0$ and as $T \to \infty$.

Hint: Determine the partition function for the system.

b. Show that, for N independent magnetic dipoles, the mean effective magnetic moment parallel to the magnetic field is

$$m = N\mu \tanh(x).$$

c. Demonstrate that the mean magnetic moment at high temperatures and/or weak magnetic fields ($x \ll 1$) is proportional to $1/T$. This is Curie's law.

d. Show that the contribution from paramagnetism to the internal energy of a crystalline solid is $U = -mB$. Determine this paramagnetic contribution at $T = \infty$. Why should this result have been expected?

e. Develop an expression for the entropy of this paramagnetic system.

PART TWO

QUANTUM MECHANICS AND SPECTROSCOPY

5 Basics of Quantum Mechanics

We found in the previous chapter that the molecular partition function is required to determine the thermodynamic properties of an ideal gas. To evaluate the partition function, specification of pertinent energy levels and degeneracies is necessary. Such knowledge demands that we investigate at least the rudiments of quantum mechanics, and especially those quantum concepts required for subsequent applications to statistical thermodynamics. For this reason, we concentrate in the next few chapters on the Schrödinger wave equation, whose various solutions provide the ε_j's and g_j's needed for the eventual calculation of thermodynamic properties. Depending on your academic background, you might thus consider reviewing classical mechanics (Appendix G) and operator theory (Appendix H) in preparation for your upcoming study of quantum mechanics.

We begin this chapter with a historical review of the developments leading to the formulation of quantum mechanics, subsequently focusing on the Bohr model for atomic hydrogen and the de Broglie hypothesis for matter waves. We then introduce the Schrödinger wave equation, the basic postulates of quantum mechanics, and salient insights from these postulates germane to the development of statistical thermodynamics. We next apply the Schrödinger wave equation to the translation energy mode of an atom or molecule. This application conveniently explains both quantum states and quantum numbers, including their relation to our previous notions of microstate and macrostate. We end this chapter by discussing the Heisenberg uncertainty principle, including its utility in defining indistinguishability and symmetry conditions for multiparticle systems.

5.1 Historical Survey of Quantum Mechanics

In most branches of physics, we explore the early work of various researchers to become familiar with those inductive processes leading to a final elegant theory. For example, studying the various laws of electricity and magnetism primes us for the acceptance of Maxwell's equations; similarly, applying the first and second laws of thermodynamics to heat engines prepares us for a postulatory approach to classical thermodynamics (Appendix F). Unfortunately, for quantum mechanics, the final postulates are so abstract that little relation apparently exists between them and those experimental results which eventually led to their formulation during the first quarter of the twentieth century. Nonetheless, given proper perspective, the development of quantum mechanics actually followed a path

typical of the evolution of any fundamental scientific theory. The following is a summary of some of these developments.

In 1900, the German physicist Max Planck (1858–1947) showed that the classical theory of oscillating electrons could not explain the behavior of blackbody radiation. Performing a thermodynamic analysis of available results at low and high wavelengths, Planck developed a general expression for emissive power that conformed to experimental data at both wavelength limits. Upon further investigation, he found that quantization of energy was required to derive his empirical relation between the emissive power of a blackbody and the frequency of its emitted radiation. In particular, he postulated that the microscopic energy, ε, emitted at a given frequency, ν, was proportional to that frequency, so that

$$\varepsilon = nh\nu,$$

where n is an integer and the proportionality constant, h (J·s), is now known as Planck's constant.

In 1905, Albert Einstein (1879–1955) published an explanation of the photoelectric effect, which occurs when electrons are ejected from a metallic surface as a result of being bombarded with ultraviolet radiation. Following Planck's lead, Einstein suggested that the incident radiation behaves, not as a classical electromagnetic wave, but as distinct entities or *photons*, with each photon having energy

$$\varepsilon = h\nu. \tag{5.1}$$

Hence, when ultraviolet light strikes a surface, the maximum kinetic energy of the escaping electrons should become

$$T_m = h\nu - \Phi,$$

where the work function, Φ, represents the minimum energy required to remove electrons from the surface of a particular material. Good agreement was eventually found between this relation and experimental data, thus verifying that the maximum kinetic energy, T_m, depends linearly not on emissive power but on its frequency.

While the corpuscular theory of light, as proposed by Isaac Newton (1642–1727), had been around for a long time, the subsequent investigations of Thomas Young (1773–1829) and Augustin Jean Fresnel (1788–1827) had shown that both diffraction and interference phenomena could be explained beautifully by modeling light as a traveling wave. The astonishing demonstration by James Clerk Maxwell (1831–1879) that light behaved as an electromagnetic wave strongly reinforced this viewpoint. Hence, Einstein's concept of the photon was actually quite revolutionary since the wave model of light, as originally developed by Christian Huygens (1629–1695), was at that time the generally accepted paradigm of classical physics.

Despite his ground-breaking work on blackbody radiation, Planck himself contended that the emitted photons should ultimately coalesce into a classical wave. However, when Einstein calculated Planck's constant using the photoelectric effect, he found excellent agreement with Planck's original value based on blackbody radiation. Einstein's seminal work thus suggested for the first time the so-called wave–particle duality of light: electromagnetic radiation can behave sometimes as a wave and sometimes as a particle. When the particle nature of light dominates, radiation is discrete rather than continuous so that,

following Eq. (5.1), the material emitting or absorbing light undergoes a distinct change in energy mirroring that for a single photon, i.e.,

$$\Delta\varepsilon = h\nu. \tag{5.2}$$

In 1911, Ernest Rutherford (1871–1937) suggested that the atom is composed of a central nucleus with orbiting electrons. This model was immediately questioned since it could not be reconciled with another basic concept of classical physics: an orbiting electron should radiate, thereby gradually losing energy and thus prompting its eventual collapse into the nucleus. Fortunately, the Danish physicist Niels Bohr (1885–1962) provided an explanation for Rutherford's model in 1913. Building on Einstein's work, he postulated that the electrons actually orbit at fixed radii and that discontinuous transitions between orbits occur only when photons are absorbed or emitted by the atom. This model, as discussed in Section 5.2, offered the first comprehensive explanation for the known spectrum of atomic hydrogen. The amazing agreement between model and experiment proved to be extremely significant, as much of the early work on quantum theory arose from the inability of classical physics to explain various spectroscopic observations.

Subsequently, the American physicist Arthur Compton (1892–1962) found that he was unable to explain classically the results of his 1922 experiments on x-ray scattering. However, by invoking Einstein's quantum model for x-rays and assuming that each photon interacted with a single electron, he was able to verify the experimental change in wavelength, λ, upon scattering as

$$\Delta\lambda = \left(\frac{h}{m_e c}\right)(1 - \cos\theta),$$

where m_e is the mass of the electron, c is the speed of light, and θ is the scattering angle. This succinct result provided further evidence for the particle nature of light and thus for an inherent wave–particle duality.

In 1924, the French physicist Louis de Broglie (1892–1985) proposed in a remarkable doctoral thesis that wave–particle duality should be as true for matter as for light. Invoking so-called matter waves, as discussed in Section 5.3, de Broglie predicted that electrons passing through a thin metallic sheet should exhibit a diffraction pattern similar to that for light waves. This suggestion was experimentally confirmed in 1927, leading to Nobel prizes ten years later for G. P. Thompson (1892–1975) in England and C. J. Davisson (1881–1958) in the United States. An interesting sidelight here is that J. J. Thomson (1856–1940), G. P. Thomson's father, received the Nobel prize for physics in 1906 after identifying electrons as fundamental particles, while his son received the identical award in 1937 for showing that these same particles can also act as waves.

As indicated by the above summary, quantum concepts were amazingly successful at explaining significant experimental results at the turn of the twentieth century. However, the resulting patchwork theory simply linked quantum ideas to well-accepted aspects of classical physics. While this loose framework provided a fruitful venue for inventive physicists, its arbitrariness proved distasteful to those who sought rigorous theories. Hence, various investigators pursued a more basic formulation that could be applied in a self-consistent manner while still explaining the major effects of quantization. In the end, the most successful theories were developed by the German physicist Werner Heisenberg (1901–1976) and by the Austrian Erwin Schrödinger (1887–1961).

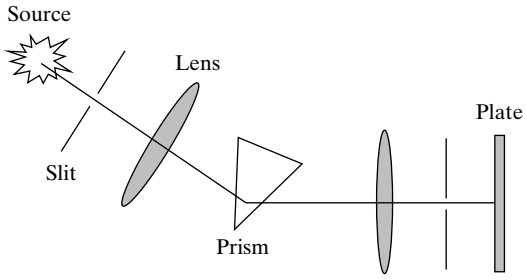

Figure 5.1 Sketch of spectrograph for determining the spectrum of atomic hydrogen.

In 1925, Heisenberg introduced his matrix mechanics. He summarily rejected descriptions in terms of classical physics and based his theory completely on selected observable properties of discrete systems. This new approach was rapidly improved and applied to several outstanding research problems. In 1926, Schrödinger set forth the basis for his wave mechanics, which is commonly known today as quantum mechanics. Schrödinger was a mathematical physicist who had done extensive work on eigenvalue problems. The matter waves proposed by de Broglie inspired him to formulate quantum theory in terms of a wave analysis. Schrödinger was later able to show that his wave mechanics gave the same results as Heisenberg's matrix mechanics.

Following Schrödinger's original work, many physicists and chemists struggled to refine the underlying structure of quantum mechanics. Nevertheless, the fundamental postulates introduced in Section 5.5 remain as a set of rules that cannot be proven, but only disproven. In other words, they cannot be understood as following from experiments or theorems in a logical way; instead, the postulates must be taken as a basic set of conjectures which can be justified only by their continual correctness in predicting the observed behavior of matter at the atomic or molecular level.

5.2 The Bohr Model for the Spectrum of Atomic Hydrogen

We now investigate the failure of classical mechanics and the success of quantum mechanics by specifically considering in some detail Bohr's model for the hydrogen atom. At the turn of the last century, much experimental work had been completed on the spectroscopy of atomic hydrogen. Typically, an emission spectrum was obtained on a photographic plate by using a hydrogen discharge lamp as the source of radiation. The resulting spectrograph of Fig. 5.1 was the forerunner of today's modern spectrometer, which employs a grating rather than a prism and a photomultiplier tube or photodiode array rather than a photographic plate. A schematic representation of the resulting spectrum for atomic hydrogen is shown in Fig. 5.2. Three series of lines can be observed, one each in the ultraviolet, visible, and infrared regions of the electromagnetic spectrum. Each series of lines displays

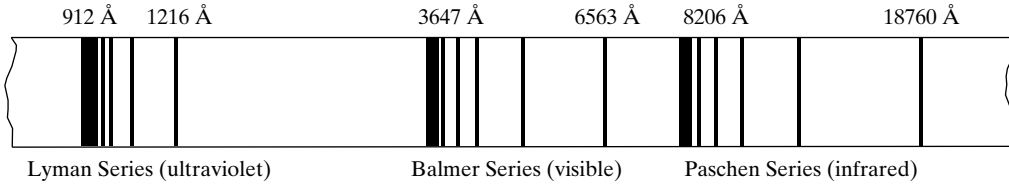

Figure 5.2 The three series of lines in the spectrum of atomic hydrogen as displayed on a logarithmic wavelength scale.

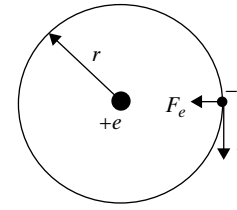

Figure 5.3 Schematic for Bohr model of the hydrogen atom.

a characteristic reduction in line spacing and thus a denser spectral region at lower wavelengths. The lower and upper limits for each spectral family range from 912 to 1216 Å for the Lyman series, from 3647 to 6563 Å for the Balmer series, and from 8206 to 18,760 Å for the Paschen series.

At this juncture, we introduce a convenient spectral definition delineating relative energy differences called the *wave number*, i.e.,

$$\tilde{\nu} \equiv \frac{\Delta\varepsilon}{hc} = \frac{\nu}{c} = \frac{1}{\lambda}, \tag{5.3}$$

where we have made use of Eq. (5.2) and recognized that the wavelength $\lambda = c/\nu$. The utility of wave number units (cm^{-1}), which indicates the number of vacuum wavelengths in one centimeter, is obvious from Eq. (5.3), in that discrete energy changes are directly related to the inverse of the measured spectral wavelength. Employing this definition, the discrete wavelengths of all spectral lines in Fig. 5.2 can be empirically correlated via the Rydberg formula,

$$\tilde{\nu}_{nm} = R_H \left(\frac{1}{m^2} - \frac{1}{n^2} \right), \tag{5.4}$$

where $m = 1, 2, 3, \ldots$ is an index representing the Lyman, Balmer, and Paschen series, respectively, while $n = m+1, m+2, m+3, \ldots$ identifies the spectral lines for each series. An adequate theory for the spectrum of atomic hydrogen must reproduce Eq. (5.4), including the *Rydberg constant*, $R_H = 109{,}678\ \text{cm}^{-1}$, which is one of the most precise physical constants in all of science. Indeed, the accurate reproduction of R_H accounts for the success of the Bohr model, which ultimately invoked energy quantization because of the two integers, m and n, in Eq. (5.4).

We initiate our discussion of the Bohr model by classically analyzing the stable circular motion of a single electron about a stationary nucleus of opposite charge, as shown in Fig. 5.3. Applying Newton's second law, a stable orbit is achieved by satisfying

$$-F_e = \frac{e^2}{4\pi\varepsilon_\circ r^2} = \frac{m_e v^2}{r},$$

where F_e is the electrostatic force and v^2/r is the centripetal acceleration. We thus obtain for the kinetic energy of the electron,

$$T_e = \frac{1}{2} m_e v^2 = \frac{e^2}{8\pi\varepsilon_\circ r}, \tag{5.5}$$

where m_e is the electron mass, v is its velocity, e its charge, r its radius, and $\varepsilon_\circ$ is the permittivity of free space. Now, for a conservative system (Appendix G), $-F_e = \partial V_e/\partial r$; thus, the potential energy of an electron orbiting about a proton can be determined from

$$V_e = \int_\infty^r \frac{e^2}{4\pi\varepsilon_\circ} \frac{dr}{r^2} = -\frac{e^2}{4\pi\varepsilon_\circ r}. \tag{5.6}$$

Combining Eqs. (5.5) and (5.6), we can express the total energy of the electron as

$$\varepsilon = T_e + V_e = -\frac{e^2}{8\pi\varepsilon_\circ r}. \tag{5.7}$$

Therefore, we find that the classical energy of the electron for atomic hydrogen is inversely proportional to its radius. Unfortunately, as indicated previously, classical electromagnetic theory indicates that an accelerating charge must emit radiation, similar to the electrons within a radio antenna. As an orbiting electron is continually accelerating, its total energy must drop and thus, according to Eq. (5.7), the electron should eventually spiral into the nucleus. This scenario is obviously contrary to experimental evidence, so that classical physics proves to be totally inadequate for predicting stable orbits of the hydrogen atom.

Refuting classical physics, Bohr courageously advocated two original postulates, which can be stated as follows. First, the electron is assumed to move in specific orbits about the nucleus, for which the orbital angular momentum, L, is quantized according to

$$L = m_e v r = n\hbar \qquad n = 1, 2, 3, \ldots \tag{5.8}$$

where $\hbar \equiv h/2\pi$. Second, the electron may emit or absorb energy only by undergoing a *transition* to an orbit of lower or higher energy, respectively. Hence, according to Eq. (5.3), the resulting energy shift in wave number units becomes

$$\tilde{\nu}_{nm} = \frac{\varepsilon_n - \varepsilon_m}{hc}, \tag{5.9}$$

where ε_n and ε_m denote the electronic energies associated with higher and lower orbits, respectively. Notice that the first postulate permits only discrete orbits while the second postulate permits only discrete wavelengths. The two postulates taken together simply deny continuous emission of electromagnetic radiation despite ongoing acceleration of the electron.

The allowed orbits can now be determined by combining Eqs. (5.5) and (5.8); i.e.,

$$T_e = \frac{1}{2}m_e v^2 = \frac{1}{2}m_e\left(\frac{n\hbar}{m_e r}\right)^2 = \frac{e^2}{8\pi\varepsilon_\circ r}.$$

Hence, if we solve for r, the allowed orbital radii become

$$r = \frac{4\pi\varepsilon_\circ\hbar^2}{m_e e^2}n^2 \qquad n = 1, 2, 3, \ldots. \tag{5.10}$$

Similarly, substituting Eq. (5.10) into Eq. (5.7), we find the allowed orbital energies to be

$$\varepsilon_n = -\frac{m_e e^4}{8\varepsilon_\circ^2 h^2}\frac{1}{n^2}, \tag{5.11}$$

or, in wave number (cm^{-1}) units,

$$\tilde{\varepsilon}_n = \frac{\varepsilon_n}{hc} = -\frac{m_e e^4}{8\varepsilon_\circ^2 ch^3}\frac{1}{n^2}, \tag{5.12}$$

where the negative values of energy indicate that the electron is bound to the nucleus. These energy values are obviously quantized through the integer n, which is called the electronic *quantum number*. Both the orbital radius and energy increase with the square of this quantum number. Hence, the lowest electronic energy occurs for $n = 1$. This minimum

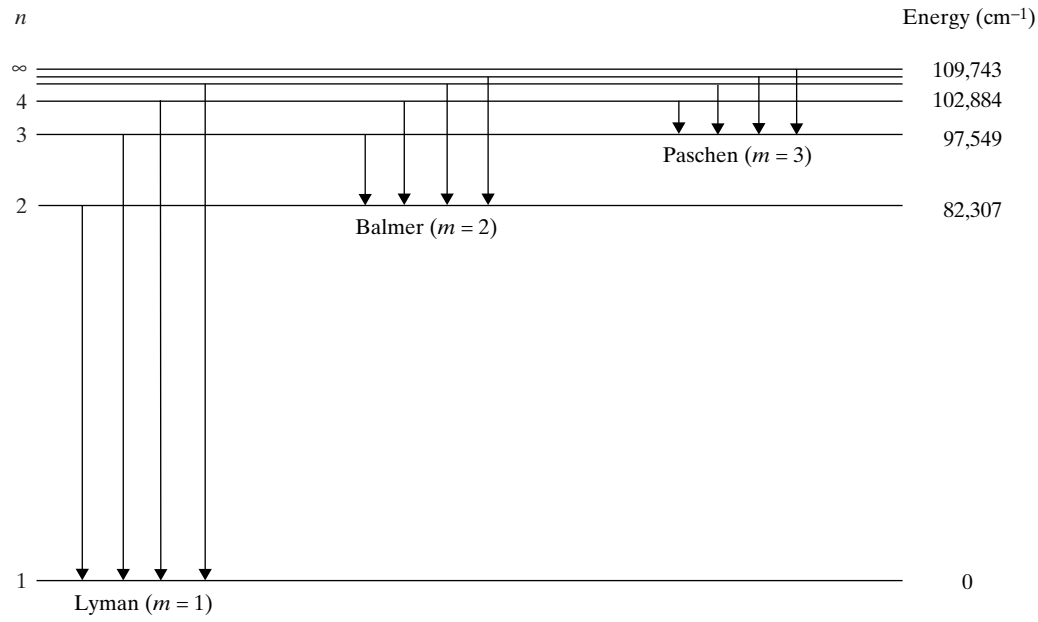

Figure 5.4 Energy-level diagram and emissive transitions for the hydrogen atom.

energy is designated as the electronic *ground state*. Higher energies ($n > 1$) are associated with less stable orbits, which are thus called *excited* electronic states.

We may now substitute Eq. (5.11) into Eq. (5.9) for two different energy levels, thus duplicating the requisite form for the Rydberg formula, i.e.,

$$\tilde{\nu}_{nm} = \frac{m_e e^4}{8\varepsilon_\circ^2 ch^3}\left(\frac{1}{m^2} - \frac{1}{n^2}\right). \tag{5.13}$$

Comparing Eqs. (5.4) and (5.13), we conclude that the Rydberg constant is given by

$$R_H = \frac{m_e e^4}{8\varepsilon_\circ^2 ch^3}, \tag{5.14}$$

from which we find that $R_H = 109{,}743\ \text{cm}^{-1}$, in excellent agreement with the experimental value of 109,678 cm^{-1}. As we will see in Chapter 6, even better agreement is obtained by using a center-of-mass coordinate system, that is, by not assuming that the nucleus is stationary. In general, despite its rather *ad hoc* linkage between classical and quantum concepts, the Bohr model proved to be incredibly successful. It provided for the first time a robust explanation for the existence of stable electronic orbits in an atom. Moreover, its predictions were in remarkable agreement with the experimental spectra for atomic hydrogen.

We close our presentation of the Bohr model by pointing out that the discrete energies predicted by Eq. (5.12) can be conveniently displayed on an *energy-level diagram*, as shown in Fig. 5.4. Such diagrams are a common feature of atomic and molecular spectroscopy, especially as applied to statistical thermodynamics. For convenience, energy-level diagrams traditionally incorporate wave number units and the ground-state energy is always set to zero; thus, for atomic hydrogen, 109,743 cm^{-1} must be added to each energy calculated from Eq. (5.12), as shown in Fig. 5.4. Note that as $n \to \infty$ the energy levels merge toward

the continuum. Consequently, the condition $n = \infty$ corresponds to the ionization energy for atomic hydrogen. In other words, the electron becomes completely removed from the atom, thereby giving continuous rather than discrete radiation. Figure 5.4 also displays the emissive transitions corresponding to the Lyman ($m = 1$), Balmer ($m = 2$), and Paschen ($m = 3$) series of spectral lines, with each family representing all transitions between the allowed sequence of higher energy levels and a specific lower level for atomic hydrogen. Therefore, the reduction in spacing at lower wavelengths for each series in the spectrum (Fig. 5.2) corresponds to an accelerating movement toward the continuum at higher orbital energies.

EXAMPLE 5.1

Using the Bohr model for atomic hydrogen, determine (a) the radius of the first allowed Bohr orbit and (b) the speed of the electron in this same orbit.

Solution

(a) From Eq. (5.10), the radius of the first Bohr orbit ($n = 1$) can be determined from

$$a_\circ = \frac{4\pi\varepsilon_\circ\hbar^2}{m_e e^2} = \frac{\varepsilon_\circ h^2}{\pi m_e e^2},$$

where we have used the common notation, $a_\circ$, for the first Bohr orbit. On this basis, we obtain

$$a_\circ = \frac{(8.854\times10^{-12}\,\mathrm{C^2/J\cdot m})(6.626\times10^{-34}\,\mathrm{J\cdot s})^2}{\pi(9.109\times10^{-31}\,\mathrm{kg})(1.602\times10^{-19}\,\mathrm{C})^2} = 5.29\times10^{-11}\,\mathrm{m}.$$

Hence, $a_\circ = 52.9$ pm, which is equivalent to 0.529 Å.

(b) Given the first Bohr radius from part (a), the speed can be determined most directly from Eq. (5.8). For $n = 1$, we thus have

$$v = \frac{h}{2\pi m_e a_\circ} = \frac{6.626\times10^{-34}\,\mathrm{J\cdot s}}{2\pi(9.109\times10^{-31}\,\mathrm{kg})(5.29\times10^{-11}\,\mathrm{m})} = 2.19\times10^{6}\,\mathrm{m/s}.$$

Hence, the speed of the electron is nearly 1% that of the speed of light.

5.3 The de Broglie Hypothesis

When Einstein modeled radiation as photons, he essentially postulated that light can act as a particle as well as a wave. In an analogous fashion, de Broglie suggested that matter can act as a wave as well as a particle. In other words, he postulated that wave–particle duality should hold for both matter and electromagnetic radiation. Therefore, for macroscopic systems, light and matter would display their traditional wave and particle properties, respectively. In contrast, for microscopic systems, light would behave as a particle while matter would behave as a wave.

From classical electromagnetic (or special relativity) theory, the linear momentum carried by a beam of parallel light is

$$p = \frac{\varepsilon}{c}, \tag{5.15}$$

where ε is the energy of the beam and c is the speed of light. Substituting Eq. (5.1) into Eq. (5.15), we find that, for a single photon,

$$p = \frac{h\nu}{c} = \frac{h}{\lambda}, \tag{5.16}$$

where we have again recognized that $\lambda\nu = c$. Therefore, according to Eq. (5.16), the wavelength of an electromagnetic wave can be linked to its momentum, although the latter concept is normally associated with particles. Similarly, de Broglie reasoned, the momentum of a particle, as imaginatively affiliated with "matter waves," can be linked in a reverse manner to the wavelength via a simple transformation of Eq. (5.16) to

$$\lambda = \frac{h}{p}. \tag{5.17}$$

Because Planck's constant is miniscule ($h = 6.6261 \times 10^{-34}\ \mathrm{J \cdot s}$), Eq. (5.17) suggests that a large mass will always produce matter waves having a wavelength much too small to affect the dynamics of classical mechanical systems. In a similar fashion, fundamental particles are more likely to be associated with much larger wavelengths approaching atomic dimensions; in this case, the behavior of the particle will be strongly influenced by its accompanying wave characteristics. For this reason, the prediction of particle behavior within atomic and molecular systems requires a probabilistic rather than deterministic approach, particularly when evaluating particle location or momentum. Such behavior comports well with our previous notion that fundamental particles are normally indistinguishable.

We end our introduction to matter waves by pointing out an important relation between de Broglie's hypothesis and the Bohr model for atomic hydrogen. Combining Eqs. (5.8) and (5.17), we obtain

$$\lambda = \frac{h}{m_e v} = \frac{2\pi r}{n},$$

so that the wavelength of a matter wave affiliated with any electronic orbit of atomic hydrogen must be an integer fraction of its orbital circumference. In short, the assigned wavelength will conform to an electronic orbit only if its associated matter wave remains in phase around the nucleus. This phase condition avoids destructive interference, which would ultimately destroy any matter waves inherently prescribing electronic behavior at atomic dimensions.

EXAMPLE 5.2

Calculate the de Broglie wavelength for (a) a golf ball with a mass of 0.04 kg traveling at 35 m/s and (b) an electron in the first Bohr orbit of atomic hydrogen.

Solution

(a) The linear momentum of the golf ball is

$$p = mv = (0.04\,\mathrm{kg})(35\,\mathrm{m/s}) = 1.40\,\mathrm{N \cdot s}.$$

Hence, the de Broglie wavelength for the golf ball becomes

$$\lambda = \frac{h}{p} = \frac{6.626 \times 10^{-34}\,\mathrm{J \cdot s}}{1.40\,\mathrm{N \cdot s}} = 4.73 \times 10^{-34}\,\mathrm{m},$$

which is obviously much smaller than its size. Consequently, matter waves can have no influence on golf dynamics, which will thus be controlled by classical mechanics.

(b) Employing the results from Example 5.1, we find the momentum of an electron at the first Bohr radius to be

$$p = m_e v = (9.109 \times 10^{-31}\,\text{kg})(2.19 \times 10^{6}\,\text{m/s}) = 1.99 \times 10^{-24}\,\text{N} \cdot \text{s}\,.$$

Hence, the de Broglie wavelength becomes

$$\lambda = \frac{h}{p} = \frac{6.626 \times 10^{-34}\,\text{J} \cdot \text{s}}{1.99 \times 10^{-24}\,\text{N} \cdot \text{s}} = 3.33 \times 10^{-10}\,\text{m}\,.$$

In this case, the de Broglie wavelength is 3.33 Å, which is comparable to the first Bohr diameter of 1.06 Å. Therefore, we must expect quantum effects for atomic hydrogen, as we have already discovered from our study of its emission spectrum.

5.4 A Heuristic Introduction to the Schrödinger Equation

We know from standard electromagnetic theory that macroscopic radiation can be modeled successfully via a classical wave equation. If, for atomic dimensions, matter behaves as a wave, should not a similar wave formulation hold for matter displaying microscopic behavior? Indeed, if an analogous expression could be developed for matter waves, might we then have a consistent rubric for quantum behavior, unlike the partly classic and partly quantum tactic used to model atomic hydrogen? By fostering such queries, de Broglie's hypothesis eventually set the stage for the mathematical prowess of Erwin Schrödinger (1887–1961). The resulting Schrödinger wave equation is now considered to be a fundamental law of quantum mechanics, similar to the primary laws of classical mechanics, thermodynamics or electromagnetics. Hence, our upcoming presentation should not be considered a derivation of the Schrödinger wave equation, but rather a heuristic rationale for its formulation. As for other fundamental laws in science, its truth must rest solely on its ultimate capability for both explaining and predicting experimental behavior.

Since we have presumed an analogy between matter waves and electromagnetic waves, we begin by considering the wave equation for electromagnetic radiation in a homogeneous, uncharged, and nonconducting medium. For a single Cartesian dimension, the electric field, E, is governed by

$$\frac{\partial^2 E}{\partial x^2} = \frac{1}{\mathsf{v}^2}\frac{\partial^2 E}{\partial t^2},$$

where v is the wave velocity and t is the time. Schrödinger reasoned that this wave equation should apply to matter waves if account is taken of the potential energy of the particle. On this basis, he defined a wave function, Ψ, for matter waves in analogy to E, so that

$$\frac{\partial^2 \Psi}{\partial x^2} = \frac{1}{\mathsf{v}^2}\frac{\partial^2 \Psi}{\partial t^2}. \tag{5.18}$$

Depending on the specific boundary conditions, many solutions are possible for this one-dimensional wave equation. For simplicity, however, we consider only the well-known solution given by

$$\Psi(x, t) = Ce^{i(kx-\omega t)}, \tag{5.19}$$

where C is a constant and the negative sign indicates wave propagation in the positive x-direction. From wave theory, the propagation number, k, is related to the wavelength, λ, by

$$k = \frac{2\pi}{\lambda} \tag{5.20}$$

and, similarly, the angular velocity, ω, is related to the frequency, ν, by

$$\omega = 2\pi\nu. \tag{5.21}$$

Because the wave velocity $v = \nu\lambda$, from Eqs. (5.20) and (5.21) we also have

$$v = \frac{\omega}{k}. \tag{5.22}$$

We can verify Eq. (5.19) by employing the method of separation of variables. Assuming a solution of the form $\Psi(x,t) = \mathrm{X}(x)\mathrm{T}(t)$ and substituting into Eq. (5.18), we find that

$$\frac{\ddot{\mathrm{X}}}{\mathrm{X}} = \frac{\ddot{\mathrm{T}}}{v^2\mathrm{T}} = -k^2, \tag{5.23}$$

where the equivalence between the spatial and temporal expressions mandates that both sides of Eq. (5.23) be given by the same constant, here introduced as $-k^2$. Both ordinary differential equations can then be solved to obtain the following specific solutions for $\mathrm{X}(x)$ and $\mathrm{T}(t)$, as can be verified by direct substitution in Eq. (5.23):

$$\mathrm{X} = Ae^{ikx} \qquad \mathrm{T} = Be^{-i\omega t}.$$

Here, A and B are constants, thus establishing the solution for $\Psi(x,t)$ given by Eq. (5.19).

Employing the Hamiltonian formulation of classical mechanics, we recall that the total energy for a particle moving in a conservative system is (Appendix G)

$$\varepsilon = H = T + V = \frac{p^2}{2m} + V, \tag{5.24}$$

where the potential energy, V, is independent of time. Now, for matter waves, Eq. (5.20) can be expressed via Eq. (5.17) as

$$k = \frac{2\pi p}{h} = \frac{p}{\hbar}, \tag{5.25}$$

where we have again defined $\hbar \equiv h/2\pi$. Solving Eq. (5.24) for the momentum and substituting into Eq. (5.25), we find on substitution for the propagation number in Eq. (5.23) that the spatial portion of the wave equation becomes

$$\ddot{\mathrm{X}} + \left[2m(\varepsilon - V)/\hbar^2\right]\mathrm{X} = 0,$$

so that after rearrangement

$$-\frac{\hbar^2}{2m}\ddot{\mathrm{X}} + V\mathrm{X} = \varepsilon\mathrm{X}.$$

Multiplying the previous expression by the time-dependent portion, $\mathrm{T}(t)$, we obtain for matter waves

$$-\frac{\hbar^2}{2m}\frac{\partial^2\Psi}{\partial x^2} + V\Psi = \varepsilon\Psi. \tag{5.26}$$

We now take the temporal derivative of Eq. (5.19) and multiply by $i\hbar$, thus obtaining

$$i\hbar\frac{\partial\Psi}{\partial t} = i\hbar(-i\omega\Psi) = \hbar\omega\Psi;$$

however, from Eqs. (5.1) and (5.21),

$$\varepsilon = \frac{h}{2\pi}(2\pi\nu) = \hbar\omega, \tag{5.27}$$

so that

$$i\hbar\frac{\partial\Psi}{\partial t} = \varepsilon\Psi. \tag{5.28}$$

Substituting Eq. (5.28) into Eq. (5.26), we obtain

$$-\frac{\hbar^2}{2m}\frac{\partial^2\Psi}{\partial x^2} + V\Psi = i\hbar\frac{\partial\Psi}{\partial t}$$

for matter waves in any single Cartesian direction. More generally, of course,

$$-\frac{\hbar^2}{2m}\nabla^2\Psi(\boldsymbol{r},t) + V(\boldsymbol{r})\Psi(\boldsymbol{r},t) = i\hbar\frac{\partial\Psi(\boldsymbol{r},t)}{\partial t}, \tag{5.29}$$

where $\boldsymbol{r}$ designates the vector location for any coordinate system. For simplicity, however, we may define the so-called Hamiltonian operator,

$$\hat{H} = -\frac{\hbar^2}{2m}\nabla^2 + V, \tag{5.30}$$

so that the *time-dependent Schrödinger wave equation* becomes

$$\hat{H}\Psi = i\hbar\frac{\partial\Psi}{\partial t}.$$

We emphasize again that the previous heuristic development does not constitute a proof for the Schrödinger wave equation but instead a rationale for its formulation. Ultimately, its veracity depends solely on its utility and versatility when addressing atomic or molecular dynamics. Fortunately, the Schrödinger wave equation in its many manifestations has proven to be extremely robust in nearly all real-world applications. For this reason, the advent of Schrödinger's famous equation signifies the real beginning of quantum mechanics as a viable field of enquiry and application in physics, chemistry, and engineering.

5.5 The Postulates of Quantum Mechanics

Any scientific equation is useless if it cannot be interpreted properly when applied to physical problems. The Schrödinger wave equation was initially plagued by this impasse owing to difficulties in assigning a practical meaning to the wave function. Defining $\Psi(\boldsymbol{r},t)$ as the amplitude of matter waves was just too vague and did not offer a clear link between model and experiment. While Schrödinger himself suggested various probabilistic interpretations, it was the German physicist Max Born (1882–1970) who ultimately realized that multiplication of the wave function by its complex conjugate defined a probability density function for particle behavior. From a more general perspective, we now know that the wave function itself offers no real insight and that physical meaning only comes when the wave function is operated on by various mathematical operators. This viewpoint

coalesced to pragmatic orthodoxy during the 1930s, thus paving the path for many robust applications of quantum mechanics.

The general procedures for identifying and assessing solutions to the Schrödinger wave equation are delineated most concisely by the following set of four basic postulates. As indicated previously, the efficacy of these postulates rests mainly on their continuing success in solving and interpreting many real-world problems in quantum mechanics since the 1930s. The four postulates are presented herewith in a form sufficient for our study of statistical thermodynamics.

I. The state of any quantum mechanical system can be specified by a function, $\Psi(\boldsymbol{r}, t)$, called the wave function of the system. The quantity $\Psi^*\Psi\, d\tau$ is the probability that the position vector $\boldsymbol{r}$ for a particle lies between $\boldsymbol{r}$ and $\boldsymbol{r} + d\boldsymbol{r}$ at time t within the volume element $d\tau$.

II. For every dynamic variable, A, a linear Hermitian operator, $\hat{A}$, can be defined as follows:
   (a) If A is r_i or t, the operator is multiplication by the variable itself;
   (b) If A is p_i, the operator is $-i\hbar\partial/\partial r_i$;
   (c) If A is a function of r_i, t, and p_i, the operator takes the same functional form as the dynamic variable, with the operators multiplication by r_i, multiplication by t, and $-i\hbar\partial/\partial r_i$ substituted for r_i, t, and p_i, respectively;
   (d) The operator corresponding to the total energy is $i\hbar\partial/\partial t$.

III. If a system state is specified by the wave function, $\Psi(\boldsymbol{r}, t)$, the average observable value of the dynamic variable A for this state is given by

$$\langle A \rangle = \frac{\int \Psi^* \hat{A} \Psi \, d\tau}{\int \Psi^* \Psi \, d\tau}. \tag{5.31}$$

IV. The wave function, $\Psi(\boldsymbol{r}, t)$, satisfies the time-dependent Schrödinger wave equation

$$\hat{H}\Psi(\boldsymbol{r}, t) = i\hbar \frac{\partial \Psi(\boldsymbol{r}, t)}{\partial t}, \tag{5.32}$$

where the Hamiltonian operator, $\hat{H}$, corresponds to the classical Hamiltonian, $H = T + V$, for which T and V are the kinetic and potential energies, respectively.

Implementing these four postulates requires some additional understanding, which we now pursue at some length. First, postulate I interprets $\Psi^*\Psi$ as a probability density function (PDF), thus indicating that this quantity must be real, positive, and *normalizable*. The real and positive conditions are automatically satisfied since the product of any variable with its complex conjugate is real and positive. More importantly, the usual normalization condition for any PDF,

$$\int \Psi^* \Psi d\tau = 1, \tag{5.33}$$

requires that the wave function be well behaved, that is, continuous, single-valued, and finite. To simplify nomenclature, volume integrals in quantum mechanics are generally written utilizing the formalism of Eq. (5.33), for which the denoted single integration over all space symbolizes the usual triple integration for any three-dimensional coordinate system. Cartesian coordinates, for example, would require the volume element, $d\tau = dx\, dy\, dz$, with all subsequent integrations occurring over the region defined by finite values of $\Psi^*\Psi$.

Postulate II implies that all mathematical transformations in quantum mechanics involve *linear Hermitian* operators. Linear operator theory and the important characteristics of Hermitian operators are discussed extensively in Appendix H. In summary, given two different wave functions, Ψ_1 and Ψ_2, a linear operator, $\hat{A}$, always obeys the rule

$$\hat{A}\{\Psi_1 + \Psi_2\} = \hat{A}\Psi_1 + \hat{A}\Psi_2.$$

Hermitian operators, moreover, prove to be most significant when applied to eigenvalue problems, as defined by

$$\hat{A}\Psi = a\Psi, \tag{5.34}$$

where the wave function, Ψ, is an *eigenfunction* and a is its associated *eigenvalue*. As we will show momentarily, the Schrödinger wave equation is actually a disguised eigenvalue problem. Consequently, all wave functions are in reality eigenfunctions of the Schrödinger equation. For Hermitian operators, *eigenfunctions always form a complete orthonormal set* and *eigenvalues are always real* (Appendix H). As a result, the normalization condition of Eq. (5.33) is essentially guaranteed by the Hermitian nature of all quantum mechanical operators.

Postulate II also defines a relation between linear Hermitian operators and dynamic variables. As we have already seen, this association comes from applying the wave equation to matter waves via the de Broglie hypothesis. However, constructing an unequivocal operator for a given dynamic variable is not always as simple as implied by this postulate. In particular, difficulties arise because multiplication is inherently commutative for dynamic variables but often not so for linear Hermitian operators (Appendix H). As shown in Section 5.8, this lack of commutation is ultimately responsible for the probabilistic nature of quantum mechanics.

Postulate III relates mean physical observations to both the PDF defined by postulate I and the linear Hermitian operator defined for a particular dynamic variable by postulate II. Based on Eq. (5.31), the resulting formalism requires that the Hermitian operator, $\hat{A}$, operate on Ψ and not on Ψ^*. In essence, mean observable values are determined by weighing the dynamical variable with its probability of occurrence at each possible location in the physical system. As for all statistical variables, the mean is also characterized by an associated standard deviation. However, for a linear Hermitian operator satisfying Eq. (5.34), we observe that

$$\langle A \rangle = \frac{\int \Psi^* a \Psi \, d\tau}{\int \Psi^* \Psi \, d\tau} = a,$$

where the denominator is, of course, unnecessary for a previously normalized wave function. In this case, we note that the mean collapses to an eigenvalue of its associated Hermitian operator. As a result, the physical observable must be both real and discrete; in other words, it has a guaranteed physical meaning but without a standard deviation. Such behavior constitutes the genesis for quantization in quantum mechanics.

Finally, postulate IV identifies Eq. (5.32) as the fundamental law of quantum mechanics. As indicated previously, this expression, known as the time-dependent Schrödinger wave equation, is in reality an eigenvalue problem. Notice from postulate II that the operator

corresponding to the total energy is $i\hbar\partial/\partial t$, as previously suggested by Eq. (5.28). Hence, Eq. (5.32) can also be written as

$$\hat{H}\Psi(\boldsymbol{r}, t) = \varepsilon\Psi(\boldsymbol{r}, t),$$

so that the energy, ε, denotes an eigenvalue for the Schrödinger wave equation. On this basis, we immediately recognize that the Schrödinger wave equation inherently offers the discrete energies expected by quantum mechanics. We are thus on our way to calculating the energy levels needed for statistical thermodynamics!

EXAMPLE 5.3

Consider a particle contained within a three-dimensional quantum mechanical system. Assuming Cartesian coordinates, determine (a) the operator corresponding to the z-component of its angular momentum and (b) an expression for the mean value of this component of angular momentum.

Solution

(a) The classical angular momentum is defined by

$$\boldsymbol{L} = \boldsymbol{r} \times \boldsymbol{p} = \begin{vmatrix} \boldsymbol{i} & \boldsymbol{j} & \boldsymbol{k} \\ x & y & z \\ p_x & p_y & p_z \end{vmatrix},$$

so that its z-component is $L_z = xp_y - yp_x$. Hence, from postulate II,

$$\hat{L}_z = -i\hbar\left(x\frac{\partial}{\partial y} - y\frac{\partial}{\partial x}\right).$$

(b) The mean value for the z-component of angular momentum can be obtained from postulate III by implementing Eq. (5.31). Assuming a normalized wave function, we have

$$\langle \mathrm{L_z} \rangle = \int \Psi^* \hat{L}_z \Psi d\tau = \iiint \Psi^* \hat{L}_z \Psi \, dx \, dy \, dz.$$

Hence, substituting for $\hat{L}_z$, we may evaluate the mean value of its z-component from

$$\langle \mathrm{L_z} \rangle = -i\hbar \iiint \Psi^* \left(x\frac{\partial \Psi}{\partial y} - y\frac{\partial \Psi}{\partial x}\right) dx \, dy \, dz.$$

5.6 The Steady-State Schrödinger Equation

We have shown that the Schrödinger wave equation can be cast as an eigenvalue problem for which the eigenfunctions constitute a complete orthonormal set of basis functions (Appendix H) and the eigenvalues designate the discrete energies required for statistical thermodynamics. The prediction of energy levels using the Schrödinger wave equation suggests an affiliation with the classical principle of energy conservation. We may verify this conjecture by considering a conservative system, for which the potential energy is a function

only of Cartesian position (Appendix G). From Eq. (5.24), the relevant Hamiltonian can be expressed as

$$H = \frac{1}{2m}\left(p_x^2 + p_y^2 + p_z^2\right) + V,$$

so that, from postulate II, the analogous operator $\hat{H}$ becomes

$$\hat{H} = (i\hbar)^2 \frac{1}{2m}\left(\frac{\partial^2}{\partial x^2} + \frac{\partial^2}{\partial y^2} + \frac{\partial^2}{\partial z^2}\right) + V = -\frac{\hbar^2}{2m}\nabla^2 + V,$$

thus confirming Eq. (5.30). Notice that because the potential energy is a function only of position, its operator is simply multiplication by V. Invoking the operational analog to the identity, $H = \varepsilon$, postulate II(d) produces the expected Schrödinger wave equation,

$$-\frac{\hbar^2}{2m}\nabla^2\Psi(\boldsymbol{r},t) + V(\boldsymbol{r})\Psi(\boldsymbol{r},t) = i\hbar\frac{\partial\Psi(\boldsymbol{r},t)}{\partial t}. \tag{5.35}$$

Therefore, we have shown that Eq. (5.35) embodies conservation of energy for a single particle in an atomic or molecular system.

5.6.1 Single-Particle Analysis

For applications to statistical thermodynamics, the most important objective when solving the Schrödinger wave equation is to predict *steady-state* expectation values for various particle properties. For this purpose, temporal information is clearly irrelevant. Hence, we now separate the temporal from the spatial portion of the wave function by again using separation of variables, so that

$$\Psi(\boldsymbol{r},t) = \psi(\boldsymbol{r})\mathrm{T}(t), \tag{5.36}$$

where $\psi(\boldsymbol{r})$ is the *steady-state* wave function. Upon substituting Eq. (5.36) into Eq. (5.32) and rearranging, we obtain

$$\frac{\hat{H}\psi(\boldsymbol{r})}{\psi(\boldsymbol{r})} = i\hbar\frac{1}{\mathrm{T}(t)}\frac{d\mathrm{T}(t)}{dt} = \kappa, \tag{5.37}$$

for which κ is the separation constant. Solving for the temporal portion of Eq. (5.37), we obtain $\mathrm{T}(t) = \exp(-i\omega t)$, where $\omega = \kappa/\hbar$. But from Eq. (5.27), $\varepsilon = \kappa = \hbar\omega$, so that, from Eq. (5.36),

$$\Psi(\boldsymbol{r},t) = \psi(\boldsymbol{r})\exp(-i\varepsilon t/\hbar). \tag{5.38}$$

Consequently, the spatial portion of Eq. (5.37) becomes

$$\hat{H}\psi(\boldsymbol{r}) = \varepsilon\psi(\boldsymbol{r}), \tag{5.39}$$

so that, substituting the Hamiltonian operator of Eq. (5.30) into Eq. (5.39), we obtain

$$-\frac{\hbar^2}{2m}\nabla^2\psi + V\psi = \varepsilon\psi \tag{5.40}$$

for any single atomic or molecular particle. Equation (5.40) is known as the *steady-state Schrödinger wave equation*. We observe that $\psi(\boldsymbol{r})$ represents an eigenfunction for the total energy operator, $\hat{H}$, and the desired steady-state energy, ε, is its associated eigenvalue. Since the Hamiltonian operator is Hermitian, the predicted energies will be physically

realistic. Therefore, solutions to Eq. (5.40) will produce the discrete energy values required for applications to statistical thermodynamics.

For completeness, we must determine the average observable value for any dynamic variable under steady-state conditions. Substituting Eq. (5.38) into Eq. (5.31), we may cancel all temporal exponential functions so that

$$\langle A \rangle = \frac{\int \psi^*(\boldsymbol{r}) \hat{A} \psi(\boldsymbol{r})\, d\tau}{\int \psi^*(\boldsymbol{r}) \psi(\boldsymbol{r})\, d\tau}. \tag{5.41}$$

Hence, we have shown that the average observable value of any dynamic variable which is explicitly independent of time can be expressed solely in terms of the steady-state wave function, $\psi(\boldsymbol{r})$. Equation (5.41) is the master expression for calculating expectation values in steady-state systems. As an example, for the Hamiltonian operator, $\hat{H}$, Eq. (5.41) becomes

$$\langle H \rangle = \frac{\int \psi^*(\boldsymbol{r}) \hat{H} \psi(\boldsymbol{r})\, d\tau}{\int \psi^*(\boldsymbol{r}) \psi(\boldsymbol{r})\, d\tau},$$

so that, from Eq. (5.39),

$$\langle H \rangle = \frac{\int \psi^*(\boldsymbol{r}) \varepsilon \psi(\boldsymbol{r})\, d\tau}{\int \psi^*(\boldsymbol{r}) \psi(\boldsymbol{r})\, d\tau} = \varepsilon. \tag{5.42}$$

Therefore, as expected, the Hamiltonian undergoes quantization, thus providing discrete particle energies for atomic or molecular systems. Notice, by the way, that $\hat{H}$ is the total energy operator only for steady-state systems. For time-dependent systems, we must still use $i\hbar\partial/\partial t$ as the total energy operator.

5.6.2 Multiparticle Analysis

For a multiparticle system composed of N independent particles, Eq. (5.35) becomes

$$-\frac{\hbar^2}{2} \sum_{i=1}^{N} \frac{1}{m_i} \nabla_i^2 \Psi + V\Psi = i\hbar \frac{\partial \Psi}{\partial t}, \tag{5.43}$$

so that, at steady state,

$$-\frac{\hbar^2}{2} \sum_{i=1}^{N} \frac{1}{m_i} \nabla_i^2 \psi + V\psi = \varepsilon \psi. \tag{5.44}$$

In a similar fashion, the Hamiltonian operator can be separated into a sum of terms,

$$\hat{H} = \hat{H}^{(1)} + \hat{H}^{(2)} + \cdots + \hat{H}^{(N)} = \sum_{i=1}^{N} \hat{H}^{(i)}, \tag{5.45}$$

such that $\hat{H}^{(i)}$ contains only the coordinates of the ith particle. Consequently, the operator $\hat{H}^{(i)}$ can be used to obtain the wave function, $\psi(\boldsymbol{r}_i)$, for this particle by solving

$$\hat{H}^{(i)} \psi(\boldsymbol{r}_i) = \varepsilon^{(i)} \psi(\boldsymbol{r}_i). \tag{5.46}$$

Similarly, the overall wave function for the system, $\psi(\boldsymbol{r})$, must satisfy Eq. (5.39).

Now, for N independent particles, we may presume that the overall wave function, $\psi(\boldsymbol{r})$, can be expressed as the continued product of single-particle wave functions, $\psi(\boldsymbol{r}_j)$, so that

$$\psi(\boldsymbol{r}) = \psi(\boldsymbol{r}_1)\,\psi(\boldsymbol{r}_2)\cdots\psi(\boldsymbol{r}_N) = \prod_{j=1}^{N}\psi(\boldsymbol{r}_j). \tag{5.47}$$

Substituting Eqs. (5.45) and (5.47) into Eq. (5.39), we obtain

$$\left[\sum_{i=1}^{N}\hat{H}^{(i)}\right]\left[\prod_{j=1}^{N}\psi(\boldsymbol{r}_j)\right] = \varepsilon\,\psi(\boldsymbol{r}). \tag{5.48}$$

Because $\hat{H}^{(k)}$ contains no coordinates other than those for the kth particle, the only term that it affects when operating on the overall wave function is $\psi(\boldsymbol{r}_k)$. Hence, we may write

$$\hat{H}^{(k)}\prod_{j}\psi(\boldsymbol{r}_j) = \left\{\prod_{j\neq k}\psi(\boldsymbol{r}_j)\right\}\varepsilon^{(k)}\psi(\boldsymbol{r}_k) = \varepsilon^{(k)}\psi(\boldsymbol{r}),$$

where we have invoked Eq. (5.46). Substituting this result into Eq. (5.48) gives

$$\left[\sum_{i=1}^{N}\varepsilon^{(i)}\right]\psi(\boldsymbol{r}) = \varepsilon\psi(\boldsymbol{r}).$$

Therefore, Eq. (5.47) has been verified, as we have previously shown in Chapter 3 that the total energy for a system of independent particles is equivalent to the sum of energies for each particle, i.e.,

$$\varepsilon = \sum_{i=1}^{N}\varepsilon^{(i)}. \tag{5.49}$$

This scenario corresponds, of course, to that for the ideal gas.

5.7 The Particle in a Box

The famous particle in a box represents the simplest quantum mechanical problem; moreover, it conveniently demonstrates the many interesting effects of quantization. The solution is also very important to statistical thermodynamics as it predicts the allowed energy levels for the translational mode of any atom or molecule. For this problem, we assume a single free particle of mass m, which is constrained to translate in a cubical box of length L. To ensure that the particle has free access to any internal location, we assign a constant potential energy, $V = 0$, inside the box. To keep the particle within the box, we also stipulate that outside the box $V = \infty$. Because particle migration cannot occur beyond the box, the PDF, $\psi^*\psi$, must be nil in this region; thus, we may further assume that the wave function is identically zero external to the box.

Employing Eq. (5.40) we may write the steady-state Schrödinger wave equation for this foundational problem as

$$-\frac{\hbar^2}{2m}\left(\frac{\partial^2\psi}{\partial x^2}+\frac{\partial^2\psi}{\partial y^2}+\frac{\partial^2\psi}{\partial z^2}\right) = \varepsilon\psi,$$

for which the boundary conditions are

$$\psi(0, y, z) = \psi(x, 0, z) = \psi(x, y, 0) = 0$$
$$\psi(L, y, z) = \psi(x, L, z) = \psi(x, y, L) = 0.$$

Upon successive application of the separation-of-variables method, i.e.,

$$\psi(x, y, z) = \psi_1(x)\psi_{23}(y, z) = \psi_1(x)\psi_2(y)\psi_3(z), \tag{5.50}$$

we eventually obtain for each of the three coordinate directions,

$$\frac{d^2\psi_i}{dx_i^2} + \frac{2m}{\hbar^2}\varepsilon_i\psi_i = 0 \qquad i = 1, 2, 3, \tag{5.51}$$

where $x_1 = x,\ x_2 = y,$ and $x_3 = z$. Similarly, the total energy becomes

$$\varepsilon = \varepsilon_1 + \varepsilon_2 + \varepsilon_3, \tag{5.52}$$

as anticipated for three independent translational energies in the x-, y-, and z-directions.

The general solution to Eq. (5.51) is

$$\psi_i = A\sin\left[(2m\varepsilon_i/\hbar^2)^{1/2}x_i\right] + B\cos\left[(2m\varepsilon_i/\hbar^2)^{1/2}x_i\right], \tag{5.53}$$

so that, with boundary conditions given by

$$\psi_i(0) = 0 \qquad \psi_i(L) = 0,$$

we find that $B = 0$ and that

$$(2m\varepsilon_i/\hbar^2)^{1/2}L = n_i\pi \qquad n_i = 1, 2, 3, \ldots. \tag{5.54}$$

The remaining constant, A, can be evaluated using the normalization condition, so that

$$\int_0^L \psi_i^*\psi_i\, dx_i = A^2\int_0^L \sin^2(n_i\pi x_i/L)\, dx_i = 1,$$

from which we obtain $A = (2/L)^{1/2}$. Hence, upon rearranging Eqs. (5.53) and (5.54), the eigenfunction and eigenvalue for any single coordinate direction can be expressed as

$$\psi_i = (2/L)^{1/2}\sin(n_i\pi x_i/L) \tag{5.55}$$

$$\varepsilon_i = \frac{h^2}{8m}\frac{n_i^2}{L^2}, \tag{5.56}$$

where we have invoked $\hbar = h/2\pi$. Therefore, substituting Eq. (5.55) into Eq. (5.50) for each coordinate direction, we obtain the overall wave function for the three-dimensional box,

$$\psi = \left(8/L^3\right)^{1/2}\sin\left(\frac{n_1\pi x}{L}\right)\sin\left(\frac{n_2\pi y}{L}\right)\sin\left(\frac{n_3\pi z}{L}\right). \tag{5.57}$$

Similarly, substituting Eq. (5.56) into Eq. (5.52) for each coordinate direction yields the total *translational energy*,

$$\varepsilon_{tr} = \frac{h^2}{8mV^{2/3}}\left(n_1^2 + n_2^2 + n_3^2\right), \tag{5.58}$$

where we have introduced the volume, $V = L^3$, and the integers, n_1, n_2, and n_3 are the three *translational quantum numbers* for the problem. Equation (5.58) is the most significant result from the above analysis; indeed, you should anticipate multiple implementations of this expression once we return to statistical thermodynamics.

We now make five important observations regarding the above solution to the steady-state Schrödinger wave equation. First, we note that three quantum numbers are generated when solving the particle in a box; moreover, instead of being introduced in an *ad hoc* fashion, these quantum numbers arise naturally from the mathematics of the problem. From a classical perspective, translational motion in a three-dimensional box is similarly characterized by three degrees of freedom (Appendix G). This concurrence is actually a general result of quantum mechanics: one quantum number always originates from each classical degree of freedom. Therefore, as might be expected, each quantum number must be specified to identify the complete state of an atomic or molecular system.

Second, we find from Eq. (5.58) that more than one combination of the three translational quantum numbers yields the same total energy. This feature is a common occurrence in quantum mechanics and gives rise to the distinction between microstates and macrostates in statistical thermodynamics. From the viewpoint of quantum mechanics, the number of independent eigenfunctions corresponding to a given eigenvalue is called the *degeneracy*. As an example, for the particle in a box, the same total energy is obtained for quantum numbers (n_1, n_2, n_3) equal to $(2, 1, 1)$, $(1, 2, 1)$, and $(1, 1, 2)$, respectively; thus, in this case, the degeneracy is three. More generally, however, every unique combination of quantum numbers represents an independent *eigenstate* for the problem. Therefore, from the perspective of statistical thermodynamics, each energy level is defined by its eigenvalue while each energy state is defined by its eigenstate.

Third, for the particle in a box, we notice that the controlling mathematics gives rise to several distinct constants, namely A, B, and ε_i. Such constants are pervasive in quantum mechanics and are typically evaluated by invoking normalization and boundary conditions. Among these parameters, the eigenvalues, ε_i, are of special importance as they provide the discrete energy levels required for statistical thermodynamics. When solving for the translation energy, we found, in particular, that discreteness arose from implementation of a second boundary condition for the problem. More generally, we deduce that mathematical boundaries of this type invariably constitute the locus for quantization in both atomic and molecular systems.

Fourth, from Eq. (5.58), we observe that

$$\varepsilon_{tr} \propto \frac{h^2}{8mV^{2/3}},$$

so that the translational energy is inherently miniscule owing to its dependence on the square of Planck's constant. For this reason, the kinetic energy of any particle appears continuous rather than discontinuous regardless of its mass or volume. Therefore, spectroscopic evidence for quantization must come from the internal energy modes of atomic or molecular systems.

Fifth, and perhaps most important, because each of the three translational quantum numbers can range from unity to infinity, the number of eigenstates accessible to the

translational energy mode is simply overwhelming. Hence, even for macroscopic systems containing a huge number of particles, the vast majority of available energy states will be unoccupied in any realistic situation. To prove this assertion, we represent each possible energy state by its own unit cube in three-dimensional, quantum-number space; i.e., with the three quantum numbers, n_1, n_2, and n_3, as coordinates. Figure 5.5 displays the positive octant of quantum-number space, including a single unit cube at the origin. Because each cube corresponds to an eigenstate of the system, one cube must exist per unit volume of quantum-number space.

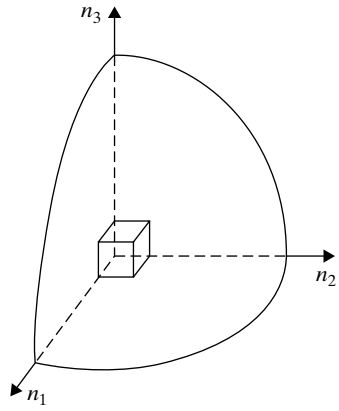

Figure 5.5 Quantum number space for the translational energy mode.

According to Eq. (5.58), the possible combinations of quantum numbers providing the same translational energy, ε_{tr}, must lie on the surface of a sphere with radius $n = (n_1^2 + n_2^2 + n_3^2)^{1/2}$ in quantum-number space. Because the three translational quantum numbers must be positive, the number of quantum states, M_ε, associated with $\varepsilon \leq \varepsilon_{tr}$ is equivalent to the volume within this space defined by the positive octant of a sphere. Therefore, from Eq. (5.58), we have

$$M_\varepsilon = \frac{\pi n^3}{6} = \frac{\pi}{6}\left[\frac{8mV^{2/3}\varepsilon_{tr}}{h^2}\right]^{3/2}, \tag{5.59}$$

which gives

$$M_\varepsilon = \frac{4\pi}{3}\left(\frac{2m}{h^2}\right)^{3/2} V\varepsilon_{tr}^{3/2}. \tag{5.60}$$

Differentiating Eq. (5.60), we obtain the associated PDF,

$$D(\varepsilon_{tr})\, d\varepsilon_{tr} = 2\pi\left(\frac{2m}{h^2}\right)^{3/2} V\varepsilon_{tr}^{1/2} d\varepsilon_{tr}, \tag{5.61}$$

which can be interpreted as the number of eigenstates per unit energy in the range ε_{tr} to $\varepsilon_{tr} + d\varepsilon_{tr}$. For simplicity in nomenclature, this important PDF is often labeled the *density of states*; the implicit understanding is that Eq. (5.61) considers only translational eigenstates. Despite the obvious restriction, we will later find significant uses for this expression in both statistical thermodynamics and kinetic theory.

Given the previous development, we are now in a position to demonstrate the incredible paucity of occupied translational energy states. For this purpose, we consider a cubic centimeter of gaseous H_2 at a temperature of 298 K. Employing Eq. (5.60), we find that the number of quantum states for which $\varepsilon_{tr} \leq \bar{\varepsilon}_{tr} = 1.5kT$ is given by $M_\varepsilon = 4.0 \times 10^{24}$. However, from the ideal gas law, the number of hydrogen molecules is only $N = 2.5 \times 10^{19}$ at atmospheric pressure. Hence, for this conservative case, we have over 10^5 translational energy states per molecule! From the perspective of statistical thermodynamics, this remarkable result essentially guarantees that any gas will satisfy the dilute limit.

EXAMPLE 5.4

Consider a free particle translating within a one-dimensional box of length L. Determine the average observable steady-state energy within this one-dimensional box.

Solution

The mean expectation value for any dynamic variable under steady-state conditions is given by Eq. (5.41). Hence, for Cartesian coordinates, the steady-state energy becomes

$$\langle H \rangle = \frac{\int \psi^* \hat{H} \psi \, dx \, dy \, dz}{\int \psi^* \psi \, dx \, dy \, dz}.$$

For a free particle ($V = 0$), the Hamiltonian operator of Eq. (5.30) becomes

$$\hat{H} = -\frac{\hbar^2}{2m} \nabla^2,$$

so that

$$\langle H \rangle = -\frac{\hbar^2}{2m} \frac{\int \psi^* \nabla^2 \psi \, dx \, dy \, dz}{\int \psi^* \psi \, dx \, dy \, dz}.$$

From Eq. (5.55), the normalized wave function for a one-dimensional box along the x-coordinate is

$$\psi = \left(\frac{2}{L}\right)^{1/2} \sin\left(\frac{n\pi x}{L}\right).$$

Hence, the mean energy becomes

$$\langle H \rangle = -\frac{\hbar^2}{2m} \int_0^\infty \psi^* \frac{d^2\psi}{dx^2} dx = \frac{\hbar^2}{2m} \left(\frac{2}{L}\right) \left(\frac{n\pi}{L}\right)^2 \int_0^\infty \sin^2\left(\frac{n\pi x}{L}\right) dx.$$

Evaluating the integral, we obtain

$$\langle H \rangle = \frac{h^2}{4\pi^2 mL} \left(\frac{n\pi}{L}\right)^2 \left(\frac{L}{2}\right) = \frac{h^2}{8m} \frac{n^2}{L^2}.$$

Therefore, as expected, the mean particle energy for a one-dimensional box is identical to its energy eigenvalue, as previously identified by Eq. (5.56). This result comports with our general expectation from quantum mechanics, as indicated by Eq. (5.42).

5.8 The Uncertainty Principle

The probabilistic nature of quantum mechanics indicates that a fundamental uncertainty must exist in the natural world at the atomic level. Consider, for example, the problem of using light to measure the position of an electron. If we wish to know its location to within a specified uncertainty, we must monitor the electron with radiation having a sufficiently small wavelength. Unfortunately, any transferred momentum owing to interaction with light will displace this electron. In other words, the measurement process itself leads to an inherent uncertainty in the position of the electron. To maintain accuracy, we might choose to use light having an even smaller wavelength. However, according to de Broglie's hypothesis, $p = h/\lambda$; hence, greater photon momentum would cause the electron to suffer an even larger displacement.

For this reason, modern microscopy has replaced photons with electrons, thus further upgrading ultimate precision. Indeed, by switching to electrons, finer matter waves can be produced by simply enhancing particle momentum. Employing this strategy, electron microscopy can typically produce images with accuracies approaching 500 pm. The downside is that metallic spray coatings are needed to stabilize many imaged objects to compensate for this higher momentum. We thus conclude that, even for electron microscopy, there is no free lunch!

By conceptually analyzing the above measurement process, the German physicist Werner Heisenberg (1901–1976) was eventually able to propose his famous uncertainty principle, which to this day remains a foundational precept in quantum mechanics. The Heisenberg uncertainty principle basically places a limit on the precision with which two dynamic variables, whose quantum mechanical operators do not commute, can be measured in any practical system. We may develop the principle by considering two arbitrary operators, $\hat{A}$ and $\hat{B}$, associated with two dynamic variables, A and B, whose commutator is given by (Appendix H)

$$[\hat{A}, \hat{B}] \equiv \hat{A}\hat{B} - \hat{B}\hat{A} = i\hat{C}. \tag{5.62}$$

The commutator can be generated by beginning with the root-mean-square deviation for both dynamic variables, which is denoted for A by

$$\Delta A = \left[\langle (A - \langle A \rangle)^2 \rangle\right]^{1/2}. \tag{5.63}$$

Employing normalized wave functions for both dynamic variables, Eqs. (5.31) and (5.63) together give

$$\Delta A \Delta B = \left[\int \Psi^* (\hat{A} - \langle A \rangle)^2 \Psi d\tau\right]^{1/2} \left[\int \Psi^* (\hat{B} - \langle B \rangle)^2 \Psi d\tau\right]^{1/2}. \tag{5.64}$$

Because $\hat{A}$ and $\hat{B}$ are quantum mechanical operators, they are unequivocally Hermitian operators; thus, $\langle A \rangle$ and $\langle B \rangle$ must be real numbers whose operators satisfy the definition of any Hermitian operator, as given by (Appendix H)

$$\int g^* \hat{D} f d\tau = \int (\hat{D} g)^* f d\tau. \tag{5.65}$$

If we apply this definition to Eq. (5.64), letting $\hat{D} = \hat{A} - \langle A \rangle$, $g = \Psi$, and $f = (\hat{A} - \langle A \rangle)\Psi$, while similarly $\hat{D} = \hat{B} - \langle B \rangle$, $g = \Psi$, and $f = (\hat{B} - \langle B \rangle)\Psi$, we obtain

$$\Delta A \Delta B = \left\{\int \left[(\hat{A} - \langle A \rangle)\Psi\right]^* (\hat{A} - \langle A \rangle)\Psi d\tau \int \left[(\hat{B} - \langle B \rangle)\Psi\right]^* (\hat{B} - \langle B \rangle)\Psi d\tau\right\}^{1/2}. \tag{5.66}$$

Employing the well-known Schwartz inequality, which states that for any two well-behaved functions, f_1 and f_2,

$$\int f_1^* f_1 d\tau \int f_2^* f_2 d\tau \geq \left|\int f_1^* f_2 d\tau\right|^2,$$

we can express Eq. (5.66) as the inequality

$$\Delta A \Delta B \geq \left|\int [(\hat{A} - \langle A \rangle)\Psi]^* (\hat{B} - \langle B \rangle)\Psi d\tau\right|. \tag{5.67}$$

In addition, for any complex number $Z = X + iY$, we have

$$|Z| \geq |Y| = \left| \frac{Z - Z^*}{2i} \right|;$$

hence, Eq. (5.67) can be rewritten as

$$\Delta A \Delta B \geq \left| \frac{1}{2i} \int [(\hat{A} - \langle A \rangle)\Psi]^* (\hat{B} - \langle B \rangle)\Psi d\tau - \frac{1}{2i} \int [(\hat{B} - \langle B \rangle)\Psi]^* (\hat{A} - \langle A \rangle)\Psi d\tau \right|.$$

Re-applying Eq. (5.65) to the two Hermitian operators, $\hat{A} - \langle A \rangle$ and $\hat{B} - \langle B \rangle$, in the above expression, we obtain

$$\Delta A \Delta B \geq \left| \frac{1}{2i} \int \Psi^* (\hat{A} - \langle A \rangle)(\hat{B} - \langle B \rangle)\Psi d\tau - \frac{1}{2i} \int \Psi^* (\hat{B} - \langle B \rangle)(\hat{A} - \langle A \rangle)\Psi d\tau \right|.$$

This result can subsequently be expressed as the single integral,

$$\Delta A \Delta B \geq \left| \frac{1}{2i} \int \Psi^* [(\hat{A} - \langle A \rangle)(\hat{B} - \langle B \rangle) - (\hat{B} - \langle B \rangle)(\hat{A} - \langle A \rangle)]\Psi d\tau \right|.$$

Expanding the operators, and making appropriate cancellations by recognizing that the various expectation values are real numbers, we have

$$\Delta A \Delta B \geq \left| \frac{1}{2i} \int \Psi^* (\hat{A}\hat{B} - \hat{B}\hat{A})\Psi d\tau \right| = \left| \frac{1}{2i} \int \Psi^* i\hat{C}\Psi d\tau \right|, \tag{5.68}$$

where we have invoked Eq. (5.62). Rewriting Eq. (5.68), we obtain finally the Heisenberg uncertainty principle,

$$\Delta A \Delta B \geq \frac{|\langle C \rangle|}{2}, \tag{5.69}$$

which confirms that two dynamic variables, whose operators do not commute, cannot be simultaneously measured with a precision greater than the expectation value of its commutator.

As a specific example, consider the simultaneous uncertainty in position and momentum for the x-direction, $\Delta x \Delta p_x$. The relevant commutator can be determined by operating on the general function, $\varphi(x)$, thus giving, from Eq. (5.62),

$$[\hat{x}, \hat{p}_x]\varphi = \left[x, \frac{\hbar}{i} \frac{\partial}{\partial x} \right] \varphi = x \frac{\hbar}{i} \frac{\partial \varphi}{\partial x} - \frac{\hbar}{i} \frac{\partial (x\varphi)}{\partial x} = i\hbar\varphi.$$

Hence, we obtain $\hat{C} = \hbar$ so that, for normalized wave functions, $\langle C \rangle$ is also given by $\hbar$. The uncertainty principle then becomes, from Eq. (5.69),

$$\Delta x \Delta p_x \geq \frac{\hbar}{2}. \tag{5.70}$$

Therefore, as expected from de Broglie's hypothesis, a lower uncertainty in position implies a higher uncertainty in momentum; similarly, a lower uncertainty in momentum implies a higher uncertainty in position.

5.9 Indistinguishability and Symmetry

Particles in classical mechanics are said to be distinguishable, not in the sense that they are visually different, but in the sense that the controlling differential equations provide

unique trajectories for all such particles. Even when collisions occur between particles, the mathematical solutions distinguish their trajectories both before and after each collision. In comparison, following particle trajectories is impossible using quantum mechanics, as suggested by its probabilistic description and the Heisenberg uncertainty principle. In other words, while we may study interactions between particles in quantum mechanics, we cannot distinguish the path of one particle from another. Therefore, we conclude that *like fundamental particles can be counted but are inherently indistinguishable*. This feature leads to natural symmetry conditions for the wave function of any multiparticle system.

These imposed symmetry conditions can be understood by solving Eq. (5.44), for which the resulting wave function for a system of N independent particles can be written as

$$\psi = \psi(\boldsymbol{r}_1, \boldsymbol{r}_2, \boldsymbol{r}_3, \ldots \boldsymbol{r}_N).$$

If we conceptually exchange two of the position vectors, say the first and second, the solution now becomes

$$\psi = \psi(\boldsymbol{r}_2, \boldsymbol{r}_1, \boldsymbol{r}_3, \ldots \boldsymbol{r}_N).$$

But this exchange is purely a mathematical operation as like particles are indistinguishable. In other words, physical observations must remain unchanged by any such virtual operation. Because physical observations depend exclusively on the PDF, we thus conclude that $\psi^*\psi$ cannot be affected by particle permutations if the particles are truly indistinguishable. This conclusion can be guaranteed if

$$\psi(\boldsymbol{r}_2, \boldsymbol{r}_1, \boldsymbol{r}_3, \ldots \boldsymbol{r}_N) = \pm\psi(\boldsymbol{r}_1, \boldsymbol{r}_2, \boldsymbol{r}_3, \ldots \boldsymbol{r}_N);$$

that is, *the wave function must be symmetric* $(+)$ *or antisymmetric* $(-)$ *with respect to the exchange of any two particles*.

For an N-particle system, there are $N!$ possible permutations. For convenience, we define the permutation operator, $\hat{P}_r$, as that operator permuting one order of position vectors $(\boldsymbol{r}_1, \boldsymbol{r}_2, \boldsymbol{r}_3, \ldots, \boldsymbol{r}_N)$ to another $(\boldsymbol{r}_2, \boldsymbol{r}_1, \boldsymbol{r}_3, \ldots, \boldsymbol{r}_N)$. For the N-particle system, the number of such operators is clearly $N!$ We may also define $|P_r|$ as the number of two-particle exchanges required to bring about the order specified by the particular operator, $\hat{P}_r$. Two successive exchanges of two particles having an antisymmetric wave function will, of course, yield the original wave function. As a more complicated example, consider the antisymmetric system containing three particles with initial order 123. Let $\hat{P}_1$ represent the 123 order; $\hat{P}_2$, 213; $\hat{P}_3$, 312; $\hat{P}_4$, 132; $\hat{P}_5$, 231; and $\hat{P}_6$, 321. By counting the number of exchanges of two particles which are necessary to give the desired order, we see that $|P_1| = 0$, $|P_2| = |P_4| = |P_6| = 1$, and $|P_3| = |P_5| = 2$. On this basis, using the permutation operator, we may write the above symmetry condition as

$$\hat{P}_r\psi = (\pm 1)^{|P_r|}\psi. \tag{5.71}$$

In general, any fundamental particle can be characterized by either a symmetric or an antisymmetric wave function. The characteristic symmetry for each particle type can be determined from experiment or deduced from relativistic quantum mechanics. Particles with symmetric wave functions are called bosons while those with antisymmetric wave functions are called fermions. Table 5.1 lists the important particle types thus obeying Bose–Einstein or Fermi–Dirac statistics. While basic material particles (electrons, protons, neutrons) always have antisymmetric wave functions, we note that nuclei of even mass

Table 5.1. *Wave function symmetries for atomic particles*

Wave function symmetry	Symmetric (+)	Antisymmetic (−)
Nomenclature	Bosons	Fermions
Statistics	Bose–Einstein	Fermi–Dirac
Particles types	Photons, phonons Nuclei of even mass number*	Electrons, protons, neutrons Nuclei of odd mass number*
Spin quantum number	Integral	Half-integral
Pauli exclusion principle?	No	Yes

* The mass number is the number of protons plus the number of neutrons in a nucleus.

number are differentiated by symmetric wave functions. In preparation for upcoming applications to quantum mechanics, spectroscopy and statistical thermodynamics, we also include for the sake of completeness in Table 5.1 the influences of symmetry on spin quantum number and the Pauli exclusion principle.

5.10 The Pauli Exclusion Principle

The Pauli exclusion principle was developed by the German physicist Wolfgang Pauli (1900–1958); the principle follows directly from the symmetry requirements on wave functions. Consider a system of independent particles, whose wave function we have previously shown can be written as a product of component wave functions. Hence, from Eq. (5.47), the overall wave function for a two-particle system can be expressed as

$$\psi(\boldsymbol{r}_1, \boldsymbol{r}_2) = \psi_i(\boldsymbol{r}_1)\psi_j(\boldsymbol{r}_2),$$

where the notation $\psi_i(\boldsymbol{r}_k)$ indicates that particle k is in quantum state i. Unfortunately, this overall wave function is neither symmetric nor antisymmetric with respect to the exchange of two particles. It is simple, however, to construct such a wave function; for example, the expression

$$\psi(\boldsymbol{r}_1, \boldsymbol{r}_2) = \psi_i(\boldsymbol{r}_1)\,\psi_j(\boldsymbol{r}_2) \pm \psi_i(\boldsymbol{r}_2)\,\psi_j(\boldsymbol{r}_1) \tag{5.72}$$

is clearly symmetric or antisymmetric, depending on whether the central sign is positive or negative, respectively. Because the Schrödinger wave equation is a linear partial differential equation, any sum of its valid solutions is also valid; thus, Eq. (5.72) satisfies the parent wave equation plus any imposed symmetry requirement.

Now, if two particles have antisymmetric wave functions, when we attempt to put them into the same quantum state (i.e., let $\psi_i = \psi_j$), Eq. (5.72) becomes

$$\psi(\boldsymbol{r}_1, \boldsymbol{r}_2) = \psi_i(\boldsymbol{r}_1)\psi_i(\boldsymbol{r}_2) - \psi_i(\boldsymbol{r}_2)\psi_i(\boldsymbol{r}_1) = 0.$$

In other words, the contemplated situation has zero probability of occurrence and is thus impossible. This important result is known as the Pauli exclusion principle: *No two like particles with antisymmetric wave functions can be in the same quantum state*. We note that the two particles in question must be in the same multiparticle system for the exclusion principle to apply. Therefore, two electrons in separate atoms can be in the same quantum state, but if those two atoms form a molecule then the two electrons must be in different quantum states.

In general, the wave function for a system of N independent particles can be written as

$$\psi(\boldsymbol{r}) = \sum_r (\pm 1)^{|P_r|}\, \hat{P}_r \psi_1(\boldsymbol{r}_1)\psi_2(\boldsymbol{r}_2)\cdots\psi_N(\boldsymbol{r}_N), \tag{5.73}$$

where the positive and negative signs are invoked, respectively, for symmetric and antisymmetric wave functions. Note that, for two particles, Eq. (5.73) duplicates Eq. (5.72). The sum in Eq. (5.73) is taken over all possible operators, $\hat{P}_r$; hence, the overall wave function, $\psi(\boldsymbol{r})$, can vanish only if the individual wave functions are antisymmetric. Therefore, particles having such wave functions must obey the exclusion principle. On this basis, Pauli was eventually able to explain satisfactorily the buildup of the periodic table, as discussed further in Chapter 6.

5.11 The Correspondence Principle

The correspondence principle was proposed by Niels Bohr in 1923. Since the laws of classical physics had been found to work well in the macroscopic domain, Bohr argued that a satisfactory quantum theory must approach classical theory when applied to macroscopic behavior. In essence, the results of quantum and classical mechanics should correspond to each other for larger masses or energies. Based on its many successful applications, the quantum theory finally developed by Schrödinger clearly satisfies this correspondence principle. As expected, the transition from quantum to classical mechanics is gradual; recall, for example, the results obtained when considering atomic hydrogen and the particle in a box. For the former, the shift from discontinuous to continuous energies occurs when the electron becomes unbound rather than bound to the proton. For the latter, the discreteness predicted by quantum mechanics for a particle bound in a box is simply too small to be observed by any instrument in the macroscopic domain.

Planck's constant, h, plays a cardinal role in the discreteness of quantum mechanics. Indeed, this fundamental constant enters explicitly or implicitly into almost every equation of quantum mechanics. Specifically, from the particle in a box, one can readily understand that the smallness of h underlies the correspondence between quantum and classical results in the macroscopic domain. Therefore, if Planck's constant were sufficiently large, we would be more likely to observe the discontinuities predicted by quantum mechanics even in our everyday world.

In summary, quantum mechanics displays two primary differences from classical mechanics: discontinuity of energies and indistinguishability of particles. These conditions must be considered in the formulation of quantum statistical mechanics. However, as we have already found in Chapter 3 and as we will see further in Chapter 8, both of these differences can be easily accounted for in certain limiting cases. Hence, classical mechanical concepts remain quite useful for many applications to statistical thermodynamics.

Problems enhancing your understanding of this chapter are combined with those for Chapters 6 and 7 in Problem Set III.

6 Quantum Analysis of Internal Energy Modes

In the previous chapter, we introduced the fundamentals of quantum mechanics and derived important expressions describing the allowed energies and degeneracies of the *external* or translational energy mode for a single-particle system. We now apply quantum mechanics to more complicated two-particle systems so as to model in a simplified manner the remaining *internal* energy modes of an atom or molecule. In so doing, we will develop equations and procedures for calculating the energies and degeneracies associated with the rotational, vibrational, and electronic motions of a diatomic molecule. Making use of basic statistical relations from Chapter 4, we will then be in a position to evaluate the partition function and thus thermodynamic properties for any given atom or molecule.

6.1 Schrödinger Wave Equation for Two-Particle System

A primary system of importance to both quantum mechanics and statistical thermodynamics is that composed of two particles, as in, for example, the two nuclei of a diatomic molecule (when neglecting its electrons) or the proton and electron of a hydrogen atom. For both cases, the total classical energy is given by the Hamiltonian,

$$H = \frac{p_1^2}{2m_1} + \frac{p_2^2}{2m_2} + V_{12}, \tag{6.1}$$

where V_{12} is the potential energy describing this two-particle system. If we convert each term of Eq. (6.1) to its corresponding quantum mechanical operator, the resulting steady-state Schrödinger wave equation becomes

$$-\frac{\hbar^2}{2m_1}\nabla_1^2\psi - \frac{\hbar^2}{2m_2}\nabla_2^2\psi + (V_{12} - \varepsilon)\psi = 0, \tag{6.2}$$

in agreement with Eq. (5.44) for a generic two-particle system. Equation (6.2) is impossible to solve in its present form; however, as in classical mechanics, we may separate the external energy mode from all internal modes by converting to a center-of-mass coordinate system. The internal motion can then be viewed as the relative motion of one particle with respect to the other particle.

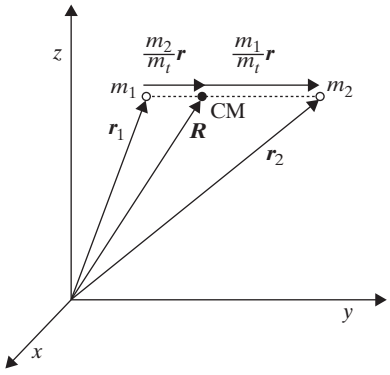

Figure 6.1 Coordinate transformation to center-of-mass system for two particles.

6.1.1 Conversion to Center-of-Mass Coordinates

The classic description of a two-particle system in terms of independent vectors, $\boldsymbol{r}_1$ and $\boldsymbol{r}_2$, associated with the two masses, m_1 and m_2, is shown in Fig. 6.1. Recall that the motion of this two-particle system can also be described in terms of its center of mass (CM). In other words, we may employ instead the independent vectors, $\boldsymbol{R}$ and $\boldsymbol{r}$, associated with absolute motion of the CM and with relative motion of the two component masses, respectively. From Fig. 6.1, we find via vector analysis that these two coordinate descriptions can be related through the basic equations

$$\boldsymbol{r}_1 = \boldsymbol{R} - (m_2/m_t)\boldsymbol{r} \tag{6.3}$$

$$\boldsymbol{r}_2 = \boldsymbol{R} + (m_1/m_t)\boldsymbol{r}, \tag{6.4}$$

where the total mass $m_t = m_1 + m_2$. Therefore, using the usual dot notation for velocity as well as Eqs. (6.3) and (6.4), the total kinetic energy can be expressed as

$$\frac{p_1^2}{2m_1} + \frac{p_2^2}{2m_2} = \frac{m_1}{2}(\dot{\boldsymbol{r}}_1 \cdot \dot{\boldsymbol{r}}_1) + \frac{m_2}{2}(\dot{\boldsymbol{r}}_2 \cdot \dot{\boldsymbol{r}}_2) = \frac{m_t}{2}(\dot{\boldsymbol{R}} \cdot \dot{\boldsymbol{R}}) + \frac{\mu}{2}(\dot{\boldsymbol{r}} \cdot \dot{\boldsymbol{r}}), \tag{6.5}$$

where the *reduced mass* is defined by

$$\mu = \frac{m_1 m_2}{m_1 + m_2}. \tag{6.6}$$

Equation (6.5) indicates that the kinetic energy of a two-particle system is equivalent to that of the total mass placed at the CM plus that of the reduced mass moving relative to the CM. Hence, from Eq. (6.2), the steady-state Schrödinger wave equation for any two-particle system becomes

$$-\frac{\hbar^2}{2m_t}\nabla_R^2\psi - \frac{\hbar^2}{2\mu}\nabla_r^2\psi + (V_{12} - \varepsilon)\psi = 0. \tag{6.7}$$

In general, however, Eq. (6.7) is still unsolvable as the potential energy, V_{12}, often depends on both $\boldsymbol{r}$ and $\boldsymbol{R}$. In other words, further assumptions are required to effect a more complete separation of the external from the internal motions of a two-particle system.

6.1.2 Separation of External from Internal Modes

We find, in fact, that full separation of the translational energy mode from the remaining internal energy modes mandates two additional hypotheses. First, we must assume that the two-particle system of interest is unaffected by other such systems so that V_{12} depends only on $\boldsymbol{r}$. Consequently, for diatomic molecules, each molecule can be considered independently of all nearby molecules within any practical macroscopic system. Second, we presume that our two-particle system experiences only a central coulombic field; i.e., $V_{12} = V(r)$, where $r = |\boldsymbol{r}_2 - \boldsymbol{r}_1|$. Therefore, Eq. (6.7) can now be written as

$$-\frac{\hbar^2}{2m_t}\nabla_R^2\psi - \frac{\hbar^2}{2\mu}\nabla_r^2\psi + V(r)\,\psi = \varepsilon\psi,$$

so that for independent external and internal coordinates, we have from the procedures of Section 5.6.2,

$$\hat{H}_{ext}\psi_{ext} = -\frac{\hbar^2}{2m_t}\nabla_R^2\psi_{ext} = \varepsilon_{ext}\psi_{ext} \tag{6.8}$$

$$\hat{H}_{int}\psi_{int} = -\frac{\hbar^2}{2\mu}\nabla_r^2\psi_{int} + V(r)\,\psi_{int} = \varepsilon_{int}\psi_{int}, \tag{6.9}$$

where $\psi = \psi_{ext}\psi_{int}$ and $\varepsilon = \varepsilon_{ext} + \varepsilon_{int}$.

We have thus shown that by converting to a center-of-mass coordinate system and assuming an independent central field, complete separation can be effected between the external and internal motions of any two-particle system. According to Section 5.7, Eq. (6.8) can be solved to determine the allowed energies and degeneracies for the translational energy mode, except that Eqs. (5.58) and (5.61) would be expressed in terms of the total mass, m_t. In a similar manner, using Eq. (6.9), we may now investigate the internal motion of any two-particle system. Specific cases of interest in this chapter include the rotation and vibration of a diatomic molecule or the electronic orbits within a hydrogen atom. By considering these two cases, we can obtain all required expressions for energies and degeneracies corresponding to the rotational, vibrational, and electronic energy modes. In doing so, we avoid mathematical fatigue by including only absolutely necessary derivations so that we can focus on those aspects of quantum mechanics explicitly needed to understand the energies and degeneracies utilized in statistical thermodynamics.

6.2 The Internal Motion for a Two-Particle System

As indicated in the previous section, Eq. (6.9) describes the internal behavior for any two-particle system characterized by an autonomous central field. The resulting complex motions are best analyzed using spherical coordinates (Appendix I). On this basis, Eq. (6.9) becomes

$$\left[\frac{1}{r^2}\frac{\partial}{\partial r}\left(r^2\frac{\partial}{\partial r}\right) + \frac{1}{r^2\sin\theta}\frac{\partial}{\partial\theta}\left(\sin\theta\frac{\partial}{\partial\theta}\right) + \frac{1}{r^2\sin^2\theta}\frac{\partial^2}{\partial\phi^2}\right]\psi_{int} + \frac{2\mu}{\hbar^2}\left[\varepsilon_{int} - V(r)\right]\psi_{int} = 0.$$

Employing separation of variables, we presume

$$\psi_{int}(r,\theta,\phi) = R(r)Y(\theta,\phi), \tag{6.10}$$

thus giving the following ordinary and partial differential equations:

$$\frac{d}{dr}\left(r^2\frac{dR}{dr}\right)+\left\{\frac{2\mu r^2}{\hbar^2}\left[\varepsilon_{int}-V(r)\right]-\alpha\right\}R=0 \tag{6.11}$$

$$\frac{1}{\sin\theta}\frac{\partial}{\partial\theta}\left(\sin\theta\frac{\partial Y}{\partial\theta}\right)+\frac{1}{\sin^2\theta}\frac{\partial^2 Y}{\partial\phi^2}+\alpha Y=0, \tag{6.12}$$

where $0\le r\le\infty$ and α is the required separation constant. Similarly,

$$Y(\theta,\phi)=\Theta(\theta)\Phi(\phi), \tag{6.13}$$

so that applying separation of variables again, but now to Eq. (6.12), we obtain

$$\frac{1}{\sin\theta}\frac{d}{d\theta}\left(\sin\theta\frac{d\Theta}{d\theta}\right)+\left(\alpha-\frac{\beta}{\sin^2\theta}\right)\Theta=0 \tag{6.14}$$

$$\frac{d^2\Phi}{d\phi^2}+\beta\,\Phi=0, \tag{6.15}$$

where $0\le\theta\le\pi$, $0\le\phi\le2\pi$ and β is a second separation constant.

Equations (6.11), (6.14), and (6.15) constitute three ordinary differential equations in terms of three unknown constants, namely, α, β, and ε_{int}. As expected, the radial portion of the internal motion depends on the central potential, $V(r)$, while the angular motion is independent of $V(r)$. Hence, for the diatomic case, Eq. (6.11) describes vibrational motion along the internuclear axis, while Eqs. (6.14) and (6.15) together define two-dimensional rotational motion. In the next section, we specifically address the diatomic molecule by solving Eqs. (6.14) and (6.15) for the allowed energies and degeneracies corresponding to the rotational energy mode. In so doing, we will determine α, thus eventually permitting solution of Eq. (6.11) for the vibrational energy mode.

6.3 The Rotational Energy Mode for a Diatomic Molecule

We begin our analysis of the rotational motion for a diatomic molecule by considering the normalized solution to Eq. (6.15),

$$\Phi(\phi)=\frac{\exp(im\phi)}{\sqrt{2\pi}}\qquad m=\sqrt{\beta}=0,\ \pm1,\ \pm2,\ldots, \tag{6.16}$$

where the integer values of m are specified by requiring that $\Phi(\phi+2\pi)=\Phi(\phi)$. As discussed in Chapter 5, such continuity conditions are often necessary to ensure well-defined probabilities for ensuing quantum calculations. By employing the transformation $w=\cos\theta$, we next convert Eq. (6.14) to

$$\frac{d}{dw}\left[(1-w^2)\frac{d\Theta}{dw}\right]+\left(\alpha-\frac{m^2}{1-w^2}\right)\Theta=0, \tag{6.17}$$

which can be identified as Legendre's equation of classical mathematical physics. When an assumed power series is invoked to solve Eq. (6.17), the series must be truncated to ensure finite solutions at $w=\pm1$. The truncation process leads to well-defined solutions only if

$$\alpha=J(J+1)\qquad J\ge|m|\,; \tag{6.18}$$

Table 6.1 *The first few spherical harmonics*

$Y_0^0 = \sqrt{\frac{1}{4\pi}}$	$Y_2^0 = \sqrt{\frac{5}{16\pi}}(3\cos^2\theta - 1)$
	$Y_2^1 = \sqrt{\frac{15}{8\pi}}\sin\theta\cos\theta\, e^{i\phi}$
$Y_1^0 = \sqrt{\frac{3}{4\pi}}\cos\theta$	$Y_2^{-1} = \sqrt{\frac{15}{8\pi}}\sin\theta\cos\theta\, e^{-i\phi}$
$Y_1^1 = \sqrt{\frac{3}{8\pi}}\sin\theta\, e^{i\phi}$	$Y_2^2 = \sqrt{\frac{15}{32\pi}}\sin^2\theta\, e^{2i\phi}$
$Y_1^{-1} = \sqrt{\frac{3}{8\pi}}\sin\theta\, e^{-i\phi}$	$Y_2^{-2} = \sqrt{\frac{15}{32\pi}}\sin^2\theta\, e^{-2i\phi}$

hence, substituting Eq. (6.18) into Eq. (6.17), we obtain after considerable effort the normalized solution

$$\Theta(w) = \left[\frac{(2J+1)}{2}\frac{(J-|m|)!}{(J+|m|)!}\right]^{1/2} P_J^{|m|}(w), \tag{6.19}$$

where $P_J^{|m|}(w)$ is the associated Legendre function of order $|m|$ and degree J, given by

$$P_J^{|m|}(w) = \frac{1}{2^J J!}(1-w^2)^{|m|/2}\frac{d^{|m|+J}}{dw^{|m|+J}}(w^2-1)^J. \tag{6.20}$$

Combining Eqs. (6.13), (6.16), and (6.19), we can express the solution for the rotational motion of a diatomic molecule as

$$Y_J^m(\theta,\phi) = \left[\frac{(2J+1)}{4\pi}\frac{(J-|m|)!}{(J+|m|)!}\right]^{1/2} P_J^{|m|}(\cos\theta)\, e^{im\phi}. \tag{6.21}$$

Because Eq. (6.21) is inherently orthonormal over a spherical surface, the various solutions for different values of the integers J and m are called spherical harmonics. The relevant integers are, of course, new quantum numbers, often called, respectively, the *rotational* and *magnetic* quantum numbers. The first few spherical harmonics are listed for clarity in Table 6.1.

From classical mechanics, we recall that the kinetic energy for a rigid two-particle system undergoing rotational motion at angular velocity ω can be expressed as

$$K = \frac{L^2}{2I}, \tag{6.22}$$

where the angular momentum $L = I\omega$ and the moment of inertia $I = \mu r^2$. Invoking Eq. (5.30), the quantum mechanical operator for the rotational kinetic energy of a two-particle system in spherical coordinates (Appendix I) is

$$\hat{K} = -\frac{\hbar^2}{2\mu}\nabla^2 = -\frac{\hbar^2}{2\mu}\left[\frac{1}{r^2}\frac{\partial}{\partial r}\left(r^2\frac{\partial}{\partial r}\right) + \frac{1}{r^2\sin\theta}\frac{\partial}{\partial\theta}\left(\sin\theta\frac{\partial}{\partial\theta}\right) + \frac{1}{r^2\sin^2\theta}\frac{\partial^2}{\partial\phi^2}\right].$$

Therefore, for a *rigid rotor*,

$$\hat{K} = -\frac{\hbar^2}{2I}\left[\frac{1}{\sin\theta}\frac{\partial}{\partial\theta}\left(\sin\theta\frac{\partial}{\partial\theta}\right) + \frac{1}{\sin^2\theta}\frac{\partial^2}{\partial\phi^2}\right] \tag{6.23}$$

as r is invariant for a hypothetical rigid molecule undergoing no vibrational motion. Comparing Eqs. (6.22) and (6.23), we conclude that the operator for the angular momentum must be

$$\hat{L}^2 = -\hbar^2 \left[\frac{1}{\sin\theta} \frac{\partial}{\partial\theta} \left(\sin\theta \frac{\partial}{\partial\theta} \right) + \frac{1}{\sin^2\theta} \frac{\partial^2}{\partial\phi^2} \right], \tag{6.24}$$

as can also be proved by directly applying operator theory to the vector definition of angular momentum.

If we now apply Eq. (6.24) to our spherical harmonics, from Eq. (6.12) we obtain

$$\hat{L}^2 Y(\theta,\phi) = -\hbar^2 \left[\frac{1}{\sin\theta} \frac{\partial}{\partial\theta} \left(\sin\theta \frac{\partial Y}{\partial\theta} \right) + \frac{1}{\sin^2\theta} \frac{\partial^2 Y}{\partial\phi^2} \right] = \alpha\hbar^2 Y(\theta,\phi). \tag{6.25}$$

From Eq. (6.18), Eq. (6.25) can be expressed more precisely as

$$\hat{L}^2 Y_J^m(\theta,\phi) = J(J+1)\hbar^2 Y_J^m(\theta,\phi). \tag{6.26}$$

Multiplying Eq. (6.26) by $R(r)$, we find from Eq. (6.10) that our original eigenvalue problem can be expressed as

$$\hat{L}^2 \psi_{int}(r,\theta,\phi) = J(J+1)\hbar^2 \psi_{int}(r,\theta,\phi);$$

hence, we conclude, following Section 5.5, that

$$L^2 = \langle L^2 \rangle = J(J+1)\hbar^2. \tag{6.27}$$

We have thus shown that the angular momentum of a rigid diatomic molecule is quantized, as for the Bohr model of atomic hydrogen.

From the point of view of statistical thermodynamics, we are, of course, more concerned with rotational energy than with angular momentum. Consequently, substituting Eq. (6.27) into Eq. (6.22), we find that the rotational energy levels for a rigid rotor are given by

$$\varepsilon_{rot} = \frac{J(J+1)\hbar^2}{2I}, \tag{6.28}$$

where, from Eqs. (6.16) and (6.18), the rotational quantum number, J, is limited to zero or any positive integer. For convenience, we convert Eq. (6.28) to wave number units, thus obtaining

$$F(J) = \frac{\varepsilon_{rot}}{hc} = J(J+1)B_e \qquad J = 0, 1, 2, \ldots, \tag{6.29}$$

where the *rotational constant* is defined as

$$B_e = \frac{h}{8\pi^2 c I_e} \tag{6.30}$$

and

$$I_e = \mu r_e^2 \tag{6.31}$$

designates the moment of inertia corresponding to the *equilibrium* internuclear distance, r_e, for a given diatomic molecule modeled as a rigid rotor.

Finally, we can determine the rotational degeneracy by recognizing that Eq. (6.21) identifies a different quantum state for every possible value of the magnetic quantum number, m, associated with any given rotational quantum number, J. Indeed, for a given J,

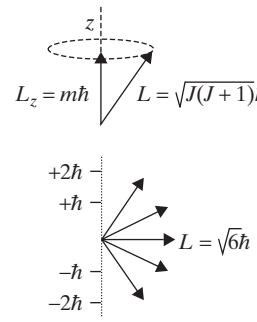

Figure 6.2 The vector model for angular momentum ($J = 2$).

Eqs. (6.16) and (6.18) indicate that $m = 0, \pm 1, \pm 2, \ldots, \pm J$; thus, the number of possible m-values for the degeneracy must be

$$g_{rot} = 2J + 1. \tag{6.32}$$

Quantum mechanics verifies that, for a given rotational energy, the above degeneracy corresponds to $2J + 1$ different values of the angular momentum along the z-coordinate. This z-component of the angular momentum, as shown schematically for $J = 2$ in Fig. 6.2, can generally be expressed as (Problem 3.3)

$$L_z = m\hbar, \tag{6.33}$$

which implies a splitting of each rotational energy level into $2J + 1$ finer levels when the z-coordinate is defined by a homogeneous magnetic field. The resulting *Zeeman effect* in the analogous atomic case (Section 6.5) is the main reason that m is called the magnetic quantum number.

EXAMPLE 6.1

Verify proper normalization for the spherical harmonic designated by Y_1^1.

Solution

Proper normalization implies that, when integrating over all space defined for any given wave function,

$$\int \psi^* \psi \, d\tau = 1,$$

where $d\tau = r^2 \sin\theta dr d\theta d\phi$ for spherical coordinates (Appendix I). Employing

$$Y_1^1 = \sqrt{\frac{3}{8\pi}} \sin\theta e^{i\phi},$$

we may write the above normalization condition as

$$\int \psi^* \psi \, d\tau = \iint Y_1^{1*} Y_1^1 \sin\theta \, d\theta \, d\phi,$$

where the r-dependence has been omitted because all spherical harmonics are functions only of the zenith and azimuthal angles, θ and ϕ. Substituting, we obtain

$$\iint Y_1^{1*} Y_1^1 \sin\theta \, d\theta \, d\phi = \frac{3}{8\pi} \int_0^{2\pi} \int_0^{\pi} \sin^3\theta \, d\theta \, d\phi = \frac{3}{4} \int_0^{\pi} \sin^3\theta \, d\theta.$$

Evaluating the remaining integral, we have

$$\iint Y_1^{1*} Y_1^1 \sin\theta \, d\theta \, d\phi = \frac{3}{4}\left[\frac{1}{3}\cos\theta(\sin^2\theta + 2)\right]_{\pi}^{0} = \frac{3}{4}\left[\frac{2}{3} + \frac{2}{3}\right] = 1.$$

Therefore, as expected, the spherical harmonic, Y_1^1, is indeed properly normalized.

6.4 The Vibrational Energy Mode for a Diatomic Molecule

The vibrational energy mode for a diatomic molecule can be analyzed by solving Eq. (6.11), which can now be expressed via Eq. (6.18) as

$$\frac{d}{dr}\left(r^2 \frac{dR}{dr}\right) + \left\{\frac{2\mu r^2}{\hbar^2}[\varepsilon_{int} - V(r)] - J(J+1)\right\} R = 0. \tag{6.34}$$

At this point, however, a further assumption is required as, realistically, ε_{int} includes the energy of all moving electrons within the molecule, which obviously cannot be described solely in terms of a single r-coordinate. More generally, the surrounding electron cloud will surely complicate the rotational and vibrational motions of the atomic nuclei comprising any such molecule. Fortunately, we can separate the electronic and nuclear motions of a diatomic molecule by invoking the so-called *Born–Oppenheimer approximation*. This somewhat intuitive presumption is based on the fact that the mass of each surrounding electron is much less than that of either vibrating nucleus. For this reason, the rapidly moving electrons undergo many orbits during a single vibration or rotation of the two nuclei. Consequently, we can analyze the electronic motion within a diatomic molecule by assuming that the nuclei are stationary. The internuclear distance still varies, of course, owing to the characteristic vibration and rotation of the molecule. Therefore, the electronic energy must be determined for every possible internuclear separation, which inherently affects the strong coupling between available electrons and protons.

In essence, the Born–Oppenheimer approximation permits separation of the electronic from the combined rotational–vibrational wave functions so that $\psi_{int} = \psi_{el}\psi_{rv}$. Subsequently, using Eq. (6.9), the Schrödinger wave equations describing the electronic and rovibrational modes become

$$\hat{H}_{el}\psi_{el} = \varepsilon_{el}\psi_{el} \tag{6.35}$$

$$\hat{H}_{rv}\psi_{rv} = \varepsilon_{rv}\psi_{rv}, \tag{6.36}$$

where the internal energy can now be expressed as a sum of independent electronic and rovibrational energies, i.e.,

$$\varepsilon_{int} = \varepsilon_{el} + \varepsilon_{rv}. \tag{6.37}$$

Conceptually, Eq. (6.35) is solved for all possible fixed separations between the atomic nuclei in a particular electronic state, thus determining $\varepsilon_{el}(r)$. The overall potential function needed for this incredibly complex solution must account for all interactions among the electrons and nuclei of a given molecular system. The continuous distribution of

resulting eigenvalues, $\varepsilon_{el}(r)$, then provides the internuclear potential, $V(r)$, needed to solve Eq. (6.36) for the chosen electronic state. In other words, $V(r) = \varepsilon_{el}(r)$, so that, as expected, the calculated rovibrational energies, ε_{rv}, must depend strongly on the specific electronic arrangement actually binding any diatomic molecule.

Because the Born–Oppenheimer approximation separates rovibrational from electronic motion, Eq. (6.36) can be rendered as Eq. (6.34) by using ε_{rv} rather than ε_{int}. Hence, the radial portion of the Schrödinger wave equation becomes

$$\frac{d}{dr}\left(r^2\frac{dR}{dr}\right) + \frac{2\mu r^2}{\hbar^2}\left[\varepsilon_{rv} - V(r) - \frac{\hbar^2}{2\mu r^2}J(J+1)\right]R = 0,$$

where electronic motion is now accounted for through $V(r)$. However, from Eq. (6.28), we subsequently obtain

$$\frac{d}{dr}\left(r^2\frac{dR}{dr}\right) + \frac{2\mu r^2}{\hbar^2}\left[\varepsilon_{vib} - V(r)\right]R = 0, \tag{6.38}$$

so that we have clearly separated the rotational from the vibrational energy modes, as indicated by

$$\varepsilon_{rv} = \varepsilon_{rot} + \varepsilon_{vib}. \tag{6.39}$$

On this basis, Eq. (6.38) may be solved for the vibrational energy mode once we have developed a suitable expression for the internuclear potential, $V(r)$.

Because Eq. (6.35) offers no hope of an analytical solution for $V(r)$, a power-series solution known as the Dunham potential has been developed that eventually produces via Eq. (6.36) a related power-series expression for the allowed energy levels describing the combined rotational and vibrational movements of a diatomic molecule. Mathematical convenience, however, has spurred the search for analytical models that reproduce the essential features of the Dunham potential. The most popular and accurate choice for such a model is the *Morse potential*,

$$V(r) = \mathrm{D}_e\left[1 - e^{-\beta(r-r_e)}\right]^2, \tag{6.40}$$

where D_e and β are associated fitting constants while r_e is the internuclear separation at thermodynamic equilibrium. Physically, the Morse potential reflects the chemical bond created by the electrostatic forces within the molecule. Figure 6.3 displays the Morse potential, as compared to the classic harmonic oscillator potential,

$$V(r) = \tfrac{1}{2}k_0(r - r_e)^2, \tag{6.41}$$

where the force constant, k_0, resulting from Hooke's law ($F = k_0 x$) is related to the conventional oscillator frequency, ν, by

$$k_0 = \mu(2\pi\nu)^2. \tag{6.42}$$

The most significant aspect of this comparison is the good agreement between the harmonic oscillator and Morse potentials at internuclear distances $r \simeq r_e$.

We can easily verify that both potentials comport with the expected vibrational motion of a diatomic molecule. Recall that, for a conservative system (Appendix G), a force is related to its potential via $F = -\partial V/\partial r$. Hence, for $r > r_e$ in Fig. 6.3, the force is negative

or attractive while, for $r < r_e$, the force is positive or repulsive. Both the strong repulsive force and the weaker attractive force arise from the electrostatic behavior of positive nuclei embedded within a negative electron cloud. More importantly, the alternating attractive and repulsive forces create oscillatory motion of the nuclei near r_e, as indicated by the minimum in either potential. However, in contrast to the harmonic oscillator potential, the Morse potential asymptotically approaches the dissociation limit, D_e, as $r \to \infty$. In other words, given sufficient energy D_e, a diatomic molecule can eventually be split into two free atoms. For this reason, the Morse potential produces vibrational motion only when $V(r) < D_e$, i.e., when a reasonably stable bond is maintained between the two nuclei of the diatomic molecule.

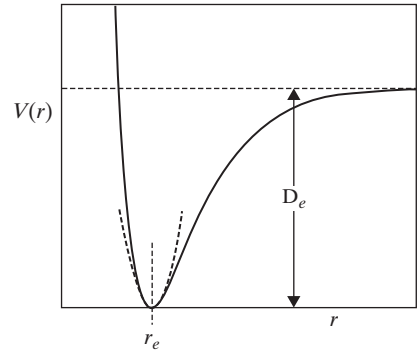

Figure 6.3 The Morse (solid line) and harmonic oscillator (dashed line) potential energy functions.

Despite this distinction, the harmonic oscillator potential remains a good approximation to the Morse potential at lower electronic energies associated with internuclear separations near r_e. On this basis, we may substitute Eq. (6.41) into Eq. (6.38), thus obtaining, after several variable transformations,

$$\frac{d^2S}{dx^2} + \frac{2\mu}{\hbar^2}\left(\varepsilon_{vib} - \frac{1}{2}k_0x^2\right)S = 0, \tag{6.43}$$

where $S(r) = r\,R(r)$ and $x = r - r_e$. Some additional transformations give

$$\frac{d^2H}{dy^2} - 2y\frac{dH}{dy} + (\lambda - 1)H = 0, \tag{6.44}$$

where $H(y) = S(y)\exp(y^2/2)$, $y = (2\pi\mu\nu/\hbar)^{1/2}x$, and

$$\lambda = \frac{2\varepsilon_{vib}}{h\nu}. \tag{6.45}$$

Equation (6.44) is another well-known differential equation from classical mathematical physics, whose solution is the Hermite polynomial of degree v,

$$H_v(y) = (-1)^v \exp(y^2)\frac{d^v}{dy^v}\exp(-y^2), \tag{6.46}$$

for which continuity requires

$$v = \tfrac{1}{2}(\lambda - 1) \qquad v = 0, 1, 2, \ldots. \tag{6.47}$$

Consequently, after proper normalization, the complete solution to Eq. (6.43) becomes

$$S_v(\alpha^{1/2}x) = \frac{1}{(2^v v!)^{1/2}}\left(\frac{\alpha}{\pi}\right)^{1/4}\exp(-\alpha x^2/2)H_v(\alpha^{1/2}x), \tag{6.48}$$

where $\alpha = 2\pi\mu\nu/\hbar$ for the harmonic oscillator. For mathematical clarity, the first few solutions representing Eq. (6.48) are provided in Table 6.2.

Table 6.2 *The first few solutions,* $S_v(\alpha^{1/2}x)$, *for the harmonic oscillator*

$S_0 = \left(\frac{\alpha}{\pi}\right)^{1/4} \exp(-\alpha x^2/2)$
$S_1 = \left(\frac{\alpha}{4\pi}\right)^{1/4} (2\alpha^{1/2}x) \exp(-\alpha x^2/2)$
$S_2 = \left(\frac{\alpha}{4\pi}\right)^{1/4} (2\alpha x^2 - 1) \exp(-\alpha x^2/2)$
$S_3 = \left(\frac{\alpha}{9\pi}\right)^{1/4} (2\alpha^{3/2}x^3 - 3\alpha^{1/2}x) \exp(-\alpha x^2/2)$

If we now combine Eqs. (6.45) and (6.47), the vibrational energy becomes

$$\varepsilon_{vib} = \left(v + \tfrac{1}{2}\right) h\nu \qquad v = 0, 1, 2, \ldots, \tag{6.49}$$

where v denotes the *vibrational quantum number*. Equation (6.49) represents the prescribed, equally-spaced energy levels for the harmonic oscillator. Note that

$$\varepsilon_{vib}(v = 0) = \tfrac{1}{2}h\nu,$$

so that a vibrational *zero-point energy* exists even at the lowest or *ground* vibrational level. This zero-point energy is a consequence of the Heisenberg uncertainty principle. Because the total energy for any harmonic oscillator can be written in terms of its kinetic and potential contributions as $(p^2/2\mu) + (k_0x^2/2)$, we immediately recognize that zero energy would require zero expectation values for both the momentum and position, which would clearly violate the uncertainty principle. If we subsequently convert to wave number units, from Eq. (6.49) we obtain

$$G(v) = \frac{\varepsilon_{vib}}{hc} = \left(v + \tfrac{1}{2}\right) \omega_e \qquad v = 0, 1, 2, \ldots, \tag{6.50}$$

where the *vibrational frequency* (cm^{-1}) can be defined, using Eq. (6.42), as

$$\omega_e = \frac{\nu}{c} = \frac{1}{2\pi c}\sqrt{\frac{k_0}{\mu}}. \tag{6.51}$$

Finally, because Eq. (6.46) depends solely on the vibrational quantum number, the vibrational degeneracy is obviously

$$g_{vib} = 1. \tag{6.52}$$

In summary, Eqs. (6.29) and (6.50) constitute simplified expressions for the rotational and vibrational energies of a diatomic molecule when modeled as a combined rigid rotor and harmonic oscillator. A rigid rotor presumes a fixed internuclear distance, which mandates small vibrational energies, so that the actual internuclear separation deviates insignificantly from its equilibrium value, r_e. Similarly, small oscillations about r_e ensure that the Morse potential is well approximated by the harmonic oscillator. In reality, of course, the vibrational and rotational motions affect one another, while the combined rigid-rotor/harmonic-oscillator model assumes no such coupling. For this reason, Eqs. (6.29) and (6.50) should be considered useful approximations eventually requiring further improvements, as discussed later in Chapter 7.

EXAMPLE 6.2

The steady-state Schrödinger wave equation for a one-dimensional harmonic oscillator in Cartesian coordiates is given by

$$\frac{d^2\psi}{dx^2} + \frac{2\mu}{\hbar^2}\left(\varepsilon_{vib} - \frac{1}{2}k_0x^2\right)\psi = 0,$$

which duplicates Eq. (6.43). Hence, the wave function, ψ_v, describing the one-dimensional harmonic oscillator is equivalent to S_v. On this basis, show that ψ_0 and ψ_1 are orthonormal.

Solution

The wave functions, ψ_0 and ψ_1, are orthonormal if they are both normalized and orthogonal. Proper normalization requires that

$$\int_{-\infty}^{\infty} \psi^*\psi\, dx = 1.$$

Hence, from Table 6.2, for $v = 0$ we have

$$\int_{-\infty}^{\infty} \psi_0^2\, dx = \left(\frac{\alpha}{\pi}\right)^{1/2}\int_{-\infty}^{\infty} \exp(-\alpha x^2)\, dx = \left(\frac{\alpha}{\pi}\right)^{1/2}\left[\frac{\pi}{\alpha}\right]^{1/2} = 1.$$

Similarly, for $v = 1$,

$$\int_{-\infty}^{\infty} \psi_1^2\, dx = 4\alpha\left(\frac{\alpha}{4\pi}\right)^{1/2}\int_{-\infty}^{\infty} x^2\exp(-\alpha x^2)\, dx = 2\alpha\left(\frac{\alpha}{\pi}\right)^{1/2}\left[\frac{\pi^{1/2}}{2\alpha^{3/2}}\right] = 1.$$

Consequently, both wave functions have been properly normalized. Now, we recall that two wave functions are orthogonal if

$$\int_{-\infty}^{\infty} \psi_0\psi_1 dx = 0.$$

Evaluating this integral, we verify that

$$\int_{-\infty}^{\infty} \psi_0\psi_1 dx = \alpha\left(\frac{2}{\pi}\right)^{1/2}\int_{-\infty}^{\infty} x\exp(-\alpha x^2)dx = 0,$$

as the above integrand is clearly an odd function of x.

6.5 The Electronic Energy Mode for Atomic Hydrogen

Our analysis of the diatomic molecule has led to important expressions for the allowed energy levels and degeneracies characterizing both the rigid rotor and harmonic oscillator. We now begin our investigation of the electronic energy mode by revisiting the prototypic hydrogen atom. Specifically, because atomic hydrogen is composed of one proton and one electron, we can essentially employ the same two-body analysis that we previously used for the diatomic molecule. Therefore, we may again separate the external and internal energy modes by transforming to a CM and relative coordinate system, except in this case the only viable internal mode arises from the electronic structure of the hydrogen atom. Repeating the usual separation-of-variables procedure, we thus obtain, once more,

$$\psi_{el}(r, \theta, \phi) = R(r)Y(\theta, \phi), \tag{6.53}$$

so that Eq. (6.11) now becomes, for the r-direction,

$$\frac{d}{dr}\left(r^2\frac{dR}{dr}\right)+\left\{\frac{2\mu r^2}{\hbar^2}\left[\varepsilon_{el}-V(r)\right]-\alpha\right\}R=0, \tag{6.54}$$

while the spherical harmonics, $Y(\theta,\phi)$, still hold for the θ and ϕ directions.

Consequently, recalling Eq. (6.21), we obtain the analogous solution,

$$Y_l^m(\theta,\phi)=\left[\frac{(2l+1)}{4\pi}\frac{(l-|m|)!}{(l+|m|)!}\right]^{1/2}P_l^{|m|}(\cos\theta)\,e^{im\phi}, \tag{6.55}$$

so that, from Eq. (6.18),

$$\alpha=l(l+1)\quad l\geq|m|\,. \tag{6.56}$$

Invoking Eq. (6.27), we introduce the *orbital angular momentum quantum number*, l, thus defining the quantized angular momentum via the analogous expression

$$L^2=l(l+1)\hbar^2. \tag{6.57}$$

Finally, from Eq. (6.56), we recall that the *magnetic quantum number*, m, can take on $2l+1$ possible values given by

$$m=0,\pm1,\pm2,\ldots,\pm l; \tag{6.58}$$

hence, we again define via Eq. (6.33) the z-component of the angular momentum, but this time for atomic hydrogen rather than for a diatomic molecule.

Based on the above development, the distinctive mathematical feature for atomic hydrogen, as compared to diatomic molecules, is the radial component of the Schrödinger wave equation. Pursuing this feature, we invoke Eqs. (5.6) and (6.56), thus expressing Eq. (6.54) as

$$\frac{1}{r^2}\frac{d}{dr}\left(r^2\frac{dR}{dr}\right)-\left\{\frac{l(l+1)}{r^2}-\frac{2\mu}{\hbar^2}\left[\varepsilon_{el}+\frac{e^2}{4\pi\varepsilon_\circ r}\right]\right\}R=0. \tag{6.59}$$

After several transformations, Eq. (6.59) becomes

$$\frac{1}{\rho^2}\frac{d}{d\rho}\left(\rho^2\frac{dR}{d\rho}\right)-\left[\frac{l(l+1)}{\rho^2}-\frac{n}{\rho}+\frac{1}{4}\right]R=0, \tag{6.60}$$

where

$$\rho=\frac{2r}{na_\circ} \tag{6.61}$$

and

$$n^2=-\frac{\hbar^2}{2\mu\,a_\circ^2\varepsilon_{el}}, \tag{6.62}$$

for which a corrected Bohr radius can now be defined as

$$a_\circ=\frac{\varepsilon_\circ h^2}{\pi\mu e^2}. \tag{6.63}$$

Table 6.3 *The first few associated Laguerre polynomials and radial functions for the hydrogen atom*

$n = 1, l = 0$	$L_1^1(\rho) = -1$	$R_{10} = \left(\frac{1}{a_\circ}\right)^{3/2} 2\exp\left(-\frac{r}{a_\circ}\right)$
$n = 2, l = 0$	$L_2^1(\rho) = -2!\,(2-\rho)$	$R_{20} = \left(\frac{1}{2a_\circ}\right)^{3/2} 2\left(1-\frac{r}{2a_\circ}\right)\exp\left(-\frac{r}{2a_\circ}\right)$
$n = 2, l = 1$	$L_3^3(\rho) = -3!$	$R_{21} = \left(\frac{1}{2a_\circ}\right)^{3/2} \frac{2}{\sqrt{3}}\left(\frac{r}{2a_\circ}\right)\exp\left(-\frac{r}{2a_\circ}\right)$
$n = 3, l = 0$	$L_3^1(\rho) = -3!(3-3\rho+\frac{1}{2}\rho^2)$	$R_{30} = \left(\frac{1}{3a_\circ}\right)^{3/2} 2\left[1-\frac{2r}{3a_\circ}+\frac{2}{3}\left(\frac{r}{3a_\circ}\right)^2\right]\exp\left(-\frac{r}{3a_\circ}\right)$
$n = 3, l = 1$	$L_4^3(\rho) = -4!\,(4-\rho)$	$R_{31} = \left(\frac{1}{3a_\circ}\right)^{3/2} \frac{4\sqrt{2}}{3}\left(\frac{r}{3a_\circ}\right)\left(1-\frac{r}{6a_\circ}\right)\exp\left(-\frac{r}{3a_\circ}\right)$
$n = 3, l = 2$	$L_5^5(\rho) = -5!$	$R_{32} = \left(\frac{1}{3a_\circ}\right)^{3/2} \frac{2\sqrt{2}}{3\sqrt{5}}\left(\frac{r}{3a_\circ}\right)^2\exp\left(-\frac{r}{3a_\circ}\right)$

The usual power-series approach eventually leads to a normalized solution for Eq. (6.60), as given by the radial function

$$R_{nl}(\rho) = -\left\{\frac{(n-l-1)!}{2n\left[(n+l)!\right]^3}\right\}^{1/2}\left(\frac{2}{na_\circ}\right)^{3/2}\rho^l\exp(-\rho/2)\;\;L_{n+l}^{2l+1}(\rho), \tag{6.64}$$

where

$$L_{n+l}^{2l+1}(\rho) = \sum_{k=0}^{n-l-1}(-1)^{k+1}\frac{[(n+l)!]^2}{(n-l-1-k)!\,(2l+1+k)!k!}\rho^k$$

is the associated Laguerre polynomial, whose continuity demands that the *principal quantum number*, n, obey

$$n = 1, 2, 3, \ldots, l < n, \tag{6.65}$$

so that $l = 0, 1, 2, \ldots, n-1$. The first few associated Laguerre polynomials and radial functions are listed for clarification in Table 6.3. As expected, each tabulated radial function, R_{nl}, has been normalized by integrating with respect to the radial portion of the differential volume in spherical coordinates, $d\tau = r^2\sin\theta\,dr\,d\theta\,d\phi$, so that

$$\int_0^\infty R_{nl}^* R_{nl} r^2\,dr = 1. \tag{6.66}$$

The probability density functions associated with Table 6.3 are shown in Fig. 6.4. We find, in contrast with the Bohr model, that the electron can wander over a range of radial positions, thus fostering mathematically the concept of an electron cloud. Nevertheless, if the orbital angular momentum quantum number, l, is zero, the most probable locations in Fig. 6.4 duplicate the electronic orbits originally suggested by Bohr. Therefore, while confirming the basic spectral features of the Bohr model, quantum mechanics obviously adds incredible depth and richness to our semiclassical understanding of atomic structure.

Having determined the radial contribution, we can now obtain the complete wave functions for atomic hydrogen from Eq. (6.53), thus giving

$$\psi_{nlm}(r,\theta,\phi) = R_{nl}(\rho)Y_l^m(\theta,\phi), \tag{6.67}$$

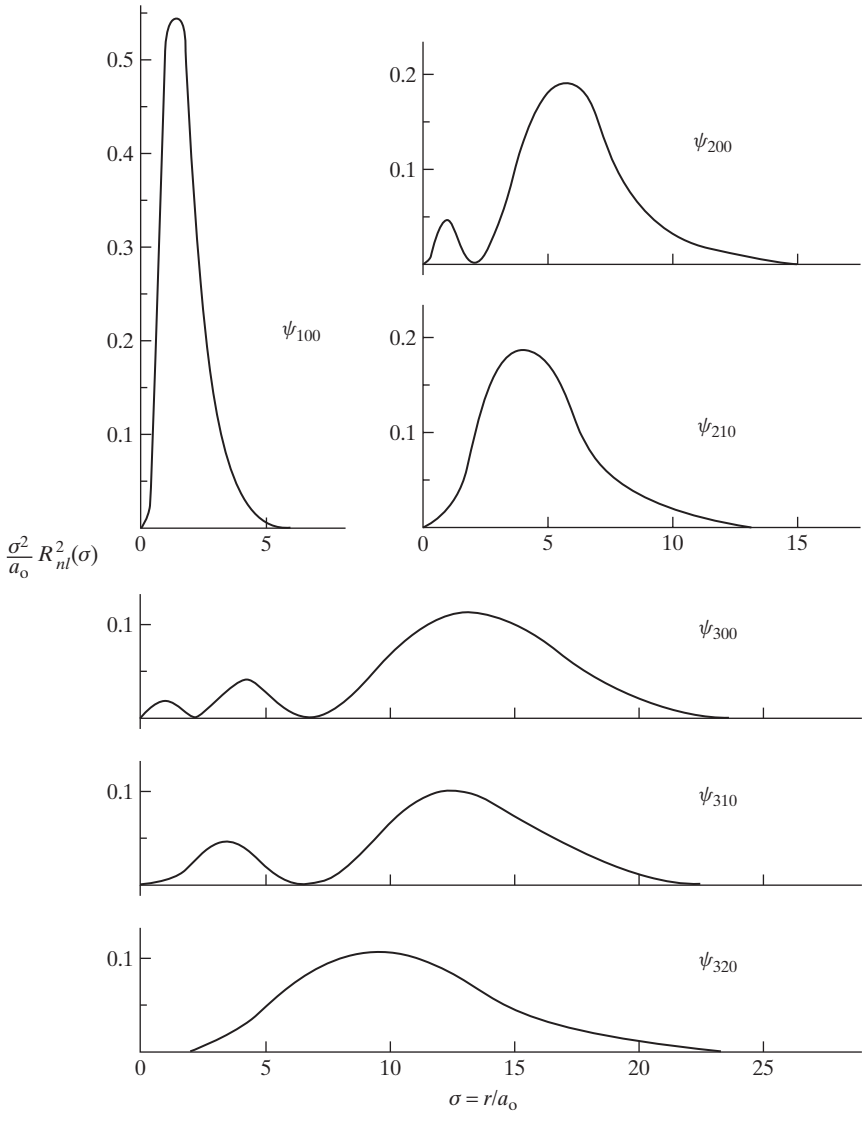

Figure 6.4 The dimensionless probability density function, $\sigma^2 R_{nl}^2(\sigma)/a_\circ$, associated with the radial portion of various wave functions for atomic hydrogen, where $\sigma = r/a_\circ$.

for which Eqs. (6.55) and (6.64) provide $Y_l^m(\theta, \phi)$ and $R_{nl}(\rho)$, respectively. From Tables 6.1 and 6.3, the wave functions for any hydrogen-like atom can be expressed in terms of the atomic number, Z, as shown in Table 6.4. We note that a hydrogen-like atom implies a single valence electron, such as for He^{+1} or Li^{+2}. Moreover, in contrast to the simpler radial functions of Table 6.3, the complete wave functions of Table 6.4 inherently describe through their angular dependencies complicated, three-dimensional electron clouds, especially if both l and m are nonzero. Some examples of electron clouds representing $\psi^*\psi$ are displayed in Fig. 6.5. By comparing Figs. 6.4 and 6.5, we observe that, for spherically symmetric wave functions ($l = 0$), the electron cloud mirrors its radial probability distribution. However, the permitted spatial distribution is obviously much more

Table 6.4 *The wave functions for atomic hydrogen, including hydrogen-like species with Z protons* ($n = 1, n = 2, n = 3$)

$n = 1, l = 0, m = 0$	$\psi_{100} = \frac{1}{\sqrt{\pi}}(\frac{Z}{a_\circ})^{3/2} \exp(-Zr/a_\circ)$
$n = 2, l = 0, m = 0$	$\psi_{200} = \frac{1}{4\sqrt{2\pi}}(\frac{Z}{a_\circ})^{3/2} [2 - (Zr/a_\circ)] \exp(-Zr/2a_\circ)$
$n = 2, l = 1, m = 0$	$\psi_{210} = \frac{1}{4\sqrt{2\pi}}(\frac{Z}{a_\circ})^{3/2} (Zr/a_\circ) \exp(-Zr/2a_\circ) \cos\theta$
$n = 2, l = 1, m = \pm 1$	$\psi_{211} = \frac{1}{8\sqrt{\pi}}(\frac{Z}{a_\circ})^{3/2} (Zr/a_\circ) \exp(-Zr/2a_\circ) \sin\theta\, e^{\pm i\phi}$
$n = 3, l = 0, m = 0$	$\psi_{300} = \frac{1}{81\sqrt{3\pi}}(\frac{Z}{a_\circ})^{3/2} [27 - 18(Zr/a_\circ) + 2(Zr/a_\circ)^2] \exp(-Zr/3a_\circ)$
$n = 3, l = 1, m = 0$	$\psi_{310} = \frac{\sqrt{2}}{81\sqrt{\pi}}(\frac{Z}{a_\circ})^{3/2} [6(Zr/a_\circ) - (Zr/a_\circ)^2] \exp(-Zr/3a_\circ) \cos\theta$
$n = 3, l = 1, m = \pm 1$	$\psi_{311} = \frac{1}{81\sqrt{\pi}}(\frac{Z}{a_\circ})^{3/2} [6(Zr/a_\circ) - (Zr/a_\circ)^2] \exp(-Zr/3a_\circ) \sin\theta\, e^{\pm i\phi}$
$n = 3, l = 2, m = 0$	$\psi_{320} = \frac{1}{81\sqrt{6\pi}}(\frac{Z}{a_\circ})^{3/2} (Zr/a_\circ)^2 \exp(-Zr/3a_\circ)(3\cos^2\theta - 1)$
$n = 3, l = 2, m = \pm 1$	$\psi_{321} = \frac{1}{81\sqrt{\pi}}(\frac{Z}{a_\circ})^{3/2} (Zr/a_\circ)^2 \exp(-Zr/3a_\circ) \sin\theta \cos\theta\, e^{\pm i\phi}$
$n = 3, l = 2, m = \pm 2$	$\psi_{322} = \frac{1}{162\sqrt{\pi}}(\frac{Z}{a_\circ})^{3/2} (Zr/a_\circ)^2 \exp(-Zr/3a_\circ) \sin^2\theta\, e^{\pm 2i\phi}$

complicated and surely rather unexpected for most three-dimensional wave functions ($l \neq 0$).

From the perspective of statistical thermodynamics, the most significant contribution from quantum mechanics is its specification of allowed energies and degeneracies. For atomic hydrogen, the electronic energy levels (cm^{-1}) can be determined by combining

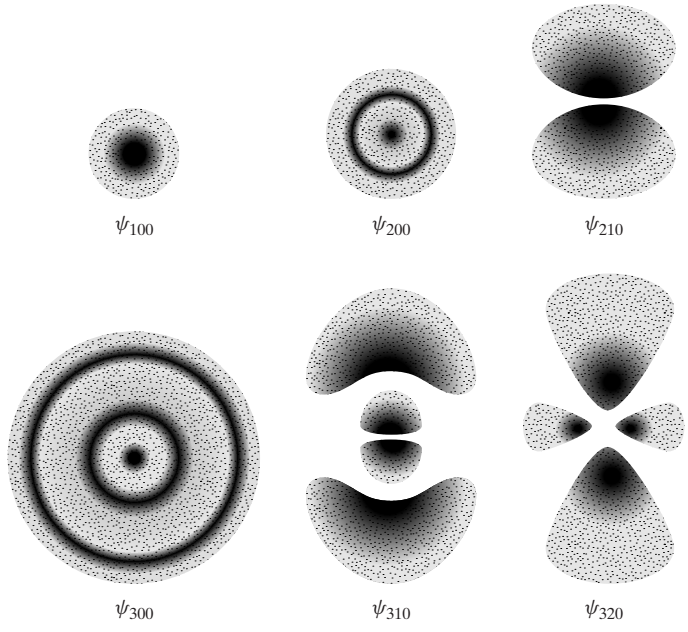

Figure 6.5 Probability density plots represented as electron clouds for various wave functions of atomic hydrogen. The darker regions indicate a higher probability of finding an electron.

Eqs. (6.62) and (6.63), thus obtaining

$$\tilde{\varepsilon}_{el} = \frac{\varepsilon_{el}}{hc} = -\frac{\mu e^4}{8\varepsilon_\circ^2 ch^3}\frac{1}{n^2}. \tag{6.68}$$

We note that Eq. (6.68) differs from Eq. (5.12) for the Bohr model only by replacement of the electron mass with its corresponding reduced mass, as expected when converting to a more accurate CM coordinate system. On this basis, a revised Rydberg constant becomes

$$R_H = \frac{\mu e^4}{8\varepsilon_\circ^2 ch^3} = 109{,}683 \text{ cm}^{-1}, \tag{6.69}$$

which is in remarkable agreement with the experimental value of 109,678 cm^{-1}. We recognize, in addition, that Eqs. (6.68) and (6.69) have been verified by employing a robust quantum mechanical theory rather than the *ad hoc* approach used in the early development of the Bohr model. Consequently, the Schrödinger wave equation can now be applied with some confidence to more complicated atomic and molecular systems.

EXAMPLE 6.3

Determine radial probability density functions for atomic hydrogen corresponding to (a) $n = 1, l = 0, m = 0$ and (b) $n = 2, l = 1, m = 0$. (c) Plot the probability density functions for these two cases on a single graph; discuss the implications of your plot.

Solution

(a) From the first postulate of quantum mechanics, the three-dimensional differential probability in spherical coordinates is given by

$$dP(r, \theta, \phi) = \psi^* \psi \, r^2 \sin\theta \, dr \, d\theta \, d\phi,$$

so that the radial differential probability can be obtained by integrating over all possible zenith and azimuthal angles:

$$dP(r) = \int_0^{2\pi}\int_0^{\pi} \psi^* \psi \, r^2 \sin\theta \, dr \, d\theta \, d\phi.$$

Hence, for the $n = 1, l = 0, m = 0$ case, from Table 6.4 ($Z = 1$) we obtain

$$\psi_{100} = \frac{1}{\sqrt{\pi}}\left(\frac{1}{a_\circ}\right)^{3/2} \exp(-r/a_\circ),$$

so that

$$dP(r) = \frac{1}{\pi a_\circ^3}\int_0^{2\pi}\int_0^{\pi} r^2 \exp(-2r/a_\circ)dr \, \sin\theta \, d\theta \, d\phi = \frac{4r^2}{a_\circ^3}\exp(-2r/a_\circ)dr.$$

Defining $\sigma = r/a_\circ$ and substituting into the previous expression, we may write $dP(\sigma) = f(\sigma)d\sigma$, so that the radial probability density function becomes

$$f(\sigma) = 4\sigma^2 \exp(-2\sigma).$$

(b) Similarly, for the $n = 2, l = 1, m = 0$ case, from Table 6.4 ($Z = 1$) we obtain

$$\psi_{210} = \frac{1}{4\sqrt{2\pi}} \left(\frac{1}{a_\circ}\right)^{3/2} (r/a_\circ) \exp(-r/2a_\circ) \cos\theta,$$

and thus

$$dP(r) = \frac{1}{32\pi a_\circ^3} \int_0^{2\pi} \int_0^{\pi} r^2 (r/a_\circ)^2 \exp(-r/a_\circ) dr \cos^2\theta \sin\theta \, d\theta \, d\phi$$
$$= \frac{r^2}{24a_\circ^3} (r/a_\circ)^2 \exp(-r/a_\circ) dr.$$

Again defining $\sigma = r/a_\circ$, the radial probability density function for this case becomes

$$f(\sigma) = \frac{\sigma^4}{24} \exp(-\sigma).$$

(c) The two radial probability density functions describing the position of the electron within atomic hydrogen are shown on the accompanying plot. As expected, the most probable radius is significantly smaller when the principal quantum number is unity rather than two. Moreover, uncertainty in the position of the electron is considerably less for the $n = 1$ case as compared to the $n = 2$ case. Because of the greater uncertainty for $n = 2$, its peak probability is significantly less than that for $n = 1$.

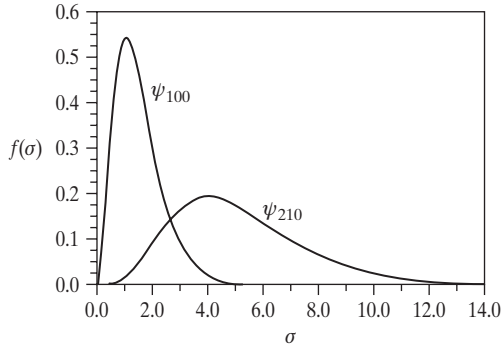

Equation (6.68) demonstrates that the allowed energy levels for atomic hydrogen are functions solely of the principal quantum number, n. In comparison, Eq. (6.67) indicates that the associated wave functions depend on the orbital angular momentum and magnetic quantum numbers, as well as the principal quantum number. Hence, the number of possible values for l and m corresponding to any given value of n must define the degeneracy for the electronic energy mode. Because Eqs. (6.58) and (6.65) show that $m = 0, \pm 1, \pm 2, \ldots, \pm l$ and $l = 0, 1, 2, \ldots, n - 1$, we expect the electronic degeneracy for atomic hydrogen to be

$$g_n = \sum_{l=0}^{n-1} (2l + 1) = n^2. \tag{6.70}$$

However, Eq. (6.70) is actually incorrect because, as suggested by Wolfgang Pauli (1900–1958) in 1925, an electron executes not only orbital motion but also spins about its own axis. This *intrinsic spin* was subsequently found to explain satisfactorily the famous

Stern–Gerlach experiment, which established that a beam of silver atoms could be split into two beams by an inhomogeneous magnetic field. More generally, the English physicist Paul Dirac (1902–1984) eventually demonstrated that electron spin arises quite naturally from relativistic quantum mechanics.

Therefore, in analogy with our previous quantum description of the orbital angular momentum, new quantum numbers can be defined for both the spin angular momentum and its z-component. From Eq. (6.57), the spin angular momentum becomes

$$S^2 = s(s+1)\hbar^2, \tag{6.71}$$

where s is the *spin quantum number* for an electron. Now, for atomic hydrogen, Eq. (6.33) for the z-component of the orbital angular momentum can be expressed as

$$L_z = m_l \hbar, \tag{6.72}$$

where m_l is the *orbital magnetic quantum number*. By analogy, the z-component of the spin angular momentum becomes

$$S_z = m_s \hbar, \tag{6.73}$$

where m_s is called the *spin magnetic quantum number*. For an electron, the spin quantum number is restricted by relativistic quantum mechanics to a single value of $s = 1/2$; thus, by analogy with Eq. (6.56), we have $s \geq |m_s|$, so that

$$m_s = \pm\tfrac{1}{2}, \tag{6.74}$$

which implies either an "up" or "down" orientation ($\uparrow\downarrow$) of the spin quantum number.

In summary, the electronic state of the hydrogen atom is specified by four quantum numbers. The principal quantum number, n, determines the electronic energy; the orbital angular momentum quantum number, l, defines the orbital angular momentum; the orbital magnetic quantum number, m_l, specifies the z-component of the orbital angular momentum; and the spin magnetic quantum number, m_s, specifies the z-component of the spin angular momentum. Because Eq. (6.70) already accounts for quantum states defined by l and m_l, while Eq. (6.74) permits two possible values for the fourth quantum number, m_s, the electronic degeneracy for the hydrogen atom becomes

$$g_{el} = 2n^2, \tag{6.75}$$

where n is the principal quantum number. Therefore, we have demonstrated from Eqs. (6.68) and (6.75) that quantum mechanics is capable of providing succinct expressions for both the electronic energy and degeneracy of atomic hydrogen. Unfortunately, the same cannot be said for multielectron atoms and molecules.

6.6 The Electronic Energy Mode for Multielectron Species

The steady-state Schrödinger wave equation for a generic N-electron atom with nuclear charge, Z, at the origin can be written as

$$\left(-\frac{\hbar^2}{2m_e}\sum_{i=1}^{N}\nabla_i^2 - \sum_{i=1}^{N}\frac{Ze^2}{4\pi\varepsilon_\circ r_i} + \sum_{i=1}^{N}\sum_{j>i}^{N}\frac{e^2}{4\pi\varepsilon_\circ r_{ij}}\right)\psi = \varepsilon\psi,$$

where the first term accounts for the motion of the N electrons, the second term accounts for hydrogen-like interactions between electrons and protons, and the third term accounts for repulsive forces among the various electrons making up the atom. Implementing the so-called Hartree–Fock procedure, accurate solutions for many atoms can be obtained by expressing the overall wave function as a product of independent wave functions,

$$\psi = \prod_{i=1}^{N} \varphi_i(r_i),$$

similar to those for atomic hydrogen, specifically

$$\varphi_i(r_i) = \sum_j N_{ij} C_{ij} \exp(-\zeta_{ij} r_i),$$

where N_{ij} is a normalization constant, while C_{ij} and ζ_{ij} are variational parameters used to obtain the final solution. In essence, the trial wave functions, $\varphi(r_i)$, represent specific solutions to the Schrödinger wave equation for independent electrons moving in an effective potential created by the combined nuclei and electrons. The final solution is obtained iteratively by guessing values for the above parameters, determining effective potentials, using these potentials to evaluate new parameter values, and so on until convergence. The resulting *self-consistent field method* leads to calculations of orbital energies and thus to allowed electronic energies for multielectron atoms. Typically, the self-consistent field method provides Hartree–Fock energies to within a percent or two of measured electronic energies for atoms having $Z < 40$. Unfortunately, similar calculations are quite ineffective for larger atoms and even more so for diatomic molecules.

Based on this discussion, we conclude that operational limitations prevent the Schrödinger wave equation from providing accurate electronic energies for multielectron atoms or molecules. Hence, these energies must be obtained experimentally via either atomic or molecular spectroscopy. Extensive tabulations of such electronic energy levels are available in the spectroscopic literature and, more recently, on websites maintained by the National Institute of Standards and Technology (Washington, DC). Each electronic energy level is characterized by an associated *term symbol* from which we can extract the electronic degeneracy required for statistical mechanical calculations. On this basis, our major goal in the remainder of this chapter is to develop an understanding and appreciation for such terms symbols as applied to both multielectron atoms and molecules.

6.6.1 Electron Configuration for Multielectron Atoms

While predicted electronic energies using the self-consistent field method are inevitably inaccurate for multielectron atoms, an important result of the Hartree–Fock orbital procedure is that the constituent electrons perpetuate the same set of quantum numbers as that employed for the hydrogen atom. Consequently, for each electron of a multielectron atom, we may still specify four controlling quantum numbers, as summarized in Table 6.5. A significant difference, however, is the strong dependence of the electronic energy for such atoms on the orbital angular momentum quantum number as well as on the principal quantum number. As for atomic hydrogen, the quantum numbers, m_l and m_s, denoting the z-components of the orbital and spin angular momenta, respectively, preserve their limitation to $2l + 1$ and two values, respectively. Taken together, these four quantum

Table 6.5 *Quantum numbers for the electrons of a multielectron atom*

n	$n = 1, 2, 3, \ldots$
l	$l = 0, 1, 2, \ldots, n-1$
m_l	$m_l = 0, \pm 1, \pm 2, \ldots, \pm l$
m_s	$m_s = \pm 1/2$

numbers must specify a single quantum state. Furthermore, according to the Pauli exclusion principle (Section 5.10), only a single electron can occupy any given quantum state. Therefore, each electron of a multielectron atom can be identified by a unique combination of the four quantum numbers listed in Table 6.5.

On this basis, we now introduce the so-called *configuration* of an atom, which specifies in a convenient fashion the number of electrons occupying each *shell* ($n = 1, 2, 3, \ldots$) and *subshell* ($l = 0, 1, 2, \ldots, n-1$) of a multielectron atom. The shell is specified by the numerical value of the principal quantum number, n, while the subshell is specified by the letters s, p, d, f, corresponding to the orbital angular momentum quantum numbers, $l = 0, 1, 2, 3$, respectively. Given this nomenclature, the number of electrons in each subshell is indicated via the format

$$nl^k,$$

where n indicates the shell number, l indicates the subshell letter, and k indicates the number of electrons per subshell. As an example, for the eleven electrons composing atomic sodium ($Z = 11$), the configuration for the ground electronic state is written as $1s^2 2s^2 2p^6 3s$, where the number of electrons per subshell is limited by m_l and m_s to $2(2l+1)$. By identifying the available subshells of lowest energy for each atomic number (Problem 3.9), we may determine the ground-state configuration of each element, as listed for hydrogen through argon in Table 6.6. We note from this tabulation that the number of electrons per shell is consistent with the degeneracy predicted by Eq. (6.75). Employing the periodic table of Appendix C, Table 6.6 could easily be extended to atoms having $Z > 18$ by heeding the appropriate rules embodied in Problem 3.9.

Table 6.6 *Electron configurations and term symbols for the ground states of atomic hydrogen through argon* ($Z = 1 - 18$)

Z	Atom	Electron configuration	Term symbol	Z	Atom	Electron configuration	Term symbol
1	H	$1s$	$^2S_{1/2}$	10	Ne	[He] $2s^2 2p^6$	$^1S_0$
2	He	$1s^2$	$^1S_0$	11	Na	[Ne] $3s$	$^2S_{1/2}$
3	Li	[He] $2s$	$^2S_{1/2}$	12	Mg	[Ne] $3s^2$	$^1S_0$
4	Be	[He] $2s^2$	$^1S_0$	13	Al	[Ne] $3s^2 3p$	$^2P_{1/2}$
5	B	[He] $2s^2 2p$	$^2P_{1/2}$	14	Si	[Ne] $3s^2 3p^2$	$^3P_0$
6	C	[He] $2s^2 2p^2$	$^3P_0$	15	P	[Ne] $3s^2 3p^3$	$^4S_{3/2}$
7	N	[He] $2s^2 2p^3$	$^4S_{3/2}$	16	S	[Ne] $3s^2 3p^4$	$^3P_2$
8	O	[He] $2s^2 2p^4$	$^3P_2$	17	Cl	[Ne] $3s^2 3p^5$	$^2P_{3/2}$
9	F	[He] $2s^2 2p^5$	$^2P_{3/2}$	18	Ar	[Ne] $3s^2 3p^6$	$^1S_0$

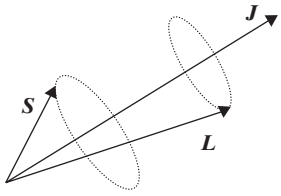

Figure 6.6 Vector model for Russell–Saunders (L–S) coupling.

6.6.2 Spectroscopic Term Symbols for Multielectron Atoms

The four quantum numbers used to determine the electron configuration do not account for what turn out to be significant interactions among the various orbital and spin angular momentum vectors of a multielectron atom. These additional interactions can be modeled by introducing the resultant orbital and spin angular momentum vectors,

$$\boldsymbol{L} = \sum_i \boldsymbol{l}_i \qquad \boldsymbol{S} = \sum_i \boldsymbol{s}_i,$$

where $\boldsymbol{l}_i$ and $\boldsymbol{s}_i$ indicate corresponding individual vectors for each electron. Invoking Eqs. (6.57) and (6.71), magnitudes for the orbital and spin angular momentum vectors can be written as

$$|\boldsymbol{L}| = \sqrt{L(L+1)}\,\hbar \quad |\boldsymbol{S}| = \sqrt{S(S+1)}\,\hbar,$$

where L and S are the resultant *orbital* and *spin angular momentum quantum numbers*, respectively. Implementing so-called *spin–orbit* (Russell–Saunders) *coupling*, which dominates for multielectron atoms having $Z < 40$, we may define the *total angular momentum vector* as

$$\boldsymbol{J} = \boldsymbol{L} + \boldsymbol{S}. \tag{6.76}$$

Because of this spin–orbit coupling (Fig. 6.6), the orbital, spin, and total angular momentum vectors exercise a pronounced effect on the allowed energy levels and thus the spectrum of a multielectron atom. The *spectroscopic term classification* is a nomenclature that describes this effect and thus provides a scheme for labeling those energy levels associated with any atomic spectrum.

The above coupling process can be understood in greater depth by recalling from basic electromagnetic theory that a rotating charge produces an induced magnetic field. Hence, an electron rotating around its orbit or about its own axis will generate a corresponding magnetic dipole moment vector. Coupling between such vectors induces a natural torque; hence, $\boldsymbol{L}$ and $\boldsymbol{S}$ will precess about $\boldsymbol{J}$, as shown in Fig. 6.6. This induced precession obviously affects the electronic energy of a multielectron atom. In particular, because of this coupling, the total angular momentum vector becomes quantized so that

$$|\boldsymbol{J}| = \sqrt{J(J+1)}\,\hbar \qquad J = |L-S|,\ |L-S|+1, \ldots L+S-1,\ L+S \tag{6.77}$$

$$J_z = M_J\,\hbar \qquad M_J = -J, -J+1, \ldots J-1, J, \tag{6.78}$$

where J is the *total angular momentum quantum number* and M_J is, of course, its quantized z-component. The various J-values permitted by Eq. (6.77) reflect the process of vector quantization, as demonstrated in Fig. 6.7 for the case in which L and S are both unity.

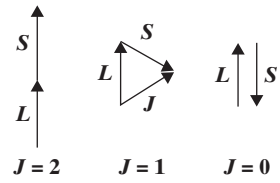

Figure 6.7 Addition of angular momentum vectors for $L = 1$ and $S = 1$.

Now, as indicated previously, the electronic energy of a multielectron atom is determined mainly by the n and l values for each constituent electron (shell and subshell). However, the overall electron cloud, as described by L, S, and J, exerts an important secondary influence. Therefore, both the electron configuration and its associated angular momentum quantum numbers must be known to properly specify an electronic energy level. Moreover, since the total angular momentum quantum number, J, influences the electronic energy while its z-component, M_J, does not, Eq. (6.78) indicates that the electronic degeneracy must be

$$g_{el} = g_J = 2J + 1. \tag{6.79}$$

As suggested by our previous discussion, the term classification for the electronic state of a multielectron atom is predicated on the above need to specify L, S, and J. In general, the *atomic term symbol* is given by

$$^{2S+1}L_J, \tag{6.80}$$

where $L = 0, 1, 2, 3$ is represented by S, P, D, F, respectively. For example, if $L = 1$ and $S = 1/2$, Eq. (6.77) indicates that $J = 1/2, 3/2$. Hence, the relevant term symbols are $^2P_{1/2}$ and $^2P_{3/2}$, often written as $^2P_{1/2,3/2}$; in other words, we have doublet P-states, which are characteristic of all alkali metals such as sodium or potassium. More generally, each electronic energy level of an atom requires a specific term symbol. Hence, for completeness, term symbols representing ground electronic states are included for all 18 elements in Table 6.6. We note from Eqs. (6.58) and (6.74) that, for any completed subshell, the z-components of L and S become by definition

$$M_L = \sum_i m_{li} = 0 \qquad M_S = \sum_i m_{si} = 0.$$

As a result, $L = S = 0$, so that the associated term symbol for any completed subshell is always $^1S_0$. Therefore, as suggested by the electron configurations of Table 6.6, we may safely ignore all quantum numbers affiliated with completely filled inner subshells when determining relevant term symbols. Empirical rules established for identification of the ground-state term symbols in Table 6.6 are outlined in Problem 3.9.

6.6.3 Electronic Energy Levels and Degeneracies for Atoms

The electronic energy levels for a multielectron atom can be determined via various spectroscopic measurements. Typically, excitation above the ground electronic state occurs because of a chemical or radiative process that excites a single valence electron to a more energetic subshell. Each energy level is identified by providing both the configuration (which specifies n and l) and the term symbol (which specifies L, S, and J). As an example, Table 6.7 lists the configuration, the term symbol, and the electronic energy for the first eleven electronic states of the potassium atom ($Z = 19$). Similar tabulations for some additional elements are provided in Appendix J.1. A more complete graphical description of

Table 6.7 *Energy levels and associated degeneracies for atomic potassium*

Configuration	Term symbol	Energy (cm^{-1})	Effective degeneracy
[Ar]4*s*	$^2S_{1/2}$	0	2
[Ar]4*p*	$^2P_{1/2,3/2}$	12985.2 13042.9	6
[Ar]5*s*	$^2S_{1/2}$	21026.6	2
[Ar]3*d*	$^2D_{3/2,5/2}$	21534.7 21537.0	10
[Ar]5*p*	$^2P_{1/2,3/2}$	24701.4 24720.1	6
[Ar]4*d*	$^2D_{3/2,5/2}$	27397.1 27398.1	10
[Ar]6*s*	$^2S_{1/2}$	27450.7	2

electronic energies for potassium is portrayed by the *energy level diagram* of Fig. 6.8. This diagram also indicates the allowed electronic transitions, including the wavelengths (Å) of the resulting spectral lines. The intense resonance lines at 7665 and 7699 Å are readily observed in emission even at very low potassium concentrations. A comparable doublet at 5890 and 5896 Å for sodium is known as the Na D-lines. Much can be learned about the rich relationship between electronic energy levels and atomic spectroscopy by studying together Table 6.7 and Fig. 6.8.

If we employ Eq. (6.79), the electronic degeneracy can be calculated from the *J*-value specified via a given term symbol. However, as demonstrated in Table 6.7, the shifts in energy among levels with only changes in *J* are usually so small that we can define an

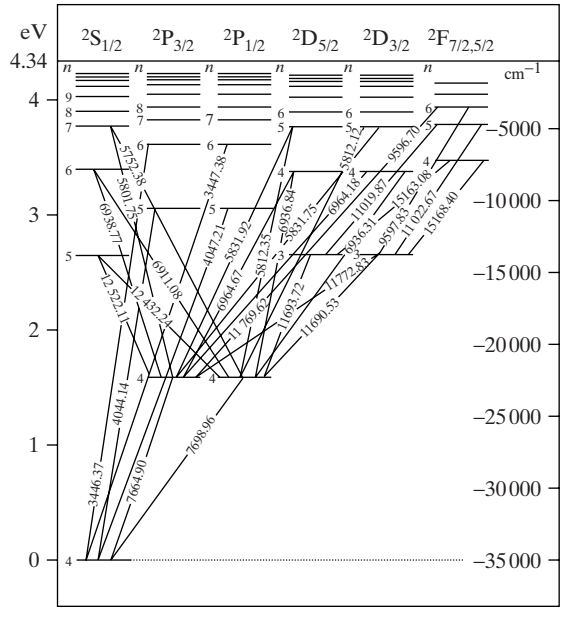

Figure 6.8 Energy-level diagram for the potassium atom. Wavelengths of transitions are shown in angstrom units.

average energy and thus an *effective degeneracy* corresponding to all J-values with the same L and S; hence,

$$g_{el,eff} = \sum_J g_J = \sum_J (2J + 1). \tag{6.81}$$

Effective degeneracies for the $4p$, $3d$, $5p$, and $4d$ levels of potassium are identified in Table 6.7. The number of J-values for given values of L and S is called the *multiplicity*. In most cases, differing J-values give rise to closely-lying lines in the spectrum, which together constitute a *multiple*t. Figure 6.8 indicates that potassium is characterized by doublets; typical spectral features for other atoms include triplets, quartets, quintets, and sextets. In fact, as indicated by Eq. (6.81), the effective degeneracy can generally be obtained by summing over an associated multiplet.

6.6.4 Electronic Energy Levels and Degeneracies for Diatomic Molecules

From a quantum mechanical viewpoint, molecules have much in common with multielectron atoms. All molecules, for example, display suitable orbital and spin angular momentum vectors, L and S. However, for a diatomic molecule, only the components of L and S along the internuclear axis undergo quantization owing to a cylindrically rather than spherically symmetric electronic potential. On this basis, we can define two new angular momentum components along internuclear axis AB, as shown in Fig. 6.9, so that

$$L_{AB} = \pm\Lambda\hbar \qquad \Lambda = 0, 1, 2, \ldots \tag{6.82}$$

$$S_{AB} = \Sigma\hbar \qquad \Sigma = -S, -S+1, \ldots S-1, S. \tag{6.83}$$

The $\pm$ symbol in Eq. (6.82) represents clockwise or counterclockwise circulation of electrons about the internuclear axis; thus, Λ is the component of the orbital angular momentum quantum number along AB. Similarly, in Eq. (6.83), for every value of the spin quantum number, S, we have $2S + 1$ values for its component, Σ, along the internuclear axis. Hence, as displayed in Fig. 6.9, we recognize that $\boldsymbol{L}$ and $\boldsymbol{S}$ must precess about this axis, similar to their precession about $\boldsymbol{J}$ for L–S coupling in multielectron atoms.

For a molecule, the electronic energy ultimately depends on the quantum numbers Λ and S, similar to the secondary dependence on L and S for an atom. Therefore, the *molecular term symbol*, in analogy with that for atoms, is labeled as

$$^{2S+1}\Lambda_{\Omega}, \tag{6.84}$$

where $\Lambda = 0, 1, 2$ is represented by Σ, Π, Δ, respectively. The subscript, $\Omega = \Lambda + \Sigma$, is often appended to identify a particular spin component, similar to J for atomic systems. For all molecules, the *multiplicity* is defined by $2S + 1$. Similar to the atomic case, the influence

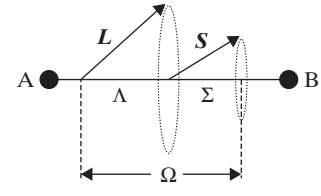

Figure 6.9 Angular momentum components for a diatomic molecule.

Table 6.8 *Electronic energy levels and degeneracies for O_2*

Term	T_e (cm^{-1})	$g_{el.eff}$
$X\,^3\Sigma_g^-$	0	3
$a\,^1\Delta_g$	7918.1	2
$b\,^1\Sigma_g^+$	13195.1	1
$A\,^3\Sigma_u^+$	35397.8	3
$B\,^3\Sigma_u^-$	49793.3	3

of spin–orbit coupling is usually small enough that we can define an *effective degeneracy*. Therefore, we obtain from Eqs. (6.80) and (6.81)

$$g_{el.eff} = \phi(2S + 1), \tag{6.85}$$

where $\phi = 1$ for $\Lambda = 0$ and $\phi = 2$ for $\Lambda > 0$, thus accounting for two possible vector directions along the internuclear axis when $L_{AB} > 0$. This factor of two is called Λ-*doubling*; the $2S + 1$ factor is called *spin-splitting*. The degeneracy defined by Eq. (6.85) is clearly effective as spin-splitting and Λ-doubling lead to spectral lines having slightly different wavelengths, although the energy difference caused by Λ-doubling is usually much smaller than that produced by spin-splitting.

Akin to the atomic case, electronic energies for diatomic molecules are typically derived from spectroscopic measurements, as discussed more completely in Chapter 7. Term symbols are again needed to identify the various electronic energy levels. As an example, the ground and first four excited electronic states for O_2 are listed in Table 6.8. Each electronic state is defined by a unique Morse potential, reflecting its own spatial charge distribution, as indicated by the associated energy-level diagram of Fig. 6.10. The energy, T_e, represents the energy gap between minima in the Morse potential describing the ground electronic

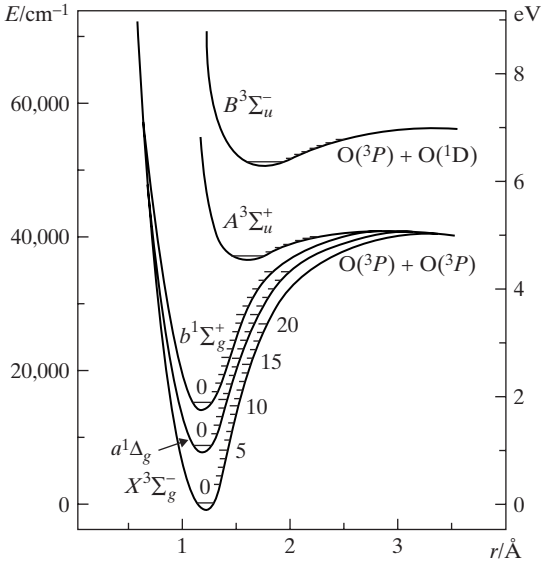

Figure 6.10 Potential energy diagram for low-lying electronic states of O_2.

state and that defining each excited electronic state. Table 6.8 also includes the effective degeneracy for each term symbol, as calculated from Eq. (6.85). Additional tabulations of electronic energies for selected diatomic molecules are provided in Appendix J.2.

For molecules, the ground electronic state is denoted by the symbol X, and each higher electronic state with the same multiplicity is labeled A, B, C, ..., respectively. Similarly, excited electronic states with different multiplicity are given the related nomenclature, a, b, c, ..., in order of increasing energy. The *g/u* subscripts are attached to the molecular term symbol only when dealing with homonuclear diatomics; these subscripts (*g/u*) denote the symmetry of the wave function (*even/odd*) upon reflection through the midpoint of its identical nuclei. Finally, the superscripts for the $\Lambda = 0$ case (Σ^-, Σ^+) indicate the symmetry of the wave function when reflected through an arbitrary plane passing through both nuclei of any diatomic molecule.

6.7 Combined Energy Modes for Atoms and Diatomic Molecules

Having applied the steady-state Schrödinger wave equation to the electronic, vibrational, and rotational motions of atoms and diatomic molecules, we now integrate our knowledge by combining their derived energy levels on an energy-level diagram. For atoms, our task is easy as electronic motion underlies the only internal energy mode. Typically, as indicated previously, energy-level diagrams are constructed by setting the energy of the ground electronic state to zero. Considering again Fig. 6.8 for atomic potassium, we note that the left-hand ordinate (eV) has its zero of energy at the ground electronic state, although the right-hand ordinate (cm^{-1}) places its zero of energy at the ionization condition. As a further example, we may use Eqs. (6.68) and (6.69) to obtain the electronic energies from the Schrödinger wave equation for the hydrogen atom; i.e.,

$$\tilde{\varepsilon}_{el} = -\frac{R_H}{n^2}, \tag{6.86}$$

where R_H is the Rydberg constant (cm^{-1}). Setting the zero of energy to that of the ground electronic state ($n = 1$), from Eq. (6.86) we obtain

$$\tilde{\varepsilon}_{el} = R_H\left(1 - \frac{1}{n^2}\right), \tag{6.87}$$

which could easily be used to construct an energy-level diagram for atomic hydrogen (Fig. 5.4).

In contrast to monatomic species, the total internal energy of a diatomic molecule can be obtained by summing contributions from the electronic, vibrational, and rotational energy modes. If we assume a combined rigid rotor and harmonic oscillator, for which the rotational and vibrational parameters, B_e and ω_e, are independent of electronic state, we obtain from Eqs. (6.29) and (6.50)

$$\tilde{\varepsilon}_{int} = T_e + \left(v + \tfrac{1}{2}\right)\omega_e + J(J+1)B_e.$$

An associated energy-level diagram for the ground and first excited electronic states of this prototypical diatomic molecule is shown in Fig. 6.11. As compared with the atomic case, the electronic energy for molecular systems is portrayed by the Morse potential, with T_e identifying the sizable energy gap between the bottoms of the potential wells for the A and X states. The ground vibrational level occurs above the bottom of each well

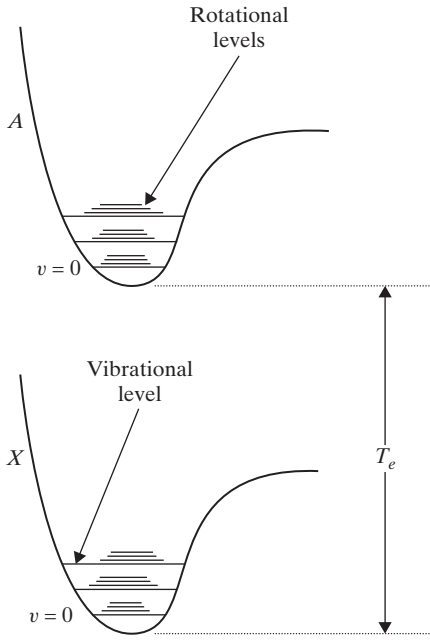

Figure 6.11 Prototypical energy-level diagram for diatomic molecule.

owing to its zero-point energy. Hence, additional vibrational and rotational energies can be denoted for each Morse potential by a sequence of energy levels above the ground vibrational state. Given such energy-level diagrams, we might surmise that spectral lines would arise corresponding to all possible energy gaps shown in Fig. 6.11. Fortunately, spectral signatures are usually much simpler owing to the applicability of so-called *selection rules* for both atoms and molecules.

6.8 Selection Rules for Atoms and Molecules

Selection rules are restrictions that govern the possible or *allowed* transitions between rotational, vibrational, or electronic states. For each energy mode, such rules are typically stated in terms of permitted changes in characteristic quantum numbers defining the internal energy states. In general, we observe that the spectral intensity of an allowed transition is much greater than that for a disallowed or *forbidden* transition. For the electronic mode, the term symbols distinguishing atoms and molecules generally provide the basic nomenclature needed for the construction of relevant selection rules. In this case, allowed transitions normally involve the jump of a single electron from one orbital to another. While selection rules have typically been deduced experimentally, significant theoretical confirmation has accrued from the application of perturbation theory to the time-dependent Schrödinger wave equation. Employing this approach, we now analyze a generic two-level system, thus eventually defining transition probabilities associated with rotational, vibrational, or electronic spectroscopy.

We begin with the time-dependent Schrödinger wave equation; i.e., from Eq. (5.32),

$$\hat{H}\Psi = i\hbar\frac{\partial \Psi}{\partial t}. \tag{6.88}$$

Considering two rotational, vibrational, or electronic states, we find that the solution to Eq. (6.88) is given by Eq. (5.38), which becomes for each state

$$\Psi_1 = \psi_1 \exp(-i\varepsilon_1 t/\hbar) \qquad \Psi_2 = \psi_2 \exp(-i\varepsilon_2 t/\hbar), \tag{6.89}$$

where ε_1 and ε_2 represent particle energies for the lower and upper levels, respectively. Assuming that any spectral transition is inherently a weak temporal process, we can define the time-dependent portion of the Hamiltonian operator, $\hat{H}'$, as a small perturbation about its steady-state manifestation, $\hat{H}_\circ$, i.e.,

$$\hat{H} = \hat{H}_\circ + \hat{H}', \tag{6.90}$$

so that, from Eq. (6.88), stationary solutions must obey

$$\hat{H}_\circ \Psi_n = i\hbar \frac{\partial \Psi_n}{\partial t}. \tag{6.91}$$

This strategy is the essential tactic used when implementing *time-dependent perturbation theory*.

For our application, the interaction energy between the perturbing electromagnetic field and the atom or molecule arises through its electric dipole moment, $\boldsymbol{\mu}$, as given by

$$\boldsymbol{\mu} = \sum_i q_i \boldsymbol{r}_i, \tag{6.92}$$

where q_i represents the charge and $\boldsymbol{r}_i$ the location for each constituent proton or electron. Presuming a uniform electric field, $\boldsymbol{E}$, we can express the time-dependent portion of the Hamiltonian operator as

$$\hat{H}' = -\boldsymbol{\mu} \cdot \boldsymbol{E}. \tag{6.93}$$

For simplicity, we take both the dipole moment and the oscillating electric field to be in the same direction, so that Eq. (6.93) becomes

$$\hat{H}' = -\mu E_\circ \cos \omega t, \tag{6.94}$$

where the radial frequency, from Eq. (5.27), can be written as

$$\omega = \frac{\varepsilon_2 - \varepsilon_1}{\hbar}. \tag{6.95}$$

We note, from Eq. (6.95), that the radial frequency of the incoming radiation corresponds to the spectral transition for a two-level system, as required if we are to investigate the transition probability.

We now model the temporal behavior of this two-level system as a dynamic perturbation about its stationary solution, so that

$$\Psi(t) = a_1(t)\Psi_1(t) + a_2(t)\Psi_2(t), \tag{6.96}$$

where a_1 and a_2 must be determined from the perturbation analysis. If we substitute Eq. (6.96) into Eq. (6.88) and invoke Eq. (6.90), we obtain

$$a_1 \hat{H}' \Psi_1 + a_2 \hat{H}' \Psi_2 = i\hbar(\Psi_1 \dot{a}_1 + \Psi_2 \dot{a}_2), \tag{6.97}$$

where all terms involving $\hat{H}_\circ$ have been eliminated through implementation of Eq. (6.91). Multiplying Eq. (6.97) by $\psi_2^* \exp(i\varepsilon_2 t/\hbar)$ and substituting from Eqs. (6.89), we have

$$a_1 e^{-i(\varepsilon_1-\varepsilon_2)t/\hbar}\,\psi_2^*\hat{H}'\psi_1 + a_2\psi_2^*\hat{H}'\psi_2 = i\hbar\dot{a}_1 e^{-i(\varepsilon_1-\varepsilon_2)t/\hbar}\,\psi_2^*\psi_1 + i\hbar\dot{a}_2\psi_2^*\psi_2.$$

Integrating over all spatial coordinates and recognizing that the wave functions are orthonormal, we then find, after utilizing Eq. (6.95),

$$i\hbar\dot{a}_2 = a_1 e^{i\omega t}\int\psi_2^*\hat{H}'\psi_1 d\tau + a_2\int\psi_2^*\hat{H}'\psi_2 d\tau. \tag{6.98}$$

According to our perturbation analysis, states 1 and 2 will differ little from their initial populations, so that we have $a_1 \simeq 1$ and $a_2 \simeq 0$. Therefore, Eq. (6.98) becomes

$$i\hbar\frac{da_2}{dt} = e^{i\omega t}\int\psi_2^*\hat{H}'\psi_1\,d\tau. \tag{6.99}$$

Finally, upon substitution from Eq. (6.94), Eq. (6.99) can be expressed as

$$i\hbar\frac{da_2}{dt} = -M_{12}E_\circ e^{i\omega t}\cos\omega t, \tag{6.100}$$

for which

$$M_{12} \equiv \int\psi_2^*\mu\psi_1 d\tau. \tag{6.101}$$

Equation (6.101) defines the *transition dipole moment*, which more generally becomes

$$\boldsymbol{M}_{ij} = \int\psi_i^*\boldsymbol{\mu}\psi_j d\tau, \tag{6.102}$$

where the wave functions, ψ_i and ψ_j, identify the two states participating in any spectral transition. Returning to our two-level system, we observe from Eq. (6.96) that $a_2(t)$ represents the extent of participation in state 2. Therefore, the temporal derivative, $\dot{a}_2$, can be interpreted as the transition rate from state 1 to state 2.

On this basis, we conclude from Eq. (6.100) that a transition between two rotational, vibrational, or electronic states is impossible if M_{12} is zero. In other words, a spectral line emerges only when its transition dipole moment is nonzero. The various selection rules thus reflect their transition dipole moments so that the more intense lines in the spectrum are generally associated with greater values of $\boldsymbol{M}_{ij}$. Fortunately, determining the selection rules themselves does not require evaluation of all possible transition dipole moments. Indeed, the mathematical symmetry of any wave function is typically defined through its quantum numbers, so that distinguishing between zero and nonzero values of Eq. (6.102) can usually be done by inspection. For this reason, primary selection rules can be expressed quite simply in terms of allowed changes in characteristic quantum numbers. Table 6.9 lists selection rules derived from Eq. (6.102) when utilizing wave functions for the rigid rotor, harmonic oscillator, and hydrogen atom.

The selection rule for the rigid rotor, $\Delta J = \pm 1$, arises directly from the mathematical properties of spherical harmonics. Since spherical harmonics depend only on θ and ϕ, Eqs. (6.92) and (6.102) together imply that rotational transitions can occur only for molecules having a permanent dipole moment ($\mu \neq 0$). Unfortunately, nonzero dipole moments are impossible for molecules endowed with spatial symmetry; for this reason,

Table 6.9 *Primary selection rules for rotational, vibrational, and electronic energy modes*

Energy mode	Model	Selection rules
Rotation	Rigid rotor	$\Delta J = \pm 1$
Vibration	Harmonic oscillator	$\Delta v = \pm 1$
Electronic	Atoms $^{2S+1}L_J$	$\Delta J = 0, \pm 1 \quad \Delta L = \pm 1 \quad \Delta S = 0$
Electronic	Molecules $^{2S+1}\Lambda_\Omega$	$\Delta \Lambda = 0, \pm 1 \quad \Delta S = 0$

homonuclear diatomics are forbidden from undergoing rotational transitions. In a similar fashion, the selection rule for the harmonic oscillator, $\Delta v = \pm 1$, depends on the mathematical properties of the Hermite polynomial. For such polynomials, evaluation of $\boldsymbol{M}_{ij}$ requires a Taylor expansion of the dipole moment about its equilibrium nuclear separation. Using this procedure, we find that any vibrational transition mandates a spatial variation in the electric dipole moment ($d\mu/dr \neq 0$). Because all homonuclear diatomics have zero dipole moments, they are thus prevented from undergoing vibrational as well as rotational transitions.

Employing calculated transition dipole moments and measured spectral signatures, spectroscopists have found that electronic selection rules can be based solely on term symbols affiliated with the energy levels involved in any electronic transition. For this reason, the electronic selection rules listed in Table 6.9 are purposefully cast in terms of atomic or molecular term symbols. Hence, for atomic spectra, the generic term symbol and associated primary selection rules are

$$^{2S+1}L_J: \quad \Delta J = 0, \pm 1 \quad \Delta L = \pm 1 \quad \Delta S = 0. \tag{6.103}$$

We note, however, that $\Delta J = 0$ is *forbidden* if both electronic levels correspond to $J = 0$ states. Moreover, while the ΔJ rule is mandatory, the ΔL and ΔS rules become less so for $Z > 40$. In comparison, for diatomic spectra, the generic term symbol and primary selection rules are

$$^{2S+1}\Lambda_\Omega: \quad \Delta \Lambda = 0, \pm 1 \quad \Delta S = 0. \tag{6.104}$$

Subsidiary selection rules when needed are as follows: $\Delta\Omega = 0, \pm 1$; $\Sigma^+ \leftrightarrow \Sigma^+$ or $\Sigma^- \leftrightarrow \Sigma^-$, but not $\Sigma^+ \leftrightarrow \Sigma^-$; only $g \leftrightarrow u$ for homonuclear diatomics.

Implementing Eq. (6.104), we note, from Table 6.8 and Fig. 6.10, that most transitions from the ground to the upper electronic states of O_2 are forbidden. The only allowed transition corresponds to the so-called Schumann–Runge system ($B^3\Sigma_u^- - X^3\Sigma_g^-$), which accounts for absorption of ultraviolet light at wavelengths below 200 nm in the earth's atmosphere. Given this electronic transition for O_2, we realize that a permanent dipole moment is unnecessary for homonuclear diatomics. This general conclusion is quite significant for two reasons. First, as might be expected for shifts between electronic orbitals, the transition dipole moment depends preferentially on that portion of the dipole moment established by the electrons and not by the two nuclei. Second, because their rotational and vibrational transitions are inherently forbidden, access to the molecular properties of homonuclear diatomics is possible only through electronic spectroscopy.

EXAMPLE 6.4

Consider the following queries concerning the atomic structure and spectrum for elemental potassium.

(a) Only four intense transitions occur between the ground state and those upper energy levels of potassium listed in Table 6.7. Identify these four electronic transitions.

(b) Verify the term symbols given in Table 6.7 for the [Ar]4p and the [Ar]3d electron configurations.

(c) Using Table 6.7, substantiate the wavelengths indicated in Fig. 6.8 for the intense doublet corresponding to the electronic transitions between the $4s\text{-}^2S_{1/2}$ and $4p\text{-}^2P_{1/2,3/2}$ states.

Solution

(a) The intense lines in the electronic spectrum for potassium must comport with those selection rules identified for all atomic spectra. Given the $4s\text{-}^2S_{1/2}$ ground state, the $\Delta S = 0$ rule is inherently obeyed by all the upper energy levels of Table 6.7. However, the $\Delta L = \pm 1$ rule favors only those four upper energy levels labeled $4p\text{-}^2P_{1/2,3/2}$ and $5p\text{-}^2P_{1/2,3/2}$. In addition, because these energy levels are identified by $J = 1/2$ or $J = 3/2$, consistency is automatically ensured with the selection rule, $\Delta J = 0, \pm 1$. Hence, we find that, among the ten upper levels of Table 6.7, only four electronic transitions satisfy all three selection rules. Moreover, the only effective rule for potassium is $\Delta L = \pm 1$.

(b) For the [Ar]4p configuration, we have only one valence electron so that $L = 1$ and $S = 1/2$. Hence, from Eq. (6.77), $J = 1/2, 3/2$. In addition, we note that $2S + 1 = 2$ and thus the term symbol for this configuration becomes $^2P_{1/2,3/2}$. In a similar fashion, for the [Ar]3d configuration, $L = 2$ and $S = 1/2$ so that $J = 3/2, 5/2$. Therefore, the term symbol for this second configuration becomes $^2D_{5/2,3/2}$.

(c) From Table 6.7, the gaps in electronic energy associated with this intense doublet are 12985.2 and 13042.9 cm^{-1}. Therefore, from Eq. (5.3), the associated wavelengths in vacuum are 7701.1 and 7667.0 Å, respectively. However, the wavelengths specified in Fig. 6.8 have surely been measured in air rather than in vacuum. Now, from $\lambda\nu = c$, we observe that for the same frequency, $\lambda = \lambda_\circ / n$, where the subscript indicates vacuum conditions and the index of refraction, $n = c_\circ / c$. For air at room temperature, the index of refraction is $n = 1.000275$ near the above vacuum wavelengths. Hence, dividing the vacuum wavelengths by n, we find that the spectral doublet should occur at wavelengths of 7699.0 and 7664.9 Å, respectively, in air. These two computed wavelengths are in excellent agreement with those indicated in Fig. 6.8.

Problems enhancing your understanding of this chapter are combined with those for Chapters 5 and 7 in Problem Set III.

7 The Spectroscopy of Diatomic Molecules

In Chapter 6, we presented a quantum mechanical analysis of the internal energy modes for a diatomic molecule. A significant aspect of this analysis was full separation of the rotational, vibrational, and electronic energy modes. In other words, by successively implementing the rigid-rotor model, the Born–Oppenheimer approximation, and the harmonic-oscillator model, we demonstrated that the internal energy of a diatomic molecule can be expressed as

$$\varepsilon_{int} = \varepsilon_{el} + \varepsilon_{vib} + \varepsilon_{rot}. \tag{7.1}$$

This uncoupling of internal energy modes creates a rudimentary model for the diatomic molecule and thus offers the simplest explanation for its various spectral features. In particular, if we convert Eq. (7.1) to wave number units (cm^{-1}), we obtain

$$\tilde{\varepsilon}_{int} = T_e + G(v) + F(J), \tag{7.2}$$

where, from Eqs. (6.29) and (6.50),

$$G(v) = \left(v + \tfrac{1}{2}\right)\omega_e \qquad v = 0, 1, 2, \ldots \tag{7.3}$$

$$F(J) = J(J+1)B_e \qquad J = 0, 1, 2, \ldots. \tag{7.4}$$

On this basis, our primary goal in this chapter is to explore how each term of Eq. (7.2) can produce spectroscopic information. This knowledge is the foundation for tabular values of T_e, ω_e, and B_e, which are fundamental for the statistical calculations of thermodynamic properties that we shall return to in Chapters 8 and 9.

In preparation for our exploration of spectroscopy, we first review the various regions of the electromagnetic spectrum, as outlined in Table 7.1. These regions are delineated in terms of both wavelength (nm) and wave number (cm^{-1}); however, you should recognize that the indicated borders are approximate and are only meant to serve as a guide for future discussions. Similarly, the molecular motions and thus the spectral transitions associated with each region are only representative. In other words, some notable exceptions exist to the general behavior indicated in Table 7.1; thus, basic calculations are often needed to ensure proper spectral assignments. Finally, you should note that spectroscopists typically report all infrared, visible, and near-ultraviolet wavelengths in air. Vacuum wavelengths are used only in the far ultraviolet, as measurements in air are not possible below 200 nm.

Table 7.1 *Significant regions in the electromagnetic spectrum for molecular spectroscopy*

Region	Wavelength (nm)	Wave number (cm^{-1})	Transitions
Far ultraviolet	10–200	1,000,000–50,000	Electronic
Near ultraviolet	200–400	50,000–25,000	Electronic
Visible	400–800	25,000–12,500	Electronic
Near infrared	800–3000	12,500–3300	Vibrational (overtones)
Mid-infrared	3000–30,000	3300–300	Vibrational (fundamental)
Far infrared	30,000–300,000	300–30	Rotational (light molecules)
Microwave	300,000–50,000,000	30–0.2	Rotational

7.1 Rotational Spectroscopy Using the Rigid-Rotor Model

We begin by considering what happens when only the rotational energy mode undergoes transposition, with no influence whatever from the vibrational or electronic energy modes. The available rotational energies, following the rigid-rotor model of Eq. (7.4), are displayed in Fig. 7.1. From Table 6.9, the selection rule for rotational transitions is $\Delta J = \pm 1$, so that beginning at $J = 3$, absorption or emission of energy can only materialize to $J = 4$ ($J_{final} - J_{initial} = +1$) or $J = 2$ ($J_{final} - J_{initial} = -1$), respectively. Hence, as compared to the hypothetical case with no selection rule, a considerable reduction occurs in the potential complexity of rotational spectroscopy.

A convenient method for writing the rotational selection rule that proves to be very useful in spectroscopy is

$$J' - J'' = 1, \tag{7.5}$$

where a single prime refers to the upper energy level and a double prime refers to the lower energy level for any given transition, whether absorption or emission. Applying this nomenclature to Eq. (7.4), the wave number of each spectral line for pure rotational spectroscopy is given by

$$\tilde{\nu} = \Delta\tilde{\varepsilon}_{rot} = J'(J'+1)B_e - J''(J''+1)B_e. \tag{7.6}$$

Invoking Eq. (7.5), we then obtain

$$\tilde{\nu} = 2B_e\,(J''+1) \qquad J'' = 0, 1, 2, \ldots,$$

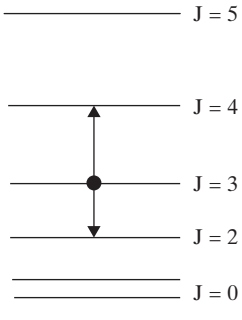

Figure 7.1 Rotational energy levels for the rigid rotor.

so that an equidistant spacing given by

$$\Delta\tilde{\nu} = 2B_e \tag{7.7}$$

occurs between all adjacent line pairs in any rotational spectrum produced by the rigid-rotor model. While an approximation, this simple but powerful prediction has nevertheless received significant confirmation in the spectroscopic literature.

Recall from Eqs. (6.30) and (6.31) that

$$B_e = \frac{h}{8\pi^2 c\, I_e}, \tag{7.8}$$

where the moment of inertia is

$$I_e = \mu r_e^2.$$

Hence, evaluation of B_e, obtained by applying Eq. (7.7) to a specific rotational spectrum, results in an experimental value for the moment of inertia, thus providing the equilibrium internuclear separation or *bond length* for a given diatomic molecule. Of course, such calculations must be tempered by the level of approximation underlying the rigid-rotor model. Nevertheless, Eq. (7.8) verifies that the average line spacing for rotational spectra becomes narrower for heavier molecules, such as AlO, and broader for lighter molecules, such as OH. Unfortunately, as discussed in Section 6.9, the transition dipole moment for homonuclear diatomics such as O_2 or N_2 is zero; the obvious result is no rotational signature. For heteronuclear diatomics, on the other hand, measured rotational constants range from 0.1 to 30 cm^{-1}. Therefore, rotational transitions appear in the microwave and far infrared portions of the electromagnetic spectrum, as indicated in Table 7.1.

7.2 Vibrational Spectroscopy Using the Harmonic-Oscillator Model

In a similar fashion, we may develop a spectral expression reflecting dominance by vibrational motion, with no influence from the rotational or electronic energy modes. Analogous to Eq. (7.5), the selection rule for the harmonic oscillator is

$$v' - v'' = 1. \tag{7.9}$$

Now, from Eq. (7.3), the wave number for pure vibrational spectroscopy when following the harmonic-oscillator model becomes

$$\tilde{\nu} = \Delta\tilde{\varepsilon}_{vib} = \left(v' + \tfrac{1}{2}\right)\omega_e - \left(v'' + \tfrac{1}{2}\right)\omega_e. \tag{7.10}$$

Substituting Eq. (7.9) into Eq. (7.10), we obtain the simple result,

$$\tilde{\nu} = \omega_e, \tag{7.11}$$

so that, for pure vibrational spectroscopy, we generate only a single spectral line at the fundamental vibrational frequency, ω_e.

Recalling Eq. (6.51), we note that

$$\omega_e = \frac{1}{2\pi c}\sqrt{\frac{k_0}{\mu}}; \tag{7.12}$$

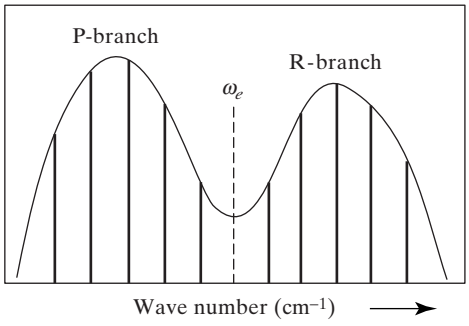

Figure 7.2 Schematic of P- and R-branches generated by combined vibration and rotation.

hence, spectral measurement of the fundamental vibrational wavelength leads to knowledge of the force constant or *bond strength* for a diatomic molecule. Typically, $\omega_e =$ 1000–3000 cm^{-1}, so that fundamental vibrational transitions appear in the mid-infrared portion of the spectrum, as indicated in Table 7.1. However, from Section 6.8, we recall that vibrational transitions mandate the generation of radial gradients in the electric dipole moment during harmonic oscillation. Such gradients are impossible for symmetric molecules; thus, as for the rotational case, homonuclear diatomics offer no spectral signatures owing to molecular vibration.

Because $\omega_e \gg B_e$, we might expect that the excessive energy accompanying vibrational motion would automatically lead to rotational excitation. In fact, if we were to inspect more carefully anticipated vibrational signatures by implementing a spectrometer with higher resolution, we would find not a single fundamental line, but rather two groups of kindred lines as indicated by the emission spectrum of Fig. 7.2. The group of lines at lower wave numbers (higher wavelengths) is called the P-branch, while the group at higher wave numbers (lower wavelengths) is called the R-branch. The dip between the branches is still centered at the fundamental vibrational wavelength; however, the simultaneous excitation of rotational motion eliminates this anticipated vibrational frequency in favor of replacement signatures on both spectral sides of ω_e.

7.3 Rovibrational Spectroscopy: The Simplex Model

We observed in the previous section that a diatomic molecule can actually never undergo vibrational motion without also undergoing rotational motion. For this reason, vibrational and rotational changes in energy must be additive, thus producing *rovibrational* spectra given by

$$\tilde{\nu} = \Delta\tilde{\varepsilon}_{rv} = (v' - v'')\omega_e + [J'(J'+1) - J''(J''+1)]B_e, \tag{7.13}$$

where we have combined Eqs. (7.6) and (7.10) to create a conjoined rigid-rotor/harmonic-oscillator model. Here, the single and double primes refer to the upper and lower vibrational levels, respectively, even when used to identify the rotational quantum numbers within each vibrational level. For this combined *simplex model*, the selection rules are

$$v' - v'' = 1 \qquad J' - J'' = \pm 1, \tag{7.14}$$

so that, as shown in the energy-level diagram of Fig. 7.3, we obtain two separate cases corresponding to $\Delta J = \pm 1$, whether for absorption or emission. For clarity in exposition, the

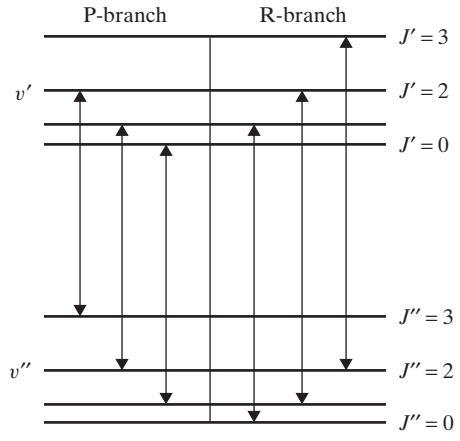

Figure 7.3 Energy-level diagram showing P- and R-branches for rovibrational spectrum.

transitions displayed from left to right in Fig. 7.3 correspond to spectral lines of increasing wave number, as portrayed in Fig. 7.2. Hence, the P-branch refers to the case for which $J' = J'' - 1$ while the R-branch refers to the case for which $J' = J'' + 1$.

Exploiting the previous development, we substitute Eq. (7.14) into Eq. (7.13) for each case, giving for the P- and R-branches,

$$\tilde{\nu}_P = \omega_e - 2B_e J'' \qquad J'' = 1, 2, 3, \ldots \tag{7.15}$$

$$\tilde{\nu}_R = \omega_e + 2B_e(J'' + 1) \qquad J'' = 0, 1, 2, \ldots, \tag{7.16}$$

respectively, so that the spectral line spacing for both branches is again

$$\Delta\nu_P = \Delta\nu_R = 2B_e. \tag{7.17}$$

Therefore, we see from Eqs. (7.15) and (7.16) that the P-branch produces a series of equidistant rovibrational lines for $\tilde{\nu} < \omega_e$ while the R-branch gives a similar series of equally-spaced rovibrational lines for $\tilde{\nu} > \omega_e$, as suggested by Fig. 7.2. We also note that the missing pure vibrational frequency in Fig. 7.2 results naturally from the addition or subtraction of rotational energy with respect to ω_e. Furthermore, because rovibrational spectroscopy encompasses both vibrational and rotational motion, a least-squares fit of Eqs. (7.15) and (7.16) to the spectrum of Fig. 7.2 would simultaneously determine both ω_e and B_e, thus providing measurements of both the bond strength and bond length.

From a more practical perspective, when discussing a particular rovibrational line, we must be able to communicate with colleagues in an unequivocal fashion. Because of this obvious need, spectroscopists have developed a rigorous notation to designate specific lines in a rovibrational spectrum. In general, the notation follows

$$B_{v'}(J'') \qquad B = P, R, \tag{7.18}$$

where $B = P$ for a line in the P-branch and $B = R$ for a line in the R-branch. Hence, $P_2(5)$ designates a transition from $v' = 2,\ J' = 4$ to $v'' = 1,\ J'' = 5$ or vice versa ($J' = J'' - 1$). Similarly, $R_1(5)$ designates a transition from $v' = 1,\ J' = 6$ to $v'' = 0,\ J'' = 5$ or vice versa ($J' = J'' + 1$). With respect to the latter, however, spectroscopists usually omit the unity subscript when describing a rovibrational transition involving the ground vibrational level.

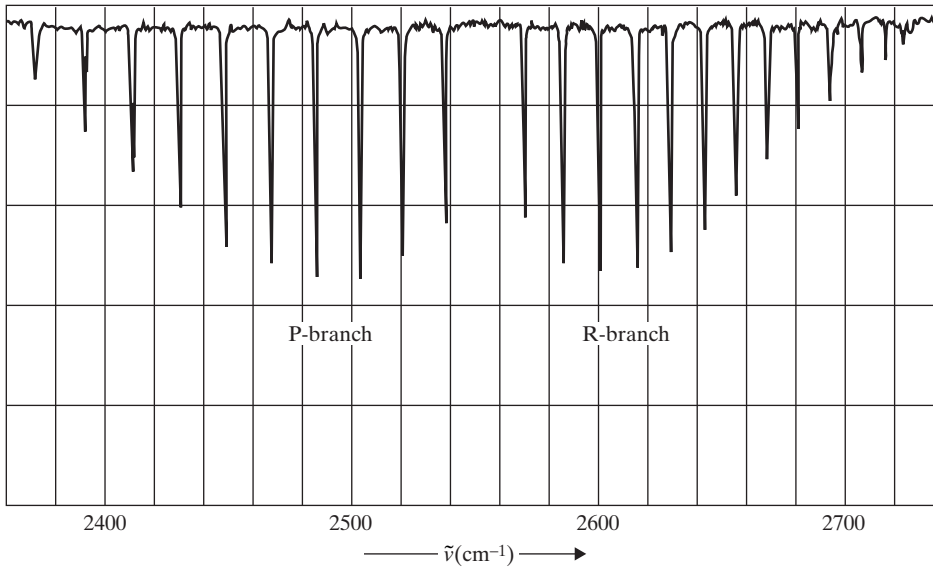

Figure 7.4 The rovibrational absorption spectrum for the $v = 0 \rightarrow 1$ transition of gaseous HBr, with the indicated P- and R-branches.

Unfortunately, the simplex model, as portrayed spectroscopically in Fig. 7.2, understates the inherent complexity of combined rotational and vibrational motion. Consider, for example, the actual infrared absorption spectrum for gaseous HBr shown in Fig. 7.4. Consistent with the simplex model, no pure vibrational line appears at $\omega_e \simeq 2555\ \text{cm}^{-1}$. Similarly, in both Figs. 7.2 and 7.4, the variations in line intensity reflect analogous differences in rotational population, as discussed further in Chapter 9. However, in comparison to the results anticipated from Eq. (7.17), the spacing between consecutive spectral lines within the P-branch drops as $\tilde{\nu} \rightarrow \omega_e$; similarly, within the R-branch, this spacing rises as $\tilde{\nu} \rightarrow \omega_e$. In other words, the simplex model cannot reproduce the actual positions for the various transitions in the rovibrational spectrum of HBr. This general result underscores the limitations of the combined rigid-rotor/harmonic-oscillator model. Given this outlook, we must now pursue a more realistic model for the combined vibrational and rotational motions of a diatomic molecule.

EXAMPLE 7.1

The Raman spectrum of a diatomic molecule can be investigated via excitation with a laser beam. The spectrum results from rovibrational modulation of scattered laser radiation to produce sideband frequencies at $\tilde{\nu}_L \pm \tilde{\nu}_R$, where $\tilde{\nu}_L$ is the laser frequency (cm^{-1}) and $\tilde{\nu}_R$ is the rovibrational frequency (cm^{-1}) of the molecule. The Stokes component at $\tilde{\nu}_L - \tilde{\nu}_R$ corresponds to the vibrational transition from $v'' = 0$ to $v' = 1$, while the anti-Stokes component at $\tilde{\nu}_L + \tilde{\nu}_R$ corresponds to the inverse transition from $v' = 1$ to $v'' = 0$. The simultaneously excited rovibrational lines are limited by the governing selection rules to $\Delta J = J' - J'' = \pm 2$, with $\Delta J = +2$ designated as the S-branch and $\Delta J = -2$ designated as the O-branch.

Consider the Stokes and anti-Stokes components of the Raman spectrum for diatomic nitrogen. The relevant spectroscopic parameters defining the harmonic oscillator and rigid rotor for the $X^1\Sigma^+$ ground electronic state of N_2 are $\omega_e = 2359\ \text{cm}^{-1}$ and $B_e = 2.0\ \text{cm}^{-1}$, respectively.

(a) Employing the simplex model, develop two expressions for the rovibrational wave number, $\tilde{\nu}_R$, defining the S-branch and the O-branch for both the Stokes and anti-Stokes spectrum.

(b) If the laser wavelength is 532 nm, determine the wavelength (nm) corresponding to the $J'' = 6$ line within the S-branch of the Stokes component for the N_2 Raman spectrum.

(c) Similarly, determine the wavelength (nm) corresponding to the $J'' = 8$ line within the O-branch of the anti-Stokes component for the N_2 Raman spectrum.

Solution

(a) For both the Stokes and anti-Stokes components of the Raman signal, the rovibrational wavenumbers can be obtained from

$$\tilde{\nu}_R = \tilde{\varepsilon}'_{rv}(v' = 1) - \tilde{\varepsilon}''_{rv}(v'' = 0),$$

where, for the simplex model,

$$\tilde{\varepsilon}_{rv} = \omega_e \left(v + \tfrac{1}{2}\right) + B_e J(J+1).$$

Therefore, for the S-branch, for which $J' = J'' + 2$,

$$\tilde{\nu}_R = \omega_e + \left[(J''+2)(J''+3) - J''(J''+1)\right] B_e = \omega_e + 2(2J''+3)\, B_e.$$

Similarly, for the O-branch, for which $J' = J'' - 2$,

$$\tilde{\nu}_R = \omega_e + \left[(J''-2)(J''-1) - J''(J''+1)\right] B_e = \omega_e - 2(2J''-1)\, B_e.$$

(b) For the $J'' = 6$ line within the S-branch,

$$\tilde{\nu}_R = \omega_e + 2(2J''+3)\, B_e = 2359 + 30(2.0) = 2419\ \text{cm}^{-1}.$$

Given a laser at $\lambda_L = 532$ nm, $\tilde{\nu}_L = \lambda_L^{-1} = 18797\ \text{cm}^{-1}$. Hence, for the Stokes component,

$$\tilde{\nu}_S = \tilde{\nu}_L - \tilde{\nu}_R = 18797 - 2419 = 16378\ \text{cm}^{-1},$$

so that $\lambda_S = \tilde{\nu}_S^{-1} = 610.6$ nm.

(c) Similarly, for the $J'' = 8$ line within the O-branch,

$$\tilde{\nu}_R = \omega_e - 2(2J''-1)\, B_e = 2359 - 30(2.0) = 2299\ \text{cm}^{-1}.$$

Hence, for the anti-Stokes component,

$$\tilde{\nu}_A = \tilde{\nu}_L + \tilde{\nu}_R = 18797 + 2299 = 21096\ \text{cm}^{-1},$$

so that $\lambda_A = \tilde{\nu}_A^{-1} = 474.0$ nm. In summary, then, for a laser at 532 nm, the $J'' = 6$ Stokes line within the S-branch is at 610.6 nm, while the $J'' = 8$ anti-Stokes line within the O-branch is at 474.0 nm.

7.4 The Complex Model for Combined Rotation and Vibration

The simplex model assumes complete separation of the vibrational and rotational energy modes, with vibration modeled as a harmonic oscillator and rotation modeled as a rigid rotor. We recognize, however, that such a model is much too simplistic. First, as we saw in Chapter 6, the harmonic oscillator approximates the more realistic Morse potential only at lower vibrational energies. Second, by imagining a diatomic molecule as two masses linked with a spring, we realize that rotation will lead to stretching of the spring, thus making a rigid rotor impossible. Third, carrying this analogy further, we also appreciate that enhanced vibration will expand the mean bond length, thus affecting the moment of inertia for rotation. In other words, an inevitable coupling must occur between vibration and rotation.

Because each electronic energy level is characterized by a unique Morse potential reflecting a prevalent bonding mechanism, Eq. (7.2) must actually be written as

$$\tilde{\varepsilon}_{int} = T_e + G(v)|_e + F_v(J)|_e, \tag{7.19}$$

where T_e is the energy for a given electronic state, the subscript e identifies a dependence of vibrational and rotational energy modes on electronic state, and the subscript v indicates that the rotational energy mode is influenced by the vibrational energy mode. From this perspective, Eq. (7.19) reminds us that, even in the ground electronic state ($T_e = 0$), the combined vibrational and rotational motions for any diatomic molecule ultimately depend on the specific internuclear potential describing its electron configuration.

Utilizing the quantum methods of Chapter 6, more realistic expressions for $G(v)$ and $F_v(J)$ could now be derived by solving the steady-state Schrödinger wave equation given the specific Morse potential,

$$V(r) = \mathrm{D}_e\left[1 - e^{-\beta(r-r_e)}\right]^2,$$

for a given electronic state. Surprisingly enough, an analytical solution based on a power-series representation of the Morse potential is still possible, though the mathematical procedures are both tedious and ponderous. Not unexpectedly, this revised solution reconstructs the basic rigid-rotor/harmonic-oscillator model, but with the inclusion of higher-order correction terms. Forsaking the mathematical intricacies, we find that the required vibrational and rotational energies can be expressed as

$$G(v) = \omega_e\left(v + \tfrac{1}{2}\right) - \omega_e x_e\left(v + \tfrac{1}{2}\right)^2 \qquad v = 0, 1, 2, \ldots \tag{7.20}$$

$$F_v(J) = B_v J(J+1) - D_e J^2(J+1)^2 \qquad J = 0, 1, 2, \ldots, \tag{7.21}$$

where

$$B_v = B_e - \alpha_e\left(v + \tfrac{1}{2}\right). \tag{7.22}$$

If we employ instead the more general *Dunham potential*, which represents a Taylor series expansion about r_e, we merely introduce further higher-order terms into Eqs. (7.20–7.22). Fortunately, these three equations are sufficiently accurate for most purposes; moreover, they include essentially all of the important physical phenomena. Furthermore, each controlling parameter in Eqs. (7.20–7.22) can be related to its Morse potential through

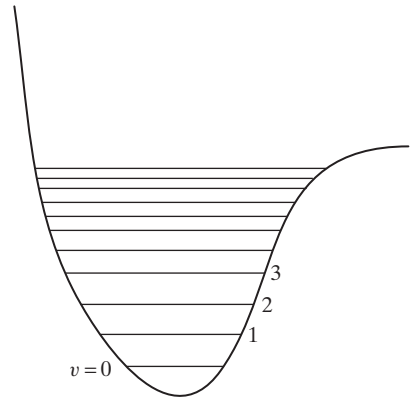

Figure 7.5 Morse potential with vibrational energy levels for the anharmonic oscillator.

a combination of Eq. (7.8) and the following suppletory expressions:

$$\omega_e = \beta\sqrt{\frac{h\mathrm{D}_e}{2\pi^2 c\mu}} \tag{7.23}$$

$$\omega_e x_e = \frac{h\beta^2}{8\pi^2 c\mu} \tag{7.24}$$

$$D_e = \frac{4B_e^3}{\omega_e^2} \tag{7.25}$$

$$\alpha_e = \frac{6B_e^2}{\omega_e}\left[\sqrt{\frac{\omega_e x_e}{B_e}} - 1\right]. \tag{7.26}$$

The second-order correction term in Eq. (7.20), as compared to Eq. (7.4) for the harmonic oscillator, represents *vibrational anharmonicity*. Hence, the new parameter, x_e, is called the *anharmonicity constant*. Typical energy levels for the *anharmonic oscillator* are displayed with their parent Morse potential in Fig. 7.5. As discussed in Chapter 6, the harmonic-oscillator potential is a useful approximation to the Morse potential at lower vibrational quantum numbers. The negative correction term in Eq. (7.20) evinces the possibility for dissociation at sufficiently high temperatures when employing the more realistic Morse potential. From a different perspective, the spacing between consecutive vibrational levels must actually decrease with higher vibrational quantum number to replicate the classical continuum upon dissociation. This behavior is quite clearly a very straightforward and robust manifestation of the correspondence principle.

The second-order correction term in Eq. (7.21), for which D_e is the *centrifugal distortion constant*, represents *rotational centrifugal stretching*. This correction term is also negative because enhanced centripetal acceleration at higher rotational quantum numbers must increase I_e, thus effectively reducing any rotational energy via the physics represented by Eq. (7.8). Note that D_e, as defined by the Kratzer relationship of Eq. (7.25), should not be confused with the *binding energy*, D_e (Eq. 6.40). Eliminating β from Eqs. (7.23) and (7.24), we find that the binding energy can be determined from spectroscopic measurements of ω_e and $\omega_e x_e$ by implementing

$$\mathrm{D}_e = \frac{\omega_e^2}{4\omega_e x_e}. \tag{7.27}$$

Finally, Eq. (7.22) represents *rotation–vibration coupling*. Here, the coupling comes from the influence of vibration on rotation and not vice versa, as typical ω_e/B_e values of 100–1000 imply many vibrations per rotation but no rotational events per vibration. The controlling effect of vibration on rotation is also implied by Fig. 7.5, which portrays an increasing average bond length with rising vibrational quantum number. This increasing bond length leads to an enhanced moment of inertia, which reduces the effective rotational energy – thus, the negative correction term involving the *coupling constant*, α_e, in Eq. (7.22).

7.5 Rovibrational Spectroscopy: The Complex Model

The combined effects of vibrational anharmonicity, rotational centrifugal stretching, and rotation–vibration coupling constitute what we shall call the *complex model*, as compared to the simplex model, which presumed an integrated harmonic oscillator and rigid rotor. Pursuing this avenue, the total rovibrational energy within a given electronic state becomes, from Eqs. (7.20) and (7.21),

$$\tilde{\varepsilon}_{rv} = G(v) + F_v(J) = \omega_e\left(v+\tfrac{1}{2}\right) - \omega_e x_e\left(v+\tfrac{1}{2}\right)^2 + B_v J(J+1) - D_e J^2(J+1)^2. \quad (7.28)$$

Furthermore, for the anharmonic oscillator, the vibrational selection rule is no longer limited to our previous $\Delta v = \pm 1$; in fact, the revised selection rules for the complex model become

$$v' - v'' = 1, 2, 3, \ldots \qquad J' - J'' = \pm 1, \quad (7.29)$$

so that, for $v'' = 0$, $v' - v'' = 1$ designates the fundamental transition, $v' - v'' = 2$ designates the first overtone, and $v' - v'' = 3$ designates the second overtone, respectively. Similarly, for $v'' > 0$, rovibrational spectra corresponding to $v' - v'' = 1, 2, 3$ would identify various *hot bands*. In general, higher overtones become progressively weaker by about a factor of ten in comparison to the fundamental transition. As their name implies, hot bands only appear at higher temperatures, when sufficient population is generated within upper vibrational energy levels.

For simplicity in our forthcoming development, we now choose to neglect rotational centrifugal stretching in Eq. (7.28), as this complication is often quite minor in comparison to the remaining contributions. Therefore, the wave numbers displayed in any rovibrational spectrum become

$$\tilde{\nu} = \Delta\tilde{\varepsilon}_{rv} = \omega_e(v' - v'') - \omega_e x_e\left[v'(v'+1) - v''(v''+1)\right] + B'_v J'(J'+1) - B''_v J''(J''+1),$$

so that, for those transitions affiliated with the ground vibrational level $(v'' = 0)$,

$$\tilde{\nu}_P = \tilde{\nu}_v - (B'_v + B''_v)J'' + (B'_v - B''_v)J''^2 \qquad J'' = 1, 2, 3\ldots \quad (7.30)$$

$$\tilde{\nu}_R = \tilde{\nu}_v + 2B'_v + (3B'_v - B''_v)J'' + (B'_v - B''_v)J''^2 \qquad J'' = 0, 1, 2\ldots \quad (7.31)$$

for the P-branch $(J' = J'' - 1)$ and R-branch $(J' = J'' + 1)$, respectively. In accord with the simplex model, Eqs. (7.30) and (7.31) show that rotational energy is either added to or subtracted from a purely vibrational contribution, specified in this case by

$$\tilde{\nu}_v = \omega_e v' - \omega_e x_e v'(v'+1). \quad (7.32)$$

On this basis, the line spacing for rovibrational spectroscopy must be independent of Eq. (7.32) and given by

$$\Delta\tilde{\nu}_P = (B'_v + B''_v) + (B''_v - B'_v)(2J'' - 1) \tag{7.33}$$

$$\Delta\tilde{\nu}_R = (3B'_v - B''_v) - (B''_v - B'_v)(2J'' + 1), \tag{7.34}$$

for the P-branch and R-branch, respectively.

Because $\alpha_e \ll B_e$, we ascertain from Eq. (7.22) that $B''_v \geq B'_v$. If $B''_v = B'_v$, Eqs. (7.33) and (7.34) merely replicate Eq. (7.17) for the simplex model. If, on the other hand, $B''_v > B'_v$, Eq. (7.33) confirms that the spacing between consecutive lines in the P-branch grows with increasing J''. Similarly, Eq. (7.34) demonstrates that the spacing between consecutive lines in the R-branch drops with increasing J''. This composite behavior comports perfectly with that displayed for HBr in Fig. 7.4. Hence, a least-squares fit of both Eqs. (7.30) and (7.31) to infrared spectra is the preferred method for determining many spectral parameters, including ω_e, $\omega_e x_e$, B_e, and α_e.

EXAMPLE 7.2

Consider the P- and R-branches for the fundamental infrared spectrum of a diatomic molecule.

(a) Show that the wave number (cm^{-1}) corresponding to the line positions for the P- and R-branches when neglecting centrifugal distortion can be expressed as

$$\tilde{\nu} = \tilde{\nu}_v + (B'_v + B''_v)K + (B'_v - B''_v)K^2,$$

where $\tilde{\nu}_v = \omega_e - 2\omega_e x_e, K = -J''$ for the P-branch, and $K = J'' + 1$ for the R-branch.

(b) Energy gaps between spectral lines that share a common upper or lower level are known as combination differences. These differences are very useful because they depend solely on the spectroscopic parameters for the lower or upper levels, respectively. Demonstrate that the specific combination differences $\Delta J'' = 2$ and $\Delta J' = 2$, as defined in the accompanying energy-level diagram, are given, respectively, by

$$\Delta_2 F''(J'') = 4B''_v\left(J'' + \tfrac{1}{2}\right) \qquad \Delta_2 F'(J'') = 4B'_v\left(J'' + \tfrac{1}{2}\right).$$

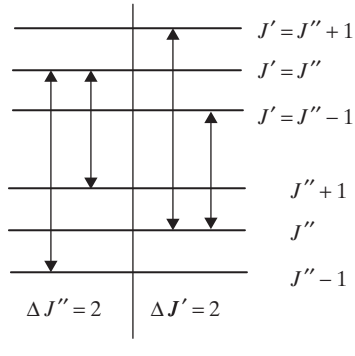

(c) The following data are available from the fundamental infrared spectrum of HI:

Rovibrational Line	Frequency (cm^{-1})	Rovibrational Line	Frequency (cm^{-1})
R(0)	2242.6	P(1)	2217.1
R(1)	2254.8	P(2)	2203.8
R(2)	2266.6	P(3)	2190.2

Employing combination differences, determine B_0, B_1, B_e, and α_e for HI from these data.

Solution

(a) For the P-branch, $K = -J''$, so that we have, from the general expression given in part (a),

$$\tilde{\nu}_P(J'') = \tilde{\nu}_v - (B'_v + B''_v)\,J'' + (B'_v - B''_v)\,J''^2,$$

which obviously replicates Eq. (7.30). Similarly, for the R-branch, $K = J'' + 1$ so that

$$\tilde{\nu}_R(J'') = \tilde{\nu}_v + (B'_v + B''_v)\,(J'' + 1) + (B'_v - B''_v)\,(J'' + 1)^2.$$

Hence,

$$\tilde{\nu}_R(J'') = \tilde{\nu}_v + (B'_v + B''_v)\,(J'' + 1) + (B'_v - B''_v)\,(2J'' + 1) + (B'_v - B''_v)\,J''^2,$$

or, in agreement with Eq. (7.31),

$$\tilde{\nu}_R(J'') = \tilde{\nu}_v + 2B'_v + (3B'_v - B''_v)\,J'' + (B'_v - B''_v)\,J''^2.$$

Finally, for the fundamental infrared spectrum, $v' = 1$, so that from Eq. (7.32) we verify that

$$\tilde{\nu}_v = \omega_e v' - \omega_e x_e v'\,(v' + 1) = \omega_e - 2\omega_e x_e.$$

(b) We observe that the combination difference for the $\Delta J'' = 2$ case can be expressed as

$$\Delta_2 F''\,(J'') = \tilde{\nu}_R\,(J'' - 1) - \tilde{\nu}_P(J'' + 1),$$

since $J' = J'' + 1$ for the R-branch while $J' = J'' - 1$ for the P-branch. Hence, setting $K = J''$ for the R-branch and $K = -(J'' + 1)$ for the P-branch,

$$\Delta_2 F''\,(J'') = (B'_v + B''_v)\,J'' + (B'_v - B''_v)\,J''^2 + (B'_v + B''_v)\,(J'' + 1) - (B'_v - B''_v)\,(J'' + 1)^2,$$

so that

$$\Delta_2 F''\,(J'') = (B'_v + B''_v)\,(2J'' + 1) - (B'_v - B''_v)\,(2J'' + 1) = 2B''_v(2J'' + 1) = 4B''_v\left(J'' + \tfrac{1}{2}\right).$$

Similarly, the combination difference for the $\Delta J' = 2$ case is

$$\Delta_2 F'\,(J'') = \tilde{\nu}_R\,(J'') - \tilde{\nu}_P\,(J'').$$

Therefore, setting $K = J'' + 1$ for the R-branch and $K = -J''$ for the P-branch,

$$\Delta_2 F'\,(J'') = (B'_v + B''_v)\,(J'' + 1) + (B'_v - B''_v)\,(J'' + 1)^2 + (B'_v + B''_v)\,J'' - (B'_v - B''_v)\,J''^2,$$

so that

$$\Delta_2 F'(J'') = (B'_v + B''_v)(2J'' + 1) + (B'_v - B''_v)(2J'' + 1) = 2B'_v(2J'' + 1) = 4B'_v\left(J'' + \tfrac{1}{2}\right).$$

(c) From the given data on the fundamental infrared spectrum of HI, the lower combination difference gives

$$\Delta_2 F''(1) = \tilde{\nu}_R(0) - \tilde{\nu}_P(2) = 2242.6 - 2203.8 = 4B_0\left(1 + \tfrac{1}{2}\right) = 6B_0,$$

so that $6B_0 = 38.8\,\text{cm}^{-1}$ or $B_0 = 6.47\,\text{cm}^{-1}$. Similarly, the upper combination difference gives

$$\Delta_2 F'(1) = \tilde{\nu}_R(1) - \tilde{\nu}_P(1) = 2254.8 - 2217.1 = 4B_1\left(1 + \tfrac{1}{2}\right) = 6B_1,$$

so that $6B_1 = 37.7\ \text{cm}^{-1}$ or $B_1 = 6.28\ \text{cm}^{-1}$. Finally, from Eq. (7.22), we may write for our two vibrational levels $B_1 = B_e - 1.5\alpha_e$ and $B_0 = B_e - 0.5\alpha_e$. Therefore, solving these two equations simultaneously, we obtain $B_e = 1.5B_0 - 0.5B_1$ and $\alpha_e = B_0 - B_1$, so that $B_e = 6.57\ \text{cm}^{-1}$ and $\alpha_e = 0.19\ \text{cm}^{-1}$.

7.6 Electronic Spectroscopy

The most complicated spectral signature arises when we have simultaneous changes in the electronic, vibrational, and rotational energy modes. From Eq. (7.19), the wave number for individual lines in a *rovibronic* spectrum can be expressed as

$$\tilde{\nu} = \Delta\tilde{\varepsilon}_{int} = \Delta T_e + \Delta G(v) + \Delta F_v(J), \tag{7.35}$$

where the three terms represent variations in the electronic, vibrational, and rotational energy, respectively. The shift in vibrational energy now depends on both the lower and upper electronic energy levels. The same applies to the change in rotational energy; moreover, this change depends on both the lower and upper vibrational energy levels. In addition, because the transition dipole moment controlling rovibronic transitions is often nonzero for symmetric species, we expect electronic spectra for all molecules – even homonuclear diatomics, such as O_2 and N_2.

If we now consider, for simplicity, the ground and excited electronic states of a diatomic molecule, Eq. (7.35) can be written in the form

$$\tilde{\nu} = \tilde{\nu}_\circ + \Delta F_v(J), \tag{7.36}$$

where the *band origin* is defined as

$$\tilde{\nu}_\circ = T_e + \Delta G(v). \tag{7.37}$$

Typically, the band origin is dominated by $T_e \approx 10^4 - 10^5\ \text{cm}^{-1}$, which corresponds to the visible or ultraviolet region of the electromagnetic spectrum, as indicated in Table 7.1. In general, the vibrational contribution to Eq. (7.37) is

$$\Delta G(v) = \left[\omega'_e\left(v' + \tfrac{1}{2}\right) - \omega'_e x'_e\left(v' + \tfrac{1}{2}\right)^2\right] - \left[\omega''_e\left(v'' + \tfrac{1}{2}\right) - \omega''_e x''_e\left(v'' + \tfrac{1}{2}\right)^2\right], \tag{7.38}$$

where the single and double primes refer to spectral parameters affiliated with the upper and lower electronic states, respectively. Analogous to the rovibrational case, the

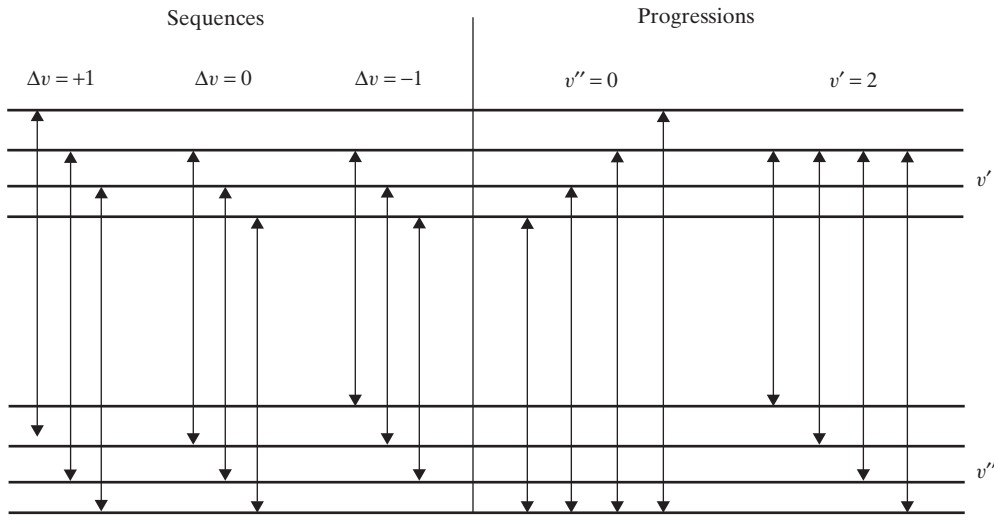

Figure 7.6 Electronic energy-level diagram, showing various sequences and progressions.

vibrational selection rule for rovibronic transitions is

$$\Delta v = v' - v'' = 0,\ \pm 1,\ \pm 2,\ \pm 3, \ldots; \tag{7.39}$$

thus, any vibrational level in an upper electronic state can be linked with any vibrational level in the ground electronic state. In particular, an electronic spectrum containing vibrational bands with constant Δv is called a *sequence*. A spectrum containing regular vibrational bands with either constant v' or v'' is called a *progression*. Such sequences and progressions are best understood via an energy-level diagram, as depicted in Fig. 7.6.

Returning to Eq. (7.36), the rotational contribution to a rovibronic spectrum can be derived by implementing Eq. (7.21); the result is

$$\Delta F_v(J) = \left[B'_v J'(J'+1) - D'_e J'^2 (J'+1)^2\right] - \left[B''_v J''(J''+1). - D''_e J''^2 (J''+1)^2\right], \tag{7.40}$$

where again the single and double primes refer to the upper and lower electronic states, respectively. In comparison to the rovibrational case, the rotational selection rule for rovibronic transitions turns out to be

$$\Delta J = J' - J'' = 0,\ \pm 1, \tag{7.41}$$

where we now entertain the possibility of a Q-branch ($\Delta J = 0$) in addition to the usual P- and R-branches. Typically, the Q-branch is intense for electronic transitions with $\Delta\Lambda = \pm 1$, weak when $\Delta\Lambda = 0$, and forbidden if $\Lambda = 0$ for both participating electronic states. In general, strong lines in a rovibronic spectrum are called *main-line* transitions, while weak spectral lines are called *satellite* transitions.

Equation (7.40) represents the rotational structure within the *vibronic* bands delineated by Eq. (7.37). In parallel with the rovibrational case, this rotational structure is defined by applying Eq. (7.41) to Eq. (7.40). Presuming again negligible rotational distortion ($D_e = 0$), we find

$$\tilde{\nu}_P = \tilde{\nu}_\circ - (B'_v + B''_v)\, J'' + (B'_v - B''_v)\, J''^2 \qquad J'' = 1, 2, 3 \ldots \tag{7.42}$$

$$\tilde{\nu}_Q = \tilde{\nu}_\circ + (B'_v - B''_v)\, J'' + (B'_v - B''_v)\, J''^2 \qquad J'' = 1, 2, 3 \ldots \tag{7.43}$$

$$\tilde{\nu}_R = \tilde{\nu}_\circ + 2B'_v + (3B'_v - B''_v)\, J'' + (B'_v - B''_v)\, J''^2 \qquad J'' = 0, 1, 2 \ldots \tag{7.44}$$

for the P-branch ($J' = J'' - 1$), Q-branch ($J' = J''$), and R-branch ($J' = J'' + 1$), respectively. We observe from Eq. (7.43) that no rovibronic signature is possible for $J' = 0 \leftrightarrow J'' = 0$; in other words, a gap will appear in the rovibronic spectrum corresponding to the band origin at $\tilde{\nu}_\circ$, in analogy with a similar gap in the infrared spectrum.

Utilizing Eqs. (7.42–7.44), we find the spacing between consecutive rovibronic lines within the P-, Q-, and R-branches to be

$$\Delta\tilde{\nu}_P = (B'_v + B''_v) + (B''_v - B'_v)(2J'' - 1) \tag{7.45}$$

$$\Delta\tilde{\nu}_Q = 2(J'' + 1)(B'_v - B''_v) \tag{7.46}$$

$$\Delta\tilde{\nu}_R = (3B'_v - B''_v) - (B''_v - B'_v)(2J'' + 1). \tag{7.47}$$

Despite the equivalence between Eqs. (7.45) and (7.33) for the P-branch and between Eqs. (7.47) and (7.34) for the R-branch, we must recognize that B'_v and B''_v can differ substantially for electronic transitions as compared to infrared transitions. Moreover, whereas $B''_v \geq B'_v$ is mandatory for infrared spectroscopy, either $B''_v \geq B'_v$ or $B''_v \leq B'_v$ can apply for visible and ultraviolet spectroscopy, as the rotational constant depends on the Morse potential for each specific electronic state. Remarkably, these features can cause the rovibronic lines within a band to crowd together and eventually reverse their spectral direction, thus creating a well-defined *bandhead*. In fact, bandheads within the P- and R-branches can be identified by setting Eqs. (7.45) and (7.47) to zero, which results in the following two expressions for the J-value in the lower electronic state defining each bandhead:

$$J''_P = \frac{1}{2}\left(\frac{B'_v + B''_v}{B'_v - B''_v} + 1\right) \tag{7.48}$$

$$J''_R = \frac{1}{2}\left(\frac{3B'_v - B''_v}{B''_v - B'_v} - 1\right). \tag{7.49}$$

We realize from Eqs. (7.48) and (7.49) that for $B''_v \leq B'_v$ the bandhead appears in the P-branch, while for $B''_v \geq B'_v$ the bandhead appears in the R-branch. Therefore, spectral analyses contingent on substantial spacings between rovibronic lines would mandate use of the R-branch for $B''_v \leq B'_v$ and the P-branch for $B''_v \geq B'_v$. On the other hand, bandheads are inevitably the most easily observable feature in any rovibronic spectrum because spectral crowding and reversal enhance spectral intensity and thus generate sharp cutoffs toward either the high- or low-wavelength end of the spectrum. Consider, for example, the ultraviolet emission spectrum of N_2, as displayed in Fig. 7.7. Here, the various bandheads clearly occur toward the high-wavelength side of the spectrum, thus indicating their occurrence within the P-branch. Such bandheads are often described as violet-degraded because of the drop in intensity toward shorter wavelengths. Similarly, a bandhead within the R-branch would be called red-degraded owing to its drop in intensity toward longer wavelengths.

For the Q-branch, we observe from Eqs. (7.43) and (7.46) that an intense pile-up of rovibronic signatures can occur at the band origin when $B''_v \simeq B'_v$. We should also note that our previous discussion of electronic spectroscopy holds exactly only for singlet–singlet transitions ($S = 0$). Visible or ultraviolet transitions involving electronic states with $S > 0$ produce somewhat more complicated spectra because of the effects of rotational structure on both the spin and orbital angular momenta. Nevertheless, the spectral signatures for such molecules can still be reasonably approximated by employing the simplified rovibronic model discussed in this chapter.

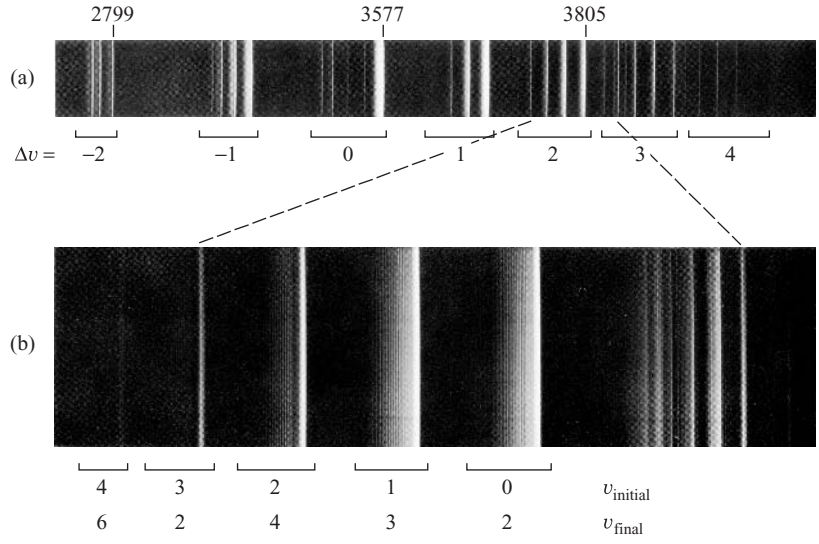

Figure 7.7 The rotational fine structure in the ultraviolet emission spectrum of N_2. The indicated wavelengths along the rovibronic sequence are in angstroms.

As might be expected, spectroscopists have developed a scheme similar to that for the rovibrational case to identify individual rovibronic transitions occurring within a visible or ultraviolet spectrum. In general, the notation invoked to designate a rotational shift follows

$$B_i(J'') \qquad B = P, Q, R \qquad i = 1, 2, 3, \ldots, \tag{7.50}$$

where $B = P$ for a line in the P-branch, $B = Q$ for a transition in the Q-branch, and $B = R$ for a line in the R-branch. The numerical subscript is less significant but is sometimes used to distinguish among closely-lying transitions linking various spin-split levels within a multiplet. For electronic spectroscopy, an additional nomenclature is obviously necessary to designate the vibrational and electronic shifts. The usual notation is

$$A(v') \rightleftarrows X(v''), \tag{7.51}$$

where only one arrow can be used, either to the left for absorption or to the right for emission. The lower vibrational level (v'') can be associated with any electronic state (X, A, B); in contrast, the upper vibrational level (v') must occur within a higher electronic state (A, B, C) permitted by the reigning selection rules. As an example, a specific transition in the ultraviolet spectrum for the hydroxyl radical could be identified via the following complete nomenclature:

$$Q_1(9) \qquad A^2\Sigma(v = 1) \leftarrow X^2\Pi(v = 0),$$

thus indicating the $J'' = J' = 9$ line in the Q-branch of OH, as produced by absorption of radiation from the $v'' = 0$ vibrational level in the ground ($^2\Pi$) electronic state to the $v' = 0$ vibrational level in the first excited ($^2\Sigma$) electronic state.

7.7 Energy-Mode Parameters for Diatomic Molecules

In summary, our purpose in this chapter has been to demonstrate the practical link through spectroscopy between quantum mechanics and statistical thermodynamics. Employing

Table 7.2 *Energy-mode parameters for the three lowest electronic states of molecular oxygen*

Term symbol	T_e (cm^{-1})	ω_e (cm^{-1})	$\omega_e x_e$ (cm^{-1})	B_e (cm^{-1})	α_e (cm^{-1})	D_e (cm^{-1})
$^3\Sigma_g^-$	0	1580.19	11.981	1.4456	0.0159	$4.839 \cdot 10^{-6}$
$^1\Delta_g$	7918.1	1483.50	12.900	1.4264	0.0171	$4.860 \cdot 10^{-6}$
$^1\Sigma_g^+$	13195.1	1432.77	14.000	1.4004	0.0182	$5.351 \cdot 10^{-6}$

statistical methods, we recall that the thermodynamic properties of atoms and molecules can be evaluated from their associated energy levels and degeneracies. These microscopic parameters can be understood and sometimes even predicted using quantum mechanics. However, as we saw in Chapter 6, quantum mechanics is usually relegated to providing basic particle models whose parameters must still be determined by experimentation. For example, in this chapter, we found that the complex model for combined rotation and vibration ultimately rests on various quantum procedures for diatomic molecules. Nevertheless, spectroscopic measurements remain essential for the determination of various energy-mode parameters, such as the fundamental vibrational frequency, ω_e, and the rotational constant, B_e.

We conclude, therefore, that the most significant aspect of atomic and molecular spectroscopy is its experimental entrée into the microscopic world. Through spectroscopy, we can determine the energies and degeneracies of electronic states, as listed in Tables 6.7 and 6.8 for atomic potassium and molecular oxygen, respectively. Similar tabulations are included in Appendix J for a potpourri of additional atoms and molecules. More generally, spectroscopic measurements permit rigorous comparisons between quantum predictions and spectral signatures, thus giving, via optimized fitting algorithms, accurate values for all energy-mode parameters. As an example, such parameter values are listed for the three lowest electronic states of molecular oxygen in Table 7.2. Similar tabulations for selected diatomic molecules are provided in Appendix K. We note from Table 7.2 that values for ω_e and B_e vary among different electronic states owing to their unique Morse potentials. In addition, because they reflect corrections to the basic harmonic-oscillator and rigid-rotor models, we observe that values for $\omega_e x_e$, α_e, and D_e are significantly less than those for ω_e and B_e. A further appreciation of the influence of molecular type and electronic state on energy-mode parameters can be gained by perusing the tables of Appendix K.

EXAMPLE 7.3

The observed spectral frequencies (cm^{-1}) corresponding to some significant vibronic transitions within the $A\,^1\Pi \leftarrow X\,^1\Sigma^+$ electronic system of PN are as follows:

Vibronic Transition	Frequency (cm^{-1})
$A\,^1\Pi\,(v=0) \leftarrow X\,^1\Sigma^+\,(v=0)$	39699.1
$A\,^1\Pi\,(v=1) \leftarrow X\,^1\Sigma^+\,(v=0)$	40786.8
$A\,^1\Pi\,(v=2) \leftarrow X\,^1\Sigma^+\,(v=0)$	41858.9

Using the given spectral data, calculate ω_e and $\omega_e x_e$ for the $A\,^1\Pi$ electronic state of PN.

Solution

Combining Eqs. (7.37) and (7.38), the band origin for any vibronic transition becomes

$$\tilde{\nu}_\circ(v',\ v'') = T_e + \left[\omega'_e\left(v'+\tfrac{1}{2}\right) - \omega'_e x'_e\left(v'+\tfrac{1}{2}\right)^2\right] - \left[\omega''_e\left(v''+\tfrac{1}{2}\right) - \omega''_e x''_e\left(v''+\tfrac{1}{2}\right)^2\right].$$

Hence, for those specific transitions indicated in the above table, we have

$$\tilde{\nu}_\circ(v'=0,\ v''=0) = T_e + \left[\tfrac{1}{2}\omega'_e - \tfrac{1}{4}\omega'_e x'_e\right] - \left[\tfrac{1}{2}\omega''_e - \tfrac{1}{4}\omega''_e x''_e\right]$$

$$\tilde{\nu}_\circ(v'=1,\ v''=0) = T_e + \left[\tfrac{3}{2}\omega'_e - \tfrac{9}{4}\omega'_e x'_e\right] - \left[\tfrac{1}{2}\omega''_e - \tfrac{1}{4}\omega''_e x''_e\right]$$

$$\tilde{\nu}_\circ(v'=2,\ v''=0) = T_e + \left[\tfrac{5}{2}\omega'_e - \tfrac{25}{4}\omega'_e x'_e\right] - \left[\tfrac{1}{2}\omega''_e - \tfrac{1}{4}\omega''_e x''_e\right].$$

Subtracting the first of these three equations from each of the remaining two equations, we may write

$$\tilde{\nu}_\circ(v'=1,\ v''=0) - \tilde{\nu}_\circ(v'=0,\ v''=0) = \omega'_e - 2\omega'_e x' = 40786.8 - 39699.1 = 1087.7$$

$$\tilde{\nu}_\circ(v'=2,\ v''=0) - \tilde{\nu}_\circ(v'=0,\ v''=0) = 2\omega'_e - 6\omega'_e x' = 41858.9 - 39699.1 = 2159.8$$

Simultaneous solution of these two expressions gives $\omega'_e = 1103.3\ \text{cm}^{-1}$ and $\omega'_e x'_e = 7.80\ \text{cm}^{-1}$.

PROBLEM SET III

Quantum Mechanics and Spectroscopy (Chapters 5–7)

3.1 Consider the Bohr model for the hydrogen atom.

a. Using the Lyman series of spectral lines, determine the first four excited energy levels and the ionization energy of the H atom (cm^{-1}).

b. Construct an energy-level diagram based on the energies computed in part (a). Determine the wavelengths (nm) of the spectral lines lying closest to the infrared for both the Lyman and Balmer series. Indicate the transitions corresponding to these two lines on your energy-level diagram.

c. If A_{21} (s^{-1}) is the probability per unit time that an atom in the first excited level of H will execute a downward transition to the ground level and N_2 is the number of atoms which occupy the first excited level at any instant, obtain an expression in terms of the Rydberg constant for the rate at which energy is emitted because of transitions from $n = 2$ to $n = 1$.

d. To a good approximation, the lifetime, τ, of an H atom in the first excited level is the reciprocal of A_{21}. If A_{21} is given by

$$A_{21} = \frac{2\pi e^2 \nu_{21}^2}{\varepsilon_\circ m_e c^3},$$

what is the value of τ? How many revolutions will an electron make before decaying radiatively to the ground level?

3.2 Despite its simplicity, the Bohr theory can be applied directly to any hydrogen-like ion such as He^+ and Li^{2+} consisting of one electron around a nucleus.

a. Using a center-of-mass coordinate system and recognizing that the charge on the nucleus is Ze where Z is the atomic number, show that the radius of allowed orbits and the change in orbital energy (cm^{-1}) are given by

$$r = \frac{\varepsilon_\circ h^2 n^2}{Z\pi\mu e^2} \qquad \Delta\tilde{\varepsilon} = \frac{Z^2 e^4 \mu}{8\varepsilon_\circ^2 c h^3}\left(\frac{1}{n_1^2} - \frac{1}{n_2^2}\right),$$

where μ is the reduced mass and n is the principal quantum number. Calculate the radius of the first Bohr orbit for He^+.

b. A spectacular success of the Bohr theory was its correct assignment of some solar spectral lines caused by He^+. These He^+ lines correspond to a set of transitions

for which the electron falls from a higher energy level into the $n = 4$ level. Derive a formula for the wave numbers of the observed lines in this so-called Pickering series. In what region of the spectrum do these lines occur?

c. Calculate the ionization energy (eV) of singly ionized helium.

3.3 For a two-particle system, we found that the steady-state Schrödinger equation in relative coordinates can be solved by expressing the normalized wave function as

$$\psi(r, \theta, \phi) = R(r)\Theta(\theta)\Phi(\phi).$$

The angular component of the wave function is given by

$$\Theta(\theta)\Phi(\phi) = AP_J^{|m|}(\cos\theta)e^{im\phi},$$

where $m = 0, \pm 1, \pm 2, \ldots, \pm J$.

a. The z-component of the orbital angular momentum is given classically by

$$L_z = xp_y - yp_x.$$

Use this expression to show that the quantum mechanical operator corresponding to the z-component of the angular momentum is given by

$$\hat{L}_z = -i\hbar\frac{\partial}{\partial\phi}.$$

b. Prove that $L_z = m\hbar$ by applying this operator to $\Phi(\phi)$.

c. Prove that $L_z = m\hbar$ by determining the expectation value for the z-component of the orbital angular momentum.

3.4 The root-mean-square deviation of a dynamic variable, $B(\boldsymbol{r}, \boldsymbol{p}, t)$, is defined as

$$\Delta B = [\langle (B - \langle B\rangle)^2\rangle]^{1/2}.$$

Hence, ΔB is a measure of the average fluctuation of a variable about its expectation value. If ΔB is zero, the variable may assume only discrete values.

a. Demonstrate that $\Delta B = [\langle B^2\rangle - \langle B\rangle^2]^{1/2}$.

b. Show that a variable B, whose operator satisfies the equation $\hat{B}\Psi = b\Psi$, where b is a real constant, may assume only discrete values. Hence, verify that the total particle energy is quantized.

3.5 Consider a free particle of mass m constrained to move on a circle of radius a.

a. Show that the Schrödinger equation for this case is given by

$$-\frac{\hbar^2}{2I}\frac{d^2\psi}{d\theta^2} = \varepsilon\psi \qquad 0 \le \theta \le 2\pi,$$

where $I = ma^2$ is the moment of inertia and θ describes the angular position of the particle.

b. Demonstrate that the normalized solution to this equation is

$$\psi(\theta) = (2\pi)^{-1/2}e^{\pm in\theta},$$

where $n = (2I\varepsilon)^{1/2}/\hbar$.

c. Using an appropriate boundary condition, show that the allowed discrete energy levels are given by

$$\varepsilon = \frac{n^2\hbar^2}{2I} \qquad n = 0, \pm 1, \pm 2, \ldots.$$

d. Prove that the above eigenfunctions form an orthonormal set.

e. These results can be used to construct a free-electron model of benzene since its six π electrons have free access to the entire doughnut-shaped electron cloud surrounding the conjugated carbon ring. Utilizing this free-electron model and the Pauli exclusion principle, show that the lowest possible absorption frequency (cm^{-1}) for benzene is

$$\tilde{\nu} = \frac{3h}{8\pi^2 cI}.$$

3.6 Consider a particle which is constrained to move in a one-dimensional box of length L. Employing the methods of quantum mechanics, determine the following properties.

a. Evaluate the average position of the particle, $\langle x \rangle$. Is your result physically reasonable? Why?

b. Calculate the uncertainty in position by finding the root-mean-square deviation, Δx.

c. Establish the average momentum of the particle, $\langle p \rangle$. Is your result physically reasonable? Why?

d. Determine the uncertainty in momentum by assessing the root-mean-square deviation, Δp.

e. Show that your standard deviations in position and momentum are consistent with the Heisenberg uncertainty principle. What happens to the uncertainties in position and momentum as $L \to 0$ and as $L \to \infty$? Explain.

3.7 The normalized wave function for a *one-dimensional* harmonic oscillator is given by

$$\psi_v(x) = \frac{1}{(2^v v!)^{1/2}} \left(\frac{\alpha}{\pi}\right)^{1/4} \mathrm{H}_v(\alpha^{1/2}x)\, \mathrm{e}^{-\alpha x^2/2},$$

where $\alpha = \sqrt{k\mu}/\hbar$, $\mathrm{H}_v(\alpha^{1/2}x)$ is the vth-degree Hermite polynomial, x denotes the displacement from the equilibrium bond length ($-\infty < x < \infty$), k is the force constant, and μ is the reduced mass. Therefore, the normalized wave functions for the ground and first excited vibrational levels are

$$\psi_0(x) = \left(\frac{\alpha}{\pi}\right)^{1/4} \mathrm{e}^{-\alpha x^2/2} \qquad \psi_1(x) = \left(\frac{\alpha}{4\pi}\right)^{1/4} (2\alpha^{1/2}x)\, \mathrm{e}^{-\alpha x^2/2}.$$

a. Employing the steady-state Schrödinger equation, verify that $\alpha = \sqrt{k\mu}/\hbar$ and hence that $\varepsilon = h\nu(v + 1/2)$, where $\nu = (2\pi)^{-1}\sqrt{k/\mu}$ for $v = 0$ and for $v = 1$.

b. The Heisenberg uncertainty principle can be expressed as

$$\sigma_p \sigma_x \geq \hbar/2,$$

where the relevant standard deviations are $\sigma_p^2 = \langle p^2 \rangle - \langle p \rangle^2$ and $\sigma_x^2 = \langle x^2 \rangle - \langle x \rangle^2$. Show that $\psi_0(x)$ and $\psi_1(x)$ give results consistent with the Heisenberg uncertainty principle.

c. To a good approximation, the microwave spectrum of HCl consists of a series of equally spaced lines separated by 20.9 cm^{-1}. In contrast, the infrared spectrum of HCl produces just one line at 2866 cm^{-1}. Determine the fractional deviation in bond length, σ_x / x_e, where x_e is the equilibrium bond length for HCl. Compare your results for $v = 0$ and $v = 1$, and discuss the relevant physical implications.

3.8 The hydrogen atom is the only chemical species which admits a closed-form solution to the Schrödinger wave equation. In general, the wave functions are expressed in spherical coordinates but fortunately they are spherically symmetric for all the *s*-orbitals. Consider the wave function for the 1*s* orbital ($n = 1,\ l = 0,\ m_l = 0$),

$$\psi(r, \theta, \phi) = \frac{1}{\sqrt{\pi}} \left(\frac{1}{a_\circ} \right)^{3/2} e^{-r/a_\circ},$$

where $a_\circ$ is the Bohr radius, given by $a_\circ = \varepsilon_\circ h^2 / \pi \mu e^2$.

a. Demonstrate that this wave function is properly normalized.

b. Show that the probability density function for the radial position of the 1*s* electron is given by

$$f(r) = \frac{4r^2}{a_\circ^3} e^{-2r/a_\circ}.$$

c. Determine the average radial position, $\bar{r}$, for the 1*s* orbital.

d. Calculate the uncertainty in radial position by determining the root-mean-square deviation, Δr.

e. Evaluate $\Delta r / \bar{r}$. Comment on the physical implications of your result.

3.9 The configuration for the ground state of a multielectron atom can be determined by using the following two rules: (1) electrons must occupy the available subshells of lowest energy; (2) the maximum number of electrons occupying any subshell is determined by the Pauli exclusion principle. The ordering of subshell energies needed to comply with the first rule has been obtained experimentally; in general, the appropriate sequence to $n = 5$ is as follows: 1*s*, 2*s*, 2*p*, 3*s*, 3*p*, 4*s*, 3*d*, 4*p*, 5*s*, 4*d*, 5*p*. Using these rules, we find the configurations for hydrogen and argon to be 1*s* and $1s^2 2s^2 2p^6 3s^2 3p^6$, respectively, where the superscript to the right of the letter designation for *l* denotes the number of electrons in a subshell. Note that the sum of the superscripts in a configuration must equal the atomic number *Z* (for hydrogen and argon, 1 and 18, respectively).

The term symbol corresponding to the lowest energy for a given configuration can also be found by using three empirical rules developed by the German spectroscopist Frederick Hund. Hund's rules are as follows: (1) the state with the largest value of *S* is most stable; (2) for states with the same value of *S*, that state with the largest value of *L* is most stable; (3) for states with the same values of *L* and *S*, that state with the smallest value of *J* is most stable when a subshell is less than

half-filled while that state with the largest value of J is most stable when a subshell is more than half-filled.

a. Construct a table listing the configuration for the ground state of those elements of the periodic table from $Z = 1$ to $Z = 18$.

b. Hund's first two rules indicate that the electronic quantum numbers $m_s = \pm 1/2$ and $m_l = 0,\ \pm 1,\ \pm 2, \ldots, \pm l$ associated with any subshell must be sequenced so that the electrons are placed in available quantum states with the highest positive values of $M_S = \sum m_{s,i}$ and $M_L = \sum m_{l,i}$, where $M_J = M_L + M_S$. On this basis, expand the table in part (a) to include the values of L and S describing the ground state for each atom.

c. Expand the table in part (b) further by including the possible J values for each atom and also the term symbol which describes the ground electronic state of each atom.

d. Based on your table, what are the common term symbols for the noble gases (He, Ne, Ar), the alkali metals (Li, Na), and halogens (F, Cl)? Hence, what feature of atomic structure is responsible for the observed periodicity of the chemical and physical properties of the elements? In particular, how would you explain the inertness of the noble gases and the high reactivity of both the alkali metals and halogens?

3.10 The following exercises are concerned with determining the degeneracy of various electronic energy levels.

a. Two low-lying but closely-spaced, excited energy levels of helium have the configuration $1s2p$. What are the values of L and S for each of these energy levels? For both levels, determine the multiplicity, the term symbol and degeneracy of each member of the multiplet, and the cumulative degeneracy (neglecting multiplet splitting).

b. Two closely-spaced, excited energy levels of atomic oxygen have the configuration $1s^2 2s^2 2p^3 3s$. What are the values of L and S for each energy level? For both levels, determine the multiplicity, the term symbol and degeneracy of each member of the multiplet, and the cumulative degeneracy.

c. Consider the following molecular term symbols: ${}^3\Sigma$, ${}^2\Pi$. List the values of S, Λ, the multiplicity, and the degeneracy for each term symbol. Provide the complete term-symbol classification (i.e., including multiplets) for each term component.

3.11 The following exercises are concerned with determining the degeneracy of various electronic energy levels.

a. Six closely-spaced, excited energy levels of atomic nitrogen have the configuration $1s^2 2s^2 2p^2 3p$. What are the values of L and S for each of these energy levels? For each level, determine the multiplicity, the term symbol and degeneracy of each member of the multiplet, and the cumulative degeneracy (neglecting multiplet splitting).

b. Consider the following molecular term symbols: ${}^1\Sigma$, ${}^3\Pi$, ${}^2\Delta$. List the values of S, Λ, the multiplicity, and the degeneracy for each term symbol. Provide the

complete term-symbol classification (i.e., including multiplets) for each term component.

3.12 The following exercises are concerned with determining the degeneracy of various electronic energy levels.

a. Two closely-spaced, excited energy levels of atomic nitrogen have the configuration $1s^2 2s^2 2p^2 3s$. What are the values of L and S for each energy level? For both levels, determine the multiplicity, the term symbol and degeneracy of each member of the multiplet, and the cumulative degeneracy (neglecting multiplet splitting).

b. Two low-lying, but closely-spaced, excited energy levels of calcium have the configuration $1s^2 2s^2 2p^6 3s^2 3p^6 4s 3d$. What are the values of L and S for each of these energy levels? For both levels, determine the multiplicity, the term symbol and degeneracy of each member of the multiplet, and the cumulative degeneracy.

c. Consider the following molecular term symbols: $^2\Sigma$, $^4\Delta$. List the values of S, Λ, the multiplicity, and the degeneracy for each term symbol. Provide the complete term-symbol classification (i.e., including multiplets) for each term component.

3.13 The following data are available for OH:

$X\ ^2\Pi$	$T_e = 0$	$\omega_e = 3737.76\ \text{cm}^{-1}$	$\omega_e x_e = 84.881\ \text{cm}^{-1}$
	$B_e = 18.911\ \text{cm}^{-1}$	$\alpha_e = 0.7242\ \text{cm}^{-1}$	$D_e = 19.38 \times 10^{-4}\ \text{cm}^{-1}$
$A\ ^2\Sigma^+$	$T_e = 32684.1\ \text{cm}^{-1}$	$\omega_e = 3178.86\ \text{cm}^{-1}$	$\omega_e x_e = 92.917\ \text{cm}^{-1}$
	$B_e = 17.358\ \text{cm}^{-1}$	$\alpha_e = 0.7868\ \text{cm}^{-1}$	$D_e = 20.39 \times 10^{-4}\ \text{cm}^{-1}$

a. Construct an energy-level diagram for the ground electronic state of OH. Consider only the energies of the first 15 rotational levels within the first two vibrational levels, i.e., $J = 0 - 15$ and $v = 0, 1$. Label the ordinate in cm^{-1} and note the *total* degeneracy of each individual rotational level on the diagram. Following standard spectroscopic practice, set the zero of energy at $v = 0$, $J = 0$ of the ground electronic state.

b. Determine the energies (cm^{-1}) of the 15 purely rotational transitions for the $v = 0$ vibrational level within the ground electronic state and plot them on a second energy-level diagram. Draw a vertical line representing $v = 0$, $J = 14 \rightarrow 13$ on your first energy-level diagram.

c. Calculate the energies (cm^{-1}) for the rovibrational transitions $P_1(1)$ through $P_1(6)$ and $R_1(0)$ through $R_1(5)$ of the ground electronic state; plot them on a third energy-level diagram. Which branch will lead to a bandhead? At what value of J'' will the bandhead form? Draw lines representing the $P_1(7)$ and $R_1(7)$ transitions on your first energy-level diagram.

d. Determine the energies (cm^{-1}) for the P(1) through P(15) and the R(0) through R(14) spectral lines for the electronic transition $A\ ^2\Sigma^+(v = 0) \leftarrow X^2\Pi(v = 0)$. Employing $K = J + 1$ for the R-branch and $K = -J$ for the P-branch, plot K versus these energies for each branch on a fourth graph, which is called a Fortrat diagram. Which branch manifests a bandhead? Why?

e. Compare typical energies for these rotational, vibrational, and electronic transitions. What does your result imply with respect to (1) ease of mode excitation and (2) location of lines for each mode in the spectrum?

3.14 The following data are available for CN:

$X\ ^2\Sigma^+$	$T_e = 0$	$\omega_e = 2068.59\ \text{cm}^{-1}$	$\omega_e x_e = 13.087\ \text{cm}^{-1}$
	$B_e = 1.8997\ \text{cm}^{-1}$	$\alpha_e = 0.0174\ \text{cm}^{-1}$	$D_e = 6.4 \times 10^{-6}\ \text{cm}^{-1}$
$B\ ^2\Sigma^+$	$T_e = 25752.0\ \text{cm}^{-1}$	$\omega_e = 2163.90\ \text{cm}^{-1}$	$\omega_e x_e = 20.200\ \text{cm}^{-1}$
	$B_e = 1.9730\ \text{cm}^{-1}$	$\alpha_e = 0.0230\ \text{cm}^{-1}$	$D_e = 6.6 \times 10^{-6}\ \text{cm}^{-1}$

a. Construct an energy-level diagram for the ground electronic state of CN. Consider only the energies of the first 15 rotational levels within the first two vibrational levels, i.e., $J = 0 - 15$ and $v = 0, 1$. Label the ordinate in cm^{-1} and indicate the *total* degeneracy of each individual rotational level on the diagram. For consistency with standard spectroscopic practice, set the zero of energy at $v = 0$, $J = 0$ of the ground electronic state.

b. Determine the energies (cm^{-1}) of the 15 purely rotational transitions for the $v = 0$ vibrational level within the ground electronic state and plot them on a second energy-level diagram. Draw a vertical line representing $v = 0$, $J = 13 \rightarrow 12$ on your first energy-level diagram.

c. Calculate the energies (cm^{-1}) for the rovibrational transitions $P_1(1)$ through $P_1(6)$ and $R_1(0)$ through $R_1(5)$ of the ground electronic state; plot them on a third energy-level diagram. Which branch will lead to a bandhead? At what value of J'' will the bandhead form? Draw lines representing the $P_1(5)$ and $R_1(5)$ transitions on your first energy-level diagram.

d. Evaluate the energies (cm^{-1}) for the $P(1 + 5n)$, $n = 0, \ldots, 9$ and the $R(5n)$, $n = 0, \ldots, 9$ spectral lines for the electronic transition $B\ ^2\Sigma^+(v = 0) \leftarrow X\ ^2\Sigma^+$ $(v = 0)$. Using $K = J + 1$ for the R-branch and $K = -J$ for the P-branch, plot K versus these energies for each branch on a fourth graph, which is called a Fortrat diagram. Which branch manifests a bandhead? Why?

e. Compare typical energies for these rotational, vibrational, and electronic transitions. What does your result imply with respect to (1) ease of mode excitation and (2) location of lines for each mode in the spectrum?

3.15 The following data are available for NO:

$X\ ^2\Pi$	$T_e = 0\ \text{cm}^{-1}$	$\omega_e = 1904.20\ \text{cm}^{-1}$	$\omega_e x_e = 14.075\ \text{cm}^{-1}$
	$B_e = 1.6720\ \text{cm}^{-1}$	$\alpha_e = 0.0171\ \text{cm}^{-1}$	$D_e = 0.54 \times 10^{-6}\ \text{cm}^{-1}$
$A\ ^2\Sigma^+$	$T_e = 43965.7\ \text{cm}^{-1}$	$\omega_e = 2374.31\ \text{cm}^{-1}$	$\omega_e x_e = 16.106\ \text{cm}^{-1}$
	$B_e = 1.9965\ \text{cm}^{-1}$	$\alpha_e = 0.0192\ \text{cm}^{-1}$	$D_e = 5.4 \times 10^{-6}\ \text{cm}^{-1}$

a. Construct an energy-level diagram for the ground electronic state of NO. Consider only the energies of the first 15 rotational levels within the first two vibrational levels, i.e., $J = 0 - 15$ and $v = 0, 1$. Label the ordinate in cm^{-1} and indicate the *total* degeneracy of each individual rotational level on the diagram.

For consistency with standard spectroscopic practice, set the zero of energy at $v = 0, J = 0$ of the ground electronic state.

b. Determine the energies (cm^{-1}) of the 15 purely rotational transitions for the $v = 0$ vibrational level within the ground electronic state and plot them on a second energy-level diagram. Draw a vertical line representing $v = 0$, $J = 12 \rightarrow 11$ on your first energy-level diagram.

c. Calculate the energies (cm^{-1}) for the rovibrational transitions $P_1(1 + 5n)$, $n = 0, \ldots, 5$ and $R_1(5n)$, $n = 0, \ldots, 5$ of the ground electronic state; plot them on a third energy-level diagram. Which branch will lead to a bandhead? At what value of J'' will the bandhead form? Draw lines representing the $P_1(6)$ and $R_1(6)$ transitions on your first energy-level diagram.

d. Determine the energies (cm^{-1}) for the P(1) through P(12) and the R(0) through R(11) spectral lines for the electronic transition $A\,^2\Sigma^+(v = 0) \leftarrow X\,^2\Pi(v = 0)$. Implementing $K = J + 1$ for the R-branch and $K = -J$ for the P-branch, plot K versus these energies for each branch on a fourth graph, which is called a Fortrat diagram. Which branch manifests a bandhead? Why?

e. Compare typical energies for these rotational, vibrational, and electronic transitions. What does your result imply with respect to (1) ease of mode excitation and (2) location of lines for each mode in the spectrum?

PART THREE

STATISTICAL THERMODYNAMICS IN THE DILUTE LIMIT

8 Interlude: From Particle to Assembly

In this chapter, we summarize and expand somewhat on those results from quantum mechanics and spectroscopy most germane to our study of statistical thermodynamics. We then prepare for revisiting intensive properties in Chapter 9 by considering the nature of thermodynamic calculations before the advent of quantum mechanics. From a pedagogical point of view, the previous three chapters have focused on the properties of a single atom or molecule. For our purposes, the most important such properties are the allowed energy levels and degeneracies corresponding to the translational, rotational, vibrational, and electronic energy modes of an independent particle. Exploiting this knowledge, we proceed to a macroscopic *assembly* of atoms or molecules, with a focus on calculations of thermodynamic properties for any pure ideal gas. Assemblies composed of different particle types subsequently permit the evaluation of properties for both nonreacting and reacting gaseous mixtures, including equilibrium constants for various chemical reactions. Finally, re-applying spectroscopy to such mixtures, we examine the utility of statistical thermodynamics for experimentally determining temperature or concentrations in realistic gaseous mixtures at high temperatures and pressures.

8.1 Energy and Degeneracy

Our foray into quantum mechanics and spectroscopy has led to relations giving the energy and degeneracy for all four energy modes – translation, rotation, vibration, and electronic. If we insist on mode independence, any consideration of diatomic molecules also mandates the simplex model, which presumes a combined rigid rotor and harmonic oscillator. The resulting expressions, summarized in Table 8.1, provide the inputs required to evaluate the partition function of any atom or diatomic molecule. As indicated in Chapter 4, knowledge of the partition function, including its various derivatives with respect to temperature, comprises a key ingredient through which statistical thermodynamics can take us from the molecular properties of individual particles to the thermodynamic properties of particle assemblies.

Perusing Table 8.1, we note that the translational energy has been converted to wave number units (cm^{-1}), thus defining α_{tr} so as to achieve dimensional consistency with the remaining internal energy modes. We also realize that the translational energy is unique in depending on the assembly volume; in contrast, no other energy mode is affected by

Table 8.1 *The energy and degeneracy for the energy modes of an atom or diatomic molecule*

Energy mode	Energy (cm^{-1})	Parameter (cm^{-1})	Degeneracy
Translation	$\alpha_{tr}\left(n_1^2+n_2^2+n_3^2\right)$	$\alpha_{tr}=\dfrac{h}{8mcV^{2/3}}$	$2\pi\left(\dfrac{2m}{h^2}\right)^{3/2}V\varepsilon_{tr}^{1/2}d\varepsilon_{tr}$
Rotation	$J(J+1)B_e$	$B_e=\dfrac{h}{8\pi^2 c\mu r_e^2}$	$2J+1$
Vibration	$\left(v+\dfrac{1}{2}\right)\omega_e$	$\omega_e=\dfrac{1}{2\pi c}\sqrt{\dfrac{k_0}{\mu}}$	1
Electronic (atoms)	T_e-tabulations	–	$\sum_J(2J+1)$
Electronic (molecules)	T_e-tabulations	–	$\phi(2S+1)$

macroscopic properties defining the particle assembly. Moreover, as compared to the internal energy modes, the degeneracy for the translational mode requires representation through a probability density function. Shifting now to the internal modes, we recall that the rotational constant, B_e, for the rigid rotor and the vibrational frequency, ω_e, for the harmonic oscillator can both be determined from spectroscopic measurements. Similarly, spectroscopic measurements provide tabulations for the electronic energies of atoms and molecules. For atoms, the required degeneracy is evaluated by summing over a multiplet caused by different J-values; in a similar vein, for molecules, we typically sum over a multiplet caused by spin-splitting and Λ-doubling. In other words, for both atoms and molecules, the relevant expressions in Table 8.1 should be recognized as representing *effective* degeneracies.

In calculating thermodynamic properties, we often find it convenient to express the energies of Table 8.1 in terms of temperature. The conversion from either energy (J) or wave number (cm^{-1}) units to temperature (K) can be effected via

$$\frac{\varepsilon}{k}=\frac{hc}{k}\tilde{\varepsilon}=(1.4387\ \text{cm-K})\,\tilde{\varepsilon}, \tag{8.1}$$

where h is Planck's constant, c is the speed of light, k is Boltzmann's constant, and $\tilde{\varepsilon}$ is the energy in cm^{-1}. Given Eq. (8.1), we may define characteristic translational, rotational, vibrational, and electronic temperatures as follows:

$$\theta_t=\frac{hc}{k}\alpha_{tr}\qquad\theta_r=\frac{hc}{k}B_e\qquad\theta_v=\frac{hc}{k}\omega_e\qquad\theta_e=\frac{hc}{k}T_e. \tag{8.2}$$

From Table 8.1, the characteristic translational temperature is $\theta_t\approx 10^{-16}$ K for one cm^3 of molecular hydrogen; even lower translational temperatures are obtained for more massive molecules or greater assembly volumes. In comparison, from Appendix K, typical characteristic temperatures for the remaining energy modes are as follows: $\theta_r\approx 10$ K, $\theta_v\approx 10^3$ K, and $\theta_e\approx 10^5$ K. Therefore, we find that both the translational and rotational modes are fully operative significantly below room temperature. The vibrational and electronic modes, however, become fully operative only at temperatures considerably above 300 K. As discussed further in Section 8.5.3, this observation proves to be very important

when comparing predicted thermodynamic properties to those expected on the basis of classical mechanics.

8.2 Separation of Energy Modes

When applying quantum mechanics to diatomic molecules in Chapter 6, we developed a protocol for full separation of the four energy modes listed in Table 8.1. We first separated the external mode from the three internal modes by converting to a coordinate system that shifted all translational motion to the molecule's center of mass. In this way, any internal particle motion could be expressed relative to the center of mass. Therefore, the Schrödinger wave equation for the molecule could be separated into two such equations, one controlling the external and the other the internal motion. Solving independently for the molecule's external and internal contributions, we thus found that

$$\psi = \psi_{ext}\psi_{int} \qquad \varepsilon = \varepsilon_{ext} + \varepsilon_{int} \qquad g = g_{ext}g_{int}. \tag{8.3}$$

Similarly, invoking the Born–Oppenheimer approximation, we found that the Morse potential describing any electronic state could be fashioned by solving the Schrödinger wave equation for the associated electronic motion. The predicted electronic energies defining the Morse potential presumed a continuum of stationary internuclear distances consistent with expected vibrational dynamics. This internuclear potential, in turn, became the primary input needed when solving the Schrödinger wave equation for combined rotational and vibrational motion. In effect, we cultivated separation of the electronic and rovibronic modes, so that

$$\psi_{int} = \psi_{el}\psi_{rv} \qquad \varepsilon_{int} = \varepsilon_{el} + \varepsilon_{rv} \qquad g_{int} = g_{el}g_{rv}. \tag{8.4}$$

Finally, we uncoupled the rotational and vibrational modes by (1) assuming a rigid rotor and (2) approximating the Morse potential with its harmonic-oscillator counterpart. On this basis, Schrödinger wave equations could be written in terms of independent potential functions for both the rigid rotor and harmonic oscillator. These two wave equations produced independent energies and degeneracies, so that

$$\psi_{rv} = \psi_{rot}\psi_{vib} \qquad \varepsilon_{rv} = \varepsilon_{rot} + \varepsilon_{vib} \qquad g_{rv} = g_{rot}g_{vib}. \tag{8.5}$$

Accumulating now all of the above approximations and assumptions, we find by combining Eqs. (8.3–8.5) that the total energy and degeneracy for a diatomic molecule become

$$\varepsilon = \varepsilon_{tr} + \varepsilon_{rot} + \varepsilon_{vib} + \varepsilon_{el} \tag{8.6}$$

$$g = g_{tr}g_{rot}g_{vib}g_{el}. \tag{8.7}$$

In other words, full separation implies independent energy modes so that the total energy is simply the sum of all component energies. Similarly, the overall degeneracy is the product of all component degeneracies, as anticipated on the basis of a probabilistic interpretation of independent events. In summary, while Eqs. (8.6) and (8.7) appear commonplace, we should understand that their validity rests on three fundamental prescriptions: (1) the Born–Oppenheimer approximation, (2) the harmonic-oscillator model, and (3) the rigid-rotor assumption.

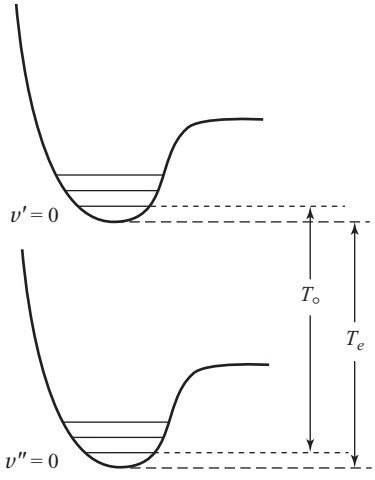

Figure 8.1 Relation between $T_\circ$ and T_e for ground and upper electronic states.

8.3 The Molecular Internal Energy

If we focus on separated internal energy modes, we find from Eqs. (8.4) and (8.5) that

$$\varepsilon_{int} = \varepsilon_{el} + \varepsilon_{vib} + \varepsilon_{rot}, \tag{8.8}$$

so that, in wave number units (cm^{-1}),

$$\tilde{\varepsilon}_{int} = T_e + \left(v + \tfrac{1}{2}\right)\omega_e + F(J). \tag{8.9}$$

Now, despite the fact that the ground vibrational level prescribes nonzero energy, this energy level obviously represents the lowest possible molecular internal energy outside electronic or rotational contributions. On this basis, we find it convenient, especially when calculating thermodynamic properties, to place the zero of energy at the lowest vibrational level within the ground electronic state. To evaluate directly the internal energy in an upper electronic state, we may define a revised electronic energy gap, $T_\circ$, as portrayed in Fig. 8.1. Consequently, Eq. (8.9) can be rewritten as

$$\tilde{\varepsilon}_{int} = T_\circ + v\omega_e + F(J), \tag{8.10}$$

where we have dispensed with the ground vibrational energy in the upper electronic state, as this zero-point energy is immaterial given the definition of $T_\circ$.

Employing this revised zero of energy, we may conveniently simplify Fig. 8.1 by displaying the various internal energy levels without their Morse potentials, as shown in Fig. 8.2. Here, we have indicated the energy levels for vibration and rotation within both the ground (X) and first excited (A) electronic states for a generic diatomic molecule. The revised electronic energy gap, $T_\circ$, which bridges the $v'' = 0$ and $v' = 0$ vibronic levels, is also shown for clarity in Fig. 8.2. The vibrational energy gap, $\Delta\varepsilon_{vib}$, is invariant for the harmonic oscillator, but actually decreases at higher vibrational levels for the anharmonic oscillator. In contrast, the rotational energy gap, $\Delta\varepsilon_{rot}$, always rises with increasing rotational quantum number. For visualization purposes, energy-level diagrams are quite

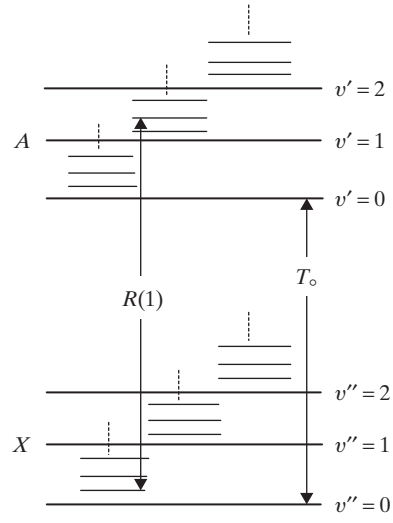

Figure 8.2 Vibrational and rotational levels in the A and X states.

convenient for displaying molecular internal energies, as enumerated via Eq. (8.10). Such diagrams are also helpful when portraying specific rovibronic lines in the spectrum, as exemplified for the $R(1)$ transition in Fig. 8.2. Finally, we note that

$$\Delta\varepsilon_{rot} < \Delta\varepsilon_{vib} < \Delta\varepsilon_{el};$$

in other words, the energy gap for the vibrational mode is less than that for the electronic mode but greater than that for the rotational mode. This result is, of course, consistent with the characteristic temperatures for the internal energy modes, as discussed in Section 8.1.

8.4 The Partition Function and Thermodynamic Properties

Separation of energy modes plays an important role not only in the evaluation of microscopic properties, but also in the evaluation of macroscopic properties. Recall from Chapter 4 that all thermodynamic properties in the dilute limit are related to the natural logarithm of the partition function. This observation is very significant because it ultimately testifies that such properties can be evaluated by simply adding the separate contributions arising from each independent energy mode. Consider, for example, the usual separation between the translational and internal energy modes, as indicated by Eq. (8.3). For this case, the partition function becomes

$$Z = \sum_j g_j e^{-\varepsilon_j/kT} = \sum_{k,l} g_{tr,k} g_{int,l} \exp\left[-\frac{\varepsilon_{tr,k} + \varepsilon_{int,l}}{kT}\right],$$

so that

$$Z = \left\{\sum_k g_{tr,k} e^{-\varepsilon_{tr,k}/kT}\right\}\left\{\sum_l g_{int,l} e^{-\varepsilon_{int,l}/kT}\right\} = Z_{tr} Z_{int}.$$

More generally, for the four independent energy modes of any diatomic molecule, we obtain

$$Z = Z_{tr} Z_{rot} Z_{vib} Z_{el} \tag{8.11}$$

$$\ln Z = \ln Z_{tr} + \ln Z_{rot} + \ln Z_{vib} + \ln Z_{el}, \tag{8.12}$$

so that the partition function is multiplicative and its logarithm is, of course, additive.

Because all thermodynamic properties in the dilute limit can be expressed in terms of $\ln Z$, Eq. (8.12) implies that such properties are also additive over the available energy modes. As an example, substituting Eq. (8.12) into Eq. (4.36), we obtain, for the specific internal energy,

$$\frac{u}{RT} = T\left(\frac{\partial \ln Z_{tr}}{\partial T}\right)_V + T\left(\frac{\partial \ln Z_{rot}}{\partial T}\right)_V + T\left(\frac{\partial \ln Z_{vib}}{\partial T}\right)_V + T\left(\frac{\partial \ln Z_{el}}{\partial T}\right)_V.$$

For the specific entropy, on the other hand, we have from Eq. (4.40)

$$\frac{s}{R} = \left(\frac{s}{R}\right)_{tr} + \left(\frac{s}{R}\right)_{rot} + \left(\frac{s}{R}\right)_{vib} + \left(\frac{s}{R}\right)_{el}, \tag{8.13}$$

where

$$\left(\frac{s}{R}\right)_{tr} = T\left(\frac{\partial \ln Z_{tr}}{\partial T}\right)_V + \ln\left(\frac{Z_{tr}}{N}\right) + 1 \tag{8.14}$$

for the translational energy mode and

$$\left(\frac{s}{R}\right)_{int} = T\left(\frac{\partial \ln Z_{int}}{\partial T}\right)_V + \ln Z_{int} \tag{8.15}$$

for each of the internal energy modes. Comparing Eqs. (8.14) and (8.15), we note that all terms independent of Z are incorporated with the translational contribution. Because these terms must be counted only once, they are included with the most easily excited mode and thus omitted from all internal modes. The same procedure must, of course, be invoked for all remaining thermodynamic properties. Given Eqs. (4.36–4.42), you should thus recognize that $h_{int} = u_{int}$, $g_{int} = a_{int}$, and $c_{p,int} = c_{v,int}$.

Separation of energy modes also facilitates probability calculations associated with statistical thermodynamics. If, for example, we wish to determine the probability of being in a specific rotational, vibrational, and electronic energy level, we obtain from Eqs. (4.14) and (8.8)

$$P_{rot,vib,el} = \frac{N_{rot,vib,el}}{N} = \frac{g_{rot} g_{vib} g_{el}}{Z_{rot} Z_{vib} Z_{el}} \exp\left[-\frac{\varepsilon_{rot} + \varepsilon_{vib} + \varepsilon_{el}}{kT}\right],$$

where the partition function and degeneracy can both be factored into their components,

$$Z_{int} = Z_{rot} Z_{vib} Z_{el} \qquad g_{int} = g_{rot} g_{vib} g_{el},$$

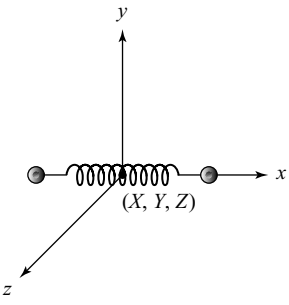

Figure 8.3 Coordinates describing the motion and thus degrees of freedom for a diatomic molecule.

from Eqs. (8.7) and (8.11). If we now wish to evaluate the probability of being in a specific rotational energy level, regardless of the possible vibrational and electronic levels, we need only sum over all possible vibrational and electronic energy levels, thus obtaining

$$P_{rot} = \frac{N_{rot}}{N} = \sum_{vib}\sum_{el} \frac{g_{rot}g_{vib}g_{el}}{Z_{rot}Z_{vib}Z_{el}} \exp\left[-\frac{\varepsilon_{rot}+\varepsilon_{vib}+\varepsilon_{el}}{kT}\right] = \frac{g_{rot}}{Z_{rot}} e^{-\varepsilon_{rot}/kT},$$

as

$$Z_{vib} = \sum_{vib} g_{vib}\, e^{-\varepsilon_{vib}/kT} \qquad Z_{el} = \sum_{el} g_{el}\, e^{-\varepsilon_{el}/kT}.$$

Therefore, for independent energy modes, the Boltzmann distribution may be applied in the same fashion to any single mode as well as to any group of such energy modes.

8.5 Energy-Mode Contributions in Classical Mechanics

In preparation for statistical thermodynamic calculations, we now consider classical contributions from various energy modes to the macroscopic internal energy and heat capacity. Our eventual goal is to compare classic and quantum allocations from each of the translational, rotational, and vibrational modes. We begin by recognizing that, from a classical perspective, each atom of a molecule can be characterized by three position coordinates. Consequently, for a molecule composed of n atoms, the temporal motion of the entire molecule requires $3n$ position coordinates. We thus say that the molecule has $3n$ *degrees of freedom*. Consider, for example, the diatomic molecule of Fig. 8.3, which must have six degrees of freedom. Based on our discussion in Chapter 6, these six degrees of freedom can be distributed in the following way. First, three degrees of freedom are needed to describe translation of the molecule's center of mass (X, Y, Z). Second, two degrees of freedom are required to describe its rotation about two orthogonal axes (y, z) perpendicular to the internuclear axis. Third, one degree of freedom is necessary to describe vibration of the molecule along the internuclear axis (x). Consistent with this description, we recall that for a diatomic molecule the translational mode leads to three quantum numbers, the rotational mode can be described by two quantum numbers, and the vibrational mode mandates one quantum number. Hence, we see that each degree of freedom can be associated with a single quantum number, thus establishing a very robust link between classical and quantum mechanics.

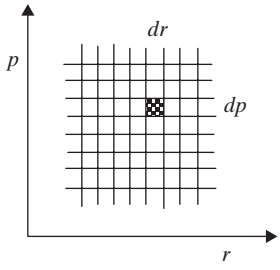

Figure 8.4 Phase-space diagram; each *dpdr* cell represents a different continuous value of energy.

8.5.1 The Phase Integral

To assess the contribution from each classic energy mode to the internal energy, u, or to the specific heat, c_v, we must develop a classical representation of the partition function. In pursuit of this goal, we introduce the concept of *phase space*, which provides the necessary link between quantum and classical mechanics. To this end, we recall that, for the one-dimensional harmonic oscillator, the Hamiltonian defining the total energy of a conservative system is given by

$$H(p, r) = \frac{p^2}{2\mu} + \frac{1}{2}k_0 r^2, \tag{8.16}$$

where p and r are the momentum and position, respectively. Now, Eq. (8.16) reflects an important result from classical mechanics, namely that each degree of freedom mandates a position and momentum coordinate (Appendix G). In fact, the central importance of momentum and position in classical mechanics is manifested by the *phase-space diagram*, as shown in Fig. 8.4. Because Eq. (8.16) signifies the Hamiltonian, we see that each cell of area $dpdr$ in phase space can be taken as representing a single classical value of continuous energy. Therefore, we may assert that the number of quantum states within a single cell in phase space must be the classical analog to the degeneracy.

The correspondence principle indicates that classical solutions must be replicated by quantum mechanics in the limit of continuous energies, i.e., when $\Delta\varepsilon \ll kT$. Therefore, for a single degree of freedom, the classical version of the partition function should become

$$Z = \sum_j g_j e^{-\varepsilon_j/kT} \simeq \int e^{-\varepsilon/kT} dg = \int e^{-H(p,r)/kT} dg, \tag{8.17}$$

where dg represents the degeneracy for one degree of freedom in the energy range, ε to $\varepsilon + d\varepsilon$. Because classical energy can always be portrayed within phase space, we presume that the classical counterpart to the differential degeneracy for one momentum and position coordinate can be expressed as

$$dg = C\, dp\, dr, \tag{8.18}$$

where the constant, C, must be chosen to ensure that the classical and quantum results agree at the classical limit. Substituting Eq. (8.18) into Eq. (8.17), we thus obtain per degree of freedom

$$Z = C\varphi = C \iint e^{-H(p,r)/kT} dp\, dr, \tag{8.19}$$

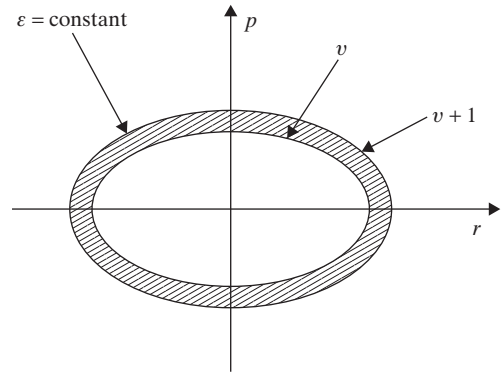

Figure 8.5 Area in phase space representing a single quantum state for the harmonic oscillator.

where the integration is carried out over all phase space, so that φ is known as the *phase integral*.

Equation (8.19) is highly significant as it relates the partition function, which implies quantum mechanics, to the phase integral, which implies classical mechanics. More importantly, while a definite point in phase space is permitted by classical mechanics, the same is not true of quantum mechanics owing to the uncertainty principle. On this basis, the value of C establishes a statistical mechanical adumbration of the correspondence principle. In particular, we note from Eq. (8.18) that C can be interpreted as the number of quantum states per area in phase space. As a result, the inverse of C must be the area in phase space corresponding to a single quantum state.

Given the above rationale, we now evaluate C by introducing a phase-space representation of the classic harmonic oscillator. From Eq. (8.16), curves of constant vibrational energy in phase space can be expressed as

$$\frac{p^2}{\alpha^2} + \frac{r^2}{\beta^2} = 1,$$

where $\alpha^2 = 2\mu\varepsilon$ and $\beta^2 = 2\varepsilon/k_0$. Therefore, for the harmonic oscillator, we find that all combinations of momentum and position giving the same total energy define an ellipse in phase space. The area circumscribed by this ellipse is given by

$$A = \pi\alpha\beta = 2\pi\varepsilon\sqrt{\mu/k_0} = \varepsilon/\nu, \tag{8.20}$$

where Eq. (6.42) has been used to express Eq. (8.20) in terms of the fundamental vibrational frequency, ν. Because the inverse of C is the area in phase space corresponding to one quantum state, we may evaluate C by determining the difference in phase-space area for two successive vibrational quantum numbers, as this incremental area identifies a single quantum state for the harmonic oscillator. Utilizing Fig. 8.5, we can determine the appropriate difference in phase-space area by substituting Eq. (6.49) into Eq. (8.20):

$$A(v+1) - A(v) = \frac{\left(v + \frac{3}{2}\right)h\nu - \left(v + \frac{1}{2}\right)h\nu}{\nu} = h.$$

Remarkably, we find that Planck's constant can be uniquely interpreted as the area in phase space corresponding to a single quantum state!

By exploiting the phase-space representation for a classic harmonic oscillator, as portrayed in Fig. 8.5, we have shown that $C = h^{-1}$. Given the magnitude of Planck's constant, we immediately recognize that the number of quantum states per area of phase space is overwhelmingly gigantic. More significantly, we find that Eq. (8.19) becomes

$$Z = \frac{1}{h} \iint e^{-H(p,r)/kT} dp\, dr \tag{8.21}$$

for a single degree of freedom. Consequently, for n degrees of freedom, the partition function can be related to the phase integral through

$$Z = \frac{\varphi}{h^n}\,, \tag{8.22}$$

where the phase integral itself can be expressed compactly as

$$\varphi = \underset{n}{\iint} e^{-H(\boldsymbol{p},\boldsymbol{r})/kT} d^n p\, d^n r. \tag{8.23}$$

As an example, for a Cartesian coordinate system having three degrees of freedom, Eq. (8.23) becomes

$$\varphi = \int_{-\infty}^{\infty}\int_{-\infty}^{\infty}\int_{-\infty}^{\infty}\int_{-\infty}^{\infty}\int_{-\infty}^{\infty}\int_{-\infty}^{\infty} e^{-H(\boldsymbol{p},\boldsymbol{r})/kT} dp_x\, dp_y\, dp_z\, dx\, dy\, dz,$$

where $H(\boldsymbol{p}, \boldsymbol{r})$ has been cast in terms of the generalized momentum and position vectors, $\boldsymbol{p}$ and $\boldsymbol{r}$, thus indicating a potential dependence on all three momentum and position coordinates.

8.5.2 The Equipartition Principle

Having defined the phase integral, we are now prepared to evaluate the classical contributions to u and c_v from the translational, rotational, and vibrational energy modes. As discussed in Chapter 9, the electronic mode cannot be considered as its input always requires the application of quantum mechanics. In general, the contribution from each classical energy mode is prescribed by the *equipartition principle*, which can be stated as follows.

> Each independent pure quadratic momentum or position term in the classical energy of a particle contributes $RT/2$ ($R/2$) to the thermodynamic internal energy (heat capacity) per mole.

To prove this principle, we again make use of the harmonic oscillator. For this case, Eq. (8.16) shows that the pure quadratic momentum term is $p^2/2\mu$ while the pure quadratic position term is $k_0 r^2/2$. Therefore, to determine allocations to u or c_v from such pure quadratic terms, we need only substitute Eq. (8.16) into Eq. (8.21). The result for a single degree of freedom is

$$Z = \frac{1}{h}\int_{-\infty}^{\infty}\int_{-\infty}^{\infty} \exp\left[-\frac{p^2}{2\mu kT} - \frac{k_0 r^2}{2kT}\right] dp\, dr = \frac{1}{h}\sqrt{2\pi\mu kT}\cdot\sqrt{2\pi kT/k_0},$$

where we have conveniently separated the contributions to the partition function from the independent momentum and position terms.

Table 8.2 *Classical contributions from the translational, rotational, and vibrational energy modes to the internal energy and heat capacity for a diatomic molecule (see Fig. 8.3)*

Contribution	Translation	Rotation	Vibration	Total
Classical energy	$\frac{1}{2m}\left(p_X^2 + p_Y^2 + p_Z^2\right)$	$\frac{1}{2I}\left(L_y^2 + L_z^2\right)$	$\frac{p_x^2}{2\mu} + \frac{k_0 x^2}{2}$	–
Degrees of freedom	3	2	1	6
Internal energy (u)	$\frac{3}{2}RT$	RT	RT	$\frac{7}{2}RT$
Heat capacity (c_v)	$\frac{3}{2}R$	R	R	$\frac{7}{2}R$

On this basis, whether derived from a pure quadratic momentum or position term, the universal contribution to the partition function in either case is given by

$$\ln Z = \frac{1}{2}\ln T + \text{constant}.$$

Hence, from Eq. (4.36), the allocation to the internal energy from either pure quadratic term is

$$\frac{u}{RT} = T\left(\frac{\partial \ln Z}{\partial T}\right)_V = \frac{1}{2}.$$

Similarly, from Eq. (4.41), the contribution to the heat capacity from either term must be

$$\frac{c_v}{R} = \left[\frac{\partial}{\partial T}T^2\left(\frac{\partial \ln Z}{\partial T}\right)\right]_V = \frac{1}{2}.$$

Therefore, at thermodynamic equilibrium, we have shown that any pure quadratic term contributes $RT/2$ to the internal energy per mole and $R/2$ to the heat capacity per mole. This conclusion is clearly unaffected by whether the pure quadratic term is based on momentum or position; thus, we have verified the classical equipartition principle.

8.5.3 Mode Contributions

By invoking the equipartition principle, we can determine the internal energy and heat capacity for a classic diatomic molecule, as summarized in Table 8.2. The translational mode is characterized by three pure quadratic momentum terms, one for each translational degree of freedom. Similarly, the rotational mode has two degrees of freedom, corresponding to two pure quadratic momentum terms. In comparison, the vibrational mode possesses a single degree of freedom, but two independent quadratic terms, one based on momentum and the other based on position. The additional quadratic term for vibration arises from its potential energy, which is totally missing from both the translational and rotational modes. In summary, the classical energy for a diatomic molecule displays seven pure quadratic terms; the implication is an internal energy and heat capacity per mole of $3.5RT$ and $3.5R$, respectively, as distributed among the three classical energy modes in Table 8.2. For a monatomic gas, comparatively, we have only three pure quadratic

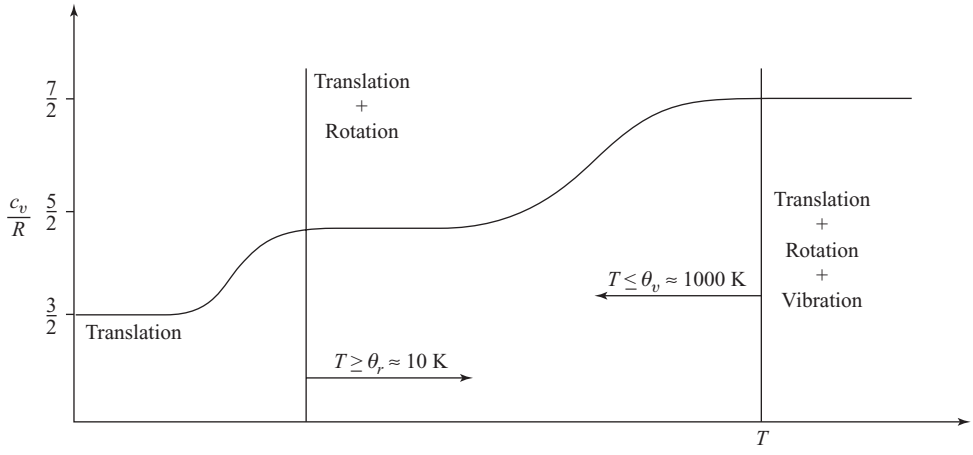

Figure 8.6 Influence of temperature on the specific heat of a typical diatomic molecule. The translational mode is fully excited at low temperatures, the rotational mode becomes fully excited at intermediate temperatures, and the vibrational mode becomes fully excited at the highest temperatures.

translational contributions, so that we would expect the internal energy per mole to be $1.5RT$ and the heat capacity per mole to be $1.5R$.

As we will see in the next chapter, classical predictions for internal energy and specific heat agree very well with quantum predictions for monatomic gases; however, the agreement is usually quite poor for diatomic gases, except at temperatures approaching 1000–2000 K. This behavior can be understood by taking into consideration the characteristic mode temperatures of Section 8.1. In particular, we recall that the translational and rotational modes have characteristic temperatures much less than 300 K, while the characteristic temperature for the vibrational mode is ordinarily much greater than 300 K. Therefore, the translational and rotational modes become *fully excited*, thus matching their classical contributions, at room temperature, while the vibrational mode approaches full excitation only at much higher temperatures. On this basis, we would expect the diatomic internal energy and heat capacity per mole to be $2.5RT$ and $2.5R$, respectively, near room temperature. More generally, the influence of temperature on specific heat for a diatomic molecule follows the behavior displayed in Fig. 8.6. Each plateau signals full excitation of an energy mode with rising temperature: first for the translational mode, then for the rotational mode, and finally for the vibrational mode. This fascinating behavior clearly reflects the importance of quantum mechanics, thus providing further motivation for our continued study of statistical thermodynamics, especially when applied to gaseous systems strongly influenced by vibrational and electronic motion.

Problems enhancing your understanding of this chapter are combined with those for Chapter 9 in Problem Set IV.

9 Thermodynamic Properties of the Ideal Gas

To this point, our study of statistical thermodynamics has provided a methodology for determining the most probable macrostate when considering an isolated system of independent particles. The most probable macrostate, in turn, has spawned mathematical definitions for both the internal energy and entropy in the dilute limit, thus producing general analytical expressions for all intensive thermodynamic properties of the ideal gas, as discussed in Chapter 4. These properties are inherently expressed in terms of the partition function, which mandates information on those energy levels and degeneracies associated with a particular atom or molecule. Obtaining such data has provided the rationale for our study of quantum mechanics and spectroscopy. Now that we have access to the necessary spectroscopic information, we are finally prepared to calculate the properties of the ideal gas. We begin, for simplicity, with the monatomic gas, which requires only knowledge connected with the translational and electronic energy modes. We then move on to the diatomic gas, which demands additional information based on the rotational and vibrational energy modes. Finally, we consider the polyatomic gas, which thus far has received little attention in our deliberations related to either statistical thermodynamics or quantum mechanics.

9.1 The Monatomic Gas

Typical monatomic gases include the noble gases, such as He and Ar, and elemental radicals, such as atomic oxygen and nitrogen. For such gases, rotation and vibration are irrelevant; thus, we need only consider the translational and electronic energy modes. Based on its extremely low characteristic temperature, the translational mode will produce thermodynamic properties that comport well with the expectations of classical mechanics. Contributions from the electronic mode, however, must build more directly on our knowledge of quantum mechanics and spectroscopy. For both modes, the entrée to property calculations rests, as expected, with their explicit linkages to the molecular partition function.

9.1.1 Translational Mode

In Section 5.7, we applied quantum mechanics to the particle in a box. The salient result, from Eq. (5.58), is an expression for the translational energy of a single gaseous

atom, namely,

$$\varepsilon_{tr} = \frac{h^2}{8mV^{2/3}}\left(n_1^2 + n_2^2 + n_3^2\right),$$

where the three spatial quantum numbers, n_1, n_2, and n_3, can each take on any value from unity to infinity. As discussed in Section 8.4, the contribution to thermodynamic properties from any independent energy mode can be ascertained by first determining its contribution to the partition function. For the translational mode, the partition function can be evaluated most directly by summing over states rather than over levels. On this basis, we obtain from Eq. (4.13)

$$Z_{tr} = \sum_{n_1=1}^{\infty}\sum_{n_2=1}^{\infty}\sum_{n_3=1}^{\infty}\exp\left[-\frac{h^2}{8mV^{2/3}kT}\left(n_1^2 + n_2^2 + n_3^2\right)\right],$$

thus giving for the translational partition function,

$$Z_{tr} = \left\{\sum_{n=1}^{\infty}\exp\left(-\frac{\theta_t n^2}{T}\right)\right\}^3, \tag{9.1}$$

where, from Eq. (8.2), we have introduced the characteristic translational temperature,

$$\theta_t = \frac{h^2}{8mkV^{2/3}}. \tag{9.2}$$

We note that the summation of Eq. (9.1) is identical for the three translational quantum numbers. Moreover, by summing over all possible values from unity to infinity, we are indeed accounting for each quantum state, as identified by its unique set of translational quantum numbers.

From Section 8.1, we recall that $\theta_t \approx 10^{-16}$ K; thus, for any realistic assembly temperature, the summation in Eq. (9.1) can be converted to an equivalent integration (Appendix D.3). In other words, because of the incredibly minute separation between consecutive translational levels, we may assume a continuous distribution of translational energies, as might be expected from classical mechanics. Consequently, from Appendix B, Eq. (9.1) becomes

$$Z_{tr} = \left\{\int_0^{\infty}\exp\left(-\frac{\theta_t n^2}{T}\right)dn\right\}^3 = \left\{\frac{1}{2}\sqrt{\frac{\pi T}{\theta_t}}\right\}^3, \tag{9.3}$$

so that, substituting Eq. (9.2) into Eq. (9.3), we obtain

$$Z_{tr} = \left(\frac{2\pi mkT}{h^2}\right)^{3/2} V. \tag{9.4}$$

The *translational partition function*, as defined by Eq. (9.4), can also be derived (Problem 4.2) by either (1) summing over energy levels using the density of states of Eq. (5.61) or (2) evaluating the phase integral, as given by Eq. (8.23). These alternatives, especially that invoking the phase integral, bespeak gargantuan numbers of energy levels separated by miniscule energy gaps, so that we can easily replace discrete with continuous energies. For this reason, quantum mechanics is actually unnecessary for the translational energy mode; hence, the equipartition principle is perfectly suitable for calculating translational contributions to thermodynamic properties.

Because the characteristic temperature for the translational mode is so much smaller than that for the various internal energy modes, the total number of quantum states for an atom or molecule is essentially equivalent to that for the translational mode. Therefore, our previous *criterion for the dilute limit*, as specified by Eq. (4.18), can be expressed as

$$\frac{Z}{N} \simeq \frac{Z_{tr}}{N} = \left(\frac{2\pi mkT}{h^2}\right)^{3/2} \left(\frac{V}{N}\right) \gg 1. \tag{9.5}$$

For an ideal gas at its standard temperature and pressure of 298.15 K and 1 bar, Eq. (9.5) typically gives $Z_{tr}/N \simeq 10^5$, which certainly supports the dilute limit. We note, however, that according to this revised criterion, dilute conditions may not exist at low temperatures or high densities, especially for particles with nearly zero mass.

Employing the translational partition function, we may now evaluate the contributions of the translational mode to the thermodynamic properties of an ideal gas. Considering, for example, the internal energy, we have from Eqs. (4.36) and (9.4)

$$\left(\frac{u}{RT}\right)_{tr} = T\left(\frac{\partial \ln Z_{tr}}{\partial T}\right)_V = \frac{3}{2}. \tag{9.6}$$

Similarly, for the specific heat at constant volume, we have from Eq. (4.41)

$$\left(\frac{c_v}{R}\right)_{tr} = \left[\frac{\partial}{\partial T} T^2 \left(\frac{\partial \ln Z_{tr}}{\partial T}\right)\right]_V = \frac{3}{2}. \tag{9.7}$$

Therefore, the translational contribution to the internal energy per mole is $1.5RT$ and that to the heat capacity per mole is $1.5R$, which is in perfect accord with our expectations from the equipartition principle. Substituting Eqs. (9.6) and (9.7) into Eqs. (4.37) and (4.42), respectively, we also find that the translational contributions to the specific enthalpy and specific heat at constant pressure are as follows:

$$\left(\frac{h}{RT}\right)_{tr} = \frac{5}{2} \qquad \left(\frac{c_p}{R}\right)_{tr} = \frac{5}{2}.$$

At this point, the pressure can be easily determined by combining aspects of classical and statistical thermodynamics. In particular, the pressure can be expressed classically (Appendix F) as

$$-P = \left(\frac{\partial A}{\partial V}\right)_{T,N}, \tag{9.8}$$

while the Helmholtz free energy, from Eq. (4.28), is

$$A = -NkT\left[\ln\left(\frac{Z}{N}\right) + 1\right].$$

Recalling that $Z = Z(T, V)$, we thus obtain the general relation

$$P = NkT\left(\frac{\partial \ln Z}{\partial V}\right)_T. \tag{9.9}$$

Applying Eq. (9.9) to the translational mode, we then obtain, by substitution from Eq. (9.4),

$$PV = NkT, \tag{9.10}$$

which is, of course, the equation of state for an ideal gas. The obvious implication here is that pressure arises solely from the translational mode, as surely expected from the momentum exchange occurring at all walls for vessels containing independent gaseous particles. On this basis, the partition function for each internal energy mode must depend solely on temperature, as verified for all such modes later in this chapter.

Finally, for the entropy, we find from Eqs. (4.40) and (9.4) that

$$\left(\frac{s}{R}\right)_{tr} = \frac{3}{2}\ln\left(\frac{2\pi mkT}{h^2}\right) + \ln\left(\frac{V}{N}\right) + \frac{5}{2},$$

which becomes, after substitution from Eq. (9.10),

$$\left(\frac{s}{R}\right)_{tr} = \ln\left[\frac{(2\pi m)^{3/2}(kT)^{5/2}}{h^3 P}\right] + \frac{5}{2}. \tag{9.11}$$

Presuming proper evaluation (Problem 4.1), Eq. (9.11) can be converted to the famous *Sackur–Tetrode equation* for translational entropy:

$$\left(\frac{s}{R}\right)_{tr} = \frac{5}{2}\ln T + \frac{3}{2}\ln M - \ln P - 1.1516, \tag{9.12}$$

where T is the temperature (K), M is the molecular weight (kg/kmol), and P is the pressure (bar). Based on Eq. (9.5), the Sackur–Tetrode equation, which holds only in the dilute limit, is obviously inappropriate for temperatures approaching absolute zero. Hence, the fact that Eq. (9.12) gives an entropy value of negative infinity at $T = 0$ should not be considered problematic.

EXAMPLE 9.1

Determine the contribution to the Helmholtz free energy (kJ/mole) from the translational energy mode at 500 K and 2 bars for monatomic helium.

Solution

From Eq. (4.38), the translational contribution to the Helmholtz free energy for an ideal gas is

$$\left(\frac{a}{RT}\right)_{tr} = -\left[\ln\left(\frac{Z_{tr}}{N}\right) + 1\right].$$

Employing Eqs. (9.4) and (9.10), we find that

$$\frac{Z_{tr}}{N} = \left(\frac{2\pi mkT}{h^2}\right)^{3/2}\left(\frac{kT}{P}\right).$$

Substituting for the given conditions and for appropriate fundamental constants, we obtain

$$\begin{aligned}\frac{Z_{tr}}{N} &= (2\pi m)^{3/2}\frac{(kT)^{5/2}}{h^3 P} \\ &= [2\pi(4.0026)(1.6605\times10^{-27})]^{3/2}\left\{\frac{[(1.3807\times10^{-23})(500)]^{5/2}}{(6.6261\times10^{-34})^3(2\times10^5)}\right\},\end{aligned}$$

from which we calculate $Z_{tr}/N = 5.808 \times 10^5$. On the other hand, because this rather cumbersome expression has already been simplified via Problem 4.1, we could also find the same answer more quickly from

$$\frac{Z_{tr}}{N} = 0.02595 \frac{T^{5/2} M^{3/2}}{P},$$

where M is the molecular weight and P is the pressure in bars. In either case, we now have

$$\left(\frac{a}{RT}\right)_{tr} = -\left[\ln\left(\frac{Z_{tr}}{N}\right) + 1\right] = -(13.272 + 1.000) = -14.272.$$

Evaluating the Hemholtz free energy, we thus obtain, for the translational mode,

$$a_{tr} = -14.272(8.3145 \text{ J/K} \cdot \text{mol})(500 \text{ K}) = -58.333 \text{ kJ/mol}.$$

9.1.2 Electronic Mode

The contribution to the partition function from the electronic energy mode requires a direct summation based on relevant term symbols and energy levels (cm^{-1}), as tabulated for selected species in Appendix J. In most cases, only the first few electronic levels need be considered because of the improbability of populating highly excited levels at typical temperatures. Nevertheless, an appropriate cutoff criterion must be established on a case-by-case basis, especially at higher temperatures. Consider, for example, data for the first three electronic levels of gaseous aluminum, as listed in Table 9.1. For this case, we would normally require only the first two levels when calculating the partition function because of the huge gap in energy between the second and third levels. Hence, from Eq. (4.12), the partition function evaluated at 1000 K would become

$$Z_{el} = g_0 + g_1 e^{-\varepsilon_1/kT} = 2 + 4 \exp\left[-\frac{(1.4387 \text{ cm} \cdot \text{K})(112.1 \text{ cm}^{-1})}{1000 \text{ K}}\right] = 5.4042.$$

Now, from Chapter 4, we recall that the contribution from any energy mode to properties such as the internal energy and heat capacity is based on the evaluation of two standard partial derivatives of the partition function with respect to temperature, namely,

$$T\left(\frac{\partial \ln Z}{\partial T}\right)_V \qquad \left[\frac{\partial}{\partial T} T^2 \left(\frac{\partial \ln Z}{\partial T}\right)\right]_V.$$

Unfortunately, for the electronic case, contributions to these two expressions can be derived only via term-by-term differentiation of Z_{el}. The salient results, following much

Table 9.1 *Electronic data for atomic aluminum*

Term symbol	T_e (cm^{-1})
$^2P_{1/2}$	0
$^2P_{3/2}$	112.1
$^2S_{1/2}$	25,347.8

algebra, are as follows:

$$T\left(\frac{\partial \ln Z_{el}}{\partial T}\right)_V = \frac{Z'_{el}}{Z_{el}} \tag{9.13}$$

$$\left[\frac{\partial}{\partial T}T^2\left(\frac{\partial \ln Z_{el}}{\partial T}\right)\right]_V = \frac{Z''_{el}}{Z_{el}} - \left(\frac{Z'_{el}}{Z_{el}}\right)^2, \tag{9.14}$$

where

$$Z_{el} = \sum_j g_j e^{-\varepsilon_j/kT} \tag{9.15}$$

$$Z'_{el} = \sum_j g_j\,(\varepsilon_j/kT)\,e^{-\varepsilon_j/kT} \tag{9.16}$$

$$Z''_{el} = \sum_j g_j\,(\varepsilon_j/kT)^2\,e^{-\varepsilon_j/kT}. \tag{9.17}$$

The immediately preceding expressions provide the requisite tools for evaluating electronic contributions to thermodynamic properties for any ideal monatomic gas. Given Eqs. (9.13) and (9.14), for example, we immediately recognize from Eqs. (4.36) and (4.41) that

$$\left(\frac{u}{RT}\right)_{el} = \left(\frac{h}{RT}\right)_{el} = \frac{Z'_{el}}{Z_{el}} \tag{9.18}$$

$$\left(\frac{c_v}{R}\right)_{el} = \left(\frac{c_p}{R}\right)_{el} = \frac{Z''_{el}}{Z_{el}} - \left(\frac{Z'_{el}}{Z_{el}}\right)^2. \tag{9.19}$$

Similarly, from Eq. (8.15), we obtain for the electronic contribution to the entropy,

$$\left(\frac{s}{R}\right)_{el} = \frac{Z'_{el}}{Z_{el}} + \ln Z_{el}. \tag{9.20}$$

EXAMPLE 9.2

Calculate the specific heat at constant volume (J/K · mol) for monatomic nitrogen at 3000 K.

Solution

From Eq. (9.7), the translational contribution to the specific heat at constant volume for any ideal gas is

$$\left(\frac{c_v}{R}\right)_{tr} = \frac{3}{2},$$

whereas the electronic contribution, from Eq. (9.19), is

$$\left(\frac{c_v}{R}\right)_{el} = \frac{Z''_{el}}{Z_{el}} - \left(\frac{Z'_{el}}{Z_{el}}\right)^2.$$

The electronic contribution to any thermodynamic property can be easily determined by setting up the following table, where from Eq. (8.1)

$$\frac{\varepsilon_j}{kT} = \frac{hc}{k}\left(\frac{\tilde{\varepsilon}_j}{T}\right) = (1.4387 \text{ cm-K})\,\frac{\tilde{\varepsilon}_j}{T}.$$

$\tilde{\varepsilon}_j(\text{cm}^{-1})$	g_j	ε_j/kT	$g_j e^{-\varepsilon_j/kT}$	$g_j(\varepsilon_j/kT)e^{-\varepsilon_j/kT}$	$g_j(\varepsilon_j/kT)^2 e^{-\varepsilon_j/kT}$
0	4	0	4	0	0
19,229	10	9.2216	9.8880×10^{-4}	9.1183×10^{-3}	8.4086×10^{-2}
28,839	6	13.830	5.9137×10^{-6}	8.1787×10^{-5}	1.1311×10^{-3}
			4.0010	9.2001×10^{-3}	8.5217×10^{-2}

Here, we consider the first three electronic energy levels of atomic nitrogen, based on the listed term symbols and energies of Appendix J.1. The energy corresponding to the fourth level is 83,322 cm^{-1}, which proves much too high to produce any further influence on thermodynamic properties at the given temperature of 3000 K. The final row of the table contains sums for the last three columns, which conveniently represent Z_{el}, Z'_{el}, and Z''_{el}, respectively. Employing the calculated data from this table, the electronic contribution to the specific heat at constant volume becomes

$$\left(\frac{c_v}{R}\right)_{el} = \frac{Z''_{el}}{Z_{el}} - \left(\frac{Z'_{el}}{Z_{el}}\right)^2 = \frac{8.5217 \times 10^{-2}}{4.0010} - \left(\frac{9.2001 \times 10^{-3}}{4.0010}\right)^2 = 0.02129.$$

Hence, summing the translational and electronic contributions, the dimensionless specific heat at constant volume for monatomic nitrogen at 3000 K is

$$\frac{c_v}{R} = \left(\frac{c_v}{R}\right)_{tr} + \left(\frac{c_v}{R}\right)_{el} = 1.5000 + 0.0213 = 1.5213,$$

so that

$$c_v = 1.5213R = 1.5213(8.3145 \text{ J/K} \cdot \text{mol}) = 12.649 \text{ J/K} \cdot \text{mol}.$$

9.2 The Diatomic Gas

Evaluation of thermodynamic properties for diatomic gases requires that we take into consideration the rotational and vibrational modes as well as the translational and electronic modes introduced during our earlier discussion of monatomic gases. For the diatomic case, complete mode separation necessitates the simplex model, i.e., the combined rigid rotor and harmonic oscillator. Using this model, property calculations are reasonably straightforward as we need only sum relevant contributions from each independent energy mode.

In particular, for any diatomic molecule, separate contributions from the rotational and vibrational modes are merely added to those previously demonstrated from the translational and electronic modes.

9.2.1 Translational and Electronic Modes

Translational and electronic contributions to the thermodynamic properties of a diatomic gas can be determined in the same manner as for the monatomic gas. However, the translational partition function must be based on a conversion to center-of-mass coordinates, so that

$$Z_{tr} = \left(\frac{2\pi mkT}{h^2}\right)^{3/2} V \qquad m = m_1 + m_2,$$

where the total mass now represents both nuclei of the chosen diatomic molecule. For the electronic mode, we observe that the upper energy levels of many diatomics tend to be substantially higher than the ground electronic level. Hence, from Eq. (9.15), the electronic partition function can often be approximated by

$$Z_{el} = \sum_j g_j e^{-\varepsilon_j/kT} \simeq g_0. \tag{9.21}$$

Care must be exercised, however, because notable exceptions, such as O_2 and NO, are inherently problematic even at modest assembly temperatures. Furthermore, any substantial electronic contribution demands adherence to a consistent zero of energy, as we discuss next before addressing the influence of rotational and vibrational modes on various thermodynamic properties.

9.2.2 The Zero of Energy

Recall from Section 8.3 that the zero of energy for a diatomic molecule can be set at either the minimum of the Morse potential defining the ground electronic state or at the ground vibrational level within this particular Morse potential. Another possibility is to set the zero of energy at the ground electronic state corresponding to those atoms produced by dissociation of the diatomic molecule. The latter requires that we define the *dissociation energy*, $D_\circ$, as well as the *binding energy*, D_e, as portrayed in Fig. 9.1. From this perspective, Table 9.2 lists the various possibilities for establishing the zero of energy and thus for defining the internal energy of any diatomic molecule. For each of the four possible cases, the vibrational and rotational energies are calculated based on mode parameters for the upper electronic state; however, if $T_\circ = 0$ or $T_e = 0$, the molecular internal energy must, of course, be defined by using only those parameters associated with the ground electronic state.

When evaluating thermodynamic properties for an assembly containing a pure ideal gas, the $T_\circ$-formulation having the zero of energy at the ground vibrational level within the ground electronic state is, by far, the most common choice. This preference derives from its conformance to spectroscopic measurements, which inherently monitor energy differences

Table 9.2 *Formulations defining the zero of energy and the internal energy for a diatomic molecule*

Formulation	Zero of energy	Internal molecular energy
$T_\circ$	Ground vibrational level within ground electronic state	$T_\circ + v\omega_e + F(J)$
T_e	Minimum of Morse potential for ground electronic state	$T_e + \left(v + \frac{1}{2}\right)\omega_e + F(J)$
$\mathrm{D}_\circ$	Ground electronic state of dissociated atoms	$T_\circ + v\omega_e + F(J) - \mathrm{D}_\circ$
D_e	Ground electronic state of dissociated atoms	$T_e + \left(v + \frac{1}{2}\right)\omega_e + F(J) - \mathrm{D}_e$

with respect to the ground vibronic level. Moreover, because the $T_\circ$-option is ubiquitous for the JANAF tables, comparative consistency demands that we follow this accepted custom. However, for an assembly containing a reactive mixture, the $\mathrm{D}_\circ$-formulation having the zero of energy at the ground electronic state of the dissociated atoms becomes mandatory, as we shall discover in Chapter 10.

We note, by the way, that the binding and dissociation energies are related through the zero-point vibrational energy within the ground electronic state, i.e.,

$$\mathrm{D}_e = \mathrm{D}_\circ + \tfrac{1}{2}\omega_e$$

when employing the harmonic-oscillator model. Nonetheless, Table 9.2 clearly indicates that the ground-state vibrational energy can be either included or excluded when choosing a zero of energy. While either is permissible, you must obviously be careful not to mix two different formulations when making thermodynamic calculations. In most cases, such problems can be avoided by simply sticking with the standard $T_\circ$-formulation established by those scientists and engineers who originally specified the thermodynamic procedures for the JANAF tables (Appendix E).

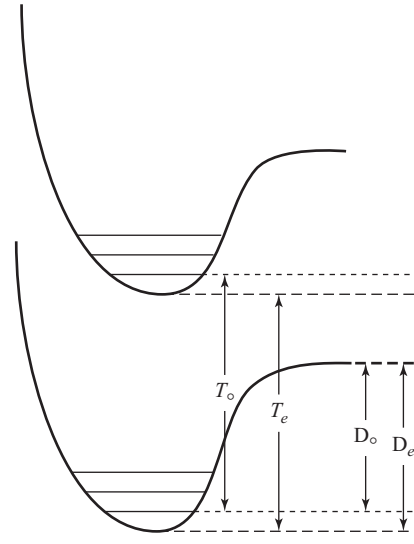

Figure 9.1 Parameters influencing the zero of energy for diatomic molecules.

9.2.3 Rotational Mode

From Table 8.1, the energy levels and degeneracies for the rigid rotor are given by

$$\tilde{\varepsilon}_{rot} = \frac{\varepsilon_{rot}}{hc} = J(J+1)B_e \qquad g_J = 2J+1$$

so that the rotational partition function becomes

$$Z_{rot} = \sum_J g_J e^{-\varepsilon_J/kT} = \sum_{J=0}^{\infty} (2J+1)\exp[-J(J+1)\theta_r/T]. \tag{9.22}$$

Here, the characteristic rotational temperature, from Eq. (8.2), is

$$\theta_r = \frac{hc}{k}B_e = \frac{h^2}{8\pi^2 k I_e}, \tag{9.23}$$

for which the moment of inertia $I_e = \mu r_e^2$. Unfortunately, for a homonuclear diatomic such as O_2 or N_2, we have inadvertently overcounted the number of available quantum states by a factor of two because of the inherent indistinguishability of the nuclear pair. This complication derives from symmetry requirements on the molecular wave function, as generated by the usual coupling between nuclear spin and orbital rotation. As a result, the partition function is restricted to only odd or even values of the rotational quantum number, a feature explored in considerably more detail in Section 9.2.4. For now, based on Eq. (9.22), we simply assert that the *rotational partition function* can be expressed more generally as

$$Z_{rot} = \frac{1}{\sigma}\sum_{J=0}^{\infty} (2J+1)\exp[-J(J+1)\theta_r/T], \tag{9.24}$$

where σ is a *symmetry factor*, which, by definition, takes values of unity for a heteronuclear and two for a homonuclear diatomic molecule.

Typically, $\theta_r < T$, so that Eq. (9.24) can be evaluated by using a standard Euler–Maclaurin expansion (Appendix D.3), thus giving (Problem 1.13)

$$Z_{rot} = \frac{T}{\sigma\theta_r}\left[1 + \frac{1}{3}\left(\frac{\theta_r}{T}\right) + \frac{1}{15}\left(\frac{\theta_r}{T}\right)^2 + \frac{4}{315}\left(\frac{\theta_r}{T}\right)^3 + \cdots\right]. \tag{9.25}$$

If, on the other hand, $\theta_r \ll T$, the summation in Eq. (9.24) can be converted to an integration, as for our evaluation of the translational partition function. The obvious result from Eq. (9.25) is

$$Z_{rot} = \frac{T}{\sigma\theta_r}. \tag{9.26}$$

Now, for nearly all diatomics, $\theta_r \simeq 2$ K, so that Eq. (9.26) is perfectly suitable for most computations. However, for molecules containing a hydrogen atom, such as HCl or OH, $\theta_r \simeq 15$ K; thus, for such cases, Eq. (9.25) becomes necessary. In contrast, direct summation via Eq. (9.24) remains a requirement for H_2, as here $\theta_r = 87.55$ K. The various scenarios are entirely consistent with Eq. (9.23), which implies a more rigorous procedure when calculating the rotational partition function for lighter molecules. In fact, based on Eq. (9.25), a cumulative error of less than 1% can be ensured when calculating Z_{rot} if we simply follow the protocol delineated by Table 9.3.

Table 9.3 *Protocol for evaluation of the rotational partition function*

Condition	Equation
$T/\theta_r \leq 3$	9.24
$3 < T/\theta_r \leq 30$	9.25
$T/\theta_r > 30$	9.26

As suggested previously, the most common scenario occurs when $T/\theta_r > 30$; here, Eq. (9.26) controls so that our two standard partial derivatives for the partition function with respect to temperature become

$$T\left(\frac{\partial \ln Z_{rot}}{\partial T}\right)_V = 1 \qquad \left[\frac{\partial}{\partial T}T^2\left(\frac{\partial \ln Z_{rot}}{\partial T}\right)\right]_V = 1.$$

Therefore, as for the translational mode, we again replicate the classical results predicted by the equipartition principle:

$$\left(\frac{u}{RT}\right)_{rot} = \left(\frac{h}{RT}\right)_{rot} = 1 \tag{9.27}$$

$$\left(\frac{c_v}{R}\right)_{rot} = \left(\frac{c_p}{R}\right)_{rot} = 1. \tag{9.28}$$

In addition, using Eq. (8.15), we obtain, for the rotational contribution to the entropy,

$$\left(\frac{s}{R}\right)_{rot} = 1 + \ln\left(\frac{T}{\sigma\theta_r}\right). \tag{9.29}$$

For heteronuclear diatomics containing atomic hydrogen, $3 < T/\theta_r \leq 30$, which implies utilization of Eq. (9.25); for this case, the rotational partition function can be expressed as

$$Z_{rot} = \frac{T}{\sigma\theta_r} Z_{rc},$$

where we have defined the rotational correction term,

$$Z_{rc} = 1 + \frac{1}{3}\left(\frac{\theta_r}{T}\right) + \frac{1}{15}\left(\frac{\theta_r}{T}\right)^2 + \frac{4}{315}\left(\frac{\theta_r}{T}\right)^3 + \cdots. \tag{9.30}$$

Evaluating our two standard partial derivatives, this time term-by-term, we find, after much algebraic manipulation,

$$T\left(\frac{\partial \ln Z_{rot}}{\partial T}\right)_V = 1 - \frac{Z'_{rc}}{Z_{rc}} \tag{9.31}$$

$$\left[\frac{\partial}{\partial T}T^2\left(\frac{\partial \ln Z_{rot}}{\partial T}\right)\right]_V = 1 + \frac{Z''_{rc} - Z'_{rc}}{Z_{rc}} - \left(\frac{Z'_{rc}}{Z_{rc}}\right)^2, \tag{9.32}$$

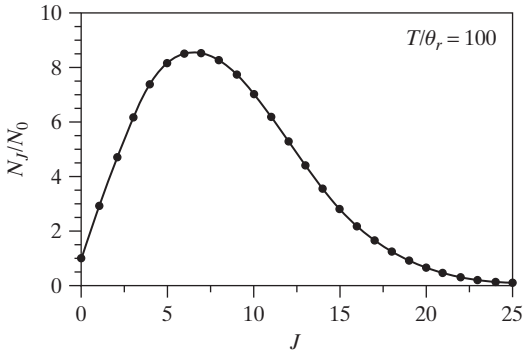

Figure 9.2 Population distribution for rotational energy mode.

where

$$Z'_{rc} = \frac{1}{3}\left(\frac{\theta_r}{T}\right) + \frac{2}{15}\left(\frac{\theta_r}{T}\right)^2 + \frac{12}{315}\left(\frac{\theta_r}{T}\right)^3 + \cdots \tag{9.33}$$

$$Z''_{rc} = \frac{1}{3}\left(\frac{\theta_r}{T}\right) + \frac{4}{15}\left(\frac{\theta_r}{T}\right)^2 + \frac{36}{315}\left(\frac{\theta_r}{T}\right)^3 + \cdots . \tag{9.34}$$

Hence, from Eqs. (9.31) and (9.32), we have for the rotational contributions to the internal energy, enthalpy, and specific heats

$$\left(\frac{u}{RT}\right)_{rot} = \left(\frac{h}{RT}\right)_{rot} = 1 - \frac{Z'_{rc}}{Z_{rc}} \tag{9.35}$$

$$\left(\frac{c_v}{R}\right)_{rot} = \left(\frac{c_p}{R}\right)_{rot} = 1 + \frac{Z''_{rc} - Z'_{rc}}{Z_{rc}} - \left(\frac{Z'_{rc}}{Z_{rc}}\right)^2 . \tag{9.36}$$

Similar expressions could be developed for all of the remaining thermodynamic properties, including the entropy, which is specifically considered in Example 9.3.

We close this section by delving into some unique features associated with the particle distribution over rotational energy levels. For simplicity, we consider a heteronuclear diatomic with a molecular distribution given, from Eq. (4.14), by

$$\frac{N_J}{N} = \frac{g_J e^{-\varepsilon_J/kT}}{Z_{rot}} = \frac{(2J+1)}{Z_{rot}} \exp\left[-\frac{J(J+1)\theta_r}{T}\right]. \tag{9.37}$$

Dividing Eq. (9.37) by its result at $J = 0$, we obtain

$$\frac{N_J}{N_0} = (2J+1) \exp\left[-\frac{J(J+1)\theta_r}{T}\right]. \tag{9.38}$$

This normalized distribution, displayed in Fig 9.2 for $T/\theta_r = 100$, accents the remarkable peak that typically arises at a rotational quantum number $J > 0$. Based on our discussion in Section 4.3.1, we would normally expect the population to peak at its ground level, with an exponentially decreasing population at higher levels. While this expectation is normally met, the rotational case demonstrates that a strongly increasing degeneracy with rising energy level can preferentially displace the maximum population away from its ground level, as shown in Fig. 9.2. A similar feature can also arise for atoms having low-lying electronic levels with degeneracies significantly greater than that for the ground electronic state. Assuming, for the moment, a continuous rather than a discrete distribution, we may

determine from Eq. (9.38) that value of the rotational quantum number corresponding to the peak in the rotational distribution, which becomes

$$J_{max} = \sqrt{\frac{T}{2\theta_r}} - \frac{1}{2}. \tag{9.39}$$

As we will discover in Chapter 11, identifying the population peak for the rotational distribution can be very important for many optical techniques used to determine the concentration or temperature in a gaseous mixture. In particular, the rotational peak usually offers the most intense signal in a rovibronic spectrum, and thus the best possible detection limit. This consideration is especially significant when contemplating pollutant measurements, for which concentrations typically occur at levels approaching a few parts per million (ppm).

EXAMPLE 9.3

Evaluate the rotational contribution to the entropy (J/K · mol) for HF at 300 K.

Solution

From Appendix K.1, we find that for HF the rotational constant $B_e = 20.956\ \text{cm}^{-1}$, so that the characteristic rotational temperature $\theta_r = (1.4387\ \text{cm} \cdot \text{K})\left(20.956\ \text{cm}^{-1}\right) = 30.1494\ \text{K}$. Therefore, at the given temperature of 300 K, $T/\theta_r = 9.9505$. From Table 9.3, we thus choose Eq. (9.25) and its related expressions to determine properly the rotational contribution to thermodynamic properties. In particular, from Eq. (8.15), the rotational contribution to the entropy is given by

$$\left(\frac{s}{R}\right)_{rot} = T\left(\frac{\partial \ln Z_{rot}}{\partial T}\right)_V + \ln Z_{rot},$$

where Z_{rot} must be obtained from Eq. (9.25) and the first-derivative term must be obtained from Eq. (9.31). On this basis, we first evaluate the rotational correction term via Eq. (9.30) and the first-derivative rotational correction term via Eq. (9.33):

$$\begin{aligned} Z_{rc} &= 1 + \frac{1}{3}\left(\frac{\theta_r}{T}\right) + \frac{1}{15}\left(\frac{\theta_r}{T}\right)^2 + \frac{4}{315}\left(\frac{\theta_r}{T}\right)^3 \\ &= 1 + 0.0335 + 0.0007 = 1.0342 \\ Z'_{rc} &= \frac{1}{3}\left(\frac{\theta_r}{T}\right) + \frac{2}{15}\left(\frac{\theta_r}{T}\right)^2 + \frac{12}{315}\left(\frac{\theta_r}{T}\right)^3 \\ &= 0.03350 + 0.00135 + 0.00004 = 0.03489. \end{aligned}$$

We now determine the rotational partition function from Eq. (9.25) and the required partial derivative from Eq. (9.31), thus obtaining

$$\begin{aligned} Z_{rot} &= \frac{T}{\sigma\theta_r} Z_{rc} = 9.9505\,(1.0342) = 10.2908 \\ T\left(\frac{\partial \ln Z_{rot}}{\partial T}\right)_V &= 1 - \frac{Z'_{rc}}{Z_{rc}} = 1 - \frac{0.03489}{1.0342} = 0.96626, \end{aligned}$$

where $\sigma = 1$ for a heteronuclear diatomic molecule. The dimensionless entropy now becomes

$$\left(\frac{s}{R}\right)_{rot} = T\left(\frac{\partial \ln Z_{rot}}{\partial T}\right)_V + \ln Z_{rot} = 0.96626 + \ln(10.2908) = 3.2976,$$

so that a final calculation gives for the rotational energy mode,

$$s_{rot} = 3.2976\,(8.3145\ \text{J/K} \cdot \text{mol}) = 27.418\ \text{J/K} \cdot \text{mol}.$$

9.2.4 Quantum Origin of Rotational Symmetry Factor

We now consider in some detail the rationale for the introduction of a symmetry factor when determining the rotational partition function of a homonuclear diatomic molecule. In short, the homonuclear issue arises owing to a combination of two factors: (1) the indistinguishability of the two identical nuclei and (2) the energy exchange that occurs owing to spin–orbit coupling. Recall from Section 5.9 that a virtual transposition of two indistinguishable particles cannot affect their joint probability density function. Therefore, the *total wave function* describing the two-particle system must be either symmetric or antisymmetric, i.e.,

$$\psi(\boldsymbol{r}_2, \boldsymbol{r}_1) = \pm\psi(\boldsymbol{r}_1, \boldsymbol{r}_2).$$

Consequently, a system composed of two identical bosons, which describe nuclei of even mass number, must display a symmetric wave function $(+)$. Similarly, as summarized in Table 5.1, a system composed of two identical fermions, which describe nuclei of odd mass number, must display an antisymmetric wave function $(-)$. Recall also, from Section 6.6.2, that any particle having both orbital and intrinsic spin generates an internal exchange of energy because of the induced magnetic field resulting from each angular momentum vector. For a diatomic molecule, this spin–orbit coupling arises because each nucleus spins about its own axis while simultaneously rotating about the molecule's center of mass.

Assuming mode separation, we may express the total wave function for a homonuclear diatomic molecule as

$$\psi = \psi_{tr}\psi_{rot}\psi_{vib}\psi_{el}\psi_{nuc}, \tag{9.40}$$

where we have now introduced a nuclear wave function to account for the spin associated with each of the identical nuclei. The translational wave function in Eq. (9.40) depends only on the center-of-mass coordinates and the vibrational wave function depends only on the distance between the two nuclei. Hence, these wave functions cannot influence the symmetry of the total wave function. For ease in our forthcoming analysis, we simply presume that the electronic wave function is symmetric with respect to nuclear exchange. In fact, the symmetric case represents, by far, the most common situation, although the antisymmetric case does occur and could easily be handled by inverting the logic of our upcoming arguments. Based on the above reasoning, we conclude from Eq. (9.40) that the symmetry of the total wave function, ψ, can be taken as identical to that for $\psi_{rot}\psi_{nuc}$. Therefore, for a homonuclear diatomic containing two identical bosons, $\psi_{rot}\psi_{nuc}$ must be symmetric; similarly, for a homonuclear diatomic containing two identical fermions, $\psi_{rot}\psi_{nuc}$ must be antisymmetric.

The nuclear wave function for a diatomic molecule can, of course, be either symmetric or antisymmetric. The number of symmetric wave functions is given by Bose–Einstein statistics, while the number of antisymmetric wave functions is given by Fermi–Dirac statistics. On this basis, given a nuclear degeneracy, g_n, the number of symmetric wave functions, from Eq. (2.31), is

$$M_{nuc}^{+} = \frac{(N + g_n - 1)!}{N!(g_n - 1)!} = \frac{(g_n + 1)!}{2(g_n - 1)!} = \frac{g_n(g_n + 1)}{2}, \tag{9.41}$$

since $N = 2$ for a homonculear diatomic. Similarly, from Eq. (2.30), the number of antisymmetric nuclear wave functions is given by

$$M_{nuc}^{-} = \frac{g_n!}{N!(g_n - N)!} = \frac{g_n!}{2(g_n - 2)!} = \frac{g_n(g_n - 1)}{2}. \tag{9.42}$$

We observe that g_n indicates the degeneracy corresponding to the nuclear ground state, as the enormous energy required for nuclear excitation precludes populating upper nuclear states at typical assembly temperatures. Hence, whether for bosons or fermions, the nuclear degeneracy represents the number of ground-state wave functions characterizing a single nucleus. In essence, the degeneracy occurs because of nuclear spin; indeed, as might be expected from Eq. (6.85), the nuclear degeneracy is $g_n = 2s_n + 1$, where s_n is the nuclear-spin quantum number.

The rotational wave function for a diatomic molecule was discussed at length in Section 6.3. An analysis of the resulting spherical harmonics shows that

$$\psi_{rot}(\pi - \theta, \phi + \pi) = (-1)^J \psi_{rot}(\theta, \phi);$$

hence, the rotational wave function must be symmetric for even values and antisymmetric for odd values of the rotational quantum number. Building on equivalent symmetry between the total wave function and $\psi_{rot}\psi_{nuc}$, we conclude that, if the total wave function is symmetric, the nuclear wave function must be symmetric for even J and antisymmetric for odd J. Similarly, if the total wave function is antisymmetric, the nuclear wave function must be antisymmetric for even J and symmetric for odd J. For our purposes, we invoke the latter, although the former leads to the same final result. If, therefore, ψ_{el} is symmetric and $\psi_{rot}\psi_{nuc}$ is antisymmetric, the combined rotational–nuclear partition function, Z_{rn}, arising from spin–orbit coupling becomes

$$Z_{rn} = \frac{g_n(g_n - 1)}{2} \sum_{J\,even}^{\infty} (2J + 1)\, e^{-J(J+1)\theta_r/T} + \frac{g_n(g_n + 1)}{2} \sum_{J\,odd}^{\infty} (2J + 1)\, e^{-J(J+1)\theta_r/T}.$$

Here, the first term combines an antisymmetric nuclear wave function with a symmetric rotational wave function while the second term combines a symmetric nuclear wave function with an antisymmetric rotational wave function, thus creating an antisymmetric total wave function. Constructing a symmetric total wave function, by the way, now becomes quite straightforward; we would merely exchange the nuclear wave functions between the first and second terms in the above expression for Z_{rn}.

Based on Section 9.2.3, the combined rotational–nuclear partition function can be simplified when $T/\theta_r > 30$ by converting the above summations to integrations, thus obtaining,

for either the symmetric or antisymmetric case,

$$Z_{rn} = \frac{g_n(g_n-1)}{2}\left[\frac{T}{2\theta_r}\right] + \frac{g_n(g_n+1)}{2}\left[\frac{T}{2\theta_r}\right] = g_n^2\left(\frac{T}{2\theta_r}\right). \tag{9.43}$$

The resulting statistical factor, g_n^2, represents the total number of nuclear quantum states associated with a homonuclear diatomic molecule. In other words, at higher temperatures, we have effectively uncoupled the rotational and nuclear partition functions for a diatomic molecule, so that, as expected, the total number of nuclear quantum states is just the square of the number of such states for each independent nucleus. Therefore, if we disavow nuclear reactions, we can safely ignore this factor, even during chemical reactions, because of atom conservation. In essence, by neglecting g_n^2 in Eq. (9.43), and thus Eq. (9.26), we have simply chosen to employ a zero of energy based on preservation of atomic particles, which is, of course, consistent with nearly all spectroscopic measurements.

In summary, the factor of two in the denominator of Eq. (9.43) arises from counting only even or odd values of the rotational quantum number, depending on the symmetry of the nuclear wave function. On this basis, only even or odd J-values should appear in Fig. 9.2 for a homonuclear diatomic molecule. Additionally, once having chosen to ignore g_n^2, we need only introduce a symmetry factor, $\sigma = 2$, into Eq. (9.24) to account for the quantum complications arising from homonuclear diatomics. This procedure, then, explains the existence of the symmetry factor that appears in all of the various expressions defining the rotational partition function.

9.2.5 Vibrational Mode

From Table 8.1, the energy levels and degeneracy for the harmonic oscillator are given by

$$G(v) = \left(v + \tfrac{1}{2}\right)\omega_e \qquad g_v = 1.$$

However, as discussed in Section 9.2.2, we normally place the zero of energy at the ground vibrational level within the ground electronic state so as to achieve consistency with the baseline used in developing the JANAF tables. Therefore, following Table 9.2, we must express the vibrational energy for the harmonic oscillator as

$$\tilde{\varepsilon}_{vib} = \frac{\varepsilon_{vib}}{hc} = v\omega_e, \tag{9.44}$$

so that the vibrational partition function becomes

$$Z_{vib} = \sum_v g_v e^{-\varepsilon_{vib}/kT} = \sum_{v=0}^{\infty} \exp[-\theta_v v/T], \tag{9.45}$$

where the characteristic vibrational temperature, from Eqs. (6.42) and (8.2), is

$$\theta_v = \frac{h\nu}{k} = \frac{h}{2\pi k}\sqrt{\frac{k_0}{\mu}}. \tag{9.46}$$

Typically, $\theta_v = 1000$–6000 K, so that we cannot employ an Euler–Maclaurin expansion as for the rotational energy mode. Fortunately, we may instead use the convergent

geometric series,

$$\sum_{n=0}^{\infty} x^n = (1-x)^{-1} \qquad |x| < 1;$$

thus, letting $x = \exp(-\theta_v/T)$, we obtain from Eq. (9.45) the *vibrational partition function*,

$$Z_{vib} = (1 - e^{-\theta_v/T})^{-1}. \tag{9.47}$$

Employing Eq. (9.47), our two standard partial derivatives for the partition function with respect to temperature become

$$T\left(\frac{\partial \ln Z_{vib}}{\partial T}\right)_V = \frac{\theta_v/T}{e^{\theta_v/T}-1}$$

$$\left[\frac{\partial}{\partial T}T^2\left(\frac{\partial \ln Z_{vib}}{\partial T}\right)\right]_V = \frac{(\theta_v/T)^2\, e^{\theta_v/T}}{(e^{\theta_v/T}-1)^2}.$$

On this basis, the vibrational contributions to the internal energy, enthalpy, and heat capacities can be expressed as

$$\left(\frac{u}{RT}\right)_{vib} = \left(\frac{h}{RT}\right)_{vib} = \frac{\theta_v/T}{e^{\theta_v/T}-1} \tag{9.48}$$

$$\left(\frac{c_v}{R}\right)_{vib} = \left(\frac{c_p}{R}\right)_{vib} = \frac{(\theta_v/T)^2\, e^{\theta_v/T}}{(e^{\theta_v/T}-1)^2}. \tag{9.49}$$

Similarly, for the vibrational contribution to the entropy, we obtain, from Eqs. (8.15) and (9.47),

$$\left(\frac{s}{R}\right)_{vib} = \frac{\theta_v/T}{e^{\theta_v/T}-1} - \ln\left(1 - e^{-\theta_v/T}\right). \tag{9.50}$$

The significance of these vibrational contributions to thermodynamic properties can be explored by carefully considering Eqs. (9.48) and (9.49), which are both plotted in Fig. 9.3. We observe that the specific heat does not display classical behavior until at least $T/\theta_v \simeq 2$, which corresponds to $T \simeq 2000-12{,}000$ K. In other words, full excitation of the vibrational mode so as to replicate the classical results,

$$\lim_{T\to\infty}\left(\frac{u}{RT}\right)_{vib} = 1 \qquad \lim_{T\to\infty}\left(\frac{c_v}{R}\right)_{vib} = 1,$$

requires very high temperatures. In fact, we find from Fig. 9.3 that classical behavior for the internal energy is considerably delayed in comparison to that for the specific heat. Hence, in contrast to the translational and rotational modes, the vibrational mode is typically only partially excited near room temperature. While the equipartition principle applies at sufficiently high temperatures, its predictions are obviously completely inappropriate for most vibrating molecules at 300–2500 K. As might be expected from Eq. (9.46), the

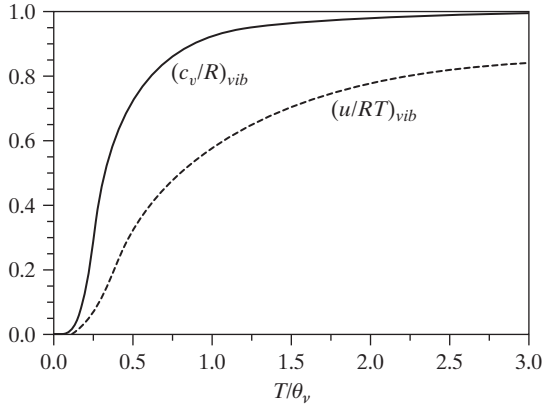

Figure 9.3 Vibrational contributions to internal energy and specific heat.

exception occurs for heavier diatomics, such as Br_2, Cl_2 and I_2, whose characteristic vibrational temperatures are near 500 K. Nevertheless, in general, the vibrational mode, more than any other, exemplifies directly the importance of quantum mechanics in the proper calculation of thermodynamic properties. Such properties can be evaluated by conveniently summing over all energy modes, as demonstrated for the internal energy in Example 9.4.

EXAMPLE 9.4

Employing the simplex model, calculate the internal energy (kJ/mole) for AlO at 2000 K.

Solution

From Section 8.4, we recognize that the internal energy can be determined by summing the contributions from all four energy modes:

$$\frac{u}{RT} = \left(\frac{u}{RT}\right)_{tr} + \left(\frac{u}{RT}\right)_{el} + \left(\frac{u}{RT}\right)_{rot} + \left(\frac{u}{RT}\right)_{vib}.$$

The translational contribution, from Eq. (9.6), is

$$\left(\frac{u}{RT}\right)_{tr} = \frac{3}{2}.$$

The electronic contribution can be obtained from the data of Appendix K.2, as evaluated based on the first two energy levels in the following table. The next level is at 20,689 cm^{-1}, which is much too high to have any further influence on the internal energy at the given temperature. Because of our choice for a zero of energy, we must convert from the T_e-formulation provided by typical spectroscopic tables to the required $T_\circ$-formulation. From Fig. 9.1, we recognize that, under the harmonic-oscillator approximation, the appropriate conversion can be made via

$$T_\circ = T_e + \tfrac{1}{2}(\omega'_e - \omega''_e).$$

$T_e(\text{cm}^{-1})$	ω_e (cm^{-1})	$T_\circ(\text{cm}^{-1})$	g_j	ε_j/kT	$g_j e^{-\varepsilon_j/kT}$	$g_j(\varepsilon_j/kT)e^{-\varepsilon_j/kT}$
0	979.2	0	2	0	2	0
5406	728.5	5281	4	3.799	0.0896	0.3404
					2.0896	0.3404

Consequently, employing the above table, we can obtain the electronic contribution from Eq. (9.18), thus giving

$$\left(\frac{u}{RT}\right)_{el} = \frac{Z'_{el}}{Z_{el}} = \frac{0.3404}{2.0896} = 0.1629.$$

The rotational contribution, from the rigid-rotor approximation, is based solely on the rotational constant, $B_e = 0.6414\ \text{cm}^{-1}$, as obtained from Appendix K.2. As a result, $T/\theta_r = (2000)/(1.4387)(0.6414) = 2167$, so that, from Table 9.3, we find that Eq. (9.27) applies; hence,

$$\left(\frac{u}{RT}\right)_{rot} = 1.$$

Finally, the vibrational contribution, employing the harmonic-oscillator approximation, depends primarily on the characteristic vibrational temperature, which is $\theta_v = (1.4387\ \text{cm} \cdot \text{K})(979.2\ \text{cm}^{-1}) = 1408.8\ \text{K}$. Therefore, from Eq. (9.48), we obtain

$$\left(\frac{u}{RT}\right)_{vib} = \frac{\theta_v/T}{e^{\theta_v/T} - 1} = 0.6888.$$

Having now evaluated the contributions from all four energy modes, we find that

$$\begin{aligned}\frac{u}{RT} &= \left(\frac{u}{RT}\right)_{tr} + \left(\frac{u}{RT}\right)_{el} + \left(\frac{u}{RT}\right)_{rot} + \left(\frac{u}{RT}\right)_{vib} \\ &= 1.5000 + 1.0000 + 0.6888 + 0.1629 = 3.3517.\end{aligned}$$

Therefore, a final calculation gives, for the total internal energy,

$$u = 3.3517(8.3145\ \text{J/K} \cdot \text{mol})\ (2000\ \text{K})\ = 55.735\ \text{kJ/mol}.$$

9.3 Rigorous and Semirigorous Models for the Diatomic Gas

Thus far, when calculating the thermodynamic properties of a diatomic molecule, we have assumed complete separation of internal energy modes. In reality, of course, accurate calculations require that the simplex model be replaced by the complex model for combined rotation and vibration. In other words, we must consider the effects of vibrational anharmonicity, rotational centrifugal stretching, and rotation–vibration coupling. Furthermore, we must account for the fact that controlling mode parameters might not be associated solely with the ground electronic state, especially for those molecules with low-lying upper electronic levels. This observation follows from Eq. (7.19), in that the rotational and vibrational mode parameters depend on their associated electronic states.

On this basis, from Section 8.4, a rigorous expression for the partition function of a diatomic gas can be given by

$$Z = Z_{tr} Z_{int}, \tag{9.51}$$

where the internal partition function is

$$Z_{\text{int}} = \sum_j g_{el,j}\, e^{-\varepsilon_{el,j}/kT} Z_{R-V,j}. \tag{9.52}$$

The *rovibronic partition function*, $Z_{R-V,j}$, which inherently implies strong rotation–vibration coupling, now depends explicitly on the jth electronic state via the influence of its Morse potential on both the vibrational and rotational energy modes. In other words, as discussed in Section 7.4 and shown by example in Table 7.2, the rovibronic energy,

$$\frac{\varepsilon_{R-V,j}}{hc} = G_j(v) + F_{vj}(J),$$

is always affected by the identity of its associated electronic energy mode. As a result, this *rigorous model* for the diatomic molecule invariably requires numerical computations so as to properly evaluate the molecular partition function. Such numerical strategies are the basis for the evaluation of all thermodynamic properties listed in the various JANAF tables (Appendix E).

Calculation of thermodynamic properties would be considerably simplified, on the other hand, if the coupled rovibrational modes could be separated from their electronic energy mode. Given this scenario, Eq. (9.52) becomes

$$Z_{int} = Z_{R-V} \sum_j g_{el,j}\, e^{-\varepsilon_{el,j}/kT}, \tag{9.53}$$

where

$$Z_{R-V} = \frac{1}{\sigma} \sum_v \sum_J (2J+1)\, e^{-(hc/kT)[G(v)+F_v(J)]}. \tag{9.54}$$

This separation can be effected if one of the following holds: (1) the excited electronic levels are unpopulated; (2) the vibrational/rotational mode parameters are essentially the same for all electronic states; or (3) the vibrational/rotational mode parameters can be suitably averaged over the populated electronic energy levels. The most common scenario, by far, is the presumption of a sufficiently low temperature so that the entire molecular population resides within the ground electronic state. For some unstable molecules, only the mode parameters associated with the ground electronic state are available in any case, owing to a lack of spectroscopic information regarding their excited electronic states.

Equations (9.51), (9.53), and (9.54) together constitute the *semirigorous model* for the partition function of a diatomic gas. The translational and electronic contributions to thermodynamic properties follow those for the simplex model. Evaluation of the rovibrational contribution via Eq. (9.54) is more convoluted, however, and thus underscores our focus for the remainder of this section.

From Eq. (7.28), the rovibrational energy for the complex model is given by

$$G(v) + F_v(J) = \omega_e\left(v+\tfrac{1}{2}\right) - \omega_e x_e\left(v+\tfrac{1}{2}\right)^2 + B_v J(J+1) - D_e J^2(J+1)^2, \tag{9.55}$$

where, from Eq. (7.22),

$$B_v = B_e - \alpha_e\left(v+\tfrac{1}{2}\right).$$

Taking the zero of energy, as usual, at $v = 0,\ J = 0$ within the ground electronic state, we obtain

$$G(0) + F_v(0) = \frac{\omega_e}{2} - \frac{\omega_e x_e}{4}. \tag{9.56}$$

Subtracting Eq. (9.56) from Eq. (9.55) yields the revised rovibrational energy,

$$G(v) + F_v(J) = \omega^* v - \omega^* x^* v\,(v-1) + B^* J(J+1) - D_e J^2 (J+1)^2 - \alpha_e v J(J+1) \tag{9.57}$$

where

$$\omega^* = \omega_e - 2\omega_e x_e \tag{9.58}$$

$$x^* = \frac{\omega_e x_e}{\omega^*} \tag{9.59}$$

and

$$B^* = B_e - \tfrac{1}{2}\alpha_e. \tag{9.60}$$

If we now define a characteristic temperature for combined rotation and vibration,

$$\theta_{R-V} = \frac{hc}{k}[G(v) + F_v(J)], \tag{9.61}$$

we have

$$\frac{\theta_{R-V}}{T} = t[v - x^* v(v-1)] + y[1 - \gamma J(J+1) - \delta v]J(J+1), \tag{9.62}$$

where

$$t = \frac{\omega^*}{\omega_e}\left(\frac{\theta_v}{T}\right) \tag{9.63}$$

$$y = \frac{B^*}{B_e}\left(\frac{\theta_r}{T}\right) \tag{9.64}$$

$$\gamma = \frac{D_e}{B^*} \tag{9.65}$$

$$\delta = \frac{\alpha_e}{B^*}. \tag{9.66}$$

We note that Eqs. (9.63) and (9.64) identify first-order corrections to the rigid-rotor/harmonic-oscillator model. As usual, ω_e, $\omega_e x_e$, B_e, α_e, and D_e are obtained from spectroscopic data, as tabulated for selected diatomics in Appendix K. If D_e or α_e are unavailable from the spectroscopy literature, they can be estimated from Eq. (7.25) or Eq. (7.26), respectively; such estimates are usually quite reliable as both equations are derived from rigorous quantum mechanical solutions based on the Morse potential.

Given Eqs. (9.54) and (9.61), the rovibrational partition function now becomes

$$Z_{R-V} = \frac{1}{\sigma}\sum_v \sum_J (2J+1) e^{-\theta_{R-V}/T}. \tag{9.67}$$

Expanding Eq. (9.67) in an Euler–Maclaurin fashion (Appendix D.3), with θ_{R-V}/T given by Eq. (9.62), we obtain after much algebra

$$Z_{R-V} = Z^{\circ}_{R-V} Z_{corr}, \tag{9.68}$$

where

$$Z^{\circ}_{R-V} = \frac{1}{\sigma} \frac{1}{y(1-e^{-t})} \tag{9.69}$$

$$Z_{corr} = 1 + \frac{y}{3} + \frac{y^2}{15} + \frac{2\gamma}{y} + \frac{\delta}{e^t - 1} + \frac{2x^* t}{(e^t-1)^2}. \tag{9.70}$$

Examining Eqs. (9.68–9.70), we note that Z°_{R-V} represents a first-order correction to the simplex solution, $Z_{rot} Z_{vib}$, and that Z_{corr} designates an auxiliary second-order correction factor. Hence, from Eqs. (9.51), (9.53), and (9.68), the total partition function becomes

$$Z = Z_{tr} Z_{el} Z^{\circ}_{R-V} Z_{corr}, \tag{9.71}$$

where, from Eq. (9.15),

$$Z_{el} = \sum_j g_{el,j}\, e^{-\varepsilon_{el,j}/kT}.$$

All terms except for Z_{corr} can be calculated in the same fashion as for the rigid-rotor/harmonic-oscillator model, except with the use of t and y rather than θ_v/T and θ_r/T, respectively.

In summary, when employing the semirigorous model, the translational and electronic contributions to thermodynamic properties follow the established simplex procedures. For the rovibrational contribution, on the other hand, we require the usual derivative expressions, which, from Eqs. (9.68–9.70), are as follows:

$$T\left(\frac{\partial \ln Z_{R-V}}{\partial T}\right)_V = 1 + \frac{t}{e^t - 1} + T\left(\frac{\partial \ln Z_{corr}}{\partial T}\right)_V \tag{9.72}$$

$$\left[\frac{\partial}{\partial T} T^2 \left(\frac{\partial \ln Z_{R-V}}{\partial T}\right)\right]_V = 1 + \frac{t^2 e^t}{(e^t-1)^2} + \left[\frac{\partial}{\partial T} T^2 \left(\frac{\partial \ln Z_{corr}}{\partial T}\right)\right]_V. \tag{9.73}$$

The first two terms of Eqs. (9.72) and (9.73) obviously arise from Z°_{R-V}. Hence, all rovibrational contributions to thermodynamic properties when using the semirigorous approach are obtained by simply adding a second-order correction term to primary terms closely affiliated with the rigid-rotor/harmonic-oscillator model.

The correction terms in Eqs. (9.72) and (9.73) can be obtained after much algebraic manipulation from Eq. (9.70). These rovibrational corrections are as follows:

$$T\left(\frac{\partial \ln Z_{corr}}{\partial T}\right)_V = \frac{Z'_{corr}}{Z_{corr}} \tag{9.74}$$

$$\left[\frac{\partial}{\partial T} T^2 \left(\frac{\partial \ln Z_{corr}}{\partial T}\right)\right]_V = \frac{4\gamma}{y} + \frac{t^2 e^t}{(e^t-1)^3}\left[\delta(e^t+1) + 8x^*(t-1) + \frac{12x^* t}{e^t - 1}\right], \tag{9.75}$$

where

$$Z'_{corr} = -\frac{y}{3} - \frac{y^2}{15} + \frac{2\gamma}{y} + \frac{t(\delta e^t - 2x^*)}{(e^t-1)^2} + \frac{4x^* t^2 e^t}{(e^t-1)^3}. \tag{9.76}$$

In essence, Eq. (9.74) corrects for the evaluation of internal energy and enthalpy; similarly, Eq. (9.75) corrects for the evaluation of specific heats.

EXAMPLE 9.5

Employing the semirigorous model, calculate the Gibbs free energy (kJ/mol) for N_2 at 3000 K and 1 bar.

Solution

From Eq. (4.39), the specific Gibbs free energy can be determined from

$$\frac{g}{RT} = -\ln\left(\frac{Z}{N}\right);$$

thus, from Eq. (9.71), we require the semirigorous evaluation,

$$\frac{Z}{N} = \frac{Z_{tr}}{N} Z_{el} Z^{\circ}_{R-V} Z_{corr}.$$

The translational contribution to the molecular partition function can be obtained most directly from the result found in Problem 4.1, i.e.,

$$\frac{Z_{tr}}{N} = 0.02595\frac{T^{5/2}M^{3/2}}{P} = 0.02595\frac{(3000)^{5/2}(28.0135)^{3/2}}{(1.0)} = 1.8965 \times 10^9.$$

The electronic contribution can be determined from the data in Appendix K.2, as evaluated in the following table. We again convert from the T_e-formulation to the $T_\circ$-formulation to account for our common zero of energy. From Fig. 9.1, we recognize that, for the complex model, the conversion can be made via

$$T_\circ = T_e + \tfrac{1}{2}(\omega'_e - \omega''_e) - \tfrac{1}{4}(\omega'_e x'_e - \omega''_e x''_e).$$

Nevertheless, because the energy corresponding to the first excited electronic level is very high, the electronic contribution to the partition function for N_2 is simply given by its ground-state degeneracy. In other words, despite a temperature of 3000 K, essentially all nitrogen molecules can be associated with the ground electronic level. Hence, only mode parameters for the ground electronic state are needed to determine contributions from the combined rotational and vibrational modes.

T_e (cm^{-1})	ω_e (cm^{-1})	$\omega_e x_e$ (cm^{-1})	$T_\circ$ (cm^{-1})	g_j	ε_j/kT	$g_j e^{-\varepsilon_j/kT}$
0	2358.6	14.32	0	1	0	1
50204	1460.6	13.87	49755	3	23.861	1.30×10^{-10}
						1.00000

The rovibronic contribution based on the semirigorous model can be evaluated from Eqs. (9.68–9.70). The required rotational temperature is, from Appendix K, $\theta_r = (1.4387)(1.9982) = 2.8748$ K. Similarly, the vibrational temperature becomes

$\theta_v = (1.4387)(2358.57) = 3393.3\,\text{K}$. Given these characteristic temperatures, the corrected rigid-rotor/harmonic-oscillator parameters for the semirigorous model are

$$y = \frac{B^*}{B_e}\left(\frac{\theta_r}{T}\right) = \frac{(B_e - 0.5\alpha_e)}{B_e}\left(\frac{\theta_r}{T}\right) = \left(\frac{1.9896}{1.9982}\right)\left(\frac{2.8748}{3000}\right) = 9.5414 \times 10^{-4}$$

$$t = \frac{\omega^*}{\omega_e}\left(\frac{\theta_v}{T}\right) = \frac{(\omega_e - 2\omega_e x_e)}{\omega_e}\left(\frac{\theta_v}{T}\right) = \left(\frac{2329.92}{2358.57}\right)\left(\frac{3393.3}{3000}\right) = 1.1174.$$

Hence, from Eq. (9.69), the corrected simplex contribution to the semirigorous model becomes

$$Z^{\circ}_{R-V} = \frac{1}{\sigma}\frac{1}{y(1-e^{-t})} = [2(9.5414 \times 10^{-4})\,(0.67287)]^{-1} = 778.80.$$

To evaluate the second-order correction term, we must first determine the required correction parameters from Eqs. (9.59), (9.65) and (9.66); i.e.,

$$x^* = \frac{\omega_e x_e}{\omega^*} = \frac{14.324}{2329.92} = 6.148 \times 10^{-3}$$

$$\gamma = \frac{D_e}{B^*} = \frac{5.76 \times 10^{-6}}{1.9896} = 2.90 \times 10^{-6}$$

$$\delta = \frac{\alpha_e}{B^*} = \frac{0.0173}{1.9896} = 8.695 \times 10^{-3}.$$

Consequently, from Eq. (9.70), the second-order correction term is

$$Z_{corr} = 1 + \frac{y}{3} + \frac{y^2}{15} + \frac{2\gamma}{y} + \frac{\delta}{e^t - 1} + \frac{2x^*t}{(e^t-1)^2} = 1 + 13.872 \times 10^{-3} = 1.0139.$$

As a result, the total partition function for the semirigorous model can now be expressed as

$$\frac{Z}{N} = \frac{Z_{tr}}{N} Z^{\circ}_{R-V} Z_{corr} Z_{el} = (1.8965 \times 10^9)\,(778.80)\,(1.0139)\,(1.0000) = 1.4975 \times 10^{12}.$$

Therefore, the dimensionless Gibbs free energy becomes

$$\frac{g}{RT} = -\ln\left(\frac{Z}{N}\right) = -\ln(1.4975 \times 10^{12}) = -28.035,$$

so that

$$g = -28.035\ (8.3145\ \text{J/K} \cdot \text{mol})\,(3000\ \text{K}) = -699.29\ \text{kJ/mol}.$$

9.4 The Polyatomic Gas

The evaluation of thermodynamic properties for a gaseous assembly composed of polyatomic molecules depends on whether the associated molecular structure is linear or nonlinear. For linear molecules, the relevant atoms are arranged along a single Cartesian coordinate; examples are CO_2, N_2O, and C_2H_2. Purely geometrical considerations restrict linear polyatomics to two rotational degrees of freedom (as for diatomics), while nonlinear polyatomics exhibit three such degrees of freedom. Hence, for a polyatomic molecule

Table 9.4 *Degrees of freedom for a polyatomic molecule with n atoms*

Mode	Linear	Nonlinear
Translation	3	3
Rotation	2	3
Vibration	$3n-5$	$3n-6$

composed of n individual atoms, the number of vibrational modes must be $3n-5$ for the linear case and $3n-6$ for the nonlinear case, as summarized in Table 9.4.

Each vibrational mode of a polyatomic molecule designates an internuclear distance or angle whose oscillation reflects a local electronic potential. Hence, stable molecular configurations for complex molecules must correspond to minima on a multidimensional potential surface. This perspective, however, is much too difficult to handle from a quantum mechanical viewpoint; therefore, as for the diatomic case, we seek a simpler model reflecting available spectroscopic data. On this basis, we again employ the rigid-rotor/harmonic-oscillator model, thus fostering complete separation of energy modes. A fully complex model, including any rovibrational coupling, must obviously be employed for more rigorous calculations.

Assuming complete mode separation, the molecular partition function for a polyatomic molecule follows Eq. (8.11), thus giving

$$Z = Z_{tr} Z_{el} Z_{rot} Z_{vib}.$$

The translational contribution, similar to that for a diatomic molecule, is given by

$$Z_{tr} = \left(\frac{2\pi mkT}{h^2}\right)^{3/2} V \qquad m = \sum_i m_i,$$

where the total mass, m, is simply the sum of all atomic masses composing the molecule. Therefore, we conclude that the contribution of the translational mode to thermodynamic properties is essentially the same for a polyatomic molecule as for the monatomic gas.

For nearly all polyatomics, the energy ascribed to the first excited electronic level is sufficiently high that only the ground electronic state is necessary for most property calculations. Hence, from Eq. (9.15), the electronic partition function becomes

$$Z_{el} = \sum_j g_j e^{-\varepsilon_j/kT} \simeq g_0, \tag{9.77}$$

so that, from Eqs. (4.36–4.42), the resulting contribution to thermodynamic properties is nonzero only for the entropy and free energies. The required electronic degeneracy can be obtained, as usual, from the term symbol associated with the ground electronic state. For linear polyatomics, the term symbol and degeneracy follow the recipes previously developed for diatomic molecules. However, for nonlinear polyatomics, the degeneracy is always

$$g_{el} = 2S+1, \tag{9.78}$$

as obtained from the associated term symbol

$$^{2S+1}A_i \text{ or } ^{2S+1}B_i \qquad i = 1,\ 2.$$

Here, A indicates a symmetric while B implies a nonsymmetric molecular wave function. Similarly, the index $i = 1,\ 2$ designates whether this wave function is symmetric or asymmetric, respectively, with respect to the chemical structure of the polyatomic molecule.

9.4.1 Rotational Contribution

For a polyatomic molecule, the rotational contribution to thermodynamic properties clearly depends on whether the molecule is linear or nonlinear. As indicated previously, a linear polyatomic has the same two rotational degrees of freedom as for a diatomic molecule. In addition, because of the greater mass of typical polyatomic species, invariably $T/\theta_r > 30$ so that the rotational partition function, following Eq. (9.26), becomes

$$Z_{rot} = \frac{T}{\sigma \theta_r}. \tag{9.79}$$

As might be expected, the symmetry factor in Eq. (9.79) reflects the chemical structure of a linear polyatomic; thus, as examples, $\sigma = 1$ for N_2O (N–N–O) and $\sigma = 2$ for CO_2 (O–C–O). Based on the diatomic case, the characteristic rotational temperature, θ_r, is given by Eq. (9.23), except that the moment of inertia must be evaluated from

$$I_e = \sum_i m_i x_i^2,$$

where x_i represents the distance of each constituent atom from the molecule's center of mass. Consequently, from Eq. (9.79), the rotational contributions to the internal energy and specific heat for a linear polyatomic are

$$\left(\frac{u}{RT}\right)_{rot} = T\left(\frac{\partial \ln Z_{rot}}{\partial T}\right)_V = 1 \tag{9.80}$$

$$\left(\frac{c_v}{R}\right)_{rot} = \left[\frac{\partial}{\partial T} T^2 \left(\frac{\partial \ln Z_{rot}}{\partial T}\right)\right]_V = 1, \tag{9.81}$$

which, of course, duplicates our previous results for the diatomic molecule.

In comparison to the linear polyatomic, the nonlinear polyatomic has three rotational degrees of freedom and thus three principal moments of inertia:

$$I_x = \sum_i m_i \left(y_i^2 + z_i^2\right)$$

$$I_y = \sum_i m_i \left(x_i^2 + z_i^2\right)$$

$$I_z = \sum_i m_i \left(x_i^2 + y_i^2\right),$$

where x_i, y_i, and z_i are atomic distances from the molecule's center of mass, as determined via the usual formulation,

$$\sum_i m_i x_i = \sum_i m_i y_i = \sum_i m_i z_i = 0.$$

The common methodology used here to define the center of mass and the principal moments of inertia is discussed in depth in any textbook on classical mechanics. For our purposes, we need only recall that the principal coordinates can ordinarily be established

Table 9.5 *Types of polyatomic molecules*

Type	Definition	Example
Spherical top	$I_x = I_y = I_z$	CH_4
Symmetric top	$I_x = I_y \neq I_z$	C_6H_6
Asymmetric top	$I_x \neq I_y \neq I_z$	H_2O

by defining one of the three Cartesian axes to be along a line of symmetry within the molecular structure.

Based on possible relations among the magnitudes of the principal moments of inertia, we may define three types of polyatomic molecules, as listed in Table 9.5. For the simple spherical top ($I_x = I_y = I_z$), quantum mechanics can be applied to determine rotational energies and degeneracies, as for the diatomic molecule of Chapter 6. The result is

$$\varepsilon_{rot} = \frac{J\,(J+1)\,\hbar^2}{2I} \qquad g_J = (2J+1)^2\,;$$

thus, from Eq. (4.12), the associated rotational partition function becomes

$$Z_{rot} = \frac{\sqrt{\pi}}{\sigma}\left(\frac{T}{\theta_r}\right)^{3/2}.$$

Similarly, for the asymmetric top, we find that

$$Z_{rot} = \frac{1}{\sigma}\sqrt{\frac{\pi\,T^3}{\theta_{rx}\theta_{ry}\theta_{rz}}}, \tag{9.82}$$

where, from Eq. (8.2), each characteristic temperature specifying rotational motion about a single Cartesian coordinate can be related to a rotational constant, B_{ei}, and thus to a moment of inertia, I_{ei}, for a given principal coordinate via

$$\theta_{ri} = \frac{hc}{k}B_{ei} = \frac{h^2}{8\pi^2 k\,I_{ei}}. \tag{9.83}$$

Clearly, both the symmetric and spherical tops can be considered special cases of the asymmetric top, so that the rotational partition function for all three cases can be determined via Eq. (9.82). As usual, the symmetry factor must be calculated from structural considerations so as to correct for any repeated counting of indistinguishable configurations. In essence, the symmetry factor indicates the number of ways that a molecule can be rotated to achieve the same orientation in three-dimensional space. Typical examples are given in Table 9.6, with structural clarifications provided for NH_3, CH_4, and C_6H_6 in Fig. 9.4. The

Table 9.6 *Symmetry factors for polyatomic molecules*

Molecule	Symmetry factor
H_2O	2
NH_3	3
C_2H_4	4
CH_4	12
C_6H_6	12

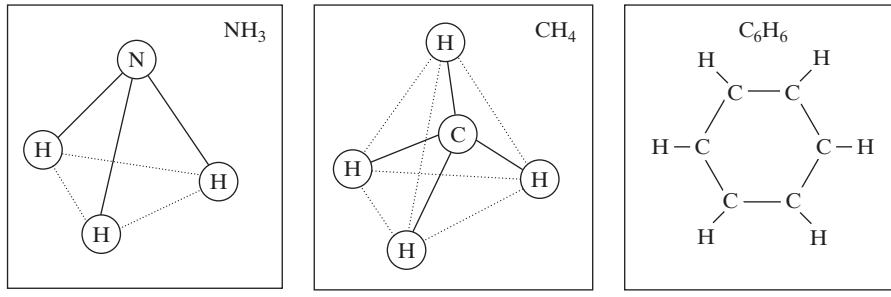

Figure 9.4 Molecular structure of selected nonlinear polyatomic molecules.

symmetry factor of three for NH_3 arises from successive 120° rotations of the pyramidal plane produced by its three hydrogen atoms. Similarly, the symmetry factor of 12 for CH_4 originates from its four tetrahedral planes, each composed of three hydrogen atoms. For C_6H_6, the symmetry factor of 12 is a manifestation of its planar hexagonal structure.

Regardless of the symmetry factor, Eq. (9.82) indicates that the rotational contributions to the internal energy and specific heat for a nonlinear polyatomic are

$$\left(\frac{u}{RT}\right)_{rot} = T\left(\frac{\partial \ln Z_{rot}}{\partial T}\right)_V = \frac{3}{2} \tag{9.84}$$

$$\left(\frac{c_v}{R}\right)_{rot} = \left[\frac{\partial}{\partial T}T^2\left(\frac{\partial \ln Z_{rot}}{\partial T}\right)\right]_V = \frac{3}{2}. \tag{9.85}$$

Therefore, we find that, compared to the linear polyatomic of Eqs. (9.80) and (9.81), the rotational mode for a nonlinear polyatomic contributes an additional $RT/2$ to the internal energy and an additional $R/2$ to the specific heat. In other words, the rotational contribution to internal energy and heat capacity for both linear and nonlinear polyatomics is in exact agreement with that expected from classical equipartition theory.

9.4.2 Vibrational Contribution

According to Table 9.4, linear and nonlinear polyatomics contain $3n - 5$ and $3n - 6$ vibrational modes, respectively. Unfortunately, because of the plethora of such modes for large polyatomics, their identification is hardly straightforward. Building again on our analogy of masses connected with springs, we obviously have an enormous variety of possible internal motions, depending on molecular structure and initial bond displacement. However, by choosing special coordinates labeled normal coordinates, the kinetic and potential energy terms become pure quadratics so that we can ensure simple harmonic motion. As for classic Fourier decompositions, any complex molecular ambulation can always be described in terms of these primary oscillations. In particular, the specification of pure harmonic motions supported by a given molecular structure is called *normal mode analysis*, as described for a simple linear triatomic in Appendix L.

The pivotal result from normal mode analysis is identification of the independent vibrational modes for any polyatomic molecule. Significantly, displacement along the identified normal coordinates causes all nuclei to move in phase with the same harmonic frequency. Hence, we can model the inherently complex vibration of a polyatomic molecule

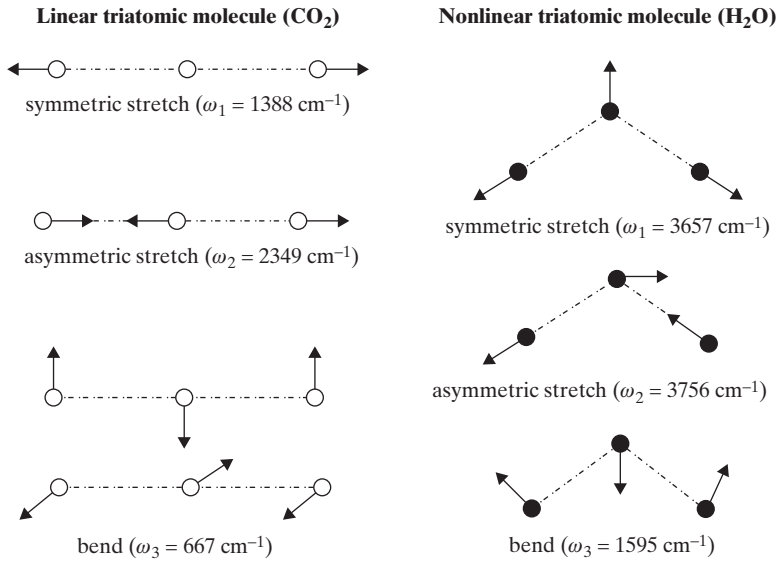

Figure 9.5 Vibrational energy modes for linear and nonlinear triatomic molecules.

with the same harmonic oscillator equations that we previously used for the diatomic molecule. Operating again with the zero of energy at the ground vibrational level, we have from Eq. (9.47)

$$Z_{vib} = \prod_{i=1}^{m} \frac{1}{1 - e^{-\theta_{vi}/T}}, \tag{9.86}$$

where m is $3n - 5$ for a linear and $3n - 6$ for a nonlinear polyatomic. From Eq. (8.2), the characteristic vibrational temperature for each normal mode is

$$\theta_{vi} = \frac{hc}{k}\omega_{ei}, \tag{9.87}$$

where ω_{ei} is a so-called *normal frequency* (cm^{-1}). As with our previous rotational constants, B_{ei}, these normal vibrational frequencies are usually obtained from the analysis of spectroscopic data. For computational purposes, B_{ei} and ω_{ei} values associated with the ground electronic state of selected polyatomic species are tabulated in Appendix K.3.

Given Eq. (9.86), we find from Eqs. (9.48) and (9.49) that the vibrational contributions to the internal energy and heat capacity, respectively, for any polyatomic molecule are

$$\left(\frac{u}{RT}\right)_{vib} = T\left(\frac{\partial \ln Z_{vib}}{\partial T}\right)_V = \sum_{i=1}^{m} \frac{\theta_{vi}/T}{e^{\theta_{vi}/T} - 1} \tag{9.88}$$

$$\left(\frac{c_v}{R}\right)_{vib} = \left[\frac{\partial}{\partial T}T^2\left(\frac{\partial \ln Z_{vib}}{\partial T}\right)\right]_V = \sum_{i=1}^{m} \frac{(\theta_{vi}/T)^2 e^{\theta_{vi}/T}}{(e^{\theta_{vi}/T} - 1)^2}. \tag{9.89}$$

Each term of Eqs. (9.88) or (9.89) entails an independent characteristic temperature; the required θ_{vi} values are based on Eq. (9.87) and tabulated values of ω_{ei}, as elaborated for CO_2 and H_2O in Fig. 9.5. Typically, for a linear triatomic such as CO_2, we identify a symmetric stretch mode, an asymmetric stretch mode, and two identical bending modes.

In comparison, for a nonlinear triatomic such as H_2O, we again have a symmetric and an asymmetric stretch mode, but only one bending mode. As might be expected from structural considerations, owing to a smaller Hooke constant (k_0), the energy stored by bending modes is usually considerably smaller than that associated with symmetric or asymmetric stretch modes.

We note, by the way, that the molecular structure of linear triatomics having $\sigma = 2$ is analogous to that for homonuclear diatomics. For this reason, the symmetric stretch mode for CO_2 is infrared inactive owing to the impossibility of changes in its molecular dipole moment. In comparison, the unbalanced molecular structure of CO_2 generated during asymmetric stretch promotes infrared activity; indeed, the resulting absorption band near 4.3 μm is undoubtedly a key factor in producing the so-called greenhouse effect.

9.4.3 Property Calculations for Polyatomic Molecules

As for the monatomic and diatomic cases, separation of energy modes implies that we may determine thermodynamic properties for polyatomic gases by summing over the contributions from each energy mode. As an example, the internal energy for a nonlinear polyatomic can be evaluated by summing the translational contribution from Eq. (9.6), the rotational contribution from Eq. (9.84), and the vibrational contribution from Eq. (9.88), thus obtaining

$$\frac{u}{RT} = 3 + \sum_{i=1}^{3n-6} \frac{\theta_{vi}/T}{e^{\theta_{vi}/T} - 1}.$$

For the entropy, we must carefully allocate contributions from the translational and the three internal energy modes, so that from Eqs. (8.14) and (8.15), we have

$$\frac{s}{R} = \left\{ T \left(\frac{\partial \ln Z_{tr}}{\partial T} \right)_V + \ln \left(\frac{Z_{tr}}{N} \right) + 1 \right\} + \sum_{i=1}^{3} \left\{ T \left(\frac{\partial \ln Z_{int,i}}{\partial T} \right)_V + \ln Z_{int,i} \right\}, \quad (9.90)$$

where the summation occurs over the rotational, vibrational, and electronic modes. Implementing Eqs. (9.11), (9.77), (9.82), (9.84), (9.86), and (9.88), Eq. (9.90) becomes

$$\frac{s}{R} = 4 + \ln g_0 + \ln \left\{ \frac{(2\pi m)^{3/2} (kT)^{5/2}}{h^3 P} \right\} + \ln \left\{ \frac{1}{\sigma} \sqrt{\frac{\pi T^3}{\theta_{rx}\theta_{ry}\theta_{rz}}} \right\} + \sum_{i=1}^{3n-6} \left\{ \frac{\theta_{vi}/T}{e^{\theta_{vi}/T} - 1} - \ln(1 - e^{-\theta_{vi}/T}) \right\}.$$

In summary, given the knowledge established in this chapter, analogous expressions could be obtained for any thermodynamic property of an ideal gas by using appropriate contributions relevant to monatomic, diatomic, linear polyatomic, or nonlinear polyatomic molecules.

EXAMPLE 9.6

Evaluate the entropy for NO_2 (J/K · mol) at 500 K and 1 bar.

Solution

From Section 8.4, we recognize that the entropy can be determined by summing the various contributions from all four energy modes, i.e.,

$$\frac{s}{R} = \left(\frac{s}{R}\right)_{tr} + \left(\frac{s}{R}\right)_{el} + \left(\frac{s}{R}\right)_{rot} + \left(\frac{s}{R}\right)_{vib}.$$

The translational contribution, from Eq. (9.11), is

$$\left(\frac{s}{R}\right)_{tr} = \ln\left[\frac{(2\pi m)^{3/2}(kT)^{5/2}}{h^3 P}\right] + \frac{5}{2}$$

so that

$$\left(\frac{s}{R}\right)_{tr} = \ln\left\{\frac{[2\pi(46.0055)(1.6605\times10^{-27})]^{3/2}[(1.3807\times10^{-23})(500)]^{5/2}}{(6.6261\times10^{-34})^3(1.0\times10^5)}\right\} + \frac{5}{2}$$
$$= 20.1280.$$

A more direct procedure is to use Eq. (9.12), i.e., the Sackur–Tetrode equation, thus obtaining

$$\left(\frac{s}{R}\right)_{tr} = \frac{5}{2}\ln T + \frac{3}{2}\ln M - \ln P - 1.1516 = \frac{5}{2}\ln(500) + \frac{3}{2}\ln(46.0055) - 1.1516$$
$$= 20.1280.$$

From Eq. (8.15), the contribution from all internal energy modes is

$$\frac{s_{int}}{R} = T\left(\frac{\partial \ln Z_{int}}{\partial T}\right)_V + \ln Z_{int}.$$

Hence, the electronic contribution, as obtained by using Eqs. (9.77) and (9.78) with the NO_2 term symbol ($^2A_1$) from Appendix K.3, becomes

$$\left(\frac{s}{R}\right)_{el} = \ln g_0 = \ln 2 = 0.6931.$$

The rotational contribution can be determined from Eqs. (9.82) and (9.84); the result is

$$\left(\frac{s}{R}\right)_{rot} = \frac{3}{2} + \ln\left[\frac{1}{\sigma}\sqrt{\frac{\pi T^3}{\theta_{rx}\theta_{ry}\theta_{rz}}}\right].$$

From Appendix K.3, the three rotational constants for NO_2 follow: $B_{e1} = 8.0012\ \text{cm}^{-1}$, $B_{e2} = 0.4336\ \text{cm}^{-1}$, and $B_{e3} = 0.4104\ \text{cm}^{-1}$. The resulting characteristic rotational temperatures, as obtained from Eq. (9.83), are $\theta_{rx} = 11.511$ K, $\theta_{ry} = 0.6238$ K, and $\theta_{rz} = 0.5904$ K. Hence, the rotational contribution to the entropy becomes

$$\left(\frac{s}{R}\right)_{rot} = \frac{3}{2} + \ln\left[\frac{1}{2}\sqrt{\frac{\pi(500)^3}{(11.511)(0.6238)(0.5904)}}\right] = 9.9789,$$

where $\sigma = 2$ from the V-shaped molecular structure of O–N–O. Finally, the vibrational contribution, from Eqs. (9.86) and (9.88), is

$$\left(\frac{s}{R}\right)_{vib} = \sum_{i=1}^{3} \left\{ \frac{\theta_{vi}/T}{e^{\theta_{vi}/T} - 1} - \ln(1 - e^{-\theta_{vi}/T}) \right\}.$$

The three vibrational frequencies, extracted from Appendix K.3, are $\omega_{e1} = 1616.8\ \text{cm}^{-1}$, $\omega_{e2} = 1319.7\ \text{cm}^{-1}$, and $\omega_{e3} = 749.65\ \text{cm}^{-1}$. The resulting characteristic vibrational temperatures, as obtained from Eq. (9.87), are $\theta_{v1} = 2326.1\ \text{K}$, $\theta_{v2} = 1898.7\ \text{K}$, and $\theta_{v3} = 1078.5\ \text{K}$. Therefore, the vibrational contribution to the entropy from the three normal modes of NO_2 becomes

$$\left(\frac{s}{R}\right)_{vib} = (0.0448 + 0.0871 + 0.2821) + (0.0096 + 0.0227 + 0.1229) = 0.5692.$$

As we have now evaluated the contributions from all four energy modes, we find that

$$\begin{aligned} \frac{s}{R} &= \left(\frac{s}{R}\right)_{tr} + \left(\frac{s}{R}\right)_{el} + \left(\frac{s}{R}\right)_{rot} + \left(\frac{s}{R}\right)_{vib} \\ &= 20.1280 + 0.6931 + 9.9789 + 0.5692 = 31.3692. \end{aligned}$$

Therefore, a final calculation gives, for the total entropy,

$$s = 31.3692\,(8.3145\ \text{J/K} \cdot \text{mol}) = 260.819\ \text{J/K} \cdot \text{mol}.$$

PROBLEM SET IV

Thermodynamic Properties of the Ideal Gas (Chapters 8–9)

4.1 Consider the development of the Sackur–Tetrode equation for the translational entropy of an ideal gas.

a. Evaluate the constant C in the expression

$$\frac{Z_{tr}}{N} = C\frac{T^{5/2}M^{3/2}}{P},$$

where T is the temperature in K, M the molecular weight, and P the pressure in bars.

b. Hence, show that the translational contribution to the entropy is given by

$$\frac{s_{tr}}{R} = \frac{5}{2}\ln T + \frac{3}{2}\ln M - \ln P - 1.1516.$$

c. The experimentally measured value of the entropy for vaporous neon at its boiling point (27.1 K) and a pressure of one bar is 96.50 J/mol · K. To verify the theoretical formulation leading to the Sackur–Tetrode equation, compare your predicted value with the given experimental result.

Hint: Keep this problem in mind for future calculations.

4.2 We have shown that the total kinetic energy of a diatomic molecule can be expressed as

$$T = \frac{m}{2}(\dot{X}^2 + \dot{Y}^2 + \dot{Z}^2) + \frac{\mu}{2}(\dot{x}^2 + \dot{y}^2 + \dot{z}^2),$$

where (X, Y, Z) and (x, y, z) are the center-of-mass and relative coordinates, respectively, m is the total mass, and μ is the reduced mass.

a. By converting to relative spherical coordinates, show that

$$T = \frac{1}{2m}\left(p_x^2 + p_y^2 + p_z^2\right) + \frac{1}{2I}\left(p_\theta^2 + \frac{p_\phi^2}{\sin^2\theta}\right) + \frac{p_r^2}{2\mu},$$

where $I = \mu r^2$ is the moment of inertia and

$$p_x = m\dot{X} \qquad p_y = m\dot{Y} \qquad p_z = m\dot{Z}$$
$$p_r = \mu\dot{r} \qquad p_\theta = I\dot{\theta} \qquad p_\phi = I\sin^2\theta\dot{\phi}.$$

b. Evaluate the classical partition function for pure translation, rotation, and vibration of a diatomic molecule.

c. Compare your classical results to those based on quantum mechanics. Explain any disparity and show that in the limit of high temperature, the quantum mechanical partition function is equivalent to the classical partition function.

4.3 The relationship between atmospheric pressure and altitude is an important result in atmospheric physics.

a. Using the classical phase integral, show that for an isothermal atmosphere

$$P = P_\circ \exp\left(-\frac{mgH}{kT}\right),$$

where $P_\circ$ is the pressure at sea level, g is the gravitational acceleration, and H is the altitude above sea level.

b. At what altitude (km) does the atmospheric pressure decrease to e^{-1} of its sea-level value? Assume that the sea-level temperature is 300 K. Does your answer overestimate or underestimate the actual e^{-1} altitude? Explain.

c. In one of his fundamental experiments on sedimentation equilibrium, Perrin observed the number of gamboge particles in water at 293 K. He found that when the microscope was raised by 100 μm, the mean number of particles in his field of view decreased from 203 to 91. Assuming that the gamboge particles had a mean volume of 9.78×10^{-21} m^3 and a density of 1351 kg/m^3, determine an experimental value for Avogadro's constant if the density of water can be taken as 1000 kg/m^3.

4.4 a. Calculate the entropy (s/R), enthalpy (h/RT), and constant pressure specific heat (c_p/R) for monatomic oxygen at $P = 1.0$ bar and $T = 1000$ K. Compare your calculated property values with those in the appropriate JANAF table. What is the entropy (s/R) for monatomic oxygen at $P = 0.1$ bar and 1000 K?

b. Compute c_p/R for monatomic oxygen at 500 K and compare with your result at 1000 K. Explain the difference. Would you expect the same trend to hold for other atoms, e.g., helium, hydrogen, or argon? Explain.

4.5 Complete Problem 4.4, but at a temperature of 1500 K rather than 1000 K.

4.6 Complete Problem 4.4, but at a temperature of 2000 K rather than 1000 K.

4.7 Plot the distribution (N_j/N) of molecules among the various (a) rotational levels ($J = 0 - 20$) for CO and (b) vibrational levels ($v = 0 - 5$) for Br_2 at both 300 K and 800 K. Assume the rigid-rotor/harmonic-oscillator model for both CO and Br_2. Discuss the difference between the vibrational and rotational distributions, and the general trend of each distribution with temperature.

4.8 Consider a monatomic gas having two nondegenerate electronic states, $\varepsilon_0 = 0$ and $\varepsilon_1 = \varepsilon$.

a. Plot the electronic contribution to specific heat versus reduced temperature, kT/ε.

b. Determine analytically the value of reduced temperature at which the electronic contribution to specific heat is a maximum.

4.9 Plot the distribution (N_j/N) of molecules among the various (a) vibrational levels ($v = 0 - 5$) for Cl_2 and (b) rotational levels ($J = 0 - 30$) for NO at both 500 K and 1000 K. Assume the rigid-rotor/harmonic-oscillator model for both Cl_2 and NO. Discuss the difference between the vibrational and rotational distributions, and the general trend of each distribution with temperature.

4.10 Calculate the entropy (s/R), enthalpy (h/RT), and constant pressure specific heat (c_p/R) for molecular oxygen (O_2) at $P = 1.0$ bar and $T = 1000$ K. Separate the contributions arising from the translational, rotational, vibrational, and electronic energy modes by assuming a rigid-rotor/harmonic-oscillator model. Compare your calculated values with those in the appropriate JANAF table; explain any discrepancy. The spectroscopic parameters for the first three electronic levels of O_2 are as follows.

Term symbol	T_e (cm^{-1})	ω_e (cm^{-1})	$\omega_e x_e$ (cm^{-1})	B_e (cm^{-1})	α_e (cm^{-1})	D_e (cm^{-1})
$^3\Sigma_g^-$	0	1580.19	11.98	1.4456	0.0159	$4.84 \cdot 10^{-6}$
$^1\Delta_g$	7869.5	1483.50	12.90	1.4264	0.0171	$4.86 \cdot 10^{-6}$
$^1\Sigma_g^+$	13120.9	1432.77	14.00	1.4004	0.0182	$5.35 \cdot 10^{-6}$

4.11 Complete Problem 4.10, but at a temperature of 1500 K rather than 1000 K.

4.12 Complete Problem 4.10, but at a temperature of 2000 K rather than 1000 K.

4.13 Calculate the entropy (s/R),enthalpy (h/RT) and constant pressure specific heat (c_p/R) for H_2O at $P = 1.0$ bar and $T = 1000$ K. Compare your calculated values with those in the appropriate JANAF table; explain any discrepancy.

4.14 Complete Problem 4.13, but at a temperature of 1500 K rather than 1000 K.

4.15 Complete Problem 4.13, but at a temperature of 2000 K rather than 1000 K.

4.16 Calculate the entropy (s/R),enthalpy (h/vRT), and constant pressure specific heat (c_p/R) for molecular oxygen (O_2) at $P = 1.0$ bar and $T = 1000$ K using the semirigorous model for a diatomic gas. Compare your calculated values with those in the appropriate JANAF table; explain any discrepancy.

4.17 Complete Problem 4.16, but at a temperature of 2000 K rather than 1000 K.

4.18 Calculate the entropy (s/R), enthalpy (h/RT), and constant pressure specific heat (c_p/R) for molecular oxygen (O_2) at $P = 1.0$ bar and $T = 300$–3000 K using the semirigorous model for a diatomic gas. Compare your calculated values as a function of temperature with those listed in the appropriate JANAF table. Explain any discrepancy and indicate a revised procedure that you would use to obtain results in exact agreement with the JANAF table.

10 Statistical Thermodynamics for Ideal Gas Mixtures

Having dealt in the previous chapter with thermodynamic properties for pure ideal gases, we are now prepared to apply statistical thermodynamics to ideal gas mixtures. We begin by considering nonreactive mixtures, with assiduous attention given to equilibrium particle distributions and to the determination of mixture properties. We then move on to reacting mixtures, with a special focus on calculating equilibrium constants and mixture compositions. Specifically, equilibrium constants are developed for generic gas-phase reactions involving monatomic, diatomic, or polyatomic species, including both dissociation and ionization reactions. A useful feature of our exploration of mixture properties is the opportunity to exploit from a different perspective, and thus to review somewhat from Chapters 3 and 4 those concepts from statistical thermodynamics of most significance at the dilute limit.

10.1 Equilibrium Particle Distribution for the Ideal Gas Mixture

We begin our discussion by focusing on the equilibrium particle distribution for a nonreactive ideal gas mixture. For this purpose, let us consider M different species within the mixture, each with independent energy levels and degeneracies given by ε_{ij} and g_{ij}, respectively, where the subscript i refers to a particular species and the subscript j refers to a specific energy level for that species. As in Chapter 3, we seek the most probable macrostate, but now with the explicit goal of identifying the most probable distribution for an isolated system of M ideal gases.

Capitalizing on the Maxwell–Boltzmann method, we impose $M + 1$ constraints on our isolated system, corresponding to mass conservation for each of M species plus energy conservation among all species, so that

$$\sum_j N_{ij} = N_i \qquad i = 1, 2, \ldots, M \tag{10.1}$$

$$\sum_{i=1}^{M} \sum_j N_{ij} \varepsilon_{ij} = E, \tag{10.2}$$

where N_{ij} indicates the number of particles identified with the ith species in the jth energy level, N_i represents the total number of particles for the ith species, and E is the total

energy for the ideal gas mixture. Because we have M independent nonreacting species, the total number of microstates per macrostate is

$$W = \prod_{i=1}^{M} W_i, \tag{10.3}$$

where, in the dilute limit, the number of microstates per macrostate for the ith gas follows corrected Maxwell–Boltzmann statistics, so that, from Eq. (4.4),

$$W_i = \prod_j \frac{g_{ij}^{N_{ij}}}{N_{ij}!}. \tag{10.4}$$

Combining Eqs. (10.3) and (10.4), we obtain

$$W = \prod_{i=1}^{M} \prod_j \frac{g_{ij}^{N_{ij}}}{N_{ij}!}; \tag{10.5}$$

here, we note that, in comparison to Chapter 3, we have directly employed the known statistics for the dilute limit.

Emulating the statistical procedures of Section 3.5, we now determine $\ln W$, apply Stirling's approximation, and optimize with constraints via the Lagrange method of undetermined multipliers. Therefore, applying the logarithmic function to Eq. (10.5), we have

$$\ln W = \sum_{i=1}^{M} \sum_j [N_{ij} \ln g_{ij} - \ln N_{ij}!],$$

whereupon, following application of Stirling's approximation, we obtain

$$\ln W = \sum_{i=1}^{M} \sum_j N_{ij} \left[\ln \left(\frac{g_{ij}}{N_{ij}} \right) + 1 \right], \tag{10.6}$$

which provides a summation over energy levels identical to that given by Eq. (4.3) for a single component in the dilute limit. In preparation for applying the method of Lagrange multipliers, we now differentiate Eq. (10.6) with respect to N_{ij}, thus deriving, after some manipulation,

$$d \ln W = \sum_{i=1}^{M} \sum_j \ln \left(\frac{g_{ij}}{N_{ij}} \right) dN_{ij} = 0. \tag{10.7}$$

Likewise, differentiating Eqs. (10.1) and (10.2), we obtain the constraints in differential form:

$$\sum_j dN_{ij} = 0 \qquad i = 1, 2, \ldots, M \tag{10.8}$$

$$\sum_{i=1}^{M} \sum_j \varepsilon_{ij} dN_{ij} = 0. \tag{10.9}$$

Letting α_i be the undetermined multiplier for the ith species constraint and β the undetermined multiplier for the energy constraint, we may combine Eqs. (10.7–10.9), thus obtaining

$$\sum_{i=1}^{M} \sum_j \left[\ln \left(\frac{g_{ij}}{N_{ij}} \right) - \alpha_i - \beta \varepsilon_{ij} \right] dN_{ij} = 0. \tag{10.10}$$

We note that Eq. (10.10) contains M terms, corresponding to M different components and thus M species constraints. Within each term, an additional summation occurs over all energy levels for that particular component. We also note that each term is identical to what Eq. (3.17) would give for a single component at the dilute limit. Therefore, for each species, Eq. (10.10) mandates

$$\ln\left(\frac{g_{ij}}{N_{ij}}\right) - \alpha_i - \beta\varepsilon_{ij} = 0,$$

so that

$$N_{ij} = g_{ij}\exp\left[-(\alpha_i + \beta\varepsilon_{ij})\right] \qquad i = 1, 2, \ldots, M. \tag{10.11}$$

Comparing Eq. (10.11) to Eq. (4.9), as written for a single independent component, so that

$$N_{ij} = g_{ij}\exp\left(\frac{\mu_i - \varepsilon_{ij}}{kT}\right) \qquad i = 1, 2, \ldots, M, \tag{10.12}$$

we find, as expected, that the Lagrange multipliers in the dilute limit are still given by

$$\alpha_i = -\frac{\mu_i}{kT} \qquad \beta = \frac{1}{kT}.$$

Now, following Section 4.3, we substitute Eq. (10.12) into Eq. (10.1), thus obtaining

$$N_i = \sum_j N_{ij} = e^{\mu_i/kT}\sum_j g_{ij}e^{-\varepsilon_{ij}/kT}, \tag{10.13}$$

so that, dividing Eq. (10.12) by Eq. (10.13), we have

$$\frac{N_{ij}}{N_i} = \frac{g_{ij}e^{-\varepsilon_{ij}/kT}}{Z_i}, \tag{10.14}$$

where, in analogy with Eq. (4.12), the partition function for the ith species can be defined as

$$Z_i = \sum_j g_{ij}e^{-\varepsilon_{ij}/kT}. \tag{10.15}$$

Equation (10.14) represents the equilibrium particle distribution for each component of an ideal gas mixture. As expected for independent species, this distribution is identical to that obtained in Section 4.3 for a pure constituent at the dilute limit. In other words, independent particles are uninfluenced by other particles in an ideal gas assembly, irrespective of whether those particles are of the same species or from a different component in the mixture.

Because the partition function for each constituent of an ideal gas mixture depends on the temperature and volume of the entire assembly, the equilibrium distribution for each species must similarly depend on only the temperature and volume of the whole mixture. Consequently, *each component of an ideal gas mixture behaves as if it alone existed in an assembly at the same total volume, V, and temperature, T*. This simple observation is the proximate basis for the calculation of mixture properties in the dilute limit. From a macroscopic perspective, the same result is encapsulated by the so-called Gibbs–Dalton law, which is invoked in all classical textbooks when discussing the properties of ideal gas mixtures. Ultimately, the Gibbs–Dalton law arises because quantum mechanics dictates

that the translational energy of any independent particle is intrinsically proportional to the assembly volume (Section 5.7).

10.2 Thermodynamic Properties of the Ideal Gas Mixture

Now that we have determined the partition function and particle distribution for the components of a nonreactive ideal gas mixture, we are in a position to calculate mixture properties. Considering first the internal energy, we substitute Eq. (10.14) into Eq. (10.2), thus obtaining

$$U = \sum_{i=1}^{M} \sum_{j} N_{ij} \varepsilon_{ij} = \sum_{i=1}^{M} \frac{N_i}{Z_i} \sum_{j} g_{ij} \varepsilon_{ij} e^{-\varepsilon_{ij}/kT}. \tag{10.16}$$

Taking the partial derivative of Eq. (10.15) with respect to temperature, we find

$$\left(\frac{\partial Z_i}{\partial T} \right)_{V,N_i} = \frac{1}{kT^2} \sum_{j} g_{ij} \varepsilon_{ij} e^{-\varepsilon_{ij}/kT}, \tag{10.17}$$

so that, substituting Eq. (10.17) into Eq. (10.16), we obtain

$$U = \sum_{i=1}^{M} N_i kT^2 \frac{1}{Z_i} \left(\frac{\partial Z_i}{\partial T} \right)_{V,N_i}, \tag{10.18}$$

where the elective N_i subscript on the partial derivatives indicates nonreactive conditions. Given Eq. (4.32), we may write, for one component of an ideal gas mixture,

$$N_i k = n_i R, \tag{10.19}$$

so that Eq. (10.18) becomes

$$U = \sum_{i=1}^{M} n_i RT^2 \left(\frac{\partial \ln Z_i}{\partial T} \right)_{V,N_i}. \tag{10.20}$$

However, from Eq. (4.37) for the ith pure component,

$$u_i = RT^2 \left(\frac{\partial \ln Z_i}{\partial T} \right)_{V,N_i}; \tag{10.21}$$

thus, substituting Eq. (10.21) into Eq. (10.20), we obtain

$$U = \sum_{i=1}^{M} n_i u_i, \tag{10.22}$$

so that, as expected, the total internal energy of an ideal gas mixture is found by simply adding contributions to the internal energy from each component of the mixture at the same assembly temperature.

Shifting to the entropy, we may combine Eqs. (3.19) and (10.6), thus giving

$$S = k \ln W = k \sum_{i=1}^{M} \sum_{j} N_{ij} \left[\ln \left(\frac{g_{ij}}{N_{ij}} \right) + 1 \right]. \tag{10.23}$$

Substituting Eq. (10.14) into Eq. (10.23), we have

$$S = k\sum_{i=1}^{M}\sum_{j} N_{ij}\left[\ln\left(\frac{Z_i}{N_i}\right) + \frac{\varepsilon_{ij}}{kT} + 1\right], \tag{10.24}$$

so that, from Eqs. (10.1), (10.16), and (10.18), we eventually find

$$S = \sum_{i=1}^{M} N_i k\left[\frac{T}{Z_i}\left(\frac{\partial Z_i}{\partial T}\right)_{V,N_i} + \ln\left(\frac{Z_i}{N_i}\right) + 1\right]. \tag{10.25}$$

Upon substitution from Eq. (10.19), Eq. (10.25) becomes

$$S = \sum_{i=1}^{M} n_i R\left[T\left(\frac{\partial \ln Z_i}{\partial T}\right)_{V,N_i} + \ln\left(\frac{Z_i}{N_i}\right) + 1\right]. \tag{10.26}$$

However, from Eq. (4.40) for the ith pure component,

$$s_i = R\left[T\left(\frac{\partial \ln Z_i}{\partial T}\right)_{V,N_i} + \ln\left(\frac{Z_i}{N_i}\right) + 1\right]; \tag{10.27}$$

thus, substituting Eq. (10.27) into Eq. (10.26), we obtain

$$S = \sum_{i=1}^{M} n_i s_i. \tag{10.28}$$

Consequently, the total entropy of an ideal gas mixture can be calculated by simply adding contributions to the entropy from each component of the mixture at the same temperature and assembly volume. In other words, there is no entropy of mixing when gases are combined at the same temperature and total volume; however, as discussed in all textbooks on classical thermodynamics, an entropy of mixing *does* occur if we try to combine gases at the same temperature and total mixture *pressure*.

Because the internal energy and entropy are both additive with respect to their component contributions, all other thermodynamic properties must also be additive at the same assembly temperature and volume. On this basis, the additive rule for any ideal gas property follows analogously from Eqs. (10.22) and (10.28). As an example, for the Gibbs free energy, we may write

$$G = \sum_{i=1}^{M} n_i g_i,$$

so that the specific Gibbs free energy for the mixture becomes

$$g = \sum_{i=1}^{M} x_i g_i,$$

where x_i is the mole fraction for the ith component of the mixture.

In essence, for any thermodynamic property, this additive feature arises from the lack of atomic or molecular interactions among particles in an ideal gas mixture. Consequently, if we define the partial pressure as that pressure contributed by the ith pure component *at the same assembly temperature and volume*, we obtain, from either Eq. (9.9) or Eq. (4.31),

$$P_i = N_i kT\left(\frac{\partial \ln Z_i}{\partial V}\right)_T = \frac{N_i kT}{V}, \tag{10.29}$$

where, of course, the total number of particles is given by

$$N = \sum_{i=1}^{M} N_i. \tag{10.30}$$

Therefore, from Eqs. (4.31), (10.29), and (10.30), we have

$$P = \frac{NkT}{V} = \frac{kT}{V}\sum_{i=1}^{M} N_i = \sum_{i=1}^{M} P_i,$$

which is Dalton's law of partial pressures. Notice, again, the importance of the fact that all component properties are functions only of the assembly temperature and volume, as based on the same functional dependence for the constituent partition functions. In other words, each component of an ideal gas mixture does indeed act as if it alone occupies the total volume of the mixture at the given assembly temperature.

EXAMPLE 10.1

A pressure vessel contains a 50/50 mixture of He and Ar by volume at 500 K and 10 bar. Assuming ideal gas behavior, calculate the specific entropy of the mixture (J/K mol). Note that, for all inert gases, the first excited electronic state is at least 10 eV above the ground electronic state.

Solution

From Eq. (10.28), the specific entropy for a 50/50 mixture of He and Ar by volume is

$$\frac{s}{R} = \sum_{i=1}^{2} x_i \left(\frac{s_i}{R}\right) = 0.5\left(\frac{s_1}{R}\right) + 0.5\left(\frac{s_2}{R}\right),$$

where s_1 is the specific entropy of He and s_2 is the specific entropy of Ar. To calculate the specific entropy for these two monatomic gases, we require their translational and electronic contributions, as given by Eqs (9.12) and (9.20):

$$\left(\frac{s}{R}\right)_{tr} = \frac{5}{2}\ln T + \frac{3}{2}\ln M - \ln P - 1.1516$$

$$\left(\frac{s}{R}\right)_{el} = \frac{Z'_{el}}{Z_{el}} + \ln Z_{el} = \ln g_0.$$

From Appendix J.1, the ground-state term symbol for all noble gases is $^1S_0$, from which we conclude that the ground-state degeneracy is $g_0 = 1$. Therefore, the only effective contribution to the entropy comes from the translational mode. Now, because each component of this ideal gas mixture acts as if it alone occupies the pressure vessel at 500 K, the pressure used in the Sackur–Tetrode equation to determine the translational contribution of each component must be the partial pressure, which is $P_1 = P_2 = 5$ bar. Hence, we have

$$\frac{s_1}{R} = \frac{5}{2}\ln(500) + \frac{3}{2}\ln(4.0026) - \ln(5) - 1.1516$$

$$\frac{s_2}{R} = \frac{5}{2}\ln(500) + \frac{3}{2}\ln(39.948) - \ln(5) - 1.1516$$

for helium and argon, respectively. On this basis, the dimensionless entropy for the mixture becomes

$$\frac{s}{R} = \frac{5}{2}\ln(500) + \frac{3}{4}[\ln(4.0026) + \ln(39.948)] - \ln(5) - 1.1516 = 16.581\,.$$

Hence, evaluating the specific entropy for the mixture, we obtain

$$s = 16.581\,(8.3145\ \text{J/K}\cdot\text{mol}) = 137.865\ \text{J/K}\cdot\text{mol}.$$

10.3 The Reacting Ideal Gas Mixture

The reacting ideal gas mixture can initially be considered in a manner quite similar to that used for the nonreactive mixture, except that we must now account for two neoteric factors that will eventually produce substantially different results and conclusions. The first factor is the obvious constraint imposed by atom conservation during chemical reactions. The second factor concerns our choice for a zero of energy. Whereas for nonreactive mixtures, we can calculate the total internal energy by referencing the particle energy for each component to its lowest accessible level, the same cannot be done for reactive mixtures owing to the release or absorption of chemical energy. Therefore, if we are to properly account for this chemical energy, we must choose a zero of energy common to all species within the gaseous assembly.

As indicated in Section 9.2.2, this common zero of energy is invariably chosen to be the ground electronic state of each constituent atom in the reacting system. Recall that in Section 10.1, ε_{ij} indicated the particle energy for the jth level, as determined relative to the lowest accessible state of the ith pure component. In comparison, we now define ε'_{ij} as the particle energy, again for the jth level of the ith pure component, but now evaluated relative to a common reference level chosen at the ground electronic state of any dissociated atom in the gaseous assembly. Employing, for consistency, the $D_\circ$-formulation of Table 9.2, the particle energy for atoms or molecules, based on this common zero of energy, can then be expressed as

$$\begin{aligned} &\text{atoms:} \quad \varepsilon'_{ij} = \varepsilon_{ij} \\ &\text{molecules:} \quad \varepsilon'_{ij} = \varepsilon_{ij} - D_{\circ i}, \end{aligned} \tag{10.31}$$

where the dissociation energy, $D_{\circ i}$, accounts for any heat produced or absorbed by chemical reaction.

10.3.1 Equilibrium Particle Distribution for Reactive Ideal Gas Mixture

As in Section 10.1, the equilibrium particle distribution for a reactive mixture can always be determined by identifying the most probable macrostate. Hence, we again have from Eq. (10.7),

$$d\ln W = \sum_{i=1}^{M}\sum_{j}\ln\left(\frac{g_{ij}}{N_{ij}}\right)dN_{ij} = 0,$$

except that the Lagrange method of undetermined multipliers must now be applied to an equilibrium chemical reaction. For pedagogical reasons, we temporarily choose this reaction to be

$$\nu_A A + \nu_B B \rightleftarrows C,$$

where the ν_i are stoichiometric coefficients converting two atoms, A and B, to the molecule, C. Therefore, for the three components of this reacting assembly, we have

$$d\ln W = \sum_j \ln\left(\frac{g_{Aj}}{N_{Aj}}\right) dN_{Aj} + \sum_j \ln\left(\frac{g_{Bj}}{N_{Bj}}\right) dN_{Bj} + \sum_j \ln\left(\frac{g_{Cj}}{N_{Cj}}\right) dN_{Cj} = 0. \tag{10.32}$$

Imposing particle-conservation constraints for both atomic species plus the usual constraint on energy conservation, all in differential form, we also have

$$\sum_j dN_{Aj} + \sum_j \nu_A\, dN_{Cj} = 0 \tag{10.33}$$

$$\sum_j dN_{Bj} + \sum_j \nu_B\, dN_{Cj} = 0 \tag{10.34}$$

$$\sum_j \varepsilon'_{Aj}\, dN_{Aj} + \sum_j \varepsilon'_{Bj}\, dN_{Bj} + \sum_j \varepsilon'_{Cj}\, dN_{Cj} = 0, \tag{10.35}$$

where Eq. (10.33) denotes conservation of A-atoms, Eq. (10.34) denotes conservation of B-atoms, and Eq. (10.35) indicates conservation of energy, as based on a common zero of energy for each species involved in the chemical reaction.

From Eqs. (10.32–10.35), the Lagrange condition becomes

$$\begin{aligned} d\ln W = &\sum_j \left\{\ln\left(\frac{g_{Aj}}{N_{Aj}}\right) - \alpha_A - \beta\varepsilon'_{Aj}\right\} dN_{Aj} + \sum_j \left\{\ln\left(\frac{g_{Bj}}{N_{Bj}}\right) - \alpha_B - \beta\varepsilon'_{Bj}\right\} dN_{Bj} \\ &+ \sum_j \left\{\ln\left(\frac{g_{Cj}}{N_{Cj}}\right) - \alpha_A\nu_A - \alpha_B\nu_B - \beta\varepsilon'_{Cj}\right\} dN_{Cj} = 0, \end{aligned} \tag{10.36}$$

where we have introduced the usual Lagrange multipliers, here denoted as α_A, α_B, and β. From Eq. (10.36), we obtain the three equilibrium conditions,

$$N_{Aj} = g_{Aj} \exp\left[-(\alpha_A + \beta\varepsilon_{Aj})\right] \tag{10.37}$$

$$N_{Bj} = g_{Bj} \exp\left[-(\alpha_B + \beta\varepsilon_{Bj})\right] \tag{10.38}$$

$$N_{Cj} = g_{Cj} \exp\left\{-[\nu_A\alpha_A + \nu_B\alpha_B + \beta(\varepsilon_{Cj} - \mathrm{D}_\circ)]\right\}, \tag{10.39}$$

where Eq. (10.31) has been used to reintroduce individual zeros of energy, as normally prescribed for each pure constituent of a gaseous mixture. For simplicity, we have also eliminated the second subscript on the dissociation energy since our chosen equilibrium reaction manifests only a single molecular component.

We next sum each of the Eqs. (10.37–10.39) over all possible energy levels, thus obtaining

$$N_A = \sum_j N_{Aj} = e^{-\alpha_A} Z_A \tag{10.40}$$

$$N_B = \sum_j N_{Bj} = e^{-\alpha_B} Z_B \tag{10.41}$$

$$N_C = \sum_j N_{Cj} = e^{-\nu_A\alpha_A - \nu_B\alpha_B + \mathrm{D}_\circ/kT} Z_C, \tag{10.42}$$

where we have simultaneously invoked $\beta = 1/kT$ and the partition function for each species, in recognition of Eq. (10.15). Finally, dividing Eqs. (10.37–10.39) by Eqs. (10.40–10.42), respectively, we have

$$\frac{N_{Aj}}{N_A} = \frac{g_{Aj} e^{-\varepsilon_{Aj}/kT}}{Z_A} \tag{10.43}$$

$$\frac{N_{Bj}}{N_B} = \frac{g_{Bj} e^{-\varepsilon_{Bj}/kT}}{Z_B} \tag{10.44}$$

$$\frac{N_{Cj}}{N_C} = \frac{g_{Cj} e^{-\varepsilon_{Cj}/kT}}{Z_C}, \tag{10.45}$$

so that the particle distribution describing corrected Maxwell–Boltzmann statistics for each species is the same, whether the mixture is reactive or nonreactive.

10.3.2 Equilibrium Constant: Introduction and Development

We are now ready to introduce an expression depicting the equilibrium constant for our chosen chemical reaction. Substituting Eqs. (10.40) and (10.41) into Eq. (10.42), we have

$$\frac{N_C}{Z_C} = \left(\frac{N_A}{Z_A}\right)^{\nu_A} \left(\frac{N_B}{Z_B}\right)^{\nu_B} e^{\mathrm{D}_\circ/kT},$$

so that

$$\frac{N_C}{N_A^{\nu_A} N_B^{\nu_B}} = \frac{Z_C}{Z_A^{\nu_A} Z_B^{\nu_B}} e^{\mathrm{D}_\circ/kT}. \tag{10.46}$$

The particle number density and the species partition function per unit volume are defined by

$$n_i = \frac{N_i}{V} \tag{10.47}$$

$$\phi_i = \frac{Z_i}{V}. \tag{10.48}$$

Therefore, Eq. (10.46) can be expressed as

$$K_c(T) = \frac{n_C}{n_A^{\nu_A} n_B^{\nu_B}} = \frac{\phi_C}{\phi_A^{\nu_A} \phi_B^{\nu_B}} e^{\mathrm{D}_\circ/kT}, \tag{10.49}$$

where K_c is the *equilibrium constant based on concentration*, here in particles/cm^3. We recall, from Eq. (9.4), that the translational partition function is linearly related to the volume; thus, Eq. (10.48) shows that the species partition function per unit volume, ϕ_i, is a function only of temperature. On this basis, from Eq. (10.49), we conclude that the equilibrium constant itself is also only a function of temperature.

Although K_c is very useful for chemical kinetics, as we will see in Chapter 17, typical composition calculations and comparisons to JANAF tabulations benefit from an equilibrium constant based instead on pressure (bar). Beginning from Eq. (10.29), we note that, for a given temperature and volume,

$$N_i = \left(\frac{P_i}{P_\circ}\right) N_\circ, \tag{10.50}$$

where $N_\circ$ represents the number of particles at a chosen reference pressure, $P_\circ$, of 1 bar. Substituting Eq. (10.50) into Eq. (10.46), we obtain

$$\frac{(P_C/P_\circ)}{(P_A/P_\circ)^{\nu_A}(P_B/P_\circ)^{\nu_B}} = \frac{(Z_C/N_\circ)}{(Z_A/N_\circ)^{\nu_A}(Z_B/N_\circ)^{\nu_B}} e^{\mathrm{D}_\circ/kT}. \tag{10.51}$$

Hence, if all pressures are defined in bars, the usual dimensionless *equilibrium constant based on pressure* (Appendix F) becomes for the chosen chemical reaction,

$$K_p = \frac{(P_C/P_\circ)}{(P_A/P_\circ)^{\nu_A}(P_B/P_\circ)^{\nu_B}}.$$

On this basis, Eq. (10.51) becomes

$$K_p(T) = \frac{(Z_C/N)_\circ}{(Z_A/N)_\circ^{\nu_A}(Z_B/N)_\circ^{\nu_B}} e^{\mathrm{D}_\circ/kT}, \tag{10.52}$$

where we have defined, using Eq. (10.29), the normalized partition function for each species as

$$\left(\frac{Z_i}{N}\right)_\circ = Z_{i,tr}\, Z_{i,int} \left(\frac{kT}{P_\circ V}\right).$$

Substituting for the translational partition function from Eq. (9.4), we then have

$$\left(\frac{Z_i}{N}\right)_\circ = \frac{(2\pi m_i)^{3/2}}{h^3 P_\circ} (kT)^{5/2}\, Z_{i,int}, \tag{10.53}$$

which explicitly eliminates any volume dependence at a standard pressure of 1 bar. As a result, the normalized partition function depends only on temperature, so that, from Eq. (10.52), the equilibrium constant based on pressure must also be a function only of temperature.

Equations (10.49) and (10.52) represent equilibrium constants based on concentration and pressure, respectively, for our chosen reaction at chemical equilibrium. Analogous equilibrium constants for generic reactions can easily be derived by implementing a semiclassical approach based on the Gibbs free energy, as exploited in Section 10.4. Regardless of the particular reaction, however, *equilibrium constants always depend solely on temperature* because volumetric normalization of each species partition function effectively eliminates the linear dependence on volume introduced by the translational energy mode. Here, we see the persuasive power of statistical thermodynamics in explaining satisfactorily an equilibrium concept often misunderstood in classical thermodynamics. Finally, we note that equilibrium constants depend directly on species partition functions rather than on their logarithms, as for all previous thermodynamic properties. Therefore, in contrast to other such properties, accurate equilibrium constants mandate irrefutable calculations of all associated partition functions.

10.4 Equilibrium Constant: General Expression and Specific Examples

The equilibrium constant introduced in the previous section is peculiar to a specific chemical reaction for which a diatomic molecule is in equilibrium with its constituent atoms. We

now wish to develop a more robust K_p expression based on the general chemical reaction,

$$\sum_i \nu_i \mathrm{M}_i = 0\,,$$

where the M_i represent various chemical symbols and the ν_i are related stoichiometric coefficients, which are defined to be positive for products and negative for reactants. As an example, for the equilibrium chemical reaction $3\mathrm{H}_2 + \mathrm{N}_2 \rightleftarrows 2\mathrm{NH}_3$, the stoichiometric coefficients for ammonia, hydrogen, and nitrogen are 2, −3, and −1, respectively. Employing this nomenclature, the equilibrium constant based on pressure, from classical thermodynamics (Appendix F), is

$$K_p = \prod_i \left(\frac{P_i}{P_\circ}\right)^{\nu_i}, \tag{10.54}$$

where $P_\circ = 1$ bar, thus mandating that all partial pressures be expressed exclusively in bars. Similarly, from classical thermodynamics, the equilibrium constant can be related to standard-state chemical potentials for each reactive species by

$$\ln K_p = -\frac{\sum_i \nu_i \mu_i^\circ}{RT}, \tag{10.55}$$

where μ_i° is the chemical potential for the *ith* species, evaluated at $P_\circ = 1$ bar.

As might be expected from Eq. (10.55), the crucial connection between classical and statistical thermodynamics occurs through the chemical potential for each gaseous component, which from Eq. (4.39) is

$$\frac{\mu_i}{RT} = -\ln\left(\frac{Z_i'}{N}\right). \tag{10.56}$$

Here, we have employed a common zero of energy for both atoms and molecules, so that the partition function for the *i*th species becomes

$$Z_i' = \sum_j g_{ij} e^{-\varepsilon_{ij}'/kT}.$$

Hence, from Eqs. (10.31) and (10.56), the chemical potential at $P_\circ = 1$ bar can be expressed as

$$\mu_i^\circ = -RT\left[\ln\left(\frac{Z_i}{N}\right)_\circ + \frac{\mathrm{D}_{\circ i}}{kT}\right], \tag{10.57}$$

where, by definition, the dissociation energy is $\mathrm{D}_{\circ i} = 0$ for any atom in the reactive mixture.

Substituting Eq. (10.57) into Eq. (10.55), next we have

$$\ln K_p = \sum_i \nu_i \ln\left(\frac{Z_i}{N}\right)_\circ + \sum_i \nu_i \left(\frac{\mathrm{D}_{\circ i}}{kT}\right),$$

from which we obtain

$$K_p = \prod_i \left(\frac{Z_i}{N}\right)_\circ^{\nu_i} \exp\left(\frac{\sum_i \nu_i \mathrm{D}_{\circ i}}{kT}\right). \tag{10.58}$$

Equation (10.58) represents our desired result, i.e., the equilibrium constant based on pressure for any reaction at chemical equilibrium. We thus realize that Eq. (10.52) is merely a special case of Eq. (10.58). Finally, exploiting the similarity between Eqs. (10.49)

and (10.52), we may also establish an analogous expression for the generic equilibrium constant based on concentration, i.e.,

$$K_c = \prod_i n^{\nu_i} = \prod_i \phi_i^{\nu_i} \exp\left(\frac{\sum_i \nu_i \mathrm{D}_{\circ i}}{kT}\right). \tag{10.59}$$

EXAMPLE 10.2

The reaction $\mathrm{A}(v, J) + \mathrm{M} \rightleftarrows \mathrm{A}(v, J - \Delta J) + \mathrm{M}$ describes rotational relaxation for a generic diatomic molecule from rotational level, J, to rotational level, $J - \Delta J$, upon collision with the nonreactive species, M. Employing the simplex model, show that the equilibrium constant based on number density for this energy-transfer reaction is given by

$$K_c = \left(1 - \frac{2\Delta J}{g_J}\right) \exp\left[\frac{\theta_r \Delta J}{T}(g_J - \Delta J)\right],$$

where the rotational degeneracy is $g_J = 2J + 1$.

Solution

From Eq. (10.59), the equilibrium constant for this energy-transfer reaction is

$$K_c = \frac{n(v, J - \Delta J)}{n(v, J)}.$$

Now, from Eq. (4.14), the population ratio between the number density associated specifically with (v, J) and the total number density describing all possible rotational and vibrational levels is

$$\frac{n(v, J)}{n} = \frac{g_J}{Z_{rot} Z_{vib}} \exp\left[-\frac{J(J+1)\theta_r + v\theta_v}{T}\right].$$

Similarly, for the number density associated specifically with $(v, J - \Delta J)$, we have

$$\frac{n(v, J - \Delta J)}{n} = \frac{g_{J-\Delta J}}{Z_{rot} Z_{vib}} \exp\left[-\frac{(J - \Delta J)(J - \Delta J + 1)\theta_r + v\theta_v}{T}\right].$$

Dividing the latter by the former, we obtain for the equilibrium constant

$$K_c = \frac{n(v, J - \Delta J)}{n(v, J)} = \frac{2(J - \Delta J) + 1}{2J + 1} \times \exp\left\{\frac{[J(J+1) - (J - \Delta J)(J - \Delta J + 1)]\theta_r}{T}\right\}$$

so that

$$K_c = \frac{2J + 1 - 2\Delta J}{2J + 1} \exp\left[\frac{(2J + 1 - \Delta J)\Delta J \theta_r}{T}\right].$$

On this basis, we find that

$$K_c = \left(1 - \frac{2\Delta J}{g_J}\right) \exp\left[\frac{\theta_r \Delta J}{T}(g_J - \Delta J)\right],$$

which verifies the given expression for the equilibrium constant.

10.4.1 Dissociation of a Homonuclear Diatomic

We now discuss three special cases, so as to exercise our ability to consider various applications of Eqs. (10.58) and (10.59). We begin with the dissociation of any homonuclear diatomic,

$$A_2 + M \rightleftarrows A + A + M,$$

where M represents a species energetic enough to break the chemical bond forming A_2 and also sufficiently absorptive to permit bond formation upon collision of two A-atoms. Applying Eq. (10.59) to this equilibrium reaction, we obtain

$$K_c = \frac{\phi_A^2}{\phi_{A_2}} e^{-D_\circ/kT}, \tag{10.60}$$

where $D_\circ$ is the dissociation energy for A_2. Similarly, applying Eq. (10.58), we obtain the equilibrium constant based on pressure, as given by

$$K_p = \frac{(Z_A/N)_\circ^2}{(Z_{A_2}/N)_\circ} e^{-D_\circ/kT}. \tag{10.61}$$

Now, from Eqs. (9.4) and (10.48),

$$\phi_i = \frac{Z_{tr}}{V} Z_{int} = \left(\frac{2\pi m_i kT}{h^2}\right)^{3/2} Z_{int}\,, \tag{10.62}$$

so that, from Eq. (10.60), we have

$$K_c = \frac{(\pi m_A kT)^{3/2}}{h^3} \left(\frac{Z_{A,int}^2}{Z_{A_2,int}}\right) e^{-D_\circ/kT}. \tag{10.63}$$

Similarly, from Eq. (10.53), Eq. (10.61) becomes

$$K_p = \frac{(\pi m_A)^{3/2}}{h^3 P_\circ} (kT)^{5/2} \left(\frac{Z_{A,int}^2}{Z_{A_2,int}}\right) e^{-D_\circ/kT}. \tag{10.64}$$

Equations (10.63) and (10.64) are completely accurate since no assumptions have been made with respect to the internal partition functions. If, on the other hand, we assume that only the ground electronic states are populated for both the atom and molecule, the required internal partition functions can be approximated as

$$Z_{A,int} = g_{0,A} \tag{10.65}$$

$$Z_{A_2,int} = \frac{g_{0,A_2}}{2} \left(\frac{T}{\theta_r}\right) [1 - e^{-\theta_v/T}]^{-1}, \tag{10.66}$$

where we have invoked the simplex model by implementing Eqs. (9.26) and (9.47). On this basis, Eqs. (10.63) and (10.64) become

$$K_c = \frac{2(\pi m_A kT)^{3/2}}{h^3} \left(\frac{g_{0,A}^2}{g_{0,A_2}}\right) \left(\frac{\theta_r}{T}\right) [1 - e^{-\theta_v/T}]\, e^{-D_\circ/kT} \tag{10.67}$$

$$K_p = \frac{2(\pi m_A)^{3/2}}{h^3 P_\circ} (kT)^{5/2} \left(\frac{g_{0,A}^2}{g_{0,A_2}}\right) \left(\frac{\theta_r}{T}\right) [1 - e^{-\theta_v/T}]\, e^{-D_\circ/kT}. \tag{10.68}$$

The calculation of equilibrium compositions requires that we review some well-known procedures of classical thermodynamics. Suppose that we begin with one mole of A_2, which reacts to form an equilibrium mixture of A and A_2 at a specified temperature and pressure. For this system, the overall mass-balance reaction,

$$A_2 \rightarrow n_{A_2} A_2 + n_A A,$$

gives, through conservation of atomic species, the relation

$$2n_{A_2} + n_A = 2,$$

where n_{A_2} and n_A are the number of moles of A_2 and A, respectively. Defining the degree of dissociation as

$$\alpha \equiv \frac{n_A}{2n_{A_2} + n_A} = \frac{n_A}{2},$$

we also have

$$n_A = 2\alpha \qquad n_{A_2} = 1 - \alpha \qquad n_A + n_{A_2} = 1 + \alpha. \tag{10.69}$$

From Eqs. (10.19), (10.29), and (10.69), the partial pressures for A and A_2 can be expressed as

$$P_A = \left(\frac{2\alpha}{1+\alpha}\right) P \qquad P_{A_2} = \left(\frac{1-\alpha}{1+\alpha}\right) P,$$

where P is the total pressure. Hence, the equilibrium constant, from Eq. (10.54), becomes

$$K_p = \frac{(P_A/P_\circ)^2}{(P_{A_2}/P_\circ)} = \frac{4\alpha^2}{1-\alpha^2}\left(\frac{P}{P_\circ}\right), \tag{10.70}$$

so that the only unknown quantity is the degree of dissociation. Combining Eqs. (10.64) and (10.70), the degree of dissociation can be obtained implicitly from

$$\frac{\alpha^2}{1-\alpha^2} = \frac{(\pi m_A)^{3/2}}{4h^3 P}(kT)^{5/2}\left(\frac{Z_{A,int}^2}{Z_{A_2,int}}\right) e^{-\mathrm{D}_\circ/kT}. \tag{10.71}$$

Therefore, though K_p is a function solely of temperature, the degree of dissociation depends on both temperature and pressure, as expected from classical thermodynamics. Having solved for the degree of dissociation, the number of moles for each species and thus their mole fractions can ultimately be determined from Eq. (10.69). On this basis, the equilibrium composition during homonuclear dissociation is clearly influenced by both temperature and pressure. In summary, for all chemical reactions, once K_p is determined from statistical thermodynamics, classical thermodynamics can always be used to calculate the equilibrium composition.

EXAMPLE 10.3

Calculate the equilibrium constant based on pressure for the reaction, $N_2 + M \rightleftarrows N + N + M$, at 3000 K.

Solution

From Eq. (10.64), the equilibrium constant is

$$K_p = \frac{(\pi m_N)^{3/2}}{h^3 P_\circ}(kT)^{5/2}\left(\frac{Z_{N,int}^2}{Z_{N_2,int}}\right) e^{-\mathrm{D}_\circ/kT}.$$

Now, from Examples 9.2 and 9.5, the internal contributions to the partition function at 3000 K are

$$Z_{N,int} = Z_{N,el} = 4.0010$$

$$Z_{N_2,int} = Z_{el}\, Z^{\circ}_{R-V}\, Z_{corr} = (1.0000)\,(778.80)\,(1.0139) = 789.63.$$

From Appendix K.1, the dissociation energy for molecular nitrogen is

$$D_{\circ} = 9.759 \text{ eV}\left(1.602 \times 10^{-19} \text{ J/eV}\right) = 1.5634 \times 10^{-18} \text{ J}.$$

Hence, we have

$$\left(\frac{Z^2_{N,int}}{Z_{N_2,int}}\right) e^{-\mathrm{D}_{\circ}/kT} = \frac{(4.0010)^2}{(789.63)} \exp\left[-\frac{1.5634 \times 10^{-18}}{(1.3807 \times 10^{-23})\,(3000)}\right] = 8.2211 \times 10^{-19}.$$

Evaluating the equilibrium constant, we thus obtain

$$K_p = \frac{\left[\pi\,(14.0067)\,(1.6605 \times 10^{-27})\right]^{3/2}}{(6.6261 \times 10^{-34})^3\,(1.0 \times 10^5)} \left[(1.3807 \times 10^{-23})\,(3000)\right]^{5/2} \times \left(8.2211 \times 10^{-19}\right) = 1.949 \times 10^{-10}.$$

10.4.2 The Homonuclear–Heteronuclear Conversion Reaction

The conversion from two homonuclear diatomics to a single heteronuclear diatomic can be represented at chemical equilibrium by

$$\mathrm{A_2} + \mathrm{B_2} \rightleftarrows 2\mathrm{AB}.$$

From Eq. (10.58), the equilibrium constant based on pressure for this reaction becomes

$$K_p = \frac{(Z_{AB}/N)^2_{\circ}}{(Z_{A_2}/N)_{\circ}\,(Z_{B_2}/N)_{\circ}} \exp\left(-\frac{\Delta h^{\circ}_0}{RT}\right), \tag{10.72}$$

where, for convenience, we have converted to the classic enthalpy of reaction for the hypothetical ideal gas at absolute zero (kJ/mol),

$$\Delta h^{\circ}_0 = -N_A \sum_i \nu_i \mathrm{D}_{\circ i} = N_A\,(\mathrm{D}_{\circ,A_2} + \mathrm{D}_{\circ,B_2} - 2\mathrm{D}_{\circ,AB}), \tag{10.73}$$

for which N_A is Avagadro's number. Based on Eqs. (10.53) and (10.66), the normalized partition function for any diatomic molecule confined to its ground electronic state can be written as

$$\left(\frac{Z_i}{N}\right)_{\circ} = \frac{(2\pi m_i)^{3/2}}{h^3 P_{\circ}} (kT)^{5/2} \left(\frac{g_{0,i}\,T}{\sigma_i \theta_{ri}}\right) [1 - e^{-\theta_{vi}/T}]^{-1}, \tag{10.74}$$

where we have again presumed the simplex model with $T/\theta_r > 30$. Substituting Eq. (10.74) into Eq. (10.72) for each species, we eventually find that

$$K_p = \left(\frac{m^2_{AB}}{m_{A_2} m_{B_2}}\right)^{3/2} \left(\frac{g^2_{0,AB}}{g_{0,A_2} g_{0,B_2}}\right) \left(\frac{4\theta_{r,A_2}\theta_{r,B_2}}{\theta^2_{r,AB}}\right) \times \frac{\left[1 - e^{-\theta_{v,A_2}/T}\right]\left[1 - e^{-\theta_{v,B_2}/T}\right]}{\left[1 - e^{-\theta_{v,AB}/T}\right]^2} \exp\left(-\frac{\Delta h^{\circ}_0}{RT}\right).$$

Because the total number of moles is invariant for this particular equilibrium reaction, we find, as might have been expected from Eqs. (10.58) and (10.59), that the above K_p expression is equivalent to that for K_c.

10.4.3 The Ionization Reaction

The ionization of an atomic species, for example in a plasma or flame, can be represented chemically by the reversible reaction

$$\mathrm{A} \rightleftarrows \mathrm{A}^+ + e^-,$$

for which the equilibrium constant based on concentration becomes, from Eq. (10.59),

$$K_c = \frac{\phi_e \phi_{A^+}}{\phi_A} \exp\left(-\frac{I}{kT}\right), \tag{10.75}$$

where I is called the ionization potential. From Eqs. (10.62) and (10.65), the partition function per unit volume for either atomic species is

$$\phi_i = \left(\frac{2\pi m_i kT}{h^2}\right)^{3/2} g_{0,i}. \tag{10.76}$$

Similarly, for the electron,

$$\phi_e = 2\left(\frac{2\pi m_e kT}{h^2}\right)^{3/2}, \tag{10.77}$$

where here the factor of two accounts for the two possible intrinsic spin states of an electron. Recognizing that the masses of the ionized and parent atom are essentially equivalent, we obtain, by combining Eqs. (10.75–10.77),

$$K_c = 2\left(\frac{2\pi m_e kT}{h^2}\right)^{3/2} \left(\frac{g_{0,A^+}}{g_{0,A}}\right) e^{-I/kT}. \tag{10.78}$$

EXAMPLE 10.4

Using the simplex model, show that the equilibrium constant for the chemical reaction $\mathrm{O_2} + \frac{1}{2}\mathrm{N_2} \rightleftarrows \mathrm{NO_2}$ is given by

$$K_p = \kappa_1 \Lambda_{\mathrm{N_2}}^{3/2} \left(\frac{P_\circ}{kT}\right)^{1/2} \frac{Z_{\mathrm{NO_2},int}}{Z_{\mathrm{O_2},int} Z_{\mathrm{N_2},int}^{1/2}} \exp\left(-\frac{\kappa_2}{T}\right),$$

where the thermal de Broglie wavelength is

$$\Lambda_i = \frac{h}{\sqrt{2\pi m_i kT}},$$

and the constants $\kappa_1 = 1.724$ and $\kappa_2 = 4320$ K.

Solution

From Eqs. (10.58) and (10.73), the equilibrium constant based on pressure is

$$K_p = \prod_i \left(\frac{Z_i}{N}\right)_\circ^{\nu_i} \exp\left(\frac{\sum_i \nu_i \mathrm{D}_{\circ i}}{kT}\right) = \prod_i \left(\frac{Z_i}{N}\right)_\circ^{\nu_i} \exp\left(-\frac{\Delta h_0^\circ}{RT}\right),$$

where, from Eq. (10.53),

$$\left(\frac{Z_i}{N}\right)_\circ = \left(\frac{2\pi m_i kT}{h^2}\right)^{3/2}\left(\frac{kT}{P_\circ}\right) Z_{i,int} = \left(\frac{kT}{\Lambda_i^3 P_\circ}\right) Z_{i,int}.$$

Applying these expressions to $O_2 + \frac{1}{2}N_2 \rightleftarrows NO_2$, we obtain

$$K_p = \frac{(Z_{NO_2}/N)_\circ}{(Z_{O_2}/N)_\circ (Z_{N_2}/N)_\circ^{1/2}} \exp\left(-\frac{\Delta h_0^\circ}{RT}\right),$$

so that, via substitution, we may verify

$$K_p = \kappa_1 \Lambda_{N_2}^{3/2}\left(\frac{P_\circ}{kT}\right)^{1/2} \frac{Z_{NO_2,int}}{Z_{O_2,int} Z_{N_2,int}^{1/2}} \exp\left(-\frac{\kappa_2}{T}\right),$$

where

$$\kappa_1 = \frac{\Lambda_{O_2}^3}{\Lambda_{NO_2}^3}$$

$$\kappa_2 = \frac{\Delta h_0^\circ}{R}.$$

On this basis, κ_1 and κ_2 may be evaluated as follows:

$$\kappa_1 = \left(\frac{m_{NO_2}}{m_{O_2}}\right)^{3/2} = \left(\frac{46.008}{32.000}\right)^{3/2} = 1.724$$

$$\kappa_2 = \frac{\Delta h_0^\circ}{R} = \frac{35927\ \text{J/mol}}{8.3145\ \text{J/K} \cdot \text{mol}} = 4320\ \text{K},$$

where here Δh_0° is the standard enthalpy of formation for NO_2 at absolute zero, as obtained from the appropriate JANAF table in Appendix E. Hence, we have verified the given numerical values for κ_1 and κ_2.

Problems enhancing your understanding of this chapter are combined with those for Chapter 11 in Problem Set V.

11 Concentration and Temperature Measurements

To this point, we have applied statistical mechanics and spectroscopy to the calculation of thermodynamic properties for both nonreactive and reactive mixtures of ideal gases. From a diagnostic perspective, spectroscopy and statistical thermodynamics can also be linked to determine the concentration and temperature in a gaseous mixture. The fundamental strategy is to deduce from a given spectroscopic measurement the number density (particles/cm^3) associated with a chosen internal energy level, $n_{int,j}$, and then to apply relevant Maxwell–Boltzmann distributions to evaluate concentration or temperature. From Eq. (4.14), we may thus determine the total number density, n, for an atom or molecule by invoking

$$\frac{n_{int,j}}{n} = \frac{g_{int,j}}{Z_{int}} \exp\left(-\frac{\varepsilon_{int,j}}{kT}\right), \tag{11.1}$$

where, from Section 8.4, the degeneracy and partition function need include only those internal energy modes accessed by the implemented spectroscopic technique. Similarly, from Eq. (4.15), the temperature can be determined from a ratio of level populations via

$$\frac{n_{int,m}}{n_{int,n}} = \frac{g_{int,m}}{g_{int,n}} \exp\left(-\frac{\varepsilon_{int,m} - \varepsilon_{int,n}}{kT}\right), \tag{11.2}$$

where the subscripts m and n refer to specific energy levels of an atom or molecule.

In general, the number density corresponding to a specific energy level can be obtained by optically probing suitable transitions with an available light source, such as a Xe-arc lamp, a pulsed laser, or a continuous wave laser. Equation (11.2) indicates that the temperature can be evaluated by simultaneously or sequentially probing two different signatures in the spectrum, while Eq. (11.1) implies that only a single spectral line is required to determine the number density, although knowledge of the temperature appears necessary. Fortunately, in many cases, an energy level can be chosen whose population is relatively insensitive to wide variations in temperature. Nonetheless, whether exploiting Eq. (11.1) or (11.2), a fundamental relation is required between $n_{int,j}$ and an optical parameter of the chosen measurement. Such relations can be developed once we understand mode temperatures and the basic theory describing the various interactions of radiation with matter.

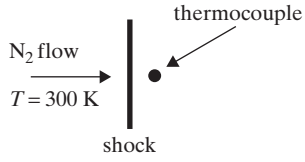

Figure 11.1 Measurement of T_{tr} behind a shock wave.

11.1 Mode Temperatures

The specific temperature characterizing a single energy mode can be defined by applying Eq. (11.2) to the population distribution for that mode. Hence, the rotational temperature becomes

$$T_{rot} = \frac{\varepsilon_{rot,n} - \varepsilon_{rot,m}}{k \ln\left(\dfrac{g_{rot,n} n_{rot,m}}{g_{rot,m} n_{rot,n}}\right)}, \tag{11.3}$$

where the indices n and m now refer to two different rotational energies, whether these levels are monitored via microwave, infrared, visible, or ultraviolet spectroscopy. Analogous definitions, of course, exist for the remaining energy modes, whether translation, vibration, or electronic.

The significance of such *mode temperatures* can be understood by considering the thermal history of N_2 upon its passage through a shock wave. Suppose that this shock is stabilized in a tube by flowing N_2 in an opposite direction, such that the temperature sufficiently far downstream can be measured by an appropriate thermocouple, as shown in Fig. 11.1. Suppose, also, that the initial N_2 temperature is 300 K and that a final equilibrium temperature can be achieved rather promptly behind the shock wave. Since a thermocouple monitors the kinetic energy of molecular motion, it inherently provides the translational temperature, T_{tr}. Nevertheless, at thermal equilibrium, only a single temperature is possible, so that the mode temperatures are related through $T_{el} = T_{vib} = T_{rot} = T_{tr}$. In other words, at thermal equilibrium, a thermocouple also measures the rotational, vibrational, and electronic temperatures.

If, however, the thermocouple were used to monitor the translational temperature as a function of distance behind the shock wave, we would find that T_{tr} follows the schematic profile shown in Fig. 11.2. Because the temperature ratio across a normal shock can be expressed in terms of the specific heat ratio, $\gamma = c_p/c_v$, the latter can be evaluated at each plateau, as also displayed in Fig. 11.2. Neglecting both dissociation and electronic

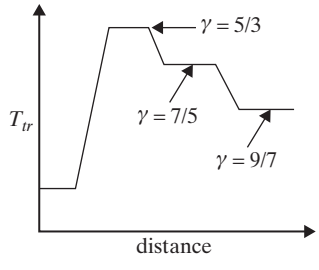

Figure 11.2 T_{tr} versus distance behind a shock wave.

Table 11.1 *Excited modes for N_2*

γ	c_v	Excited modes
$\frac{5}{3}$	$\frac{3}{2}R$	tr
$\frac{7}{5}$	$\frac{5}{2}R$	tr + rot
$\frac{9}{7}$	$\frac{7}{2}R$	tr + rot + vib

excitation, which is certainly reasonable for N_2 at temperatures below 3000 K, the indicated specific heat ratios can be converted to c_v values via the well-known relation

$$\gamma = \frac{c_v + R}{c_v}.$$

From classical equipartition theory, these c_v values may be interpreted in terms of mode excitations, as delineated in Table 11.1. We thus recognize that thermal equilibration is a dynamic process; that is, the rotational and vibrational temperatures ultimately coalesce with the translational temperature, but in distinct temporal stages. Hence, the c_v value designating the first plateau of Fig. 11.2 represents only translational excitation, as insufficient collisions have occurred to pass kinetic energy to the rotational and vibrational modes. Further collisions eventually produce equivalent rotational and translational temperatures ($\gamma = 7/5$), followed by full equilibration with the vibrational mode ($\gamma = 9/7$). We thus conclude that the rotational mode inherently responds much more rapidly than the vibrational mode to changes in the translational temperature. This behavior reflects more effective collisional energy exchange with the rotational as compared to the vibrational mode, which should be expected based on the much smaller energies for the former as compared to the latter. Therefore, we conclude that spectroscopic measurements monitoring T_{rot} are normally preferable for practical thermometry, as compared to those monitoring T_{vib} or T_{el}.

11.2 Radiative Transitions

Concentration and temperature measurements are usually conducted by employing UV–visible spectroscopy, although infrared spectroscopy is adopted in some cases. For atoms, electronic transitions must obviously be exploited, while, for molecules, rovibronic lines are typically used within a chosen electronic system. Among potential atoms, those with low-lying electronic levels are preferable, thus bolstering the opportunity for thermal equilibration. Similarly, for molecules, rovibronic levels are favored because of the enhanced probability of equilibration between the rotational and translational energy modes.

Whether the transitions involved are electronic or rovibronic, a conceptual framework is obviously mandatory for the fundamental analysis of radiative transitions. To this end, we now introduce the required nomenclature by considering the simple two-level model

shown in Fig. 11.3, where u indicates the upper and l the lower energy level. For an atom, electronic transitions are, of course, well represented by this two-level model. For a molecule, on the other hand, a two-level model holds only at exceedingly short excitation times (~2 ns), as thermal collisions can quickly provide the kinetic energy needed to shift population within the upper rovibronic level to other rotational levels within the same electronic state.

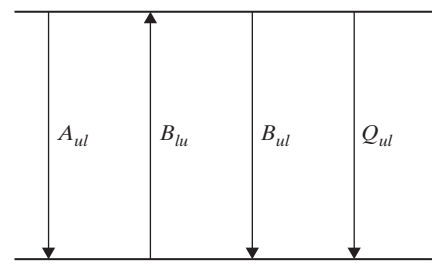

Figure 11.3 Rate coefficients for radiative and nonradiative transitions.

In general, the rate of population transfer into or out of the lower and upper energy levels, respectively, can be written as

$$\frac{dn_l}{dt} = n_u A_{ul} - n_l B_{lu}\rho_\nu + n_u B_{ul}\rho_\nu + Q_{ul} n_u \tag{11.4}$$

$$\frac{dn_u}{dt} = -n_u A_{ul} + n_l B_{lu}\rho_\nu - n_u B_{ul}\rho_\nu - Q_{ul} n_u, \tag{11.5}$$

where the first term in each rate equation represents spontaneous emission, the second term stimulated absorption, the third stimulated emission, and the last nonradiative quenching owing to collisions with nearby atoms or molecules. Here, n_l and n_u represent number densities in the lower and upper energy levels, while the parameters A_{ul}, B_{lu}, and B_{ul} are denoted as the Einstein coefficients for spontaneous emission, absorption, and stimulated emission, respectively. In essence, A_{ul} represents the probability per unit time that an atom or molecule in the upper level will undergo a radiative transition to the lower level. Similar definitions apply to $B_{ul}\rho_\nu$ and $B_{lu}\rho_\nu$, where ρ_ν is the radiative energy density at frequency ν ($J/m^3 \cdot s^{-1}$). On this basis, the rate coefficients for spontaneous emission, A_{ul}, and quenching, Q_{ul}, have units of s^{-1}. Similarly, the Einstein coefficients for stimulated absorption and emission, B_{lu} and B_{ul}, have units of $m^3/J \cdot s^2$.

As for the Bohr model of Chapter 5, spontaneous emission and stimulated absorption represent energy shifts for an atom or molecule upon release or absorption of a single photon. Hence, the upper and lower energy levels, ε_u and ε_l, are related to the transition frequency, ν_{ul}, by

$$\varepsilon_u - \varepsilon_l = h\nu_{ul},$$

where the discrete energies represent electronic or rovibronic levels for atoms or molecules, respectively. While spontaneous emission inherently produces isotropic radiation, stimulated emission, by comparison, generates an additional coherent photon in phase with the incident photon. More importantly, electronic quenching is inevitably exacerbated at higher pressures because of the greater rate of binary collisions, as discussed further in Section 16.1.

If we now sum Eqs. (11.4) and (11.5), we obtain

$$\frac{d}{dt}(n_u + n_l) = 0 \tag{11.6}$$

so that

$$n_u + n_l = n_l^\circ, \tag{11.7}$$

where n_l° represents the initial number density within the lower energy level prior to radiative interaction. Equation (11.7) is basically a statement of conservation of mass. In general, n_l° can also be taken as the total number density in the nascent two-level system, since nearly the entire population before excitation is typically associated with the lower energy level.

11.2.1 Spectral Transfer of Radiation

If we now consider only optical transitions, we may demonstrate that the temporal change in number density within the lower energy level is related to an accompanying change in spectral energy density, ρ_ν. To ensure only radiative interactions, we require $Q_{ul} n_u = 0$, so that Eq. (11.4) represents the effective photon emission rate per unit volume (photons/s $\cdot$ m^3). This underlying condition typically holds for either low pressures ($Q_{ul} \simeq 0$) or weak transitions ($n_u \simeq 0$). Recognizing that the energy per photon is $h\nu$, we may thus convert Eq. (11.4) to a local spectral power density, p_ν (W/m$^3 \cdot$ s^{-1}), so that

$$p_\nu = h\nu \left(\frac{dn_l}{dt} \right) Y(\nu) = h\nu A_{ul} n_u Y(\nu) + h\nu \left[B_{ul} n_u - B_{lu} n_l \right] \rho_\nu Y(\nu), \tag{11.8}$$

where $Y(\nu)$ is a *line profile function*, which accounts for the inevitable variation in transition probability owing to energy quantization. On this basis, $Y(\nu)$ can be taken as a probability density function, normalized in the usual way via

$$\int Y(\nu)\, d\nu = 1, \tag{11.9}$$

where, here, we need integrate only over the spectral line width. As discussed in Section 11.2.3, the line profile function simply affirms that absorption and emission of light do not occur precisely at ν_{lu} owing to both Doppler and collisional broadening of the spectral transition.

Preferentially, Eq. (11.8) can be cast in terms of the *spectral irradiance*, I_ν (W/m$^2 \cdot$ s^{-1}), by considering a differential length along some optical path, ds. We thus obtain

$$dI_\nu = p_\nu\, ds = h\nu \left(\Omega_c / 4\pi \right) A_{ul} n_u Y(\nu)\, ds + (h\nu/c) \left[B_{ul} n_u - B_{lu} n_l \right] I_\nu Y(\nu)\, ds, \tag{11.10}$$

where Ω_c represents a small solid angle that takes into account the isotropic nature of spontaneous emission. In developing Eq. (11.10), we have made use of the fundamental relation

$$I_\nu = \rho_\nu c, \tag{11.11}$$

which is derived in nearly all textbooks on electromagnetic theory. Dividing through by Ω_c, Eq. (11.10) can finally be converted into the steady-state, one-dimensional radiative transfer equation

$$\frac{dJ_\nu}{ds} = \left(\frac{h\nu}{4\pi} \right) A_{ul} n_u Y(\nu) + \frac{h\nu}{c} \left[B_{ul} n_u - B_{lu} n_l \right] J_\nu Y(\nu), \tag{11.12}$$

where J_ν is the *spectral radiance* or *intensity* ($\mathrm{W/m^2 \cdot sr \cdot s^{-1}}$), which is equivalent to the spectral irradiance per unit solid angle. For most applications, propagation of radiation is confined to a small solid angle, Ω_c. Hence, the $\Omega_c/4\pi$ factor in Eq. (11.10) is the fraction of the total spontaneous emission that falls within the solid angle of the propagating beam.

11.2.2 The Einstein Coefficients

Relations among the Einstein coefficients for spontaneous emission, stimulated absorption, and stimulated emission can be developed by assuming both thermodynamic and radiative equilibrium. Given radiative equilibrium, Eq. (11.8) becomes

$$A_{ul} n_u + [B_{ul} n_u - B_{lu} n_l]\ \rho_\nu = 0. \tag{11.13}$$

At thermal equilibrium, n_u and n_l are related by Eq. 4.15, so that

$$\frac{n_u}{n_l} = \frac{g_u}{g_l}\ \exp\left[-\frac{(\varepsilon_u - \varepsilon_l)}{kT}\right] = \frac{g_u}{g_l}\ e^{-h\nu/kT}, \tag{11.14}$$

as $\varepsilon_u - \varepsilon_l = h\nu$ for interaction with light at resonant frequency ν. Combining Eqs. (11.13) and (11.14), we obtain for the spectral energy density

$$\rho_\nu = \frac{A_{ul}}{(g_l/g_u)\ B_{lu} e^{h\nu/kT} - B_{ul}} \tag{11.15}$$

or

$$\rho_\nu = \frac{(A_{ul}/B_{ul})}{\left(\dfrac{g_l B_{lu}}{g_u B_{ul}}\right)\ e^{h\nu/kT} - 1}. \tag{11.16}$$

For radiative equilibrium, the spectral energy density follows the Planck distribution for a blackbody, which, from Eq. 14.17, is

$$\rho_\nu^B = \frac{8\pi h\nu^3/c^3}{e^{h\nu/kT} - 1}. \tag{11.17}$$

Comparing Eqs. (11.16) and (11.17), we find that

$$A_{ul} = \frac{8\pi h\nu^3}{c^3}\ B_{ul} \tag{11.18}$$

and also

$$\frac{B_{lu}}{B_{ul}} = \frac{g_u}{g_l}. \tag{11.19}$$

Although Eqs. (11.18) and (11.19) have been derived by invoking thermodynamic and radiative equilibrium, these expressions also hold away from equilibrium as the Einstein coefficients are fundamental microscopic parameters. Because A_{ul}, B_{ul}, and B_{lu} are thus interrelated, only A_{ul} values (s^{-1}) are typically compiled in the literature. Such values are generally determined from spectroscopic measurements, time-dependent solutions to the Schrödinger wave equation, or a combination thereof. Indeed, the Einstein coefficient for spontaneous emission is fundamentally related to the transition dipole moment, $\boldsymbol{M}_{ul}$, i.e.,

$$A_{ul} = \frac{16\pi^3\nu^3}{3\varepsilon_\circ hc^3} M_{ul}^2, \tag{11.20}$$

where $\boldsymbol{M}_{ul}$ is given quantum mechanically by Eq. 6.102. From this quantum viewpoint, we recognize that the Einstein coefficients are sizable for allowed transitions and nearly negligible for forbidden transitions. Equation (11.20) also attests that spectroscopic signals become more intense at greater frequencies, so that ultraviolet spectroscopy is normally much more useful than infrared spectroscopy for most diagnostic purposes.

11.2.3 Line Broadening

As indicated previously, the line profile function, $Y(\nu)$, varies with the mechanism of line broadening. For our purposes, a simple introduction to the two most important line-broadening mechanisms is sufficient. These two mechanisms are Doppler broadening, which gives a Gaussian profile, and collisional broadening, which gives a Lorentzian profile. Typically, Doppler broadening dominates at lower pressures while collisional broadening dominates at higher pressures.

Doppler broadening is a manifestation of the Doppler effect of classical physics. The random translational motion of gaseous particles implies that atoms or molecules can be moving toward or away from an observer. A distribution of radiative frequencies thus occurs because of the resulting Doppler shift. By averaging this Doppler shift over the possible particle speeds, which we will discuss in Section 15.2, the line profile function for this case can be shown to be

$$Y_D(\nu) = \frac{2}{\Delta\nu_D}\sqrt{\frac{\ln 2}{\pi}}\exp\left[-4\ln 2\frac{(\nu-\nu_\circ)^2}{\Delta\nu_D^2}\right], \tag{11.21}$$

where the full-width at half-maximum (FWHM) for the Doppler profile is

$$\Delta\nu_D = \frac{2\nu_\circ}{c}\sqrt{\frac{2\ln 2\,kT}{m}}. \tag{11.22}$$

The resulting Gaussian profile is shown in Fig. 11.4. We note, from Eq. (11.22), that a careful measurement of the line profile can be employed to determine the temperature. It also turns out that the center frequency, $\nu_\circ$, shifts notably with changes in flow velocity, so that any displacement in center frequency could also be used to measure the fluid flow rate.

In contrast to Doppler broadening, collisional broadening is a manifestation of the disruption of radiation by collisions. In essence, a greater collision rate produces shorter wave packets, which inherently broaden the spectral signal. This behavior can be understood from Fourier analysis, in that more Fourier overtones are needed to describe a sharper temporal pulse. The resulting line profile accounts for the statistical distribution of possible collision times, so that

$$Y_C(\nu) = \frac{\Delta\nu_C}{2\pi}\frac{1}{(\nu-\nu_\circ)^2+(\Delta\nu_C/2)^2}. \tag{11.23}$$

Here, the collisional FWHM is

$$\Delta\nu_C = \frac{2Z^*}{\pi}, \tag{11.24}$$

where Z^* is the collisional frequency (collisions per second). In comparison to the Doppler case, the collisional FWHM broadens substantially with increasing pressure owing to an enhanced collision rate at greater density (see Section 16.2.1). Therefore, careful measurements of the collisional profile can sometimes be used to monitor the pressure of a gaseous assembly. We note, finally, that the Lorentzian profile resulting from collisional broadening displays broader wings than the Gaussian profile produced by Doppler broadening, as shown in Fig. 11.4.

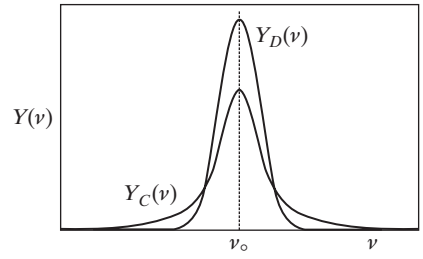

Figure 11.4 Line profile functions for Doppler and collisional broadening.

11.3 Absorption Spectroscopy

In absorption spectroscopy, a beam of light is passed through the medium of interest and its decay is monitored by a suitable detector, as shown in Fig. 11.5. For the sake of simplicity, we undertake our analysis of spectral absorption by beginning with the atomic rather than the molecular case. On this basis, the upper and lower levels can be taken as denoting the first excited and ground electronic states, respectively, so that $n_u/n_l << 1$ at thermodynamic equilibrium. Consequently, for a weak light source, Eq. (11.10) becomes

$$\frac{dI_\nu}{I_\nu} = -k_\nu ds, \tag{11.25}$$

where the *spectral absorption coefficient* (cm^{-1}) is defined by

$$k_\nu = (h\nu/c)\, B_{lu} n_l Y(\nu). \tag{11.26}$$

Assuming a homogeneous medium, we may integrate Eq. (11.25) over the interaction length L, thus obtaining the familiar Beer–Lambert attenuation law,

$$I_\nu(L) = I_\nu(0)\, e^{-k_\nu L}, \tag{11.27}$$

where $I_\nu(0)$ is the incoming irradiance at $L = 0$.

The experimentally measured quantity of interest in absorption spectroscopy is the integrated absorption, W_{lu} (s^{-1}), defined by

$$W_{lu} = \int \left[1 - \frac{I_\nu(L)}{I_\nu(0)}\right] d\nu = \int [1 - e^{-k_\nu L}]\, d\nu, \tag{11.28}$$

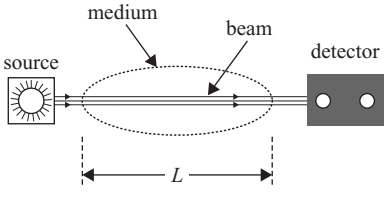

Figure 11.5 Typical experimental setup for absorption spectroscopy.

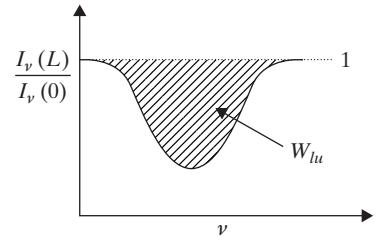

Figure 11.6 Typical line profile obtained in absorption spectroscopy.

as displayed in Fig. 11.6. For typical experiments, we employ a weakly absorbing line and either a broad-band or a scanning narrow-band light source, so that integration over the spectral line profile gives

$$W_{lu} = \int k_\nu L d\nu \tag{11.29}$$

since $e^{-k_\nu L} \simeq 1 - k_\nu L$. Hence, substituting from Eq. (11.26), we have

$$W_{lu} = K_{lu} L, \tag{11.30}$$

where K_{lu} is the *line strength* (integrated absorption coefficient), expressed by

$$K_{lu} = \int k_\nu \, d\nu = \left(\frac{h\nu_{ul}}{c}\right) B_{lu} n_l. \tag{11.31}$$

The desired quantity is n_l, which can be determined by combining Eqs. (11.30) and (11.31), thus giving

$$n_l = \frac{c W_{lu}}{h\nu_{ul} B_{lu} L}, \tag{11.32}$$

where W_{lu} is evaluated from the normalized area under the absorption line and the Einstein coefficient, B_{lu}, is obtained from appropriate tabulations in the literature. The total number density, n, can then be determined from n_l via Eq. (11.1), so that

$$n = \frac{n_l}{g_l} Z_{el} \exp\left(\frac{\varepsilon_l}{kT}\right). \tag{11.33}$$

By employing another low-lying electronic energy level, a second population density, n_k, can be determined in the same way, and thus the electronic temperature can be obtained from Eq. (11.2), i.e.,

$$T_{el} = \frac{\varepsilon_k - \varepsilon_l}{k \ln(g_k n_l / g_l n_k)}. \tag{11.34}$$

Moving now to molecules, we can apply the same two-level model to individual rovibronic levels within two different electronic states. Hence, from Eqs. (11.30) and (11.31), we may write

$$n(J'') = \frac{K_{J''J'}}{h\tilde{\nu} B_{J''J'}}, \tag{11.35}$$

where $\tilde{\nu}$ is the wave number corresponding to the line center and J'' is the rotational quantum number identifying the rovibronic level in the lower electronic state. The

total number density can then be obtained from Eqs. (7.19), (9.53), and (11.1), so that

$$n = \frac{Z_{el} Z_{R\text{–}V} n(J'')}{\phi(2S+1)(2J''+1)} \exp\left\{\frac{hc}{kT}\left[T_e + G(v) + F_v(J'')\right]\right\}, \tag{11.36}$$

where we have presumed an electronic degeneracy, $g_{el} = \phi(2S+1)$. However, we note that the electronic degeneracy should be unity if the rovibronic transition used in the measurements actually corresponds to an individual spin-split, Λ-doubled level.

Analogous to the atomic case, the rotational temperature can be determined by using two different rotational levels within the same lower vibronic level. Hence, assuming equivalent rotational and translational temperatures, we have from Eq. (11.36)

$$\frac{n(J_1'')}{(2J_1''+1)} \exp\left\{\frac{hc}{kT}\left[T_e + G(v) + F_v(J_1'')\right]\right\} = \frac{n(J_2'')}{(2J_2''+1)} \exp\left\{\frac{hc}{kT}\left[T_e + G(v) + F_v(J_2'')\right]\right\}$$

so that

$$\frac{n(J_1'')}{n(J_2'')} = \frac{(2J_1''+1)}{(2J_2''+1)} \exp\left\{\frac{hc}{kT_{rot}}\left[F_v(J_2'') - F_v(J_1'')\right]\right\}. \tag{11.37}$$

Substituting Eq. (11.35) into Eq. (11.37) for each rovibronic level, we find that

$$\ln\left[\frac{K_{J''J'}}{(2J''+1)B_{J''J'}}\right]_1 - \ln\left[\frac{K_{J''J'}}{(2J''+1)B_{J''J'}}\right]_2 = \frac{hc}{kT_{rot}}\left[F_v(J_2'') - F_v(J_1'')\right], \tag{11.38}$$

where we have presumed that $\tilde{\nu}_1 \simeq \tilde{\nu}_2$. Therefore, manipulating Eq. (11.38), the rotational temperature becomes

$$T_{rot} = \frac{\dfrac{hc}{k}\left[F_v(J_2'') - F_v(J_1'')\right]}{\ln\left[\dfrac{K_{J''J'}}{(2J''+1)B_{J''J'}}\right]_1 - \ln\left[\dfrac{K_{J''J'}}{(2J''+1)B_{J''J'}}\right]_2}. \tag{11.39}$$

While Eq. (11.39) provides the rotational temperature when using two rovibronic transitions, a more accurate rotational temperature can usually be determined by employing a large number of rovibronic lines in the spectrum. From Eq. (11.38), we find that, for multiple lines,

$$F_v(J'') \propto -\frac{kT_{rot}}{hc} \ln\left[\frac{K_{J''J'}}{(2J''+1)B_{J''J'}}\right], \tag{11.40}$$

so that the resulting *Boltzmann plot* shown in Fig. 11.7 offers a straightforward method by which a linear slope can be used to determine the rotational temperature. However, we should understand that while a nonlinear Boltzmann plot surely indicates nonequilibrium conditions, the anticipated linear plot does not necessarily guarantee rotational equilibrium, as intense chemical reactions, for example, can sometimes produce a "rotationally hot"

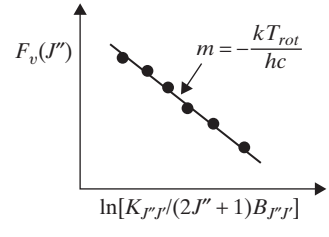

Figure 11.7 Boltzmann plot.

population distribution. Therefore, as in most optical experiments, caution is required so as to properly interpret the measured rotational temperature.

EXAMPLE 11.1

Atomic magnesium is monitored using a broad-band absorption measurement taken across the two-meter smokestack of an incinerator at 1 bar. At a measured exhaust temperature of 500 K, the integrated absorption at 4571 Å is found to be 1.35×10^{11} s^{-1}. If the Einstein A-coefficient for the electronic transition at this wavelength is known to be 2.2×10^4 s^{-1}, determine the concentration of atomic magnesium, in parts per million (ppm), leaving the incinerator.

Solution

The given wavelength of 4571 Å indicates a wave number of $(4571 \times 10^{-8})^{-1} = 21877$ cm^{-1}, which, from Appendix J.1, clearly corresponds to an electronic transition from the ground $3s^2 - {}^1S_0$ state (l) to the first excited $3s3p - {}^3P_{0,1,2}$ state (u). At ppm levels of atomic magnesium, the number density for Mg in the ground state can be related to the integrated absorption via Eq. (11.32), i.e.,

$$n_l = \frac{cW_{lu}}{h\nu_{ul} B_{lu} L},$$

thus indicating that B_{lu} must be evaluated from A_{ul}. Hence, from Eqs. (11.18) and (11.19),

$$B_{lu} = \frac{g_u}{g_l} B_{ul} = \frac{g_u c^3}{8\pi g_l h\nu^3} A_{ul} = \frac{g_u}{8\pi g_l h\tilde{\nu}^3} A_{ul}.$$

Now, from the above term symbols, $g_l = 1$ and $g_u = 1 + 3 + 5 = 9$. Hence,

$$B_{lu} = \frac{(9)(2.2 \times 10^4 \text{ s}^{-1})}{8\pi (6.6261 \times 10^{-34} \text{ J} \cdot \text{s})(21877 \text{ cm}^{-1})^3} = 1.135 \times 10^{24} \text{ cm}^3/\text{J} \cdot \text{s}^2.$$

Given $W_{lu} = 1.35 \times 10^{11}$ s^{-1} and $L = 200$ cm, the number density in the ground electronic state is

$$\begin{aligned} n_l &= \frac{W_{lu}}{h\tilde{\nu}_{ul} B_{lu} L} \\ &= \frac{(1.35 \times 10^{11} \text{ s}^{-1})}{(6.6261 \times 10^{-34} \text{ J} \cdot \text{s})\,(21877 \text{ cm}^{-1})\,(1.135 \times 10^{24} \text{ cm}^3/\text{J} \cdot \text{s}^2)\,(200 \text{ cm})} \\ &= 4.103 \times 10^{13} \text{ cm}^{-3}. \end{aligned}$$

For atomic spectroscopy, the electronic mode is obviously the only internal energy mode of significance. Hence, from Eq. (11.33), the total number density in the exhaust stream can be determined from

$$n = Z_{el} \exp\left(\frac{\varepsilon_l}{kT}\right) n_l = Z_{el} n_l,$$

as $\varepsilon_l = 0$ for the ground electronic state. From the data of Appendix J.1, the electronic partition function for atomic magnesium at 500 K is

$$Z_{el} = g_0 + g_1 \exp\left(-\frac{\varepsilon_1}{kT}\right) = 1 + 9\exp\left[-\frac{(1.4387)\,(21877)}{500}\right] = 1 + 4.13 \times 10^{-27} \simeq 1.$$

Consequently, for atomic magnesium at this temperature, the total number density is the same as that in the ground electronic state, so that $n = 4.103 \times 10^{13}$ particles/cm^3. To convert to parts per million (ppm), we invoke Eq. (9.10) to determine the total number density for an ideal gas at 500 K and 1 bar; thus,

$$n = \frac{P}{kT} = \frac{(1.0 \times 10^6 \text{ dyne/cm}^2)}{(1.3807 \times 10^{-16} \text{ dyne} \cdot \text{cm/K})(500 \text{ K})} = 1.449 \times 10^{19} \text{ cm}^{-3}.$$

Therefore, the exhaust concentration of atomic magnesium, in ppm, is

$$C_{ppm} = \frac{4.103 \times 10^{13}}{1.449 \times 10^{19}}(10^6) = 2.83 \text{ ppm}.$$

11.4 Emission Spectroscopy

A potential problem for absorption spectroscopy is that the measured concentration or temperature is averaged along a line of sight through the medium. In contrast, emission spectroscopy normally permits point measurements, as the isotropic emission can be focused onto a suitable detector, as shown in Fig. 11.8. Unfortunately, because an emissive signal inherently reflects nonequilibrium conditions, emission spectroscopy can be plagued by the invalidity of Eqs. (11.1) and (11.2). On the other hand, at high temperatures and pressures, such as in plasmas, the emissive signal is not only more intense, but equilibration is more likely, so that emission spectroscopy can sometimes be applied quite successfully to both concentration and temperature measurements.

11.4.1 Emissive Diagnostics

For purely emissive conditions, we have no large external source of radiation so that $\rho_\nu = 0$; hence, Eq. (11.8) becomes

$$p_\nu = h\nu A_{ul} n_u Y(\nu). \tag{11.41}$$

However, as in Fig. 11.8, the measured signal is obtained by focusing only a portion of the isotropic emission onto a suitable photodetector. The power, $P_d(W)$, at the detector is given by

$$P_d = (\Omega_c/4\pi)\, V_c \int p_\nu \, d\nu, \tag{11.42}$$

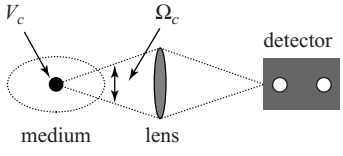

Figure 11.8 Typical experimental setup for emission spectroscopy.

where Ω_c is the solid angle of the collection optics and V_c is the collection volume, which usually is less than 0.1 mm^3. Combining Eqs. (11.41) and (11.42), we have for the number density in the upper level

$$n_u = \frac{4\pi P_d}{h\nu_{ul} A_{ul} \Omega_c V_c}. \tag{11.43}$$

In general, $n_u/n_l << 1$; thus, an emissive signal should intuitively be much less than an absorptive signal. However, an absorptive signal must be recovered from the pervasive background caused by its light source, whereas an emissive signal is essentially free of background radiation. Hence, emission spectroscopy typically offers a much larger signal-to-background ratio and thus a lower detection limit.

Equation (11.43) implies that a concentration measurement using emission spectroscopy requires careful calibration, as knowledge of the collection volume, V_c, is very difficult to obtain in any reasonable experiment. Fortunately, in comparison, an emissive measurement of temperature is usually quite straightforward. In particular, when employing two emitting lines with the same optical setup, the ratio

$$\frac{n_m}{n_n} = \frac{\nu_{nl} A_{nl} P_{d,m}}{\nu_{ml} A_{ml} P_{d,n}}, \tag{11.44}$$

derived from Eq. (11.43), proves to be independent of all unknown calibration factors. Therefore, temperature can be easily determined from a combination of Eqs. (11.2) and (11.44).

11.4.2 The Problem of Self-Absorption

A problem that must be considered for any emissive measurement is the potential for radiative trapping or self-absorption. In developing Eq. (11.42), we assumed that $\rho_\nu = 0$. However, for strong emission, ρ_ν becomes significant owing to emissive radiation so that the signal can be reabsorbed by the surrounding gas. This particular situation can be understood by casting Eq. (11.12) in the form

$$\frac{dJ_\nu}{ds} = \varepsilon_\nu - \kappa_\nu J_\nu, \tag{11.45}$$

where

$$\varepsilon_\nu = \frac{h\nu}{4\pi} A_{ul} n_u Y(\nu) \tag{11.46}$$

is called the *spectral emission coefficient* and

$$\kappa_\nu = \frac{h\nu}{c} \left[B_{lu} n_l - B_{ul} n_u \right] Y(\nu) \tag{11.47}$$

is the *effective spectral absorption coefficient*. Comparing Eqs. (11.26) and (11.47), we observe that $\kappa_\nu = k_\nu$ when $n_u/n_l << 1$, which represents the usual situation at reasonable temperatures.

Defining the *optical depth* corresponding to a path length L,

$$\tau = \int_0^L \kappa_\nu \, ds, \tag{11.48}$$

we have

$$d\tau = \kappa_\nu \, ds. \tag{11.49}$$

Hence, Eq. (11.45) can be converted to

$$\frac{dJ_\nu}{d\tau} = \frac{\varepsilon_\nu}{\kappa_\nu} - J_\nu. \tag{11.50}$$

Presuming a homogeneous medium (n_l and n_u independent of position), the solution to Eq. (11.50) is

$$J_\nu = J_\nu(0)\, e^{-\kappa_\nu L} + \frac{\varepsilon_\nu}{\kappa_\nu}\,[1 - e^{-\kappa_\nu L}]. \tag{11.51}$$

Based on Eq. (11.51), the behavior of the spectral intensity depends critically on the optical depth, $\kappa_\nu L$. If $\kappa_\nu L << 1$, we say that the medium is *optically thin*, while if $\kappa_\nu L >> 1$, we say that it is *optically thick*. For an unexcited medium ($\varepsilon_\nu = 0$), we again obtain the Beer–Lambert law, as given by Eq. (11.27). In comparison, for the emissive case with no external illumination, Eq. (11.51) becomes

$$J_\nu = \frac{\varepsilon_\nu}{\kappa_\nu}\,[1 - e^{-\kappa_\nu L}]. \tag{11.52}$$

Hence, for an optically thin medium, expansion of the exponential factor gives $J_\nu = \varepsilon_\nu L$, which is essentially equivalent to Eq. (11.41). As a result, we find that radiative trapping can always be eliminated by creatively ensuring optically thin conditions.

If, on the other hand, the optical depth of the medium rises, Eq. (11.51) indicates that the spectral distribution of the observed radiation departs from that of the radiating species and instead approaches that for the source function, $\varepsilon_\nu/\kappa_\nu$, over a progressively wider range of frequencies. Given a nonuniform medium, in which the temperature decreases toward the boundary, self-absorption can lead to a noticeable dip in the center of the line profile for the emitted radiation. In the worst-case scenario, we find, from Eqs. (11.46), (11.47), and (11.52), that a homogeneous medium in thermal equilibrium under optically thick conditions ($\kappa_\nu L >> 1$) has spectral radiance

$$J_\nu = \frac{\varepsilon_\nu}{\kappa_\nu} = \frac{c}{4\pi}\frac{A_{ul}}{B_{lu}\,(n_l/n_u) - B_{ul}}. \tag{11.53}$$

However, at thermodynamic equilibrium, Eq. (11.14) holds, so that

$$J_\nu = \frac{(c\,A_{ul}/4\pi\,B_{ul})}{\left(\dfrac{g_l\,B_{lu}}{g_u\,B_{ul}}\right)\, e^{h\nu/kT} - 1}; \tag{11.54}$$

thus, from Eqs. (11.17–11.19),

$$J_\nu = \frac{c}{4\pi}\rho_\nu^B = \frac{I_\nu^B}{4\pi} = J_\nu^B, \tag{11.55}$$

where, for a blackbody, $J_\nu^B = I_\nu^B/4\pi$ because of the isotropic nature of its radiation. Hence, a homogeneous, optically-thick gas at constant temperature will generate the spectral radiance of a blackbody. A massive, gaseous source such as the Sun displays blackbody behavior at all wavelengths owing to a combination of collisional broadening and optically-thick conditions.

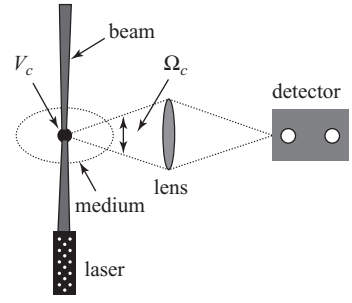

Figure 11.9 Typical experimental setup for fluorescence spectroscopy.

11.5 Fluorescence Spectroscopy

Emission spectroscopy is inherently a powerful analytical tool because of its high signal-to-background ratio as compared to absorption spectroscopy, but unfortunately spontaneous emission occurs only for a sufficiently high upper-level population, that is, in a very hot medium. Fluorescence spectroscopy, on the other hand, can exploit the analytical advantages of emission spectroscopy at all temperatures via the excitation of atoms or molecules with an intense radiative source, such as a laser. For this technique, as displayed in Fig. 11.9, thermal equilibration before excitation is usually not an issue, but interpretation of the resulting signal can be problematic. In particular, the induced population in the upper level, n_u, must somehow be related to the initial population in the lower level, n_l°, and thus to the total number density. As for all emissive methods, fluorescence spectroscopy can be complicated by radiative trapping; thus, fluorescence signals must always be examined carefully to ensure the existence of optically-thin conditions ($\kappa_\nu L << 1$).

If an atom or molecule is excited by a laser beam of the appropriate wavelength, steady-state conditions are generally achieved within approximately 100 psec. Hence, for a typical pulsed laser, Eq. (11.5) becomes

$$n_u = \frac{B_{lu}\rho_\nu n_l}{A_{ul} + Q_{ul} + B_{ul}\rho_\nu}, \tag{11.56}$$

where ρ_ν represents the spectral energy density of the light source. For our two-level model, Eq. (11.7) holds; thus, substituting for n_l in Eq. (11.56), we obtain, after some manipulation,

$$\frac{n_u}{n_l^\circ} = \left[1 + \frac{B_{ul}}{B_{lu}} + \frac{A_{ul} + Q_{ul}}{B_{lu}\rho_\nu}\right]^{-1}, \tag{11.57}$$

where n_l° is the number density affiliated with the lower level before laser excitation.

Two distinct cases are now possible. For low laser energies, Eq. (11.57) becomes

$$n_u = \frac{B_{lu}\rho_\nu}{A_{ul} + Q_{ul}} n_l^\circ, \tag{11.58}$$

whereas, for high laser energies, we obtain

$$n_u = \frac{B_{lu}}{B_{lu} + B_{ul}} n_l^\circ. \tag{11.59}$$

Equation (11.58) represents the linear fluorescence method favored by analytical chemists; in comparison, Eq. (11.59) represents saturated fluorescence spectroscopy. In either case, we have successfully related the number density in the upper energy level after excitation

to that in the lower level prior to laser excitation. Because the measured fluorescence signal arises from emission caused by laser-induced population in the upper level, we may solve for the desired quantity, n_l°, by utilizing Eq. (11.43). We then obtain

$$n_l^\circ = \left(1 + \frac{Q_{ul}}{A_{ul}}\right) \frac{4\pi P_d}{h\nu_{ul}\Omega_c V_c B_{lu}\rho_\nu} \tag{11.60}$$

for linear fluorescence and

$$n_l^\circ = \left(1 + \frac{g_l}{g_u}\right) \frac{4\pi P_d}{h\nu_{ul} A_{ul}\Omega_c V_c} \tag{11.61}$$

for saturated fluorescence, where we have also used Eq. (11.19). In each case, P_d represents the measured fluorescence signal at the detector, which remains proportional to n_l°.

The total number density can now be obtained by using Eq. (11.1) combined with either Eq. (11.60) or Eq. (11.61), depending on the chosen fluorescence method. In both cases, utilization of two transitions can again provide the temperature from Eq. (11.2). As in emission spectroscopy, determination of the total number density requires calibration, whereas determination of the temperature does not when based on a common calibration factor for the ratio of populations. As an example, employing saturated fluorescence, Eq. (11.61) gives quite simply

$$\frac{n_m^\circ}{n_n^\circ} = \frac{\nu_{un} A_{un} P_{d,m}}{\nu_{um} A_{um} P_{d,n}},$$

if we assume that the degeneracy ratio, g_l/g_u, is the same for both transitions.

For linear laser-induced fluorescence (LIF), typically $Q_{ul}/A_{ul} >> 1$, so that Eq. (11.60) can be expressed as

$$P_d = h\nu_{ul}\left(\frac{A_{ul}B_{lu}}{Q_{ul}}\right)\frac{\Omega_c}{4\pi} V_c n_l^\circ \rho_\nu. \tag{11.62}$$

Consequently, we find that the fluorescence signal, P_d, is proportional to the energy density of the laser, ρ_ν, and inversely proportional to the quenching coefficient, Q_{ul}. Because Q_{ul} is linearly related to pressure and also depends on the identity of the collision species, LIF is best used under laboratory conditions, for which we can either measure or predict the pressure, temperature, and quenching environment. Such is the case for most applications in analytical spectroscopy. In comparison, utilization of fluorescence spectroscopy under practical conditions often requires laser-saturated fluorescence (LSF). Equation (11.61) shows that, in this case, n_l° is independent of both Q_{ul} and any variation in the irradiance of the laser. However, a problem with LSF concerns the large laser powers needed to fully saturate molecular transitions. Required laser irradiances at atmospheric pressure are on the order of 10^8 W/cm^2, with even greater irradiances needed at higher pressures. Another difficulty is that fully saturated conditions are never achieved across the entire spatial irradiance profile created by any actual laser beam.

EXAMPLE 11.2

Laser-saturated fluorescence measurements of the hydroxyl radical (OH) are performed in a combustion system. The fluorescence signals for the $P_1(11)$ and $P_1(16)$ rovibronic lines within the electronic transition $X^2\Pi(v = 0) \rightarrow A^2\Sigma(v = 0)$ are found to be 11.5 and

1.45 mV, respectively. The wave number and transition probability for each of these lines are

$$\begin{aligned} P_1(11): &\quad 31869.5\ \text{cm}^{-1} \quad A_{ul} = 3.54 \times 10^5\ \text{s}^{-1} \\ P_1(16): &\quad 31492.1\ \text{cm}^{-1} \quad A_{ul} = 2.98 \times 10^5\ \text{s}^{-1}. \end{aligned}$$

Determine the flame temperature. For consistency with the two-level model, assume that fluorescence detection occurs at the same wavelength as laser excitation for each spectral line.

Solution

From Eq. (11.61), the number density in the lower rovibronic level for either transition before laser excitation is given by

$$n_l^\circ = \left(1 + \frac{g_l}{g_u}\right) \frac{4\pi P_d}{h\nu_{ul} A_{ul} \Omega_c V_c}.$$

From Eqs. (6.32) and (6.85), the total degeneracy for any rovibronic level is

$$g = g_{el} g_{rot} = \phi(2S+1)(2J+1),$$

presuming that each rovibronic transition incorporates all spin-split, Λ-doubled sublevels. On this basis, the degeneracies for the lower and upper levels associated with the $P_1(11)$ line are

$$g_l = (2)\,(2)\,(2 \cdot 11 + 1) = 92 \qquad g_u = (1)\,(2)\,(2 \cdot 10 + 1) = 42.$$

Similarly, for the $P_1(16)$ line, the degeneracies for the lower and upper levels become

$$g_l = (2)\,(2)\,(2 \cdot 16 + 1) = 132 \qquad g_u = (1)\,(2)\,(2 \cdot 15 + 1) = 62.$$

If we assume that the fluorescence power at the detector is converted to an electrical signal with equal efficiency at the two spectral wavelengths, we may form the ratio,

$$\begin{aligned} \frac{n_l^\circ(16)}{n_l^\circ(11)} &= \frac{[1 + (g_l/g_u)]_{16}}{[1 + (g_l/g_u)]_{11}} \frac{(\nu_{ul} A_{ul})_{11}}{(\nu_{ul} A_{ul})_{16}} \left(\frac{P_{d,16}}{P_{d,11}}\right) \\ &= \left(\frac{3.129}{3.190}\right)\left(\frac{31869.5}{31492.1}\right)\left(\frac{3.54 \times 10^5}{2.98 \times 10^5}\right)\left(\frac{1.45}{11.5}\right) = 0.1487. \end{aligned}$$

From Eq. (11.37), the ratio of rovibronic populations in the ground vibrational level for the ground electronic state of OH before laser excitation can be expressed as

$$\frac{n_l^\circ(16)}{n_l^\circ(11)} = \frac{(2 \cdot 16 + 1)}{(2 \cdot 11 + 1)} \exp\left\{-\frac{hc}{kT}\left[F_0(16) - F_0(11)\right]\right\}.$$

Now, from Eq. (7.21), the rotational energy in the ground vibrational level of the ground electronic state for either transition is

$$F_0(J) = B_0 J(J+1) - D_e J^2 (J+1)^2,$$

where, from Appendix K.1,

$$B_0 = B_e - 0.5\alpha_e = 18.911 - 0.5(0.7242) = 18.549\ \text{cm}^{-1}.$$

Hence, the rotational energies for the two rovibronic levels are

$$F_0(16) = (18.549)(16)(17) - \left(19.4 \times 10^{-4}\right)(16)^2(17)^2 = 4901.8 \text{ cm}^{-1}$$
$$F_0(11) = (18.549)(11)(12) - \left(19.4 \times 10^{-4}\right)(11)^2(12)^2 = 2414.7 \text{ cm}^{-1}.$$

Therefore, substituting for the rotational energies, the calculated ratio of rovibronic populations becomes

$$\frac{n_l^\circ(16)}{n_l^\circ(11)} = 0.1487 = \left(\frac{33}{23}\right) \exp\left\{-\frac{(1.4387)[4901.8 - 2414.7]}{T}\right\}.$$

Solving for the flame temperature, we obtain

$$T = \frac{3578.2}{\ln(9.6488)} = 1578 \text{ K}.$$

11.6 Sodium D-Line Reversal

Flame and plasma temperatures are often measured using the sodium D-line reversal method. Here, NaCl is added to the flame or plasma to create sodium atoms at high temperatures (1000–3000 K). Under such conditions, sodium emits radiation at two wavelengths, 5890 and 5896 Å, the so-called D-lines. If a tungsten strip lamp is used to backlight the flame, as shown in Fig. 11.10, the flame temperature can be accurately measured by visually looking for the *reversal point* through an inexpensive spectrometer. The reversal point corresponds to that radiance from the tungsten lamp which causes the intensity of the D-lines to be equal to that of the strip lamp. For lamp intensities less than the reversal intensity, the D-lines appear in emission; for lamp intensities greater than the reversal intensity, the D-lines appear in absorption. Hence, at the reversal point, the spectrum shows no emission or absorption.

We may demonstrate that a thermodynamic temperature can be measured via this method by considering Eq. (11.51), which was derived for an externally radiated, emissive, and homogeneous medium. At the reversal point $J_\nu = J_\nu(0)$, so that

$$J_\nu(0) = J_\nu(0)\, e^{-\kappa_\nu L} + \frac{\varepsilon_\nu}{\kappa_\nu}[1 - e^{-\kappa_\nu L}], \tag{11.63}$$

where $J_\nu(0)$ is the incident spectral radiance from the strip lamp. Equation (11.63) indicates that

$$J_\nu(0) = \frac{\varepsilon_\nu}{\kappa_\nu} \tag{11.64}$$

and thus the measured temperature is independent of the optical thickness of the medium. Furthermore, we have previously shown that at thermal equilibrium (Eqs. 11.53–11.55)

$$J_\nu^B = \frac{\varepsilon_\nu}{\kappa_\nu}, \tag{11.65}$$

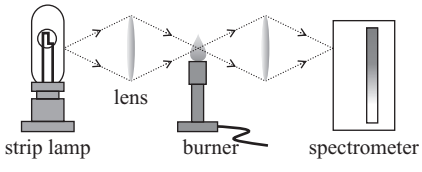

Figure 11.10 Experimental setup for sodium D-line reversal method.

so that, from Eq. (11.64), $J_\nu^B = J_\nu(0)$. Hence, the flame temperature must be equal to the temperature of a blackbody at the radiance of the strip lamp. This temperature, often called the *brightness temperature*, can be determined by calibrating the tungsten lamp with an optical pyrometer.

The sodium D-line method is useful, not because of the pair of D-lines, but because the D-lines appear in the yellow, where detectors, including the human eye, are very sensitive to small changes in the spectral radiance. Typically, a temperature of 2000 K can be measured with an accuracy of ± 40 K. Nevertheless, because sodium line reversal is a line-of-sight method, we must never forget that the measured temperature for a nonuniform profile will always be weighted toward the highest temperatures along the optical path.

11.7 Advanced Diagnostic Techniques

This chapter has been concerned with absorption, emission, and fluorescence methods for determining species concentrations and temperature. These techniques represent the simplest approaches that can be used to monitor the above properties in gaseous mixtures. However, you should realize that advanced diagnostic strategies are often available which are more suitable for specific applications. While such methods were not considered in this elementary discussion, many have actually become quite robust in the past few decades owing to the commercialization of tunable lasers. Examples of reliable coherent sources for diagnostic purposes include injection-seeded Nd:YAG lasers, diode lasers, and picosecond lasers.

The plethora of advanced diagnostic techniques built on statistical thermodynamics and spectroscopy has been reviewed by Eckbreth (1996). Among these techniques, Rayleigh scattering has traditionally been employed for density and temperature measurements, spontaneous Raman scattering for temperature and major species concentrations, and planar LIF for images of selected species distributions. Laser-induced breakdown spectroscopy can be used to determine the atomic composition of complex mixtures; similarly, atomic concentrations have been monitored successfully via methods based on multiphoton photoionization or LIF. In comparison, cavity ring-down spectroscopy, laser-induced polarization spectroscopy, and degenerate four-wave mixing can be employed specifically for determining concentrations of minor molecular species. Coherent anti-Stokes Raman scattering is generally applied to measurements of temperature and major species concentrations in turbulent reactive flows. Finally, laser-induced incandescence is often used for monitoring particle sizes and number densities.

PROBLEM SET V

Chemical Equilibrium and Diagnostics (Chapters 10–11)

5.1 A vessel contains an ideal monatomic gas at constant temperature T. The vessel is initially divided into two equal parts by a partition, such that each part contains N atoms at volume V. The partition is then removed.

a. Using the methods of statistical thermodynamics, determine the change in entropy accompanying this isothermal mixing process.

b. Provide a physical explanation for your answer in part (a). In particular, carefully distinguish between those conditions for which the mixing process is reversible versus irreversible.

c. Determine the above entropy of mixing by assuming that the atoms are distinguishable rather than indistinguishable. The difference between this result and that obtained in part (a) was the first historical indication of the inadequacy of classical vis-a-vis quantum mechanics. The predicted disagreement with reality constitutes the famous Gibbs paradox of the nineteenth century.

d. What is the source of the Gibbs paradox from a quantum mechanical viewpoint? A classical thermodynamics viewpoint?

5.2 A vessel of volume V contains an ideal monatomic gas at temperature T. The number of atoms of mass m within the vessel is N. The electronic partition function for the gas can be taken as $Z_{el} = g_\circ$.

a. Determine the chemical potential for this gas assembly.

b. Thermodynamic adsorption on a surface can be modeled by confining $N_s \ll N$ atoms of the above gas to a surface of area $A = L^2$ and temperature T located within the vessel. If the adsorbed atoms are free to move anywhere on the surface, show that the translational partition function for this two-dimensional ideal gas is

$$Z_{tr} = \left(\frac{2\pi mkT}{h^2}\right) A.$$

c. The force binding an atom to this surface can be modeled by an harmonic oscillator normal to the surface. If the potential well of the oscillator can be

characterized by a binding energy ε_b and a characteristic binding temperature $\theta_b = h\nu/k$, determine the chemical potential of the adsorbed ideal gas.

d. According to classical thermodynamics, the chemical potentials of the above two- and three-dimensional ideal gases must be equal to one another at phase equilibrium. Use this condition to determine the equilibrium number of atoms adsorbed per unit area of the surface when the pressure of the surrounding gas is P.

5.3 Two dissimilar ideal gases, A and B, are initially separated by a partition within an insulated tank. There are N_A molecules of A in volume V_A and N_B molecules of B in volume V_B. The two gases are at the same pressure and temperature. The partition is then broken and the gases are permitted to mix.

a. Employing appropriate partition functions, show that the entropy change upon mixing is given by

$$\Delta S = -R \sum_i n_i \ln x_i ,$$

where n_i and x_i are the number of moles and mole fraction, respectively, for the ith gas.

b. If gases A and B are identical, demonstrate that no change in entropy occurs when the partition is broken.

5.4 Consider the equilibrium reaction $O_2 \rightleftarrows 2O$.

a. Determine the equilibrium constant K_p at 1000 K. Compare with the JANAF value and explain any discrepancy.

Hint: See Problem Set IV.

b. Find the degree of dissociation for an equilibrium mixture of O_2 and O at a pressure of 0.01 bar. Determine the partial pressure of oxygen atoms under these conditions.

5.5 Complete Problem 5.4, but at a temperature of 1500 K rather than 1000 K.

5.6 Complete Problem 5.4, but at a temperature of 2000 K rather than 1000 K.

5.7 Consider the chemical reaction $H_2O + M \rightleftarrows H + OH + M$.

a. Using the rigid-rotor/harmonic-oscillator model, show that the equilibrium constant for this reaction is given by

$$K_p(T) = \frac{\kappa T^2}{(1 - e^{-\theta_v / T})} \prod_{i=1}^{3} (1 - e^{-\theta_{vi} / T}) \exp\left(-\frac{\Delta h_0^\circ}{RT}\right),$$

where κ is a constant, θ_v is the characteristic vibrational temperature for OH, θ_{vi} are the characteristic vibrational temperatures for H_2O, and Δh_0° is the standard enthalpy of reaction at absolute zero.

b. Develop an expression for κ in terms of appropriate parameters from statistical thermodynamics. The ground electronic state for each species in the above reaction is as follows: (1) H, $^2S_{1/2}$; (2) OH, $^2\Pi$; (3) H_2O, $^1A_1$.

5.8 The molecular hydrogen–deuterium exchange reaction is given by

$$H_2 + D_2 \rightleftarrows 2HD,$$

where atomic deuterium (D) is that isotope of atomic hydrogen (H) having a molecular weight $M = 2$ gm/gmol. Using the rigid-rotor/harmonic-oscillator model and assuming a temperature $T \gg \theta_r$, show that the equilibrium constant for this particular reaction is given by $K_p = 3\sqrt{2}\kappa(T)$, where

$$\kappa(T) = \frac{[1 - \exp(-\theta_{v,H_2}/T)][1 - \exp(-\theta_{v,D_2}/T)]}{[1 - \exp(-\theta_{v,HD}/T)]^2} \times \exp\left(-\frac{2\theta_{v,HD} - \theta_{v,H_2} - \theta_{v,D_2}}{2T}\right).$$

Hint: Because of the Born–Oppenheimer approximation, the isotopic molecules H_2, D_2, and HD have the same ground-state internuclear potential and term symbol.

5.9 Consider the equilibrium gas-phase reaction

$$I_2 + M \rightleftarrows 2I + M,$$

where the term symbols for the ground electronic states of atomic and diatomic iodine are ${}^2P_{3/2}$ and ${}^1\Sigma_g^+$, respectively. The main vibrational and rotational parameters for diatomic iodine are $\omega_e = 214.50\ \text{cm}^{-1}$ and $B_e = 0.03737\ \text{cm}^{-1}$; the dissociation energy $D_\circ = 1.542$ eV.

a. Show that if the zero of energy is placed at the bottom of the harmonic oscillator potential, the vibrational partition function for a diatomic molecule can be expressed as

$$Z_{vib} = \frac{1}{2\sinh(\theta_v/2T)},$$

where $\theta_v = hc\omega_e/k$.

b. Using the rigid-rotor/harmonic-oscillator model, show that the equilibrium constant for this reaction is given by

$$K_p = AT^{3/2}\sinh(B/T)\exp(-C/T),$$

where A, B, and C are constants. Assume that $Z_{el} = g_\circ$ for both atomic and diatomic iodine.

c. Evaluate the constants A, B, and C.

5.10 An excellent approximation to the rovibrational energy levels of many diatomic molecules can be obtained by considering vibrational anharmonicity, but neglecting centrifugal stretching and rotation–vibration coupling.

a. Employing these assumptions, develop a suitable expression for the difference in energy, $\Delta G(v) + \Delta F(J)$, between any two rovibrational levels in terms of $\Delta v = v' - v''$, $\Delta J = J' - J''$, $\Delta v^2 = (v')^2 - (v'')^2$, and $\Delta J^2 = (J')^2 - (J'')^2$.

b. The number densities associated with selected rovibronic levels in the ground electronic state of the hydroxyl radical have been measured in a flame using the laser absorption method. The results are as follows:

v	J	n_{vJ} (molecules/cm^3)	v	J	n_{vJ} (molecules/cm^3)
0	5	2.4×10^{14}	1	5	–
0	10	1.1×10^{14}	1	10	7.2×10^{12}

The rotational and vibrational temperatures are defined to be those temperatures that describe the equilibrium distribution among the rotational and vibrational energy levels, respectively. Determine these temperatures for OH using the measured number densities. Is the OH molecule in thermal equilibrium?

c. Determine the missing value of n_{vJ}.

5.11 Analytical chemists often determine the concentrations of metal impurities in a liquid sample by vaporizing the sample into a small flat-flame burner. Suppose that an absorption measurement is to be made of atomic calcium on a burner that has an effective optical path length of 1 cm. The integrated absorption for the $4s^2(^1S_0) \rightarrow 4s4p(^1P_1)$ transition of calcium is found to be 0.17 cm^{-1}. The Einstein A-coefficient for the associated spectral line is 2.18×10^8 s^{-1}.

a. Determine the flame temperature at which 1% of the total population of calcium atoms would reside in the first excited electronic state.

b. Show that the number density in the ground electronic state is given by

$$n_l = \frac{g_l}{g_u}\left(\frac{8\pi W_{lu}}{A_{ul}\lambda^2 L}\right),$$

where W_{lu} (s^{-1}) is the integrated absorption, λ (cm) is the wavelength of the electronic transition, and L (cm) is the optical path length.

c. Determine the total number density of atomic calcium in the flame (atoms/cm^3).

5.12 The National Institute of Standards and Technology provides tabulations of the electronic energy levels and associated Einstein coefficients, A_{ul}, for a large number of atomic species. The following table gives relevant data for selected electronic levels of the hydrogen atom.

Configuration	Classification	Energy (cm^{-1})	Transition	Wavelength (Å)	A_{ul} (s^{-1})
$1s$	$^2S_{1/2}$	0			
$2p$	$^2P_{1/2,3/2}$	82,259	$2p \rightarrow 1s$	1216	6.27×10^8
$3p$	$^2P_{1/2,3/2}$	97,492	$3p \rightarrow 1s$	1026	1.67×10^8

a. An emission spectrum obtained from a hydrogen plasma shows that the intensity of the spectral line corresponding to the $3p$-$1s$ transition is 0.57% of that from the $2p$-$1s$ transition. Determine the temperature of the plasma. Assume that induced emission and absorption are negligible.

b. What assumption is required to calculate the plasma temperature?

5.13 Laser-induced fluorescence (LIF) measurements of the sodium atom are to be used to determine the flame temperature in a laboratory combustor. The following table provides relevant data for selected electronic transitions of sodium.

Configuration	Classification	Energy (cm^{-1})	Transition	Wavelength (Å)	A_{ul} (s^{-1})
$3s$	$^2S_{1/2}$	0			
$3p$	$^2P_{1/2}$	16,956	$3p\ (^2P_{3/2}) \rightarrow 3s$	5890.0	6.22×10^7
$3p$	$^2P_{3/2}$	16,973			
$5s$	$^2S_{1/2}$	33,201	$5s \rightarrow 3p\ (^2P_{1/2})$	6154.2	2.60×10^6

a. Demonstrate that, for normal LIF, the fluorescence signal (V) is given by

$$S_f = \eta G \left(\frac{\Omega_c}{4\pi}\right)\left(\frac{V_c}{8\pi Q_{ul}}\right)\left(\frac{g_u}{g_l}\right)(\lambda_{ul} A_{ul})^2 n_l^\circ I_\nu,$$

where η is the optical efficiency, G is the gain of the detector (V/W), Ω_c is the solid angle of the collection optics, V_c is the collection volume, Q_{ul} is the rate coefficient for collisional quenching, g_u and g_l are the relevant degeneracies, λ_{ul} is the laser wavelength, A_{ul} is the Einstein coefficient for spontaneous emission, n_l° is the initial population of the lower level, and I_ν is the spectral irradiance of the laser beam.

b. The LIF signals at 5890.0 Å and 6154.2 Å are found to be 8.64 V and 74.2 nV, respectively. If I_ν and Q_{ul} are invariant with laser wavelength, determine the flame temperature. For consistency with the two-level model, you may assume that fluorescence detection occurs at the same wavelength as laser excitation for each spectral line.

5.14 Laser-saturated fluorescence measurements of the potassium atom are performed in a coal combustion system. The following table provides relevant data for selected electronic transitions of potassium.

Configuration	Classification	Energy (cm^{-1})	Transition	Wavelength (Å)	A_{ul} (s^{-1})
$4s$	$^2S_{1/2}$	0	$4p\ (^2P_{1/2}) \rightarrow 4s\ (^2S_{1/2})$	7699.0	3.82×10^7
$4p$	$^2P_{1/2}$	12,989	$4p\ (^2P_{3/2}) \rightarrow 4s\ (^2S_{1/2})$	7664.9	3.87×10^7
$4p$	$^2P_{3/2}$	13,046	$6s\ (^2S_{1/2}) \rightarrow 4p\ (^2P_{3/2})$	6938.8	5.40×10^6
$6s$	$^2S_{1/2}$	27,459	$6s\ (^2S_{1/2}) \rightarrow 4p\ (^2P_{1/2})$	6911.1	2.72×10^6

If the LIF signals at 6938.8 Å and 7699.0 Å are found to be 0.14 mV and 8.92 V, respectively, determine the flame temperature. For consistency with the two-level model, you may assume that fluorescence detection occurs at the same wavelength as laser excitation for each spectral line.

5.15 Absorption measurements of the hydroxyl radical (OH) are performed on a flat-flame burner having an effective length of 6 cm. The integrated absorptions for the $P_1(6)$ and $Q_1(9)$ rovibronic lines of the $X^2\Pi(v = 0) \rightarrow A^2\Sigma^+(v = 0)$ electronic

transition are found to be 0.39 cm^{-1} and 0.51 cm^{-1}, respectively. The frequency and transition probability for each of these lines are

$$P_1(6): \quad \tilde{\nu} = 32180.8 \text{ cm}^{-1} \qquad A_{ul} = 4.15 \times 10^5 \text{ s}^{-1}$$
$$Q_1(8): \quad \tilde{\nu} = 32297.4 \text{ cm}^{-1} \qquad A_{ul} = 6.36 \times 10^5 \text{ s}^{-1}.$$

Hint: The given A_{ul} values represent each spin-split, Λ-doubled line in the OH spectrum.

a. Show that the population in the ground-state rovibronic level is given by

$$n_l = \frac{g_l}{g_u}\left(\frac{8\pi W_{lu}}{A_{ul}\lambda^2 L}\right),$$

where W_{lu} (s^{-1}) is the integrated absorption, A_{ul} (s^{-1}) is the Einstein coefficient for spontaneous emission, λ (cm) is the wavelength of the rovibronic transition, and L (cm) is the optical path length.

b. Evaluate the flame temperature (K).

c. Determine the total number density for the hydroxyl radical (cm^{-3}). For simplicity, evaluate the OH partition function by using the rigid-rotor/harmonic-oscillator model.

d. What assumptions are required for your calculations?

PART FOUR

STATISTICAL THERMODYNAMICS BEYOND THE DILUTE LIMIT

12 Thermodynamics and Information

Having applied statistical mechanics to nonreactive and reactive gaseous mixtures, we now shift from our study of the dilute limit to fundamental statistical interpretations of undoubtedly the three most salient concepts in classical thermodynamics, namely, work, heat, and entropy. We first introduce a unified microscopic viewpoint for reversible work and heat, followed by an exploration of the statistical foundations underlying the second law of thermodynamics. We then develop a more robust statistical definition of the entropy, which leads directly to a novel interpretation of this pivotal property in terms of statistical information. We complete this chapter by showing how such information can provide a more general stochastic formulation for physical phenomena, with statistical thermodynamics being a particularly cogent example of the power of *information theory*.

12.1 Reversible Work and Heat

We recall from classical thermodynamics that, for a simple closed system, reversible work can be evaluated via

$$\delta W_{rev} = -P\,dV, \tag{12.1}$$

while reversible heat can be expressed as

$$\delta Q_{rev} = T\,dS. \tag{12.2}$$

On this basis, the first law of thermodynamics becomes (Appendix F)

$$dU = \delta Q_{rev} + \delta W_{rev} = T\,dS - P\,dV. \tag{12.3}$$

In comparison, from Eq. (4.19), statistical thermodynamics gives

$$dU = d\left\{\sum_j N_j \varepsilon_j\right\} = \sum_j \varepsilon_j\,dN_j + \sum_j N_j\,d\varepsilon_j. \tag{12.4}$$

However, from Eq. (3.30), we may write, for any system of independent particles,

$$P = -\sum_j N_j \left(\frac{d\varepsilon_j}{dV}\right),$$

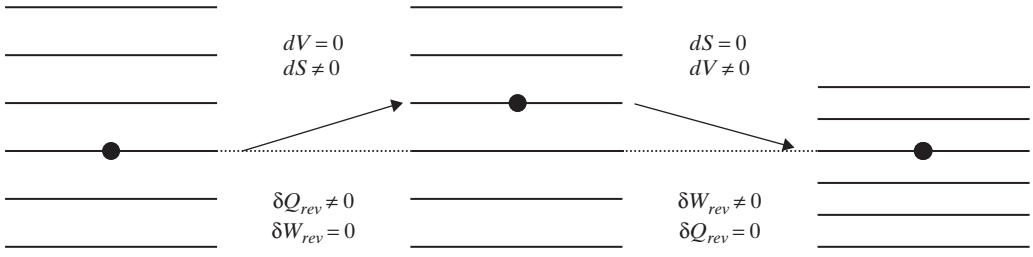

Figure 12.1 Influence of reversible heat addition followed by reversible adiabatic expansion on the energy and population of depicted energy levels for an ideal gas. The large black dot identifies the most probable energy level.

for which ε_j is solely a function of volume. Consequently, from Eq. (12.1), reversible work can be expressed as

$$\delta W_{rev} = \sum_j N_j \, d\varepsilon_j. \tag{12.5}$$

Comparing Eqs. (12.3) and (12.4), we then have, for reversible heat,

$$\delta Q_{rev} = \sum_j \varepsilon_j \, dN_j. \tag{12.6}$$

Despite their apparent simplicity, Eqs. (12.5) and (12.6), when taken together, admit some striking implications. Equation (12.5) shows that, from a microscopic viewpoint, reversible work occurs via a change in quantized energy, but with no change in population. In contrast, Eq. (12.6) indicates that reversible heat manifests itself microscopically through a change in population, but with no change in quantized energy. Moreover, these interpretations for reversible heat and work apply to all independent particles, whether such particles are distinguishable or indistinguishable.

12.2 The Second Law of Thermodynamics

We now apply the microscopic interpretation of reversible heat and work in the previous section to the development of a wholly statistical foundation for the second law of thermodynamics. Consider an ideal gas undergoing a two-step reversible process, composed of (1) reversible heat addition at constant volume followed by (2) reversible adiabatic expansion. For clarity in our upcoming discussion, the influence of these two subprocesses on both the energy and population of the quantized levels associated with any gaseous assembly is displayed in Fig. 12.1. We note that, for analytical convenience, no work is permitted in the first subprocess while no heat is exchanged in the second subprocess.

Recall that reversible heat addition intimates no change in energy, ε_j, for the quantized levels, but an increase in energy of the most probable level owing to the resulting rise in temperature. For simplicity, this energy enhancement for the most probable level is portrayed in Fig. 12.1 by the upward displacement of a large black dot upon completion of the heat-transfer process. In contrast, reversible adiabatic expansion implies no change in the quantum number identifying the most probable level, but a decrease in energy, ε_j, for all levels owing to the resulting rise in volume. Therefore, in Fig. 12.1, the large black dot identifying the most probable level is displaced downward upon completion of

the expansion process. Comparing these two subprocesses, we note that any variation in entropy is apparently accompanied microscopically by a change in particle distribution among the available energy levels for the system.

Remarkably, the stark two-step process portrayed in Fig. 12.1 can engender new insights regarding the second law of thermodynamics. Our approach here is to presume that the most probable energy is the same at the beginning and end of this two-step process. On this basis, we observe that all of the heat energy provided to the system during the first subprocess must be converted to work energy during the second subprocess. However, from Fig. 12.1, we also find that, despite specifying the same initial and final temperatures, the original state of the system is actually unrecoverable because of irreversible changes in both the energy and population of each quantized level. Hence, we must conclude that no cyclic process is possible whose sole result is the absorption of heat from a single reservoir and the conversion of all this heat into work external to the system. From classical thermodynamics, we recognize this conclusion as the Kelvin–Planck statement of the second law of thermodynamics. Therefore, from a microscopic perspective, we have verified that the full conversion of heat to work is impossible in a cyclic process because the working substance can never be brought back to its initial thermodynamic state. Consequently, a reversible cyclic process always mandates the loss of heat to a second reservoir. From classical thermodynamics, the unfortunate outcome from this conclusion is a limited thermodynamic efficiency for heat engines and, similarly, a limited coefficient of performance for refrigerators.

12.3 The Boltzmann Definition of Entropy

We now explore analytically the implied relation between entropy and population distribution suggested by Fig. 12.1. From Eq. (4.14), the probability of occurrence for any energy state is

$$P_i = \frac{N_i}{N} = \frac{e^{-\varepsilon_i / kT}}{Z}, \tag{12.7}$$

where the partition function, from Eq. (4.13), can be expressed as

$$Z = \sum_i e^{-\varepsilon_i / kT}.$$

Combining Eqs. (12.2) and (12.6), followed by multiple implementation of Eq. (12.7), we can relate the entropy to the probability of each state by

$$dS = \frac{1}{T} \sum_i \varepsilon_i \, dN_i = -k \sum_i \ln(P_i Z) \, d(P_i N). \tag{12.8}$$

After appropriate mathematical manipulations, Eq. (12.8) becomes

$$dS = -Nk \left\{ \sum_i \ln P_i \, dP_i + \ln Z \sum_i dP_i \right\} = -Nk \sum_i \ln P_i \, dP_i$$

$$= -Nk \, d \left[\sum_i P_i \ln P_i \right] \tag{12.9}$$

for any isolated system, as

$$\sum_i P_i \, d \ln P_i = \sum_i d P_i = 0$$

follows from

$$\sum_i P_i = 1.$$

Hence, based on Eq. (12.9), we have

$$S = -Nk \sum_i P_i \ln P_i, \tag{12.10}$$

which is called the *Boltzmann definition of entropy*. From Problem 2.5, we may show that this important expression holds, as expected, for both distinguishable and indistinguishable particles. More importantly, Eq. (12.10) demonstrates conclusively that the entropy depends solely on the probability of occurrence for each quantum state. In other words, the entropy of an isolated system undergoes change only when the state probabilities, P_i, shift owing to an increase or decrease in temperature.

12.4 Information Theory

In 1948, Claude Shannon postulated an entirely new approach to chaotic processes through his development of what we now call information theory. At that time, the electronics industry was concerned with the limitations posed by various communication schemes, particularly their susceptibility to random errors. In response to this concern, Shannon proposed that the uncertainty owing to possible errors in any message could be encapsulated by

$$\mathcal{U}(W) = \ln W, \tag{12.11}$$

where W is the number of possible ways for coding random information. As might be expected from this rather heuristic strategy, Eq. (12.11) is actually quite intuitive; the defined uncertainty increases with rising W, can be easily summed for independent events, and becomes zero if $W = 1$.

By considering the number of ways that N distinguishable letters can be arranged to provide any coded message, we find from Eq. (2.28) that

$$W = \frac{N!}{\prod_{i=1}^{M} N_i!}, \tag{12.12}$$

where M represents the number of letters in the alphabet and N_i indicates the expected number of appearances for each letter in typical prose, given that

$$\sum_i N_i = N. \tag{12.13}$$

Substituting Eq. (12.12) into Eq. (12.11) and applying Stirling's approximation (Appendix D.2), we obtain

$$\mathcal{U}(W) = N \ln N - \sum_i N_i \ln N_i,$$

so that, from Eq. (12.13),

$$\mathcal{U}(W) = -\sum_i N_i \ln(N_i/N) = -N\sum_i P_i \ln P_i, \tag{12.14}$$

where $P_i = N_i/N$ defines the probability or relative frequency for each possible letter. The clear analogy between Eqs. (12.14) and (12.10) prompted Shannon to dub $\mathcal{U}(W)$ the *information entropy*. On this basis, Shannon defined *information* as

$$I = \sum_i P_i \ln P_i, \tag{12.15}$$

where, from Eq. (12.14), we note that I is simply the negative of the mean uncertainty per symbol, so that information itself always regresses with rising uncertainty.

Employing information theory, we are now in a position to identify the specific conditions leading to minimum information about any thermodynamic system. Our strategy is to use again the method of Lagrange multipliers, along with the obvious constraint

$$\sum_i P_i = 1, \tag{12.16}$$

which, in differential form, becomes

$$\sum_i dP_i = 0. \tag{12.17}$$

Introducing the usual Lagrange multiplier, α, from Eqs. (12.15) and (12.17) we obtain

$$dI = \sum_i [\ln P_i - \alpha]\, dP_i = 0,$$

so that

$$P_i = e^{\alpha} = \text{constant}. \tag{12.18}$$

Hence, we find, from Eq. (12.18), that the least information or greatest uncertainty about a system occurs when we are forced to assume that all events are equally likely. This totally random situation is, of course, the impetus for our basic statistical assumption of equal *a priori* probabilities. From the viewpoint of information theory, any explicit knowledge of various probabilities delimiting the system of interest constitutes greater information. Therefore, shifting to a thermodynamic perspective, we have shown that maximizing the entropy, in essence, identifies that isolated system characterized by the greatest possible uncertainty.

Finally, an interesting question at this point is what happens to the entropy defined by Eq. (12.10) when we invoke total randomness, as presumed for thermodynamic equilibrium. Based on Eq. (12.18), the probability of each state at equilibrium is simply the inverse of the total number of states in the system, which is equivalent to the total degeneracy, g, as summed over all energy levels. Consequently, from Eqs. (12.10) and (12.16) we have

$$S = -Nk\sum_i P_i \ln (g^{-1}) = Nk \ln g,$$

so that

$$S = k \ln g^N = k \ln W, \tag{12.19}$$

where W represents the total number of microstates for a system composed of N independent particles. Equation (12.19) is identical to Eq. (3.19); hence, we have derived from Eq. (12.10) and information theory the Boltzmann relation introduced in Chapter 3. More fundamentally, we have shown that, at thermodynamic equilibrium, the Boltzmann relation follows naturally from its more general formulation, as its associated equilibrium states are inherently those displaying the greatest randomness or, if you will, the least information.

12.5 Spray Size Distribution from Information Theory

In the previous section, we showed that statistical thermodynamics can be formulated alternatively in terms of information theory. We also suggested that information theory could offer greater analytical utility as compared to statistical mechanics. Hence, information theory might be applicable to a wider variety of physical phenomena governed by stochastic processes. As an example, we consider here the distribution of droplet sizes in liquid sprays (Li and Tankin, 1987), a subject of importance to many industrial processes such as spray painting and fuel injection.

For a liquid spray, we have two constraints, one given by Eq. (12.16) and the other by

$$\dot{m} = \sum_i \rho \dot{n} V_i P_i, \tag{12.20}$$

where $\dot{m}$ is the total mass flow rate for the spray, ρ the liquid density, $\dot{n}$ the total number of droplets produced per unit time, V_i the volume for an individual droplet, and P_i the fraction of total droplets having that volume. While $\dot{n}$ varies considerably for a given nozzle, it mainly depends on the pressure drop through the nozzle and the liquid viscosity. Applying next the Lagrange method of undetermined multipliers, Eqs. (12.15), (12.16), and (12.20) can be summed in differential form, thus giving, via information theory,

$$dI = \sum_i \left[\ln P_i + \alpha + \beta \rho \dot{n} V_i\right] dP_i = 0, \tag{12.21}$$

where, as usual, α and β are the Lagrange multipliers. From Eq. (12.21), we find that

$$P_i = \exp\left[-(\alpha + \beta \rho \dot{n} V_i)\right], \tag{12.22}$$

so that, substituting Eq. (12.22) into Eqs. (12.16) and (12.20), we obtain from these constraints

$$e^{-\alpha} \sum_i \exp\left[-\beta \rho \dot{n} V_i\right] = 1 \tag{12.23}$$

$$e^{-\alpha} \sum_i \rho \dot{n} V_i \exp\left[-\beta \rho \dot{n} V_i\right] = \dot{m}. \tag{12.24}$$

Combining Eqs. (12.23) and (12.24), we thus have for the total mass flow rate

$$\dot{m} = \frac{\sum_i \rho \dot{n} V_i \exp[-\beta \rho \dot{n} V_i]}{\sum_i \exp[-\beta \rho \dot{n} V_i]}. \tag{12.25}$$

Converting, for convenience, to continuous variables, we can express the volume for any droplet as

$$V = \frac{\pi D^3}{6}, \tag{12.26}$$

where D is the diameter of the droplet. On this basis, the probability for droplets having volumes between V and $V + dV$ becomes, from Eq. (12.22),

$$P(V)\,dV = e^{-\alpha} \exp\left[-\beta\rho\dot{n}V\right] dV.$$

Hence, from Eq. (12.26), the probability of obtaining diameters between D and $D + dD$ can be expressed as

$$P(D)\,dD = \frac{\pi}{2} D^2 e^{-\alpha} \exp\left[-\frac{\pi\beta\rho\dot{n}D^3}{6}\right] dD. \tag{12.27}$$

After integration over all possible droplet sizes, Eq. (12.23) becomes

$$e^{\alpha} = \int_0^{\infty} \exp\left[-\beta\rho\dot{n}V\right] dV,$$

so that, from Eq. (12.26) and Appendix B,

$$e^{\alpha} = \frac{\pi}{2}\int_0^{\infty} D^2 \exp\left[-\frac{\pi\beta\rho\dot{n}D^3}{6}\right] dD = \frac{\pi}{3}\int_0^{\infty} x \exp\left[-\frac{\pi\beta\rho\dot{n}x^2}{6}\right] dx = \frac{1}{\beta\rho\dot{n}}. \tag{12.28}$$

Similarly, from Eq. (12.25),

$$\dot{m} = \frac{\int_0^{\infty} \rho\dot{n}V \exp\left[-\beta\rho\dot{n}V\right] dV}{\int_0^{\infty} \exp\left[-\beta\rho\dot{n}V\right] dV};$$

substituting again from Eq. (12.26) and utilizing Appendix B, we have

$$\dot{m} = \frac{\frac{\pi}{6}\int_0^{\infty} \rho\dot{n}D^5 \exp\left[-\frac{\pi\beta\rho\dot{n}D^3}{6}\right] dD}{\int_0^{\infty} D^2 \exp\left[-\frac{\pi\beta\rho\dot{n}D^3}{6}\right] dD} = \frac{\frac{\pi\rho\dot{n}}{6}\int_0^{\infty} x^3 \exp\left[-\frac{\pi\beta\rho\dot{n}x^2}{6}\right] dx}{\int_0^{\infty} x \exp\left[-\frac{\pi\beta\rho\dot{n}x^2}{6}\right] dx} = \frac{1}{\beta}. \tag{12.29}$$

Now, combining Eqs. (12.28) and (12.29), we obtain

$$e^{\alpha} = \frac{\dot{m}}{\rho\dot{n}}, \tag{12.30}$$

which, from Eq. (12.20), defines the mean volume of the droplets in the spray. Upon substitution of Eqs. (12.29) and (12.30) into Eq. (12.27), the desired probability density function, based on our criterion of least information, becomes

$$P(D) = \frac{\pi}{2}\left(\frac{\rho\dot{n}}{\dot{m}}\right) D^2 \exp\left[-\frac{\pi\rho\dot{n}D^3}{6\dot{m}}\right]. \tag{12.31}$$

Consequently, Eq. (12.31) would be the expected droplet-size distribution based on a completely random spray formation process. Surprisingly enough, this expression is replicated by the so-called Nukiyama–Tanasawa distribution, which has received considerable experimental confirmation. Therefore, we have verified that a steady-state spray is

often best understood by invoking a random rather than an evolutionary model. The triumph of this statistical approach demonstrates the power of information theory when dealing with physical phenomena not amenable to description using classical conservation equations. Indeed, for this reason, thermodynamic properties can be calculated with substantial success by employing a close cousin of information theory – statistical thermodynamics.

13 Elements of the Solid State

Our applications of statistical thermodynamics have thus far been mainly concerned with the gaseous state. We now move on to the solid state, with a particular focus in this chapter on metallic crystals, such as copper and silver. While semiconductors are, of course, very significant in an electronic age, their study is beyond the purview of this book, although our introduction to the solid state will surely pave the path for any future work that you might contemplate in this lucrative field.

In general, metallic crystals display a *lattice structure*, which features lattice sites occupied by metallic ions, but with their accompanying electrons migrating throughout the crystal. Because these ions are immobilized within a crystalline structure, they can vibrate about their equilibrium positions but they clearly cannot rotate or translate. Contrastingly, the electrons can surely translate, as indicated by their movement through any electrically conducting solid. In fact, as for individual metallic ions, electrons can be taken as independent particles because the electrostatic forces created between electrons and ions or among the electrons themselves are so long range that the electrons essentially move within a constant potential throughout the lattice structure. On the other hand, the mass of the electron is so tiny that our criterion for the dilute limit cannot possibly hold in this case, as verified by Eq. (9.5). Therefore, for the electron gas, we have no recourse but to summon basic Fermi–Dirac statistics.

13.1 Statistical Thermodynamics of the Crystalline Solid

We begin our study of the solid state by analyzing a *crystalline solid* – a lattice of vibrating metallic ions without its penetrating sea of conducting electrons. As for the diatomic gas, each metallic ion stationed within the lattice structure can vibrate, except that the vibrations can occur in any of three coordinate directions, as portrayed schematically in Fig. 13.1. Consequently, for N individual ions, each with three mutually independent vibrational motions, we have the equivalent of $3N$ linear harmonic oscillators. On this basis, from the classical equipartition principle, we would anticipate a specific internal energy of $3RT$ and a specific heat of $3R$. In fact, surprisingly enough, this simple classical supposition found good agreement with the early experimental work of Dulong and Petit (1819).

Subsequent measurements below room temperature, however, demonstrated a considerable reduction in specific heat as compared to the expected $3R$. From our study of

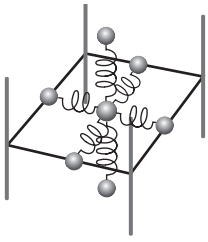

Figure 13.1 Lattice structure of a crystalline solid.

the diatomic molecule, we now realize, of course, that this result arises naturally from less than full excitation of the vibrational energy mode. In comparison, modern cryogenic experiments in the early twentieth century showed that

$$\lim_{T\to 0} \frac{c_v}{R} \propto T^3,$$

which could never have been anticipated based on the harmonic oscillator model. Therefore, the stage was set for the work of Albert Einstein (1879–1955) and Peter Debye (1884–1966), as they sought to develop statistical models to explain the behavior of crystalline solids.

In preparation for our study of such models, we must recognize that the $3N$ oscillators of a crystalline solid are inherently *distinguishable* rather than indistinguishable because of their association with specific lattice sites. Therefore, in contrast to the ideal gas, a solid lattice follows uncorrected rather than corrected Maxwell–Boltzmann statistics. For this reason, before pursuing either Einstein or Debye theory, we synthesize general thermodynamic expressions identifying pertinent solid-state properties for any assembly composed of distinguishable particles.

We begin by recalling that, for N distinguishable particles, the number of microstates per macrostate, from Eq. (4.7), is

$$W_{MB} = N! \prod_j \frac{g_j^{N_j}}{N_j!}. \tag{13.1}$$

Taking the logarithm of Eq. (13.1) and implementing Stirling's approximation (Appendix D.2) yields

$$\ln W_{MB} = N \ln N + \sum_j N_j \ln\left(\frac{g_j}{N_j}\right). \tag{13.2}$$

Applying next the Lagrange method of undetermined multipliers (Appendix D.1), with the usual constraints for an isolated system given by

$$\sum_j N_j = N \tag{13.3}$$

$$\sum_j N_j \varepsilon_j = E, \tag{13.4}$$

we have from Eqs. (13.2–13.4)

$$d \ln W_{MB} = \sum_j \left\{ \ln\left(\frac{g_j}{N_j}\right) - \alpha - \beta\varepsilon_j \right\} dN_j = 0, \tag{13.5}$$

where α and β are, of course, the Lagrange multipliers. From Eq. (13.5), we thus obtain, in the normal manner, the most probable distribution,

$$N_j = g_j \exp\left[-(\alpha + \beta\varepsilon_j)\right]. \tag{13.6}$$

The Lagrange multipler, α, may now be eliminated in favor of β by substituting Eq. (13.6) into Eq. (13.3). Accordingly, we have

$$N = e^{-\alpha} \sum_j g_j e^{-\beta\varepsilon_j}, \tag{13.7}$$

so that, dividing Eq. (13.6) by Eq. (13.7), we obtain the probability for the jth level as

$$\frac{N_j}{N} = \frac{g_j e^{-\beta\varepsilon_j}}{\sum_j g_j e^{-\beta\varepsilon_j}}. \tag{13.8}$$

In analogy with Section 4.3, we define the molecular partition function

$$Z = \sum_j g_j e^{-\beta\varepsilon_j} = \sum_j g_j e^{-\varepsilon_j/kT},$$

where we have invoked, as usual (Problem 2.3),

$$\beta = \frac{1}{kT}.$$

On this basis, the equilibrium particle distribution becomes, as expected from corrected Maxwell–Boltzmann statistics,

$$\frac{N_j}{N} = \frac{g_j e^{-\varepsilon_j/kT}}{Z}. \tag{13.9}$$

If we next substitute Eq. (13.9) into Eq. (13.4), we have for the internal energy

$$U = \sum_j N_j\varepsilon_j = NkT^2 \left(\frac{\partial \ln Z}{\partial T}\right)_V, \tag{13.10}$$

as derived previously in Section 4.4 for indistinguishable particles in the dilute limit. Similarly, for the specific heat, we obtain, from Eq. (4.33),

$$C_V = \left(\frac{\partial U}{\partial T}\right)_V = Nk\left[\frac{\partial}{\partial T}T^2\left(\frac{\partial \ln Z}{\partial T}\right)\right]_V. \tag{13.11}$$

The entropy, on the other hand, requires that we combine Eqs. (3.19), (13.2), and (13.9), thus giving

$$S = k\ln W_{MB} = kN\ln N + k\sum_j N_j\left[\ln\left(\frac{Z}{N}\right) + \frac{\varepsilon_j}{kT}\right],$$

so that, from Eq. (13.10),

$$S = Nk\left[T\left(\frac{\partial \ln Z}{\partial T}\right)_V + \ln Z\right]. \tag{13.12}$$

At this point, it is instructive to compare Eqs. (13.10) and (13.12), for distinguishable particles, to Eqs. (4.21) and (4.23), respectively, for indistinguishable particles in the dilute limit. We find, unsurprisingly, that the internal energy has remained the same; however,

the current expression for entropy has changed owing to the different statistics associated with distinguishability. Equation (13.12), on the other hand, duplicates Eq. (8.15), thus verifying that the contribution to the entropy from any internal energy mode is identical for distinguishable and indistinguishable particles. In other words, the resulting difference in entropy can be associated, as expected, with the translational energy mode. Therefore, in summary, statistical relations for properties such as the internal energy, enthalpy, and heat capacities will be the same while those for the entropy and free energies will be different for distinguishable particles as compared to indistinguishable particles in the dilute limit.

13.2 Einstein Theory for the Crystalline Solid

Einstein (1907) made the very reasonable assumption that a crystalline lattice can be modeled as an assembly of $3N$ identical, noninteracting harmonic oscillators. In addition, because of the tightly-bound structure of crystalline solids, he presumed that all $3N$ vibrational modes would oscillate at the same fundamental frequency. On this basis, from Eq. (9.47), the molecular partition function for a single harmonic oscillator can be written as

$$Z_{vib} = (1 - e^{-\theta_E/T})^{-1}, \tag{13.13}$$

where $\theta_E = h\nu_E/k$ is the so-called Einstein temperature, which is simply a characteristic vibrational temperature for the crystalline solid. In essence, θ_E is an adjustable parameter that can be used to best match predicted and experimental thermodynamic data for a given metal.

Because the partition function for distinguishable particles is the same as that for indistinguishable particles in the dilute limit, we find from Eqs. (13.10) and (13.11) that, for $3N$ oscillators having the same characteristic temperature,

$$U = 3NkT^2 \left(\frac{\partial \ln Z_{vib}}{\partial T} \right)_V \tag{13.14}$$

$$C_V = 3Nk \left[\frac{\partial}{\partial T} T^2 \left(\frac{\partial \ln Z_{vib}}{\partial T} \right) \right]_V . \tag{13.15}$$

Therefore, in analogy with Eqs. (9.48) and (9.49), we obtain from Eqs. (13.13–13.15)

$$\frac{u}{RT} = \frac{3\theta_E/T}{e^{\theta_E/T} - 1} \tag{13.16}$$

$$\frac{c_v}{R} = \frac{3\,(\theta_E/T)^2\, e^{\theta_E/T}}{(e^{\theta_E/T} - 1)^2}. \tag{13.17}$$

Similarly, for the entropy, we find from Eq. (13.12)

$$S = 3Nk \left[T \left(\frac{\partial \ln Z_{vib}}{\partial T} \right)_V + \ln Z_{vib} \right], \tag{13.18}$$

so that from Eqs. (13.13), (13.16), and (13.18) we have, for $3N$ harmonic oscillators,

$$\frac{s}{R} = 3 \left[\frac{\theta_E/T}{e^{\theta_E/T} - 1} - \ln (1 - e^{-\theta_E/T}) \right]. \tag{13.19}$$

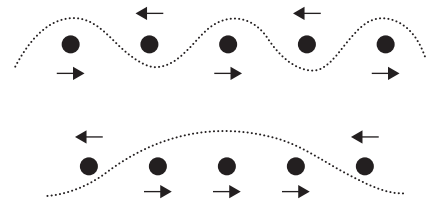

Figure 13.2 Normal mode structure within a crystalline solid at higher and lower frequencies.

For comparative purposes, we close this section by analyzing the limiting behavior for specific heat at high and low temperatures, as predicted by the Einstein theory. At the high-temperature limit we have, upon invoking series expansions for the exponential terms in Eq. (13.17),

$$\lim_{\theta_E/T\to 0}\frac{c_v}{R}=\frac{3(\theta_E/T)^2\left[1+(\theta_E/T)+\cdots\right]}{(1+(\theta_E/T)+\cdots-1)^2}\simeq 3,$$

so that we have successfully reproduced the expected result from equipartition theory. On the other hand, at the low-temperature limit, we obtain

$$\lim_{\theta_E/T\to\infty}\frac{c_v}{R}=\frac{3(\theta_E/T)^2e^{\theta_E/T}}{e^{2\theta_E/T}}=3(\theta_E/T)^2e^{-\theta_E/T},$$

which obviously disagrees with the observed T^3-dependence near absolute zero. This failure of Einstein theory arises because of a collective coupling among the lattice sites at lower temperatures, as we will now explore by turning to the more successful Debye theory.

13.3 Debye Theory for the Crystalline Solid

Because the energy of an oscillator is proportional to its frequency, an improved statistical model for the crystalline solid at lower temperatures mandates a better understanding of vibrational energy modes at lower frequencies. As for the single atom of a polyatomic gas, the normal frequencies in a crystal describe the concerted harmonic motion of all metallic ions within the lattice structure. At lower frequencies, the resulting wavelengths are long compared to the atomic spacing within the lattice; thus, these frequencies must be determined by analyzing the crystal as a continuous elastic medium. In other words, at lower temperatures, the behavior of a crystalline solid displays features more appropriately described by classical rather than quantum mechanics. At higher frequencies, on the other hand, the wavelength must eventually be limited by the internuclear spacing within the lattice structure, as indicated in Fig. 13.2. The upshot is that neighboring ions tend to move collectively in phase at lower frequencies while ionic pairs gravitate toward out-of-phase motion at higher frequencies.

Based on this distinction between low- and high-frequency behavior, Debye (1912) postulated a continuous distribution of oscillator frequencies, but with a maximum frequency identified with a characteristic internuclear spacing, thus defining the so-called *Debye frequency*. From this postulate, we may write

$$dN=g(\nu)\,d\nu \qquad 0\le\nu\le\nu_D, \tag{13.20}$$

where dN is the number of normal vibrators in the frequency range ν to $\nu+d\nu$, $g(\nu)$ is a frequency distribution function, and ν_D is the Debye frequency. Here, we note that $g(\nu)$

is not the usual probability density function, as integration of Eq. (13.20) over all possible frequencies gives the total number of oscillators for a crystalline solid, so that

$$\int_0^{\nu_D} g(\nu)\, d\nu = 3N. \tag{13.21}$$

At this point, the required distribution function could be obtained by determining the number of standing acoustic waves produced by thermally excited vibrations within a specified elastic medium. Fortunately, an analogous procedure is needed to determine the number of standing electromagnetic waves in a blackbody cavity, as we will discuss in Chapter 14. From this type of analysis, we find that

$$g(\nu) = \frac{12\pi V}{v_s^3}\nu^2, \tag{13.22}$$

where V represents the volume of the elastic medium and v_s is the average speed of sound in the metallic crystal. Substituting Eq. (13.22) into Eq. (13.21), we obtain

$$g(\nu) = \frac{9N\nu^2}{\nu_D^3}, \tag{13.23}$$

so that the Debye frequency can be related to fundamental crystalline parameters via

$$\nu_D^3 = \frac{3Nv_s^3}{4\pi V}. \tag{13.24}$$

If we now assume that the properties of a crystalline solid can be determined by superimposing the contributions from each normal mode, we then have from Eqs. (13.14) and (13.15)

$$U = \int_0^{\nu_D} g(\nu)kT^2 \left(\frac{\partial \ln Z_{vib}}{\partial T}\right)_V d\nu \tag{13.25}$$

$$C_V = \int_0^{\nu_D} g(\nu)k\left[\frac{\partial}{\partial T}T^2\left(\frac{\partial \ln Z_{vib}}{\partial T}\right)\right]_V d\nu, \tag{13.26}$$

where, in each case, we have integrated over all possible frequencies after weighing the relevant property per vibrator with its frequency distribution function. Generalizing Eq. (13.13), we may write the vibrational partition function for any frequency as

$$Z_{vib} = (1 - e^{-h\nu/kT})^{-1}, \tag{13.27}$$

so that, substituting Eq. (13.27) into Eqs. (13.25) and (13.26), we obtain

$$U = \int_0^{\nu_D} g(\nu)kT\frac{h\nu/kT}{e^{h\nu/kT} - 1}d\nu \tag{13.28}$$

$$C_V = \int_0^{\nu_D} g(\nu)k\frac{(h\nu/kT)^2\, e^{h\nu/kT}}{(e^{h\nu/kT} - 1)^2}d\nu. \tag{13.29}$$

Our remaining development will be aided considerably by introducing

$$x = \frac{h\nu}{kT} \qquad x_D = \frac{h\nu_D}{kT} = \frac{\theta_D}{T},$$

where θ_D is called the *Debye temperature*. Given these definitions, Eqs. (13.28) and (13.29) become, after substitution from Eq. (13.23),

$$U = \frac{9NkT}{x_D^3}\int_0^{x_D}\frac{x^3}{e^x-1}dx \tag{13.30}$$

$$C_V = \frac{9Nk}{x_D^3}\int_0^{x_D}\frac{x^4e^x}{(e^x-1)^2}dx. \tag{13.31}$$

Defining the *Debye function*,

$$D(x_D) = \frac{3}{x_D^3}\int_0^{x_D}\frac{x^3}{e^x-1}dx, \tag{13.32}$$

and integrating Eq. (13.31) by parts, we obtain finally the specific internal energy and heat capacity as

$$\frac{u}{RT} = 3D(x_D) \tag{13.33}$$

$$\frac{c_v}{R} = 3\left[4D(x_D) - \frac{3x_D}{e^{x_D}-1}\right]. \tag{13.34}$$

To expedite the evaluation of Eqs. (13.33) and (13.34), the Debye function has been numerically integrated and the results tabulated in Appendix M. Note that both the internal energy and specific heat are functions solely of $x_D = \theta_D/T$. In general, the Debye temperature, θ_D, is obtained by fitting Eq. (13.34) to experimental data, although good results can also be had by using Eq. (13.24) along with the measured speed of sound within a crystalline solid. More significantly, if we explore once again the low-temperature limit for specific heat, we now find

$$\lim_{x_D\to\infty}\frac{c_v}{R} = 12\lim_{x_D\to\infty}D(x_D) = 12\left[\frac{\pi^4}{5x_D^3}\right] = \frac{12\pi^4}{5}\left(\frac{T}{\theta_D}\right)^3, \tag{13.35}$$

thus supporting the observed T^3-dependence for $T < 0.05\theta_D$.

We conclude from Eq. (13.35) that the specific heat of a crystalline solid becomes negligible as the temperature approaches absolute zero. Of more interest, however, is what happens to the entropy under such conditions. Employing the same statistical procedures invoked previously to derive Eqs. (13.33) and (13.34), we have, from Eq. (13.18),

$$S = \int_0^{\nu_D} g(\nu)k\left[T\left(\frac{\partial \ln Z_{vib}}{\partial T}\right)_V + \ln Z_{vib}\right]d\nu. \tag{13.36}$$

Hence, substituting from Eqs. (13.23) and (13.27), we obtain

$$S = \frac{9Nk}{x_D^3}\int_0^{x_D}\left[\frac{x^3}{e^x-1} - x^2\ln(1-e^{-x})\right]dx, \tag{13.37}$$

which becomes, after integration by parts,

$$\frac{s}{R} = 4D(x_D) - 3\ln(1-e^{-x_D}). \tag{13.38}$$

Table 13.1 *Debye temperatures for some selected metallic crystals*

Element	$\theta_D(K)$	Element	$\theta_D(K)$
Pb	86	Zn	240
K	99	Cu	308
Bi	111	Al	398
Na	160	Cr	405
Sn	165	Co	445
Ag	215	Fe	453
Pt	225	Ni	456
Ca	230	Be	980

Consequently, as for Eq. (13.35), we may now evaluate the low-temperature limit for the entropy, thus finding

$$\lim_{x_D \to \infty} \frac{s}{R} = 4\left[\frac{\pi^4}{5x_D^3}\right] = \frac{4\pi^4}{5}\left(\frac{T}{\theta_D}\right)^3. \tag{13.39}$$

Therefore, we conclude that the entropy of a perfect crystalline solid becomes zero at a temperature of absolute zero. We have thus verified the famous third law of thermodynamics. Just as importantly, we now understand that this classical result occurs because all $3N$ vibrational modes must drop into their nondegenerate ground states at absolute zero.

13.4 Critical Evaluation of the Debye Formulation

Because of its obvious superiority as compared to the Einstein theory, the Debye theory has engendered widespread applications in solid-state physics. In particular, by fitting the Debye model to measured specific heat data, we may determine Debye temperatures for most crystalline solids, as verified for selected metallic crystals in Table 13.1. Using these characteristic temperatures, we may also collapse specific heat data to a common dimensionless plot based on Eq. (13.34), as demonstrated in Fig. 13.3. More importantly, Debye temperatures are especially useful when evaluating thermodynamic properties other than the specific heat for metallic crystals.

Highly accurate specific-heat measurements in recent years, however, have shown that θ_D is not perfectly constant, but actually varies by as much as 10–20% with temperature, as shown schematically in Fig. 13.4. Typically, θ_D is somewhat constant at its low- and

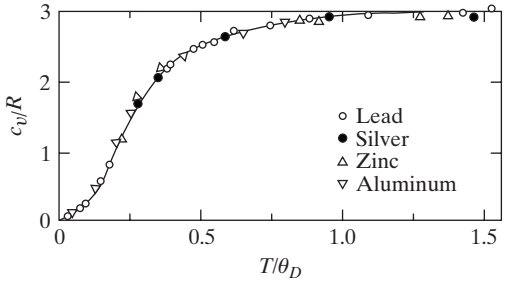

Figure 13.3 Specific heats of metallic solids following the Debye theory.

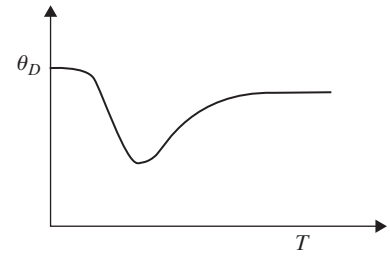

Figure 13.4 Schematic thermal variation of the Debye temperature.

high-temperature limits, with a minimum near $T = 0.1\theta_D$. This variation arises from the actual frequency distribution function for crystalline solids, which tends to exhibit less than a ν^2-dependence for $T < 0.1\theta_D$ and greater than a ν^2-dependence for $T > 0.1\theta_D$. Moreover, as indicated by Fig. 13.4, the limiting θ_D values at low and high temperatures are somewhat different, so that many tabulations of θ_D preferentially emphasize low-temperature behavior, as for those Debye temperatures listed in Table 13.1.

By comparing the previous Einstein and Debye expressions for the specific heat of a crystalline solid, we may convert the Debye temperatures of Table 13.1 to comparable Einstein temperatures for use in the Einstein formulation. The strategy here is to apply series expansions to the various functional representations in Eqs. (13.17) and (13.34), thus obtaining, after much algebra,

$$\left(\frac{c_v}{3R}\right)_E = 1 - \frac{(\theta_E/T)^2}{12} + \frac{(\theta_E/T)^4}{240} + \cdots$$

$$\left(\frac{c_v}{3R}\right)_D = 1 - \frac{(\theta_D/T)^2}{20} + \frac{(\theta_D/T)^4}{560} + \cdots.$$

On this basis, the specific heats for the Debye and Einstein models should be equivalent, at least up through the quadratic term, if

$$\theta_E = \left(\frac{3}{5}\right)^{1/2} \theta_D. \tag{13.40}$$

Hence, by using Eq. (13.40) to determine an Einstein temperature, thermodynamic properties can also be evaluated via the Einstein model, which often proves beneficial at higher temperatures.

Finally, we must comment that, just as classical electromagnetic waves can be interpreted quantum mechanically via the photon, classical acoustic waves can be treated in a quantized fashion through introduction of the so-called *phonon*. From this alternative viewpoint, the lattice structure of a crystalline solid can be modeled as a set of $3N$ phonon vibrations. In recent years, phonons have been studied directly through the inelastic scattering of neutrons. In comparison to the basic Debye model, such experiments have shown that phonons have dispersion; that is, their acoustic velocity within metallic crystals actually depends on the wavelength. This defect in the Debye model, along with its several other weaknesses, is primarily due to an overly simplistic modeling of the crystalline solid as a purely elastic medium. In fact, the discrete atomic structure of the solid state must be especially accounted for when encountering the world of semiconductors.

EXAMPLE 13.1

From the Debye theory, determine (a) the temperature (K) at which the internal energy of metallic copper is two-thirds of its classical value. Employing this temperature, evaluate the entropy (J/mole · K) of copper by applying (b) the Debye model and (c) the Einstein model.

Solution

(a) From Eq. (13.33), the internal energy for a Debye solid is given by

$$u = 3RTD(x_D),$$

so that u is two-thirds of its classical value when $D(x_D) = 0.667$. Hence, from Appendix M,

$$x_D = \frac{\theta_D}{T} \simeq 1.0.$$

On this basis, from Table 13.1, $T = \theta_D = 308$ K.

(b) From Eq. (13.38), the entropy of copper using the Debye model is

$$\frac{s}{R} = 4D(x_D) - 3\ln(1 - e^{-x_D}).$$

Evaluating this expression at $x_D = 1.0$, we obtain

$$\frac{s}{R} = 4(0.667) + 3(0.459) = 4.045.$$

Hence,

$$s = 4.045(8.3145) = 33.632 \text{ J/mol} \cdot \text{K}.$$

(c) From Eq. (13.40), the Einstein temperature is

$$\theta_E = \left(\frac{3}{5}\right)^{1/2} \theta_D = 238 \text{ K}.$$

Hence, from Eq. (13.19), the entropy of copper using the Einstein model gives

$$\frac{s}{R} = 3\left[\frac{\theta_E/T}{e^{\theta_E/T} - 1} - \ln(1 - e^{-\theta_E/T})\right] = 3(0.663 + 0.619) = 3.846.$$

Therefore,

$$s = 3.846(8.3145) = 31.978 \text{ J/mol} \cdot \text{K},$$

which is only about 5% less than the Debye evaluation for the entropy of copper.

13.5 The Band Theory of Metallic Solids

In Chapter 7, we introduced nomenclature identifying the electronic energy levels of individual atoms. As compared to gaseous particles, the ions in a metallic crystal are confined to a lattice, so that their electronic energies cannot be considered in such an autonomous fashion. In fact, as shown in Fig. 13.5, as the distance between atoms progressively drops,

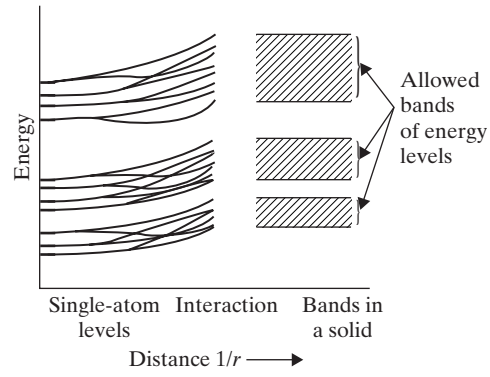

Figure 13.5 The evolution of energy bands in a crystalline solid.

their discrete energy levels split and coalesce so that, in a crystalline lattice, *energy bands* are formed with each band composed of a huge number of electronic levels. More dominantly, between these bands, forbidden regions emerge which cannot be accessed by potential electronic states.

Previously, starting from Eq. (9.5), we found that electrons cannot satisfy our criterion for the dilute limit (Problem 2.7). Similarly, in Chapter 5, we concluded, based on the Pauli exclusion principle, that electrons follow Fermi–Dirac statistics, so that they are constrained to only one particle per energy state. For such statistics, the equilibrium particle distribution, based on Eq. (3.31), is given by

$$N_j = \frac{g_j}{\exp[(\varepsilon_j - \mu)/kT] + 1}, \tag{13.41}$$

where, obviously, $N_j/g_j \leq 1$. From Eq. (13.41), we observe that as the temperature approaches zero there are only two possibilities for the number of particles per energy state:

$$\begin{aligned} (\varepsilon_j - \mu_0) > 0 \qquad & N_j/g_j = 0 \\ (\varepsilon_j - \mu_0) < 0 \qquad & N_j/g_j = 1, \end{aligned}$$

where μ_0 is the chemical potential at absolute zero. Therefore, a critical energy, $\varepsilon_F = \mu_0$, exists that near absolute zero neatly separates totally filled from completely empty electronic states, as displayed graphically in Fig. 13.6. Consequently, unlike either corrected or uncorrected Maxwell–Boltzmann statistics, Fermi–Dirac statistics implies nonzero internal energy, even at absolute zero, because the exclusion principle forces available electrons to occupy states of progressively higher energy. The maximum energy, ε_F, needed to house all such electrons is called the *Fermi energy*.

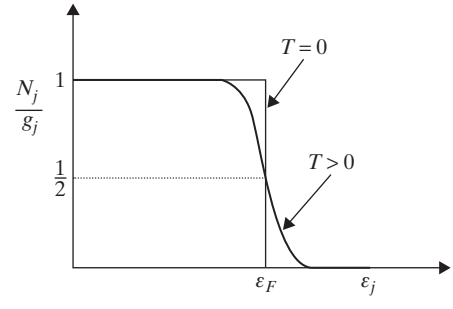

Figure 13.6 The Fermi–Dirac distribution.

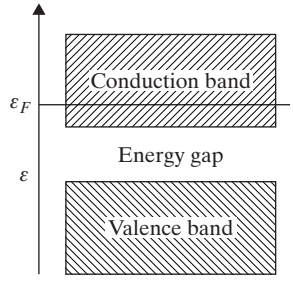

Figure 13.7 Band structure for a metallic crystal.

In contrast to the energy, the entropy for a Fermi–Dirac system, from Eqs. (3.10) and (3.19), is given very simply by

$$S = k \ln W_{FD} = k \ln \left\{ \prod_j \frac{g_j!}{N_j!\,(g_j - N_j)!} \right\}. \tag{13.42}$$

From Fig. 13.6, we note that for $\varepsilon < \varepsilon_F$, $N_j = g_j$; thus, from Eq. (13.42), we find that $W_j = 1$. Similarly, for $\varepsilon > \varepsilon_F$, $N_j = 0$ so that again $W_j = 1$. As a result, only one way exists by which to place N_j indistinguishable fermions in g_j energy states. The inescapable conclusion is that, despite the required Fermi energy, the entropy at absolute zero always vanishes for Fermi–Dirac statistics.

Based on Figs. 13.5 and 13.6, we presume that available electrons fill the lowest accessible energy levels and thus the lowest energy bands up to the Fermi energy. Hence, any energy levels existing above the Fermi energy must be empty. In general, the highest populated band is called the *valence band* while the next highest band is called the *conduction band*. For an insulator, a large energy gap exists between the Fermi energy within the valence band and the empty conduction band. Therefore, at ordinary temperatures, no flowing electrons can be associated with the conduction band.

For a metal, however, the Fermi level occurs in the middle of the conduction band, as shown in Fig. 13.7. The ensuing availability of electrons within the conduction band, even at room temperature, results in migration of electrons throughout the crystal and thus electrical conductivity. For this reason, the electrons in a metallic crystal can usually be modeled as an electron gas. In comparison, semiconductors are characterized by band gaps considerably smaller than those for an insulator. Hence, appropriate impurities can normally be added to create either mobile electrons within the conduction band or mobile "holes" just above the valence band. This extra complication effectively couples the behavior of metallic ions with their accompanying electrons, thus making the electron-gas model inappropriate for semiconductors, as discussed at length in more advanced treatises concerned with solid-state physics.

13.6 Thermodynamic Properties of the Electron Gas

The electron gas is clearly significant as it provides the primary mechanism for the electrical conductivity of metallic crystals. Moreover, the Debye theory for a crystalline solid proves to be inadequate at temperatures below approximately 5 K because electronic deportment adds materially to thermodynamic properties under such conditions. As indicated previously, the electrons can be treated as independent particles owing to a roughly

constant potential throughout the lattice structure. This relatively constant potential arises from rather long-range forces both among the electrons themselves and also between the electrons and the metallic ions located at the various lattice sites.

Continuing the previous development for a crystalline solid, we seek to determine the thermodynamic properties of its electron gas, particularly the internal energy and specific heat. The only significant energy mode in this case is translation within the conduction band. Consequently, identifying the number of energy states associated with an electron of mass m_e for translational energies between ε and $\varepsilon + d\varepsilon$, we have from Eq. (5.61)

$$D(\varepsilon)\, d\varepsilon = 4\pi \left(\frac{2m_e}{h^2}\right)^{3/2} V\varepsilon^{1/2}\, d\varepsilon, \tag{13.43}$$

except that we have multiplied the usual density of translational states by a factor of two to account for the intrinsic spin of each electron. Because the Pauli exclusion principle permits only one electron per state, Eq. (13.43) also represents the number of electrons with translational energies between ε and $\varepsilon + d\varepsilon$ at absolute zero. Therefore, from Eq. (13.41), the electronic distribution function at any temperature must be

$$N(\varepsilon) = \frac{D(\varepsilon)}{\exp[(\varepsilon - \mu)/kT] + 1}, \tag{13.44}$$

so that the total number of electrons becomes

$$N = \int_0^\infty N(\varepsilon)\, d\varepsilon = \int_0^\infty \frac{D(\varepsilon)\, d\varepsilon}{\exp[(\varepsilon - \mu)/kT] + 1}. \tag{13.45}$$

Substituting Eq. (13.43) into Eq. (13.45), and recognizing from Fig. 13.6 that $0 < \varepsilon < \varepsilon_F$, we obtain

$$N = 4\pi \int_0^{\varepsilon_F} \left(\frac{2m_e}{h^2}\right)^{3/2} V\varepsilon^{1/2}\, d\varepsilon \tag{13.46}$$

at absolute zero. Performing the indicated integration, we find from Eq. (13.46)

$$\varepsilon_F = \mu_0 = \frac{h^2}{8m_e}\left(\frac{3N}{\pi V}\right)^{2/3}, \tag{13.47}$$

so that the Fermi energy has now been shown to depend on the number density of free electrons, which is, of course, affected by the number of valence electrons provided by each atom in the metallic crystal. In general, we also have, for the internal energy,

$$U = \int_0^\infty \varepsilon N(\varepsilon)\, d\varepsilon, \tag{13.48}$$

so that, at absolute zero, Eq. (13.48) becomes

$$U_0 = 4\pi \int_0^{\varepsilon_F} \left(\frac{2m_e}{h^2}\right)^{3/2} V\varepsilon^{3/2}\, d\varepsilon = \frac{3}{5} N\varepsilon_F. \tag{13.49}$$

In other words, as expected, the internal energy cannot be zero, even at absolute zero, owing to the Pauli exclusion principle. Similarly, for the pressure, we have from Problem 2.2

$$PV = \frac{2}{3}E_{tr} = \frac{2}{3}U, \tag{13.50}$$

so that, at absolute zero,

$$P_0 = \frac{2}{5}\left(\frac{N\varepsilon_F}{V}\right). \tag{13.51}$$

Remarkably, Eq. (13.51) shows that fermions produce positive pressure, even at absolute zero.

We find it convenient at this point to define the Fermi temperature,

$$\theta_F = \frac{\varepsilon_F}{k}, \tag{13.52}$$

which is typically 10^5 K, and thus several orders of magnitude greater than normal metal temperatures. Therefore, despite being evaluated at absolute zero, the internal energy and pressure from Eqs. (13.49) and (13.51), respectively, turn out to be simply huge. Moreover, even at substantial temperatures, $T \ll \theta_F$ and thus thermodynamic properties for an electron gas should differ insignificantly from those evaluated at absolute zero. On this basis, we may determine the chemical potential at higher temperatures by manipulating Eq. (13.45) via a series expansion for μ about μ_0. Similarly, the internal energy can be determined by solving Eq. (13.48) via the implementation of a Taylor expansion about U_0. Forsaking algebraic shenanigans, involving ponderous Fermi–Dirac integrals both below and above the Fermi energy, we can eventually show that (Davidson, 1962)

$$\mu = \varepsilon_F\left[1 - \frac{\pi^2}{12}\left(\frac{kT}{\varepsilon_F}\right)^2 + \cdots\right] \tag{13.53}$$

$$U = U_0\left[1 + \frac{5\pi^2}{12}\left(\frac{kT}{\varepsilon_F}\right)^2 + \cdots\right]. \tag{13.54}$$

Hence, the chemical potential decreases and the internal energy increases, but ever so slightly compared to their respective values at absolute zero. From Fig. 13.6, we observe that the chemical potential drops because the energy level at which half the quantum states become filled declines at greater temperatures, as electrons move to higher energy states. This movement to higher energy levels also causes, of course, an accompanying increase in the internal energy of the electron gas.

From Eqs. (13.49) and (13.54), we also obtain

$$C_V = \left(\frac{\partial U}{\partial T}\right)_{V,N} = \frac{\pi^2}{2}Nk\left(\frac{kT}{\varepsilon_F}\right),$$

so that the specific heat contributed by the electron gas becomes

$$\frac{c_v}{R} = \frac{\pi^2}{2}\left(\frac{T}{\theta_F}\right). \tag{13.55}$$

In essence, Eq. (13.55) implies that only electrons near the Fermi energy become sufficiently agitated thermally to contribute to the specific heat. Moreover, given typical values of the Fermi temperature, this contribution is not $1.5R$, as for the ideal gas, but on the order of $10^{-2}R$. For most scenarios, electronic contributions of this magnitude are negligible, except as compared to the minuscule input from the lattice structure at very low temperatures. Nonetheless, the contribution of the electron gas to solid-state physics remains otherwise quite significant across the entire temperature range, especially with respect to modeling the thermionic properties of metals and also their electrical and thermal conductivities.

EXAMPLE 13.2

Show that the specific entropy for the electron gas can be expressed as

$$\frac{s}{R} = \frac{\pi^2}{2}\left(\frac{kT}{\varepsilon_F}\right),$$

thus proving once again that its entropy vanishes at temperatures approaching absolute zero.

Solution

From classical thermodynamics (Appendix F), the entropy can be expressed as

$$S = \frac{H - G}{T} = \frac{U + PV - G}{T}.$$

Employing Eq. (13.50), we have

$$PV = \frac{2}{3}U,$$

so that, by combining the two previous equations, the entropy becomes

$$S = \frac{1}{T}\left(\frac{5}{3}U - G\right).$$

From Eq. (13.53), the Gibbs free energy can be represented by

$$G = N\mu = N\varepsilon_F\left[1 - \frac{\pi^2}{12}\left(\frac{kT}{\varepsilon_F}\right)^2 + \cdots\right],$$

while, from Eqs. (13.49) and (13.54), the internal energy is

$$U = \frac{3}{5}N\varepsilon_F\left[1 + \frac{5\pi^2}{12}\left(\frac{kT}{\varepsilon_F}\right)^2 + \cdots\right].$$

As a result, the entropy for the electron gas becomes

$$S = \frac{N\varepsilon_F}{T}\left\{\left[1 + \frac{5\pi^2}{12}\left(\frac{kT}{\varepsilon_F}\right)^2 + \cdots\right] - \left[1 - \frac{\pi^2}{12}\left(\frac{kT}{\varepsilon_F}\right)^2 + \cdots\right]\right\} = \frac{N\varepsilon_F}{T}\left(\frac{\pi^2}{2}\right)\left(\frac{kT}{\varepsilon_F}\right)^2.$$

Therefore, the specific entropy is found to be

$$\frac{s}{R} = \frac{\varepsilon_F}{kT}\left(\frac{\pi^2}{2}\right)\left(\frac{kT}{\varepsilon_F}\right)^2 = \frac{\pi^2}{2}\left(\frac{kT}{\varepsilon_F}\right),$$

thus verifying that the entropy for an electron gas is zero at absolute zero.

13.7 The Metallic Crystal near Absolute Zero

If we now superimpose the separate contributions from vibrating metallic ions and migrating electrons within the lattice structure, the specific heat of a metallic crystal, from Eqs. (13.35) and (13.55), can be expressed near absolute zero as

$$\frac{c_v}{R} = \frac{12\pi^4}{5}\left(\frac{T}{\theta_D}\right)^3 + \eta\frac{\pi^2}{2}\left(\frac{T}{\theta_F}\right), \tag{13.56}$$

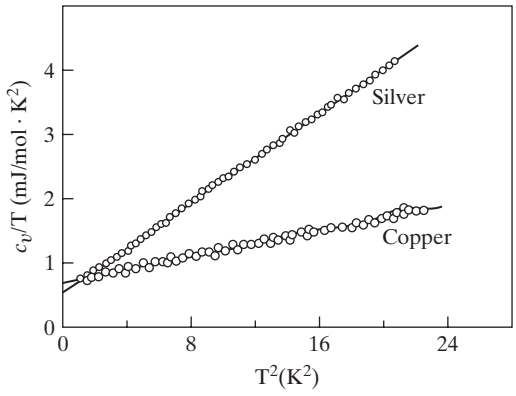

Figure 13.8 The low-temperature specific heat of metallic crystals.

where η represents the number of valence electrons per atom. The additional parameter, η, is mandatory in Eq. (13.56) because the specific heat contribution from the crystalline solid is calculated per mole of atoms, while that from the electron gas is evaluated per mole of electrons. Based on Eq. (13.56), a plot of c_v/T versus T^2 should give a straight line whose slope indicates the contribution from metallic ions and whose intercept indicates that from migrating electrons. Figure 13.8 provides such plots based on careful measurements for silver and copper; the excellent results verify our statistical analyses identifying both the ionic and electronic contributions to the properties of a metallic crystal. Moreover, from a practical perspective, the slope can be exploited to determine the Debye temperature, while the intercept can be used to evaluate the Fermi temperature. The former permits exploration of the low-temperature behavior for a crystalline solid while the latter provides information on the density of states for an electron gas near the Fermi level.

Problems enhancing your understanding of this chapter are combined with those for Chapter 14 in Problem Set VI.

14 Equilibrium Radiation

In this chapter, we examine equilibrium radiation, which represents our third and final application of statistical mechanics to independent particles beyond the dilute limit. For simplicity in mathematically modeling the radiant field, we apply the methods of statistical thermodynamics to electromagnetic waves enclosed in a cubical blackbody cavity. The enclosed radiation is at both thermal and radiative equilibrium if the walls of the cavity are at constant temperature with equal rates of emission and absorption, respectively.

14.1 Bose–Einstein Statistics for the Photon Gas

From a quantum perspective, the electromagnetic radiation within a blackbody cavity can be modeled as an assembly of independent photons. Given this representation, we recall from Section 5.9 that photons are particles of zero spin; hence, a *photon gas* must follow Bose–Einstein statistics, whose equilibrium particle distribution, following Eq. (3.31), is normally given by

$$N_j = \frac{g_j}{\exp[(\varepsilon_j - \mu)/kT] - 1}. \tag{14.1}$$

However, in comparison to the usual assumptions associated with Eq. (14.1), photons do not obey particle conservation as they are constantly being formed and destroyed at the walls of a blackbody cavity. Of course, thermodynamic equilibrium still mandates conservation of energy at these same walls. As a result, nothing prevents, for example, the replacement of one incoming photon with two outgoing photons, each having half its energy. Consequently, the chemical potential must vanish from Eq. (14.1) as this thermodynamic property ultimately arises from that Lagrange multiplier representing particle conservation, which we now know is irrelevant for photons; thus, for the photon gas,

$$N_j = \frac{g_j}{\exp(\varepsilon_j/kT) - 1}. \tag{14.2}$$

Mathematically, Eq. (14.2) provides no substantive limit on the number of photons per energy state, as anticipated from both the nature of electromagnetic radiation and Bose–Einstein statistics. Nevertheless, for any photon, $\varepsilon = h\nu$, so that we actually have a

continuous distribution of photon energies. Consequently, we may convert Eq. (14.2) to

$$N(\nu)\,d\nu = \frac{g(\nu)\,d\nu}{\exp\,(h\nu/kT) - 1}, \tag{14.3}$$

where $N(\nu)\,d\nu$ represents the number of photons and $g(\nu)\,d\nu$ the number of photon states in the frequency range ν to $\nu + d\nu$.

14.2 Photon Quantum States

Because the only operative energy mode for the photon gas is kinetic, Eq. (14.3) requires that we identify the number of *translational* quantum states for any photon in the frequency range ν to $\nu + d\nu$. This determination is actually quite similar to that used when deriving the density of translational states for the particle in a box, as developed in Section 5.7. In particular, based on Eq. (5.59), the total number of translational quantum states encompassed by all frequencies less than a chosen frequency ν is

$$M_\nu = \frac{\pi n^3}{6}, \tag{14.4}$$

where n is the total translational quantum number, as represented by the usual volumetric radius in three-dimensional, quantum-number space (see Fig. 5.5).

Reproducing our previous density of states analysis, we now differentiate Eq. (14.4), thus obtaining the number of quantum states in the frequency range ν to $\nu + d\nu$, i.e.,

$$g(\nu)\,d\nu = \pi n^2 dn, \tag{14.5}$$

where we have also multiplied by a factor of two to account for the two independent polarizations of an electromagnetic wave. Substituting Eq. (14.5) into Eq. (14.3), the number of photons in the frequency range ν to $\nu + d\nu$ thus becomes

$$N(\nu)d\nu = \frac{\pi n^2 dn}{\exp\,(h\nu/kT) - 1}. \tag{14.6}$$

Because $N(\nu)$ is basically a photon distribution function, you should recognize at this point that the total translational quantum number, n, must eventually be related to the photon frequency, ν.

14.3 The Planck Distribution Law

As intimated above, the crucial step in our development of the radiant energy distribution for a blackbody cavity is, in fact, deriving an explicit relation for $n(\nu)$. The fundamental difficulty is that, in this case, we cannot directly associate n with its kinetic energy, as for the ideal or electron gas, because photons have zero rest mass. Instead, we must approach the problem classically by considering electromagnetic radiation trapped in a cubical cavity of volume $V = L^3$, with wall temperature, T. As discussed shortly, owing to internal reflections, traveling electromagnetic waves become standing electromagnetic waves when confined to a blackbody cavity. Our overall strategy, therefore, is to determine the number of standing electromagnetic waves in a cubical cavity, which will eventually allow us to complete the evolution of Eq. (14.6).

We begin by recalling that standing waves can always be produced through a proper combination of traveling waves. An electromagnetic wave traveling in the positive x-direction, for example, can be represented by the electric-field expression

$$E_+ = E_\circ \sin(k_x x - \omega t), \tag{14.7}$$

where, from Eq. (5.20), the propagation number associated with the x-direction can be written artificially in terms of the spatial frequency, ν_x, and the speed of light, c, so that

$$k_x = \frac{2\pi \nu_x}{c}. \tag{14.8}$$

Now, for an enclosed cavity, we require standing electromagnetic waves with their nodes placed at the walls of the cubical cavity for all three Cartesian coordinates. We can construct such standing waves via the superposition of two traveling waves moving in opposite directions. Hence, in the x-direction, we have, from Eq. (14.7),

$$E_s = E_+ + E_- = E_\circ \left[\sin(k_x x - \omega t) + \sin(k_x x + \omega t)\right] = 2E_\circ \sin k_x x \ \cos \omega t. \tag{14.9}$$

The standing wave represented by Eq. (14.9) is, of course, subject to the required boundary conditions, $E_s = 0$ at $x = 0$ and at $x = L$. On this basis, we obtain, as usual,

$$k_x L = n_x \pi \qquad n_x = 1,\ 2,\ 3, \ldots, \tag{14.10}$$

where n_x indicates the number of standing waves in the x-direction.

Shifting next to three-dimensional standing waves, the propagation number for this more realistic scenario becomes, from Eq. (14.10),

$$k^2 = k_x^2 + k_y^2 + k_z^2 = \frac{\pi^2}{L^2}\left(n_x^2 + n_y^2 + n_z^2\right) = \left(\frac{\pi}{L}\right)^2 n^2, \tag{14.11}$$

where n is the desired total translational quantum number. We observe, very significantly, that this total quantum number arises quite naturally from counting all possible standing waves because of the obvious analogy between the classical problem of electromagnetic radiation in a cavity and the quantum mechanical problem of the particle in a box. Pursuing this analogy, we may rewrite Eq. (14.8) for a three-dimensional wave, so that

$$k^2 = \left(\frac{2\pi}{c}\right)^2 \nu^2. \tag{14.12}$$

Consequently, comparing Eqs. (14.11) and (14.12), we can at last express the total quantum number, n, in terms of the frequency, ν, so that

$$n^3 = \left(\frac{2L}{c}\right)^3 \nu^3 = \frac{8V}{c^3}\nu^3. \tag{14.13}$$

If we now differentiate Eq. (14.13), we obtain

$$n^2 dn = \frac{8V}{c^3}\nu^2 d\nu, \tag{14.14}$$

where V is the volume of a cubical cavity. Substituting Eq. (14.14) into Eq. (14.5), we have

$$g(\nu) = \frac{8\pi V}{c^3}\nu^2, \tag{14.15}$$

so that the number of photon states is proportional to ν^2, as also indicated for phonons in Chapter 13. This same proportionality holds for phonons as well as photons, as previously anticipated, because of the physical and mathematical analogy between standing acoustic waves in a cubical crystal and standing electromagnetic waves in a cubical cavity.

Finally, substituting Eq. (14.15) into Eq. (14.3), we find that the number of photons in the frequency range ν to $\nu + d\nu$ becomes

$$N(\nu)\,d\nu = \frac{8\pi V}{c^3}\frac{\nu^2 d\nu}{\exp\,(h\nu/kT) - 1}. \tag{14.16}$$

If we now multiply by the energy per photon, $\varepsilon = h\nu$, the radiant energy per unit volume in the frequency range ν to $\nu + d\nu$ can be expressed as

$$\rho_\nu\,d\nu = \frac{h\nu N(\nu)\,d\nu}{V}.$$

Hence, from Eq. (14.16), the *spectral energy density*, ρ_ν, becomes

$$\rho_\nu = \frac{8\pi h}{c^3}\frac{\nu^3}{\exp\,(h\nu/kT) - 1}, \tag{14.17}$$

which is the desired *Planck distribution law* for equilibrium radiation.

14.4 Thermodynamics of Blackbody Radiation

Equation (14.17) is our required entrée to the many thermodynamic relations, both classical and statistical, describing blackbody radiation. For example, beginning with the spectral energy density, $\rho_\nu\,(\mathrm{J/m^3 \cdot s^{-1}})$, we may determine the internal energy per unit volume by simply integrating over all frequencies, so that

$$\frac{U}{V} = \int_0^\infty \rho_\nu\,d\nu = \frac{8\pi h}{c^3}\left(\frac{kT}{h}\right)^4 \int_0^\infty \frac{x^3}{e^x - 1}dx, \tag{14.18}$$

where, for convenience in upcoming manipulations, we have defined

$$x \equiv \frac{h\nu}{kT}. \tag{14.19}$$

Employing Appendix B, we may now evaluate the integral in Eq. (14.18), thus obtaining, for the internal energy per unit volume,

$$\frac{U}{V} = \frac{8\pi^5}{15}\frac{(kT)^4}{(hc)^3}. \tag{14.20}$$

Similarly, we can determine the *spectral emissive power*, $E_\nu(\mathrm{W/m^2 \cdot s^{-1}})$, by recognizing that, for the photon gas, energy flux is related to energy density by

$$\text{energy flux (energy/time} \cdot \text{area)} = \frac{c}{4} \times \text{energy density (energy/volume)},$$

as we will verify via basic kinetic theory in Section 15.4. Hence, from Eq. (14.17), we have

$$E_\nu = \frac{c}{4}\rho_\nu = \frac{2\pi h}{c^2}\frac{\nu^3}{\exp\,(h\nu/kT) - 1}. \tag{14.21}$$

Integrating Eq. (14.21) over all frequencies, the *total emissive power* can then be expressed as

$$E = \int_0^\infty E_\nu\,d\nu = \frac{2\pi k^4}{h^3c^2}T^4\int_0^\infty \frac{x^3}{e^x - 1}dx = \sigma T^4, \tag{14.22}$$

so that the well-known Stefan–Boltzmann constant becomes

$$\sigma = \frac{2\pi^5 k^4}{15h^3c^2}. \tag{14.23}$$

Equation (14.22) is, of course, recognizable as the famous Stefan–Boltzmann law of radiative heat transfer. Evaluation of the Stefan–Boltzmann constant via the fundamental physical parameters of Appendix A gives $\sigma = 5.6716 \times 10^{-8}$ W/m$^2 \cdot$ K^4, which proves to be in excellent agreement with radiant measurements. Hence, we are once again amazed by the power of statistical thermodynamics, here with respect to the development of basic theoretical formulations for both the Stefan–Boltzmann law and the Stefan–Boltzmann constant. We note, by the way, that, while this law is universally used for heat transfer calculations, Eq. (14.22) basically presumes both thermodynamic and radiative equilibrium.

Finally, employing Bose–Einstein statistics, we can write the entropy, from Eq. (3.29), as

$$S = \frac{U - \mu N}{T} - k\sum_j g_j \ln\left\{1 - \exp\left[-\left(\frac{\varepsilon_j - \mu}{kT}\right)\right]\right\}. \tag{14.24}$$

Now, for the photon gas, $\mu = 0$, so that for a continuous distribution Eq. (14.24) becomes

$$S = \frac{U}{T} - k\sum_j g_j \ln\left(1 - e^{-\varepsilon_j/kT}\right) = \frac{U}{T} - k\int_0^\infty g(\nu)\ln\left(1 - e^{-h\nu/kT}\right)d\nu, \tag{14.25}$$

where, as usual, we have invoked $\varepsilon = h\nu$. Upon substitution from Eq. (14.15), Eq. (14.25) can be expressed as

$$S = \frac{U}{T} - 8\pi kV\left(\frac{kT}{hc}\right)^3 \int_0^\infty x^2 \ln\left(1 - e^{-x}\right)dx, \tag{14.26}$$

where we have again used Eq. (14.19). Substituting from Eq. (14.20) and integrating by parts, we obtain from Eq. (14.26)

$$S = \frac{8\pi^5 kV}{15}\left(\frac{kT}{hc}\right)^3 + \frac{8\pi kV}{3}\left(\frac{kT}{hc}\right)^3 \int_0^\infty \frac{x^3}{e^x - 1}dx = 8\pi^5 kV\left(\frac{1}{15} + \frac{1}{45}\right)\left(\frac{kT}{hc}\right)^3,$$

so that

$$S = \frac{32}{45}\pi^5 kV\left(\frac{kT}{hc}\right)^3. \tag{14.27}$$

Therefore, as for the electron gas, the entropy of the photon gas vanishes at absolute zero.

EXAMPLE 14.1

Demonstrate that the electromagnetic pressure at radiative equilibrium can be related to its internal energy per unit volume by

$$P = \frac{U}{3V}.$$

Discuss the implications of this result.

Solution

From classical thermodynamics (Appendix F), the pressure can always be obtained from the Helmholtz free energy by invoking

$$P = -\left(\frac{\partial A}{\partial V}\right)_T$$

for a closed thermodynamic system. Now, the Hemholtz free energy is

$$A = U - TS,$$

so that, from Eqs. (14.20) and (14.27), we have

$$A = \frac{8\pi^5}{15}\frac{(kT)^4}{(hc)^3}V - \frac{32\pi^5}{45}\frac{(kT)^4}{(hc)^3}V = -\frac{8\pi^5}{45}\frac{(kT)^4}{(hc)^3}V.$$

Differentiating with respect to volume, we obtain

$$P = -\left(\frac{\partial A}{\partial V}\right)_T = \frac{8\pi^5}{45}\frac{(kT)^4}{(hc)^3}.$$

Comparing with Eq. (14.20), we find the pressure to be

$$P = \frac{8\pi^5}{45}\frac{(kT)^4}{(hc)^3} = \frac{U}{3V}.$$

This result for the photon gas should be compared to Eq. (13.50),

$$P = \frac{2U}{3V},$$

which is the accepted relation between pressure and internal energy per unit volume for both the ideal and electron gases. The observed reduction by a factor of two for the photon gas indicates the importance of relativistic effects caused by a zero rest mass.

14.5 The Influence of Wavelength for the Planck Distribution

We end our discussion of equilibrium radiation by investigating how the Planck distribution is affected by the wavelength of electromagnetic waves. Converting the spectral energy density from frequency to wavelength, ρ_λ (J/m^4), we have, from $\lambda\nu = c$ and Eq. (14.17),

$$\rho_\lambda = \rho_\nu \left|\frac{d\nu}{d\lambda}\right| = \frac{8\pi}{\lambda^5}\frac{hc}{\exp(hc/\lambda kT) - 1}. \tag{14.28}$$

At deep infrared wavelengths, Eq (14.28) becomes

$$\lim_{\lambda\to\infty}\rho_\lambda = \frac{8\pi}{\lambda^5}\frac{hc}{[1 + hc/\lambda kT] - 1} = \frac{8\pi}{\lambda^4}kT, \tag{14.29}$$

which is the classic Rayleigh–Jeans law. Similarly, at deep ultraviolet wavelengths,

$$\lim_{\lambda\to 0}\rho_\lambda = \frac{8\pi hc}{\lambda^5}e^{-hc/\lambda kT}, \tag{14.30}$$

which is called Wien's law. Defining once again $x \equiv hc/\lambda kT$, we obtain for each case

$$\rho_\lambda = 8\pi\frac{(kT)^5}{(hc)^4}\frac{1}{x^5(e^x - 1)} \qquad \text{Planck's law} \tag{14.31}$$

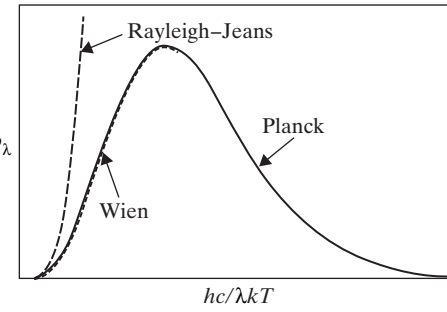

Figure 14.1 The Planck, Rayleigh–Jeans, and Wien blackbody distributions.

$$\rho_\lambda = 8\pi \frac{(kT)^5}{(hc)^4} x^4 \qquad \text{Rayleigh–Jeans law} \tag{14.32}$$

$$\rho_\lambda = 8\pi \frac{(kT)^5}{(hc)^4} x^5 e^{-x} \qquad \text{Wien law.} \tag{14.33}$$

These three expressions are plotted in Fig. 14.1, which clearly identifies those regions where the Rayleigh–Jeans law and Wien law are suitable approximations. In general, Planck's law is required at most intermediate wavelengths, including the visible portion of the electromagnetic spectrum.

We recall from radiative heat transfer that the spectral energy density emitted from any surface can be related to that of a blackbody via the spectral emissivity ε_λ, so that

$$\rho_\lambda = \varepsilon_\lambda \rho_\lambda^B, \tag{14.34}$$

where ρ_λ^B now specifically identifies Eq. (14.28) as the spectral energy density for a blackbody. For a so-called gray surface, the spectral emissivity can be taken to be independent of wavelength, so that, from Eqs. (14.28) and (14.34), the ratio of spectral energy densities becomes

$$\frac{\rho_{\lambda 1}}{\rho_{\lambda 2}} = \left(\frac{\lambda_2}{\lambda_1}\right)^5 \left[\frac{\exp(hc/\lambda_2 kT) - 1}{\exp(hc/\lambda_1 kT) - 1}\right]. \tag{14.35}$$

Equation (14.35) defines the so-called *two-color method* for determining surface temperature. In general, if we measure a ratio of spectral energy densities at two chosen wavelengths from the same region on a gray or black surface, we note that Eq. (14.35) provides the surface temperature. Indeed, this relatively simple approach to surface thermometry has been used extensively in recent years to determine soot temperatures in laboratory and industrial flames. Typically, infrared wavelengths must be avoided because of background problems caused by nearby hot surfaces. In particular, by invoking ultraviolet wavelengths, Wien's law can often be implemented, thus simplifying the temperature measurements, as obtained from

$$\frac{\rho_{\lambda 1}}{\rho_{\lambda 2}} = \left(\frac{\lambda_2}{\lambda_1}\right)^5 \exp\left[\frac{hc}{kT}\left(\frac{\lambda_1 - \lambda_2}{\lambda_1 \lambda_2}\right)\right]. \tag{14.36}$$

Nevertheless, we note from Eq. (14.36) that the accuracy of such measured temperatures ultimately depends on a judicious choice for λ_1 and λ_2. In other words, some care must be taken in selecting the monitored wavelengths for any given range of expected surface temperatures.

PROBLEM SET VI

The Solid State and Radiation (Chapters 13–14)

6.1 The Debye temperature of solid copper is 308 K.

a. Using the Debye model, determine the temperature (K) at which the internal energy of metallic copper is two-thirds of its classical value.

b. Employing the Debye model, evaluate the specific heat (J/mol · K) and the entropy (J/mol · K) of copper at the temperature found in part (a).

c. Using the Einstein model, calculate the specific heat of copper (J/mol · K) at this same temperature. What are the implications of your calculation?

6.2 The specific heat of gold is 0.1203 J/g · K at a temperature of 165 K.

a. Estimate the Einstein and Debye temperatures for gold.

b. Verify that your calculated values of θ_E and θ_D are consistent with one another.

c. Use both the Einstein and Debye models to find the specific heat of gold at 100 K.

d. Determine the specific heat of gold at 100 K using appropriate series expansions for both the Einstein and Debye models. Discuss the implications of your result.

6.3 A crystalline solid has a frequency distribution function given by

$$g(\nu) = C\nu \qquad 0 \leq \nu \leq \nu_m,$$

where C is a constant and ν_m is the maximum oscillator frequency.

a. Show that the specific heat of the solid is

$$\frac{c_v}{R} = \frac{6}{x_m^2} \int_0^{x_m} \frac{x^3 e^x}{(e^x - 1)^2}\, dx,$$

where $x = h\nu/kT$.

b. Develop an expression for the entropy (s/R) of this solid.

6.4 The gravitational collapse of a white dwarf star is prevented by the high internal pressure produced by an electron gas near the center of the star, where the temperature is approximately 2×10^7 K. Sirius B is a typical white dwarf star; its estimated

mass and radius are 2.1×10^{30} kg and 5.6×10^3 km, respectively. Assume that thermonuclear reactions have converted all the hydrogen in Sirius B to helium and that the helium has undergone complete ionization.

a. Determine the total number of electrons in Sirius B.

b. Neglecting any relativistic effects, calculate the Fermi temperature (K) of Sirius B.

c. Estimate the pressure (bar) at the center of this star.

6.5 Consider an electron gas within a metallic solid having one conduction electron per atom of metal and a metal density of 0.1 mole/cm^3.

a. Calculate the Fermi energy and the pressure exerted by this electron gas at 0 K.

b. Using the thermodynamic relation

$$P = -\left(\frac{\partial A}{\partial V}\right)_T,$$

show that, at room temperature,

$$PV = \frac{2}{3}U.$$

c. Calculate the chemical potential and the pressure for this electron gas at 300 K.

6.6 Employing a metal density of 10.5 g/cm^3 and assuming one conduction electron per atom, calculate the lattice and electronic contributions to the specific heat of silver (J/mol · K) at both 30 K and 300 K. What are the implications of your calculations?

6.7 Experimental data for the low-temperature heat capacity of silver ($\rho =$ 10.5 gm/cm^3) can be correlated by the equation

$$c_v = 0.6\ T + 0.18\ T^3,$$

where c_v is in mJ/mol · K and T is in K. Find the Debye temperature, the effective number of free electrons per atom, and the Fermi energy for silver.

6.8 Silver has a Debye temperature of 210 K and a Fermi energy of 5.3 eV.

a. If the density of silver can be taken as 10.5 gm/cm^3, determine the effective number of valence electrons per silver atom.

b. What are the contributions to the specific heat (J/mol · K) owing to lattice vibrations and to electronic motion at 300 K? Discuss your results.

c. At what temperature will the electronic contribution to the specific heat be equal to that from the lattice vibrations?

6.9 We have previously shown the pressure,

$$P = -\sum_j N_j \left(\frac{\partial \varepsilon_j}{\partial V}\right)_{T,N},$$

for Bose–Einstein statistics. Hence, this expression can be applied to equilibrium radiation in a blackbody cavity.

a. Employing the above expression, show that $PV = U/3$ for the photon gas.

b. Determine U/V and thus P. Why is P independent of volume?

c. Find the Helmholtz free energy for a photon gas.

d. Using part (c), determine S and μ for the photon gas.

6.10 Consider a blackbody cavity at radiative equilibrium.

a. Develop an expression for the total number of photons/volume in the cavity.

Hint :
$$\int_0^\infty \frac{x^2}{(e^x - 1)} dx \cong \frac{12}{5}.$$

b. Determine the mean energy of the photons in the cavity.

c. Explain how the result of part (b) reflects the uncertainty principle.

6.11 The spectral distribution of blackbody radiation is strongly influenced by the temperature.

a. Beginning with the spectral energy density, ρ_ν, verify that
$$\rho_\lambda = \frac{8\pi}{\lambda^5} \frac{hc}{\exp(hc/\lambda kT) - 1}.$$

b. Show that the wavelength corresponding to the maximum value of ρ_λ for a given temperature can be determined from $\lambda_{\max} T = 0.29 \text{ cm} \cdot \text{K}$. This expression is called Wien's displacement law.

c. At what wavelength is ρ_λ a maximum for $T = 5800$ K (the approximate temperature of the sun)? What color in the visible spectrum does this wavelength represent? Discuss the implications of your result.

PART FIVE

NONEQUILIBRIUM STATISTICAL THERMODYNAMICS

15 Elementary Kinetic Theory

We have previously shown that the translational energy mode for an ideal gas, even through a shock wave, invariably displays classical equilibrium behavior. In contrast, the rotational, vibrational, and electronic modes generally require significant time for re-equilibration upon disturbances in their equilibrium particle distributions. On this basis, we may expand our statistical discourse to nonequilibrium topics by grounding any dynamic redistribution on the presumption of translational equilibrium. For this reason, we now shift to elementary kinetic theory, which focuses solely on the translational motion of a gaseous assembly. Specifically, in this chapter, we consider equilibrium kinetic theory and its applications to velocity distributions, surface collisions, and pressure calculations. We then proceed to nonequilibrium kinetic theory with particular emphasis on calculations of transport properties and chemical reaction rates, as pursued in Chapters 16 and 17, respectively.

15.1 The Maxwell–Boltzmann Velocity Distribution

In Section 9.1, we showed that the translational energy mode for a dilute assembly displays classical behavior because of the inherently minute spacing between its discrete energy levels ($\Delta\varepsilon \ll kT$). Under such conditions, the partition function can be expressed in terms of the phase integral, φ, thus giving, from Eqs. (8.22) and (8.23),

$$Z = \frac{\varphi}{h^n} = \frac{1}{h^n} \iint_n e^{-H(\boldsymbol{p},\boldsymbol{r})/kT} d^n p \, d^n r. \tag{15.1}$$

Therefore, for a single particle circumscribed by three Cartesian coordinates, the translational partition function becomes, from Eq. (15.1),

$$Z_{tr} = \frac{\varphi_{tr}}{h^3} = \frac{1}{h^3} \int_{-\infty}^{\infty}\int_{-\infty}^{\infty}\int_{-\infty}^{\infty}\int_{-\infty}^{\infty}\int_{-\infty}^{\infty}\int_{-\infty}^{\infty} e^{-H(\boldsymbol{p},\boldsymbol{r})/kT} dp_x \, dp_y \, dp_z \, dx \, dy \, dz, \tag{15.2}$$

where

$$H(\boldsymbol{p}, \boldsymbol{r}) = \frac{\left(p_x^2 + p_y^2 + p_z^2\right)}{2m}. \tag{15.3}$$

Now, from our statistical development in Section 4.3, the probability of taking on any quantized energy, ε_j, can be expressed as

$$P_j = \frac{N_j}{N} = \frac{g_j e^{-\varepsilon_j/kT}}{Z}, \tag{15.4}$$

where the molecular partition function is

$$Z = \sum_j g_j e^{-\varepsilon_j/kT}.$$

By analogy with Eq. (15.4), we conclude that the probability of assuming continuous energies within the range $H(\boldsymbol{p}, \boldsymbol{r})$ to $H(\boldsymbol{p}, \boldsymbol{r}) + dH(\boldsymbol{p}, \boldsymbol{r})$ can be written, from Eq. (15.1), as

$$dP = e^{-H(\boldsymbol{p}, \boldsymbol{r})/kT} \frac{d^n p \, d^n r}{\varphi}. \tag{15.5}$$

Hence, for a translating particle, from Eqs. (15.3) and (15.5) we obtain

$$dP = \frac{1}{\varphi_{tr}} \exp\left[-\frac{p_x^2 + p_y^2 + p_z^2}{2mkT}\right] dp_x \, dp_y \, dp_z \, dx \, dy \, dz, \tag{15.6}$$

where, from Eqs. (9.4) and (15.2), the phase integral for the translational mode is

$$\varphi_{tr} = (2\pi mkT)^{3/2} V. \tag{15.7}$$

From a probabilistic perspective, Eq. (15.6) can be interpreted as the fraction of particles expected in the momentum and position ranges, $\boldsymbol{p}$ to $\boldsymbol{p} + d\boldsymbol{p}$ and $\boldsymbol{r}$ to $\boldsymbol{r} + d\boldsymbol{r}$, respectively. We note that this fractional population is independent of Planck's constant; thus, quantum mechanical effects are irrelevant, as expected when considering the translational energy mode.

Defining a probability density function (PDF) for the momentum and position vectors, $f(\boldsymbol{p}, \boldsymbol{r})$, Eq. (15.6) can equivalently be expressed as

$$dP = f(\boldsymbol{p}, \boldsymbol{r}) \, dp_x \, dp_y \, dp_z \, dx \, dy \, dz, \tag{15.8}$$

so that, from Eqs. (15.6–15.8),

$$f(\boldsymbol{p}, \boldsymbol{r}) = \frac{1}{V}\left(\frac{1}{2\pi mkT}\right)^{3/2} \exp\left[-\frac{p_x^2 + p_y^2 + p_z^2}{2mkT}\right]. \tag{15.9}$$

In general, a new PDF can always be constructed using selected variables associated with a more comprehensive PDF by integrating over the remaining independent variables of the system. Hence, employing Eq. (15.8), we may define the related PDF, $f(\boldsymbol{p})$, associated only with momentum by integrating over all possible positions:

$$f(\boldsymbol{p}) \, dp_x \, dp_y \, dp_z = \iiint_V f(\boldsymbol{p}, \boldsymbol{r}) \, dp_x \, dp_y \, dp_z \, dx \, dy \, dz, \tag{15.10}$$

so that, from Eq. (15.9),

$$f(\boldsymbol{p}) = \left(\frac{1}{2\pi mkT}\right)^{3/2} \exp\left[-\frac{p_x^2 + p_y^2 + p_z^2}{2mkT}\right]. \tag{15.11}$$

Similarly, substituting for $\boldsymbol{p} = m\boldsymbol{V}$, we may define

$$f(\boldsymbol{V})\,dV_x\,dV_y\,dV_z = f(\boldsymbol{p})\,dp_x\,dp_y\,dp_z, \tag{15.12}$$

and thus the PDF for velocity, $f(\boldsymbol{V})$, becomes, from Eqs. (15.11) and (15.12),

$$f(\boldsymbol{V}) = \left(\frac{m}{2\pi kT}\right)^{3/2} \exp\left[-\frac{m\left(V_x^2 + V_y^2 + V_z^2\right)}{2kT}\right]. \tag{15.13}$$

In honor of its co-discoverers, Eq. (15.13) is usually called the *Maxwell–Boltzmann velocity distribution*. This PDF is most significant as it defines the velocity distribution existing at thermodynamic equilibrium among the atoms or molecules of a perfect gas assembly.

In line with our previous deliberations, the velocity PDF for any single Cartesian direction can be constructed by integrating the differential probability, $f(\boldsymbol{V})\,dV_x\,dV_y\,dV_z$, over its remaining two components. For example, integrating over the y- and z-coordinates, we obtain for the x-direction

$$f(V_x)\,dV_x = \left(\frac{m}{2\pi kT}\right)^{3/2} \exp\left(-\frac{mV_x^2}{2kT}\right) dV_x \int_{-\infty}^{\infty}\int_{-\infty}^{\infty} \exp\left[-\frac{m\left(V_y^2 + V_z^2\right)}{2kT}\right] dV_y\,dV_z,$$

so that, upon evaluating the associated Gaussian integrals (Appendix B),

$$f(V_x)\,dV_x = \left(\frac{m}{2\pi kT}\right)^{1/2} \exp\left(-\frac{mV_x^2}{2kT}\right) dV_x. \tag{15.14}$$

Because the coordinate choice specified by Eq. (15.14) is surely arbitrary, the resulting Gaussian distribution holds for each Cartesian component. Moreover, because $f(\boldsymbol{V})$ depends solely on the magnitude of particle velocity, we have

$$f(\boldsymbol{V})\,dV_x\,dV_y\,dV_z = f(V_x)\,f(V_y)\,f(V_z)\,dV_x\,dV_y\,dV_z,$$

so that the particle velocity in any gaseous assembly contains no preferred direction. For this reason, the Maxwell–Boltzmann velocity distribution, $f(\boldsymbol{V})$, exhibits totally random particle behavior and is thus *isotropic*. Consequently, we would expect the mean velocity at a given temperature to be zero for any Cartesian direction; indeed, from Eq. (15.14),

$$\overline{V}_x = \int_{-\infty}^{\infty} V_x\,f(V_x)\,dV_x = \left(\frac{kT}{2\pi m}\right)^{1/2} \int_{\infty}^{\infty} \exp\left(-\frac{mV_x^2}{2kT}\right) d\left(\frac{mV_x^2}{2kT}\right) = 0.$$

In other words, particles are as likely to be moving in a positive as in a negative direction along any of the three Cartesian coordinates.

15.2 The Maxwell–Boltzmann Speed Distribution

While the Maxwell–Boltzmann velocity distribution accounts for both the speed and direction of assembly particles, we are often interested more in their speed than in their direction. For this purpose, it proves convenient to introduce spherical coordinates in *velocity space*, as illustrated by Fig. 15.1. In analogy with the usual spatial analysis, the conversion from

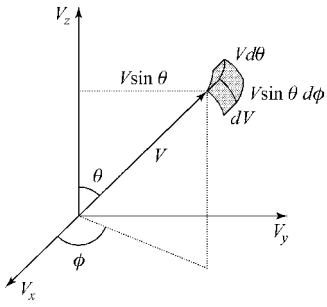

Figure 15.1 Spherical velocity space.

Cartesian to spherical coordinates can be accomplished by invoking the transformation

$$dV_x\, dV_y\, dV_z = (V d\theta)(V \sin\theta\, d\phi)(dV) = V^2 \sin\theta\, dV d\theta\, d\phi, \tag{15.15}$$

where V is the particle speed, θ is the zenith angle, and ϕ is the azimuthal angle in spherical velocity space. Following our previous development, the speed PDF can now be determined from the velocity PDF by converting to spherical velocity coordinates and then integrating over all possible solid angles. Converting first to spherical coordinates, we obtain, from Eq. (15.15),

$$f(\boldsymbol{V})\, dV_x\, dV_y\, dV_z = f(\boldsymbol{V})\, V^2 \sin\theta\, dV d\theta\, d\phi.$$

For an isotropic velocity distribution, $f(\boldsymbol{V})$ is unaffected by either θ or ϕ; thus, directly integrating over all zenith and azimuthal angles, we find that

$$f(V)\, dV = f(\boldsymbol{V})\, V^2 dV \int_0^{\pi} \sin\theta\, d\theta \int_0^{2\pi} d\phi = 4\pi V^2 f(\boldsymbol{V})\, dV, \tag{15.16}$$

where $f(V)$ represents the derived speed PDF.

From Eq. (15.16), we observe that the PDF for any isotropic velocity distribution can be converted to its corresponding speed PDF by employing

$$f(V) = 4\pi V^2 f(\boldsymbol{V}). \tag{15.17}$$

Hence, substituting from Eq. (15.13), we determine the PDF representing the *Maxwell–Boltzmann speed distribution* as

$$f(V) = \frac{4}{\sqrt{\pi}} \left(\frac{m}{2kT}\right)^{3/2} V^2 \exp\left(-\frac{mV^2}{2kT}\right). \tag{15.18}$$

On this basis, the most probable speed can be determined by implementing

$$\frac{df(V)}{dV} = 0,$$

from which we obtain

$$V_{mp} = \left(\frac{2kT}{m}\right)^{1/2}. \tag{15.19}$$

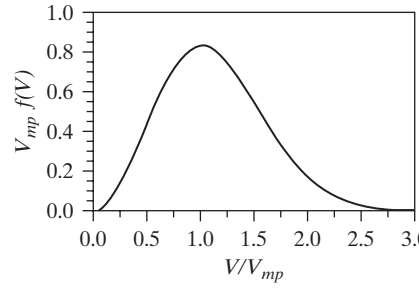

Figure 15.2 Maxwell–Boltzmann speed distribution.

Consequently, Eq. (15.18) can be reformulated as (Problem 7.3)

$$f(V) = \frac{4}{\sqrt{\pi} V_{mp}} \left(\frac{V}{V_{mp}}\right)^2 \exp\left[-\left(\frac{V}{V_{mp}}\right)^2\right], \tag{15.20}$$

which is clearly non-Gaussian compared to $f(V_x)$, as demonstrated by Fig. 15.2.

Given the speed PDF for a gaseous assembly, the mean for any function of particle speed, $G(V)$, can be determined by evaluating

$$\overline{G(V)} = \int_0^\infty G(V)\, f(V)\, dV.$$

Therefore, for $G(V) = V^n$, from Eq. (15.20) we obtain

$$\overline{V^n} = \frac{4}{\sqrt{\pi}} \left(\frac{2kT}{m}\right)^{n/2} \int_0^\infty \left(\frac{V}{V_{mp}}\right)^{n+2} \exp\left[-\left(\frac{V}{V_{mp}}\right)^2\right] d\left(\frac{V}{V_{mp}}\right). \tag{15.21}$$

Applying the Gaussian integrals of Appendix B, we thus find that the mean and root-mean-square speeds for a given assembly temperature become

$$\overline{V} = \left(\frac{8kT}{\pi m}\right)^{1/2} \tag{15.22}$$

$$V_{rms} = \sqrt{\overline{V^2}} = \left(\frac{3kT}{m}\right)^{1/2}. \tag{15.23}$$

Comparing Eqs. (15.19), (15.22), and (15.23), we see that, at translational equilibrium,

$$V_{rms} > \overline{V} > V_{mp},$$

which confirms the non-Gaussian nature of the speed PDF for Maxwell–Boltzmann statistics.

EXAMPLE 15.1

Gaseous nitrogen at thermodynamic equilibrium is contained in a vessel at 1 bar and 300 K.

(a) Determine the most probable mean and rms speeds for diatomic nitrogen at 1 bar and 300 K.

(b) Evaluate the speed of sound for gaseous nitrogen at these same conditions. Why should this speed be comparable to the various molecular speeds of part (a)?

Solution

(a) Employing Eqs. (15.19), (15.22), and (15.23), we find the requested particle speeds for nitrogen:

$$V_{mp} = \left(\frac{2kT}{m}\right)^{1/2} = \left[\frac{2(1.3807 \times 10^{-23}\,\text{kg} \cdot \text{m}^2/s^2 \cdot \text{K})(300\,\text{K})}{(28)(1.6605 \times 10^{-27}\,\text{kg})}\right]^{1/2} = 422\ \text{m/s}$$

$$\overline{V} = \left(\frac{8kT}{\pi m}\right)^{1/2} = \frac{2}{\sqrt{\pi}} V_{mp} = 476\ \text{m/s}$$

$$V_{rms} = \left(\frac{3kT}{m}\right)^{1/2} = \left(\frac{3}{2}\right)^{1/2} V_{mp} = 517\ \text{m/s}.$$

Would you have expected molecular speeds of such astounding magnitudes?

(b) The speed of sound for an ideal gas can be evaluated by applying classical thermodynamics to an isentropic process, for which $P \propto \rho^{\gamma}$ and $\gamma = c_p/c_v$. Hence, recognizing that

$$\rho = \frac{mP}{kT},$$

we obtain for this case

$$V_s = \left(\frac{\partial P}{\partial \rho}\right)_s^{1/2} = \left(\frac{\gamma kT}{m}\right)^{1/2}.$$

On this basis,

$$V_s = \left[\frac{1.4(1.3807 \times 10^{-23}\,\text{kg} \cdot \text{m}^2/\text{s}^2 \cdot \text{K})(300\,\text{K})}{(28)(1.6605 \times 10^{-27}\,\text{kg})}\right]^{1/2} = 353\ \text{m/s}.$$

The speed of sound is comparable to the various molecular speeds because sound must propagate via a kinetic mechanism. However, we also note that $V_{rms} > \overline{V} > V_{mp} > V_s$ so that some loss apparently occurs when random molecular motion converts to a spherically directional speed of sound.

15.3 The Maxwell–Boltzmann Energy Distribution

The Maxwell–Boltzmann speed distribution given by Eq. (15.18) can easily be converted to an associated energy distribution since translational energy and speed are related through

$$\varepsilon = \frac{1}{2}mV^2. \tag{15.24}$$

On this basis, the probability of a single particle having speed in the range V to $V + dV$ is equivalent to that having energy in the corresponding range ε to $\varepsilon + d\varepsilon$. Consequently, we recognize that $f(\varepsilon)\,d\varepsilon = f(V)\,dV$, so that, combining Eqs. (15.18) and (15.24), we obtain

$$f(\varepsilon)\,d\varepsilon = \frac{4}{\sqrt{\pi}}\left(\frac{m}{2kT}\right)^{3/2}\left(\frac{2\varepsilon}{m}\right)\exp\left(-\frac{\varepsilon}{kT}\right)\left(\frac{1}{2m\varepsilon}\right)^{1/2} d\varepsilon,$$

which for a given temperature becomes

$$f(\varepsilon)\,d\varepsilon = \frac{2}{\sqrt{\pi}}\left(\frac{\varepsilon}{kT}\right)^{1/2}\exp\left(-\frac{\varepsilon}{kT}\right)\,d\left(\frac{\varepsilon}{kT}\right). \tag{15.25}$$

Equation (15.25) can be interpreted as the probability that any single particle will have translational energy between ε and $\varepsilon + d\varepsilon$; thus, the particle fraction associated with any prescribed energy interval can be evaluated by appropriate integration. Equation (15.25) can also be derived by employing either the phase integral or the momentum distribution given by Eq. (15.11). Such strategies are explored via Problem 7.1. A more compelling option is to invoke the statistical chi-square distribution, as discussed in Appendix N.

Employing Eq. (15.25), we may now determine the mean translational energy, i.e.,

$$\overline{\varepsilon} = \int_0^\infty \varepsilon f(\varepsilon)\,d\varepsilon = \frac{2kT}{\sqrt{\pi}}\int_0^\infty \left(\frac{\varepsilon}{kT}\right)^{3/2}\exp\left(-\frac{\varepsilon}{kT}\right)d\left(\frac{\varepsilon}{kT}\right),$$

which becomes, upon substituting for $x^2 \equiv \varepsilon/kT$ and evaluating the appropriate Gaussian integral (Appendix B),

$$\overline{\varepsilon} = \frac{4kT}{\sqrt{\pi}}\int_0^\infty x^4 e^{-x^2}dx = \frac{4kT}{\sqrt{\pi}}\left(\frac{3\sqrt{\pi}}{8}\right) = \frac{3}{2}kT. \tag{15.26}$$

Equation (15.26) is identical to the mean translational energy obtained from either statistical thermodynamics or the equipartition principle of classical thermodynamics (Table 8.2). Alternatively, the mean energy could have been determined by combining Eqs. (15.23) and (15.24) so that

$$\bar{\varepsilon} = \frac{1}{2}m\overline{V^2} = \frac{1}{2}m\,V_{rms}^2 = \frac{1}{2}m\left(\frac{3kT}{m}\right) = \frac{3}{2}kT,$$

which again provides the expected translational energy per particle for a gaseous assembly.

15.4 Molecular Effusion

Experimental verification of the Maxwell–Boltzmann speed distribution requires that we sample molecular velocities. This can be done by permitting gas to escape from a vessel through a small orifice and into a vacuum, as shown schematically in Fig. 15.3. The vacuum is, of course, needed to avoid molecular collisions once the particles leave the hole. Similarly, the size of the orifice must be small enough to minimize collisions near its exit. If the hole is too large, the pressure drop in the vessel will be controlled not by kinetic theory but by continuum fluid mechanics. In general, this loss of gas through a sufficiently small orifice is called molecular *effusion*.

To analyze the effusion process, let us consider a small hole in the x–y plane of area dA, as illustrated in Fig. 15.4. We begin by assuming that a certain class of particles having speed V moves at angular direction (θ, ϕ) toward the orifice. We also assume that such particles have already experienced their last collision so that no further impacts occur in the differential time dt. As a result, all particles within the slanted cylinder shown in Fig. 15.4 must eventually undergo molecular effusion.

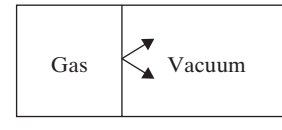

Figure 15.3 Effusion apparatus.

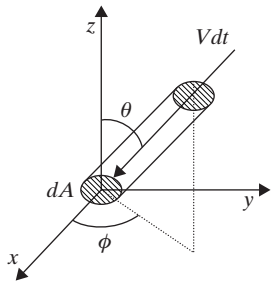

Figure 15.4 Spherical geometry for description of effusion process.

Now, the total number of particles within this slanted cylinder is given by

$$n\,(V\,dt)(dA\cos\theta),$$

where n is the particle density. Of these particles, the fraction having speed V and moving toward the hole at angular direction (θ, ϕ) can be represented within a Cartesian framework as

$$f(\boldsymbol{V})\,dV_x\,dV_y\,dV_z.$$

Therefore, the number of particles that will strike dA in time dt with speed V from angular direction (θ, ϕ) is

$$n(V\cos\theta\,dA\,dt)\,f(\boldsymbol{V})\,dV_x\,dV_y\,dV_z. \tag{15.27}$$

On this basis, the *flux of particles* (particles/$\mathrm{m}^2 \cdot \mathrm{s}$) with speed V approaching the hole from angular direction (θ, ϕ) must be

$$nV\cos\theta f(\boldsymbol{V})\,dV_x\,dV_y\,dV_z, \tag{15.28}$$

so that the *total flux* when integrated over all possible hemispherical directions (θ, ϕ) can be expressed as

$$J = n\iiint_{\cap} V\cos\theta f(\boldsymbol{V})\,dV_x\,dV_y\,dV_z. \tag{15.29}$$

From Eq. (15.15), Eq. (15.29) may be converted to spherical coordinates so that the total flux (particles/$\mathrm{m}^2 \cdot \mathrm{s}$) for any velocity PDF, $f(\boldsymbol{V})$, becomes

$$J = n\iiint_{\cap} V^3\sin\theta\cos\theta f(\boldsymbol{V})\,dV d\theta\,d\phi.$$

If, however, $f(\boldsymbol{V})$ is isotropic, we may substitute from Eq. (15.17) with subsequent integration over all (θ, ϕ) values defining a hemisphere, i.e.,

$$J = \frac{n}{4\pi}\int_0^{2\pi} d\phi \int_0^{\pi/2} \sin\theta\cos\theta\,d\theta \int_0^{\infty} Vf(V)\,dV. \tag{15.30}$$

Performing the indicated operations in Eq. (15.30), we obtain the total flux

$$J = \frac{n}{4}\int_0^{\infty} Vf(V)\,dV = \frac{n\overline{V}}{4} \tag{15.31}$$

for any isotropic velocity distribution. In particular, for the Maxwell–Boltzmann speed distribution, we have from Eq. (15.22)

$$J = n\left(\frac{kT}{2\pi m}\right)^{1/2}. \tag{15.32}$$

Hence, invoking the ideal gas law,

$$n = \frac{N}{V} = \frac{P}{kT}, \tag{15.33}$$

we obtain from Eq. (15.32)

$$J = \frac{P}{\sqrt{2\pi mkT}}, \tag{15.34}$$

so that the total effusive flux for an ideal gas can be determined by knowing only the pressure and temperature in the vessel. Significantly, Eq. (15.34) demonstrates that the total flux scales inversely with the square root of particle mass. Therefore, lighter particles will exit the vessel into a vacuum more quickly than heavier particles. This conclusion is the basis for several practical devices, including the time-of-flight mass spectrometer for sensitive chemical analyses and isotopic enrichment facilities for the nuclear industry. The former is especially relevant for pollutant concentration measurements in the parts-per-billion range.

EXAMPLE 15.2

Molecular effusion occurs into a well-established vacuum from a one-liter vessel at 300 K via a precision orifice having an area $A = 10^{-6}$ cm^2.

(a) Show that the loss of pressure, P, from the vessel as a function of time, t, is given by $P = P_\circ \exp(-t/\tau)$, where $P_\circ$ is the initial pressure and τ is a time constant for the process.

(b) Develop an expression for τ in terms of appropriate molecular parameters.

(c) If the pressure drops to 90% of its initial value in 3.08 hours, determine the molecular weight of the gas within the vessel.

Solution

(a) Beginning with the total flux, J, the particle loss rate from the vessel can be expressed as

$$\frac{dN}{dt} = -JA.$$

Invoking the ideal gas law at constant temperature, we obtain

$$\left(\frac{V}{kT}\right)\frac{dP}{dt} = -JA,$$

where V is the volume of the vessel. However, from Eqs. (15.31) and (15.33),

$$J = \frac{n\overline{V}}{4} = \frac{P\overline{V}}{4kT},$$

so that

$$\left(\frac{V}{kT}\right)\frac{dP}{dt} = -\left(\frac{\overline{V}A}{4kT}\right)P,$$

where V is the mean molecular speed. Therefore,

$$\frac{dP}{P} = -\frac{dt}{\tau},$$

where the time constant for the process becomes

$$\tau = \frac{4V}{\overline{V}A}.$$

For this first-order ordinary differential equation, the solution is clearly

$$\frac{P}{P_\circ} = \exp\left(-\frac{t}{\tau}\right),$$

where $P_\circ$ is the initial pressure within the vessel.

(b) Combining the derived expression for τ from part (a) with Eq. (15.22), we obtain

$$\tau = \frac{4V}{\overline{V}A} = \frac{4V}{A}\left(\frac{\pi m}{8kT}\right)^{1/2} = \left(\frac{2\pi m}{kT}\right)^{1/2}\frac{V}{A}.$$

(c) The time constant can be evaluated from the given conditions using the specified expression, i.e.,

$$\tau = -\frac{t}{\ln(P/P_\circ)} = \frac{3.08(3600)}{\ln(0.9)} = 1.05 \times 10^5 \text{ s}.$$

Solving for the molecular mass from part (b), we obtain

$$\begin{aligned} m &= \left(\frac{kT}{2\pi}\right)\left(\frac{\tau A}{V}\right)^2 \\ &= \left[\frac{(1.3807 \times 10^{-16} \text{ g} \cdot \text{cm}^2/\text{s}^2 \cdot \text{K})(300 \text{ K})}{2\pi}\right]\left[\frac{(1.05 \times 10^5 \text{ s})(10^{-6} \text{ cm}^2)}{1000 \text{ cm}^3}\right]^2 \\ &= 7.3 \times 10^{-23} \text{ g}. \end{aligned}$$

Hence, the molecular weight of the gas leaving the vessel is

$$M = \frac{7.3 \times 10^{-23} \text{ g}}{1.6605 \times 10^{-24} \text{ g/amu}} = 44 \text{ amu}.$$

15.5 The Ideal Gas Pressure

The procedures employed in Section 15.4 to determine the particle flux can also be used to develop expressions for the flux of momentum or energy. In particular, if we eliminate the orifice of Fig. 15.3, the exchange of momentum at the solid wall can be analyzed to produce an expression for the ideal gas pressure. We now undertake this analysis to demonstrate the utility of kinetic theory for calculating the flux of momentum. A similar analysis for determining the flux of energy, as generated during molecular effusion, is considered in Problem 7.5.

From Newton's law, the pressure created by particles moving with speed V from angular direction (θ, ϕ) can be expressed as

$$P(V, \theta, \phi) = \frac{\Delta G_{\perp}(V, \theta, \phi)}{dA\, dt}, \tag{15.35}$$

where $\Delta G_{\perp}(V, \theta, \phi)$ represents the exchange of momentum perpendicular to the differential area dA for particles affiliated with the independent variables (V, θ, ϕ). Now, the number of particles striking dA in time dt with speed V coming from angular direction (θ, ϕ) is given by Eq. (15.27). From conservation of momentum, the exchange of momentum perpendicular to the wall for such particles is $2mV\cos\theta$. Therefore, simple multiplication with Eq. (15.27) gives

$$\Delta G_{\perp} = 2mn\, V^2 \cos^2\theta\, dA\, dt\; f(\boldsymbol{V})\, dV_x\, dV_y\, dV_z. \tag{15.36}$$

Substituting Eq. (15.36) into Eq. (15.35) and integrating over a hemisphere, we obtain for the total pressure exerted by the gaseous assembly,

$$P = 2mn \iiint_{\Omega} V^2 \cos^2\theta\, f(\boldsymbol{V})\, dV_x\, dV_y\, dV_z. \tag{15.37}$$

Applying Eqs. (15.15) and (15.17), we next convert Eq. (15.37) to spherical coordinates while simultaneously invoking isotropic conditions, thus obtaining

$$P = \frac{mn}{2\pi} \int_0^{2\pi} d\phi \int_0^{\pi/2} \cos^2\theta \sin\theta d\theta \int_0^{\infty} V^2 f(V)\, dV. \tag{15.38}$$

Performing the indicated operations, Eq. (15.38) becomes

$$P = \frac{mn}{3} \int_0^{\infty} V^2 f(V)\, dV = \frac{1}{3} mn\overline{V^2}, \tag{15.39}$$

so that, from Eq. (15.23),

$$P = \frac{mn}{3}\left(\frac{3kT}{m}\right) = nkT, \tag{15.40}$$

which may also, of course, be written in the familiar form,

$$P = \frac{NkT}{V}.$$

Therefore, we find that the Maxwell–Boltzmann speed distribution leads to an ideal gas equation of state, as might be expected for translational equilibrium. Combining Eqs. (15.24) and (15.39), we also deduce that

$$P = \frac{mn}{3}\left(\frac{2\bar{\varepsilon}_{tr}}{m}\right) = \frac{2}{3}\frac{E_{tr}}{V}; \tag{15.41}$$

hence, as for the translational energy, the pressure is an additive property. In other words, Eq. (15.41) provides the theoretical framework for Dalton's law of partial pressures, as discussed previously in Section 10.2.

EXAMPLE 15.3

A pressure vessel contains particles with number density n and molecular mass m, which are characterized by the hypothetical speed distribution

$$f(V) = \frac{6V(V_m - V)}{V_m^3},$$

where V_m is the maximum particle speed.
(a) What is the mean speed for these particles?
(b) Determine the pressure in this vessel.

Solution

(a) The mean speed is given by

$$\overline{V} = \int_0^{V_m} V f(V)\, dV,$$

so that

$$\overline{V} = \frac{6}{V_m^3}\int_0^{V_m} V^2(V_m - V)\, dV = \frac{6}{V_m^3}\left(\frac{1}{3}V_m^4 - \frac{1}{4}V_m^4\right) = \frac{V_m}{2}.$$

(b) The given speed distribution is isotropic as its PDF is independent of both θ and ϕ. On this basis, from Eq. (15.39),

$$P = \frac{mn}{3}\int_0^{\infty} V^2 f(V)\, dV = \frac{2mn}{V_m^3}\int_0^{V_m} V^3(V_m - V)\, dV.$$

Therefore, the pressure within the vessel must be

$$P = \frac{2mn}{V_m^3}\left(\frac{1}{4}V_m^5 - \frac{1}{5}V_m^5\right) = \frac{2mn}{V_m^3}\left(\frac{V_m^5}{20}\right) = \frac{1}{10}mnV_m^2.$$

Problems enhancing your understanding of this chapter are combined with those for Chapters 16 and 17 in Problem Set VII.

16 Kinetics of Molecular Transport

Having assimilated equilibrium kinetic theory in Chapter 15, we may now apply basic kinetic notions to nonequilibrium processes. In this chapter, the nonequilibrium phenomena of interest include molecular transport of momentum, energy, and mass. We begin our investigation of such processes with binary collision theory, as elementary collision rates ultimately determine molecular transport in all laminar flows. Collision rates also limit the kinetics of bimolecular chemical reactions, as we shall see in Chapter 17.

16.1 Binary Collision Theory

The goal of binary collision theory is to determine the collision rate between two independent particles making up an ideal gas. As a first approximation, the particles can be treated as rigid spheres admitting no intermolecular potential. In other words, we assume that the atoms or molecules experience no attractive forces and that they undergo only elastic collisions. On this basis, we begin our analysis by considering dual particles having masses m_1 and m_2 with velocities $\boldsymbol{V}_1$ and $\boldsymbol{V}_2$, respectively. Transforming to center-of-mass (CM) and relative coordinates in velocity space, as portrayed in Fig. 16.1, we obtain

$$\boldsymbol{V}_c = \frac{m_1 \boldsymbol{V}_1 + m_2 \boldsymbol{V}_2}{m_1 + m_2} \tag{16.1}$$

$$\boldsymbol{V}_r = \boldsymbol{V}_1 - \boldsymbol{V}_2, \tag{16.2}$$

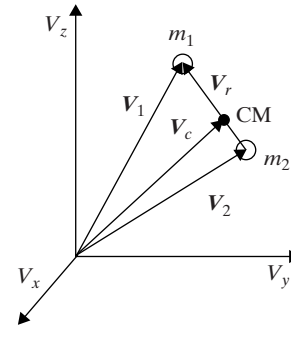

Figure 16.1 Velocity space for binary collisions.

where $\boldsymbol{V}_c$ is the velocity of the CM and $\boldsymbol{V}_r$ is the relative velocity between the two particles. We may now solve for $\boldsymbol{V}_1$ and $\boldsymbol{V}_2$ using Eqs. (16.1) and (16.2), thus realizing

$$\boldsymbol{V}_1 = \boldsymbol{V}_c + \left(\frac{m_2}{m_1 + m_2}\right)\boldsymbol{V}_r \tag{16.3}$$

$$\boldsymbol{V}_2 = \boldsymbol{V}_c - \left(\frac{m_1}{m_1 + m_2}\right)\boldsymbol{V}_r. \tag{16.4}$$

Squaring Eqs. (16.3) and (16.4), we may also express conservation of kinetic energy for this two-particle system as

$$\tfrac{1}{2}m_1 V_1^2 + \tfrac{1}{2}m_2 V_2^2 = \tfrac{1}{2}(m_1 + m_2)V_c^2 + \tfrac{1}{2}\mu V_r^2, \tag{16.5}$$

for which the *reduced mass* becomes

$$\mu = \frac{m_1 m_2}{m_1 + m_2}. \tag{16.6}$$

Because momentum is conserved for any system bearing no external forces, we find, from Eq. (16.1), that our two-particle system undergoes uniform rectilinear motion, so that its CM moves with constant velocity, $\boldsymbol{V}_c$. As a result, from Eq. (16.5), conservation of kinetic energy mandates that the relative speed, V_r, also remain invariant. Consequently, relative to its defined CM, the motion of two particles, m_1 and m_2, is in all respects equivalent to that of a single particle of mass μ moving with constant relative speed, V_r. Moreover, because $\boldsymbol{V}_1$ and $\boldsymbol{V}_2$ inherently conform to Maxwell–Boltzmann velocity distributions, we observe that $\boldsymbol{V}_c$ and $\boldsymbol{V}_r$ must also both be isotropic. For this reason, as we will see shortly, collision processes can generally be analyzed in terms of probability density functions based on speed rather than on velocity.

For analytical simplicity, let us fix our relative coordinate system on mass m_2 so that this particle is now at rest while mass m_1 moves with speed V_r, as shown in Fig. 16.2. From this perspective, a collision between m_1 and m_2 will always occur when m_1 appears inside the so-called sphere of influence of m_2, as constructed in Fig. 16.2 by placing a virtual image of m_1 tangent to m_2. The cross-sectional area of this sphere of influence is clearly $\pi\sigma_{12}^2$, where $\sigma_{12} = r_1 + r_2$ represents the average diameter for these two rigid-sphere particles. On this basis, as mass m_1 travels, it sweeps out a collision volume per unit time equal to $\pi\sigma_{12}^2 V_r$ relative to mass m_2. Therefore, by definition, particle m_1 must undergo collision with every random particle m_2 encountered within this delimited collision volume.

If dn_2 is the number density of particle type m_2 within the velocity class $\boldsymbol{V}_2$ to $\boldsymbol{V}_2 + d\boldsymbol{V}_2$, we then find that the collision rate (collisions/s) for one m_1 particle moving through a sea of m_2 particles within this velocity class is $\pi\sigma_{12}^2 V_r\, dn_2$. In a similar fashion, if dn_1 is the number density of particle type m_1 within the velocity class $\boldsymbol{V}_1$ to $\boldsymbol{V}_1 + d\boldsymbol{V}_1$, the total number of collisions per unit volume (collisions/cm$^3 \cdot$ s) between particles m_1 and m_2 within the

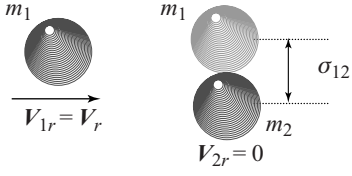

Figure 16.2 Sphere of influence for binary collisions.

velocity classes $\boldsymbol{V}_1$ to $\boldsymbol{V}_1 + d\boldsymbol{V}_1$ and $\boldsymbol{V}_2$ to $\boldsymbol{V}_2 + d\boldsymbol{V}_2$ must be

$$dZ_{12} = \pi \sigma_{12}^2 V_r \, dn_1 \, dn_2. \tag{16.7}$$

From Chapter 15, the number density dn_i for either particle, whether atom or molecule, within the velocity class $\boldsymbol{V}_i$ to $\boldsymbol{V}_i + d\boldsymbol{V}_i$ can be expressed as

$$dn_i = n_i \, f(\boldsymbol{V}_i) \, d\boldsymbol{V}_i, \tag{16.8}$$

where $f(\boldsymbol{V}_i)$ is the probability density function (PDF) representing a Maxwell–Boltzmann velocity distribution. Therefore, after substitution for dn_1 and dn_2 using Eq. (16.8), Eq. (16.7) becomes

$$dZ_{12} = \pi n_1 n_2 \sigma_{12}^2 V_r \, f(\boldsymbol{V}_1) \, f(\boldsymbol{V}_2) \, d\boldsymbol{V}_1 \, d\boldsymbol{V}_2. \tag{16.9}$$

Applying Maxwell–Boltzmann velocity PDFs from Eq. (15.13), we can subsequently express Eq. (16.9) as

$$dZ_{12} = \pi n_1 n_2 \sigma_{12}^2 \frac{(m_1 m_2)^{3/2}}{(2\pi kT)^3} V_r \exp\left[-\frac{m_1 V_1^2 + m_2 V_2^2}{2kT} \right] d\boldsymbol{V}_1 \, d\boldsymbol{V}_2. \tag{16.10}$$

The total collision rate per unit volume (collisions/cm$^3 \cdot$s) can be obtained from Eq. (16.10) by integrating over all possible collisions. However, to effect this integration, we must convert from the original ($\boldsymbol{V}_1$, $\boldsymbol{V}_2$) coordinate system to a comparable ($\boldsymbol{V}_r$, $\boldsymbol{V}_c$) coordinate system in velocity space. For the kth Cartesian component (x, y, or z), the procedure for effecting this transformation with respect to any function g requires

$$\iint g(V_{1k}, V_{2k}) \, dV_{1k} \, dV_{2k} = \iint g(V_{rk}, V_{ck}) \, |J_k| \, dV_{rk} \, dV_{ck}, \tag{16.11}$$

where the relevant Jacobian, as evaluated from Eqs. (16.3) and (16.4), becomes

$$J_k = \frac{\partial(V_{1k}, V_{2k})}{\partial(V_{rk}, V_{ck})} = \begin{vmatrix} \dfrac{\partial V_{1k}}{\partial V_{rk}} & \dfrac{\partial V_{1k}}{\partial V_{ck}} \\ \dfrac{\partial V_{2k}}{\partial V_{rk}} & \dfrac{\partial V_{2k}}{\partial V_{ck}} \end{vmatrix} = 1.$$

Therefore, if we apply Eq. (16.11) to Eq. (16.10) for all three Cartesian components, the complete coordinate transformation gives

$$dZ_{12} = \pi n_1 n_2 \sigma_{12}^2 \frac{(m_1 m_2)^{3/2}}{(2\pi kT)^3} V_r \exp\left[-\frac{(m_1 + m_2) V_c^2 + \mu V_r^2}{2kT} \right] d\boldsymbol{V}_r \, d\boldsymbol{V}_c, \tag{16.12}$$

where we have simultaneously invoked Eq. (16.5).

We now account for all possible collisions by integrating over the three spherical coordinates in velocity space (V, θ, ϕ) for both $\boldsymbol{V}_r$ and $\boldsymbol{V}_c$. Happily, for the Maxwell–Boltzmann velocity distribution, isotropic conditions prevail; moreover, because neither the zenith nor azimuthal angles appear in Eq. (16.12), we find, from Eq. (15.15) that, for either $\boldsymbol{V}_r$ or $\boldsymbol{V}_c$,

$$\int_0^{2\pi} \int_0^{\pi} V_i^2 dV_i \sin\theta d\theta d\phi = 4\pi V_i^2 dV_i. \tag{16.13}$$

Consequently, when integrating Eq. (16.12) over all six spherical coordinates, we simply apply Eq. (16.13) to $\boldsymbol{V}_r$ and $\boldsymbol{V}_c$, so that we are left with only two speed distributions

in CM and relative coordinates. The integrated result, after some algebraic manipulation, becomes

$$Z_{12} = \pi n_1 n_2 \sigma_{12}^2 \int_0^\infty \frac{4}{\sqrt{\pi}} \left(\frac{m_1 + m_2}{2kT}\right)^{3/2} V_c^2 \exp\left[-\frac{(m_1 + m_2)V_c^2}{2kT}\right] dV_c$$
$$\times \int_0^\infty \frac{4}{\sqrt{\pi}} \left(\frac{\mu}{2kT}\right)^{3/2} V_r^3 \exp\left[-\frac{\mu V_r^2}{2kT}\right] dV_r.$$

Recalling Eq. (15.18), we next recognize the resulting Maxwell–Boltzmann speed distributions with respect to both CM and relative coordinates, thus obtaining

$$Z_{12} = \pi n_1 n_2 \sigma_{12}^2 \int_0^\infty f(V_c)\, dV_c \int_0^\infty V_r f(V_r)\, dV_r. \tag{16.14}$$

For a properly normalized speed PDF, the first integration in Eq. (16.14) obviously gives unity. The resulting disappearance of CM coordinates might certainly have been anticipated as the volumetric collision rate only depends on the *relative* speed between particles. Indeed, from Eq. (16.14), our final result for the volumetric collision rate (collisions/cm$^3 \cdot$ s) is simply

$$Z_{12} = \pi n_1 n_2 \sigma_{12}^2 \overline{V}_r. \tag{16.15}$$

We previously found that, relative to the CM, the motion of any particle pair is equivalent to that for a single particle of reduced mass, μ, moving at relative speed, V_r. For such systems, the mean relative speed, from Eq. (15.22), can be expressed as

$$\overline{V}_r = \left(\frac{8kT}{\pi\mu}\right)^{1/2}. \tag{16.16}$$

Hence, from Eqs. (16.15) and (16.16), the binary collision rate per unit volume becomes

$$Z_{12} = 2 n_1 n_2 \sigma_{12}^2 \left(\frac{2\pi kT}{\mu}\right)^{1/2}, \tag{16.17}$$

so that Z_{12} depends on the reduced mass rather than on either m_1 or m_2 directly, as expected for binary motion within a relative coordinate system. For a pure gas, on the other hand, each collision within the context of Eq. (16.17) has been counted twice. Moreover, we notice from Eq. (16.6) that the reduced mass $\mu = m/2$; thus, the volumetric collision rate (collisions/cm$^3 \cdot$ s) for a pure gas takes on the simplified form,

$$Z = 2 n^2 \sigma^2 \left(\frac{\pi kT}{m}\right)^{1/2}. \tag{16.18}$$

EXAMPLE 16.1

A vessel containing gaseous argon is maintained at 300 K and 1 atm. Presuming a hard-sphere diameter of 3.42 Å, calculate the volumetric collision rate between argon atoms within the vessel. Discuss the implications of your result.

Solution

From Appendices A and C, the mass of an argon atom is

$$m = (39.948)(1.6605 \times 10^{-24}\ \text{g}) = 6.63 \times 10^{-23}\ \text{g},$$

while its hard-sphere diameter is given as

$$\sigma = 3.42 \times 10^{-8}\ \text{cm}.$$

From Eq. (15.33), the number density within the vessel is

$$n = \frac{P}{kT} = \frac{(1.013 \times 10^{6}\ \text{erg/cm}^3)}{(1.3807 \times 10^{-16}\ \text{erg/K})(300\ \text{K})} = 2.45 \times 10^{19}\ \text{cm}^{-3}.$$

Substituting into Eq. (16.18),

$$Z = 2n^2\sigma^2\left(\frac{\pi kT}{m}\right)^{1/2};$$

we find that the volumetric collision rate becomes

$$Z = 2(2.45 \times 10^{19}\ \text{cm}^{-3})^2(3.42 \times 10^{-8}\ \text{cm})^2\left[\frac{\pi(300)(1.38 \times 10^{-16}\ \text{g} \cdot \text{cm}^2/\text{s}^2)}{(6.63 \times 10^{-23}\ \text{g})}\right]^{1/2}$$
$$= 6.22 \times 10^{28}\ \text{collisions/cm}^3 \cdot \text{s}.$$

In other words, we have determined that, at room temperature and pressure, over 10^{28} collisions occur between argon atoms every second in a volume of only one cubic centimeter. This unfathomable number still represents over 10^{16} collisions per picosecond! Obviously, a binary collision rate of this magnitude will be very effective in maintaining local thermodynamic equilibrium.

16.2 Fundamentals of Molecular Transport

Having considered binary collision theory, we are now ready to formulate a basic framework for the molecular transport of momentum, energy, or mass. The similarity among these three classical transport mechanisms arises from their common underlying connection to binary collision theory. Preparatory to our central development, we first introduce the concept of a mean free path, which describes in a straightforward fashion the mean distance traveled by any given particle between collisions. Specifying this distance will prove to be crucial in developing a fundamental theory for all transport phenomena.

16.2.1 The Mean Free Path

Given the volumetric collision rate for an ideal gas assembly from Eq. (16.15), the total number of collisions per unit time experienced by a single particle of mass m_1 must be

$$Z_{12}^{*} = \frac{Z_{12}}{n_1} = \pi n_2 \sigma_{12}^2 \overline{V}_r. \tag{16.19}$$

Defining the *mean free path* as the average distance, ℓ_{12}, traveled by particle m_1 between collisions with particle m_2, we observe that $\ell_{12}/\overline{V}_1$ must similarly represent a mean time

between collisions for m_1. Because this mean time is just the reciprocal of Z_{12}^*, the mean free path for particle m_1 can thus be expressed as

$$\ell_{12} = \frac{\overline{V}_1}{Z_{12}^*} = \frac{1}{\pi n_2 \sigma_{12}^2}\left(\frac{\overline{V}_1}{\overline{V}_r}\right) = \left(\frac{m_2}{m_1 + m_2}\right)^{1/2} \frac{1}{\pi n_2 \sigma_{12}^2}, \tag{16.20}$$

where $\overline{V}_1$ is the mean speed of particle m_1.

Combining Eqs. (16.16) and (16.19), the collision rate (collisions/s) for a pure gas becomes

$$Z^* = \frac{2Z}{n} = 4n\sigma^2\left(\frac{\pi kT}{m}\right)^{1/2}, \tag{16.21}$$

as verified by Eq. (16.18). Similarly, for a pure gas, the mean free path can be expressed as

$$\ell = \frac{\overline{V}}{Z^*} = \frac{1}{\sqrt{2}\pi n\sigma^2}. \tag{16.22}$$

Substituting from Eq. (15.33) for the number density in Eq. (16.22), we obtain finally

$$\ell = \frac{kT}{\sqrt{2}\pi\sigma^2 P}, \tag{16.23}$$

so that, as expected, lower pressures and higher temperatures imply a greater mean free path based on a larger average distance between atoms or molecules in a gaseous assembly.

If we now consider continuum flow through a typical nozzle, we expect $\sigma \ll \ell \ll d$, where d represents the throat diameter for the nozzle. Hence, in this case, we presume that the so-called Knudsen number is

$$Kn = \frac{\ell}{d} < 0.1.$$

If, on the other hand,

$$Kn = \frac{\ell}{d} > 10, \tag{16.24}$$

we would anticipate much fewer collisions near the orifice, as required for molecular effusion. Therefore, $Kn > 10$ constitutes a suitable criterion distinguishing molecular from continuum flow.

EXAMPLE 16.2

A vessel contains gaseous argon at 300 K and 1 atm.

(a) Calculate the collision rate (collisions/s) for a typical argon atom within the vessel.
(b) Determine the mean free path for argon in this vessel.

Solution

(a) Employing Eq. (16.21), we can determine the collision rate for any labeled argon atom by using appropriate parameters available from Example 16.1. Hence, from

$$Z^* = 4n\sigma^2\left(\frac{\pi kT}{m}\right)^{1/2}$$

we obtain

$$Z^* = 4(2.45 \times 10^{19}\ \text{cm}^{-3})(3.42 \times 10^{-8}\ \text{cm})^2 \times \left[\frac{\pi(300)(1.38 \times 10^{-16}\ \text{g} \cdot \text{cm}^2/\text{s}^2)}{(6.63 \times 10^{-23}\ \text{g})}\right]^{1/2} = 5.08 \times 10^9\ \text{collisions/s}.$$

(b) The mean free path can be obtained from Eq. (16.22). Using parameters previously calculated in Example 16.1, we find that

$$\ell = \frac{1}{\sqrt{2}\pi n\sigma^2} = \frac{1}{\sqrt{2}\pi(2.45 \times 10^{19}\ \text{cm}^{-3})(3.42 \times 10^{-8}\ \text{cm})^2} = 7.85 \times 10^{-6}\ \text{cm}.$$

We note again the huge collision rate experienced by any single argon atom, approximately five collisions per nanosecond. For these typical conditions, the mean free path is remarkably only about 100 times greater than the size of the atom itself.

16.2.2 The Molecular Flux

The similarity among macroscopic expressions for transfer of momentum, energy, and mass in laminar flows suggests a common molecular mechanism for all transport phenomena. Table 16.1 lists macroscopic equations defining Newton's, Fourier's, and Fick's laws, including their respective transported microscopic properties. In each case, the flux of a microscopic property (momentum, energy, or mass), expressed in generic SI units as property/$\text{m}^2 \cdot \text{s}$, is linearly related to the first derivative of this property, as ultimately connected to the bulk flow velocity, U_y, the temperature, T, or the mass fraction of the ith species, Y_i. Considering Newton's law, for example, we note that the momentum flux is related to a spatial gradient in bulk velocity through the dynamic viscosity, η ($\text{N} \cdot \text{s/m}^2$). Similarly, for Fourier's law, the heat flux is associated with a spatial gradient in temperature through the thermal conductivity, λ ($\text{W/m} \cdot \text{K}$). Finally, for Fick's law, the mass flux per unit density, ρ (kg/m^3), is related to a spatial gradient in mass fraction through a diffusion coefficient, D (m^2/s).

In general, each transported microscopic property in Table 16.1 identifies a characteristic physical entity per particle. For simplicity in our initial development, we take these physical entities as those for *pure monatomic gases*. Therefore, only the translational energy

Table 16.1 *Common features among transport processes for momentum, energy, and mass*

Transport quantity	Macroscopic flux	Microscopic property
Momentum	$\tau_{yz} = -\eta\dfrac{\partial U_y}{\partial z}$	mU_y
Energy	$q_z = -\lambda\dfrac{\partial T}{\partial z}$	$\overline{\varepsilon}_{tr}$
Mass	$J_{zi} = -\rho D\dfrac{\partial Y_i}{\partial z}$	$Y_i m$

mode is represented in Table 16.1. In a similar vein, the diffusion coefficient is in reality a self-diffusion coefficient, so that Y_i represents the mass fraction of virtually tagged particles in the flow. As you might anticipate, our results will be generalized later in this chapter; hence, we will eventually consider transport properties for polyatomic gases as well as for binary gaseous mixtures.

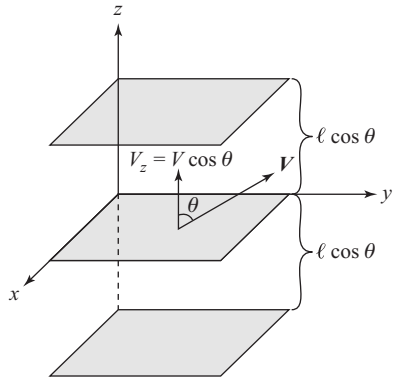

Figure 16.3 Planes marking sequential collisions during transport processes.

At this stage, however, we may proceed by performing a perturbation analysis for molecular transport in the z-direction of a typical microscopic property, $P(z)$. For this purpose, we consider a baseline x–y plane at $z = 0$, with two additional x–y planes approximately one mean free path above and below that at $z = 0$. Hence, as defined in Fig. 16.3, each plane represents an x–y surface at which we anticipate the next collision. From the perspective of molecular transport, any flux in the z-direction depends solely on the molecular speed in that direction, which can be represented by $V_z = V\cos\theta$. Furthermore, because $\overline{V}_z = 0$, the mean particle flow through any x–y plane has to be zero under steady-state conditions. Therefore, as might have been expected from the macroscopic equations of Table 16.1, we conclude that net transport of $P(z)$ in the z-direction is only possible if a gradient exists in $P(z)$ itself!

Continuing with our perturbation analysis, we note that Fig. 16.3 portrays a particle with velocity, $\boldsymbol{V}$, which travels an average distance, ℓ, between collisions. For this reason, the three x–y planes marking sequential collisions in the z-direction must be separated from one another by a mean distance, $\ell\cos\theta$. Given any monatomic gas, we presume that previous collisions have ensured local thermodynamic equilibrium, so that we can define all microscopic properties. On this basis, we may apply a Taylor expansion to the microscopic property, $P(z)$, thus obtaining

$$P(z) = P(0) - \ell\cos\theta\frac{dP}{dz}, \tag{16.25}$$

where $0 \le \theta \le \pi/2$ and $\pi/2 \le \theta \le \pi$ designate identifiable conditions for which the last collision before passage through the baseline plane occurred either below or above this plane, respectively. Hence, from Eq. (16.25), if $dP/dz > 0$, any previous collision from above ($\cos\theta < 0$) must transfer property $P(z > 0) > P(0)$, so that its flux reduces the initial gradient in $P(z)$. In a similar fashion, if $dP/dz < 0$, any previous collision from below ($\cos\theta > 0$) transports $P(z < 0) > P(0)$, so that its flux again reduces the initial gradient in $P(z)$. Consequently, we confirm that the negative sign in Eq. (16.25) establishes a flux in $P(z)$ which always occurs in a direction opposite to its gradient, thus ensuring the proper dissipation of all such gradients during equilibration processes.

We next recognize that the particle flux (particles/m$^2 \cdot$ s) crossing the x–y plane at $z = 0$ can be represented by nV_z, where n is the local number density (particles/m^3) and V_z is the particle speed in the z-direction (m/s). From this perspective, the flux of particles crossing the baseline plane with particle velocities from $\boldsymbol{V}$ to $\boldsymbol{V} + d\boldsymbol{V}$ must be $nV_z f(\boldsymbol{V})\, dV_x\, dV_y\, dV_z$. Therefore, multiplying this differential particle flux by $P(z)$ and integrating over all

possible velocities, the net flux for any microscopic property, $P(z)$, in the z-direction can be expressed as

$$F(z) = n \iiint P(z) V_z f(\boldsymbol{V})\, dV_x\, dV_y\, dV_z. \tag{16.26}$$

Substituting for $P(z)$ from Eq. (16.25), Eq. (16.26) can be converted to

$$F(z) = nP(0) \iiint V_z f(\boldsymbol{V})\, dV_x\, dV_y\, dV_z - n\ell \frac{dP}{dz} \iiint V cos^2\theta f(\boldsymbol{V})\, dV_x\, dV_y\, dV_z, \tag{16.27}$$

as the specified property gradient at $z = 0$ is inherently independent of velocity space.

Because the integral dominating the first term of Eq. (16.27) represents $\overline{V}_z$, this entire term is obviously zero. Having implemented $V_z = V\cos\theta$ in the second term, we may invoke the usual isotropic velocity distribution, thus obtaining from Eqs. (15.15) and (15.17)

$$f(\boldsymbol{V})\, dV_x\, dV_y\, dV_z = \frac{1}{4\pi} f(V) \sin\theta\, dV d\theta\, d\phi, \tag{16.28}$$

so that, from Eq. (16.27),

$$F(z) = -\frac{n\ell}{4\pi} \frac{dP}{dz} \int_0^{2\pi} d\phi \int_0^{\pi} \cos^2\theta \sin\theta\, d\theta \int_0^{\infty} V f(V)\, dV. \tag{16.29}$$

Finally, performing the requisite integrations established for Eq. (16.29), the total property flux in the z-direction becomes

$$F(z) = -\frac{1}{3} n\ell \overline{V} \frac{dP}{dz}, \tag{16.30}$$

which clearly holds for any microscopic property, $P(z)$, regardless of whether that property describes the molecular transport of momentum, energy, or mass.

16.2.3 Transport Properties

Having developed a general expression for the macroscopic flux associated with any microscopic property, we may now formulate statistical relations for the various transport properties by comparing Eq. (16.30) to each flux equation in Table 16.1. Beginning with the flux in momentum, for which the relevant microscopic property $P(z) = mU_y$, we obtain

$$\tau_{yz} = -\eta \frac{\partial U_y}{\partial z} = -\frac{1}{3} n\ell \overline{V} \frac{\partial}{\partial z} (mU_y).$$

As a result, the dynamic viscosity can be expressed quite simply as

$$\eta = \frac{1}{3} nm\ell \overline{V}; \tag{16.31}$$

hence, η can be evaluated directly from well-established molecular parameters, such as the mean free path, ℓ, and the mean speed, $\overline{V}$.

In a similar fashion, for the energy flux, the microscopic property of interest is $P(z) = \bar{\varepsilon}_{tr}$, so that

$$q_z = -\lambda \frac{\partial T}{\partial z} = -\frac{1}{3} n \ell \overline{V} \frac{\partial}{\partial z} (\bar{\varepsilon}_{tr}) .$$

Furthermore, for a monatomic gas,

$$\bar{\varepsilon}_{tr} = \frac{3}{2} kT = \left(\frac{c_v}{N_A} \right) T,$$

where $c_v = 3R/2$ is the molar heat capacity provided by the translational energy mode and N_A is Avagadro's number. On this basis, the thermal conductivity becomes

$$\lambda = \frac{1}{3} \left(\frac{n c_v}{N_A} \right) \ell \overline{V}; \tag{16.32}$$

we recognize, however, that the specific heat in Eq. (16.32) requires modification for polyatomic gases, as discussed later in Section 16.3.1.

Finally, for the mass flux, the relevant microscopic property $P(z) = Y_i m$, so that from Eq. (16.30)

$$J_{zi} = -\rho D \frac{\partial Y_i}{\partial z} = -\frac{1}{3} n \ell \overline{V} \frac{\partial}{\partial z} (Y_i m).$$

Because the gravimetric density is

$$\rho = \frac{mP}{kT} = mn, \tag{16.33}$$

we find that the self-diffusion coefficient can be expressed very simply as

$$D = \frac{1}{3} \ell \overline{V}. \tag{16.34}$$

Therefore, in comparison to the dynamic viscosity and thermal conductivity, the diffusion coefficient can be related solely to the mean free path and mean molecular speed. Perhaps more poetically, considering our rather intricate exposition of transport theory, we might certainly be forgiven for momentarily waxing eloquent regarding the delightful austerity of Eq. (16.34)!

In general, Eqs. (16.31), (16.32), and (16.34) offer a common microscopic interpretation of macroscopic transport properties based on fundamental collision theory. If we substitute for the mean speed from Eq. (15.22), the mean free path from Eq. (16.23), and the particle density from Eq. (16.33), these three equations can be cast in the analogous formulations

$$\eta = \frac{2\sqrt{mkT}}{3\pi^{3/2}\sigma^2} \tag{16.35}$$

$$\lambda = \frac{2\sqrt{mkT}}{3\pi^{3/2}\sigma^2} \left(\frac{c_v}{M} \right) \tag{16.36}$$

$$D = \frac{2\sqrt{mkT}}{3\pi^{3/2}\sigma^2 \rho}, \tag{16.37}$$

where M represents the molecular weight for the chosen monatomic gas. We note from Eqs. (16.35–16.37) that the dynamic viscosity and thermal conductivity are independent of

pressure, whereas the self-diffusion coefficient is inversely proportional to pressure. Moreover, whereas η and λ depend on temperature as $T^{1/2}$, the diffusion coefficient depends more acutely on temperature as $T^{3/2}$.

EXAMPLE 16.3

Employing basic transport theory, determine the following transport properties for gaseous argon: (a) its dynamic viscosity at 300 K, (b) its thermal conductivity at 300 K, and (c) its self-diffusion coefficient at 300 K and 1 atm.

Solution

(a) From Eq. (15.22), the mean particle speed for argon at 300 K is

$$\overline{V} = \left(\frac{8kT}{\pi m}\right)^{1/2} = \left[\frac{8(1.3807 \times 10^{-23}\,\text{kg} \cdot \text{m}^2/\text{s}^2 \cdot \text{K})(300\,\text{K})}{\pi(39.948)(1.6605 \times 10^{-27}\,\text{kg})}\right]^{1/2} = 398.8\ \text{m/s}.$$

Hence, from Eq. (16.31) and previously calculated parameters taken from Examples 16.1 and 16.2, we find that the dynamic viscosity becomes

$$\begin{aligned}\eta &= \frac{1}{3}nm\ell\overline{V} \\ &= \frac{1}{3}(2.45 \times 10^{25}\ \text{m}^{-3})(6.63 \times 10^{-26}\ \text{kg})(7.85 \times 10^{-8}\ \text{m})(398.8\text{m/s}) \\ &= 1.70 \times 10^{-5}\ \text{kg/m} \cdot \text{s},\end{aligned}$$

which is equivalent to $1.70 \times 10^{-5}\ \text{N} \cdot \text{s/m}^2$.

(b) From Eqs. (16.31) and (16.32), the thermal conductivity for argon at 300 K is

$$\begin{aligned}\lambda &= \left(\frac{c_v}{M}\right)\eta = \frac{3}{2}\left(\frac{R}{M}\right)\eta \\ &= \frac{3}{2}\left(\frac{8.3145 \times 10^3\ \text{J/K} \cdot \text{kmol}}{39.948\ \text{kg/kmol}}\right)(1.70 \times 10^{-5}\ \text{kg/m} \cdot \text{s}) \\ &= 5.31 \times 10^{-3}\ \text{W/m} \cdot \text{K}.\end{aligned}$$

(c) From Eq. (16.34), the self-diffusion coefficient for argon at 300 K and 1 atm becomes

$$D = \frac{1}{3}\ell\overline{V} = \frac{1}{3}(7.85 \times 10^{-8}\ \text{m})(398.8\ \text{m/s}) = 1.04 \times 10^{-5}\ \text{m}^2/\text{s}\,.$$

16.3 Rigorous Transport Theory

Our derivation of microscopic relations for transport properties, as explicated in Section 16.2, is both physically correct and mathematically consistent, but not fully rigorous. The rigorous procedure requires the so-called *Chapman–Enskog solution* to the *Boltzmann equation*, the latter constituting, in essence, an equation of motion for the general PDF, $f(\boldsymbol{V}, \boldsymbol{r}, t)$. This very ponderous and mathematically cumbersome procedure is necessary not only for a more realistic consideration of intermolecular forces but also for a more accurate development of the classic hard-sphere solution (Hirschfelder *et al.*,

Table 16.2 *Comparison between basic and rigorous solutions for transport properties*

Transport property	Approximate rigid sphere model	Rigorous rigid sphere model	Rigorous intermolecular potential model
$\dfrac{\eta\sqrt{\pi}\sigma^2}{(mkT)^{1/2}}$	$\dfrac{2}{3\pi}$	$\dfrac{5}{16}$	$\dfrac{5}{16\Omega^{(2,2)^*}}$
$\dfrac{\lambda\sqrt{\pi}\sigma^2}{(mkT)^{1/2}}\left(\dfrac{M}{c_v}\right)$	$\dfrac{2}{3\pi}$	$\dfrac{25}{32}$	$\dfrac{25}{32\Omega^{(2,2)^*}}$
$\dfrac{D\sqrt{\pi}\sigma^2\rho}{(mkT)^{1/2}}$	$\dfrac{2}{3\pi}$	$\dfrac{3}{8}$	$\dfrac{3}{8\Omega^{(1,1)^*}}$

1967). Fortunately, in both cases, such plausible elaborations merely end up multiplying our previous results by an additional factor of order unity. Considering that these rigorous solutions offer serious mathematical challenges with few attendant rewards in terms of further physical insights, we elect to simply tabulate the final Chapman–Enskog results in Table 16.2. Note that the rigorous rigid-sphere model merely replaces the universal factor of $2/3\pi$ from Section 16.2.3 with three new factors that now differ among the various transport properties. The additional functional forms, $\Omega^{(1,1)^*}$ and $\Omega^{(2,2)^*}$, constitute *collision integrals*, which represent more sophisticated corrections arising from the inclusion of an intermolecular potential, as discussed in Section 16.3.2.

16.3.1 Dimensionless Transport Parameters

Dimensionless parameters relating various transport properties can be readily obtained from Table 16.2. We begin by recognizing that, for either the rigorous rigid-sphere or intermolecular potential model, thermal conductivity can be related to dynamic viscosity via

$$\lambda = \frac{5}{2}\left(\frac{c_v}{M}\right)\eta. \tag{16.38}$$

While fully appropriate for monatomic gases, Eq. (16.38) proves to be unsuitable for polyatomic species owing to the opportunity for additional energy storage within rotational and vibrational energy modes. For such gases, the thermal conductivity can be evaluated quite satisfactorily using the so-called Eucken correction (Problem 7.10),

$$\lambda = \frac{1}{4}(9\gamma - 5)\tilde{c}_v\eta, \tag{16.39}$$

where $\gamma = \tilde{c}_p/\tilde{c}_v$ is the ratio of gravimetric specific heats, the latter given by $\tilde{c}_p = c_p/M$ and $\tilde{c}_v = c_v/M$ at constant pressure and volume, respectively (J/kg · K).

Employing the Eucken correction, we may now define characteristic dimensionless parameters traditionally employed for scaling transport phenomena in fluid mechanics, heat transfer, and mass transfer. As an example, for the rigorous rigid-sphere model, the

Table 16.3 *Transport parameters for air at 300 K*

Parameter	Model	Experiment
Pr	0.737	0.707
Sc	0.833	0.883
Le	1.13	1.25

Prandtl, Schmidt, and Lewis numbers become

$$Pr = \frac{\tilde{c}_p \eta}{\lambda} = \frac{4\gamma}{(9\gamma - 5)} \tag{16.40}$$

$$Sc = \frac{\eta}{\rho D} = \frac{5}{6} \tag{16.41}$$

$$Le = \frac{\lambda}{\rho \tilde{c}_p D} = \frac{5}{24\gamma}(9\gamma - 5). \tag{16.42}$$

On this basis, we may calculate approximate values of *Pr*, *Sc* and *Le* for air at 300 K by simply invoking $\gamma \simeq 1.4$ in Eqs. (16.40), (16.41), and (16.42), respectively. The resulting predictions are shown in Table 16.3, along with corresponding experimental values. Despite the rather bold approximations, the comparisons are quite reasonable, especially as we have not yet accounted for the influence of attractive forces during molecular collisions.

16.3.2 Collision Integrals

Considering the simplicity of a rigid-sphere model, the utility of our previous results for transport properties has been nothing short of remarkable. However, if we are to make further progress, we must clearly account for the existence of intermolecular potentials. Such potentials should incorporate both attractive forces between molecules at long range and repulsive forces between these same molecules at short range. Unfortunately, while engendering greater reality, an attractive potential makes the mean free path ill defined in any practical scenario. On the other hand, accounting for both attractive and repulsive forces ultimately creates an opportunity for improved predictions of transport properties. Similar considerations will pave the path for our eventual study of nonideal gases in Chapter 19.

In general, an intermolecular potential describing the interaction between two particles depends not only on their separation distance but also on their relative orientation. The latter is especially significant for molecules with permanent dipole moments. Nevertheless, we presume for convenience an intermolecular potential, $\phi(r)$, that depends only on the distance, r, separating the two particles. For such systems, the resulting particle trajectory can be completely described by utilizing a relative coordinate system, as shown in Fig. 16.4.

From our previous discussion in Section 16.1, conservation of momentum indicates that the relative speed, V_r, must be the same sufficiently before and after impact for this two-body problem. Employing polar coordinates, we define the impact parameter, b, as the distance of closest approach, presuming no intermolecular potential, while χ represents the angle of deflection caused by interaction between the particles. In general, the typical

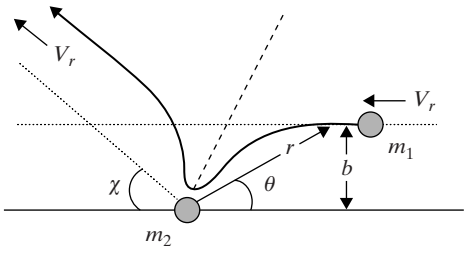

Figure 16.4 Particle trajectory in impact region for intermolecular potential $\phi(r)$.

trajectory shown in Fig. 16.4 implies that we are seeking the distance, r, and the angle, θ, as functions of time. This goal can be achieved by implementing both conservation of energy and conservation of angular momentum, as described by

$$\tfrac{1}{2}\mu V_r^2 = \tfrac{1}{2}\mu(\dot{r}^2 + r^2\dot{\theta}^2) + \phi(r) \tag{16.43}$$

$$\mu b V_r = \mu r^2 \dot{\theta}, \tag{16.44}$$

where μ is the reduced mass. These fundamental equations confirm that the intermolecular potential plays its most significant role during an inelastic collision and that $\phi(r)$ is quite irrelevant far from the impact region. Indeed, for the rigorous rigid-sphere model, $\phi(r) = 0$.

If we now combine Eqs. (16.43) and (16.44), we obtain

$$\dot{r}^2 + V_r^2\left(\frac{b}{r}\right)^2 + \frac{2\phi(r)}{\mu} = V_r^2. \tag{16.45}$$

Given V_r, $\phi(r)$, μ, and b as input parameters, Eqs. (16.44) and (16.45) can be sequentially solved at a given temperature to determine r and θ as functions of time. From this solution, we may determine the angle of deflection, χ, at a given temperature, which proves to be expressible in the functional form, $\chi(\alpha, \phi, b)$, where

$$\alpha = \left(\frac{\mu}{2kT}\right)^{1/2} V_r.$$

From the Chapman–Enskog solution, we may then obtain appropriate collision integrals defined as

$$\Omega^{(l,s)} = \left(\frac{2\pi kT}{\mu}\right)^{1/2} \int_0^\infty \int_0^\infty e^{-\alpha^2} e^{2s+3}(1 - \cos^l \chi) b\, db\, d\alpha. \tag{16.46}$$

In essence, Eq. (16.46) implies that by integrating over all α and b, we may account for all possible impact scenarios for a given intermolecular potential. According to Table 16.2, reliable collision integrals defined by Eq. (16.46) comprise key factors when correcting rigorous rigid-sphere results, thus permitting more accurate predictions of transport properties. In anticipation of such improvements, we now turn to our final missing ingredient, i.e., a sufficiently complete and reliable model for the intermolecular potential.

16.3.3 The Lennard–Jones Potential

A numerical solution to Eq. (16.46) obviously requires a model for the intermolecular potential, $\phi(r)$. To avoid unwarranted complications, it proves useful to restrict our choice to those models established for no more than two independent parameters. Among such

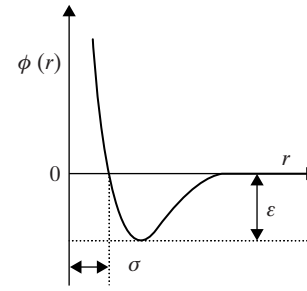

Figure 16.5 Lennard–Jones 6–12 potential with force constants.

models, substantial investigations have demonstrated that by far the best is the Lennard–Jones 6–12 potential, as defined by

$$\phi(r) = 4\varepsilon \left\{ \left(\frac{\sigma}{r}\right)^{12} - \left(\frac{\sigma}{r}\right)^{6} \right\}, \tag{16.47}$$

where Fig. 16.5 identifies the two associated Lennard–Jones parameters, ε and σ. In essence, ε indicates the energy at the bottom of the potential well that accounts for molecular attraction, while σ establishes the particle radius that provides a barrier for molecular repulsion. Although the sixth-order attraction term in Eq. (16.47) can be derived based on quadrupole–quadrupole interactions, the twelfth-order term is less crucial and has been chosen merely to ensure sufficiently robust repulsion. Nevertheless, the Lennard–Jones potential is quite realistic, even furnishing a practical entrée to real gas behavior, as discussed later in Chapter 19.

When implementing the Lennard–Jones (L–J) potential, the calculation of collision integrals using Eq. (16.46) can be facilitated by defining a dimensionless or reduced temperature,

$$T^* = \frac{kT}{\varepsilon}. \tag{16.48}$$

On this basis, the L–J force constants are generally tabulated as ε/k (K) and σ (Å). Parameter values can be established for any gas by least-squares fitting L–J predictions to either viscosity or second virial coefficient data near room temperature. L–J parameters derived in this manner are provided for some common gases in Appendix O. Given these L–J force constants, transport properties can be evaluated at substantially higher or lower temperatures for which transport data are generally unavailable. Such calculations no doubt constitute the most practical application of transport theory based on the L–J 6–12 intermolecular potential.

If we implement the dimensionless temperature of Eq. (16.48), reduced collision integrals can also be established, as defined by

$$\Omega^{(l,s)*}(T^*) = \frac{\Omega^{(l,s)}}{\Omega^{(l,s)}_{RS}}, \tag{16.49}$$

where the denominator of Eq. (16.49) represents normalization based on the rigorous rigid-sphere model. Because of this normalization, reduced collision integrals for the latter case are by definition unity, as indicated in Table 16.2. On the other hand, for more accurate calculations of transport properties, we require evaluations of both

$\Omega^{(1,1)*}$ and $\Omega^{(2,2)*}$ utilizing the L–J 6–12 potential. Suitable tabulations are provided in Appendix P.

16.3.4 Rigorous Expressions for Transport Properties

Rigorous calculations of transport properties require application of an intermolecular potential model, based here on the L–J 6–12 potential. For the viscosity, we need only invoke the rigorous expression defined in Table 16.2. Consequently, converting the particle mass to a molecular weight, evaluating known constants, and applying appropriate conversion factors, we have

$$\eta = \frac{5}{16}\frac{(mkT)^{1/2}}{\sqrt{\pi}\sigma^2\Omega^{(2,2)*}} = \frac{5(1.6605\times10^{-27}\ \text{kmol})^{1/2}(1.3807\times10^{-23}\ \text{kg}\cdot\text{m}^2/\text{s}^2\cdot\text{K})^{1/2}}{16\sqrt{\pi}(10^{-10}\ \text{m/Å})^2}\frac{\sqrt{MT}}{\sigma^2\Omega^{(2,2)*}},$$

thus obtaining

$$\eta = 2.6696\times10^{-6}\frac{\sqrt{MT}}{\sigma^2\Omega^{(2,2)*}}\quad \text{N}\cdot\text{s/m}^2, \tag{16.50}$$

where the temperature, T, must be in K, the molecular weight, M, must be in kg/kmol, and the L–J parameter, σ, must be in Å. Now, knowing η, we may convert Eq. (16.39) to appropriate SI units, giving for the thermal conductivity

$$\lambda = 250(9\gamma - 5)\tilde{c}_v\eta \quad \text{W/m}\cdot\text{K}, \tag{16.51}$$

where the gravimetric specific heat, $\tilde{c}_v$, must be in units of kJ/kg · K.

Beginning once more from Table 16.2, we find that the self-diffusion coefficient, after substitution for density using Eq. (16.33), becomes

$$D = \frac{3}{8}\frac{(mkT)^{1/2}}{\sqrt{\pi}\rho\sigma^2\Omega^{(1,1)*}} = \frac{3}{8}\frac{(kT)^{3/2}}{\sqrt{\pi m}P\sigma^2\Omega^{(1,1)*}}.$$

As for the viscosity, we again convert particle mass to molecular weight, evaluate known constants, and apply appropriate conversion factors, i.e.,

$$D = \frac{3(1.3807\times10^{-23}\ \text{kg}\cdot\text{m}^2/\text{s}^2\cdot\text{K})^{3/2}}{8\sqrt{\pi}(1.6605\times10^{-27}\ \text{kmol})^{1/2}(1.013\times10^5\ \text{kg/m}\cdot\text{s}^2\cdot\text{atm})(10^{-10}\ \text{m/Å})^2}\frac{T^{3/2}}{\sqrt{M}P\sigma^2\Omega^{(1,1)*}},$$

thus obtaining

$$D = 2.6295\times10^{-7}\frac{T^{3/2}}{\sqrt{M}P\sigma^2\Omega^{(1,1)*}}\quad \text{m}^2/\text{s}, \tag{16.52}$$

where the pressure must be expressed in atm.

Based on Eq. (16.52), the binary diffusion coefficient describing the diffusion of species A through species B can be evaluated from

$$D_{AB} = 2.6295\times10^{-7}\frac{T^{3/2}}{\sqrt{M_{AB}}P\sigma_{AB}^2\Omega_{AB}^{(1,1)*}}\quad \text{m}^2/\text{s}, \tag{16.53}$$

where, by definition,

$$M_{AB} = \frac{2M_A M_B}{(M_A + M_B)} \tag{16.54}$$

ensures that Eq. (16.53) becomes equivalent to Eq. (16.52) for a pure gas. Evaluation of the reduced collision integral in Eq. (16.53) requires knowledge of the L–J force constants for a binary gas mixture. From empirical studies, these parameters are found to be best evaluated using

$$\sigma_{AB} = \frac{1}{2}(\sigma_A + \sigma_B) \tag{16.55}$$

$$\varepsilon_{AB} = \sqrt{\varepsilon_A \varepsilon_B}. \tag{16.56}$$

Finally, we note that, for binary diffusion, Eq. (16.54) implies that only a single reduced molecular weight is necessary for mixture calculations. This result conforms to our previous conclusion that the relative motion of two particles can always be transformed to that of a single particle by using the reduced mass of a two-particle system.

EXAMPLE 16.4

Employing rigorous transport theory, determine the following transport properties for gaseous argon:

(a) its dynamic viscosity at 300 K;
(b) its thermal conductivity at 300 K;
(c) its self-diffusion coefficient at 300 K and 1 atm.

Solution

(a) From Appendix O, $\varepsilon/k = 124$ K and $\sigma = 3.42$ Å for argon. Hence, from Eq. (16.48), the reduced temperature is

$$T^* = \frac{kT}{\varepsilon} = \frac{300}{124} = 2.42.$$

Consequently, from Appendix P, the normalized collision integral is $\Omega^{(2,2)*} = 1.104$. On this basis, from Eq. (16.50), the dynamic viscosity becomes

$$\eta = 2.6696 \times 10^{-6} \frac{\sqrt{MT}}{\sigma^2 \Omega^{(2,2)*}} = 2.6696 \times 10^{-6} \frac{\sqrt{(39.948)(300)}}{(3.42)^2(1.104)}$$
$$= 2.263 \times 10^{-5} \text{ N} \cdot \text{s/m}.$$

(b) For any atomic species, the specific heat ratio is $\gamma = 5/3$. Moreover, the gravimetric specific heat at constant volume for argon is

$$\tilde{c}_v = \frac{3}{2}\left(\frac{R}{M}\right) = \frac{3}{2}\left(\frac{8.3145 \text{ kJ/kmol} \cdot \text{K}}{39.948 \text{ kg/kmol}}\right) = 0.3122 \text{ kJ/kg} \cdot \text{K}.$$

Hence, from Eq. (16.51), the thermal conductivity for argon at 300 K is

$$\lambda = 250(9\gamma - 5)\tilde{c}_v \eta = 2500(0.3122)(2.263 \times 10^{-5}) = 1.766 \times 10^{-2} \text{ W/m} \cdot \text{K}.$$

(c) From the reduced temperature of part (a) and Appendix P, the normalized collision integral $\Omega^{(1,1)*} = 1.010$. Therefore, from Eq. (16.52), the self-diffusion coefficient for argon at 300 K and $P = 1$ atm becomes

$$D = 2.6295 \times 10^{-7} \frac{T^{3/2}}{\sqrt{M} P \sigma^2 \Omega^{(1,1)*}} = 2.6295 \times 10^{-7} \frac{(300)^{3/2}}{\sqrt{39.948}(3.42)^2(1.010)}$$

$$= 1.830 \times 10^{-5} \text{ m}^2/\text{s}.$$

While the dynamic viscosity evaluated when using the L–J potential is only 33% higher than that obtained in Example 16.3 when using the rigid-sphere model, the thermal conductivity is a whopping 232% greater and the self-diffusion coefficient is 76% greater than the associated rigid-sphere calculations.

Problems enhancing your understanding of this chapter are combined with those for Chapters 15 and 17 in Problem Set VII.

17 Chemical Kinetics

In this chapter, we apply kinetic theory and statistical thermodynamics to the fundamentals of chemical kinetics. Our goal is to provide a basic understanding of how gas-phase chemical reactions occur in the natural world. In particular, we focus on bimolecular chemical reactions, which typically describe reactive collisions as they actually occur between an individual atom and molecule. In our short introduction to chemical kinetics, we consider both a hard-sphere collision model and a more accurate formulation based on so-called activated complex theory.

17.1 The Bimolecular Reaction

The high-temperature reversible reaction,

$$O + H_2 \rightleftarrows OH + H,$$

is an example of an elementary chemical event – in this case, one that occurs in most flames. By definition, an *elementary* reaction describes a chemical interaction as it actually takes place on a microscopic level. Therefore, for this reaction, O and H_2 directly collide to produce OH and H. Many such elementary reactions are involved in any realistic chemical process. For example, combustion of the simplest fuel, H_2, requires a complex amalgamation of over 20 reversible elementary reactions, involving a variety of both expected and unexpected species such as H_2, O_2, OH, O, H, HO_2, and H_2O_2.

A typical interaction between two gaseous species participating in an elementary chemical reaction involves the breaking and forming of a single chemical bond. The *molecularity* specifies the number of reactant species in an elementary chemical reaction which combine to generate its products. In particular, an elementary reaction with a molecularity of two is called a *bimolecular* chemical reaction. For $O + H_2 \rightleftarrows OH + H$, both the forward and backward chemical steps are bimolecular. Such reversible bimolecular processes are by far the most common type of high-temperature, gas-phase chemical reactions.

17.2 The Rate of Bimolecular Reactions

In general, a reversible bimolecular reaction can be represented by

$$\mathrm{A} + \mathrm{B} \rightleftarrows \mathrm{C} + \mathrm{D},$$

where A, B, C, and D denote various chemical species. Because a bimolecular reaction portrays an actual physical event, we anticipate that its rate of occurrence should be proportional to an effective collision rate and thus, from binary collision theory, to the concentrations of both reactant species. This expectation has been confirmed experimentally, and has therefore been generalized into what is called the *law of mass action*. This empirical law suggests that chemical reaction rates can be expressed as

$$r_f = k_f[\mathrm{A}][\mathrm{B}] \tag{17.1}$$

$$r_b = k_b[\mathrm{C}][\mathrm{D}], \tag{17.2}$$

where r_f and r_b describe specific reaction rates, in mol/cm$^3 \cdot$ s, for the forward and backward directions, respectively; k_f and k_b are specific rate coefficients for these reversible reactions; and $[\mathrm{M}_i]$ denotes the concentration of the ith species in mol/cm^3.

Forward and backward rate coefficients are usually considered to be temperature-dependent properties for a given elementary chemical reaction. Hence, they can be tabulated as functions of temperature, similar to thermodynamic equilibrium constants in the JANAF tables (Appendix E). Indeed, at chemical equilibrium, the forward and backward reaction rates must be equal so that, from Eqs. (17.1) and (17.2),

$$K_c = \frac{k_f}{k_b} = \frac{[\mathrm{C}][\mathrm{D}]}{[\mathrm{A}][\mathrm{B}]}. \tag{17.3}$$

where K_c is, of course, the equilibrium constant based on concentration. Therefore, given K_c, Eq. (17.3) indicates that fundamental knowledge of either k_f or k_b inherently provides the reverse rate coefficient for any chosen bimolecular reaction. Of course, information will always be necessary regarding a specific rate coefficient in either the forward or backward direction. From this perspective, our goal in this chapter is to develop theoretical expressions for the specific rate coefficient describing any bimolecular chemical reaction.

The interpretation of such theoretical expressions can be facilitated by considering in an empirical fashion the influence of temperature when describing the bimolecular rate coefficient. For simplicity, we begin by applying the law of mass action to the general irreversible reaction,

$$\mathrm{A} + \mathrm{B} \rightarrow \mathrm{C} + \mathrm{D},$$

so that the gas-phase chemical reaction rate (mol/cm$^3 \cdot$ s) can be written as

$$r = k[\mathrm{A}][\mathrm{B}]. \tag{17.4}$$

From our previous discussion, the rate coefficient, k, encapsulates the known effect of temperature on chemical reaction rates. The governing empirical correlation, labeled the *Arrhenius law*, is given by

$$k = Ae^{-E/RT}, \tag{17.5}$$

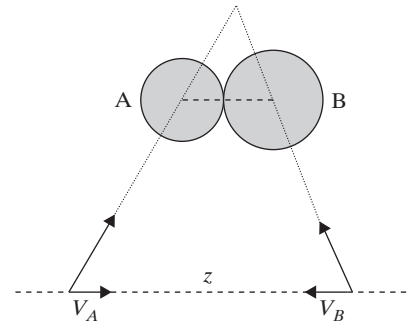

Figure 17.1 Coordinate for line of centers (z) during collision between A and B.

where A identifies a *pre-exponential factor* and E is called the *activation energy*. While the exponential term in Eq. (17.5) usually dominates, the pre-exponential factor nevertheless displays a residual dependence on temperature, which becomes especially significant for small values of E. This temperature influence is usually modeled via

$$A = BT^n, \tag{17.6}$$

where B indicates a pre-exponential constant and n is its temperature coefficient. Combining Eqs. (17.4–17.6), we then have

$$r = BT^n e^{-E/RT}[\mathrm{A}][\mathrm{B}], \tag{17.7}$$

which represents an empirical rate coefficient based on both the Arrhenius law and the law of mass action. A crowning achievement in the field of chemical kinetics is the derivation of Eq. (17.7) from first principles. Such derivations constitute our overriding objective for the remainder of this chapter.

17.3 Chemical Kinetics from Collision Theory

The bimolecular rate for the irreversible reaction $\mathrm{A} + \mathrm{B} \rightarrow \mathrm{C} + \mathrm{D}$ can be estimated from collision theory by recognizing that the rate of reacting collisions is equal to the total collision rate multiplied by the fraction of such collisions with sufficient energy to cause chemical reaction. From binary collision theory, the total collision rate (collisions/cm$^3 \cdot$ s) between species A and B, based on Eq. (16.17), is

$$Z_{AB} = 2n_A n_B \sigma_{AB}^2 \left(\frac{2\pi kT}{\mu}\right)^{1/2}, \tag{17.8}$$

where n_A and n_B are the number densities (particles/cm^3) of species A and B, respectively, σ_{AB} is the mean hard-sphere diameter for species A and B, and μ represents their reduced mass. Given Eq. (17.8), we may now turn our attention to the fraction of collisions with sufficient energy to cause chemical reaction. This development, however, is not at all straightforward and will thus occupy considerable effort before we can return to the bimolecular rate coefficient.

We initiate our exploration of sufficiently energetic collisions by considering the motion of two particles, A and B, which approach each other along the trajectories established in Fig. 17.1. At the moment of impact, the direction along the line of particle centers (z) defines that portion of the total translational energy which should be effective in breaking

a chemical bond. Hence, we can safely neglect any remaining energy associated with sideswiping motion, as this energy merely accounts for particle velocities after collision. From Fig. 17.1, V_A and V_B identify the velocity components of A and B, respectively, along the line of particle centers. Therefore, the fraction of collisions for which the incoming velocities of A and B in the impact direction lie between V_A and $V_A + dV_A$ plus V_B and $V_B + dV_B$, respectively, is given by

$$f(V_A)\,dV_A \cdot f(V_B)\,dV_B, \tag{17.9}$$

where, from Eq. (15.14), we invoke for either particle

$$f(V_z)\,dV_z = \left(\frac{m}{2\pi kT}\right)^{1/2} \exp\left(-\frac{mV_z^2}{2kT}\right) dV_z \tag{17.10}$$

along this single coordinate direction (z).

We now convert Eq. (17.10) to energy along the line of particle centers by implementing

$$\varepsilon_z = \tfrac{1}{2}mV_z^2$$

and multiplying by a factor of two, thus accounting for both positive and negative values of V_z. As a result, we find

$$f(\varepsilon_z)\,d\varepsilon_z = 2\left(\frac{m}{2\pi kT}\right)^{1/2}\left(\frac{1}{2m\varepsilon_z}\right)^{1/2} e^{-\varepsilon_z/kT} d\varepsilon_z$$

so that

$$f(\varepsilon_z)\,d\varepsilon_z = \left(\frac{1}{\pi kT}\right)^{1/2} \varepsilon_z^{-1/2} e^{-\varepsilon_z/kT} d\varepsilon_z, \tag{17.11}$$

which can be verified by checking for proper normalization:

$$\int_0^\infty f(\varepsilon_z)\,d\varepsilon_z = 1.$$

Consequently, from Eqs. (17.9) and (17.11), the fraction of collisions displaying cumulative energy along the impact direction within the range ε_A to $\varepsilon_A + d\varepsilon_A$ plus ε_B to $\varepsilon_B + d\varepsilon_B$ becomes

$$f(\varepsilon_A)\,f(\varepsilon_B)\,d\varepsilon_A\,d\varepsilon_B = \left(\frac{1}{\pi kT}\right)(\varepsilon_A\varepsilon_B)^{-1/2} \exp\left[-\frac{\varepsilon_A + \varepsilon_B}{kT}\right] d\varepsilon_A\,d\varepsilon_B. \tag{17.12}$$

Because we require the fraction of collisions having sufficient total energy, $\varepsilon = \varepsilon_A + \varepsilon_B$, along the line of particle centers, we apply the coordinate transformation

$$\varepsilon_A = \varepsilon - \xi \qquad \varepsilon_B = \xi,$$

whose Jacobian is

$$|J| = \begin{vmatrix} \dfrac{\partial \varepsilon_A}{\partial \varepsilon} & \dfrac{\partial \varepsilon_A}{\partial \xi} \\ \dfrac{\partial \varepsilon_B}{\partial \varepsilon} & \dfrac{\partial \varepsilon_B}{\partial \xi} \end{vmatrix} = 1.$$

Therefore, Eq. (17.12) becomes

$$f(\varepsilon)\, f(\xi)\, d\varepsilon\, d\xi = \left(\frac{1}{\pi kT}\right)(\varepsilon - \xi)^{-1/2}\, \xi^{-1/2} e^{-\varepsilon/kT} d\varepsilon\, d\xi. \tag{17.13}$$

Upon integration of Eq. (17.13) over all possible values of ξ, the probability of obtaining a total collision energy in the range ε to $\varepsilon + d\varepsilon$ becomes

$$f(\varepsilon)\, d\varepsilon = \left(\frac{1}{\pi kT}\right) e^{-\varepsilon/kT} d\varepsilon \int_0^{\varepsilon} (\varepsilon - \xi)^{-1/2}\, \xi^{-1/2} d\xi. \tag{17.14}$$

Applying next the integrating factor $\xi = \varepsilon \sin^2 \alpha$, we may evaluate the above integral, giving

$$\int_0^{\varepsilon} (\varepsilon - \xi)^{-1/2}\, \xi^{-1/2} d\xi = \int_0^{\pi/2} \left(\frac{2\varepsilon \sin\alpha \cos\alpha}{\varepsilon \cos\alpha \sin\alpha}\right) d\alpha = \pi,$$

so that Eq. (17.14) becomes

$$f(\varepsilon)\, d\varepsilon = \left(\frac{1}{kT}\right) e^{-\varepsilon/kT} d\varepsilon. \tag{17.15}$$

The fraction of collisions of sufficient energy can finally be determined by integrating Eq. (17.15) from the minimum energy required for chemical reaction, say $\varepsilon_\circ$, to infinity. The result is

$$\int_{\varepsilon_\circ}^{\infty} f(\varepsilon)\, d\varepsilon = \left(\frac{1}{kT}\right) \int_{\varepsilon_\circ}^{\infty} e^{-\varepsilon/kT} d\varepsilon = e^{-\varepsilon_\circ/kT}, \tag{17.16}$$

which clearly represents the exponential temperature dependence anticipated from the empirical Arrhenius law.

We now recall that the rate for a bimolecular reaction, $\mathrm{A} + \mathrm{B} \rightarrow \mathrm{C} + \mathrm{D}$, can be determined by multiplying the total collision rate, Z_{AB}, by the fraction of collisions with sufficient energy to cause chemical reaction. Hence, we have from Eq. (17.16)

$$r^* = Z_{AB} e^{-\varepsilon_\circ/kT},$$

where r^* is the specific reaction rate expressed as particles/cm$^3 \cdot$ s. On this basis, the chemical reaction rate expressed macroscopically in mol/cm$^3 \cdot$ s becomes

$$r = \left(\frac{Z_{AB}}{N_A}\right) e^{-E/RT}, \tag{17.17}$$

where N_A is Avagadro's number and E is the activation energy (kJ/mol). If we substitute for Z_{AB} from Eq. (17.8), Eq. (17.17) may be expressed as

$$r = 2N_A \sigma_{AB}^2 \left(\frac{2\pi kT}{\mu}\right)^{1/2} e^{-E/RT}[\mathrm{A}][\mathrm{B}]. \tag{17.18}$$

Finally, comparing Eq. (17.18), as derived from collision theory, with its empirical analog represented by Eq. (17.7), we find that the pre-exponential constant becomes

$$B = 2N_A \sigma_{AB}^2 \left(\frac{2\pi k}{\mu}\right)^{1/2}, \tag{17.19}$$

and that the associated temperature exponent $n = 1/2$. Consequently, we have successfully provided a theoretical formulation that explains both the activation energy and the

pre-exponential factor for bimolecular chemical reactions. The activation energy represents the *minimum energy required for bond breakage* while the pre-exponential factor, $A = BT^n$, arises from the total binary collision rate. Unfortunately, in most cases, the activation energy can only be estimated from semiempirical correlations or perhaps chemical intuition, although improvements have recently become possible through more sophisticated calculations based on either quantum mechanics or Monte Carlo simulations. Nevertheless, the striking similarity between Eqs. (17.7) and (17.18) is certainly compelling, thus warranting further confidence in the many physical insights provided by kinetic theory.

EXAMPLE 17.1

The pre-exponential factor for the elementary reaction $O + H_2 \rightarrow OH + H$ has been determined experimentally to be 8.04×10^{11} cm^3/mol·s at 500 K. Calculate the pre-exponential factor for this elementary chemical reaction at the same temperature using collision theory and compare your result with the given experimental value.

Solution

From Eqs. (17.6) and (17.19), the pre-exponential factor provided by kinetic theory is

$$A = 2N_A\sigma_{AB}^2\left(\frac{2\pi kT}{\mu}\right)^{1/2}.$$

From Appendix O, we may take the rigid-sphere diameter of H_2 to be 2.92 Å and that for atomic oxygen to be half of its value for O_2 or 1.72 Å. On this basis, we obtain, from Eq. (16.55),

$$\sigma_{AB} = \frac{\sigma_A + \sigma_B}{2} = \frac{2.92 + 1.72}{2} = 2.32\,\text{Å}.$$

From Eq. (16.6), the reduced mass for this binary reaction is

$$\mu = \frac{m_A m_B}{m_A + m_B} = \frac{(2)(16)}{2+16}(1.6605 \times 10^{-24}\,\text{g}) = 2.952 \times 10^{-24}\,\text{g}.$$

Therefore, the pre-exponential factor from kinetic theory becomes

$$A = 2(6.022 \times 10^{23}\,\text{mol}^{-1})(2.32 \times 10^{-8}\,\text{cm})^2 \times \sqrt{\frac{2\pi(1.381 \times 10^{-16}\,\text{g}\cdot\text{cm}^2/\text{s}^2\cdot\text{K})(500\text{K})}{2.952 \times 10^{-24}\,\text{g}}}$$

$$= 2.48 \times 10^{14}\,\text{cm}^3/\text{mol}\cdot\text{s}.$$

The calculated pre-exponential factor from kinetic theory is over 300 times greater than that provided by experiment. This huge discrepancy arises from the internal energy modes of molecular hydrogen, which are not accounted for in a purely kinetic model.

17.4 The Significance of Internal Energy Modes

Despite qualitative agreement between collision theory and empirical correlations, quantitative agreement when evaluating bimolecular reaction rates is usually quite poor.

While this behavior partially arises from the disruption of Maxwell–Boltzmann velocity distributions upon preferential depletion of energetic particles, the far more important issue is the pervasive influence of internal energy modes, which are totally neglected by kinetic theory. In particular, vibrational and rotational modes can easily absorb translational energy during collisions, thus dispersing the available energy that could be effective in rupturing a critical chemical bond. The upshot is that fewer collisions provide the requisite activation energy for initiating a chemical reaction. Hence, kinetic theory invariably overestimates the rate of bimolecular reactions, with the exception of those chemical systems involving essentially atomic rather than molecular species.

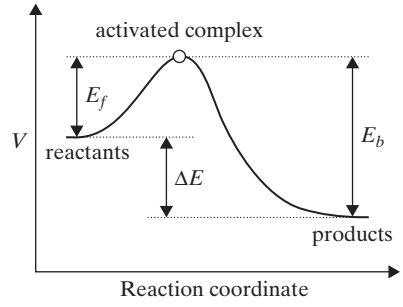

Figure 17.2 Energy along reaction coordinate for elementary chemical reaction.

Fortunately, the inherent weakness of kinetic theory with respect to internal energy modes can be addressed quite successfully by invoking transition state theory, which is, in essence, an equilibrium formulation founded on the edifice of statistical thermodynamics. The important innovation in transition state theory is quantum modeling of a preferentially energized reaction path that activates a chemical complex uniquely composed of all atomic constituents. This *activated complex* is characterized by a weak vibrational bond so that rupture occurs upon every oscillation. As a result, the bimolecular reaction rate can be directly related to the vibrational frequency of this critical molecular bond. In general, the concept of an activated complex proves quite fruitful as compared to collision theory; however, as we will see in Example 17.2, modeling the chemical structure of an activated complex poses a continuing challenge for transition state theory.

17.5 Chemical Kinetics from Transition State Theory

The basic presumption of transition state theory is that elementary chemical reactions occur along a preferred reaction coordinate associated with a particular chemical bond. In reality, of course, a chemical process represents the cumulative result arising from many possible reaction paths. However, for elementary reactions, a single reaction coordinate dominated by the weakest chemical bond is often significantly more likely than all remaining reaction paths. While the latter can be considered using Monte Carlo simulations, transition state theory works best for those elementary chemical reactions characterized by a dominant reaction coordinate.

The preferred reaction path across a local minimum on a typical potential energy surface is depicted for an elementary chemical reaction in Fig. 17.2. The basic notion is that the reactant species merge to create a metastable activated complex which is sufficiently energetic to undergo chemical reaction. The activation energy, whether in the forward (E_f) or backward (E_b) direction, indicates the energy required to create this activated complex. In a sense, the reaction coordinate displayed in Fig. 17.2 represents a microscopic progress variable for an elementary chemical reaction. Therefore, the activation energy can only be associated with reaction along a single preferred molecular bond.

The fundamentals of transition state theory were developed by Henry Eyring and his co-workers at the University of Utah around 1935. The basic assumptions of the theory are as follows:

1. The concentration of activated complexes converting reactants to products is the same as it would be at chemical equilibrium.
2. The total reaction rate can be approximated by the rate at which activated complexes pass along the most probable reaction coordinate.
3. The activated complex undergoes conversion to products via the transformation of an unstable vibrational degree of freedom into translational energy.

The first assumption implies that the number of activated complexes passing over the energy barrier in the forward direction is independent of that passing in the backward direction. The fact that measured rate coefficients prove to be the same regardless of their remoteness from chemical equilibrium verifies this supposition. More recent theoretical work, however, suggests that the first assumption might be too restrictive and that equilibration of mode temperatures among the reactants is probably sufficient for most purposes. In comparison, the second assumption simply reiterates the importance of a dominant reaction coordinate while the third assumption identifies a suitable mechanism for determining the frequency with which complexes pass to products. The latter two assumptions taken together provide the basic procedure for determining chemical reaction rates using transition state theory.

If we now apply the first assumption to our usual bimolecular chemical reaction,

$$\mathrm{A} + \mathrm{B} \rightarrow \mathrm{C} + \mathrm{D},$$

chemical equilibrium can be presumed between the reactants and the activated complex so that

$$\mathrm{A} + \mathrm{B} \rightleftarrows \mathrm{X}^{\ddagger},$$

where $\mathrm{X}^{\ddagger}$ denotes the activated complex. On this basis, the concentration of activated complexes can be determined from the concentrations of A and B using

$$[\mathrm{X}^{\ddagger}] = K_c^{\ddagger}[\mathrm{A}][\mathrm{B}], \tag{17.20}$$

where $K_c^{\ddagger}$ is an associated equilibrium constant based on concentration (mol/cm^3). Invoking the third assumption, we may designate ν_D as the frequency (s^{-1}) of an unstable vibrational bond characteristic of the activated complex. Consequently, the specific rate for a bimolecular reaction can be written as

$$r = \nu_D[\mathrm{X}^{\ddagger}] = \nu_D K_c^{\ddagger}[\mathrm{A}][\mathrm{B}], \tag{17.21}$$

where each oscillation must pass the activated complex from reactants to products along a preferred reaction coordinate. From Eqs. (17.4) and (17.21), we thus find that the rate coefficient characteristic of any bimolecular chemical reaction obeys the amazingly simple relation,

$$k = \nu_D K_c^{\ddagger}. \tag{17.22}$$

Hence, our fundamental problem is to develop an expression for $K_c^{\ddagger}$ in terms of appropriate partition functions via the methods of statistical thermodynamics.

A suitable equation for the required equilibrium constant, $K_c^{\ddagger}$, can be derived by applying Eq. (10.59) to the equilibrium reaction, $\mathrm{A} + \mathrm{B} \rightleftarrows \mathrm{X}^{\ddagger}$, thus obtaining

$$K_c^{\ddagger} = \frac{n_{\mathrm{X}^{\ddagger}}}{n_{\mathrm{A}} n_{\mathrm{B}}} = \frac{\phi_{\mathrm{X}^{\ddagger}}}{\phi_{\mathrm{A}} \phi_{\mathrm{B}}} \exp\left(\frac{\mathrm{D}_{\circ \mathrm{X}^{\ddagger}} - \mathrm{D}_{\circ \mathrm{A}} - \mathrm{D}_{\circ \mathrm{B}}}{kT}\right), \tag{17.23}$$

where

$$\phi_i = \frac{Z_i}{V} \tag{17.24}$$

is the partition function per unit volume for the ith species. In conformance with the protocol established in Chapter 10, each Z_i is calculated in the usual manner by setting its zero of energy at the ground vibrational level within the ground electronic state. Converting next from number density (particles/cm^3) to concentration (mol/cm^3), the required molar equilibrium constant becomes, from Eq. (17.23),

$$K_c^{\ddagger} = \frac{[\mathrm{X}^{\ddagger}]}{[\mathrm{A}][\mathrm{B}]} = N_A \frac{\phi_{\mathrm{X}^{\ddagger}}}{\phi_{\mathrm{A}} \phi_{\mathrm{B}}} \exp\left(-\frac{\Delta E_0}{kT}\right), \tag{17.25}$$

where N_A is Avagadro's number and

$$\Delta E_0 = \mathrm{D}_{\circ \mathrm{A}} + \mathrm{D}_{\circ \mathrm{B}} - \mathrm{D}_{\circ \mathrm{X}^{\ddagger}} \tag{17.26}$$

defines the chemical energy needed at absolute zero to produce the activated complex.

Equation (17.25) requires the partition function per unit volume for the activated complex, which can be written as

$$\phi_{\mathrm{X}^{\ddagger}} = \phi^{\ddagger} \phi_D. \tag{17.27}$$

Here, $\phi^{\ddagger}$ is the volumetric partition function associated with the complex's standard translational and internal degrees of freedom while ϕ_D defines the partition function per unit volume associated with its unstable vibrational mode along the reaction coordinate. According to transition state theory, chemical reaction occurs when the ultraweak vibrational mode represented by ϕ_D manifests translational behavior. Given this presumption, the vibrational mode defining any dominant reaction coordinate must approach its classical translational limit. On this basis, from Eq. (6.49), the weak vibrational bond must obey

$$\frac{\Delta \varepsilon}{kT} = \frac{h\nu}{kT} \ll 1,$$

so that, using Eqs. (9.46) and (9.47), we have

$$\phi_D = \lim_{h\nu/kT \to 0} Z_{vib} = \lim_{h\nu/kT \to 0} (1 - e^{-h\nu/kT})^{-1} = \frac{kT}{h\nu_D}, \tag{17.28}$$

where ν_D is a characteristic vibrational frequency associated with the controlling reaction coordinate. This same result for ϕ_D could also have been obtained by determining the classical phase integral for the harmonic oscillator, as exploited in Problem 4.2.

Having determined ϕ_D, we may substitute Eqs. (17.27) and (17.28) into Eq. (17.25), thus obtaining

$$K_c^{\ddagger} = N_A \left(\frac{kT}{h\nu_D}\right) \frac{\phi^{\ddagger}}{\phi_{\mathrm{A}} \phi_{\mathrm{B}}} \exp\left(-\frac{\Delta E_0}{kT}\right). \tag{17.29}$$

Therefore, combining Eqs. (17.22) and (17.29), we obtain the rate coefficient for our standard bimolecular chemical reaction,

$$k = N_A \left(\frac{kT}{h}\right) \frac{\phi^{\ddagger}}{\phi_A \phi_B} \exp\left(-\frac{\Delta E_0}{kT}\right). \tag{17.30}$$

Comparing Eqs. (17.5) and (17.30), we find from transition state theory that the empirical activation energy can be explained from Eq. (17.26) in terms of dissociation energies evaluated at absolute zero. More interestingly, the remaining temperature dependence incorporated into the pre-exponential factor,

$$A = N_A \left(\frac{kT}{h}\right) \frac{\phi^{\ddagger}}{\phi_A \phi_B}, \tag{17.31}$$

can now be understood through the influence of temperature on partition functions for the reactants and activated complex. In general, the quantitative relationship displayed by Eq. (17.31) surely constitutes a triumph for transition state theory. Nevertheless, determining $\phi^{\ddagger}$ remains a major challenge, as we are always faced with developing a robust model for the molecular structure of a given activated complex. In practice, the modeling procedure is mostly based on structural analogies with successful complexes – in other words, those which have previously produced good agreement with experiments when dealing with similar elementary chemical reactions.

EXAMPLE 17.2

The pre-exponential factor for the elementary chemical reaction, $O + H_2 \rightarrow OH + H$, has been determined experimentally to be 8.04×10^{11} cm^3/mol · s at 500 K. Calculate the pre-exponential factor for this reaction at the same temperature using transition state theory and compare your result with the given experimental value.

Solution

From Eq. (17.31), the pre-exponential factor provided by transition state theory is

$$A = N_A \left(\frac{kT}{h}\right) \frac{\phi^{\ddagger}}{\phi_A \phi_B},$$

where the required partition functions per unit volume can be determined via Eq. (10.62):

$$\phi_i = \left(\frac{2\pi m_i kT}{h^2}\right)^{3/2} Z_{int}.$$

Hence, for atomic oxygen, we obtain

$$\phi_A = \phi_{tr}^{\circ} Z_{el} = \left(\frac{2\pi m_A kT}{h^2}\right)^{3/2} Z_{el},$$

so that, given the associated term symbol from Appendix J.1, we get $Z_{el} = 9$ and thus

$$\phi_A = 9\left[\frac{2\pi(16)(1.66 \times 10^{-24}\,\text{g})(1.38 \times 10^{-16}\,\text{g} \cdot \text{cm}^2/\text{s}^2 \cdot \text{K})(500\text{K})}{(6.626 \times 10^{-27}\,\text{g} \cdot \text{cm}^2/\text{s})^2}\right]^{3/2}$$

$$= 9(1.34 \times 10^{26}) = 1.21 \times 10^{27}\ \text{cm}^{-3}.$$

Similarly, for molecular hydrogen, we have, for the rigid-rotor/harmonic-oscillator model,

$$\phi_{\mathrm{B}} = \left(\frac{2\pi m_{\mathrm{B}} kT}{h^2}\right)^{3/2} Z_{rot} Z_{vib} Z_{el}.$$

Accordingly, from Appendix K.1, the ground electronic state for molecular hydrogen mandates $Z_{el} = 1$. For the rotational mode of H_2, $B_e = 60.853\ \mathrm{cm}^{-1}$ so that $\theta_r = (1.4387)(60.853) = 87.55$ K. Similarly, for the vibrational mode of H_2, $\omega_e = 4401\ \mathrm{cm}^{-1}$ and thus $\theta_v = (1.4387)(4401) = 6332$ K. Therefore, from Eqs. (9.25) and (9.47),

$$Z_{rot} Z_{vib} Z_{el} = \left(\frac{T}{2\theta_r}\right)\left(1 + \frac{\theta_r}{3T}\right)(1 - e^{-\theta_v / T})^{-1} Z_{el} = \frac{(500\ \mathrm{K})}{2(87.55\ \mathrm{K})}(1.058)(1)(1) = 3.02.$$

On this basis, the molecular partition function per unit volume for H_2 is

$$\begin{aligned}\phi_{\mathrm{B}} &= 3.02\left(\frac{2\pi m_{\mathrm{B}} kT}{h^2}\right)^{3/2} = 3.02\left(\frac{m_{\mathrm{B}}}{m_{\mathrm{A}}}\right)^{3/2} \phi_{tr}^{\circ} = 3.02\left(\frac{2}{16}\right)^{3/2}(1.34 \times 10^{26}) \\ &= 1.79 \times 10^{25}\ \mathrm{cm}^{-3}.\end{aligned}$$

Now, for the activated complex, we assume a linear triatomic, i.e.,

$$\mathrm{O—H}\cdots\cdots\mathrm{H},$$

with only three vibrational modes, as the fourth such mode represents the weak bond that ruptures during chemical reaction. For simplicity in our analysis, we model the rotational mode of the activated complex using its analogous OH structure; hence, from Appendix K.1, $B_e = 18.911\ \mathrm{cm}^{-1}$ and thus $\theta_r = 27.21$ K. In a similar fashion, we model the vibrational modes based on H_2O so that, from Appendix K.3, we have a single stretch mode at $\omega_e \simeq 3700\ \mathrm{cm}^{-1}$ and two bending modes at $\omega_e \simeq 1600\ \mathrm{cm}^{-1}$. Therefore, the characteristic vibrational temperatures for the activated complex are $\theta_{v1} = 5323$ K and $\theta_{v2} = 2302$ K, respectively. Similarly, from Appendix K.3, the ground electronic state for H_2O indicates that $Z_{el} = 1$. Based on this model for the activated complex, its partition function per unit volume becomes

$$\phi^{\ddagger} = \left(\frac{2\pi m_{\mathrm{X}^{\ddagger}} kT}{h^2}\right)^{3/2} Z_{rot} Z_{vib} Z_{el} = Z_{rot} Z_{vib} Z_{el}\left(\frac{m_{\mathrm{X}^{\ddagger}}}{m_{\mathrm{A}}}\right)^{3/2} \phi_{tr}^{\circ}.$$

Evaluating the above internal partition functions, we have, from Eqs. (9.26) and (9.47),

$$Z_{rot} Z_{vib} Z_{el} = \left(\frac{T}{\theta_r}\right)(1 - e^{-\theta_{v1} / T})^{-1}(1 - e^{-\theta_{v2} / T})^{-2} Z_{el} = \frac{(500\ \mathrm{K})}{(27.21\ \mathrm{K})}(1)(1.01)^2(1) = 18.75.$$

Consequently, for the activated complex,

$$\phi^{\ddagger} = 18.75\left(\frac{m_{\mathrm{X}^{\ddagger}}}{m_{\mathrm{A}}}\right)^{3/2} \phi_{tr}^{\circ} = 18.75\left(\frac{18}{16}\right)^{3/2}(1.34 \times 10^{26}) = 3.00 \times 10^{27}\ \mathrm{cm}^{-3}.$$

Having determined all relevant partition functions, we may finally calculate the pre-exponential factor, thus obtaining

$$\begin{aligned}A = N_A\left(\frac{kT}{h}\right)\frac{\phi^{\ddagger}}{\phi_{\mathrm{A}}\phi_{\mathrm{B}}} &= (6.022 \times 10^{23}\ \mathrm{mol}^{-1}) \\ &\times \frac{(1.38 \times 10^{-16}\ \mathrm{erg/K})(500\ \mathrm{K})(3.00 \times 10^{27}\ \mathrm{cm}^{-3})}{(6.626 \times 10^{-27}\ \mathrm{erg \cdot s})(1.21 \times 10^{27}\ \mathrm{cm}^{-3})(1.79 \times 10^{25}\ \mathrm{cm}^{-3})},\end{aligned}$$

so that our result from transition state theory becomes

$$A = 8.69 \times 10^{11}\ \text{cm}^3/\text{mol} \cdot \text{s}.$$

Remarkably, the pre-exponential factor based on transition state theory for this elementary chemical reaction agrees with that based on experiment to within 8%, which is probably fortuitous given our rather simplified model for the activated complex. On the other hand, we must not forget in the midst of these long-winded calculations that transition state theory inherently accounts for all internal energy modes, thus providing predictions for chemical reaction rates that are undeniably much more realistic than those determined from collision theory.

PROBLEM SET VII

Kinetic Theory and Molecular Transport (Chapters 15–17)

7.1 The following exercises explore relationships among momentum, speed, and energy in classical kinetic theory.

a. Starting with $f(\boldsymbol{p})$ for the momentum, derive the probability density function, $f(p)$, for the magnitude of the momentum. How is this distribution related to the speed distribution?

b. From $f(p)$, derive an expression for $f(\varepsilon/kT)$, where ε is the kinetic energy. Show that the probability, $P(a \leq \varepsilon/kT \leq b)$, does not depend on particle mass or temperature.

c. Employing the phase integral, verify that the classical degeneracy for a single translating particle is given by

$$dg = \frac{4\pi mV}{h^3}(2m\varepsilon)^{1/2}d\varepsilon.$$

d. Using the degeneracy of part (c), obtain $f(\varepsilon/kT)$ and compare your result to that of part (b).

7.2 Consider a two-dimensional gas constrained to the x–y plane so that the velocity distribution function becomes

$$f(\boldsymbol{V}) = \left(\frac{m}{2\pi\, kT}\right) \exp\left[-\frac{m\left(V_x^2 + V_y^2\right)}{2kT}\right],$$

where m is the particle mass.

a. Determine the corresponding speed distribution function, $f(V)$.

b. Verify that the total flux of particles at the walls of a two-dimensional enclosure is given by $J = n\langle \mathrm{V} \rangle/\pi$, where n is the particle surface density (molecules/cm^2).

c. Evaluate the particle flux, J, for the speed distribution function of part (a).

d. Demonstrate that the pressure for a two-dimensional gas is $P = nkT$. Why would you expect this result?

7.3 By definition, an assembly of atoms follows the Maxwell–Boltzmann velocity distribution at thermodynamic equilibrium.

a. On this basis, show that the fraction of atoms having speeds between 0 and V at thermal equilibrium can be expressed as

$$\frac{N_{0-V}}{N} = \text{erf}(x) - \frac{2}{\sqrt{\pi}} x \exp(-x^2),$$

where $x = V/V_{mp}$ and V_{mp} is the most probable speed for the atomic assembly.

b. Calculate the fraction of argon atoms at 300 K with speeds less than 500 m/s.

7.4 Consider the following exercises associated with the mean free path, ℓ, of an ideal-gas assembly.

a. By defining a suitable collision coefficient, α, derive the so-called survival equation

$$N = N_\circ \exp(-\alpha x),$$

which represents the number of molecules, N, out of an initial number, $N_\circ$, that has not yet experienced a collision after traveling a distance x.

b. Show that the survival equation can also be expressed as

$$P(x) = \exp(-x/\ell),$$

where $P(x)$ is the probability that an individual molecule has a free path of at least x.

c. What is the probability of finding a free path $x \geq 100$ nm for air at STP conditions?

d. Verify that the probability density function describing the possible free paths for an individual molecule is given by

$$f(x) = \frac{\exp(-x/\ell)}{\ell}.$$

e. Using this distribution function, show that ℓ does indeed represent the mean free path.

f. Determine the root-mean-square free path, ξ, in terms of the mean free path, ℓ.

7.5 A miniscule pinhole develops in the wall of a tank so that every molecule of gas within the tank striking the hole escapes from the pressure vessel. Demonstrate that the average translational energy per particle escaping from the tank is $2kT$. Why is this mean translational energy different from that inside the pressure vessel?

7.6 Consider the effusion of a perfect gas from a small hole in the wall of a container. Show that the fraction of escaping particles with speeds greater than W is given by

$$F = (x^2 + 1) \exp(-x^2),$$

where $x = W/V_{mp}$ and V_{mp} is the most probable speed for the contained particles. Using the above expression, determine the fraction of escaping particles with speeds greater than the mean molecular speed, $\overline{V}$, within the container.

7.7 Translation is the only important energy mode for the electron gas; thus, we can apply the procedures of kinetic theory to the conduction electrons in a metal.

a. Demonstrate that the probability distribution for the translational energy of an electron gas can be expressed as

$$f(\varepsilon)d\varepsilon = \frac{8\pi m_e}{h^3}\left(\frac{V}{N}\right)\frac{(2m_e\varepsilon)^{1/2}d\varepsilon}{e^{(\varepsilon-\mu)/kT}+1},$$

where V is the volume, m_e is the mass of an electron, and N is the total number of electrons within the system.

b. Prove that the mean speed of the conduction electrons at absolute zero is

$$\overline{V}_0 = \frac{3}{4}\sqrt{\frac{2\mu_0}{m_e}},$$

where μ_0 is the Fermi energy.

c. Why is $\overline{V}_0$ not equal to zero?

7.8 Kinetic theory can be employed to estimate the influence of quenching collisions on the efficacy of laser-induced fluorescence (LIF) measurements.

a. Demonstrate that, for normal LIF, the fluorescence signal (V) is given by

$$S_f = \eta(h\nu_{ul})\left(\frac{\Omega_c}{4\pi}\right)\left(\frac{A_{ul}}{A_{ul}+Q_{ul}}\right)\left(\frac{B_{lu}V_c}{c}\right)n_l^\circ I_\nu,$$

where η is the detector efficiency (V/W), ν_{ul} is the laser frequency, Ω_c is the solid angle of the collection optics, A_{ul} and B_{lu} are the relevant Einstein coefficients, Q_{ul} is the rate coefficient for collisional quenching, V_c is the collection volume, n_l° is the initial population for the lower level, and I_ν is the spectral irradiance of the laser beam.

b. The Stern–Volmer factor, $A_{ul}/(A_{ul}+Q_{ul})$, is a measure of the fluorescence efficiency. Assuming that every collision leads to quenching of the excited electronic state, show that

$$Q_{ul} = \frac{2\sqrt{2}\sigma_e P}{(\pi\mu kT)^{1/2}},$$

where $\sigma_e = \pi\sigma_{12}^2$ is the relevant cross section for electronic quenching, T is the temperature, and P is the ambient pressure.

c. Consider a reaction vessel containing small quantities of NO in a bath of O_2. The chemical kinetics of NO oxidation can be studied via LIF measurements of NO. The quenching cross section for NO in O_2 must be known to assess the fluorescence efficiency. Calculate σ_e (Å^2) using the so-called hard-sphere approximation.

d. The Einstein A-coefficient for a typical rovibronic line of NO is 4×10^5 s^{-1}. Determine the relevant Stern–Volmer factor for a reaction vessel temperature and pressure of 500 K and 1 bar, respectively. What is the physical implication of your result? What reaction vessel parameter should you change to increase the fluorescence efficiency?

7.9 An ideal gas, composed of molecules with mass m, is maintained at temperature T inside an enclosure. The molecules emit light along the x-direction through

a window of the enclosure and into a spectrometer. A stationary molecule would emit light at a sharply defined frequency, $\nu_\circ$, but owing to the Doppler effect the frequency of observed light from a molecule with an x-component of velocity, V_x, is

$$\nu = \nu_\circ \left(1 + \frac{V_x}{c}\right),$$

where c is the velocity of light. As a result, the light arriving at the spectrometer displays a spectral line profile, $Y(\nu)$, which is defined as the fraction of light in the frequency range between ν and $\nu + d\nu$.

a. Determine $Y(\nu)$ for a Doppler-broadened spectral line.

b. Verify that the mean frequency of the light observed by the spectrometer is $\nu_\circ$.

c. The root-mean-square deviation, $\Delta\nu$, defines the spectral line width arising from the Doppler effect. Show that this line width is given by

$$\Delta\nu = \sqrt{\frac{kT}{mc^2}}\,\nu_\circ.$$

d. Provide an expression for the spectral line profile, $Y(\nu)$, in terms of the parameters $\nu_\circ$ and $\Delta\nu$.

7.10 We have shown that $\lambda = \delta\eta c_v$, where c_v is the gravimetric specific heat at constant volume, $\delta = 1$ for simple kinetic theory, and $\delta = 5/2$ from rigorous kinetic theory. The physical explanation for $\delta > 1$ was first pointed out by Eucken in 1913. For translational motion, molecules with greater velocities have larger mean free paths. Because these molecules travel farther and carry more kinetic energy, the transport of kinetic energy by the faster molecules is more effective, thus giving $\delta > 1$. Eucken further argued that for polyatomic molecules δ should remain at unity for the internal energy modes as they are independent of velocity. He thus formulated the following nonrigorous extension of the above formula:

$$\lambda = \left(\tfrac{5}{2}c_{v,tr} + c_{v,\text{int}}\right)\eta.$$

a. Show that this formulation leads to the so-called Eucken correction,

$$\lambda = \tfrac{1}{4}(9\gamma - 5)\eta c_v,$$

where $\gamma = c_p/c_v$.

b. Show that the Eucken correction reduces to the rigorous result for a monatomic gas.

7.11 The Lennard–Jones parameters for molecular oxygen based on viscosity data are $\sigma = 3.43$ Å and $\varepsilon/k = 113$ K.

a. Calculate the dynamic viscosity, η (N · s/m^2), at 300 K.

b. Redo part (a) by using instead Lennard–Jones parameters based on virial coefficient data. Compare your calculated viscosities with tabulated data. Comment on the significance of your comparisons.

c. Evaluate the remaining transport properties, namely, the thermal conductivity, λ (W/m · K), and the binary diffusion coefficient, D_{AB}, for O_2 in N_2 (m^2/s) at 300 K and 1 atm. Compare your results with tabulated data.

d. Calculate η and λ at 1000 K. Comment on specific comparisons of your results with tabulated data.

7.12 The Lennard–Jones parameters for molecular hydrogen based on viscosity data are $\sigma = 2.92$ Å and $\varepsilon/k = 38.0$ K.

a. Calculate the three transport properties η, λ, and D (H_2–N_2) at 300 K and 1 atm. Compare your results with available tabulations.

b. In most cases, transport properties are unavailable at flame temperatures. Calculate η, λ, and D (H_2–N_2) at 1500 K and 0.1 atm. To the extent that you can, compare your results with available data.

c. Why did we use Lennard–Jones parameters based on viscosity data rather than on virial coefficient data?

7.13 The Lennard–Jones parameters for carbon dioxide based on viscosity data are $\sigma = 4.00$ Å and $\varepsilon/k = 190$ K.

a. Why are these parameters different from those based on virial coefficient data (Appendix O)? Which set of parameters should be used for calculations of thermodynamic properties? For calculations of transport properties?

b. Evaluate the three transport properties, η (N · s/m^2), λ (W/m · K), and D_{AB} (m^2/s), for CO_2 in air at 300 K and 1 atm. Compare your results with available tabulations.

c. Describe how you would obtain the parameters σ and ε/k from experimental viscosity data.

7.14 An estimate is to be made for the rate of the bimolecular reaction,

$$O_2 + N_2 \rightarrow O + O + N_2,$$

using collision theory. The binary diffusion coefficient for mass transport of O_2 in N_2 is known to be 0.18 cm^2/s at 1 atm and 273 K.

a. Using the empirical rate expression

$$r = BT^n e^{-E/RT}[O_2][N_2] \quad \text{mol/cm}^3 \cdot \text{s},$$

estimate B, n and E (kJ/mol) for this elementary reaction.

b. Determine the rate coefficient for the above reaction at 2500 K. Compare with the measured rate coefficient given by

$$k = 1.9 \times 10^{11}\ T^{1/2} \exp(-48100/T) \quad \text{cm}^3/\text{mol} \cdot \text{s}.$$

Explain why reasonable agreement between theory and experiment is obtained in this case.

7.15 An estimate is to be made for the rate of the bimolecular reaction,

$$H_2 + N_2 \rightarrow H + H + N_2,$$

using collision theory. The binary diffusion coefficient for mass transport of H_2 in N_2 is known to be 0.68 cm^2/s at 1 atm and 273 K.

a. Using the empirical rate expression

$$r = BT^n e^{-E/RT}[H_2][N_2] \quad \text{mol/cm}^3 \cdot \text{s},$$

estimate B, n and E (kJ/mol) for this elementary reaction.

b. Determine the rate coefficient for this reaction at 2500 K. Compare with the measured rate coefficient given by

$$k = 4.4 \times 10^{13} \exp(-48300/T) \quad \text{cm}^3/\text{mol} \cdot \text{s}.$$

Explain why reasonable agreement between theory and experiment is obtained in this case.

7.16 An estimate is to be made for the rate of the bimolecular reaction

$$\text{H} + \text{O}_2 \rightarrow \text{OH} + \text{O}$$

using collision theory. The binary diffusion coefficient for mass transport of H in O_2 is known to be 1.35 cm^2/s at 1 atm and 294 K.

a. Using the empirical rate expression

$$r = B(T/K)^n e^{-E/RT}[\text{H}][\text{O}_2] \quad \text{mol/cm}^3 \cdot \text{s},$$

estimate B, n, and E (kJ/mol) for this elementary reaction.

b. Determine the rate coefficient for the above reaction at 2000 K. Compare with the measured rate coefficient, as given by the rate parameters $B = 1.2 \times 10^{17}$ $\text{cm}^3/\text{mol} \cdot \text{s}$, $n = -0.9$, and $E = 69.1$ kJ/mol. Discuss reasons for the level of agreement or disagreement obtained for this particular reaction.

PART SIX

THE ENSEMBLE METHOD OF STATISTICAL THERMODYNAMICS

18 The Canonical and Grand Canonical Ensembles

To this point, we have dealt exclusively with systems composed of independent particles and thus we have utilized the Maxwell–Boltzmann method of statistical thermodynamics. We know, however, that at a sufficiently high pressure or low temperature any gas will begin demonstrating nonideal behavior. For such *real gases*, and also for liquids, centralized forces arise among constituent particles owing to shorter intermolecular distances. Consequently, we are eventually confronted with systems composed of *dependent* rather than independent particles. Such systems mandate that we forsake the Maxwell–Boltzmann method and turn instead to a more robust computational procedure known as the Gibbs or ensemble method of statistical thermodynamics.

18.1 The Ensemble Method

We recall from Section 3.2 that an ensemble is a mental collection of a huge number of identical systems, each of which replicates *macroscopically* the thermodynamic system under investigation. Because such replication occurs at the macroscopic and not at the microscopic level, every member of the ensemble may be associated with a possibly different *system quantum state*. In essence, the independent particles required for the Maxwell–Boltzmann method are replaced with independent systems for the ensemble method. As a result, when using the latter, we inherently retain independent events proffered for statistical analyses, while accounting for the intermolecular forces needed to model real gases and liquids. In so doing, we shift our focus from a consideration of particle quantum states to a consideration of system quantum states.

As discussed previously, the utility of the Gibbs method rests on two fundamental postulates of statistical thermodynamics. The *ergodic hypothesis* presumes that any thermodynamic property defined by taking a temporal average for a single system can be equivalently defined by an ensemble average over its replicated members. On this basis, all quantum states temporally accessible within a single system must be mirrored by the same number of representations within the formulated ensemble. The *principle of equal a priori probability*, on the other hand, presumes that various system quantum states are equally likely only for unperturbed thermodynamic conditions. For this reason, the imposed constraints used in the Maxwell–Boltzmann method are always those for an isolated system;

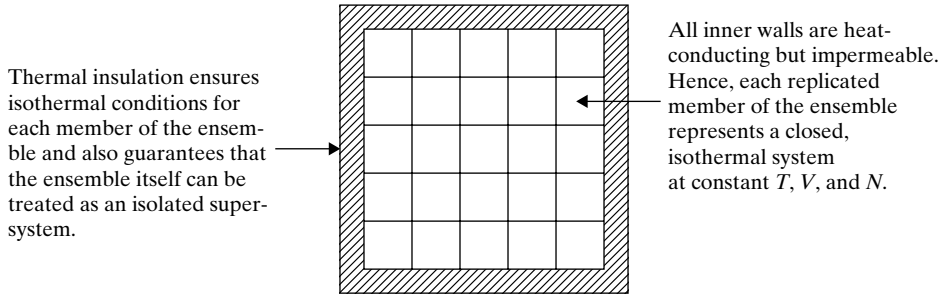

Figure 18.1 A representation of the canonical ensemble.

analogously, the imposed constraints for the Gibbs method must be those for an *isolated ensemble*. In other words, the ensemble itself must be isolated from its surroundings, so that no mass or energy crosses its boundary. This important feature will become clearer as we subsequently discuss the canonical and grand canonical ensembles.

18.2 The Canonical Ensemble

While a variety of ensembles are definable, depending on the type of replicated system, the so-called *canonical ensemble* proves to be the most pertinent for comparing with salient results established via the Maxwell–Boltzmann method of statistical thermodynamics. For this case, each member of the ensemble represents the same *closed, isothermal system*, as specified by an identical number of particles, volume, and temperature. Moreover, by implementing the canonical ensemble and imposing independent particles in the dilute limit, we can easily mimic our previous results for the ideal gas. Therefore, the canonical ensemble can be utilized to verify the Maxwell–Boltzmann method of statistical thermodynamics.

A schematic representation of the canonical ensemble is provided in Fig. 18.1. The number of displayed systems is, of course, miniscule as compared to that required to account for all system quantum states. Thermal insulation surrounds the entire ensemble and conductive, impermeable walls define each replicated system, thus ensuring constant T, V, and N for all members of the ensemble. Thermal insulation also guarantees that the ensemble itself can be modeled as an *isolated supersystem*, thus fulfilling a fundamental requirement for applying the principle of equal *a priori* probability. On this basis, suitable constraints on mass and energy for the ensemble can be represented by

$$\sum_i \eta_i = \eta \tag{18.1}$$

$$\sum_i \eta_i E_i = E, \tag{18.2}$$

where η_i is the number of members affiliated with the ith system quantum state, E_i indicates the energy associated with this quantum state, η is the total number of members within the ensemble, and E identifies the total energy of the isolated supersystem.

Analogous to the particle distribution over energy states for the Maxwell–Boltzmann method, the *system distribution* for the ensemble method is defined by specifying the number of members associated with each system quantum state. According to the principle

of equal *a priori* probability, any statistical operation providing this distribution is equally likely, as identifying system quantum states for every member of the ensemble is equivalent to specifying an overall quantum state for the isolated supersystem. To account for all possible system quantum states, η must, of course, approach infinity. Therefore, when counting over all available quantum states, the various eigenvalues, E_i, must inevitably be repeated many times when evaluating Eq. (18.2).

18.2.1 The Equilibrium Distribution for the Canonical Ensemble

If we imagine the kth possible system distribution for the canonical ensemble, designated as η_{ki}, we are immediately confronted with the reality that this explicit distribution can be achieved in many possible ways. In fact, because each member of the canonical ensemble represents a replicated *macroscopic* system, the number of ways that the kth distribution can be realized is given by the number of ways that η identical, *distinguishable* objects can be arranged into identifiable groups, each associated with a specific system quantum state, such that η_{ki} objects occupy the ith group. From Eq. (2.28), we thus find that the thermodynamic probability for the kth distribution becomes

$$W_k = \frac{\eta!}{\prod_i \eta_{ki}!}\,, \tag{18.3}$$

which, in retrospect, is actually a simpler statistical expression for this quantity as compared to those developed for indistinguishable particles when using the Maxwell–Boltzmann method of statistical thermodynamics.

Because the canonical ensemble is also an isolated supersystem, every ensemble quantum state is equally likely; thus, each way of obtaining the kth distribution must be given equal weight in performing ensemble averages. Consequently, the probability, P_i, that any given member of the ensemble is in its ith system quantum state can be determined by suitably averaging over all system distributions; i.e.,

$$P_i = \frac{\overline{\eta}_i}{\eta} = \frac{\sum_k W_k \eta_{ki}}{\eta \sum_k W_k}. \tag{18.4}$$

We recognize, of course, that this summation over all possible system distributions poses, in reality, an insurmountable task. Fortunately, as for the Maxwell–Boltzmann method, the thermodynamic probability for the most probable distribution is overwhelmingly huge as compared to that for all remaining distributions owing to the gigantic value of η. Therefore, Eq. (18.4) can be expressed more simply as

$$P_i = \frac{\eta_{i,mp}}{\eta},$$

where $\eta_{i,mp}$ identifies the number of members associated with the ith system quantum state for the most probable distribution of the canonical ensemble.

This most probable distribution can be found, as in Chapter 3, by first taking the natural logarithm of Eq. (18.3) and applying Stirling's formula (Appendix D.2) so that

$$\ln W_{mp} = \eta \ln \eta - \sum_i \eta_i \ln \eta_i\,, \tag{18.5}$$

where we have now identified, in anticipation, the most probable distribution. From Eqs. (18.1) and (18.2), the constraints in differential form for the isolated ensemble become

$$\sum_i d\eta_i = 0 \tag{18.6}$$

$$\sum_i E_i d\eta_i = 0\,. \tag{18.7}$$

Applying the method of Lagrange multipliers (Appendix D.1), we next differentiate Eq. (18.5) with respect to η_i while invoking Eqs. (18.6) and (18.7), thus obtaining

$$\sum_i (\ln \eta_i + \alpha + \beta E_i)\, d\eta_i = 0, \tag{18.8}$$

where α and β are appropriate Lagrange multipliers.

From Eq. (18.8), the most probable distribution for the systems making up the canonical ensemble can be expressed in terms of α and β as

$$\eta_i = e^{-\alpha} \exp(-\beta E_i). \tag{18.9}$$

Substituting Eq. (18.9) into Eq. (18.1), we have

$$\eta = e^{-\alpha} \sum_i \exp(-\beta E_i); \tag{18.10}$$

hence, eliminating $e^{-\alpha}$ between Eqs. (18.9) and (18.10), we obtain

$$\frac{\eta_i}{\eta} = \frac{\exp(-\beta E_i)}{Q}, \tag{18.11}$$

where the *canonical partition function* has been defined as

$$Q = \sum_i \exp(-\beta E_i). \tag{18.12}$$

Equation (18.11) represents the most probable distribution for the systems of the canonical ensemble, an expression which is clearly analogous to the equilibrium particle distribution previously identified when using the Maxwell–Boltzmann method of statistical thermodynamics.

18.2.2 Equilibrium Properties for the Canonical Ensemble

The thermodynamic properties describing a closed isothermal system can be obtained, following the Maxwell–Boltzmann method, by first deriving equilibrium expressions for the mean internal energy and mean entropy of the canonical ensemble. For the mean internal energy, we have from Eq. (18.2)

$$\overline{U} = \frac{E}{\eta} = \frac{1}{\eta} \sum_i \eta_i E_i. \tag{18.13}$$

If we substitute for the equilibrium distribution from Eq. (18.11), Eq. (18.13) becomes

$$\overline{U} = \frac{1}{Q} \sum_i E_i \exp(-\beta E_i). \tag{18.14}$$

However, from Eq. (18.12),

$$\left(\frac{\partial Q}{\partial \beta}\right)_{V,N} = -\sum_i E_i \exp(-\beta E_i)$$

as $E_i(V, N)$, so that the mean internal energy becomes, from Eq. (18.14),

$$\overline{U} = -\left(\frac{\partial \ln Q}{\partial \beta}\right)_{V,N}. \tag{18.15}$$

Considering next the mean entropy for the canonical ensemble, we have from Eq. (3.20)

$$\overline{S} = \frac{k}{\eta} \ln W_{mp} \tag{18.16}$$

so that, from Eqs. (18.5) and (18.11), we obtain

$$\overline{S} = k \ln \eta - \frac{k}{Q} \sum_i \exp(-\beta E_i) \ln\left(\frac{\eta}{Q} e^{-\beta E_i}\right) \tag{18.17}$$

for the most probable distribution. Equations (18.12) and (18.17) then yield

$$\overline{S} = k \ln \eta - k \ln\left(\frac{\eta}{Q}\right) + \frac{k\beta}{Q} \sum_i E_i \exp(-\beta E_i)$$

and thus, from Eq. (18.14), the mean entropy can be expressed as

$$\overline{S} = k \ln Q + k\beta \overline{U}. \tag{18.18}$$

Equations (18.15) and (18.18) provide desired expressions for the mean internal energy and entropy at thermodynamic equilibrium, but in terms of the unknown Lagrange multiplier, β. To identify β, we differentiate Eq. (18.18) with respect to $\overline{U}$ for this ensemble, thus obtaining

$$\left(\frac{\partial \overline{S}}{\partial \overline{U}}\right)_{V,N} = k\left(\frac{\partial \ln Q}{\partial \overline{U}}\right)_{V,N} + k\beta + k\overline{U}\left(\frac{\partial \beta}{\partial \overline{U}}\right)_{V,N},$$

so that, substituting for $\overline{U}$ from Eq. (18.15), we find that

$$\left(\frac{\partial \overline{S}}{\partial \overline{U}}\right)_{V,N} = k\beta. \tag{18.19}$$

However, from classical thermodynamics (Appendix F), the time-averaged values of entropy and internal energy are related by

$$\left(\frac{\partial \overline{S}}{\partial \overline{U}}\right)_{V,N} = \frac{1}{T}, \tag{18.20}$$

and thus, from Eqs. (18.19) and (18.20),

$$\beta = \frac{1}{kT}. \tag{18.21}$$

Equation (18.21) establishes the same inverse relation between β and T as derived previously (Section 3.6) from the Maxwell–Boltzmann method of statistical thermodynamics. This anticipated compatibility thus confirms that Eq. (18.21) represents an essential and universal relation linking microscopic and macroscopic thermodynamics.

Substituting, finally, Eq. (18.21) into Eq. (18.12), we have for the canonical partition function

$$Q = \sum_i \exp(-E_i/kT), \tag{18.22}$$

which implies that Q must be a function of T, V, and N. Similarly, substituting Eq. (18.21) into Eqs. (18.15) and (18.18), we can express the mean internal energy and entropy for the canonical ensemble as

$$\overline{U} = kT^2 \left(\frac{\partial \ln Q}{\partial T} \right)_{V,N} \tag{18.23}$$

$$\overline{S} = kT \left(\frac{\partial \ln Q}{\partial T} \right)_{V,N} + k \ln Q. \tag{18.24}$$

Therefore, the mean Helmholtz free energy becomes

$$\overline{A}(T, V, N) = \overline{U} - T\overline{S} = -kT \ln Q, \tag{18.25}$$

which confirms that Q is a function of T, V, and N. We thus find that the natural independent variables for both the canonical partition function and Helmholtz free energy are the temperature, volume, and number of particles in a molecular assembly. On this basis, Eq. (18.25) can be taken as the primary analytical connection between classical thermodynamics and the canonical ensemble. Similar fundamental expressions in terms of natural thermodynamic variables exist for all ensembles, as we will see later when we introduce the grand canonical ensemble.

All remaining thermodynamic variables can now be expressed in terms of the canonical partition function by invoking additional macroscopic relations from Appendix F. We may, for example, obtain for the mean pressure and chemical potential,

$$\overline{P} = -\left(\frac{\partial \overline{A}}{\partial V} \right)_{T,N} = kT \left(\frac{\partial \ln Q}{\partial V} \right)_{T,N} \tag{18.26}$$

$$\overline{\mu} = \left(\frac{\partial \overline{A}}{\partial N} \right)_{T,V} = -kT \left(\frac{\partial \ln Q}{\partial N} \right)_{T,V}. \tag{18.27}$$

Hence, based on Eqs. (18.23–18.27), we conclude that any thermodynamic property of interest can be determined from knowledge of the canonical partition function. Recall that an analogous conclusion was reached in Chapter 4 when using the Maxwell–Boltzmann method of statistical thermodynamics. In that case, any thermodynamic property could be evaluated for the ideal gas from knowledge of the molecular rather than the canonical partition function.

EXAMPLE 18.1

Demonstrate that the mean entropy for the canonical ensemble can be expressed as

$$\overline{S} = -k \sum_i P_i \ln P_i,$$

where P_i is the probability of the ith system quantum state at thermodynamic equilibrium.

Solution

The mean entropy at thermodynamic equilibrium for the canonical ensemble is provided by Eq. (18.16), where $\ln W_{mp}$ is given by Eq. (18.5) for the most probable distribution over system quantum states. Combining these two expressions, we obtain

$$\overline{S} = \frac{k}{\eta}\left(\eta \ln \eta - \sum_i \eta_i \ln \eta_i\right),$$

where η_i represents the number of members in the ith system quantum state at thermodynamic equilibrium. Employing Eq. (18.1), the mean entropy can also be expressed as

$$\overline{S} = -\left(\frac{k}{\eta}\right)\sum_i \eta_i \ln\left(\frac{\eta_i}{\eta}\right);$$

consequently,

$$\overline{S} = -k\sum_i \left(\frac{\eta_i}{\eta}\right)\ln\left(\frac{\eta_i}{\eta}\right).$$

The probability for the ith system quantum state is given by η_i / η, and thus we confirm that

$$\overline{S} = -k\sum_i P_i \ln P_i.$$

This expression for the mean entropy of the canonical ensemble is consistent with the Boltzmann definition of entropy and also with information theory, as discussed in Chapter 12. Therefore, appropriately understood, the Boltzmann definition of entropy can be applied to both independent and dependent particles.

18.2.3 Independent Particles in the Dilute Limit

Given the canonical ensemble, we can now analyze effectively various thermodynamic systems involving intermolecular forces, such as real gases and liquids. Nevertheless, this more robust approach should, of course, duplicate in the appropriate limit ideal gas relations previously derived via the Maxwell–Boltzmann method. We offer proof for this statement by initially considering an assembly composed of N identical, independent, and *distinguishable* particles. For this assembly, the energy corresponding to the ith system quantum state can be expressed as

$$E_i = \varepsilon_k + \varepsilon_l + \varepsilon_m \cdots, \tag{18.28}$$

where ε_k, for example, represents the energy affiliated with any permissible quantum state for the kth independent particle. On this basis, the canonical partition function for N distinguishable particles can be determined by substituting Eq. (18.28) into Eq. (18.22). Since the N identifiable terms in Eq. (18.28) can be associated with N different particles, we have

$$Q = \sum_k \exp(-\varepsilon_k/kT)\cdot\sum_l \exp(-\varepsilon_l/kT)\cdot\sum_m \exp(-\varepsilon_m/kT)\cdot\cdots$$

so that, from Eq. (4.13),

$$Q = Z^N \tag{18.29}$$

for N distinguishable particles.

While Eq. (18.29) may be appropriate for a crystalline solid, it is surely inappropriate for an ideal gas composed of N *indistinguishable* particles. Furthermore, for a dilute assembly, we recall from Section 5.7 that the number of particle quantum states is five orders of magnitude greater than the number of particles. In essence, then, each indistinguishable particle within the gaseous assembly represents a different particle quantum state. We thus find that $k \neq l \neq m \neq \ldots$ for all quantum states in Eq. (18.28), so that the resulting permutation of N different subscripts to generate an additional $N!$ states is actually irrelevant if the particles are indeed indistinguishable. Therefore, we have

$$Q = \frac{Z^N}{N!} \tag{18.30}$$

when dealing with indistinguishable particles in the dilute limit. In addition, we recall that the molecular partition function is $Z(T, V)$, so that we again find that Q is a function of T, V, and N. More importantly, Eq. (18.30) shows that the canonical partition function for a closed ideal gas assembly can be related directly to the molecular partition function for a single particle within that same assembly.

Equation (18.30) can now be used to relate the mean internal energy and entropy for the canonical ensemble to the molecular partition function. Presumably, the resulting expressions will be identical to those developed in Chapter 4 for the ideal gas. We begin by determining $\ln Q$ from Eq. (18.30), thus obtaining, after implementation of Stirling's approximation,

$$\ln Q = N \ln \left(\frac{Z}{N} \right) + N. \tag{18.31}$$

After substitution of Eq. (18.31) into Eq. (18.23), the mean internal energy becomes

$$\overline{U} = NkT^2 \left(\frac{\partial \ln Z}{\partial T} \right)_V, \tag{18.32}$$

which is identical to Eq. (4.21) for the case of independent particles in the dilute limit. Similarly, for the mean entropy, we have from Eq. (18.24)

$$\overline{S} = Nk \left[T \left(\frac{\partial \ln Z}{\partial T} \right)_V + \ln \left(\frac{Z}{N} \right) + 1 \right], \tag{18.33}$$

which is again identical to Eq. (4.23) for the ideal gas.

Based on this development, we conclude that all equilibrium thermodynamic properties for an ideal gas could have been derived by implementing the canonical ensemble. In other words, for independent particles, the Maxwell–Boltzmann method is equivalent to the ensemble method of statistical thermodynamics. Indeed, we note from Eq. (18.30) that $Q = Z$ when each member of the ensemble contains a single particle. For this unique scenario, each particle is confined to its own replicated system so that it cannot interact with other particles in the ensemble. Such particles are, by definition, independent and thus amenable to analysis via the Maxwell–Boltzmann method of statistical thermodynamics.

18.2.4 Fluctuations in Internal Energy

The standard deviation for a thermodynamic variable is an accepted statistical indicator of random fluctuations about its mean ensemble value. From our discussion of classical properties in Chapter 3, we expect such fluctuations to be miniscule at thermodynamic equilibrium. If we can demonstrate the veracity of this supposition, we will have the crucial evidence needed to finally prove that the most probable distribution is indeed the only *significant* distribution. Such proof is impossible when using the Maxwell–Boltzmann method, but can be pursued quite easily via the ensemble method of statistical thermodynamics. We now undertake this crucial proof, thus confirming the robustness of the Gibbs method as compared to the Maxwell–Boltzmann method of statistical thermodynamics.

Before beginning our analysis, we should recognize that, while property fluctuations generally occur within any thermodynamic assembly, they cannot be determined for those specific properties defining the natural variables of a particular ensemble. As an example, replications within the canonical ensemble are defined to be those for an isothermal, closed system; hence, the temperature, volume, and number of particles remain fixed for each member of the ensemble. Therefore, for this case, fluctuations in temperature, volume, or number of particles are inaccessible, but fluctuations can be evaluated for any remaining thermodynamic properties such as the entropy or pressure.

Specifically, for the canonical ensemble, it proves especially convenient to investigate fluctuations in internal energy, which can be defined via the standard deviation, σ_U, as

$$\sigma_U^2 = \langle U^2 \rangle - \langle U \rangle^2. \tag{18.34}$$

From Eqs. (18.14) and (18.21), the mean internal energy becomes

$$\langle U \rangle = \frac{1}{Q} \sum_i E_i \exp(-E_i/kT). \tag{18.35}$$

Similarly, the mean squared internal energy for the canonical ensemble is given by

$$\langle U^2 \rangle = \frac{1}{Q} \sum_i E_i^2 \exp(-E_i/kT). \tag{18.36}$$

If we then differentiate Eq. (18.35) with respect to temperature, we obtain

$$\left(\frac{\partial \overline{U}}{\partial T} \right)_{V,N} = \frac{1}{kT^2 Q} \sum_i E_i^2 \exp(-E_i/kT) - \frac{1}{Q} \left(\frac{\partial \ln Q}{\partial T} \right)_{V,N} \sum_i E_i \exp(-E_i/kT),$$

so that the mean specific heat becomes, from Eqs. (18.23), (18.35), and (18.36),

$$\overline{C}_v = \frac{\langle U^2 \rangle}{kT^2} - \frac{\langle U \rangle^2}{kT^2}. \tag{18.37}$$

Comparing Eqs. (18.34) and (18.37), we find that

$$\sigma_U^2 = kT^2 \overline{C}_v,$$

so that the *fractional fluctuation* in internal energy can be defined as

$$\frac{\sigma_U}{\overline{U}} = \frac{(kT^2 \overline{C}_v)^{1/2}}{\overline{U}}. \tag{18.38}$$

For independent particles in the dilute limit, we recall from Eqs. (4.21) and (4.33), respectively, that the mean internal energy scales with NkT and that the mean specific heat scales with Nk. Hence, the fractional fluctuation in internal energy for the ideal gas obeys

$$\frac{\sigma_U}{\bar{U}} \propto \frac{1}{\sqrt{N}}, \tag{18.39}$$

which portends remarkable behavior when applied to a typical ideal gas assembly. If, for example, $N = 10^{20}$, the fractional fluctuation in internal energy is only 10^{-10}. Given this astonishing outcome, we can safely presume that the most probable distribution is indeed the only significant distribution for the canonical ensemble. Therefore, the most probable distribution can be taken as defining all relevant properties at thermodynamic equilibrium.

Pictorially, we may assert that the range of possible particle distributions follows a Dirac delta function centered near the most probable distribution. From a different perspective, we find that $N = 1$ gives a standard deviation for the internal energy comparable to the internal energy itself, a result surely consistent with the Heisenberg uncertainty principle. Finally, further investigation shows that Eq. (18.39) holds universally for other thermodynamic properties and also for other ensembles. Therefore, we conclude that a sufficiently large number of particles, whether distinguishable or indistinguishable, guarantees well-defined equilibrium properties, namely, those possessing no measurable fluctuations and thus appearing essentially constant in time.

EXAMPLE 18.2

A crystalline solid can be modeled as an assembly of $3N$ identical, independent harmonic oscillators. The molecular partition function for each oscillator is given by

$$Z = \left(1 - e^{-\theta_E/T}\right)^{-1},$$

where θ_E is a relevant Einstein temperature.

(a) Determine the canonical partition function for this solid.
(b) Derive suitable relations for its internal energy and entropy.
(c) What is the chemical potential for this crystalline solid?
(d) Develop an expression for its fractional fluctuation in internal energy.

Solution

(a) The canonical partition function for $3N$ independent and distinguishable harmonic oscillators can be derived from Eq. (18.29), thus giving

$$Q = \left(1 - e^{-\theta_E/T}\right)^{-3N}.$$

(b) Using the above expression for the canonical partition function, we can determine the mean internal energy and entropy from

$$\ln Q = -3N \ln\left(1 - e^{-\theta_E/T}\right).$$

Substituting ln Q into Eqs. (18.23) and (18.24), we obtain

$$\overline{U} = 3Nk\left(\frac{\theta_E}{e^{\theta_E/T}-1}\right)$$

$$\overline{S} = 3Nk\left[\frac{\theta_E/T}{e^{\theta_E/T}-1} - \ln\left(1-e^{-\theta_E/T}\right)\right].$$

These relations duplicate Eqs. (13.16) and (13.19), which were previously derived from the Einstein theory for a crystalline solid and the Maxwell–Boltzmann method of statistical thermodynamics.

(c) The chemical potential can be determined from Eq. (18.27). Substituting again for ln Q, we obtain

$$\overline{\mu} = 3kT\ln\left(1-e^{-\theta_E/T}\right).$$

(d) The fractional fluctuation in internal energy, defined by Eq. (18.38), is

$$\frac{\sigma_U}{\overline{U}} = \frac{(kT^2\overline{C}_v)^{1/2}}{\overline{U}}.$$

The mean specific heat can be determined by suitable differentiation of the expression for mean internal energy, which gives

$$\overline{C}_v = \left(\frac{\partial\overline{U}}{\partial T}\right)_{V,N} = 3Nk\frac{(\theta_E/T)^2 e^{\theta_E/T}}{(e^{\theta_E/T}-1)^2}.$$

If we substitute for $\overline{C}_v$ and $\overline{U}$, the fractional fluctuation becomes

$$\frac{\sigma_U}{\overline{U}} = \frac{\exp(\theta_E/2T)}{\sqrt{3N}},$$

so that, analogously with the ideal gas, the fractional fluctuation in internal energy for the crystalline solid scales inversely with the square root of the number of independent harmonic oscillators.

18.3 The Grand Canonical Ensemble

We now proceed to a fully interactive thermodynamic system that can exchange both energy and mass with its surroundings. Because of this extra complication, the required mathematical maneuverings are more cumbersome; however, as we will see in Chapter 19, the final results ultimately prove advantageous when developing equations of state for real gases. Previously, we demonstrated that the canonical ensemble can be modeled as replicated isothermal systems separated by heat-conducting but impermeable walls. In comparison, for the *grand canonical ensemble*, the walls separating the replicated isothermal systems are heat-conducting *and* permeable so that both mass and energy can migrate among members of the ensemble. Therefore, while temperature and volume are still invariable, we no longer have a constant number of particles in each replicated system but instead equilibration of particle concentrations, as portrayed schematically in Fig. 18.2.

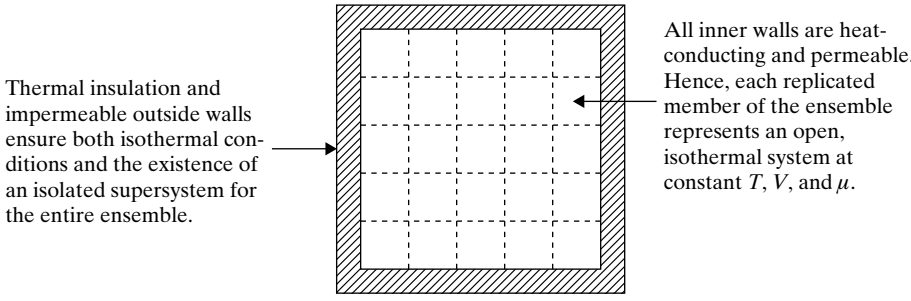

Figure 18.2 A representation of the grand canonical ensemble.

From classical thermodynamics (Appendix F), we recall that the chemical potential represents the driving force for species or phase equilibration in analogy with temperature as the driving force for thermal equilibration. Therefore, each member of the grand canonical ensemble must represent an open thermodynamic system at constant temperature, volume, and chemical potential. In other words, we have shifted from replication of a closed isothermal system for the canonical ensemble to replication of an open isothermal system for the grand canonical ensemble. Nevertheless, the overall ensemble, whether canonical or grand canonical, must still be modeled as an isolated supersystem to ensure consistency with the principle of equal *a priori* probability. On this basis, we continue requiring suitable constraints consistent with conservation of energy and mass for the entire ensemble.

The evolution of the grand canonical ensemble follows that of the canonical ensemble except that, for the former, each member is specified by both its number of particles and its system quantum state for that number of particles. Hence, constraints analogous to those defined by Eqs. (18.1) and (18.2) for the canonical case can be conveniently represented for the grand canonical ensemble as

$$\sum_N \sum_i \eta_{Ni} = \eta \tag{18.40}$$

$$\sum_N \sum_i \eta_{Ni} E_{Ni} = E, \tag{18.41}$$

where η_{Ni} is the number of members containing N particles and also identified with the ith system quantum state, E_{Ni} is the energy for a replicated system containing N particles in the ith system quantum state, η indicates the total number of members for the ensemble, and E identifies the total energy of the isolated supersystem. We note that, for Eqs. (18.40) and (18.41), N is always specified before i as the system quantum state depends on the value of N. Because the grand canonical ensemble replicates an open thermodynamic system, we clearly require an additional constraint for overall mass conservation, as given by

$$\sum_N \sum_i \eta_{Ni} N = \boldsymbol{N}, \tag{18.42}$$

where N indicates the number of particles affiliated with each member of the ensemble and $\boldsymbol{N}$ represents the total number of particles for the isolated supersystem.

18.3.1 The Equilibrium Distribution for the Grand Canonical Ensemble

The opportunity for any specific distribution of members within the grand canonical ensemble can be investigated in analogy with our previous statistical analysis for the canonical ensemble. In particular, we require the number of ways that η identical, distinguishable objects can be arranged such that η_{Ni} objects occupy the ith subgroup among those groups identified with N particles. Invoking Eq. (18.3), the number of ways of arriving at any given system distribution can be expressed as

$$W = \frac{\eta!}{\prod_N \prod_i \eta_{Ni}!}, \tag{18.43}$$

from which the most probable distribution can again be found by first taking the natural logarithm of Eq. (18.43) and applying Stirling's formula, thus obtaining

$$\ln W_{mp} = \eta \ln \eta - \sum_N \sum_i \eta_{Ni} \ln \eta_{Ni}. \tag{18.44}$$

Expressing Eqs. (18.40–18.42) in differential form, the three constraints for the grand canonical ensemble become

$$\sum_N \sum_i d\eta_{Ni} = 0 \tag{18.45}$$

$$\sum_N \sum_i E_{Ni}\, d\eta_{Ni} = 0 \tag{18.46}$$

$$\sum_N \sum_i N d\eta_{Ni} = 0. \tag{18.47}$$

Applying the method of Lagrange multipliers, we differentiate Eq. (18.44) with respect to η_{Ni} and subsequently introduce Eqs. (18.45–18.47) for an isolated supersystem, thereby getting

$$\sum_N \sum_i (\ln \eta_{Ni} + \alpha + \beta E_{Ni} - N \ln \lambda)\, d\eta_{Ni} = 0, \tag{18.48}$$

where α, β, and $\ln \lambda$ are chosen as convenient Lagrange multipliers. From Eq. (18.48), the most probable distribution for the systems of the grand canonical ensemble can thus be expressed as

$$\eta_{Ni} = e^{-\alpha} \lambda^N \exp(-\beta E_{Ni}). \tag{18.49}$$

Finally, substituting Eq. (18.49) into Eq. (18.40), we have

$$\eta = e^{-\alpha} \sum_N \sum_i \lambda^N \exp(-\beta E_{Ni}), \tag{18.50}$$

so that, eliminating $e^{-\alpha}$ between Eqs. (18.49) and (18.50), we obtain

$$\frac{\eta_{Ni}}{\eta} = \frac{\lambda^N \exp(-\beta E_{Ni})}{\Xi}, \tag{18.51}$$

where the *grand canonical partition function* has been defined as

$$\Xi = \sum_N \sum_i \lambda^N \exp(-\beta E_{Ni}). \tag{18.52}$$

Based on our previous insights, Eq. (18.51) represents the system distribution at thermodynamic equilibrium for the grand canonical ensemble. The additional multiplier, λ, as compared to the two usual multipliers for the canonical ensemble, arises from the requirement for mass conservation in an open system. We thus expect this parameter to be related to the chemical potential. This indeed turns out to be the case, as we will see in the next section; for this reason, λ is labeled the *absolute activity*.

18.3.2 Equilibrium Properties for the Grand Canonical Ensemble

The thermodynamic properties for the grand canonical ensemble can be determined, as for the canonical ensemble, by starting with expressions describing the mean internal energy and the mean entropy. For the mean internal energy, we have, analogously to Eq. (18.13),

$$\overline{U} = \frac{E}{\eta} = \frac{1}{\eta} \sum_N \sum_i \eta_{Ni} E_{Ni}. \tag{18.53}$$

After substitution for the equilibrium distribution from Eq. (18.51), Eq. (18.53) becomes

$$\overline{U} = \frac{1}{\Xi} \sum_N \sum_i \lambda^N E_{Ni} \exp(-\beta E_{Ni}); \tag{18.54}$$

however, from Eq. (18.52),

$$\left(\frac{\partial \Xi}{\partial \beta}\right)_{V,\lambda} = -\sum_N \sum_i \lambda^N E_{Ni} \exp(-\beta E_{Ni})$$

as $\Xi(V, \beta, \lambda)$. Therefore, from Eq. (18.54), the mean internal energy for the grand canonical ensemble becomes

$$\overline{U} = -\left(\frac{\partial \ln \Xi}{\partial \beta}\right)_{V,\lambda}. \tag{18.55}$$

As for a closed isothermal system, the mean entropy for an open isothermal system can once again be determined from Eq. (18.16). Substituting from Eqs. (18.44) and (18.51), we thus have for the most probable distribution,

$$\overline{S} = k \ln \eta - \frac{k}{\Xi} \sum_N \sum_i \lambda^N \exp(-\beta E_{Ni}) \ln\left(\frac{\eta \lambda^N}{\Xi} e^{-\beta E_{Ni}}\right). \tag{18.56}$$

Employing Eq. (18.52), we can rewrite Eq. (18.56) as

$$\overline{S} = k \ln \eta - k \ln\left(\frac{\eta}{\Xi}\right) - \frac{k \ln \lambda}{\Xi} \sum_N \sum_i \lambda^N N \exp(-\beta E_{Ni}) + \frac{k\beta}{\Xi} \sum_N \sum_i \lambda^N E_{Ni} \exp(-\beta E_{Ni})$$

and hence, from Eq. (18.54),

$$\overline{S} = k \ln \Xi - \frac{k \ln \lambda}{\Xi} \sum_N \sum_i \lambda^N N \exp(-\beta E_{Ni}) + k\beta \overline{U}. \tag{18.57}$$

We note, however, that the mean number of particles for the ensemble is

$$\overline{N} = \frac{1}{\eta} \sum_N \sum_i \eta_{Ni} N, \tag{18.58}$$

so that, from Eq. (18.51),

$$\overline{N} = \frac{1}{\Xi} \sum_N \sum_i \lambda^N N \exp\left(-\beta E_{Ni}\right). \tag{18.59}$$

Therefore, if we identify $\overline{N}$ from Eq. (18.59), Eq. (18.57) becomes

$$\overline{S} = k \ln \Xi - k\overline{N} \ln \lambda + k\beta \overline{U}, \tag{18.60}$$

which represents quite nicely the mean entropy for the grand canonical ensemble.

Proceeding as for the canonical ensemble, the Lagrange multiplier, β, can be determined by first differentiating Eq. (18.60) with respect to $\overline{U}$, thus obtaining

$$\left(\frac{\partial \overline{S}}{\partial \overline{U}}\right)_{V,N} = k\left(\frac{\partial \ln \Xi}{\partial \overline{U}}\right)_{V,N} - k\overline{N}\left(\frac{\partial \ln \lambda}{\partial \overline{U}}\right)_{V,N} + k\beta + k\overline{U}\left(\frac{\partial \beta}{\partial \overline{U}}\right)_{V,N}. \tag{18.61}$$

Differentiating Eq. (18.52) with respect to λ, we find from Eq. (18.59) that

$$\left(\frac{\partial \Xi}{\partial \lambda}\right)_{V,\beta} = \frac{1}{\lambda} \sum_N \sum_i \lambda^N N \exp(-\beta E_{Ni}) = \frac{\Xi \overline{N}}{\lambda},$$

as $E_{Ni}(V, N)$ is invariant for any N of the indicated summation; hence, upon rearrangement,

$$\overline{N} = \left(\frac{\partial \ln \Xi}{\partial \ln \lambda}\right)_{V,\beta}. \tag{18.62}$$

We now substitute for $\overline{U}$ and $\overline{N}$ from Eqs. (18.55) and (18.62), respectively, so that Eq. (18.61) becomes

$$\left(\frac{\partial \overline{S}}{\partial \overline{U}}\right)_{V,N} = k\beta + k\left(\frac{\partial \ln \Xi}{\partial \overline{U}}\right)_{V,N} - k\left(\frac{\partial \ln \Xi}{\partial \ln \lambda}\right)_{V,\beta}\left(\frac{\partial \ln \lambda}{\partial \overline{U}}\right)_{V,N} - k\left(\frac{\partial \ln \Xi}{\partial \beta}\right)_{V,\lambda}\left(\frac{\partial \beta}{\partial \overline{U}}\right)_{V,N}.$$

Therefore, using the chain rule for partial differentiation at constant volume, we obtain

$$\left(\frac{\partial \overline{S}}{\partial \overline{U}}\right)_{V,N} = k\beta$$

and so, from Eq. (18.20), we again find that

$$\beta = \frac{1}{kT}. \tag{18.63}$$

Substituting Eq. (18.63) into Eq. (18.52), we obtain, for the grand canonical partition function,

$$\Xi = \sum_N \sum_i \lambda^N \exp(-E_{Ni}/kT). \tag{18.64}$$

Similarly, substituting Eq. (18.63) into Eqs. (18.55) and (18.60), we can express the mean internal energy and entropy for the grand canonical ensemble as

$$\overline{U} = kT^2 \left(\frac{\partial \ln \Xi}{\partial T}\right)_{V,\lambda} \tag{18.65}$$

$$\overline{S} = kT\left(\frac{\partial \ln \Xi}{\partial T}\right)_{V,\lambda} - k\overline{N}\ln\lambda + k\ln\Xi. \tag{18.66}$$

Consequently, for the Helmholtz free energy, we have

$$\overline{A} = \overline{U} - T\overline{S} = \overline{N}kT\ln\lambda - kT\ln\Xi. \tag{18.67}$$

The chemical potential can now be obtained via classical thermodynamics (Appendix F) by differentiation of Eq. (18.67):

$$\mu = \left(\frac{\partial \overline{A}}{\partial \overline{N}}\right)_{V,T} = kT\ln\lambda + \overline{N}kT\left(\frac{\partial \ln\lambda}{\partial \overline{N}}\right)_{V,T} - kT\left(\frac{\partial \ln\Xi}{\partial \overline{N}}\right)_{V,T}. \tag{18.68}$$

Substituting for $\overline{N}$ via Eq. (18.62), we may express Eq. (18.68) as

$$\mu = kT\ln\lambda, \tag{18.69}$$

so that, as expected from our previous development, the absolute activity can be related to the chemical potential, which is, of course, a specified independent variable for the grand canonical ensemble. In fact, given that the grand canonical ensemble embodies replicated systems at constant T, V, and μ, we note that the partial derivatives in Eqs. (18.65) and (18.66) might more properly be evaluated at constant volume and chemical potential rather than at constant volume and absolute activity.

Finally, from classical thermodynamics (Appendix F), we recall that

$$\overline{P}V = \overline{G} - \overline{A} = \overline{N}\mu - \overline{A}. \tag{18.70}$$

Hence, after substitution from Eqs. (18.67) and (18.69), Eq. (18.70) becomes

$$\overline{P}V = kT\ln\Xi, \tag{18.71}$$

which is the fundamental relation for the grand canonical ensemble. The significance of this relation can be understood by first differentiating Eq. (18.70), thus giving

$$d(\overline{P}V) = \overline{N}\,d\mu + \mu\,d\overline{N} - d\overline{A}. \tag{18.72}$$

From classical thermodynamics (Appendix F),

$$d\overline{A} = -\overline{P}\,dV - \overline{S}\,dT + \mu\,d\overline{N},$$

so that Eq. (18.72) can then be expressed as

$$d(\overline{P}V) = \overline{S}\,dT + \overline{P}\,dV + \overline{N}\,d\mu. \tag{18.73}$$

Given Eq. (18.73), we find from classical thermodynamics that the natural independent variables for $\overline{P}V$ are temperature, volume, and chemical potential, which is in agreement with the independent thermodynamic properties specified for the grand canonical partition function. While this link can be verified through Eq. (18.71), a more utilitarian role for this same expression is the generation of equations of state for real gases, as exploited in Chapter 19.

18.3.3 Independent Particles in the Dilute Limit Revisited

We now reconsider the ideal gas assembly, with a focus on demonstrating equivalent thermodynamic properties based on the canonical and grand canonical ensembles. Utilizing Eq. (18.64), we may write

$$\Xi = \sum_N \lambda^N \sum_i \exp(-E_{Ni}/kT);$$

hence, substituting from Eq. (18.22) for any given number of particles, N, we obtain

$$\Xi = \sum_N \lambda^N Q(T, V, N). \tag{18.74}$$

Equation (18.74) provides a general relation between the grand canonical and canonical partition functions. For the special case of independent particles in the dilute limit, the canonical partition function can, in turn, be related to the molecular partition function by implementing Eq. (18.30). On this basis, Eq. (18.74) becomes

$$\Xi = \sum_N \frac{(\lambda Z)^N}{N!},$$

which can be expressed more succinctly as

$$\Xi = \exp(\lambda Z). \tag{18.75}$$

Equation (18.75) conveniently casts the grand canonical partition function in terms of the molecular partition function for a system of independent particles in the dilute limit. Given this expression, we next determine the mean internal energy and mean entropy for an ideal gas assembly using the grand canonical ensemble.

In preparation for determining $\overline{U}$ and $\overline{S}$, we first rewrite Eq. (18.62) as

$$\overline{N} = \lambda \left(\frac{\partial \ln \Xi}{\partial \lambda} \right)_{T,V}, \tag{18.76}$$

so that, from both Eqs. (18.75) and (18.76), we obtain

$$\ln \Xi = \overline{N} = \lambda Z. \tag{18.77}$$

Hence, for the ideal gas, $\ln \Xi$ leads directly to the mean number of particles in the grand canonical ensemble. On this basis, the mean internal energy becomes, from Eq. (18.65),

$$\overline{U} = kT^2 \lambda \left(\frac{\partial Z}{\partial T} \right)_V,$$

so that, reusing Eq. (18.77), we find that $\overline{U}$ in the dilute limit for the grand canonical ensemble becomes

$$\overline{U} = \overline{N} kT^2 \left(\frac{\partial \ln Z}{\partial T} \right)_V, \tag{18.78}$$

which is in agreement with Eq. (18.32) for the ideal gas assembly.

Similarly, for the mean entropy, Eq. (18.66) can be written as

$$\overline{S} = \overline{N} kT \left(\frac{\partial \ln Z}{\partial T} \right)_V - \overline{N} k \ln \lambda + k \ln \Xi.$$

Substituting once again from Eq. (18.77), we obtain

$$\overline{S} = \overline{N}k\left[T\left(\frac{\partial \ln Z}{\partial T}\right)_V + \ln\left(\frac{Z}{\overline{N}}\right) + 1\right], \tag{18.79}$$

which is in agreement with Eq. (18.33) for the ideal gas assembly. Therefore, whether we employ the canonical or the grand canonical ensemble, we derive the same results for $\overline{U}$ and $\overline{S}$ in terms of the molecular partition function. While this feature has been demonstrated here for the internal energy and entropy of an ideal gas, the same conclusion holds for any other thermodynamic property and for any ensemble. In other words, from the viewpoint of statistical thermodynamics, we may assert that all ensembles are equivalent with respect to the calculation of thermodynamic properties.

Finally, from Eqs. (18.71) and (18.77), we also find that

$$\overline{P}V = \overline{N}kT, \tag{18.80}$$

which is the expected equation of state for independent particles in the dilute limit. While Eq. (18.80) is certainly unsurprising at this juncture, the crucial inference is that robust equations of state for systems containing dependent particles could equivalently be derived from Eq. (18.71) given knowledge of $\ln \Xi$. This important conclusion paves the path for determining the thermodynamic properties of real gases, as pursued in Chapter 19.

EXAMPLE 18.3

A hypothetical system contains an assembly of N identical, independent harmonic oscillators. The oscillators are indistinguishable with a molecular partition function for each oscillator given by

$$Z = \left(1 - e^{-\theta_v/T}\right)^{-1},$$

where θ_v is a characteristic vibrational temperature.

(a) Determine the absolute activity for this hypothetical assembly.
(b) Using part (a), develop an expression for the mean internal energy of the system.

Solution

(a) For N independent and indistinguishable harmonic oscillators, the absolute activity can be determined directly from Eq. (18.77). On this basis, we find that

$$\lambda = \frac{N}{Z} = N\left(1 - e^{-\theta_v/T}\right).$$

(b) Employing the grand canonical ensemble, we can find the mean internal energy by using Eqs. (18.65) and (18.77). The resulting expression becomes

$$\overline{U} = kT^2\left(\frac{\partial \ln \Xi}{\partial T}\right)_{V,\lambda} = kT^2\lambda\left(\frac{\partial Z}{\partial T}\right)_V.$$

Performing the required differentiation via the given molecular partition function, we obtain

$$\left(\frac{\partial Z}{\partial T}\right)_V = \frac{\theta_v \exp(-\theta_v/T)}{T^2\left(1 - e^{-\theta_v/T}\right)^2}.$$

Substituting for the absolute activity from part (a) and employing the above partial derivative, we may write our previous expression for the mean internal energy as

$$\overline{U} = Nk\left(\frac{\theta_v}{e^{\theta_v/T} - 1}\right),$$

which is essentially equivalent to Eq. (9.48). This result should have been expected based on the vibrational contribution to the internal energy of a diatomic gas from an assembly of N harmonic oscillators.

Problems enhancing your understanding of this chapter are combined with those for Chapter 19 in Problem Set VIII.

19 Applications of Ensemble Theory to Real Gases

As indicated in Chapter 18, ensemble theory is especially germane when calculating thermodynamic properties for systems composed of dependent rather than independent particles. Potential applications include real gases, liquids, and polymers. In this chapter, we focus on the thermodynamic properties of nonideal gases. Our overall approach is to develop an equation of state using the grand canonical ensemble. From classical thermodynamics, equilibrium properties can always be determined by suitably operating on such equations of state. As shown later in this chapter, typical evaluations require an accurate model for the intermolecular forces underlying any macroscopic assembly. This requirement is endemic to all applications of ensemble theory, including those for liquids and polymers. As a matter of fact, by mastering the upcoming procedures necessary for the statistics of real gases, you should be prepared for many pertinent applications to other tightly-coupled thermodynamic systems.

19.1 The Behavior of Real Gases

As the density of a gas rises, its constituent particles interact more vigorously so that their characteristic intermolecular potential exercises a greater influence on macroscopic behavior. Accordingly, the gas becomes less ideal and more real; i.e., its particles eventually display greater contingency owing to enhanced intermolecular forces. This deviation from ideal behavior is reflected through a more complicated equation of state for real gases.

An equation of state, you recall, describes a functional relation among the pressure, specific volume, and temperature of a given substance. For a real gas, perhaps the most fundamental such relation is the so-called *virial equation of state*, as given by

$$\frac{Pv}{RT} = 1 + \frac{B(T)}{v} + \frac{C(T)}{v^2} + \cdots, \tag{19.1}$$

where Pv/RT is the *compressibility factor*, v denotes the molar specific volume, $B(T)$ is the second virial coefficient, and $C(T)$ the third virial coefficient. According to Eq. (19.1), the various virial coefficients depend only on the temperature and identity of a particular gas. Hence, for a specified temperature and substance, plotting $(Pv/RT - 1)$ vs. $1/v$ for a suitable range of specific volumes permits evaluation of $B(T)$ and $C(T)$ from the resulting intercept and slope, respectively. Ideal gas behavior, of course, occurs

when the compressibility factor is unity, that is, when all virial coefficients are negligible. From classical thermodynamics, we know that such behavior occurs preferentially at low pressures and high temperatures.

In the remainder of this chapter, we will be concerned with those statistical procedures needed to derive thermodynamic expressions for the second and third virial coefficients. As indicated previously, such derivations require information on the intermolecular potential for real gases. Utilizing the Lennard–Jones potential, we find that predicted values for the second virial coefficient compare well with thermodynamic data. Similar comparisons for the third virial coefficient are reasonable but certainly less satisfactory. For this reason, we will focus on the second virial coefficient in our upcoming statistical analyses.

Typically, including $B(T)$ in Eq. (19.1) accounts for deviations from ideal gas behavior up to about 10 bar near room temperature. Similarly, $C(T)$ must be included to deal with pressures up to about 100 bar. Higher virial coefficients must, of course, be considered to account for even greater pressures. Regardless of pressure, however, we recall from classical thermodynamics that the compressibility factor is almost universally invoked to model real gas behavior. Therefore, our goal is to determine Pv/RT by utilizing the methods of statistical thermodynamics. Because Eq. (19.1) represents a dimensionless correlation, we also note that the compressibility factor can be taken to define both classically and statistically the *principle of corresponding states*.

19.2 Equation of State for Real Gases

The theoretical formulation of an equation of state from statistical thermodynamics is best established using the grand canonical rather than the canonical partition function. According to Eq. (18.71), when employing the former, the compressibility factor may be evaluated directly from $\ln \Xi$. In contrast, from Eq. (18.26), determining the compressibility factor when using the latter requires partial differentiation of $\ln Q$ with respect to volume. Therefore, eschewing any additional complexity, we obtain from Eqs. (18.71) and (18.74)

$$\frac{PV}{kT} = \ln\left[\sum_{N=0}^{\infty} \lambda^N Q(T, V, N)\right], \tag{19.2}$$

where, for convenience, all over bars denoting mean ensemble values are henceforth eliminated in recognition of their ultimate identification with classical thermodynamic properties.

Despite beginning with the grand canonical ensemble, we recognize that any equation of state vindicated through Eq. (19.2) requires evaluation of the canonical partition function. From Eq. (18.30), the canonical partition function for independent particles in the dilute limit is

$$Q = \frac{Z^N}{N!}, \tag{19.3}$$

so that $Q(T, V, N)$ must be unity for $N = 0$. Hence, at this point, we can rewrite Eq. (19.2) as

$$\frac{PV}{kT} = \ln\left[1 + \sum_{N=1}^{\infty} \lambda^N Q(T, V, N)\right]. \tag{19.4}$$

Further progress mandates that we properly account for intermolecular forces when mathematically describing the canonical partition function.

19.2.1 Canonical Partition Function for Real Gases

Given a thermodynamic system composed of identifiable but interacting particles, the system energy associated with the *i*th system quantum state can be expressed as

$$E_i(T, V, N) = E_i^* + \Phi\left(\boldsymbol{r}_1, \boldsymbol{r}_2, \ldots \boldsymbol{r}_N\right), \tag{19.5}$$

where E_i^* denotes the corresponding energy for a hypothetical assembly of independent particles and $\Phi(\boldsymbol{r}_1, \boldsymbol{r}_2, \ldots \boldsymbol{r}_N)$ defines the *configuration energy*, which corrects E_i^* for nonideality based on the location of all N particles in the macroscopic assembly. For simplicity, we assume that the configuration energy is essentially unaffected by secondary influences arising from particle orientation. Hence, our overall approach works best for nonpolar species, although it has often been used with good success for moderately polar molecules.

If we now substitute Eq. (19.5) into Eq. (18.22), the canonical partition function becomes

$$Q(T, V, N) = \sum_i \exp(-E_i^*/kT) \cdot \frac{1}{V^N} \iint \cdots \int e^{-\Phi/kT} d\boldsymbol{r}_1 \, d\boldsymbol{r}_2 \ldots d\boldsymbol{r}_N, \tag{19.6}$$

where the volumetric integration conforms with the configuration energy, which is a continuous function of all particle positions. Indeed, for this reason, the configuration factor in Eq. (19.6) can be conveniently evaluated by integrating over each particle location rather than by summing over each particle quantum state. This procedure is analogous to that employed for evaluation of the phase integral, as discussed in Section 8.5.

By definition, ideal gases are unperturbed by molecular interactions; hence, the summation factor in Eq. (19.6) must represent the canonical partition function for an assembly of independent particles in the dilute limit. On this basis, we obtain from Eqs. (19.3) and (19.6)

$$Q(T, V, N) = \frac{Z^N}{N!} \left(\frac{Q_N}{V^N} \right), \tag{19.7}$$

where the *configuration integral* has been defined for convenience as

$$Q_N = \iint \cdots \int \exp\left[-\frac{\Phi(\boldsymbol{r}_1, \boldsymbol{r}_2, \ldots, \boldsymbol{r}_N)}{kT} \right] d\boldsymbol{r}_1 d\boldsymbol{r}_2 \ldots d\boldsymbol{r}_N. \tag{19.8}$$

Because Eq. (19.8) embodies a classical evaluation, we have inherently neglected quantum effects, which prove to be significant for very light species, such as He and H_2. Accordingly, for these two gases, we require a direct summation beginning with Eq. (18.22). In all other cases, we find from Eqs. (19.7) and (19.8) that, when the configuration energy approaches zero, $Q_N = V^N$, so that the canonical partition function becomes, as expected, that for the ideal gas.

19.2.2 The Virial Equation of State

Returning now to our equation of state for real gases, we obtain, after substituting Eq. (19.7) into Eq. (19.4),

$$\frac{PV}{kT} = \ln\left[1 + \sum_{N=1}^{\infty}\left(\frac{Q_N}{N!}\right)z^N\right], \tag{19.9}$$

where, for convenience, we have defined

$$z \equiv \frac{\lambda Z}{V}, \tag{19.10}$$

with Z as the usual molecular partition function for the hypothetical ideal gas assembly. Combining Eqs. (18.77) and (19.10), we find that $z = N/V$ for independent particles in the dilute limit, so that the expansion parameter, z, represents particle number density for the ideal gas. Hence, we should anticipate an eventual expansion of Eq. (19.9) in terms of particle number density for real as well as for ideal gases.

Employing the usual logarithmic series, $\ln(1+x) \simeq x - x^2/2 + x^3/3 - \cdots$, we find that Eq. (19.9) becomes, after some rather tedious algebra,

$$\frac{PV}{kT} = Q_1 z + \frac{1}{2!}\left(Q_2 - Q_1^2\right)z^2 + \frac{1}{3!}\left(Q_3 - 3Q_1Q_2 + 2Q_1^3\right)z^3 + \cdots. \tag{19.11}$$

If we now invoke an expansion in particle number density of the form

$$\frac{P}{kT} = \sum_{\ell=1}^{\infty} b_\ell z^\ell, \tag{19.12}$$

a term-by-term comparison between Eqs. (19.11) and (19.12) gives

$$b_1 = \frac{Q_1}{V} = 1 \tag{19.13}$$

$$b_2 = \frac{Q_2 - Q_1^2}{2!V} \tag{19.14}$$

$$b_3 = \frac{Q_3 - 3Q_1Q_2 + 2Q_1^3}{3!V}. \tag{19.15}$$

Because of their connection to various configuration integrals through Eqs. (19.13–19.15), the coefficients, b_ℓ, in Eq. (19.12) are known as *cluster integrals*. We note, from Eq. (19.14), that determination of b_2 requires the evaluation of configuration integrals for at most two particles. Similarly, from Eq. (19.15), determination of b_3 involves configuration integrals for at most three particles. Hence, at moderate densities, we have effectively separated our original N-particle problem to one involving a series of one-, two-, or three-body problems!

Further evolution toward a virial equation of state requires that Eq. (19.12) be expressed in terms of the number density for a real gas rather than the parameter, z, which represents number density for an ideal gas. This process can be initiated by using Eq. (18.76), thus expressing the actual number density as

$$n = \frac{N}{V} = \frac{\lambda}{V}\left(\frac{\partial \ln \Xi}{\partial \lambda}\right)_{T,V}. \tag{19.16}$$

Recalling that $Z(T, V)$, we may eliminate λ from Eq. (19.16) by implementing Eq. (19.10); hence,

$$n = \frac{z}{V}\left(\frac{\partial \ln \Xi}{\partial z}\right)_{T,V},$$

whereupon, substituting for $\ln \Xi$ from Eq. (18.71), we find that

$$n = \frac{z}{kT}\left(\frac{\partial P}{\partial z}\right)_{T,V}. \tag{19.17}$$

Finally, substituting for the pressure from Eq. (19.12), Eq. (19.17) can be written as

$$n = \sum_{\ell=1}^{\infty} \ell b_\ell z^\ell, \tag{19.18}$$

which constitutes, in essence, a series for the number density of a real gas in terms of that corresponding to the ideal gas.

For our purposes, we next invert the series represented by Eq. (19.18), so that

$$z = \sum_{\ell=1}^{\infty} a_\ell n^\ell. \tag{19.19}$$

This inversion process can be accomplished by simply substituting Eq. (19.19) into Eq. (19.18), thus eventually obtaining

$$n = a_1 b_1 n + \left(a_2 b_1 + 2a_1^2 b_2\right) n^2 + \left(a_3 b_1 + 4a_1 a_2 b_2 + 3a_1^3 b_3\right) n^3 + \cdots,$$

from which we find, to third order,

$$\begin{aligned} a_1 b_1 &= 1 \\ a_2 b_1 + 2a_1^2 b_2 &= 0 \\ a_3 b_1 + 4a_1 a_2 b_2 + 3a_1^3 b_3 &= 0. \end{aligned}$$

Beginning with Eq. (19.13), we may solve the above expressions sequentially to determine the unknown coefficients of Eq. (19.19) in terms of cluster integrals. The result is

$$\begin{aligned} a_1 &= 1 \\ a_2 &= -2b_2 \\ a_3 &= 8b_2^2 - 3b_3. \end{aligned}$$

Consequently, from Eq. (19.19), the inverted series becomes, to third order,

$$z = n - 2b_2 n^2 + \left(8b_2^2 - 3b_3\right) n^3 + \cdots. \tag{19.20}$$

Our penultimate step requires substitution of Eq. (19.20) into Eq. (19.12), thus obtaining, after some additional algebra,

$$\frac{P}{kT} = n - b_2 n^2 + \left(4b_2^2 - 2b_3\right) n^3 + \cdots. \tag{19.21}$$

We then convert from number density to molar specific volume, v, by recognizing that

$$n = \frac{N_A}{v}. \tag{19.22}$$

Substituting Eq. (19.22) into Eq. (19.21), we have to third order

$$\frac{Pv}{RT} = 1 - b_2\left(\frac{N_A}{v}\right) + \left(4b_2^2 - 2b_3\right)\left(\frac{N_A}{v}\right)^2 + \cdots, \tag{19.23}$$

which is our long-sought virial equation of state. Finally, comparing Eq. (19.23) with Eq. (19.1), we find that the second and third virial coefficients can be expressed in terms of cluster integrals as

$$B(T) = -b_2 N_A \tag{19.24}$$

$$C(T) = \left(4b_2^2 - 2b_3\right) N_A^2. \tag{19.25}$$

Linking Eqs. (19.14) and (19.24), we observe that the second virial coefficient requires information on only the first two configuration integrals. Similarly, from Eqs. (19.15) and (19.25), we find that the third virial coefficient demands, in addition, the third configuration integral. Hence, the second virial coefficient can be associated exclusively with binary collisions, while the third virial coefficient includes both binary and tertiary collisions. From a different perspective, we have shown that the virial equation of state rests solely on two-particle interactions at lower densities, but must account for three-particle interactions at moderate densities. Greater densities could, of course, be handled by expanding Eq. (19.23) in terms of higher virial coefficients.

19.3 The Second Virial Coefficient

We now focus our attention on the second virial coefficient, which, according to Eq. (19.24), is defined in terms of the second cluster integral, b_2. Given this relation, Eq. (19.14) further demonstrates that evaluation of $B(T)$ requires both the first and second configuration integrals, Q_1 and Q_2. From Eq. (19.8), the first configuration integral is simply

$$Q_1 = \int_V d\boldsymbol{r}_1 = V. \tag{19.26}$$

Given a central intermolecular potential, $\phi(r_{12})$, that depends solely on the separation distance between any two particles, r_{12}, the configuration energy $\Phi(\boldsymbol{r}_1, \boldsymbol{r}_2)$ obviously becomes $\phi(r_{12})$. Hence, once again using Eq. (19.8), we can represent the second configuration integral by

$$Q_2 = \iint_V \exp\left[-\frac{\phi(r_{12})}{kT}\right] d\boldsymbol{r}_1\, d\boldsymbol{r}_2. \tag{19.27}$$

Upon substitution of Eqs. (19.26) and (19.27) into Eq. (19.14), the required second cluster integral may thus be expressed as

$$b_2 = \frac{1}{2V}\iint_V \left[e^{-\phi(r_{12})/kT} - 1\right] d\boldsymbol{r}_1\, d\boldsymbol{r}_2. \tag{19.28}$$

For convenience, we now introduce the so-called *Mayer cluster function*,

$$f_{ij} = e^{-\phi(r_{ij})/kT} - 1, \tag{19.29}$$

so that Eq. (19.28) becomes

$$b_2 = \frac{1}{2V} \iint_V f_{12}\, d\boldsymbol{r}_1\, d\boldsymbol{r}_2. \tag{19.30}$$

Converting to relative coordinates in a manner similar to that used in Section 16.1, we find that Eq. (19.30) can be written as

$$b_2 = \frac{1}{2V} \int_V d\boldsymbol{r}_c \int_V f_{12}\, d\boldsymbol{r}_{12}, \tag{19.31}$$

where the first integration occurs with respect to the center of mass and the second with respect to the relative distance between any two particles. The first integration can be evaluated as in Eq. (19.26); hence, from Eq. (19.31), our simplified expression for the second cluster integral becomes

$$b_2 = \frac{1}{2} \int_V f_{12}\, d\boldsymbol{r}_{12}, \tag{19.32}$$

and thus, from Eq. (19.24), the second virial coefficient can be expressed quite succinctly as

$$B(T) = -\frac{N_A}{2} \int_V f_{12}\, d\boldsymbol{r}_{12}. \tag{19.33}$$

For practical calculations, we typically favor the intermolecular potential, $\phi(r_{12})$, rather than the Mayer cluster function, f_{12}. Therefore, substituting from Eq. (19.29), Eq. (19.33) becomes

$$B(T) = \frac{N_A}{2} \int_V \left[1 - e^{-\phi(\boldsymbol{r}_{12})/kT}\right] d\boldsymbol{r}_{12}. \tag{19.34}$$

Finally, given that $d\boldsymbol{r}_{12} = 4\pi r^2 dr$, the second virial coefficient may be rewritten in a more convenient fashion as

$$B(T) = 2\pi N_A \int_0^\infty \left[1 - e^{-\phi(r)/kT}\right] r^2 dr, \tag{19.35}$$

where integration to infinity is permitted as the intermolecular potential drops to zero for r-values greater than a few molecular diameters. In general, the second virial coefficient can be easily derived from Eq. (19.35) given a suitable model for $\phi(r)$. Alternatively, information on the intermolecular potential can be developed from experimental measurements of $B(T)$.

Typically, as shown schematically in Fig. 19.1, $B(T)$ is negative at lower temperatures owing to attractive forces, becomes positive with rising temperature because of repulsive forces, then flattens out while dropping slowly toward zero at significantly higher temperatures. In the following subsections, we determine the second virial coefficient based on three different models for the intermolecular potential. As might be expected, we find better agreement with experiment for those potentials displaying both an attractive and repulsive component.

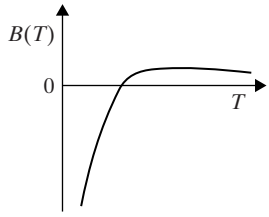

Figure 19.1 Effect of temperature on $B(T)$ behavior.

19.3.1 Rigid-Sphere and Square-Well Potentials

A cornerstone of simplified kinetic theory is the rigid-sphere potential, which can be easily represented by

$$\phi(r) = \begin{cases} \infty & r \leq \sigma \\ 0 & r > \sigma \end{cases},$$

where σ is an appropriate radius for the chosen atom or molecule. In this billiard-ball case, we have an infinitely repulsive potential at $r \leq \sigma$ and no attractive potential for $r > \sigma$. Consequently, from Eq. (19.35), we obtain for the second virial coefficient

$$B(T) = 2\pi N_A \int_0^\sigma r^2 dr = \frac{2\pi}{3} N_A \sigma^3, \tag{19.36}$$

which is usually designated as

$$b_\circ = \frac{2\pi}{3} N_A \sigma^3 \tag{19.37}$$

because of its universal appearance in virial-coefficient expressions, even those affiliated with more rigorous intermolecular potentials. In general, the second virial coefficient is inherently a function of temperature; here, however, $B(T)$ is simply a nonzero constant owing to the infinitely repulsive nature of the rigid-sphere potential. Guided by Fig. 19.1, we thus conclude that the rigid-sphere model should only be used for gases at very high temperatures.

As compared to the rigid-sphere potential, the square-well potential amplifies on the former by including a negative trough; hence, this model duplicates quite nicely experimental behavior for the second virial coefficient. Figure 19.2 illustrates the square-well potential, which can be represented mathematically by

$$\phi(r) = \begin{cases} \infty & r \leq \sigma \\ -\varepsilon & \sigma < r \leq \lambda\sigma \\ 0 & r > \lambda\sigma. \end{cases}$$

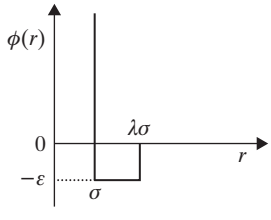

Figure 19.2 Schematic of the square-well potential.

As for the Lennard–Jones model, the negative well for this potential simulates attractive behavior. For this case, Eq. (19.35) gives

$$B(T) = 2\pi N_A \left\{ \int_0^{\sigma} r^2 dr + \int_{\sigma}^{\lambda\sigma} (1 - e^{\varepsilon/kT}) r^2 dr \right\},$$

which becomes

$$B(T) = b_\circ \left[1 - (\lambda^3 - 1)(e^{\varepsilon/kT} - 1) \right]. \tag{19.38}$$

In contrast to Eq. (19.36), Eq. (19.38) displays a clear dependence on temperature, as expected for the second virial coefficient. This temperature dependence reflects the combined attractive and repulsive components of the square-well potential.

Remarkably enough, the second virial coefficient for the square-well case is actually in good accord with the typical behavior shown in Fig. 19.1. At lower temperatures, the second term in Eq. (19.38) ensures that $B(T)$ takes on large negative values; thus, from Eq. (19.1), the pressure is less than that for an ideal gas at the same density and temperature. This behavior reflects the influence of weak but long-range attractive forces at lower temperatures, which would muster particles and thus reduce the pressure. In comparison, at higher temperatures, the second term in Eq. (19.38) approaches zero so that the billiard-ball component of the square-well potential overcomes its attractive component. As a result, $B(T)$ approaches $b_\circ$ so that at sufficiently high temperatures the gas behaves like one displaying a simple hard-sphere potential. For such conditions, the pressure, from Eq. (19.1), would be greater than that for an ideal gas at the same density and temperature. Unfortunately, this behavior departs somewhat from that shown in Fig. 19.1, thus posing a significant limitation for the square-well potential at extremely high temperatures.

19.3.2 Implementation of Lennard–Jones Potential

As discussed in Section 16.3, a more realistic potential having both attractive and repulsive components is the Lennard–Jones 6–12 potential, given by

$$\phi(r) = 4\varepsilon \left[\left(\frac{\sigma}{r} \right)^{12} - \left(\frac{\sigma}{r} \right)^{6} \right], \tag{19.39}$$

where the positive and negative terms model strong repulsive and weak attractive forces, respectively, as suggested in part from quantum mechanical perturbation theory. The functional form manifested by Eq. (19.39) can be represented generically by

$$\phi(r) = \varepsilon f(r/\sigma),$$

from which, using Eq. (19.35), we find that the second virial coefficient can be expressed as

$$B(T) = 2\pi N_A \int_0^{\infty} \left\{ 1 - \exp\left[-\left(\frac{\varepsilon}{kT} \right) \cdot f\left(\frac{r}{\sigma} \right) \right] \right\} r^2 dr. \tag{19.40}$$

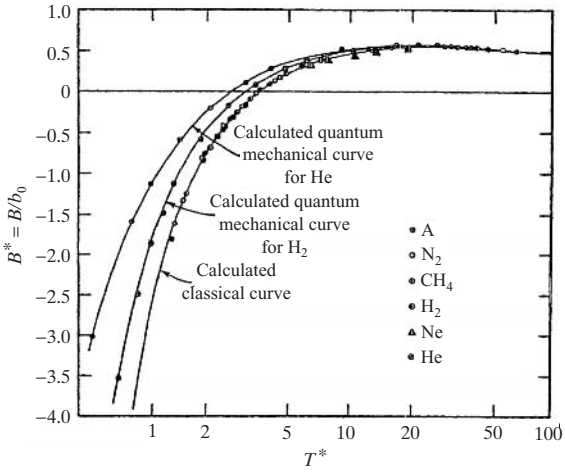

Figure 19.3 Reduced second virial coefficient for Lennard–Jones potential.

If we now introduce reduced properties, namely,

$$r^* \equiv \frac{r}{\sigma} \tag{19.41}$$

$$T^* \equiv \frac{kT}{\varepsilon}, \tag{19.42}$$

Eq. (19.40) can be rewritten as

$$B(T) = 2\pi N_A \sigma^3 \int_0^\infty \{1 - \exp[f(r^*)/T^*]\} r^{*2} dr^*. \tag{19.43}$$

Finally, defining a reduced second virial coefficient, we have

$$B^*(T^*) \equiv \frac{B(T)}{b_\circ}, \tag{19.44}$$

so that, by implementing Eq. (19.37), Eq. (19.43) becomes

$$B^*(T^*) = 3 \int_0^\infty \{1 - \exp[f(r^*)/T^*]\} r^{*2} dr^*, \tag{19.45}$$

which can be used to numerically evaluate B^* as a function of T^* for the Lennard–Jones potential.

While the square-well potential can often be used to predict second virial coefficients (Problem 8.7), the Lennard–Jones 6–12 potential is more universal and thus imbeds the most complete tabulation of input parameters for practical calculations of real gas behavior. The required force constants, ε/k and σ, are tabulated for this purpose in Appendix O for a variety of gaseous species. These constants are determined for each substance based on both transport and virial coefficient data near room temperature. Numerically integrated values of B^* versus T^* for the Lennard–Jones potential based on Eq. (19.45) are tabulated in Appendix Q. Employing these appendices, we can determine accurate values of the second virial coefficient for any chosen gas and temperature. Typical results are displayed in Fig. 19.3, which indicates the reduced second virial coefficient as a function of reduced temperature when using the Lennard–Jones potential. Experimental data are included to demonstrate the utility of the principle of corresponding states when

using the above reduced properties. As expected, the data for He and H_2 generate their own distinctive curves owing to quantum effects unique to each gaseous species.

EXAMPLE 19.1

Employing the Lennard–Jones 6–12 potential, determine the second virial coefficient, in cm^3/mol, for CH_4 at 222 K.

Solution

From Appendix O, the force constants for CH_4 are $\varepsilon/k = 148$ K and $\sigma = 3.81$ Å. Hence, from Eq. (19.42), the reduced temperature is

$$T^* = \frac{kT}{\varepsilon} = \frac{222}{148} = 1.5.$$

Consequently, from Appendix Q, the reduced second virial coefficient, $B^*(T^*)$, is -1.20. On this basis, the second virial coefficient, in $cm^3/mole$, can be determined from Eqs. (19.37) and (19.44), i.e.,

$$B(T) = \frac{2\pi}{3} N_A \sigma^3 B^*(T^*).$$

Evaluating this expression, we have

$$B(T) = \frac{2\pi}{3}(6.02 \times 10^{23}\ \text{mol}^{-1})(3.81 \times 10^{-8}\ \text{cm})^3\,(-1.20)$$

and thus

$$B(T) = -1.20(69.7\ \text{cm}^3/\text{mol}) = -83.7\ \text{cm}^3/\text{mol}\,.$$

The negative value of $B(T)$ in this case underscores the importance of attractive forces at low temperatures, as confirmed by Fig. 19.3.

19.4 The Third Virial Coefficient

According to Eq. (19.25), the third virial coefficient can be defined in terms of the cluster integrals, b_2 and b_3. Therefore, from Eq. (19.15), evaluation of $C(T)$ requires the third configuration integral in addition to the first and second configuration integrals. If we invoke again a central intermolecular potential that depends only on the separation distance between any two particles, r_{ij}, we can approximate the configuration energy as

$$\Phi(\boldsymbol{r}_1, \boldsymbol{r}_2, \boldsymbol{r}_3) \simeq \phi(r_{12}) + \phi(r_{13}) + \phi(r_{23}), \tag{19.46}$$

where we have boldly assumed pair-wise additivity for all possible intermolecular potentials in the three-particle system. On this basis, from Eq. (19.8), we initially have for the third configuration integral

$$Q_3 = \iiint_V \exp\left[-\frac{\phi(r_{12}) + \phi(r_{13}) + \phi(r_{23})}{kT}\right] d\boldsymbol{r}_1 d\boldsymbol{r}_2\, d\boldsymbol{r}_3. \tag{19.47}$$

The required third cluster integral can now be obtained from Q_1, Q_2, and Q_3. Hence, using the configuration integrals from Eqs. (19.26), (19.27), and (19.47), Eq. (19.15) can be expressed as

$$b_3 = \frac{1}{6V} \iiint_V \Big[e^{-\phi(r_{12})/kT} e^{-\phi(r_{13})/kT} e^{-\phi(r_{23})/kT} - e^{-\phi(r_{12})/kT} - e^{-\phi(r_{13})/kT} - e^{-\phi(r_{23})/kT} + 2 \Big] d\boldsymbol{r}_1\, d\boldsymbol{r}_2\, d\boldsymbol{r}_3.$$

Employing Eq. (19.29), we may convert to Mayer cluster functions, thus obtaining

$$b_3 = \frac{1}{6V} \iiint_V \left[(f_{12}+1)(f_{13}+1)(f_{23}+1) - f_{12} - f_{13} - f_{23} - 1 \right] d\boldsymbol{r}_1\, d\boldsymbol{r}_2\, d\boldsymbol{r}_3$$

or

$$b_3 = \frac{1}{6V} \iiint_V \left[f_{12} f_{13} f_{23} + f_{12} f_{13} + f_{12} f_{23} + f_{13} f_{23} \right] d\boldsymbol{r}_1\, d\boldsymbol{r}_2\, d\boldsymbol{r}_3. \tag{19.48}$$

If we also consider the integral

$$\iiint_V f_{12} f_{13}\, d\boldsymbol{r}_1\, d\boldsymbol{r}_2\, d\boldsymbol{r}_3 = \int_V d\boldsymbol{r}_c \cdot \int_V f_{12}\, d\boldsymbol{r}_{12} \cdot \int_V f_{13}\, d\boldsymbol{r}_{13},$$

we find, from Eq. (19.32), that the b_2^2 relation needed in Eq. (19.25) for the third coefficient is

$$b_2^2 = \frac{1}{4V} \iiint_V f_{12} f_{13}\, d\boldsymbol{r}_1\, d\boldsymbol{r}_2\, d\boldsymbol{r}_3, \tag{19.49}$$

where similar expressions, of course, exist when using the 12–23 or 13–23 particle pairs.

Finally, substituting Eqs. (19.48) and (19.49) into Eq. (19.25), we may write

$$C(T) = \frac{N_A^2}{3V} \iiint_V \left[f_{12} f_{13} + f_{12} f_{23} + f_{13} f_{23} \right] d\boldsymbol{r}_1\, d\boldsymbol{r}_2\, d\boldsymbol{r}_3 - \frac{N_A^2}{3V} \iiint_V \left[f_{12} f_{13} f_{23} + f_{12} f_{13} + f_{12} f_{23} + f_{13} f_{23} \right] d\boldsymbol{r}_1\, d\boldsymbol{r}_2\, d\boldsymbol{r}_3,$$

so that the third virial coefficient becomes

$$C(T) = -\frac{N_A^2}{3V} \iiint_V f_{12} f_{13} f_{23}\, d\boldsymbol{r}_1\, d\boldsymbol{r}_2\, d\boldsymbol{r}_3. \tag{19.50}$$

While numerical integration of Eq. (19.50) is considerably more difficult than that of Eq. (19.33), calculations for third virial coefficients based on the Lennard–Jones potential have nevertheless permitted comparisons to experimental data, as for the second virial coefficient. In contrast to the latter, the former unfortunately leads to more substantial disagreement. Better results can be obtained by including a nonadditivity term in Eq. (19.46); however, this tactic surely constitutes a rather cavalier approach to developing robust procedures for evaluation of the configuration energy. A further problem, of

course, is the lurking issue of relative orientation during particle interactions, especially for highly polar molecules, such as water or carbon dioxide.

19.5 Properties for Real Gases

We now investigate the utility of virial equations of state for the calculation of thermodynamic properties. For this purpose, we begin by defining the *property defect* for any generic property of a real gas, $P(T, v)$, as

$$\Delta P_T \equiv P(T, v) - P^\circ(T, v), \tag{19.51}$$

where $P^\circ(T, v)$ represents the identical property, but evaluated for a hypothetical ideal gas at the same T and v. Because ideal gas conditions are guaranteed when the specific volume approaches infinity, Eq. (19.51) may be rewritten as

$$\Delta P_T = [P(T, v) - P(T, \infty)] - [P^\circ(T, v) - P^\circ(T, \infty)],$$

so that

$$\Delta P_T = \int_\infty^v \left[\left(\frac{\partial P}{\partial v}\right)_T - \left(\frac{\partial P^\circ}{\partial v}\right)_T\right] dv \tag{19.52}$$

for any isothermal path. Therefore, once we have evaluated the property defect from Eq. (19.52), we may easily determine the value of that property at a realistic temperature and specific volume from Eq. (19.51). Similarly, any property difference can be obtained from

$$\begin{aligned} P(T_2, v_2) - P(T_1, v_1) = {} & [P^\circ(T_2, v_2) - P^\circ(T_1, v_1)] \\ & + [\Delta P_T(T_2, v_2) - \Delta P_T(T_1, v_1)], \end{aligned} \tag{19.53}$$

where the required property difference for the hypothetical ideal gas can be determined from an appropriate JANAF table in Appendix E.

As an example, let us consider the defect in specific entropy, Δs_T, which can be written, from Eq. (19.52), as

$$\Delta s_T = \int_\infty^v \left[\left(\frac{\partial s}{\partial v}\right)_T - \left(\frac{\partial s^\circ}{\partial v}\right)_T\right] dv. \tag{19.54}$$

However, from macroscopic thermodynamics (Appendix F), a Maxwell relation is available linking entropy to pressure, namely,

$$\left(\frac{\partial s}{\partial v}\right)_T = \left(\frac{\partial P}{\partial T}\right)_v, \tag{19.55}$$

so that, for the hypothetical ideal gas, we have from the ideal gas law, $Pv = RT$,

$$\left(\frac{\partial s^\circ}{\partial v}\right)_T = \frac{R}{v}. \tag{19.56}$$

Similarly, for moderate densities, we have from Eq. (19.1)

$$P = \frac{RT}{v} + \frac{BRT}{v^2}, \tag{19.57}$$

and thus, from Eqs. (19.55) and (19.57),

$$\left(\frac{\partial s}{\partial v}\right)_T = \frac{R}{v}\left(1 + \frac{B}{v}\right) + \frac{RT}{v^2}\frac{dB}{dT}. \tag{19.58}$$

Given Eqs. (19.56) and (19.58), the specific entropy defect can be determined via substitution into Eq. (19.54). We thus obtain

$$\Delta s_T = R\left(B + T\frac{dB}{dT}\right)\int_\infty^v \frac{dv}{v^2},$$

so that, following the above integration, the specific entropy defect becomes

$$\Delta s_T = -\frac{R}{v}\left(B + T\frac{dB}{dT}\right). \tag{19.59}$$

From Eq. (19.51), the specific entropy for a real gas can be expressed as

$$s(T, v) = s^\circ(T, v) + \Delta s_T, \tag{19.60}$$

so that, after substituting Eq. (19.59) into Eq. (19.60), we have

$$s(T, v) = s^\circ(T, v) - \frac{R}{v}\left(B + T\frac{dB}{dT}\right), \tag{19.61}$$

where $s^\circ(T, v)$ can be determined from an appropriate JANAF table. Defect quantities and associated real gas values can, of course, be determined in a similar fashion for other thermodynamic properties such as the internal energy, enthalpy, or the specific heats. In this way, we can easily correct ideal gas properties for both the attractive and repulsive effects associated with any intermolecular potential representative of real gas behavior.

EXAMPLE 19.2

Consider the evaluation of specific entropy using a virial equation of state based on the square-well potential. Presume conditions for which the third virial coefficient is unnecessary for property calculations.

(a) Provide a suitable expression for the specific entropy defect.
(b) Using part (a), develop a relation for the specific entropy of a real gas under these conditions.

Solution

(a) According to Eq. (19.38), the second virial coefficient based on the square-well potential is

$$B(T) = b_\circ\left[1 - (\lambda^3 - 1)(e^{\varepsilon/kT} - 1)\right].$$

From Eq. (19.59), the specific entropy defect requires the derivative of $B(T)$ with respect to temperature. Using the above expression, we thus obtain

$$\frac{dB}{dT} = b_\circ\left(\frac{\varepsilon}{kT^2}\right)(\lambda^3 - 1)\, e^{\varepsilon/kT}.$$

Hence, substituting into Eq. (19.59), the specific entropy defect can be expressed as

$$\Delta s_T = -\frac{Rb_\circ}{v}\left[\lambda^3 + (\lambda^3 - 1)\left(\frac{\varepsilon}{kT} - 1\right)\exp\left(\frac{\varepsilon}{kT}\right)\right].$$

(b) The specific entropy of a real gas can be obtained from Eq. (19.60):

$$s(T, v) = s^{\circ}(T, v) + \Delta s_T.$$

Therefore, substituting for the specific entropy defect, we obtain

$$s(T, v) = s^{\circ}(T, v) - \frac{Rb_{\circ}}{v}\left[\lambda^3 + (\lambda^3 - 1)\left(\frac{\varepsilon}{kT} - 1\right)\exp\left(\frac{\varepsilon}{kT}\right)\right].$$

Evaluation of $s(T, v)$ requires the specific entropy for the hypothetical ideal gas from an appropriate JANAF table as well as relevant parameters describing the square-well potential for the chosen real gas.

PROBLEM SET VIII

Ensemble Theory and the Nonideal Gas (Chapters 18–19)

8.1 The canonical ensemble is composed of closed, isothermal systems (*T, V, N*) while the grand canonical ensemble is composed of open, isothermal systems (*T, V,* μ). Another ensemble, called the microcanonical ensemble, is composed of isolated systems (*E, V, N*).

a. Provide a sufficient argument to show that the only constraint for the microcanonical ensemble is $\sum_i \eta_i = \eta$.

b. If $\Omega(E)$ is the number of system states, prove that the equilibrium distribution for the microcanonical ensemble is given by

$$\frac{\eta_i}{\eta} = \frac{1}{\Omega(E)}.$$

c. How does the above expression relate to the principle of equal *a priori* probability? What limitation must then be imposed on η, the total number of systems in the microcanonical ensemble?

d. Note that the constraint $\sum_i \eta_i = \eta$ is, in essence, common to the microcanonical, canonical, and grand canonical ensembles. For the canonical ensemble, we impose the constraint $\sum_i \eta_i E_i = E$; for the grand canonical ensemble, we instead replace $\sum_i \eta_i = \eta$ with $\sum_i \sum_N \eta_{Ni} = \eta$ and impose $\sum_i \sum_N \eta_{Ni} E_{Ni} = E$ and $\sum_i \sum_N \eta_{Ni} N = \boldsymbol{N}$. Employing this information, show that the canonical and grand canonical partition functions can be written in terms of the microcanonical partition function by summing over the thermodynamic variables (E, N) included in the constraints.

8.2 The canonical partition function for a dense gas can be approximated by

$$Q = \frac{1}{N!}\left(\frac{2\pi mkT}{h^2}\right)^{3N/2}(V - Nb)^N \exp\left(\frac{aN^2}{VkT}\right),$$

where a and b are constants which represent known molecular parameters.

a. Show that this partition function gives the van der Waals equation of state.

b. Develop relations for the internal energy and specific heat (c_v) of this gas.

c. Develop expressions for the entropy and chemical potential of a van der Waals gas.

d. Determine the corresponding partition function for the grand canonical ensemble.

8.3 The canonical partition function for the photon gas can be expressed as

$$Q = \exp(aT^3V),$$

where $a = (8\pi^5/45)(k/hc)^3$, T is the absolute temperature, and V is the volume.

a. Verify that the internal energy derived from Q is that of the photon gas.

b. Employing Q, determine the entropy and pressure for the photon gas.

c. Show that the partition function for the grand canonical ensemble is identical to that for the canonical ensemble in the case of the photon gas. Explain this result.

d. Employing the partition function for the grand canonical ensemble, verify your expression for the entropy obtained in part (b).

8.4 Consider a monatomic ideal gas having the molecular partition function

$$Z = g_\circ \left(\frac{2\pi mkT}{h^2}\right)^{3/2} V,$$

where $g_\circ$ is the degeneracy of the ground electronic state.

a. Develop expressions for both $\ln Q$ and $\ln \Xi$, where Q is the canonical partition function and Ξ is the grand canonical partition function.

b. For the canonical ensemble, the primary statistical and classical relations are

$$A = -kT \ln Q \qquad dA = -SdT - PdV + \mu dN.$$

Employing the canonical partition function, develop expressions for S, P, and μ for the monatomic ideal gas.

c. Show that the ideal gas equation of state is obtained if $Q = f(T)\, V^N$, where $f(T)$ is any function of temperature. What are the implications of this result?

d. For the grand canonical ensemble, the primary statistical and classical relations are

$$PV = kT \ln \Xi \qquad d(PV) = SdT + Nd\mu + PdV.$$

Using the grand canonical ensemble, develop expressions for N, P, and S for the monatomic ideal gas. Show that your results are the same as those obtained using (1) the canonical ensemble and (2) the Maxwell–Boltzmann method.

8.5 A vessel contains an ideal monatomic gas of mass m at temperature T and pressure P. The electronic partition function for the gas is $Z_{el} = g_\circ$.

a. Determine the chemical potential, $\mu(T, P)$, for this gas assembly.

b. Suppose that the above gas is in equilibrium with the surface of a solid within the vessel. Some of the atoms will then be adsorbed onto the surface. A simple model for this system is to picture the solid surface as a two-dimensional lattice of M sites, each of which can be either unoccupied or occupied by a single atom. If an adsorbed atom is bound to the surface, its molecular partition function, Z, can depend only on the surface temperature. Making appropriate assumptions,

show that the canonical partition function for an assembly of N atoms adsorbed onto M sites is given by

$$Q = \frac{M!}{N!(M-N)!} Z^N.$$

c. Determine the chemical potential, $\mu(T, N, M)$, for the adsorbed ideal gas.

d. By invoking equilibrium between the adsorbed and gaseous atoms, show that the fractional surface coverage, $\theta = N/M$, is given by the so-called Langmuir adsorption isotherm,

$$\theta(P, T) = \frac{\chi(T)P}{1 + \chi(T)P},$$

which represents the amount of gas adsorbed as a function of pressure for a fixed temperature. Provide a suitable expression for the temperature coefficient, $\chi(T)$.

8.6 An ideal gas in a container of volume V is in diffusive contact with a reservoir at absolute temperature, T.

a. Starting with the canonical partition function for a system of independent, indistinguishable particles, show that the grand canonical partition function can be expressed as

$$\ln \Xi = \langle N \rangle,$$

where $\langle N \rangle$ is the average number of molecules in the container.

b. Demonstrate that the probability for the existence of N molecules in the container is given by

$$P(N) = \langle N \rangle^N \frac{\exp(-\langle N \rangle)}{N!},$$

which is just the Poisson distribution function.

c. Confirm that $\sum_N P(N) = 1$ and that $\sum_N NP(N) = \langle N \rangle$.

d. Show that the fractional standard deviation for the number of molecules is

$$\frac{\sigma_N}{\langle N \rangle} = \left(\frac{1}{\langle N \rangle} \right)^{1/2}.$$

Discuss the implications of this result.

8.7 Sherwood and Prausnitz (*J. Chem. Phys.* **41**, 429, 1964) have determined relevant parameters for both the square-well and Lennard–Jones potentials applicable to a large number of gases from second virial coefficient data. For argon, $\lambda = 1.70$, $\sigma = 3.067$ Å, $\varepsilon/k = 93.3$ K for the square-well potential and $\sigma = 3.504$ Å, $\varepsilon/k = 117.7$ K for the Lennard–Jones potential.

a. Plot the second virial coefficient, $B(T)$, versus temperature in the range 200–1200 K for both the square-well and Lennard–Jones potentials.

b. Discuss any similarities or differences between the two curves. What are the implications of your result?

8.8 Consider the second virial coefficient for the Sutherland potential, defined by

$$\phi(r) = \infty \quad r < \sigma \qquad \phi(r) = -\varepsilon(\sigma/r)^6 \quad r > \sigma.$$

a. Sketch the Sutherland potential, $\phi(r)$, versus r. Is this potential reasonable? That is, does it include both an attractive and a repulsive portion?

b. Show that the second virial coefficient is given by

$$B(T) = b_\circ \left[1 - \sum_{n=1}^{\infty} \frac{1}{n!(2n-1)} (\varepsilon/kT)^n \right],$$

where $b_\circ = 2\pi N_A \sigma^3/3$.

c. Determine the compressibility factor if higher order virial coefficients are neglected and if $B(T)$ is approximated by using only the first term in the above summation.

d. Compare your compressibility factor with that developed from the van der Waals equation of state. This represents the most satisfactory "derivation" of the van der Waals equation.

Hint: Expand $RT/(v-b)$ *using a binomial series.*

8.9 Consider the second virial coefficient for the Feinberg–DeRocco potential, defined by

$$\begin{aligned} \phi(r) &= \infty & r &< \sigma \\ \phi(r) &= \frac{\varepsilon}{\sigma(\lambda-1)}[r - \lambda\sigma] & \sigma &< r < \lambda\sigma \\ \phi(r) &= 0 & r &> \lambda\sigma. \end{aligned}$$

a. Sketch the Feinberg–DeRocco potential, $\phi(r)$, versus r. Is this potential reasonable, that is, does it include both an attractive and a repulsive portion?

b. Develop a closed-form expression for the second virial coefficient, $B(T)$. Show that this expression is of the form $B(T) = b_\circ B^*(T^*)$, where $b_\circ = 2\pi N_A \sigma^3/3$ and $T^* = kT/\varepsilon$.

8.10 The real gas behavior of the specific heat, c_v, can be investigated by evaluating the isothermal specific heat defect, $\Delta c_{v,T}$.

a. Develop an expression for $\Delta c_{v,T}$ in terms of the second virial coefficient, $B(T)$.

Hint: $(\partial c_v/\partial v)_T = T(\partial^2 P/\partial T^2)_v$ *from classical thermodynamics.*

b. Employing the square-well potential, show that

$$\Delta c_{v,T} = \frac{Rb_\circ}{v}(\lambda^3 - 1)\left(\frac{\varepsilon}{kT}\right)^2 e^{\varepsilon/kT},$$

where $b_\circ = 2\pi N_A \sigma^3/3$.

c. The square-well parameters from second virial coefficient data for carbon dioxide are $\varepsilon/k = 284$ K, $\sigma = 3.57$ Å, and $\lambda = 1.44$. Determine the specific heat, c_v(J/mol·K), for CO_2 at a temperature of 300 K and a specific volume of 2.5 m^3/kgmol.

20 Whence and Whither

We have come a long way together on this journey through the intricacies of statistical thermodynamics. Did the voyage meet your expectations? Were there any surprises along the way? While such questions are part and parcel of any journey, sober reflection on your itinerary offers convincing evidence that macroscopic thermodynamics can indeed be built on a solid foundation of microscopic thermodynamics. More importantly, you have surely found that new insights, deeper understanding, and novel applications follow from a statistical approach to basic thermodynamics. In this concluding chapter, we review highlights from our journey and muse on future experiences awaiting you in the realm of statistical thermodynamics. A significant outcome of this first excursion is that you are now prepared for many new journeys to come. I encourage you to be open to this further understanding and to explore the multitude of evolving venues which seek to exploit both the fundamentals and applications of statistical thermodynamics.

20.1 Reprising the Journey

We began our quest by introducing the two basic postulates of statistical thermodynamics: the ergodic hypothesis and the principle of equal *a priori* probability. The first postulate asserts that any thermodynamic variable characterizing an isolated system of independent particles can be evaluated by suitably averaging over all possible microstates, that is, over all feasible distributions of particles among energy states. The required statistical perspective is encapsulated by the second postulate, which holds that all microstates are equally likely. Consequently, the thermodynamic probability of any macrostate, representing any distribution of particles among energy levels, can be delineated by its number of microstates. For thermodynamic assemblies containing innumerable particles, probability theory also dictates that nearly all microstates can be associated with the most probable macrostate. In other words, the most probable macrostate must represent the equilibrium particle distribution. This conclusion is pivotal as it ultimately defines the underlying viewpoint propounded by the Maxwell–Boltzmann method of statistical thermodynamics.

By applying combinatorial analysis in tandem with the method of Lagrange multipliers, we subsequently identified the most probable macrostate for an isolated system of indistinguishable particles, both with and without limitations on the number of particles per energy state. From this identification, equilibrium particle distributions can be found

for fermions or bosons, which describe, respectively, particles following Fermi–Dirac or Bose–Einstein statistics. If, however, the number of particles is much less than the number of energy states, the particle distribution becomes the same for either fermions or bosons. In this dilute limit, the equilibrium particle distribution among energy levels is equivalent to that found when using classical Maxwell–Boltzmann statistics, which holds for distinguishable particles with no limitation on the number of particles per energy state. Accordingly, the equilibrium distribution for an ideal gas is usually called the Maxwell–Boltzmann particle distribution. We find, however, that classical statistics must be corrected for particle indistinguishability when calculating entropies or free energies in the dilute limit. For this reason, such thermodynamic properties are often said to follow corrected Maxwell–Boltzmann statistics.

Employing the Maxwell–Boltzmann distribution, we next defined the molecular partition function,

$$Z = \sum_i e^{-\varepsilon_i / kT},$$

which represents an effective sum of energy states for thermodynamic systems in the dilute limit. Because each state is weighed by its accessibility at a given temperature, the partition function reflects the thermal behavior of any equilibrium particle distribution. Presuming that the entropy is related to thermodynamic probability through the Boltzmann relation,

$$S = k \ln W,$$

and that the internal energy is found by summing state energies for all particles,

$$U = \sum_i \varepsilon_i,$$

we can develop expressions for the entropy and internal energy of an ideal gas in terms of the partition function. On this basis, the molecular partition function becomes the crucial parameter needed to calculate all thermodynamic properties for the ideal gas.

The evaluation of thermodynamic properties via the partition function ultimately demands that we have information on various energy levels and degeneracies for an atom or molecule. Suitable expressions for particle energy and degeneracy can be obtained through the methods of quantum mechanics. In particular, the steady-state Schrödinger wave equation can be solved for each of the translational and electronic energy modes of an atom, or for each of the translational, rotational, vibrational, and electronic modes of a molecule. For any energy mode, the discrete eigenvalues provided by the Schrödinger wave equation identify the required energy levels while the number of eigenstates associated with a specific energy level defines its degeneracy.

Because the rotational or vibrational energies dispensed by quantum mechanics are generally expressed in terms of derived molecular parameters, spectroscopic techniques must be relied upon to convert energy correlations to energy values. Rotational parameters, for example, can be determined from microwave or far infrared spectroscopy. Similarly, rotational and vibrational information can be determined from near infrared spectroscopy, while rotational, vibrational, and electronic parameters can be evaluated from visible or ultraviolet spectroscopy. While a combined rigid-rotor/harmonic-oscillator model can be used for simplicity, the complexity of actual spectroscopic signatures requires consideration

of rotational centrifugal stretching, vibrational anharmonicity, and rotation–vibration coupling. Typically, for either atoms or molecules, electronic energy levels are obtained from measured electronic transitions. Electronic degeneracies, on the other hand, are usually accessed indirectly through spectroscopic term symbols.

Given particle energies and degeneracies from a combination of quantum mechanics and spectroscopy, the thermodynamic properties of an ideal gas or an ideal gas mixture can be evaluated from knowledge of the molecular partition function. Typical properties include the internal energy, entropy and enthalpy, specific heats, and free energies. Simplified calculations for monatomic, diatomic, and polyatomic species can be undertaken by assuming separation of energy modes. In comparison, a rigorous or semirigorous model provides more accurate results, thus prompting extensive tabulations exemplified by the JANAF tables. For the translational and rotational modes, contributions to the internal energy and heat capacities emulate those expected from the classical phase integral, as summarized by the equipartition principle. This classical approach, however, is quite inappropriate when considering vibrational or electronic modes, as their characteristic temperatures are usually considerably above 300 K. In general, partition functions for various species can also be used to determine equilibrium constants for reactive mixtures, including those for dissociation or ionization reactions.

Spectroscopic measurements can also be invoked for the purpose of determining either temperature or species concentrations via the equilibrium particle distribution. Several techniques are possible depending on unique spectral signatures related to the fundamental equation of photon transfer. Typical methods include those based on absorption, emission, or fluorescence spectroscopy. For any of these techniques, the goal is to determine the population of specified energy levels affiliated with selected vibrational or electronic transitions. For this purpose, Einstein coefficients must be implemented to account for characteristic transition strengths, thus separating the influences of population and dipole moment on measured spectral signatures. Utilizing the Boltzmann fraction, we may then determine the total number density for a particular gaseous species or perhaps its rotational, vibrational, or electronic temperature.

At this juncture, our journey through statistical mechanics took a noticeable turn; we shifted to assemblies of independent particles beyond the dilute limit, with a focus on the thermodynamic properties of the solid state. Specifically, we found that metallic crystals can be modeled as a lattice structure composed of vibrating metallic ions within a sea of translating electrons. Because the crystalline solid implies distinguishable rather than indistinguishable particles, its properties mimic those for a collection of three-dimensional oscillators, but based on uncorrected rather than corrected Maxwell–Boltzmann statistics. In comparison, the conducting electrons surrounding the lattice structure follow Fermi–Dirac statistics. Fortunately, because of high Fermi energies within the conduction band, the thermodynamic properties of an electron gas differ insignificantly from those evaluated at absolute zero. In fact, near absolute zero, the specific heat of a metallic crystal displays a cubic dependence on rising temperature owing to its lattice structure, with a secondary linear dependence owing to the electron gas.

If we heat a metallic crystal, an isothermal cavity within its surface will always generate blackbody radiation. This equilibrium radiation can be represented by a photon gas, which follows Bose–Einstein statistics. However, by considering electromagnetic radiation

trapped within a cubical cavity, translational quantum numbers for the photon gas can be expressed in terms of the frequency of accompanying electromagnetic waves. Hence, we may determine the number of photons in a given frequency range and thus the spectral energy density, which defines the Planck distribution law for equilibrium radiation. When expressed in terms of wavelength, this energy distribution can also be used to determine the temperature at grey surfaces, usually via the so-called two-color method for surface thermometry.

Having traveled beyond the dilute limit, we next explored the rudiments of nonequilibrium statistical thermodynamics. We began with equilibrium kinetic theory, focusing on the Maxwell–Boltzmann velocity and speed distributions for an ideal gas assembly. Exploiting geometrical aspects of molecular effusion, we identified particle flux as the underlying mechanism for transport of momentum, energy, and mass in laminar flows. From the Lennard–Jones intermolecular potential, fundamental relations were then developed for the dynamic viscosity, thermal conductivity, and binary diffusion coefficient. Similarly, employing binary collision theory, we derived a useful relation for the rate coefficient of a bimolecular chemical reaction that duplicates empirical behavior based on both the Arrhenius law and the law of mass action. Nevertheless, to properly account for both vibrational and rotational energetics during collisions, a more robust model was proposed based on the existence of an activated complex along a single reaction coordinate of the chemical system. The resulting transition state theory provides a significantly improved model for the bimolecular rate coefficient in terms of partition functions per unit volume for the reactants as well as for the activated complex.

We completed our journey by migrating beyond systems of independent particles, thus exploiting the Gibbs method of statistical thermodynamics. Here, independent particles were replaced with independent systems, so that we could now invoke system rather than particle quantum states. On this basis, we proposed statistical models for a closed, isothermal system using the canonical ensemble and for an open, isothermal system using the grand canonical ensemble. The utility of the ensemble method was demonstrated by replicating the equilibrium particle distribution and thermodynamic properties of an ideal gas, beginning with either the canonical or the grand canonical ensemble. Further exploiting ensemble theory, we found that statistical fluctuations in thermodynamic properties scale inversely with the square root of the number of particles in an assembly, thus confirming the efficacy of the Maxwell–Boltzmann method when dealing with macroscopic systems composed of independent particles.

As an example of the practical utility of the ensemble method, we employed the grand canonical partition function to develop a fundamental equation of state for real gases. By comparing our theoretical formulation to the classic virial equation of state, we showed that the second virial coefficient can be determined through a configuration integral based on either the square-well or Lennard–Jones potential. We then demonstrated how thermodynamic properties for real gases can be calculated using so-called defect quantities, which essentially model property differences between real and ideal gases through their multiple virial coefficients. Since real gases manifest interactive particle behavior, we appropriately ended our journey with a practical thermodynamic system whose analysis demands the ensemble method. Challenging systems of this type include liquids, semiconductors, and plasmas, which are more usefully studied via advanced courses in statistical thermodynamics.

20.2 Preparing for New Journeys

As implied in the previous section, a second course in statistical thermodynamics invariably builds on the ensemble method. Hence, given this introductory textbook, you might rightly infer that an advanced course would revisit ideal gas behavior, except beginning with the canonical ensemble rather than the Maxwell–Boltzmann method of statistical thermodynamics. The same holds true for the crystalline solid and the photon gas, although the grand canonical ensemble is usually a better entrée for studying the electron gas, real gases, or surface adsorption. Beyond these subjects, typically considered during a first course, we now explore new adventures open to you when applying the ensemble method to a variety of thermodynamic systems composed of dependent rather than independent particles.

An obvious extension to our investigation of real gas behavior is that of the liquid state. You should recognize, however, that the cluster-expansion method adopted for dense gases in Chapter 19 cannot be applied to liquids, as the resulting particle interactions are too intense to be represented by a power series delineating collisions among only a few particles. Nevertheless, evaluation of the canonical partition function using a combination of the configuration integral and Lennard–Jones potential remains appropriate for the liquid state. The trick, in comparison to the gaseous state, is to account satisfactorily for deviations between local and bulk densities owing to intermolecular forces. This can be accomplished by defining a radial distribution function that accounts for particle interactions in the fluid, thus equivalently specifying a mean intermolecular potential. The key point here is that any thermodynamic property can ultimately be expressed in terms of this so-called pair-correlation function. In addition, the mathematical form of the distribution function can be verified experimentally by using well-established x-ray diffraction techniques.

Unfortunately, evaluating the radial distribution function generally requires cumbersome numerical procedures for solving various nonlinear integral equations. For this reason, perturbation theories have been developed based on the fact that short-range repulsive forces dominate in liquids. In other words, the attractive portion of the mean intermolecular potential can be effectively modeled as a small perturbation about the rigid-sphere potential. On this basis, the canonical partition function can be expressed in terms of a simplified pair-correlation function, thus generating liquid properties in good agreement with experiment.

Similar procedures have been developed for electrolytic solutions, which are very important in various biological systems. As might be expected, cluster expansions prove unworkable because of long-range coulombic forces generated by charged particles. Therefore, perturbation techniques must again be employed, but now based on a charge rather than a particle distribution function. Such methods are, in essence, improvements on basic Debye–Hückel theory, which holds only for ions having nearly identical hard-sphere diameters. In comparison, however, the virial approach remains quite valid for dilute solutions involving nonelectrolytes. A good example is the calculation of osmotic pressure via McMillan–Mayer theory, which necessarily represents a more robust formulation of the cluster-expansion technique.

Statistical procedures based on the canonical partition function can also be applied to organic polymers. Researchers have evaluated, for example, mean chain lengths arising from chaotic entanglement, thus modeling the elastic behavior of linear polymeric chains. Surprisingly, as for dense gases, polymer configurations can often be handled through a

second virial coefficient. In essence, the intermolecular potential encapsulates the force needed to bring together two isolated polymeric molecules. A complete lattice model is required, however, when dealing with polymeric solutions, the most famous of which is that due to Flory and Huggins.

Extensive work has, of course, been done during the last half-century in applying statistical thermodynamics to the solid state. Theories have been developed for electrical conductivity, thermionic emission, and magnetism, with a particular focus on the electronic behavior of semiconductors. As compared with the simple electron gas, modern applications to solid-state physics make use of the famous Kronig–Penney model, which features electronic responses created via repetitive potentials induced by the ionic structure of crystalline solids. Strong electrostatic interactions among electrons surrounding atomic nuclei are especially significant in ferromagnetic materials. For this reason, the canonical ensemble can also be invoked to explain ferromagnetism, especially through the implementation of so-called Ising models.

Three-dimensional Ising models in combination with modern renormalization techniques can be used to predict phase changes and various critical phenomena such as opalescence. The famous Landau–Ginsburg model for phase transitions employs the canonical partition function, although tractable calculations mandate powerful mathematical transformations made possible by Wilson renormalization theory. These approaches are extremely abstract and complicated, constituting a leading edge in modern statistical thermodynamics. Other approaches to modeling phase transitions include mean-field approximations, which neglect statistical correlations between neighboring particles, or Monte Carlo simulations, which can be used to generate sampling sequences for the canonical ensemble based on the principle of detailed balance.

During the last several decades, particularly significant innovations have occurred in the arena of nonequilibrium statistical thermodynamics. Most researchers in this field have, of course, been concerned with dynamic behavior, with a focus on equilibration to the most probable macrostate. Typically, various time series are generated, so that the statistical quantities of interest become the autocorrelation function and the power spectral density. Exploiting this tactic, transport properties can ultimately be expressed in terms of time-averaged rather than ensemble-averaged correlation functions.

With respect to nonequilibrium behavior, the most famous indicator of gas-phase relaxation to thermodynamic equilibrium is the Boltzmann equation, which describes the probability density function for particle momentum as a function of time. While this integrodifferential equation is nearly impossible to solve, it nevertheless identifies a crucial connection between entropy and time, thus rationalizing temporal progression in the universe. Indeed, modern cosmology suggests that the second law of thermodynamics can be associated with the expansion of our universe since the big bang. In other words, prior to the big bang, the universe must have been highly ordered and thus incredibly improbable according to the second law. We are thus confronted with deciding whether life in the universe is a statistical anomaly or evidence for the hand of God. Statistical thermodynamics has once again given us much to ponder!

Finally, while we have focused in this section on novel applications of ensemble theory, you might actually be more intrigued by a deeper understanding of specialized topics rather than by an advanced course devoted exclusively to statistical thermodynamics. For example, you may be interested in a full course dealing with quantum mechanics

or spectroscopy, which are available in physics and chemistry departments of most universities. More advanced work could also be pursued in specific subjects such as chemical kinetics, transport phenomena, or solid-state physics. Classes in these disciplines are offered in many chemical, mechanical, or electrical engineering departments, as well as through the chemistry or physics curriculum. Recent applications of statistical thermodynamics are often covered in courses dealing with laser-based diagnostics, remote sensing, laser processing, or various aspects of nanotechnology. Regardless of your particular interests, however, you can rest assured that this first venture in statistical thermodynamics has prepared you well for any of the numerous and exciting manifestations of the subject that you might encounter during future academic journeys.

20.3 The Continuing Challenge of Thermodynamics

We close by restating the obvious. Statistical thermodynamics is a challenging discipline, a verity recognized by anyone who has completed his or her first adventure through its richness, versatility, and utility. It demands an incredible diversity of skills, from probability theory to quantum mechanics to molecular modeling. Furthermore, it requires a fundamental knowledge of classical thermodynamics, transport phenomena, and physical optics. Nevertheless, because of its breadth and depth, you should be convinced by now of its importance in establishing a clear understanding of equilibrium behavior, especially on those aspects related to the second law of thermodynamics. Therefore, with continuing study and reflection, you can rest assured that a practical symbiosis will eventually bloom that simultaneously reinforces and expands your appreciation of both microscopic and macroscopic thermodynamics.

If, as is probably likely, you still feel unsure about certain aspects of either statistical or classical thermodynamics, you might take solace in a cryptic remark often attributed to the great physicist Arnold Sommerfeld. Upon being asked why he had never written a book on thermodynamics, he responded somewhat as follows. “It’s a funny subject. The first time you go through it, you don’t understand it at all. The second time through you think you do except for one or two minor points. The third time you know you don’t understand it, but by then you are so used to it, it doesn’t bother you.” So be it!

PART SEVEN

APPENDICES

APPENDIX A

Physical Constants and Conversion Factors

Constant	MKS Units	CGS Units
Avagadro's Number (N_A)	6.0221×10^{26} kmol^{-1}	6.0221×10^{23} mol^{-1}
Boltzmann's Constant (k)	1.3807×10^{-23} J/K	1.3807×10^{-16} erg/K
Universal Gas Constant ($R = N_A k$)	8.3145 J/K · mol	8.3145×10^{7} erg/K · mol
Planck's Constant (h)	6.6261×10^{-34} J · s	6.6261×10^{-27} erg · s
Speed of Light in Vacuum (c)	2.9979×10^{8} m/s	2.9979×10^{10} cm/s
Atomic Mass Unit (m_u)	1.6605×10^{-27} kg	1.6605×10^{-24} g
Electron Rest Mass (m_e)	9.1094×10^{-31} kg	9.1094×10^{-28} g
Proton Rest Mass (m_p)	1.6726×10^{-27} kg	1.6726×10^{-24} g
Electron Charge (e)	1.6022×10^{-19} C	1.6022×10^{-19} C
Permittivity of Vacuum ($\varepsilon_\circ$)	8.8542×10^{-12} C^2/J · m	8.8542×10^{-21} C^2/erg · cm

1 J = 1 N · m = 1 kg · m^2/s^2
1 W = 1 J/s
1 bar = 10^5 N/m^2
1 J = 10^7 erg
1 N = 10^5 dyne
1 erg = 1 dyne · cm = 1 g · cm^2/s^2
1 atm = 1.013 bar = 1.013×10^6 dyne/cm^2
1 eV = 1.602×10^{-19} J
1 cal = 4.184 J
1 Å = 10^{-8} cm

APPENDIX B

Series and Integrals

$$e^x = 1 + x + \tfrac{1}{2}x^2 + \tfrac{1}{6}x^3 + \cdots$$

$$\ln\,(1+x) = x - \tfrac{1}{2}x^2 + \tfrac{1}{3}x^3 - \tfrac{1}{4}x^4 + \cdots \quad |x| < 1$$

$$\int_0^\infty x^n e^{-ax}dx = \frac{\Gamma(n+1)}{a^{n+1}} \quad \Gamma(n+1) = n\Gamma(n) \quad \Gamma(1) = 1 \quad \Gamma\left(\tfrac{1}{2}\right) = \sqrt{\pi} \quad n > 0$$

$\int_0^\infty x^n e^{-a\,x^2}dx$		$\int_0^\infty x^p(e^x-1)^{-1}dx$	
$n=0$	$\frac{1}{2}\sqrt{\pi}a^{-1/2}$	$p=0.5$	$1.306\sqrt{\pi}$
$n=1$	$(2a)^{-1}$	$p=1.0$	$\pi^2/6$
$n=2$	$\frac{1}{4}\sqrt{\pi}a^{-3/2}$	$p=1.5$	$1.006\sqrt{\pi}$
$n=3$	$(2a^2)^{-1}$	$p=2.0$	2.404
$n=4$	$\frac{3}{8}\sqrt{\pi}a^{-5/2}$	$p=3.0$	$\pi^4/15$
$n=5$	$(a^3)^{-1}$	$p=5.0$	$8\pi^6/63$

$$\int_{-\infty}^{\infty} x^n e^{-a\,x^2}dx = 0 \quad (n \text{ odd})$$

$$\int_{-\infty}^{\infty} x^n e^{-a\,x^2}dx = 2\int_0^\infty x^n e^{-a\,x^2}dx \quad (n \text{ even})$$

$$\text{Error function: } \operatorname{erf}(x) = \frac{2}{\sqrt{\pi}}\int_0^x e^{-t^2}dt$$

APPENDIX C

Periodic Table

The atomic number (top left) is the number of protons in the nucleus. The atomic mass (bottom) is weighted by mean isotopic abundances in the earth's surface. Atomic masses are relative to the mass of the carbon-12 isotope, defined to be exactly 12 atomic mass units (amu). If sufficiently stable isotopes do not exist for an element, the mass of its longest-lived isotope is indicated in parentheses. For elements 110–112, the mass numbers of the known isotopes are given. Reference: Schroeder (2000) as extracted from *The European Physical Journal* **C3**, 73 (1998).

Periodic Table of the Elements

1 IA	2 IIA	3 IIIB	4 IVB	5 VB	6 VIB	7 VIIB	8	9 VIII	10	11 IB	12 IIB	13 IIIA	14 IVA	15 VA	16 VIA	17 VIIA	18 VIIIA
1 **H** Hydrogen 1.00794																	2 **He** Helium 4.002602
3 **Li** Lithium 6.941	4 **Be** Beryllium 9.012182											5 **B** Boron 10.811	6 **C** Carbon 12.0107	7 **N** Nitrogen 14.00674	8 **O** Oxygen 15.9994	9 **F** Fluorine 18.9984032	10 **Ne** Neon 20.1797
11 **Na** Sodium 22.989770	12 **Mg** Magnesium 24.3050											13 **Al** Aluminum 26.981538	14 **Si** Silicon 28.0855	15 **P** Phosph. 30.973761	16 **S** Sulfur 32.066	17 **Cl** Chlorine 35.4527	18 **Ar** Argon 39.948
19 **K** Potassium 39.0983	20 **Ca** Calcium 40.078	21 **Sc** Scandium 44.955910	22 **Ti** Titanium 47.867	23 **V** Vanadium 50.9415	24 **Cr** Chromium 51.9961	25 **Mn** Manganese 54.938049	26 **Fe** Iron 55.845	27 **Co** Cobalt 58.933200	28 **Ni** Nickel 58.6934	29 **Cu** Copper 63.546	30 **Zn** Zinc 65.39	31 **Ga** Gallium 69.723	32 **Ge** German 72.61	33 **As** Arsenic 74.92160	34 **Se** Selenium 78.96	35 **Br** Bromine 79.904	36 **Kr** Krypton 83.80
37 **Rb** Rubidium 85.4678	38 **Sr** Strontium 87.62	39 **Y** Yttrium 88.90585	40 **Zr** Zlrconium 91.224	41 **Nb** Niobium 92.90638	42 **Mo** Molybd. 95.94	43 **Tc** Technet. (97.907215)	44 **Ru** Ruthen. 101.07	45 **Rh** Rhodium 102.90550	46 **Pd** Palladium 106.42	47 **Ag** Silver 107.8682	48 **Cd** Cadmium 112.411	49 **In** Indium 114.818	50 **Sn** Tin 118.710	51 **Sb** Antimony 121.760	52 **Te** Tellurium 127.60	53 **I** Iodine 126.90447	54 **Xe** Xenon 131.29
55 **Cs** Cesium 132.90545	56 **Ba** Barium 137.327	57-71 Lantha-nides	72 **Hf** Hafnium 178.49	73 **Ta** Tantaium 180.9479	74 **W** Tungsten 183.84	75 **Re** Rhenium 186.207	76 **Os** Osmium 190.23	77 **Ir** Iridium 192.217	78 **Pt** Platinum 195.078	79 **Au** Gold 196.96655	80 **Hg** Mercury 200.59	81 **Tl** Thalillum 204.3833	82 **Pb** Lead 207.2	83 **Bi** Bismuth 208.98038	84 **Po** Polonium (208.982415)	85 **At** Astatine (209.987131)	86 **Rn** Radon (222.017570)
87 **Fr** Francium (223.019731)	88 **Ra** Radium (226.025402)	89–103 Actinides	104 **Rf** Rutherford (261.1089)	105 **Db** Dubnium (262.1144)	106 **Sg** Seaborg. (263.1186)	107 **Bh** Bohrium (262.1231)	108 **Hs** Hassium (265.1306)	109 **Mt** Meltner. (266.1378)	110 (269.273)	111 (272)	112 (277)						

Lanthanide series	57 **La** Lantbanum 138.9055	58 **Ce** Cerium 140.116	59 **Pr** Praseodym. 140.90765	60 **Nd** Neodym 144.24	61 **Pm** Prometh. (144.912745)	62 **Sm** Samarium 150.36	63 **Eu** Europium 151.964	64 **Gd** Gadolin. 157.25	65 **Tb** Terbium 158.92534	66 **Dy** Dyspros. 162.50	67 **Ho** Holmium 164.93032	68 **Er** Erbium 167.26	69 **Tm** Thulium 168.93421	70 **Yb** Ytterbium 173.04	71 **Lu** Lutetium 174.967

Actinide series	89 **Ac** Actinium (227.027747)	90 **Th** Thorium 232.0381	91 **Pa** Protactin. 231.03588	92 **U** Uranium 238.0289	93 **Np** Neptunium (237.048166)	94 **Pu** Plutonium (244.064197)	95 **Am** Americium (243.061372)	96 **Cm** Curium (247.070346)	97 **Bk** Berkelium (247.070298)	98 **Cf** Californ. (251.079579)	99 **Es** Einstein. (252.08297)	100 **Fm** Fermium (257.095096)	101 **Md** Mendelev. (258.098427)	102 **No** Nobelium (259.1011)	103 **Lr** Lawrenc. (262.1098)

APPENDIX D

Mathematical Procedures

D.1 Method of Lagrange Multipliers

Consider a continuous function, $f(x, y, z)$, which depends on the three independent variables, x, y, and z. To determine the maximum or minimum of this function, we normally invoke

$$df = \left(\frac{\partial f}{\partial x}\right) dx + \left(\frac{\partial f}{\partial y}\right) dy + \left(\frac{\partial f}{\partial z}\right) dz = 0, \tag{D.1}$$

which simply requires

$$\left(\frac{\partial f}{\partial x}\right) = \left(\frac{\partial f}{\partial y}\right) = \left(\frac{\partial f}{\partial z}\right) = 0.$$

Now, suppose that x, y, and z are not independent variables but are instead related through two independent and continuous constraints,

$$g_1(x, y, z) = 0 \tag{D.2}$$

$$g_2(x, y, z) = 0. \tag{D.3}$$

Since g_1 and g_2 are each constant, the differential of each must be zero so that

$$\left(\frac{\partial g_1}{\partial x}\right) dx + \left(\frac{\partial g_1}{\partial y}\right) dy + \left(\frac{\partial g_1}{\partial z}\right) dz = 0 \tag{D.4}$$

$$\left(\frac{\partial g_2}{\partial x}\right) dx + \left(\frac{\partial g_2}{\partial y}\right) dy + \left(\frac{\partial g_2}{\partial z}\right) dz = 0. \tag{D.5}$$

Multiplying Eqs. (D.4) and (D.5) by the constants λ_1 and λ_2, respectively, and adding the results to Eq. (D.1) yields the combined requirement,

$$\left(\frac{\partial f}{\partial x} + \lambda_1 \frac{\partial g_1}{\partial x} + \lambda_2 \frac{\partial g_2}{\partial x}\right) dx + \left(\frac{\partial f}{\partial y} + \lambda_1 \frac{\partial g_1}{\partial y} + \lambda_2 \frac{\partial g_2}{\partial y}\right) dy + \left(\frac{\partial f}{\partial z} + \lambda_1 \frac{\partial g_1}{\partial z} + \lambda_2 \frac{\partial g_2}{\partial z}\right) dz = 0. \tag{D.6}$$

Given the two applied constraints, two of the three variables, say x and y, must depend on the remaining variable, z. Consequently, the first two terms of Eq. (D.6) can be zero

only by choosing λ_1 and λ_2 so that

$$\left(\frac{\partial f}{\partial x}+\lambda_1\frac{\partial g_1}{\partial x}+\lambda_2\frac{\partial g_2}{\partial x}\right)=0 \tag{D.7}$$

$$\left(\frac{\partial f}{\partial y}+\lambda_1\frac{\partial g_1}{\partial y}+\lambda_2\frac{\partial g_2}{\partial y}\right)=0. \tag{D.8}$$

Having selected λ_1 and λ_2, the only way that Eq. (D.6) can be zero for any arbitrary value of dz is for its coefficient to be identically zero, or

$$\left(\frac{\partial f}{\partial z}+\lambda_1\frac{\partial g_1}{\partial z}+\lambda_2\frac{\partial g_2}{\partial z}\right)=0. \tag{D.9}$$

Analogous arguments hold for any arbitrary choice of the independent variable. Hence, in general, the extremum is defined in all cases by the same three expressions, namely, Eqs. (D.7), (D.8), and (D.9). Including the two constraints, Eqs. (D.2) and (D.3), we have finally five equations in the five unknowns, x_o, y_o, z_o, λ_1, and λ_2, where (x_o, y_o, z_o) defines the extremum condition.

The parameters λ_1 and λ_2 are called Lagrange multipliers. In essence, the maximum or minimum with constraints is obtained from the above procedure by finding the extremum of the auxiliary function

$$\varphi = f+\lambda_1 g_1+\lambda_2 g_2$$

with no imposition of constraints. This procedure works because $g_1=0$ and $g_2=0$. Therefore, for n independent constraints, $g_1=0, g_2=0, \ldots, g_n=0$, the auxiliary function becomes

$$\varphi = f+\lambda_1 g_1+\lambda_2 g_2+\cdots+\lambda_n g_n$$

where $\lambda_1, \lambda_2, \ldots, \lambda_n$ are the unknown Lagrange multipliers, the number of which must, of course, be less than the number of system variables.

D.2 Stirling's Formula

Stirling's formula provides an excellent estimate for the natural logarithm of the factorial of a large number. Taking the natural logarithm of $N!$, we obtain

$$\ln N! = \sum_{n=1}^{N}\ln n,$$

which can be approximated by the integral

$$\ln N! = \int_0^N \ln n\, dn \tag{D.10}$$

for very large N. Evaluating the integral of Eq. (D.10), we obtain

$$\ln N! = N\ln N - N, \tag{D.11}$$

where l'Hospital's rule has been used to properly evaluate $n\ln n$ at $n=0$. A somewhat better approximation, especially at lower values of N, is (Reif, 1965)

$$\ln N! = N\ln N - N + \tfrac{1}{2}\ln(2\pi N) \tag{D.12}$$

or

$$N! = \sqrt{2\pi N}\, N^N e^{-N}. \tag{D.13}$$

Equation (D.11) is accurate to within 1% for $N > 10^2$ and to within 0.01% for $N > 10^4$. For statistical mechanical applications, N is extremely large and thus, for all practical purposes, Eq. (D.11) is exact. On the other hand, Eq. (D.12) is preferable for lower values of N; similarly, Eq. (D.13) should be used for direct evaluation of $N!$.

D.3 Euler–Maclaurin Summation Formula

It often proves convenient in statistical mechanics to approximate the summation of a function over a discrete variable by an analogous integration over a continuous variable. The accuracy of this procedure can be assessed by implementation of the Euler–Maclaurin summation formula.

Consider a function $f(n)$ that changes only gradually with increasing integer values, $0 \le n \le \infty$. If, in addition,

$$\lim_{n\to\infty} f(n) = 0,$$

we may show via contour integration in the complex plane (Hecht, 1990) that

$$\sum_{n=0}^{\infty} f(n) = \int_0^{\infty} f(n)\, dn + \frac{1}{2} f(0) - \frac{1}{12} f'(0) + \frac{1}{720} f'''(0) + \cdots, \tag{D.14}$$

where $f(0)$ is $f(n)$ evaluated at $n = 0$, $f'(0)$ is its first derivative evaluated at $n = 0$, and $f'''(0)$ is its third derivative evaluated at $n = 0$.

APPENDIX E

Thermochemical Data for Ideal Gases

The thermochemical data for the ideal gases of this appendix are taken directly from the Third Edition of the JANAF Thermochemical Tables, as tabulated by Chase *et al*. (1985). The twelve atoms and molecules selected are frequently cited in papers dealing with the chemistry and physics of flames and plasmas. For the sake of brevity, the plethora of possible hydrocarbons are not included in this appendix, but many of them can, of course, be found in the complete JANAF tables, which are available in the reference section of most science and engineering libraries.

The ordered listing of the twelve chosen gases is as follows: H_2, H, O_2, O, H_2O, OH, CO, CO_2, N_2, N, NO, and NO_2. Each table describes the formation of one mole of the subject species from its elements in their natural physical state at 298.15 K and 1 bar. The reader should refer to the original JANAF tables for a listing of the quantum mechanical and spectroscopic data used to effect the statistical mechanical calculations for each species. The reference state for all of these compounds is the hypothetical ideal gas at a temperature of 298.15 K (T_r) and a pressure of 1 bar (0.1 MPa). The logarithm of the equilibrium constant is to the base 10. By definition, both the enthalpy and Gibbs free energy of formation are identically zero for any ideal gas reference compound, such as H_2, O_2, or N_2.

Hydrogen (H_2), ideal gas reference state, mol. wt. = 2.01588

Enthalpy Reference Temperature = T_r = 298.15 K				Standard State Pressure = P° = 0.1 MPa			
	J K^{-1} mol^{-1}			kJ mol^{-1}			
T/K	C_p°	S°	$-[G^\circ - H^\circ(T_r)]/T$	$H^\circ - H^\circ(T_r)$	$\Delta_f H^\circ$	$\Delta_f G^\circ$	Log K_f
0	0.	0.	INFINITE	−8.467	0.	0.	0.
100	28.154	100.727	155.408	−5.468	0.	0.	0.
200	27.447	119.412	133.284	−2.774	0.	0.	0.
250	28.344	125.640	131.152	−1.378	0.	0	0.
298.15	28.836	130.680	130.680	0.	0.	0.	0.
300	28.849	130.858	130.680	0.053	0.	0.	0.
350	29.081	135.325	131.032	1.502	0.	0.	0.
400	29.181	139.216	131.817	2.959	0.	0.	0.
450	29.229	142.656	132.834	4.420	0.	0.	0.
500	29.260	145.737	133.973	5.882	0.	0.	0.
600	29.327	151.077	138.392	8.811	0.	0.	0.
700	29.441	155.606	138.822	11.749	0.	0.	0.
800	29.624	159.548	141.171	14.702	0.	0.	0.
900	29.881	163.051	143.411	17.676	0.	0.	0.
1000	30.205	166.216	145.536	20.680	0.	0.	0.
1100	30.581	169.112	147.549	23.719	0.	0.	0.
1200	30.992	171.790	149.459	26.797	0.	0.	0.
1300	31.423	174.288	151.274	29.918	0.	0.	0.
1400	31.861	176.633	153.003	33.082	0.	0.	0.
1500	32.298	178.846	154.652	36.290	0.	0.	0.
1600	32.725	180.944	156.231	39.541	0.	0.	0.
1700	33.139	182.940	157.743	42.835	0.	0.	0.
1800	33.537	184.846	159.197	46.169	0.	0.	0.
1900	33.917	186.669	160.595	49.541	0.	0.	0.
2000	34.280	188.418	161.943	52.951	0.	0.	0.
2100	34.624	190.099	163.244	56.397	0.	0.	0.
2200	34.952	191.718	164.501	59.876	0.	0.	0.
2300	35.263	193.278	165.719	63.387	0.	0.	0.
2400	35.559	194.785	166.899	68.928	0.	0.	0.
2500	35.842	196.243	168.044	70.498	0.	0.	0.
2600	36.111	197.654	169.155	74.096	0.	0.	0.
2700	36.370	199.021	170.236	77.720	0.	0.	0.
2800	36.618	200.349	171.288	81.369	0.	0.	0.
2900	36.856	201.638	172.313	85.043	0.	0.	0.
3000	37.087	202.891	173.311	88.740	0.	0.	0.
3100	37.311	204.111	174.285	92.460	0.	0.	0.
3200	37.528	205.299	175.236	96.202	0.	0.	0.
3300	37.740	206.457	176.164	99.966	0.	0.	0.
3400	37.946	207.587	177.072	103.750	0.	0.	0.
3500	38.149	206.690	177.960	107.555	0.	0.	0.
3600	38.348	209.767	178.828	111.380	0.	0.	0.
3700	38.544	210.821	179.679	115.224	0.	0.	0.
3800	38.738	211.851	180.512	119.089	0.	0.	0.
3900	38.928	212.860	161.328	122.972	0.	0.	0.
4000	39.116	213.848	182.129	126.874	0.	0.	0.
4100	39.301	214.816	182.915	130.795	0.	0.	0.
4200	39.484	215.765	183.686	134.734	0.	0.	0.
4300	39.685	216.696	184.442	138.692	0.	0.	0.
4400	39.842	217.610	185.186	142.667	0.	0.	0.
4500	40.017	218.508	185.916	146.660	0.	0.	0.
4600	40.188	219.389	186.635	150.670	0.	0.	0.
4700	40.355	220.255	187.341	154.698	0.	0.	0.
4800	40.518	221.106	188.035	158.741	0.	0.	0.
4900	40.676	221.943	188.719	162.801	0.	0.	0.
5000	40.829	222.767	189.392	166.876	0.	0.	0.
5100	40.976	223.577	190.054	170.967	0.	0.	0.
5200	41.117	224.374	190.706	175.071	0.	0.	0.
5300	41.252	225.158	191.349	179.190	0.	0.	0.
5400	41.379	225.931	191.982	183.322	0.	0.	0.
5500	41.498	226.691	192.606	187.465	0.	0.	0.
5600	41.609	227.440	193.222	191.621	0.	0.	0.
5700	41.712	228.177	193.829	195.787	0.	0.	0.
5800	41.806	228.903	194.427	199.963	0.	0.	0.
5900	41.890	229.619	195.017	204.148	0.	0.	0.
6000	41.965	230.323	195.600	208.341	0.	0.	0.

Hydrogen, monatomic (H), ideal gas, mol. wt. = 1.00794

Enthalpy Reference Temperature = T_r = 298.15 K				Standard State Pressure = P° = 0.1 MPa			
	J K^{-1} mol^{-1}			kJ mol^{-1}			
T/K	C_p°	S°	$-[G^\circ - H^\circ(T_r)]/T$	$H^\circ - H^\circ(T_r)$	$\Delta_f H^\circ$	$\Delta_f G^\circ$	Log K_f
0	0.	0.	INFINITE	−6.197	216.035	216.035	INFINITE
100	20.786	92.009	133.197	−4.119	216.614	212.450	−110.972
200	20.786	106.417	116.618	−2.040	217.346	208.004	−54.325
250	−20.786	111.055	115.059	−1.001	217.687	205.629	−42.964
298.15	20.786	114.716	114.716	0.	217.999	203.278	−35.613
300	20.786	114.845	114.717	0.038	218.011	203.186	−35.378
350	20.786	118.049	114.970	1.078	218.326	200.690	−29.951
400	20.786	120.825	115.532	2.117	218.637	198.150	−25.876
450	20.786	123.273	116.259	3.156	218.946	195.570	−22.701
500	20.786	125.463	117.072	4.196	219.254	192.957	−20.158
600	20.786	129.253	118.796	6.274	219.868	187.640	−16.335
700	20.786	132.457	120.524	8.353	220.478	182.220	−13.597
800	20.788	135.232	122.193	10.431	221.080	176.713	−11.538
900	20.786	137.681	123.781	12.510	221.671	171.132	−9.932
1000	20.786	139.871	125.282	14.589	222.248	165.485	−8.644
1100	20.786	141.852	126.700	16.667	222.807	159.782	−7.587
1200	20.786	143.660	128.039	18.746	223.346	154.028	−6.705
1300	20.786	145.324	129.305	20.824	223.865	148.230	−5.956
1400	20.788	146.865	130.505	22.903	224.361	142.394	−5.313
1500	20.786	148.299	131.644	24.982	224.836	136.522	−4.754
1600	20.786	149.640	132.728	27.060	225.289	130.620	−4.264
1700	20.786	150.900	133.760	29.139	225.721	124.689	−3.831
1800	20.786	152.088	134.745	31.217	226.132	118.734	−3.446
1900	20.786	153.212	135.688	33.296	226.525	112.757	−3.100
2000	20.786	154.278	136.591	35.375	226.898	106.760	−2.788
2100	20.786	155.293	137.458	37.453	227.254	100.744	−2.506
2200	20.786	156.260	138.291	39.532	227.593	94.712	−2.249
2300	20.786	157.184	139.092	41.610	227.916	88.664	−2.014
2400	20.786	158.068	139.864	43.689	228.224	82.603	−1.798
2500	20.786	158.917	140.610	45.768	228.518	76.530	−1.599
2600	20.786	159.732	141.330	47.846	228.798	70.444	−1.415
2700	20.786	160.516	142.026	49.925	229.064	84.349	−1.245
2800	20.786	161.272	142.700	52.004	229.318	58.243	−1.087
2900	20.786	162.002	143.353	54.082	229.560	52.129	−0.939
3000	20.786	162.706	143.986	56.161	229.790	46.007	−0.801
3100	20.786	183.388	144.601	58.239	230.008	39.877	−0.672
3200	20.786	164.048	145.199	60.318	230.216	33.741	−0.551
3300	20.786	164.688	145.780	62.397	230.413	27.598	−0.437
3400	20.786	165.308	146.345	64.475	230.599	21.449	−0.330
3500	20.786	165.911	145.895	66.554	230.776	15.295	−0.228
3600	20.786	166.496	147.432	68.632	230.942	9.136	−0.133
3700	20.786	167.066	147.955	70.711	231.098	2.973	−0.042
3800	20.786	187.620	148.465	72.790	231.244	−3.195	0.044
3900	20.786	168.160	148.963	74.868	231.381	−9.366	0.125
4000	20.786	168.686	149.450	76.947	231.509	−15.541	0.203
4100	20.786	169.200	149.925	79.025	231.627	−21.718	0.277
4200	20.786	169.700	150.390	81.104	231.736	−27.899	0.347
4300	20.786	170.190	150.845	83.183	231.836	−34.082	0.414
4400	20.786	170.667	151.290	85.261	231.927	−40.267	0.478
4500	20.786	170.135	151.726	87.340	232.009	−46.454	0.539
4600	20.786	171.591	152.153	89.418	232.082	−52.643	0.598
4700	20.786	172.038	152.571	91.497	232.147	−58.834	0.654
4800	20.786	172.476	152.981	93.576	232.204	−65.025	0.708
4900	20.786	172.905	153.383	95.654	232.253	−71.218	0.759
5000	20.786	173.325	153.778	97.733	232.294	−77.412	0.809
5100	20.786	173.736	154.165	99.811	232.327	−83.606	0.856
5200	20.786	174.140	154.546	101.890	232.353	−89.801	0.902
5300	20.786	174.536	154.919	103.969	232.373	−95.997	0.946
5400	20.786	174.924	155.286	106.047	232.386	−102.192	0.989
5500	20.786	175.306	155.646	108.126	232.392	−108.389	1.029
5600	20.786	175.680	156.001	110.204	232.393	−114.584	1.069
5700	20.786	176.048	156.349	112.283	232.389	−120.780	1.107
5800	20.786	176.410	156.692	114.362	232.379	−126.976	1.144
5900	20.786	176.765	157.029	116.440	232.365	−133.172	1.179
6000	20.786	177.114	157.361	118.519	232.348	−139.368	1.213

Oxygen (O_2), ideal gas reference state, mol. wt. = 31.9988

Enthalpy Reference Temperature = T_r = 298.15 K				Standard State Pressure = P° = 0.1 MPs			
	J K^{-1} mol^{-1}			kJ mol^{-1}			
T/K	C_p°	S°	$-[G^\circ - H^\circ(T_r)]/T$	$H^\circ - H^\circ(T_f)$	$\Delta_f H^\circ$	$\Delta_f G^\circ$	Log K_f
0	0.	0.	INFINITE	−8.683	0.	0.	0.
100	29.106	173.307	231.094	−5.779	0.	0.	0.
200	29.126	193.485	207.823	−2.868	0.	0.	0.
250	29.201	199.990	205.630	−1.410	0.	0.	0.
298.15	29.376	205.147	205.147	0.	0.	0.	0.
300	29.385	205.329	205.148	0.054	0.	0.	0.
350	29.694	209.880	205.506	1.531	0.	0.	0.
400	30.106	213.871	206.308	3.025	0.	0.	0.
450	30.584	217.445	207.350	4.543	0.	0.	0.
500	31.091	220.693	208.524	6.084	0.	0.	0.
600	32.090	226.451	211.044	9.244	0.	0.	0.
700	32.981	231.466	213.611	12.499	0.	0.	0.
800	33.733	235.921	216.126	15.835	0.	0.	0.
900	34.355	239.931	218.552	19.241	0.	0.	0.
1000	34.870	243.578	220.875	22.703	0.	0.	0.
1100	35.300	246.922	223.093	26.212	0.	0.	0.
1200	35.667	250.010	225.209	29.761	0.	0.	0.
1300	35.988	252.878	227.229	33.344	0.	0.	0.
1400	36.277	255.556	229.158	36.957	0.	0.	0.
1500	36.544	258.068	231.002	40.599	0.	0.	0.
1600	38.796	260.434	232.768	44.266	0.	0.	0.
1700	37.040	262.672	234.462	47.958	0.	0.	0.
1800	37.277	264.796	236.089	51.673	0.	0.	0.
1900	37.510	268.818	237.653	55.413	0.	0.	0.
2000	37.741	268.748	239.160	59.175	0.	0.	0.
2100	37.969	270.595	240.613	62.961	0.	0.	0.
2200	38.195	272.366	242.017	66.769	0.	0.	0.
2300	38.419	274.069	243.374	70.600	0.	0.	0.
2400	38.639	275.709	244.687	74.453	0.	0.	0.
2500	38.856	277.290	245.959	78.328	0.	0.	0.
2600	39.068	278.819	247.194	82.224	0.	0.	0.
2700	39.276	280.297	248.393	86.141	0.	0.	0.
2800	39.478	281.729	249.558	90.079	0.	0.	0.
2900	39.674	283.118	250.691	94.036	0.	0.	0.
3000	39.864	284.466	251.795	98.013	0.	0.	0.
3100	40.048	285.776	252.870	102.009	0.	0.	0.
3200	40.225	287.050	253.918	106.023	0.	0.	0.
3300	40.395	288.291	254.941	110.054	0.	0.	0.
3400	40.559	289.499	255.940	114.102	0.	0.	0.
3500	40.716	290.677	256.916	118.165	0.	0.	0.
3600	40.868	291.826	257.870	122.245	0.	0.	0.
3700	41.013	292.948	258.802	126.339	0.	0.	0.
3800	41.154	294.044	259.716	130.447	0.	0.	0.
3900	41.289	295.115	260.610	134.569	0.	0.	0.
4000	41.421	298.162	261.485	138.705	0.	0.	0.
4100	41.549	297.186	262.344	142.854	0.	0.	0.
4200	41.674	298.189	263.185	147.015	0.	0.	0.
4300	41.798	299.171	264.011	151.188	0.	0.	0.
4400	41.920	300.133	264.821	155.374	0.	0.	0.
4500	42.042	301.076	265.616	159.572	0.	0.	0.
4600	42.164	302.002	266.397	163.783	0.	0.	0.
4700	42.287	302.910	267.164	168.005	0.	0.	0.
4800	42.413	303.801	267.918	172.240	0.	0.	0.
4900	42.542	304.677	268.660	178.488	0.	0.	0.
5000	42.675	305.538	269.389	180.749	0.	0.	0.
5100	42.813	306.385	270.106	185.023	0.	0.	0.
5200	42.956	307.217	270.811	189.311	0.	0.	0.
5300	43.105	308.037	271.506	193.614	0.	0.	0.
5400	43.262	308.844	272.190	197.933	0.	0.	0.
5500	43.426	309.639	272.884	202.267	0.	0.	0.
5600	43.599	310.424	273.527	206.618	0.	0.	0.
5700	43.781	311.197	274.181	210.987	0.	0.	0.
5800	43.973	311.960	274.826	215.375	0.	0.	0.
5900	44.175	312.713	275.462	219.782	0.	0.	0.
6000	44.387	313.457	276.089	224.210	0.	0.	0.

Oxygen, monatomic (O), ideal gas, mol. wt. = 15.9994

Enthalpy Reference Temperature = T_r = 298.15 K				Standard State Pressure = P° = 0.1 MPa			
	J K^{-1} mol^{-1}			kJ mol^{-1}			
T/K	$\overline{C}^\circ_p$	S°	$-[G^\circ - H^\circ(T_r)]/T$	$H^\circ - H^\circ(T_r)$	$\Delta_f H^\circ$	$\Delta_f G^\circ$	Log K_f
0	0.	0.	INFINITE	−6.725	246.790	246.790	INFINITE
100	23.703	135.947	181.131	−4.518	247.544	242.615	−126.729
200	22.734	152.153	165.085	−2.186	248.421	237.339	−61.986
250	22.246	157.170	161.421	−1.063	248.816	234.522	−49.001
298.15	21.911	161.058	161.058	0.	249.173	231.736	−40.599
300	21.901	161.194	161.059	0.041	249.187	231.628	−40.330
350	21.657	164.551	161.324	1.129	249.537	228.673	−34.128
400	21.482	167.430	161.912	2.207	249.868	225.670	−29.469
450	21.354	169.953	162.668	3.278	250.180	222.626	−25.542
500	21.257	172.197	163.511	4.343	250.474	219.549	−22.936
600	21.124	176.060	165.291	6.462	251.013	213.312	−18.570
700	21.040	179.310	167.067	8.570	251.494	206.990	−15.446
800	20.984	182.116	168.777	10.671	251.926	200.602	−13.098
900	20.944	184.585	170.399	12.767	252.320	194.163	−11.269
1000	20.915	186.790	171.930	14.860	252.682	187.681	−9.803
1100	20.893	188.782	173.373	16.950	253.018	181.165	−8.603
1200	20.877	190.599	174.734	19.039	253.332	174.619	−7.601
1300	20.864	192.270	176.019	21.126	253.627	168.047	−6.752
1400	20.853	193.816	177.236	23.212	253.906	161.453	−6.024
1500	20.845	195.254	178.390	25.296	254.171	154.840	−5.392
1600	20.838	196.599	179.486	27.381	254.421	148.210	−4.639
1700	20.833	197.862	180.530	29.464	254.659	141.564	−4.350
1800	20.830	199.053	181.527	31.547	254.884	134.905	−3.915
1900	20.827	200.179	182.479	33.630	255.097	128.234	−3.525
2000	20.826	201.247	183.391	35.713	255.299	121.552	−3.175
2100	20.827	202.263	184.266	37.796	255.488	114.860	−2.857
2200	20.830	203.232	185.106	39.878	255.667	108.159	−2.568
2300	20.835	204.158	185.914	41.962	255.835	101.450	−2.304
2400	20.841	205.045	186.693	44.045	255.992	94.734	−2.062
2500	20.851	205.896	187.444	46.130	256.139	88.012	−1.839
2600	20.862	206.714	188.170	48.216	256.277	81.284	−1.633
2700	20.877	207.502	188.871	50.303	256.405	74.551	−1.442
2800	20.894	208.261	189.550	52.391	256.525	67.814	−1.265
2900	20.914	208.995	190.208	54.481	256.637	61.072	−1.100
3000	20.937	209.704	190.846	56.574	256.741	54.327	−0.946
3100	20.963	210.391	191.466	58.669	256.838	47.578	−0.802
3200	20.991	211.057	192.068	60.767	256.929	40.826	−0.666
3300	21.022	211.704	192.653	62.867	257.014	34.071	−0.539
3400	21.056	212.332	193.223	64.971	257.094	27.315	−0.420
3500	21.092	212.943	193.777	67.079	257.169	20.555	−0.307
3600	21.130	213.537	194.318	69.190	257.241	13.794	−0.200
3700	21.170	214.117	194.845	71.305	257.309	7.030	−0.099
3800	21.213	214.682	195.360	73.424	257.373	0.265	−0.004
3900	21.257	215.234	195.862	75.547	257.436	−6.501	0.087
4000	21.302	215.772	196.353	77.675	257.496	−13.270	0.173
4100	21.349	216.299	196.834	79.808	257.554	−20.010	0.255
4200	21.397	216.814	197.303	81.945	257.611	−26.811	0.333
4300	21.445	217.318	197.763	84.087	257.666	−33.583	0.408
4400	21.495	217.812	198.213	86.234	257.720	−40.358	0.479
4500	21.545	218.295	198.654	88.386	257.773	−47.133	0.547
4600	21.596	218.769	199.086	90.543	257.825	−53.909	0.612
4700	21.647	219.234	199.510	92.705	257.876	−60.687	0.674
4800	21.697	219.690	199.925	94.872	257.926	−67.465	0.734
4900	21.748	220.138	200.333	97.045	257.974	−74.244	0.791
5000	21.799	220.578	200.734	99.222	258.021	−81.025	0.846
5100	21.849	221.010	201.127	101.405	258.066	−87.808	0.899
5200	21.899	221.435	201.514	103.592	258.110	−94.589	0.950
5300	21.949	221.853	201.893	105.784	258.150	−101.371	0.999
5400	21.997	222.264	202.267	107.982	258.189	−106.155	1.046
5500	22.045	222.668	202.634	110.184	258.224	−114.940	1.092
5600	22.093	223.065	202.995	112.391	258.255	−121.725	1.135
5700	22.139	223.457	203.351	114.602	258.282	−128.510	1.178
5800	22.184	223.842	203.701	116.818	258.304	−135.296	1.218
5900	22.229	224.222	204.046	119.039	258.321	−142.083	1.258
6000	22.273	224.596	204.385	121.264	258.332	−148.889	1.296

Water (H_2O), ideal gas, mol. wt. = 18.01528

Enthalpy Reference Temperature = T_r = 298.15 K				Standard State Pressure = P° = 0.1 MPa			
	J K^{-1} mol^{-1}			kJ mol^{-1}			
T/K	C_p°	S°	$-[G^\circ - H^\circ(T_r)]/T$	$H^\circ - H^\circ(T_r)$	$\Delta_f H^\circ$	$\Delta_f G^\circ$	Log K_f
0	0.	0.	INFINITE	−9.904	−238.921	−238.921	INFINITE
100	33.299	152.388	218.534	−6.615	−240.083	−236.584	123.579
200	33.349	175.485	191.896	−3.282	−240.900	−232.766	60.792
298.15	33.590	188.834	188.834	0.	−241.826	−228.582	40.047
300	33.596	189.042	188.835	0.062	−241.844	−228.500	39.785
400	34.262	198.788	190.159	3.452	−242.846	−223.901	29.238
500	35.226	206.534	192.685	6.925	−243.826	−219.051	22.884
600	36.325	213.052	195.550	10.501	−244.758	−214.007	18.631
700	37.495	218.739	198.465	14.192	−245.632	−206.612	15.582
800	38.721	223.825	201.322	18.002	−246.443	−203.496	13.287
900	39.987	228.459	204.084	21.938	−247.185	−198.083	11.496
1000	41.268	232.738	206.738	26.000	−247.857	−192.590	10.060
1100	42.536	236.731	209.285	30.191	−248.460	−187.033	8.881
1200	43.768	240.485	211.730	34.506	−248.997	−181.425	7.897
1300	44.945	244.035	214.080	38.942	−249.473	−175.774	7.063
1400	46.054	247.407	216.341	43.493	−249.894	−170.089	6.346
1500	47.090	250.620	218.520	48.151	−250.265	−164.376	5.724
1600	48.050	253.690	220.623	52.908	−250.592	−158.639	5.179
1700	48.935	256.630	222.655	57.758	−250.881	−152.883	4.698
1800	49.749	259.451	224.621	62.693	−251.138	−147.111	4.269
1900	50.496	262.161	226.526	67.706	−251.368	−141.325	3.885
2000	51.180	264.769	228.374	72.790	−251.575	−135.528	3.540
2100	51.823	267.282	230.167	77.941	−251.762	−129.721	3.227
2200	52.408	269.706	231.909	83.153	−251.934	−123.905	2.942
2300	52.947	272.048	233.604	88.421	−252.092	−118.082	2.682
2400	53.444	274.312	235.253	93.741	−252.239	−112.252	2.443
2500	53.904	276.503	236.860	99.108	−252.379	−106.416	2.223
2600	54.329	278.625	238.425	104.520	−252.513	−100.575	2.021
2700	54.723	280.683	239.952	109.973	−252.643	−94.729	1.833
2800	55.089	282.680	241.443	115.464	−252.771	−88.878	1.658
2900	55.430	284.619	242.899	120.990	−252.897	−83.023	1.495
3000	55.748	286.504	244.321	128.549	−253.024	−77.163	1.344
3100	56.044	288.337	245.711	132.139	−253.152	−71.298	1.201
3200	56.323	290.120	247.071	137.757	−253.282	−65.430	1.086
3300	56.583	291.858	248.402	143.403	−253.416	−59.558	0.943
3400	56.828	293.550	249.705	149.073	−253.553	−53.681	0.825
3500	57.058	295.201	250.982	154.768	−253.696	−47.801	0.713
3600	57.276	296.812	252.233	160.485	−253.844	−41.916	0.608
3700	57.480	298.384	253.459	166.222	−253.997	−36.027	0.509
3800	57.675	299.919	254.661	171.980	−254.158	−30.133	0.414
3900	57.859	301.420	255.841	177.757	−254.326	−24.236	0.325
4000	58.033	302.887	256.999	183.552	−254.501	−18.334	0.239
4100	58.199	304.322	258.136	189.363	−254.684	−12.427	0.158
4200	58.357	305.726	259.252	195.191	−254.876	−6.516	0.081
4300	58.507	307.101	260.349	201.034	−255.078	−0.600	0.007
4400	58.650	308.448	261.427	206.892	−255.288	5.320	−0.063
4500	58.767	309.767	262.486	212.764	−255.508	11.245	−0.131
4600	58.918	311.061	263.528	218.650	−255.738	17.175	−0.195
4700	59.044	312.329	264.553	224.548	−255.978	23.111	−0.257
4800	59.164	313.574	265.562	230.458	−256.229	29.052	−0.316
4900	59.275	314.795	266.554	236.380	−256.491	34.998	−0.373
5000	59.390	315.993	267.531	242.313	−256.763	40.949	−0.428
5100	59.509	317.171	268.493	248.256	−257.046	46.906	−0.480
5200	59.628	318.327	269.440	254.215	−257.338	52.869	−0.531
5300	59.746	319.464	270.373	260.184	−257.639	58.838	−0.580
5400	59.864	320.582	271.293	266.164	−257.950	64.811	−0.627
5500	59.982	321.682	272.199	272.157	−258.268	70.791	−0.672
5600	60.100	322.764	273.092	278.161	−258.595	76.777	−0.716
5700	60.218	323.828	273.973	284.177	−258.930	82.769	−0.758
5800	60.335	324.877	274.841	290.204	−259.272	88.787	−0.799
5900	60.453	325.909	275.698	296.244	−259.621	94.770	−0.839
6000	60.571	326.926	276.544	302.295	−259.977	100.780	−0.877

Hydroxyl (OH), ideal gas, mol. wt. = 17.0074

Enthalpy Reference Temperature = T_r = 298.15 K				Standard State Pressure = P° = 0.1 MPa			
	J K^{-1} mol^{-1}			kJ mol^{-1}			
T/K	C_p°	S°	$-[G^\circ - H^\circ(T_r)]/T$	$H^\circ - H^\circ(T_r)$	$\Delta_f H^\circ$	$\Delta_f G^\circ$	Log K_f
0	0.	0.	INFINITE	−9.172	38.390	38.390	INFINITE
100	32.627	149.590	210.980	−6.139	38.471	37.214	−19.438
200	30.777	171.592	186.471	−2.976	38.832	35.803	−9.351
250	30.283	178.402	184.204	−1.450	38.930	35.033	−7.320
298.15	29.986	183.708	183.708	0.	38.987	34.277	−6.005
300	29.977	183.894	183.709	0.055	38.988	34.248	−5.963
350	29.780	188.499	184.073	1.549	39.019	33.455	−4.993
400	29.650	192.466	184.880	3.035	39.029	32.660	−4.265
450	29.567	195.954	185.921	4.515	39.020	31.864	−3.699
500	29.521	199.066	187.082	5.992	38.995	31.070	−3.246
600	29.527	204.447	189.542	8.943	38.902	29.493	−2.568
700	29.663	209.007	192.005	11.902	38.764	27.935	−2.085
800	29.917	212.983	194.384	14.880	38.598	26.399	−1.724
900	30.264	216.526	196.651	17.888	38.416	24.884	−1.444
1000	30.676	219.736	198.801	20.935	38.230	23.391	−1.222
1100	31.124	222.680	200.840	24.024	38.046	21.916	−1.041
1200	31.586	225.408	202.775	27.160	37.867	20.458	−0.891
1300	32.046	227.955	204.615	30.342	37.697	19.014	−0.764
1400	32.492	230.346	206.368	33.569	37.535	17.583	−0.656
1500	32.917	232.602	208.043	38.839	37.381	16.163	−0.563
1600	33.319	234.740	209.645	40.151	37.234	14.753	−0.482
1700	33.694	236.771	211.182	43.502	37.093	13.352	−0.410
1800	34.044	238.707	212.657	46.889	36.955	11.960	−0.347
1900	34.369	240.557	214.078	50.310	36.819	10.575	−0.291
2000	34.670	242.327	215.446	53.762	36.685	9.197	−0.240
2100	34.950	244.026	216.767	57.243	36.551	7.826	−0.195
2200	35.209	245.658	218.043	60.752	36.416	6.462	−0.153
2300	35.449	247.228	219.278	64.285	36.278	5.103	−0.116
2400	35.673	248.741	220.474	67.841	36.137	3.750	−0.082
2500	35.881	250.202	221.635	71.419	35.992	2.404	−0.050
2600	36.075	251.613	222.761	75.017	35.843	1.063	−0.021
2700	36.256	252.978	223.855	76.633	35.689	−0.271	0.005
2800	36.426	254.300	224.918	82.267	35.530	−1.600	0.030
2900	36.588	255.581	225.954	85.918	35.365	−2.924	0.053
3000	36.736	256.824	226.962	89.584	35.194	−4.241	0.074
3100	36.878	258.031	227.945	93.265	35.017	−5.552	0.094
3200	37.013	259.203	228.904	96.960	34.834	−6.858	0.112
3300	37.140	260.344	229.839	100.667	34.644	−8.158	0.129
3400	37.261	261.455	230.753	104.387	34.448	−9.452	0.145
3500	37.376	262.537	231.645	108.119	34.246	−10.741	0.160
3600	37.486	263.591	232.518	111.863	34.037	−12.023	0.174
3700	37.592	264.620	233.372	115.617	33.821	−13.300	0.188
3800	37.693	265.624	234.208	119.381	33.599	−14.570	0.200
3900	37.791	266.604	235.026	123.155	33.371	−15.834	0.212
4000	37.885	267.562	235.827	126.939	33.136	−17.093	0.223
4100	37.976	268.499	236.613	130.732	32.894	−18.346	0.234
4200	38.064	269.415	237.383	134.534	32.646	−19.593	0.244
4300	38.150	270.311	238.138	138.345	32.391	−20.833	0.253
4400	38.233	271.189	238.879	142.164	32.130	−22.068	0.262
4500	38.315	272.050	239.607	145.991	31.862	−23.297	0.270
4600	38.394	272.893	240.322	149.827	31.587	−24.520	0.278
4700	38.472	273.719	241.023	153.670	31.305	−25.737	0.286
4800	38.549	274.530	241.713	157.521	31.017	−26.947	0.293
4900	38.625	275.326	242.391	161.380	30.722	−28.152	0.300
5000	38.699	276.107	243.057	165.246	30.420	−29.350	0.307
5100	38.773	276.874	243.713	169.120	30.111	−30.542	0.313
5200	38.846	277.627	244.358	173.001	29.796	−31.729	0.319
5300	38.919	278.368	244.993	176.889	29.473	−32.909	0.324
5400	38.991	279.096	245.617	180.784	29.144	−34.083	0.330
5500	39.062	279.812	246.233	184.687	28.807	−35.251	0.335
5600	39.134	280.517	246.839	188.597	28.464	−36.412	0.340
5700	39.206	281.210	247.436	192.514	28.113	−37.568	0.344
5800	39.278	281.892	248.024	196.438	27.756	−38.716	0.349
5900	39.350	282.564	248.804	200.369	27.391	−39.860	0.353
6000	39.423	283.226	249.175	204.308	27.019	−40.997	0.357

Carbon monoxide (CO), ideal gas, mol. wt. = 28.0104

Enthalpy Reference Temperature = T_r = 298.15 K				Standard State Pressure = P° = 0.1 MPa			
	J K^{-1} mol^{-1}			kJ mol^{-1}			
T/K	C_p°	S°	$-[G^\circ - H^\circ(T_r)]/T$	$H^\circ - H^\circ(T_r)$	$\Delta_f H^\circ$	$\Delta_f G^\circ$	Log K_f
0	0.	0.	INFINITE	−8.671	−113.805	−113.805	INFINITE
100	29.104	165.850	223.539	−5.769	−112.415	−120.239	62.807
200	29.108	186.025	200.317	−2.858	−111.286	−128.526	33.568
298.15	29.142	197.653	197.653	0.	−110.527	−137.163	24.030
300	29.142	197.833	197.653	0.054	−110.516	−137.328	23.911
400	29.342	206.238	198.798	2.976	−110.102	−146.338	19.110
500	29.794	212.831	200.968	5.931	−110.003	−115.414	16.236
600	30.443	218.319	203.415	8.942	−110.150	−164.486	14.320
700	31.171	223.066	205.890	12.023	−110.469	−173.518	12.948
800	31.899	227.277	208.305	15.177	−110.905	−182.497	11.916
900	32.577	231.074	210.628	18.401	−111.418	−191.416	11.109
1000	33.183	234.538	212.848	21.690	−111.983	−200.275	10.461
1100	33.710	237.726	214.967	25.035	−112.586	−209.075	9.928
1200	34.175	240.679	216.988	28.430	−113.217	−217.819	9.481
1300	34.572	243.431	218.917	31.868	−113.870	−226.509	9.101
1400	34.920	246.006	220.761	35.343	−114.541	−235.149	8.774
1500	35.217	248.426	222.526	38.850	−115.229	−243.740	8.488
1600	35.480	250.707	224.216	42.385	−115.933	−252.284	8.236
1700	35.710	252.865	225.839	45.945	−116.651	−260.784	8.013
1800	35.911	254.912	227.398	49.526	−117.384	−269.242	7.813
1900	36.091	256.859	228.897	53.126	−118.133	−277.658	7.633
2000	36.250	258.714	230.342	58.744	−118.896	−286.034	7.470
2100	36.392	260.486	231.736	60.376	−119.675	−294.372	7.322
2200	36.518	262.182	233.081	64.021	−120.470	−302.672	7.186
2300	36.635	263.809	234.382	67.683	−121.278	−310.936	7.062
2400	36.321	265.359	235.641	71.324	−122.133	−319.164	6.946
2500	36.836	266.854	236.860	74.985	−122.994	−327.356	6.840
2600	36.924	268.300	238.041	78.673	−123.854	−335.514	6.741
2700	37.003	269.695	239.188	82.369	−124.731	−343.638	6.648
2800	37.083	271.042	240.302	86.074	−125.623	−351.729	6.562
2900	37.150	272.345	241.384	89.786	−126.532	−359.789	6.480
3000	37.217	273.605	242.437	93.504	−127.457	−367.816	6.404
3100	37.279	274.827	243.463	97.229	−128.397	−375.812	6.332
3200	37.338	276.011	244.461	100.960	−129.353	−383.778	6.265
3300	37.392	277.161	245.435	104.696	−130.325	−391.714	6.200
3400	37.443	278.278	246.385	108.438	−131.312	−399.620	6.139
3500	37.493	279.364	247.311	112.185	−132.313	−407.497	6.082
3600	37.543	280.421	248.216	115.937	−133.329	−415.345	6.027
3700	37.589	281.450	249.101	119.693	−134.360	−423.165	5.974
3800	37.631	282.453	249.965	123.454	−135.405	−430.956	5.924
3900	37.673	283.431	250.811	127.219	−136.464	−438.720	5.876
4000	37.715	284.386	251.638	130.989	−137.537	−446.457	5.830
4100	37.756	285.317	252.449	134.762	−138.623	−454.166	5.786
4200	37.794	286.228	253.242	138.540	−139.723	−461.849	5.744
4300	37.832	287.117	254.020	142.321	−140.836	−469.506	5.703
4400	37.869	287.988	254.782	146.106	−141.963	−477.136	5.664
4500	37.903	288.839	255.529	149.895	−143.103	−484.741	5.627
4600	37.941	289.673	256.262	153.687	−144.257	−492.321	5.590
4700	37.974	290.489	256.982	157.483	−145.424	−499.875	5.555
4800	38.007	291.289	257.688	161.282	−146.605	−507.404	5.522
4900	38.041	292.073	258.382	165.084	−147.800	−514.908	5.489
5000	38.074	292.842	259.064	168.890	−149.009	−522.387	5.457
5100	38.104	293.596	259.733	172.699	−150.231	−529.843	5.427
5200	38.137	294.336	260.392	176.511	−151.469	−537.275	5.397
5300	38.171	295.063	261.039	180.326	−152.721	−544.681	5.368
5400	38.200	295.777	261.676	184.146	−153.987	−552.065	5.340
5500	38.074	296.476	262.302	187.957	−155.279	−559.426	5.313
5600	38.263	297.164	262.919	191.775	−156.585	−566.762	5.287
5700	38.296	297.842	263.525	195.603	−157.899	−574.075	5.261
5800	38.325	298.508	264.123	199.434	−159.230	−581.364	5.236
5900	38.355	299.163	264.711	203.268	−160.579	−588.631	5.211
6000	38.388	299.808	265.291	207.106	−161.945	−595.875	5.188

Carbon dioxide (CO_2), ideal gas, mol. wt. = 44.0098

Enthalpy Reference Temperature = T_r = 298.15 K				Standard State Pressure = P° = 0.1 MPa			
	J K^{-1} mol^{-1}			kJ mol^{-1}			
T/K	C_p°	S°	$-[G^\circ - H^\circ(T_r)]/T$	$H^\circ - H^\circ(T_r)$	$\Delta_f H^\circ$	$\Delta_f G^\circ$	Log K_f
0	0.	0.	INFINITE	−9.364	−393.151	−393.151	INFINITE
100	29.208	179.009	243.568	−6.456	−393.208	−393.683	205.639
200	32.359	199.975	217.046	−3.414	−393.404	−394.085	102.924
298.15	37.129	213.795	213.795	0.	−393.522	−394.389	69.095
300	37.221	214.025	213.795	0.069	−393.523	−394.394	68.670
400	41.325	225.314	215.307	4.003	−393.583	−394.675	51.539
500	44.627	234.901	218.290	8.305	−393.666	−394.939	41.259
600	47.321	243.283	221.772	12.907	−393.803	−395.182	34.404
700	49.564	250.750	225.388	17.754	−393.983	−395.398	29.505
800	51.434	257.494	228.986	22.806	−394.168	−395.586	25.829
900	52.999	263.645	232.500	28.030	−394.405	−395.748	22.969
1000	54.308	269.299	235.901	33.397	−394.623	−395.886	20.679
1100	55.409	274.528	239.178	38.884	−394.838	−396.001	18.805
1200	56.342	279.390	242.329	44.473	−395.050	−396.098	17.242
1300	57.137	283.932	245.356	50.148	−395.257	−396.177	15.919
1400	57.802	288.191	248.265	55.896	−395.462	−398.240	14.784
1500	58.379	292.199	251.062	61.705	−395.668	−396.288	13.800
1600	56.886	295.983	253.753	67.569	−395.876	−396.323	12.939
1700	59.317	299.566	256.343	73.480	−396.090	−396.344	12.178
1800	59.701	302.968	258.840	79.431	−396.311	−396.353	11.502
1900	60.049	306.205	261.248	85.419	−396.542	−396.349	10.896
2000	60.350	309.293	263.574	91.439	−396.784	−396.333	10.351
2100	60.622	312.244	265.822	97.488	−397.039	−396.304	9.858
2200	60.865	315.070	267.996	103.562	−397.309	−396.262	9.408
2300	61.086	317.781	270.102	109.660	−397.596	−396.209	8.998
2400	61.287	320.385	272.144	115.779	−397.900	−396.142	8.622
2500	61.471	322.890	274.124	121.917	−398.222	−396.062	8.275
2600	61.647	325.305	276.046	128.073	−398.562	−395.969	7.955
2700	61.802	327.634	277.914	134.246	−398.921	−395.862	7.658
2800	61.952	329.885	279.730	140.433	−399.299	−395.742	7.383
2900	62.095	332.061	281.497	146.636	−399.695	−395.609	7.126
3000	62.229	334.169	283.218	152.852	−400.111	−395.461	6.886
3100	62.347	336.211	284.895	159.081	−400.545	−395.298	6.661
3200	62.462	338.192	286.529	165.321	−400.998	−398.122	6.450
3300	62.573	340.116	288.124	171.573	−401.470	−394.932	6.251
3400	62.681	341.986	289.681	177.836	−401.960	−394.726	6.064
3500	62.785	343.804	291.202	184.109	−402.467	−394.506	5.888
3600	62.884	345.574	292.687	190.393	−402.991	−394.271	5.721
3700	62.980	347.299	294.140	196.686	−403.532	−394.022	5.563
3800	63.074	348.979	295.561	202.989	−404.089	−393.756	5.413
3900	63.166	350.619	296.952	209.301	−404.682	−393.477	5.270
4000	63.254	352.219	298.314	215.622	−405.251	−393.183	5.134
4100	63.341	353.782	299.648	221.951	−405.856	−392.874	5.005
4200	63.426	355.310	300.955	228.290	−406.475	−392.550	4.882
4300	63.509	356.803	302.236	234.637	−407.110	−392.210	4.764
4400	63.588	358.264	303.493	240.991	−407.760	−391.857	4.652
4500	63.667	359.694	304.726	247.354	−408.426	−391.488	4.544
4600	63.745	361.094	305.937	253.725	−409.106	−391.105	4.441
4700	63.823	362.466	307.125	260.103	−409.802	−390.706	4.342
4800	63.893	363.810	308.292	266.489	−410.514	−390.292	4.247
4900	63.968	365.126	309.438	272.882	−411.242	−389.892	4.156
5000	64.046	366.422	310.585	279.283	−411.986	−389.419	4.068
5100	64.128	367.691	311.673	285.691	−412.746	−388.959	3.984
5200	64.220	368.937	312.762	292.109	−413.522	−388.486	3.902
5300	64.312	370.161	313.833	298.535	−414.314	−387.996	3.824
5400	64.404	371.364	314.888	304.971	−415.123	−387.493	3.748
5500	64.496	372.547	315.925	311.416	−415.949	−386.974	3.675
5600	64.588	373.709	316.947	317.870	−416.794	−386.439	3.605
5700	64.680	374.853	317.953	324.334	−417.658	−385.890	3.536
5800	64.772	375.979	318.944	330.806	−418.541	−385.324	3.470
5900	64.865	377.087	319.920	337.288	−419.445	−384.745	3.406
6000	64.957	378.178	320.882	343.779	−420.372	−384.148	3.344

Nitrogen (N_2), ideal gas reference state, mol. wt. = 28.0134

Enthalpy Reference Temperature = T_r = 298.15 K				Standard State Pressure = P° = 0.1 MPa			
	J K^{-1} mol^{-1}			kJ mol^{-1}			
T/K	C_p°	S°	$-[G^\circ - H^\circ(T_r)]/T$	$H^\circ - H^\circ(T_r)$	$\Delta_f H^\circ$	$\Delta_f G^\circ$	Log K_f
0	0.	0.	INFINITE	−8.670	0.	0.	0.
100	29.104	159.811	217.490	−5.768	0.	0.	0.
200	29.107	179.985	194.272	−2.857	0.	0.	0.
250	29.111	186.481	192.088	−1.402	0.	0.	0.
298.15	29.124	191.609	191.609	0.	0.	0.	0.
300	29.125	191.789	191.610	0.054	0.	0.	0.
350	29.165	196.281	191.964	1.511	0.	0.	0.
400	29.249	200.181	192.753	2.971	0.	0.	0.
450	29.387	203.633	193.774	4.437	0.	0.	0.
500	29.580	206.739	194.917	5.911	0.	0.	0.
600	30.110	212.176	197.353	8.894	0.	0.	0.
700	30.754	216.866	199.813	11.937	0.	0.	0.
800	31.433	221.017	202.209	15.046	0.	0.	0.
900	32.090	224.757	204.510	18.223	0.	0.	0.
1000	32.697	228.170	206.708	21.463	0.	0.	0.
1100	33.241	231.313	208.804	24.760	0.	0.	0.
1200	33.723	234.226	210.802	28.109	0.	0.	0.
1300	34.147	236.943	212.710	31.503	0.	0.	0.
1400	34.518	239.487	214.533	34.936	0.	0.	0.
1500	34.843	241.880	216.277	38.405	0.	0.	0.
1600	35.128	244.138	217.948	41.904	0.	0.	0.
1700	35.378	246.275	219.552	45.429	0.	0.	0.
1800	35.600	248.304	221.094	48.978	0.	0.	0.
1900	35.796	250.234	222.577	52.548	0.	0.	0.
2000	35.971	252.074	224.006	56.137	0.	0.	0.
2100	36.126	253.833	225.385	59.742	0.	0.	0.
2200	36.268	255.517	226.717	63.361	0.	0.	0.
2300	36.395	257.132	228.004	66.995	0.	0.	0.
2400	36.511	258.684	229.250	70.640	0.	0.	0.
2500	36.616	260.176	230.458	74.296	0.	0.	0.
2600	36.713	261.614	231.629	77.963	0.	0.	0.
2700	36.801	263.001	232.765	81.639	0.	0.	0.
2800	36.883	264.341	233.869	85.323	0.	0.	0.
2900	36.959	265.637	234.942	89.015	0.	0.	0.
3000	37.030	266.891	235.986	92.715	0.	0.	0.
3100	37.096	268.106	237.003	96.421	0.	0.	0.
3200	37.158	269.285	237.993	100.134	0.	0.	0.
3300	37.216	270.429	238.959	103.852	0.	0.	0.
3400	37.271	271.541	239.901	107.577	0.	0.	0.
3500	37.323	272.622	240.821	111.306	0.	0.	0.
3600	37.373	273.675	241.719	115.041	0.	0.	0.
3700	37.420	274.699	242.596	118.781	0.	0.	0.
3800	37.465	275.698	243.454	122.525	0.	0.	0.
3900	37.508	276.671	244.294	126.274	0.	0.	0.
4000	37.550	277.622	245.115	130.027	0.	0.	0.
4100	37.590	278.549	245.919	133.784	0.	0.	0.
4200	37.629	279.456	246.707	137.545	0.	0.	0.
4300	37.666	280.341	247.479	141.309	0.	0.	0.
4400	37.702	281.208	248.236	145.078	0.	0.	0.
4500	37.738	282.056	248.978	148.850	0.	0.	0.
4600	37.773	282.885	249.706	152.625	0.	0.	0.
4700	37.808	283.698	250.420	156.405	0.	0.	0.
4800	37.843	284.494	251.122	160.187	0.	0.	0.
4900	37.878	285.275	251.811	163.973	0.	0.	0.
5000	37.912	286.041	252.488	167.763	0.	0.	0.
5100	37.947	286.792	253.153	171.556	0.	0.	0.
5200	37.981	287.529	253.807	175.352	0.	0.	0.
5300	38.013	288.253	254.451	179.152	0.	0.	0.
5400	38.046	288.964	255.083	182.955	0.	0.	0.
5500	38.080	289.662	255.705	186.761	0.	0.	0.
5600	38.116	290.348	256.318	190.571	0.	0.	0.
5700	38.154	291.023	256.921	194.384	0.	0.	0.
5800	38.193	291.687	257.515	198.201	0.	0.	0.
5900	38.234	292.341	258.099	202.023	0.	0.	0.
6000	38.276	292.984	258.675	205.848	0.	0.	0.

Nitrogen, monatomic (N), ideal gas, mol. wt. = 14.0067

Enthalpy Reference Temperature = T_r = 298.15 K				Standard State Pressure = P° = 0.1 MPa			
	J K^{-1} mol^{-1}			KJ mol^{-1}			
T/K	C_p°	S°	$-[G^\circ - H^\circ(T_r)]/T$	$H^\circ - H^\circ(T_r)$	$\Delta_f H^\circ$	$\Delta_f G^\circ$	Log K_f
0	0.	0.	INFINITE	−6.197	470.820	470.820	INFINITE
100	20.786	130.593	171.780	−4.119	471.448	466.379	−243.611
200	20.786	145.001	155.201	−2.040	472.071	461.070	−120.419
250	20.786	149.639	153.642	−1.001	472.383	458.283	−95.753
296.15	20.796	153.300	153.300	0.	472.683	455.540	−79.809
300	20.788	153.429	153.300	0.038	472.694	455.434	−79.298
350	20.786	156.633	153.554	1.078	473.005	452.533	−67.537
400	20.786	159.408	154.116	2.117	473.314	449.587	−58.710
450	20.786	161.857	154.843	3.156	473.621	446.603	−51.840
500	20.786	164.047	155.655	4.196	473.923	443.584	−46.341
600	20.766	167.836	157.379	6.274	474.510	437.461	−38.084
700	20.786	171.041	159.108	8.353	475.067	431.242	−32.180
800	20.786	173.816	160.777	10.431	475.591	424.945	−27.746
900	20.786	176.264	162.364	12.510	476.081	418.584	−24.294
1000	20.786	178.454	163.866	14.589	476.540	412.171	−21.530
1100	20.786	180.436	165.284	16.667	476.970	405.713	−19.266
1200	20.786	182.244	166.623	18.746	477.374	399.217	−17.377
1300	20.788	183.908	167.889	20.824	477.756	392.688	−15.778
1400	20.786	185.448	169.089	22.903	478.118	386.131	−14.407
1500	20.786	186.882	170.228	24.982	478.462	379.548	−13.217
1600	20.786	188.224	171.311	27.060	478.791	372.943	−12.175
1700	20.786	189.484	172.344	29.139	479.107	366.318	−11.256
1800	20.787	190.672	173.329	31.218	479.411	359.674	−10.437
1900	20.788	191.796	174.272	33.296	479.705	353.014	−9.705
2000	20.790	192.863	175.175	35.375	479.990	346.339	−9.045
2100	20.793	193.877	176.042	37.454	480.266	339.650	−8.448
2200	20.797	194.844	176.874	39.534	480.536	332.947	−7.905
2300	20.804	195.769	177.676	41.614	480.799	326.233	−7.409
2400	20.813	196.655	178.448	43.695	481.057	319.507	−6.954
2500	20.826	197.504	179.194	45.777	481.311	312.770	−6.535
2600	20.843	198.322	179.914	47.860	481.561	306.024	−6.148
2700	20.864	199.109	180.610	49.945	481.809	299.268	−5.790
2800	20.891	199.868	181.285	52.033	482.054	292.502	−5.457
2900	20.924	200.601	181.938	54.124	482.299	285.728	−5.147
3000	20.963	201.311	182.572	56.218	482.543	278.946	−4.857
3100	21.010	202.000	183.188	58.317	482.789	272.155	−4.586
3200	21.064	202.667	183.786	60.420	483.036	265.357	−4.332
3300	21.126	203.317	184.368	62.530	483.286	258.550	−4.093
3400	21.197	203.948	184.935	64.646	483.540	251.736	−3.867
3500	21.277	204.564	185.487	66.769	483.799	244.915	−3.655
3600	21.365	205.164	186.025	68.902	484.064	238.086	−3.455
3700	21.463	205.751	188.550	71.043	484.335	231.249	−3.265
3800	21.569	206.325	187.063	73.194	484.614	224.405	−3.085
3900	21.685	206.887	187.564	75.357	484.903	217.554	−2.914
4000	21.809	207.437	188.054	77.532	485.201	210.695	−2.751
4100	21.941	207.977	188.534	79.719	485.510	203.829	−2.597
4200	22.082	208.508	189.003	81.920	485.830	196.955	−2.449
4300	22.231	209.029	189.463	84.136	486.164	190.073	−2.309
4400	22.388	209.542	189.913	86.367	486.510	183.183	−2.175
4500	22.551	210.047	190.355	88.614	486.871	176.285	−2.046
4600	22.722	210.544	190.788	90.877	487.247	169.379	−1.923
4700	22.899	211.035	191.214	93.158	487.638	162.465	−1.806
4800	23.081	211.519	191.632	95.457	488.046	155.542	−1.693
4900	23.269	211.997	192.043	97.775	488.471	148.610	−1.584
5000	23.461	212.469	192.447	100.111	488.912	141.670	−1.480
5100	23.658	212.935	192.844	102.467	489.372	134.721	−1.380
5200	23.858	213.397	193.235	104.843	489.849	127.762	−1.283
5300	24.061	213.853	193.619	107.238	490.345	120.794	−1.190
5400	24.266	214.305	193.998	109.655	490.860	113.817	−1.101
5500	24.474	214.752	194.371	112.092	491.394	106.829	−1.015
5600	24.682	215.195	194.739	114.550	491.947	99.832	−0.931
5700	24.892	215.633	195.102	117.028	492.519	92.825	−0.851
5800	25.102	216.068	195.460	119.528	493.110	85.808	−0.773
5900	25.312	216.499	195.813	122.049	493.720	78.780	−0.697
6000	25.521	216.926	196.161	124.590	494.349	71.742	−0.625

Nitrogen oxide (NO), ideal gas, mol. wt. = 30.0061

Enthalpy Reference Temperature = T_r = 298.15 K				Standard State Pressure = P° = 0.1 MPa			
	J K^{-1} mol^{-1}			kJ mol^{-1}			
T/K	C_p°	S°	$-[G^\circ - H^\circ(T_r)]/T$	$H^\circ - H^\circ(T_r)$	$\Delta_f H^\circ$	$\Delta_f G^\circ$	Log K_f
0	0	0.	INFINITE	−9.192	89.775	89.775	INFINITE
100	32.302	177.031	237.757	−6.073	89.991	88.944	−46.460
200	30.420	198.747	213.501	−2.951	90.202	87.800	−22.931
250	30.025	205.488	211.251	−1.441	90.256	87.193	−18.218
298.15	29.845	210.758	210.758	0.	90.291	86.600	−15.172
300	29.841	210.943	210.759	0.055	90.292	86.577	−15.074
350	29.823	215.540	211.122	1.546	90.316	85.955	−12.828
400	29.944	219.529	211.929	3.040	90.332	85.331	−11.143
450	30.175	223.068	212.974	4.542	90.343	84.705	−9.832
500	30.486	226.263	214.145	6.059	90.352	84.079	−8.784
600	31.238	231.886	216.646	9.144	90.366	82.822	−7.210
700	32.028	236.761	219.179	12.307	90.381	81.564	−6.086
800	32.767	241.087	221.652	15.548	90.398	80.303	−5.243
900	33.422	244.985	224.031	18.858	90.417	79.041	−4.587
1000	33.987	248.536	226.307	22.229	90.437	77.775	−4.063
1100	34.468	251.799	228.478	25.653	90.457	76.508	−3.633
1200	34.877	254.816	230.549	29.120	90.476	75.239	−3.275
1300	35.226	257.621	232.525	32.626	90.493	73.969	−2.972
1400	35.524	260.243	234.412	36.164	90.508	72.697	−2.712
1500	35.780	262.703	236.217	39.729	90.518	71.425	−2.487
1600	36.002	265.019	237.945	43.319	90.525	70.151	−2.290
1700	36.195	267.208	239.603	46.929	90.526	68.878	−2.116
1800	36.364	269.282	241.195	50.557	90.522	67.605	−1.962
1900	36.514	271.252	242.725	54.201	90.511	66.332	−1.824
2000	36.647	273.128	244.199	57.859	90.494	65.060	−1.699
2100	36.767	274.919	245.619	61.530	90.469	63.788	−1.587
2200	36.874	276.632	246.990	65.212	90.438	62.519	−1.484
2300	36.971	278.273	248.315	68.904	90.398	61.251	−1.391
2400	37.060	279.849	249.596	72.606	90.350	59.984	−1.306
2500	37.141	281.383	250.837	76.316	90.295	58.720	−1.227
2600	37.216	282.822	252.039	80.034	90.231	57.458	−1.154
2700	37.285	284.227	253.205	83.759	90.160	56.199	−1.087
2600	37.350	285.585	254.338	87.491	90.081	54.943	−1.025
2900	37.410	286.896	255.438	91.229	89.994	53.689	−0.967
3000	37.466	288.165	256.508	94.973	89.899	52.439	−0.913
3100	37.519	289.395	257.549	98.722	89.798	51.192	−0.863
3200	37.570	290.587	258.563	102.477	89.689	49.948	−0.815
3300	37.617	291.744	259.551	106.236	89.574	48.708	−0.771
3400	37.663	292.867	260.514	110.000	89.451	47.472	−0.729
3500	37.706	293.960	261.454	113.768	89.323	46.239	−0.690
3600	37.747	295.022	262.372	117.541	89.189	45.010	−0.653
3700	37.787	296.057	263.269	121.318	89.049	43.784	−0.618
3800	37.825	297.065	264.145	125.098	88.903	42.563	−0.585
3900	37.862	298.048	265.002	128.883	88.752	41.346	−0.554
4000	37.898	299.008	265.840	132.671	88.596	40.132	−0.524
4100	37.933	299.944	266.660	136.462	88.434	38.922	−0.496
4200	37.966	300.858	267.464	140.257	88.268	37.717	−0.469
4300	37.999	301.752	268.251	144.056	88.097	36.515	−0.444
4400	38.031	302.626	269.022	147.857	87.922	35.318	−0.419
4500	38.062	303.481	269.778	151.662	87.741	34.124	−0.396
4600	38.092	304.318	270.520	155.469	87.556	32.934	−0.374
4700	38.122	305.137	271.248	159.280	87.366	31.749	−0.353
4800	38.151	305.940	271.962	163.094	87.171	30.568	−0.333
4900	38.180	306.727	272.664	166.910	86.970	29.391	−0.313
5000	38.208	307.499	273.353	170.730	86.765	28.218	−0.295
5100	38.235	308.256	274.030	174.552	86.553	27.049	−0.277
5200	38.262	308.998	274.695	178.377	86.336	25.884	−0.260
5300	38.289	309.728	275.349	182.204	89.112	24.724	−0.244
5400	38.316	310.443	275.993	186.034	85.881	23.568	−0.228
5500	38.342	311.147	276.625	189.867	85.644	22.416	−0.213
5600	38.367	311.838	277.248	193.703	85.399	21.289	−0.198
5700	36.393	312.517	277.861	197.541	85.146	20.125	−0.184
5800	38.418	313.185	278.464	201.381	84.884	18.987	−0.171
5900	38.443	313.842	279.058	205.224	84.613	17.853	−0.158
6000	38.468	314.488	279.643	209.070	84.331	16.724	−0.146

Nitrogen dioxide (NO_2), ideal gas, mol. wt. = 46.0055

Enthalpy Reference Temperature = T_r = 298.15 K				Standard State Pressure = P° = 0.1 MPa			
	J K^{-1} mol^{-1}			KJ mol^{-1}			
T/K	C_p°	S°	$-[G^\circ \cdot H^\circ(T_r)]/T$	$H^\circ - H^\circ(T_r)$	$\Delta_f H^\circ$	$\Delta_f G^\circ$	Log K_f
0	0.	0.	INFINITE	−10.186	35.927	35.927	INFINITE
100	33.276	202.563	271.168	−6.881	34.898	39.963	−20.874
200	34.385	225.852	243.325	−3.495	33.897	45.422	−11.863
250	35.593	233.649	240.634	−1.746	33.460	48.355	−10.103
298.15	36.974	240.034	240.034	0.	33.095	51.258	−8.980
300	37.029	240.262	240.034	0.068	33.083	51.371	−8.944
350	38.583	246.086	240.491	1.958	32.768	54.445	−8.125
400	40.171	251.342	241.524	3.927	32.512	57.560	−7.517
450	41.728	256.164	242.886	5.975	32.310	60.703	−7.046
500	43.206	260.638	244.440	8.099	32.154	63.867	−6.672
600	45.834	268.755	247.830	12.555	31.959	70.230	−6.114
700	47.986	275.988	251.345	17.250	31.878	76.616	−5.717
800	49.708	282.512	254.840	22.138	31.874	83.008	−5.420
900	51.076	288.449	258.250	27.179	31.923	89.397	−5.188
1000	52.166	293.889	261.545	32.344	32.005	95.779	−5.003
1100	53.041	298.903	264.717	37.605	32.109	102.152	−4.851
1200	53.748	303.550	267.761	42.946	32.226	108.514	−4.724
1300	54.326	307.876	270.683	48.351	32.351	114.867	−4.615
1400	54.803	311.920	273.485	53.808	32.478	121.209	−4.522
1500	55.200	315.715	276.175	59.309	32.603	127.543	−4.441
1600	55.533	319.288	278.759	64.846	32.724	133.868	−4.370
1700	55.815	322.663	281.244	70.414	32.837	140.186	−4.307
1800	56.055	325.861	283.634	76.007	32.940	146.497	−4.251
1900	56.262	328.897	285.937	81.624	33.032	152.804	−4.201
2000	56.441	331.788	288.158	87.259	33.111	159.106	−4.155
2100	56.596	334.545	290.302	92.911	33.175	165.404	−4.114
2200	56.732	337.181	292.373	98.577	33.223	171.700	−4.077
2300	56.852	339.706	294.377	104.257	33.255	177.993	−4.042
2400	56.958	342.128	296.316	109.947	33.270	184.285	−4.011
2500	57.052	344.455	298.196	115.648	33.268	190.577	−3.982
2600	57.136	346.694	300.018	121.357	33.248	196.870	−3.955
2700	57.211	348.852	301.787	127.075	33.210	203.164	−3.930
2800	57.278	350.934	303.505	132.799	33.155	209.460	−3.908
2900	57.339	352.945	305.176	138.530	33.082	215.757	−3.886
3000	57.394	354.889	306.800	144.267	32.992	222.058	−3.866
3100	57.444	356.772	308.382	150.009	32.885	228.363	−3.848
3200	57.490	358.597	309.923	155.756	32.761	234.670	−3.831
3300	57.531	360.366	311.425	161.507	32.622	240.981	−3.814
3400	57.569	362.084	312.890	167.262	32.467	247.298	−3.799
3500	57.604	363.754	314.319	173.020	32.297	253.618	−3.785
3600	57.636	365.377	315.715	178.783	32.113	259.945	−3.772
3700	57.666	366.957	317.079	184.458	31.914	266.276	−3.759
3800	57.693	368.495	318.412	190.316	31.701	272.613	−3.747
3900	57.719	369.994	319.715	196.086	31.475	278.956	−3.736
4000	57.742	371.455	320.991	201.859	31.236	285.305	−3.726
4100	57.764	372.881	322.239	207.635	30.985	291.659	−3.716
4200	57.784	374.274	323.461	213.412	30.720	298.020	−3.706
4300	57.803	375.634	324.659	219.191	30.444	304.388	−3.698
4400	57.821	376.963	325.833	224.973	30.155	310.762	−3.689
4500	57.837	378.262	326.983	230.756	29.854	317.142	−3.681
4600	57.853	379.534	328.112	236.540	29.540	323.530	−3.674
4700	57.867	380.778	329.219	242.326	29.214	329.925	−3.667
4800	57.881	381.996	330.306	248.114	28.875	336.326	−3.660
4900	57.894	383.190	331.373	253.902	28.523	342.736	−3.654
5000	57.906	384.360	332.421	259.692	28.158	349.152	−3.648
5100	57.917	385.507	333.451	265.483	27.778	355.576	−3.642
5200	57.928	386.631	334.463	271.276	27.384	362.006	−3.636
5300	57.938	387.735	335.458	277.069	26.974	368.446	−3.631
5400	57.948	388.818	336.436	282.863	26.548	374.892	−3.626
5500	57.957	389.881	337.398	288.658	26.106	381.347	−3.622
5600	57.965	390.926	338.344	294.455	25.646	387.811	−3.617
5700	57.973	391.952	339.276	300.251	25.167	394.281	−3.613
5800	57.981	392.960	340.193	306.049	24.669	400.762	−3.609
5900	57.988	393.951	341.096	311.848	24.150	407.249	−3.606
6000	57.995	394.926	341.985	317.647	23.608	413.748	−3.602

APPENDIX F

Summary of Classical Thermodynamics

The basic concepts of classical thermodynamics can be summarized by invoking the following four postulates (Callen, 1985):

1. There exist particular states (called equilibrium states) of simple compressible systems that, macroscopically, are characterized completely by the internal energy, U, the volume, V, and the mole or particle numbers, $N_1, N_2, \ldots, N_k$, of the chemical components.
2. There exists a function called the entropy, S, of the extensive parameters (U, V, N_i) of any composite system, defined for all equilibrium states and having the following property: The values assumed by the extensive parameters in the absence of an internal constraint are those which maximize the entropy for the composite isolated system.
3. The entropy of a composite system is additive over the constituent subsystems. Moreover, the entropy is a continuous, differentiable, and monotonically increasing function of the internal energy.
4. The entropy of any system vanishes in the state for which $(\partial U/\partial S)_{V,N} = 0$ (i.e., at the zero of temperature).

Recall that a *simple compressible system* is defined as one that is macroscopically homogeneous, uncharged, and chemically inert, that is sufficiently large that surface effects can be neglected, and that is not acted on by electric, magnetic, or gravitational fields. Although these four basic postulates are restricted to simple compressible systems, they can readily be extended to more complex systems (Lewis and Randall, 1961).

The first and second postulates define the fundamental functional relationship,

$$S = S(U, V, N_i) \tag{F.1}$$

or

$$U = U(S, V, N_i). \tag{F.2}$$

Differentiating, we obtain

$$dU = \left(\frac{\partial U}{\partial S}\right)_{V,N_i} dS + \left(\frac{\partial U}{\partial V}\right)_{S,N_i} dV + \sum_{i=1}^{k} \left(\frac{\partial U}{\partial N_i}\right)_{S,V,N_{j\neq i}} dN_i. \tag{F.3}$$

We now make the following definitions:

$$T \equiv \left(\frac{\partial U}{\partial S}\right)_{V,N_i} \tag{F.4}$$

$$P \equiv -\left(\frac{\partial U}{\partial V}\right)_{S,N_i} \tag{F.5}$$

$$\mu_i \equiv \left(\frac{\partial U}{\partial N_i}\right)_{S,V,N_{j\neq i}}. \tag{F.6}$$

Substituting Eqs. (F.4–F.6) into Eq. (F.3), we have

$$dU = TdS - PdV + \sum_i \mu_i dN_i \tag{F.7}$$

or

$$dS = \frac{1}{T}\,dU + \frac{P}{T}\,dV - \sum_i \frac{\mu_i}{T}\,dN_i. \tag{F.8}$$

We may now verify that the above definitions for T, P, and μ_i correspond to the usual notions of temperature, pressure, and chemical potential. This can be done by showing that (1) equilibrium with respect to heat transfer comes about when the temperatures in two subsystems are equal; (2) equilibrium of a movable wall takes place when the pressures on both sides are equal; and (3) equilibrium with respect to transfer of chemical species occurs when the chemical potential in any two subsystems is the same. Hence, we see that the chemical potential, a seemingly abstruse concept, is directly analogous to the temperature. Two subsystems are thus in equilibrium with respect to their potential to interchange species A when μ_A is the same in both subsystems.

We can demonstrate the above procedure by analyzing the case of thermal equilibrium. Consider an isolated, composite system consisting of two subsystems separated by a rigid and impermeable wall that permits the flow of heat. The volumes and mole numbers of each subsystem are fixed, but their internal energies, U_1 and U_2, are free to change subject to the conservation condition

$$U_1 + U_2 = \text{constant}. \tag{F.9}$$

The second postulate states that the entropy of an isolated system reaches its maximum at equilibrium; hence, from the third postulate,

$$dS = dS_1 + dS_2 = 0. \tag{F.10}$$

Now, from Eq. (F.8),

$$dS = \frac{1}{T_1}\,dU_1 + \frac{1}{T_2}\,dU_2 = 0; \tag{F.11}$$

moreover, from Eq. (F.9),

$$dU_2 = -\,dU_1, \tag{F.12}$$

and thus

$$\frac{1}{T_1} = \frac{1}{T_2}. \tag{F.13}$$

Therefore, thermal equilibrium is defined by $T_1 = T_2$ in agreement with the usual notions of temperature. Similar developments are considered by Callen (1985) for pressure and the chemical potential.

Among the various special functions of thermodynamics, the three most useful are the enthalpy, H, the Helmholtz free energy, A, and the Gibbs free energy, G, defined, respectively, by

$$H = U + PV \tag{F.14}$$

$$A = U - TS \tag{F.15}$$

$$G = H - TS. \tag{F.16}$$

In differential form, we have, for the enthalpy,

$$dH = dU + PdV + VdP,$$

and thus, from Eq. (F.7),

$$dH = TdS + VdP + \sum_i \mu_i dN_i. \tag{F.17}$$

Similarly, for the Helmholtz free energy,

$$dA = dU - TdS - SdT$$

so that, from Eq. (F.7),

$$dA = -PdV - SdT + \sum_i \mu_i\, dN_i. \tag{F.18}$$

Lastly, for the Gibbs free energy,

$$dG = dH - TdS - SdT$$

and thus, from Eq. (F.17),

$$dG = VdP - SdT + \sum_i \mu_i\, dN_i. \tag{F.19}$$

Significant relations among thermodynamic properties, similar to those defined by Eqs. (F.4–F.6), can be obtained from Eqs. (F.18) and (F.19). We begin by comparing each equation with a parallel expression for its total derivative. Hence, for the Helmholtz free energy, we have

$$dA = \left(\frac{\partial A}{\partial V}\right)_{T,N_i} dV + \left(\frac{\partial A}{\partial T}\right)_{V,N_i} dT + \sum_{i=1}^{k} \left(\frac{\partial A}{\partial N_i}\right)_{T,V,N_{j\neq i}} dN_i, \tag{F.20}$$

which, by comparison to Eq. (F.18), gives

$$P = -\left(\frac{\partial A}{\partial V}\right)_{T,N_i} \tag{F.21}$$

$$S = -\left(\frac{\partial A}{\partial T}\right)_{V,N_i} \tag{F.22}$$

$$\mu_i = \left(\frac{\partial A}{\partial N_i}\right)_{T,V,N_{j\neq i}}. \tag{F.23}$$

Similarly, for the Gibbs free energy, we find

$$V = \left(\frac{\partial G}{\partial P}\right)_{T,N_i} \tag{F.24}$$

$$S = -\left(\frac{\partial G}{\partial T}\right)_{P,N_i} \tag{F.25}$$

$$\mu_i = \left(\frac{\partial G}{\partial N_i}\right)_{T,P,N_{j\neq i}}. \tag{F.26}$$

Finally, because the differentials for the Helmholtz and Gibbs free energies are inherently exact, their second mixed partial derivatives must be equal. Therefore, from Eqs. (F.18) and (F.19), we have the following Maxwell relations:

$$\left(\frac{\partial P}{\partial T}\right)_{V,N_i} = \left(\frac{\partial S}{\partial V}\right)_{T,N_i} \tag{F.27}$$

$$\left(\frac{\partial V}{\partial T}\right)_{P,N_i} = -\left(\frac{\partial S}{\partial P}\right)_{T,N_i}. \tag{F.28}$$

From Eqs. (F.7), (F.17), (F.18), and (F.19), we note that the natural variables for U, H, A, and G are as follows for a nonreacting system:

$$U = U(S, V)$$
$$H = H(S, P)$$
$$A = A(T, V)$$
$$G = G(T, P).$$

The equilibrium criterion for an isolated system, from the second postulate, is

$$(dS)_{U,V,N} = 0, \tag{F.29}$$

in concert with Eq. (F.8). Since P, V, and T are easily measured variables, an equilibrium criterion based on either A or G is typically more useful for practical thermodynamic systems. From Eqs. (F.18) and (F.19), the relevant equilibrium criteria are

$$(dA)_{T,V,N} = 0 \tag{F.30}$$

$$(dG)_{T,P,N} = 0. \tag{F.31}$$

Hence, for a chemically reacting system at constant pressure and temperature, the equilibrium criterion becomes, from Eqs. (F.19) and (F.31),

$$(dG)_{T,P,N} = \sum_i \mu_i dN_i = 0. \tag{F.32}$$

The variables U, S, V, and N_i are called extensive variables since they depend on the size of the system. Mathematically, such variables are called first-order homogeneous since we can write

$$U(\lambda S, \lambda V, \lambda N_i) = \lambda U(S, V, N_i)$$

for any positive constant, λ. Now, according to the Euler theorem, any first-order equation of this form, $y(\lambda x_i) = \lambda y(x_i)$, whose differential is given by $dy = \sum_i g_i dx_i$, can be written as $y = \sum_i g_i x_i$. On this basis, Eq. (F.7) can be converted to

$$U = TS - PV + \sum_i \mu_i N_i. \tag{F.33}$$

From Eqs. (F.14–F.16), we then have

$$H = TS + \sum_i \mu_i N_i \tag{F.34}$$

$$A = -PV + \sum_i \mu_i N_i \tag{F.35}$$

$$G = \sum_i \mu_i N_i. \tag{F.36}$$

Therefore, for a single-component system, the chemical potential $\mu = G/N$.

Consider now the general chemical reaction

$$\nu_A \mathrm{A} + \nu_B \mathrm{B} \rightleftarrows \nu_C \mathrm{C} + \nu_D \mathrm{D},$$

where A and B are reactants, C and D are products, and the ν_i represent multiple stoichiometric coefficients. If we define λ to be the extent of reaction, then

$$dN_i = \nu_i \, d\lambda \tag{F.37}$$

for all i, where the ν_i for products are positive and those for reactants are negative. Hence, from Eqs. (F.32) and (F.37), chemical equilibrium is defined by

$$dG = \left(\sum_i \mu_i \nu_i \right) d\lambda = 0 \tag{F.38}$$

at constant temperature and pressure.

For a single ideal gas at constant temperature, Eq. (F.19) gives

$$dG = V \, dP \tag{F.39}$$

when presuming a closed system. Hence, from Eq. (F.36), we have for the ith pure component

$$d\mu_i = \left(\frac{V}{N_i} \right) dP. \tag{F.40}$$

Now, for an ideal gas,

$$P_i V = N_i RT, \tag{F.41}$$

so that substituting Eq. (F.41) into Eq. (F.40) and integrating, we obtain, for the chemical potential of the ith component of an ideal gas mixture,

$$\mu_i(T, P) - \mu_i^\circ(T) = \int_{P_\circ}^{P_i} \frac{RT}{P_i} \, dP$$

or

$$\mu_i(T, P) = \mu_i^\circ(T) + RT \ln P_i. \tag{F.42}$$

Here, $\mu_i^\circ(T)$ is the chemical potential of the ith component at a standard state pressure of 1 bar and P_i is the partial pressure in bar. Note that the standard state chemical potential is a function only of temperature.

Substituting Eq. (F.42) into Eq. (F.38), we have at chemical equilibrium

$$\sum_i \nu_i \mu_i^\circ(T) + RT \sum_i \ln P_i^{\nu_i} = 0, \tag{F.43}$$

from which we obtain

$$\Delta\mu^\circ = -RT \ln K_p, \tag{F.44}$$

where

$$\Delta\mu^\circ = \nu_C \mu_C^\circ + \nu_D \mu_D^\circ - \nu_A \mu_A^\circ - \nu_B \mu_B^\circ \tag{F.45}$$

and

$$K_p = \frac{P_C^{\nu_C} P_D^{\nu_D}}{P_A^{\nu_A} P_B^{\nu_B}} \tag{F.46}$$

for our general chemical reaction. K_p is the equilibrium constant based on partial pressure in bar and $\Delta\mu^\circ$ is the standard state change in specific Gibbs free energy (chemical potential). From Eq. (F.44), we see that K_p is a function only of temperature.

APPENDIX G

Review of Classical Mechanics

Classical mechanics is invariably associated with Newton's second law, as expressed by

$$\boldsymbol{F} = \frac{d\boldsymbol{p}}{dt}. \tag{G.1}$$

Unfortunately, Eq. (G.1) changes in form when converting among various coordinate systems. This problem constitutes the main disadvantage of the Newtonian approach. Fortunately, however, more convenient formulations are available whose equations are invariant under coordinate transformations. These constitute the so-called Lagrangian and Hamiltonian formulations of classical mechanics.

We may investigate these two approaches by considering a three-dimensional system of n particles. Such a system is said to have $3n$ degrees of freedom, each of which must be known to determine the state of the system. A degree of freedom can be identified by specifying appropriate values for its position and momentum. Hence, we must designate $3n$ values of position and $3n$ values of momentum to determine the state of an n-particle system. In general, the three position coordinates for the ith particle are specified by the vector, $\boldsymbol{r}_i$; similarly, the three momentum coordinates for the same particle are specified by the vector, $\boldsymbol{p}_i$.

The first invariant formulation of classical mechanics utilizes the Lagrangian, defined as

$$L = T - V, \tag{G.2}$$

where T and V denote the kinetic and potential energies, respectively. The kinetic energy can generally be expressed as

$$T = \frac{1}{2} \sum_{i=1}^{3n} p_i \dot{r}_i, \tag{G.3}$$

where $p_i = m_i \dot{r}_i$, m_i is the associated mass, and $\dot{r}_i = dr_i/dt$ is the velocity in any single coordinate direction. For conservative systems, the Lagrangian is explicitly independent of time and the potential energy is a function only of position. Hence, the generalized force component in the r_i direction can be related to the potential energy through

$$-F_i = \frac{\partial V}{\partial r_i}. \tag{G.4}$$

Equations (G.2–G.4) then give

$$\frac{\partial L}{\partial \dot{r}_i} = \frac{\partial T}{\partial \dot{r}_i} = p_i \tag{G.5}$$

$$\frac{\partial L}{\partial r_i} = -\frac{\partial V}{\partial r_i} = F_i, \tag{G.6}$$

so that Eq. (G.1) in terms of the Lagrangian becomes

$$\frac{d}{dt}\left(\frac{\partial L}{\partial \dot{r}_i}\right) - \frac{\partial L}{\partial r_i} = 0 \tag{G.7}$$

for any conservative system. There are $3n$ of these equations of motion, one for each degree of freedom. Notice that the Lagrangian formulation is based on the potential energy of the system, whereas the Newtonian formulation is based on the forces acting on the system. Because it is often much easier to develop an expression for the potential energy than to recognize all relevant forces, the Lagrangian method can be more useful than the Newtonian method for solving many classical problems.

As a specific example, consider a particle of mass m constrained to move along a single coordinate direction. For this case, we have only one degree of freedom and thus

$$\frac{d}{dt}\left(\frac{\partial L}{\partial \dot{r}_i}\right) - \frac{\partial L}{\partial r_i} = \frac{d}{dt}\left[\frac{\partial}{\partial \dot{x}}\left(\frac{1}{2}m\dot{x}^2 - V(x)\right)\right] - \frac{\partial}{\partial x}\left(\frac{1}{2}m\dot{x}^2 - V(x)\right) = 0.$$

Because the position and velocity are considered to be independent variables, the indicated differentiation gives

$$\frac{d}{dt}(m\dot{x}) + \frac{\partial V(x)}{\partial x} = m\ddot{x} + \frac{\partial V}{\partial x} = 0.$$

Substituting from Eq. (G.4), we obtain $F_x = m\ddot{x}$, thus recovering the familiar form of Newton's second law for a single Cartesian direction.

The other invariant approach to the equations of motion is called the Hamiltonian formulation. This procedure is not as useful as Lagrange's method for solving problems, but it is more convenient from a theoretical viewpoint, particularly in quantum mechanics and statistical thermodynamics. The Hamiltonian formulation uses position and momentum as independent variables and is defined for both conservative and nonconservative systems by

$$H = \sum_{i=1}^{3n} p_i \dot{r}_i - L \tag{G.8}$$

when dealing with n particles. Taking the total differential of Eq. (G.8), we find that

$$dH = \sum_{i=1}^{3n} \left\{ p_i d\dot{r}_i + \dot{r}_i dp_i - \frac{\partial L}{\partial r_i} dr_i - \frac{\partial L}{\partial \dot{r}_i} d\dot{r}_i \right\}. \tag{G.9}$$

Substitution of Eq. (G.5) into Eq. (G.7) for a conservative system gives

$$\dot{p}_i = \frac{\partial L}{\partial r_i}; \tag{G.10}$$

hence, from Eqs. (G.5) and (G.10) for $\partial L/\partial \dot{r}_i$ and $\partial L/\partial r_i$, respectively, Eq. (G.9) becomes

$$dH = \sum_{i=1}^{3n} \{\dot{r}_i dp_i - \dot{p}_i dr_i\}.$$

Since H is a function of position and momentum, we can also write dH as

$$dH = \sum_{i=1}^{3n} \left\{ \frac{\partial H}{\partial p_i} dp_i + \frac{\partial H}{\partial r_i} dr_i \right\}.$$

Comparing these two expressions for dH gives

$$\frac{\partial H}{\partial p_i} = \dot{r}_i \tag{G.11}$$

$$\frac{\partial H}{\partial r_i} = -\dot{p}_i. \tag{G.12}$$

Equations (G.11) and (G.12) represent the equations of motion in Hamiltonian form.

We now show that the Hamiltonian is equal to the total energy of the system. Employing Eq. (G.2), Eq. (G.8) can be rewritten as

$$H = \sum_{i=1}^{3n} p_i \dot{r}_i - T + V.$$

Substitution from Eq. (G.3) then gives the desired result,

$$H = T + V. \tag{G.12}$$

The Hamiltonian represents the total kinetic plus potential energy of a conservative system with momentum and position as independent variables. This H-function is important as it forms the classical mechanical basis for the formulation of quantum mechanics.

APPENDIX H

Review of Operator Theory

An operator is a mathematical rule, or set or rules, which transforms one function into another without necessarily specifying any particular function. Mathematically, we define the general operator, $\hat{A}$, as

$$\hat{A} f(x) = g(x).$$

Examples of $\hat{A}$ might be (1) multiply by x or (2) take the first derivative with respect to x. In the first case, $\hat{A}$ is simply x and $g(x) = xf(x)$. In the second case, $\hat{A}$ is d/dx and $g(x) = df(x)/dx$.

Some of the basic rules of operator algebra are as follows:

$$\hat{A}C\, f(x) = C\hat{A}\, f(x) \tag{H.1}$$

$$(\hat{A} + \hat{B})\, f(x) = \hat{A} f(x) + \hat{B}\, f(x) \tag{H.2}$$

$$\hat{A}\hat{B}\, f(x) = \hat{A}\{\hat{B}\, f(x)\} \tag{H.3}$$

$$(\hat{A} + \hat{B}) + \hat{C} = \hat{A} + (\hat{B} + \hat{C}) \tag{H.4}$$

$$\hat{A} + \hat{B} = \hat{B} + \hat{A}, \tag{H.5}$$

where C is a constant. The identity operator, $\hat{I}$, is the operator which leaves the function unchanged; the null operator, $\hat{O}$, is the operator which yields zero when operating on any function:

$$\hat{I}\, f(x) = f(x) \tag{H.6}$$

$$\hat{O} f(x) = 0. \tag{H.7}$$

Note that, in Eqs. (H.4) and (H.5), we dropped any explicit reference to the function $f(x)$. This is the usual way of writing the equations of operator algebra.

Most operators encountered in the physical sciences are linear operators. An operator, $\hat{A}$, is linear if

$$\hat{A}\{f_1(x) + f_2(x)\} = \hat{A} f_1(x) + \hat{A} f_2(x). \tag{H.8}$$

An example of a nonlinear operator is the square-root execution. In general, the results from two operations do not commute, so that $\hat{A}\hat{B} \neq \hat{B}\hat{A}$. Hence, if we define the commutator, $[\hat{A}, \hat{B}]$, as

$$[\hat{A}, \hat{B}] = \hat{A}\hat{B} - \hat{B}\hat{A}, \tag{H.9}$$

the operators $\hat{A}$ and $\hat{B}$ can then be said to commute if $[\hat{A}, \hat{B}]\, f(x) = 0$. As an example, consider the commutator $[x, d/dx]$ operating on the function $\varphi(x)$:

$$\left[x, \frac{d}{dx}\right]\varphi(x) = x\frac{d\varphi}{dx} - \frac{d}{dx}(x\varphi) = x\frac{d\varphi}{dx} - x\frac{d\varphi}{dx} - \varphi = -\varphi.$$

Therefore, the operation "multiply by x" and the operation "take the first derivative with respect to x" do not commute. The Heisenberg uncertainty principle results directly from the failure of certain quantum mechanical operators to commute, as we show in Chapter 5.

Two important characteristics of operators are those of *eigenfunction* and *eigenvalue*. If an operation on a function occurs such that

$$\hat{A}f(x) = af(x), \tag{H.10}$$

where a is some number, then f is called an eigenfunction of operator $\hat{A}$ and a is labeled its eigenvalue. As an example, consider the operator d^2/dx^2, whose eigenfunctions are given by the two solutions of

$$\frac{d^2f}{dx^2} = af,$$

which we know are $f_1 = A\sin(\alpha x)$ and $f_2 = B\cos(\beta x)$. Substitution into the original differential equation shows that the eigenvalues are $-\alpha^2$ and $-\beta^2$, respectively. If $\alpha = \beta$, the eigenfunctions are said to be degenerate. Similarly, eigenvalues can be restricted by boundary conditions for the problem. If, for example, the eigenfunctions for the d^2/dx^2 operator were required to be zero at both $x = 0$ and $x = L$, we would have a set of eigenfunctions

$$f_n = A_n \sin\frac{n\pi x}{L},$$

where n is an integer and the eigenvalues corresponding to the eigenfunctions are $-n^2\pi^2/L^2$.

For quantum mechanical operators, an important additional characteristic is that such operators are always *Hermitian*. The operator $\hat{A}$ is Hermitian if it satisfies the definition

$$\int g^*\hat{A}f\, d\tau = \int (\hat{A}g)^* f\, d\tau, \tag{H.11}$$

where f and g are arbitrary functions, the superscript * denotes the complex conjugate, and $d\tau$ represents an appropriate volume element for the governing coordinate system. Spherical coordinates, for example, give $d\tau = r^2\sin\theta\, dr\, d\theta\, d\phi$ (Appendix I) so that the single integral in Eq. (H.11) is in reality a short-hand notation indicating the usual triple integral required for volumetric integration. The limits of integration for Eq. (H.11) cover the entire region for which the functions, f and g, are defined; consequently, both integrands must vanish at the boundaries of the region.

One can readily show that d/dx does not satisfy the definition of a Hermitian operator. For d/dx, the left-hand side of Eq. (H.11) becomes

$$\int g^* \hat{A} f \, d\tau = \int g^* \frac{df}{dx} dx = -\int f \frac{dg^*}{dx} \, dx,$$

where we have used integration by parts and the fact that the integrand vanishes at its upper and lower limits. For the right-hand side of Eq. (H.11), we have

$$\int (\hat{A}g)^* f \, d\tau = \int \frac{dg^*}{dx} f \, dx \neq -\int f \frac{dg^*}{dx} \, dx.$$

Hence, d/dx is not a Hermitian operator. In a similar fashion, you could readily show that id/dx and d^2/dx^2 are Hermitian operators.

Hermitian operators prove to have two additional characteristics that are very important in applications to quantum mechanics. First, the *eigenvalues* of a Hermitian operator are always *real*. Second, the associated *eigenfunctions* form a *complete, orthogonal, and normalizable set*. As shown in Chapter 5, quantum mechanics associates the eigenvalues of Hermitian operators with measurable properties of actual physical systems. Hence, the first characteristic is important as it ensures that predictions of measurable properties will always be assigned real numbers. The second characteristic is also significant since many applications of quantum mechanics involve the expansion of one function in terms of a set of basis functions; this cannot be done unless the set of functions is said to be complete. The most familiar examples of such complete sets are the functions $\sin(n\pi x/L)$ and $\cos(m\pi x/L)$, which are both used in Fourier analysis $(0 \leq n \leq \infty)$.

Mathematically, the set of eigenfunctions $u_i(x)$ is deemed orthogonal in the interval $[a,b]$ if and only if

$$\int_a^b u_n(x) \, u_m(x) \, dx = C^2 \delta_{mn}, \tag{H.12}$$

where δ_{mn} is called the Kronecker delta and has the following definition:

$$\delta_{mn} = \begin{cases} 1 & m = n \\ 0 & m \neq n \end{cases}. \tag{H.13}$$

We recall from Fourier analysis, for example, that $\sin(nx)$ and $\sin(mx)$ are orthogonal in the interval 0–2π. If, in addition, the integral in Eq. (H.12) converges, the associated eigenfunctions are said to be normalizable. Normalization occurs when we divide each function by a constant, C, thus giving $u_i' = u_i/C$, so that

$$\int_a^b u_n' \, u_m' \, dx = \delta_{mn}.$$

A complete set of functions that is both orthogonal and normalizable is called a *complete, orthonormal set*.

APPENDIX I

The Spherical Coordinate System

Developments in statistical thermodynamics, quantum mechanics, and kinetic theory often require implementation of a spherical coordinate system. Making use of Fig. I.1, we recognize that spherical coordinates can be related to Cartesian coordinates through

$$x = \rho \cos\phi \quad y = \rho \sin\phi \quad \rho = r \sin\theta$$

and thus

$$x = r \sin\theta \cos\phi \tag{I.1}$$

$$y = r \sin\theta \sin\phi \tag{I.2}$$

$$z = r \cos\theta. \tag{I.3}$$

From Eqs. (I.1) and (I.2), we have

$$x^2 + y^2 = r^2 \sin^2\theta, \tag{I.4}$$

while from Eq. (I.3)

$$z^2 = r^2 \cos^2\theta. \tag{I.5}$$

Adding Eqs. (I.4) and (I.5), we obtain, as expected,

$$r = \sqrt{x^2 + y^2 + z^2}. \tag{I.6}$$

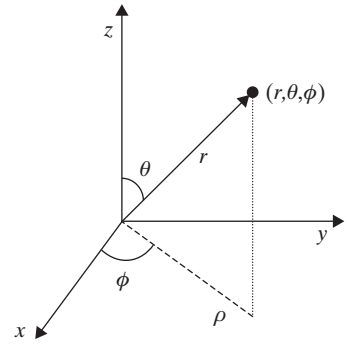

Figure I.1 Spherical and Cartesian coordinate systems.

Dividing Eq. (I.4) by Eq. (I.5), we find that

$$\theta = \tan^{-1}\left[\frac{\sqrt{x^2+y^2}}{z}\right]. \tag{I.7}$$

Similarly, dividing Eq. (I.2) by Eq. (I.1), we have

$$\phi = \tan^{-1}\left(\frac{y}{x}\right). \tag{I.8}$$

Hence, while Eqs. (I.1), (I.2), and (I.3) express Cartesian coordinates in terms of spherical coordinates, Eqs. (I.6), (I.7), and (I.8) relate spherical coordinates to Cartesian coordinates.

The gradient and Laplacian operators for any orthogonal curvilinear coordinate system (u_1, u_2, u_3) can be expressed as (Hildebrand, 1962)

$$\boldsymbol{\nabla} = \frac{\boldsymbol{u}_1}{h_1}\frac{\partial}{\partial u_1} + \frac{\boldsymbol{u}_2}{h_2}\frac{\partial}{\partial u_2} + \frac{\boldsymbol{u}_3}{h_3}\frac{\partial}{\partial u_3} \tag{I.9}$$

$$\boldsymbol{\nabla}^2 = \boldsymbol{\nabla}\cdot\boldsymbol{\nabla} = \frac{1}{h_1h_2h_3}\left[\frac{\partial}{\partial u_1}\left(\frac{h_2h_3}{h_1}\frac{\partial}{\partial u_1}\right) + \frac{\partial}{\partial u_2}\left(\frac{h_3h_1}{h_2}\frac{\partial}{\partial u_2}\right) + \frac{\partial}{\partial u_3}\left(\frac{h_1h_2}{h_3}\frac{\partial}{\partial u_3}\right)\right], \tag{I.10}$$

where $\boldsymbol{u}_i$ represents the unit vector for the ith coordinate, with an inherent scale factor given by

$$h_i = \left|\frac{\partial \boldsymbol{r}}{\partial u_i}\right|. \tag{I.11}$$

The utility of Eqs. (I.9) through (I.11) can be demonstrated by applying them to the familiar Cartesian coordinates, for which

$$\begin{aligned} u_1 &= x \quad u_2 = y \quad u_3 = z \\ \boldsymbol{u}_1 &= \boldsymbol{i} \quad \boldsymbol{u}_2 = \boldsymbol{j} \quad \boldsymbol{u}_3 = \boldsymbol{k}. \end{aligned}$$

Therefore, using

$$\boldsymbol{r} = x\boldsymbol{i} + y\boldsymbol{j} + z\boldsymbol{k}, \tag{I.12}$$

we obtain, from Eq. (I.11),

$$h_1 = 1 \quad h_2 = 1 \quad h_3 = 1.$$

Subsequently, from Eqs. (I.9) and (I.10), the gradient and Laplacian operators for the Cartesian coordinate system become, as anticipated,

$$\boldsymbol{\nabla} = \frac{\partial}{\partial x}\boldsymbol{i} + \frac{\partial}{\partial y}\boldsymbol{j} + \frac{\partial}{\partial z}\boldsymbol{k}$$

$$\boldsymbol{\nabla}^2 = \frac{\partial^2}{\partial x^2} + \frac{\partial^2}{\partial y^2} + \frac{\partial^2}{\partial z^2}.$$

Now, for spherical coordinates, we introduce in a similar fashion,

$$\begin{aligned} u_1 &= r \quad u_2 = \theta \quad u_3 = \phi \\ \boldsymbol{u}_1 &= \boldsymbol{e}_r \quad \boldsymbol{u}_2 = \boldsymbol{e}_\theta \quad \boldsymbol{u}_3 = \boldsymbol{e}_\phi\,. \end{aligned} \tag{I.13}$$

Substituting Eqs. (I.1), (I.2), and (I.3) into Eq. (I.12), we obtain

$$\boldsymbol{r} = r\sin\theta\cos\phi\,\boldsymbol{i} + r\sin\theta\sin\phi\boldsymbol{j} + r\cos\theta\,\boldsymbol{k}, \tag{I.14}$$

so that

$$\frac{\partial \boldsymbol{r}}{\partial r} = \sin\theta\cos\phi\,\boldsymbol{i} + \sin\theta\sin\phi\,\boldsymbol{j} + \cos\theta\,\boldsymbol{k} \tag{I.15}$$

$$\frac{\partial \boldsymbol{r}}{\partial \theta} = r\cos\theta\cos\phi\,\boldsymbol{i} + r\cos\theta\sin\phi\,\boldsymbol{j} - r\sin\theta\,\boldsymbol{k} \tag{I.16}$$

$$\frac{\partial \boldsymbol{r}}{\partial \phi} = -r\sin\theta\sin\phi\,\boldsymbol{i} + r\sin\theta\cos\phi\,\boldsymbol{j}. \tag{I.17}$$

Consequently, from Eq. (I.15),

$$\left|\frac{\partial \boldsymbol{r}}{\partial r}\right|^2 = \frac{\partial \boldsymbol{r}}{\partial r}\cdot\frac{\partial \boldsymbol{r}}{\partial r} = \sin^2\theta\cos^2\phi + \sin^2\theta\sin^2\phi + \cos^2\theta = 1. \tag{I.18}$$

Similarly, from Eqs. (I.16) and (I.17),

$$\left|\frac{\partial \boldsymbol{r}}{\partial \theta}\right|^2 = \frac{\partial \boldsymbol{r}}{\partial \theta}\cdot\frac{\partial \boldsymbol{r}}{\partial \theta} = r^2\cos^2\theta\cos^2\phi + r^2\cos^2\theta\sin^2\phi + r^2\sin^2\theta = r^2 \tag{I.19}$$

$$\left|\frac{\partial \boldsymbol{r}}{\partial \phi}\right|^2 = \frac{\partial \boldsymbol{r}}{\partial \phi}\cdot\frac{\partial \boldsymbol{r}}{\partial \phi} = r^2\sin^2\theta\sin^2\phi + r^2\sin^2\theta\cos^2\phi = r^2\sin^2\theta. \tag{I.20}$$

Therefore, from Eq. (I.11), the scale factors in spherical coordinates are

$$h_1 = 1 \quad h_2 = r \quad h_3 = r\sin\theta. \tag{I.21}$$

The volume element for any orthogonal curvilinear coordinate system is given by (Hildebrand, 1962)

$$d\tau = h_1\,h_2\,h_3\,du_1\,du_2\,du_3. \tag{I.22}$$

Hence, for spherical coordinates, we find, from Eqs. (I.13), (I.21), and (I.22),

$$d\tau = r^2\sin\theta\,dr\,d\theta\,d\phi. \tag{I.23}$$

Similarly, substituting Eqs. (I.13) and (I.21) into Eqs. (I.9) and (I.10), we can express the gradient and Laplacian operators for the spherical coordinate system as

$$\nabla = \frac{\partial}{\partial r}\boldsymbol{e}_r + \frac{1}{r}\frac{\partial}{\partial \theta}\boldsymbol{e}_\theta + \frac{1}{r\sin\theta}\frac{\partial}{\partial \phi}\boldsymbol{e}_\phi \tag{I.24}$$

$$\nabla^2 = \frac{1}{r^2}\frac{\partial}{\partial r}\left(r^2\frac{\partial}{\partial r}\right) + \frac{1}{r^2\sin\theta}\frac{\partial}{\partial \theta}\left(\sin\theta\frac{\partial}{\partial \theta}\right) + \frac{1}{r^2\sin^2\theta}\frac{\partial^2}{\partial \phi^2}. \tag{I.25}$$

APPENDIX J

Electronic Energy Levels

Results from a variety of spectroscopic measurements are necessary for computations in statistical thermodynamics. In particular, calculations of atomic and molecular properties usually require knowledge of electronic energy levels and their associated electronic degeneracies. This appendix provides the appropriate data in tabular form for selected atoms and molecules. The atomic tables include electron configurations, term symbols, and energies (cm^{-1}) for the ground state and five additional upper energy levels. For most degenerate energy levels, mean energies are determined from relevant closely-lying values and reported with one less significant digit. In a similar fashion, the molecular tables provide term symbols and electronic energies (cm^{-1}) for the ground state and three additional upper energy levels. The tabulated molecular energies (T_e) represent energy gaps between the minima corresponding to internuclear potentials for the ground electronic and each upper electronic state. The atomic data have been taken from compilations made available electronically by the National Institute of Standards and Technology (NIST) (http://physics.nist.gov/PhysRefData), while the molecular data have been extracted from Huber and Herzberg (1979).

J.1 Electronic Energy Levels for Atoms

Atom	Configuration	Term symbol	Energy (cm^{-1})	Atom	Configuration	Term symbol	Energy (cm^{-1})
He	$1s^2$	$^1S_0$	0	**N**	$2s^22p^3$	$^4S_{3/2}$	0
$Z = 2$	$1s2s$	$^3S_1$	159,856.1	$Z = 7$	$2s^22p^3$	$^2D_{5/2,3/2}$	19,229
	$1s2s$	$^1S_0$	166,277.5		$2s^22p^3$	$^2P_{1/2,3/2}$	28,839
	$1s2p$	$^3P_{2,1,0}$	169,087		$2s^22p^23s$	$^4P_{1/2,3/2,5/2}$	83,322
	$1s2p$	$^1P_1$	171,135.0		$2s^22p^23s$	$^2P_{1/2,3/2}$	86,179
	$1s3s$	$^3S_1$	183,236.9		$2s2p^4$	$^4P_{5/2,3/2,1/2}$	88,143
O	$2s^22p^4$	$^3P_2$	0	**Na**	$3s$	$^2S_{1/2}$	0
$Z = 8$	$2s^22p^4$	$^3P_1$	158.3	$Z = 11$	$3p$	$^2P_{1/2}$	16,956.2
	$2s^22p^4$	$^3P_0$	227.0		$3p$	$^2P_{3/2}$	16,973.4
	$2s^22p^4$	$^1D_2$	15,867.9		$4s$	$^2S_{1/2}$	25,740.0
	$2s^22p^4$	$^1S_0$	33,792.6		$3d$	$^2D_{5/2,3/2}$	29,173
	$2s^22p^33s$	$^5S_2$	73,768.2		$4p$	$^2P_{1/2,3/2}$	30,270
Mg	$3s^2$	$^1S_0$	0	**Al**	$3s^23p$	$^2P_{1/2}$	0
$Z = 12$	$3s3p$	$^3P_{0,1,2}$	21,877	$Z = 13$	$3s^23p$	$^2P_{3/2}$	112.1
	$3s3p$	$^1P_0$	35,051.3		$3s^24s$	$^2S_{1/2}$	25,347.8
	$3s4s$	$^3S_1$	41,197.4		$3s3p^2$	$^4P_{1/2,3/2,5/2}$	29,077
	$3s4s$	$^1S_0$	43,503.3		$3s^23d$	$^2D_{3/2,5/2}$	32,436
	$3s3d$	$^1D_2$	46,403.1		$3s^24p$	$^2P_{1/2,3/2}$	32,958
Si	$3s^23p^2$	$^3P_0$	0	**P**	$3s^23p^3$	$^4S_{3/2}$	0
$Z = 14$	$3s^23p^2$	$^3P_1$	77.1	$Z = 15$	$3s^23p^3$	$^2D_{3/2,5/2}$	11,369
	$3s^23p^2$	$^3P_2$	223.2		$3s^23p^3$	$^2P_{1/2,3/2}$	18,735
	$3s^23p^2$	$^1D_2$	6298.8		$3s^23p^24s$	$^4P_{1/2,3/2,5/2}$	56,123
	$3s^23p^2$	$^1S_0$	15,394.4		$3s^23p^24s$	$^2P_{1/2,3/2}$	58,026
	$3s3p^3$	$^5S_2$	33,326.0		$3s3p^4$	$^4P_{5/2,3/2,1/2}$	59,690
S	$3s^23p^4$	$^3P_2$	0	**Cl**	$3s^23p^5$	$^2P_{3/2}$	0
$Z = 16$	$3s^23p^4$	$^3P_1$	396.1	$Z = 17$	$3s^23p^5$	$^2P_{1/2}$	882.4
	$3s^23p^4$	$^3P_0$	573.6		$3s^23p^44s$	$^4P_{5/2,3/2,1/2}$	72,425
	$3s^23p^4$	$^1D_2$	9238.6		$3s^23p^44s$	$^2P_{3/2,1/2}$	74,546
	$3s^23p^4$	$^1S_0$	22,180.0		$3s^23p^44p$	$^4P_{5/2,3/2,1/2}$	83,138
	$3s^23p^34s$	$^5S_2$	52,623.6		$3s^23p^44p$	$^4D_{7/2,5/2,3/2,1/2}$	84,300
K	$4s$	$^2S_{1/2}$	0	**Ca**	$4s^2$	$^1S_0$	0
$Z = 19$	$4p$	$^2P_{1/2,3/2}$	13,014	$Z = 20$	$4s4p$	$^3P_{0,1,2}$	15,228
	$5s$	$^2S_{1/2}$	21,026.5		$3d4s$	$^3D_{1,2,3}$	20,352
	$3p^63d$	$^2D_{5/2,3/2}$	21,536		$3d4s$	$^1D_2$	21,849.6
	$5p$	$^2P_{1/2,3/2}$	24,711		$4s4p$	$^1P_1$	23,652.3
	$4d$	$^2D_{5/2,3/2}$	27,398		$4s5s$	$^3S_1$	31,539.5

J.2 Electronic Energy Levels for Molecules

Molecule	Term symbol	Energy (cm^{-1})	Molecule	Term symbol	Energy (cm^{-1})
AlO	$^2\Sigma^+$	0	**BF**	$^1\Sigma^+$	0
	$^2\Pi$	5406		$^3\Pi$	29,144
	$^2\Sigma^+$	20,689		$^1\Pi$	51,157
	$^2\Pi$	33,116		$^3\Sigma^+$	61,035
CN	$^2\Sigma^+$	0	**CO**	$^1\Sigma^+$	0
	$^2\Pi$	9245		$^3\Pi$	48,687
	$^2\Sigma^+$	25,752		$^3\Sigma^+$	55,825
	$^2\Pi$	54,486		$^3\Delta$	61,120
CuO	$^2\Pi_{3/2}$	0	**MgO**	$^1\Sigma^+$	0
	$^2\Pi_{1/2}$	279.0		$^3\Pi$	2400
	$^2\Sigma^+$	16,491		$^1\Pi$	3563
	$^2\Delta_{5/2}$	21,058		$^1\Sigma^+$	19,984
N_2	$^1\Sigma_g^+$	0	**NO**	$^2\Pi_{1/2}$	0
	$^3\Sigma_u^+$	50,204		$^2\Pi_{3/2}$	119.8
	$^3\Pi_g$	59,619		$^4\Pi$	38,440
	$^3\Delta_u$	59,808		$^2\Sigma^+$	43,966
O_2	$^3\Sigma_g^-$	0	**OH**	$^2\Pi$	0
	$^1\Delta_g$	7918		$^2\Sigma^+$	32,684
	$^1\Sigma_g^+$	13,195		$^2\Sigma^+$	69,774
	$^1\Sigma_u^-$	33,057		$^2\Sigma^+$	89,459
PO	$^2\Pi$	0	**SO**	$^3\Sigma^-$	0
	$^2\Sigma^+$	30,731		$^1\Delta$	6350
	$^2\Pi$	33,121		$^1\Sigma^+$	10,510
	$^4\Sigma^-$	34,837		$^3\Pi$	38,463

APPENDIX K

Energy-Mode Parameters for Molecules

Parameters describing internal energy modes for molecular systems are required for statistical calculations of thermodynamic properties. This appendix includes such parameters for both diatomic and polyatomic molecules. Energy-mode parameters are tabulated for selected diatomic molecules in their ground electronic states. Term symbols for these electronic states are included, along with relevant bond lengths and dissociation energies. Similar parameters are also given for diatomic molecules in accessible upper electronic states. Finally, term symbols, rotational constants, and vibrational frequencies (cm^{-1}) are tabulated for selected polyatomic molecules, with a particular focus on triatomic species. All diatomic data have been extracted from Huber and Herzberg (1978), while the polyatomic data have been taken from Herzberg (1991). Additional spectroscopic data are available electronically from NIST (http://webbook.nist.gov/chemistry/).

K.1 Diatomic Molecules in Ground Electronic State

Molecule	Term symbol	ω_e (cm^{-1})	$\omega_e x_e$ (cm^{-1})	B_e (cm^{-1})	α_e (cm^{-1})	D_e (cm^{-1})	r_e (10^{-8} cm)	$D_\circ$ (eV)
Br_2	$^1\Sigma_g^+$	325.32	1.077	0.0821	0.00032	2.09×10^{-8}	2.281	1.971
CH	$^2\Pi$	2858.50	63.020	14.457	0.534	14.5×10^{-4}	1.120	3.465
Cl_2	$^1\Sigma_g^+$	559.72	2.675	0.2440	0.0015	18.6×10^{-8}	1.988	2.479
CO	$^1\Sigma^+$	2169.81	13.288	1.9313	0.0175	6.12×10^{-6}	1.128	11.09
H_2	$^1\Sigma_g^+$	4401.21	121.336	60.853	3.062	4.71×10^{-2}	0.741	4.478
HBr	$^1\Sigma^+$	2648.98	45.218	8.4649	0.2333	3.46×10^{-4}	1.414	3.758
HCl	$^1\Sigma^+$	2990.95	52.819	10.593	0.3072	5.32×10^{-4}	1.275	4.434
HF	$^1\Sigma^+$	4138.32	89.880	20.956	0.798	21.5×10^{-4}	0.917	5.869
N_2	$^1\Sigma_g^+$	2358.57	14.324	1.9982	0.0173	5.76×10^{-6}	1.098	9.759
NO	$^2\Pi_{1/2}$	1904.20	14.075	1.6720	0.0171	0.54×10^{-6}	1.151	6.497
O_2	$^3\Sigma_g^-$	1580.19	11.981	1.4456	0.0159	4.84×10^{-6}	1.208	5.116
OH	$^2\Pi$	3737.76	84.881	18.911	0.7242	19.4×10^{-4}	0.970	4.392

K.2 Diatomic Molecules in Upper Electronic States

Molecule	Term symbol	T_e (cm^{-1})	ω_e (cm^{-1})	$\omega_e x_e$ (cm^{-1})	B_e (cm^{-1})	α_e (cm^{-1})	D_e (cm^{-1})
AlF	$X\ ^1\Sigma^+$	0	802.26	4.77	0.5525	0.0050	1.05×10^{-6}
	$a\ ^3\Pi$	27241	827.8	3.9	0.5570	0.0045	0.98×10^{-6}
	$A\ ^1\Pi$	43949.2	803.94	5.99	0.5564	0.0053	1.06×10^{-6}
AlO	$X\ ^2\Sigma^+$	0	979.23	6.97	0.6414	0.0058	1.08×10^{-6}
	$A\ ^2\Pi$	5406.0	728.5	4.15	0.5354		1.1×10^{-6}
	$B\ ^2\Sigma^+$	20689.0	870.05	3.52	0.6041	0.0045	1.16×10^{-6}
BaO	$X\ ^1\Sigma^+$	0	669.76	2.028	0.3126	0.0014	0.27×10^{-6}
	$A\ ^1\Sigma^+$	16807.2	499.70	1.64	0.2583	0.0011	0.28×10^{-6}
BeCl	$X\ ^2\Sigma^+$	0	846.7	4.85	0.7285	0.0069	2.5×10^{-6}
	$A\ ^2\Pi$	27992.0	822.11	5.24	0.7094	0.0068	2.3×10^{-6}
BeH	$X\ ^2\Sigma^+$	0	2060.78	36.31	10.3164	0.3030	10.22×10^{-4}
	$A\ ^2\Pi$	20033.2	2088.58	40.14	10.4567	0.3222	10.41×10^{-4}
	$B\ ^2\Pi$	50882	2265.94	71.52	10.8495	0.1016	10.35×10^{-4}
BF	$X\ ^1\Sigma^+$	0	1402.13	11.84	1.5072	0.0198	7.6×10^{-6}
	$a\ ^3\Pi$	29144.3	1323.86	9.20	1.4135	0.0158	6.3×10^{-6}
	$A\ ^1\Pi$	51157.5	1264.96	12.53	1.4227	0.0180	7.3×10^{-6}
CN	$X\ ^2\Sigma^+$	0	2068.59	13.087	1.8997	0.0174	6.40×10^{-6}
	$A\ ^2\Pi$	9245.3	1812.56	12.609	1.7151	0.0171	5.93×10^{-6}
	$B\ ^2\Sigma^+$	25752.0	2163.90	20.200	1.9730	0.023	6.6×10^{-6}
CO	$X\ ^1\Sigma^+$	0	2169.81	13.288	1.9313	0.0175	6.12×10^{-6}
	$a\ ^3\Pi$	48686.7	1743.41	14.36	1.6912	0.0190	6.36×10^{-6}
CuO	$X\ ^2\Pi_{3/2}$	0	640.17	4.43	0.4445	0.0046	0.85×10^{-6}
	$X\ ^2\Pi_{1/2}$	279.0	636.18	4.36	0.4442	0.0045	0.84×10^{-6}
	$A\ ^2\Sigma^+$	16491.3	631.02	6.0	0.4339	0.0048	0.79×10^{-6}
GeF	$X\ ^2\Pi_{1/2}$	0	665.67	3.150	0.3658	0.0027	44.7×10^{-8}
	$X\ ^2\Pi_{3/2}$	934.3	667.33	3.150	0.3666	0.0027	45.0×10^{-8}
	$A\ ^2\Sigma^+$	23316.7	413.03	1.124	0.3204	0.0031	77.8×10^{-8}
	$B\ ^2\Sigma^+$	35010.9	796.99	3.613	0.3944	0.0026	38.8×10^{-8}
N_2	$X\ ^1\Sigma_g^+$	0	2358.57	14.324	1.9982	0.0173	5.76×10^{-6}
	$a\ ^3\Sigma_u^+$	50203.6	1460.64	13.872	1.4546	0.0180	6.15×10^{-6}
	$b\ ^3\Pi_g$	59619.4	1733.39	14.122	1.6375	0.0179	5.9×10^{-6}
NH	$X\ ^3\Sigma^-$	0	3282.27	78.35	16.6993	0.6490	17.10×10^{-4}
	$a\ ^1\Delta$	12566	3188.0	68.0	16.439	0.660	16.2×10^{-4}
	$b\ ^1\Sigma^+$	21202	3352.4	74.24	16.705	0.591	16.0×10^{-4}
	$A\ ^3\Pi$	29807.4	3231.2	98.6	16.6745	0.7454	17.80×10^{-4}
NO	$X\ ^2\Pi_{3/2}$	0	1904.20	14.075	1.6720	0.0171	0.54×10^{-6}
	$X\ ^2\Pi_{1/2}$	119.82	1904.04	14.100	1.7202	0.0182	10.23×10^{-6}
	$A\ ^2\Sigma^+$	43965.7	2374.31	16.106	1.9965	0.0192	5.4×10^{-6}

O_2	$X\ ^3\Sigma_g^-$	0	1580.19	11.98	1.4456	0.0159	4.84×10^{-6}
	$a\ ^1\Delta_g$	7918.1	1483.50	12.90	1.4264	0.0171	4.86×10^{-6}
	$b\ ^1\Sigma_g^+$	13195.1	1432.77	14.00	1.4004	0.0182	5.35×10^{-6}
OH	$X\ ^2\Pi$	0	3737.76	84.881	18.911	0.7242	19.38×10^{-4}
	$A\ ^2\Sigma^+$	32684.1	3178.86	92.917	17.358	0.7868	20.39×10^{-4}
PbF	$X\ ^2\Pi_{1/2}$	0	502.73	2.28	0.2288	0.0015	18.3×10^{-8}
	$X\ ^2\Pi_{3/2}$	8263.5	528.75	1.50	0.2340	0.0015	17.8×10^{-8}
	$A\ ^2\Sigma^+$	22556.5	394.73	1.77	0.2076	0.0014	22.2×10^{-8}
SiH	$X\ ^2\Pi$	0	2041.80	35.51	7.4996	0.2190	3.97×10^{-4}
	$a\ ^2\Delta$	24300.4	1858.90	99.18	7.4664	0.3445	5.24×10^{-4}

K.3 Polyatomic Molecules in Ground Electronic State

Molecule	Term symbol	Rotational constants (cm^{-1})			Vibrational frequencies (cm^{-1})				
CO_2	$^1\Sigma_g^+$	0.3902			2349.2	1388.2	667.40 (2)		
HCN	$^1\Sigma^+$	1.4782			3311.5	2096.7	713.46 (2)		
N_2O	$^1\Sigma^+$	0.4190			2223.8	1284.9	588.78 (2)		
H_2O	$^1A_1$	27.877	14.512	9.285	3755.8	3657.1	1594.8		
H_2S	$^1A_1$	10.374	8.991	4.732	2627.5	2614.6	1182.7		
NO_2	$^2A_1$	8.0012	0.4336	0.4104	1616.8	1319.7	749.65		
SO_2	$^1A_1$	2.0274	0.3442	0.2935	1361.8	1151.4	517.69		
C_2H_2	$^1\Sigma_g^+$	1.1766			3372.5	3294.9	1973.5	729.15 (2)	611.70 (2)
NH_3	$^1A_1$	9.9443 (2)	6.1960		3443.6 (2)	3336.2	1626.1 (2)	932.5	
CH_4	$^1A_1$	5.2412 (3)			3019.5 (3)	2916.5	1533.3 (2)	1306.2 (3)	

APPENDIX L

Normal Mode Analysis

Normal mode analysis permits modeling each vibrational mode of a polyatomic molecule as the equivalent of a harmonic oscillator. Hence, the methods developed for assessing the vibrational contribution to thermodynamic properties of a diatomic molecule can be applied in a straightforward manner to polyatomic molecules. In particular, by choosing special coordinates called *normal coordinates*, both kinetic and potential contributions to the vibrational energy become pure quadratic terms; thus, we have simple harmonic motion. Consequently, for each normal mode, displacement along the normal coordinates leads to a pure harmonic oscillation in which all nuclei of the molecule move in phase with the same frequency.

As an example of the procedure and results from normal mode analysis, we consider a simple linear triatomic, as shown in Fig. L.1. For this case, we can easily depict the position of the three nuclear masses, m_1, m_2, and m_3, via the one-dimensional coordinates, x_1, x_2, and x_3. Therefore, this analysis only considers translation and vibration in the x-direction for two oscillators with spring constants, k_1 and k_3, respectively.

The total kinetic and potential energies for the linear triatomic in Fig. L.1 are given by

$$T = \tfrac{1}{2}m_1\dot{x}_1^2 + \tfrac{1}{2}m_2\dot{x}_2^2 + \tfrac{1}{2}m_3\dot{x}_3^2 \tag{L.1}$$

$$V = \tfrac{1}{2}k_1(x_2 - x_1)^2 + \tfrac{1}{2}k_3(x_3 - x_2)^2. \tag{L.2}$$

Note that the potential energy, V, is not composed of pure quadratic terms. Consequently, we must find a new set of normal coordinates, ξ_1, ξ_2, and ξ_3, linearly related to x_1, x_2, and x_3, such that both T and V are composed of pure quadratic terms. In this way, the motion of the system can be decomposed into independent harmonic oscillators that represent all of the allowed vibrational degrees of freedom.

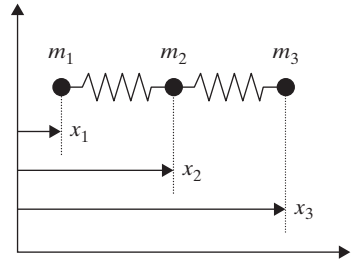

Figure L.1 Geometry for a simple linear triatomic molecule (HCN).

By applying Newton's Second Law to each nucleus, we have

$$m_1\ddot{x}_1 = k_1(x_2 - x_1) \tag{L.3}$$

$$m_2\ddot{x}_2 = -k_1(x_2 - x_1) + k_3(x_3 - x_2) \tag{L.4}$$

$$m_3\ddot{x}_3 = -k_3(x_3 - x_2). \tag{L.5}$$

Harmonic oscillation can now be forced by requiring that

$$m_i\ddot{x}_i = -\omega^2 m_i x_i, \tag{L.6}$$

as the solution to Eq. (L.6) is clearly

$$x_i = C\cos(\omega t + \phi),$$

where C is a constant, ω indicates the radial frequency, and ϕ is an arbitrary phase angle. Substituting Eq. (L.6) into Eqs. (L.3–L.5), we have the following rearranged set of linear homogeneous equations:

$$(k_1 - m_1\omega^2)x_1 - k_1x_2 = 0 \tag{L.7}$$

$$-k_1x_1 + (k_1 + k_3 - m_2\omega^2)x_2 - k_3x_3 = 0 \tag{L.8}$$

$$-k_3x_2 + (k_3 - m_3\omega^2)x_3 = 0. \tag{L.9}$$

A nontrivial solution exists only if the determinant of the coefficients vanishes, that is, if

$$\begin{vmatrix} k_1 - m_1\omega^2 & -k_1 & 0 \\ -k_1 & k_1 + k_3 - m_2\omega^2 & -k_3 \\ 0 & -k_3 & k_3 - m_3\omega^2 \end{vmatrix} = 0. \tag{L.10}$$

Therefore, solving Eq. (L.10), we obtain three normal frequencies associated with this characteristic value problem:

$$\omega_1^2 = 0 \tag{L.11}$$

$$\omega_2^2 + \omega_3^2 = k_1\left(\frac{m_1 + m_2}{m_1 m_2}\right) + k_3\left(\frac{m_2 + m_3}{m_2 m_3}\right) \tag{L.12}$$

$$\omega_2^2\omega_3^2 = k_1k_3\left(\frac{m_1 + m_2 + m_3}{m_1 m_2 m_3}\right). \tag{L.13}$$

For simplicity in the remaining analysis, we assume $m_1 = m_2 = m_3$ and $k_1 = k_3$; thus, from Eqs. (L.11–L.13), we have

$$\omega_1^2 = 0 \tag{L.14}$$

$$\omega_2^2 = k/m \tag{L.15}$$

$$\omega_3^2 = 3k/m. \tag{L.16}$$

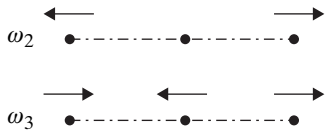

Figure L.2 Vibrational modes for a linear triatomic molecule (HCN).

Substituting Eqs. (L.14–L.16) back into Eqs. (L.7–L.9), we obtain for each mode

$$\omega_1^2 = 0 \qquad x_1 = x_2 = x_3 \tag{L.17}$$

$$\omega_2^2 = k/m \qquad x_2 = 0, \quad x_3 = -x_1 \tag{L.18}$$

$$\omega_3^2 = 3k/m \qquad x_3 = x_1 = -\tfrac{1}{2}x_2. \tag{L.19}$$

Obviously, the mode denoted by $\omega_1^2 = 0$ represents translation. The two vibrational modes, as represented by Eqs. (L.18) and (L.19), are shown in Fig. L.2. From these results, we have clearly identified the vibrational motion for each allowed normal vibrational mode.

Because we have forced harmonic motion, the new coordinates, ξ_1, ξ_2, and ξ_3, must lead to pure quadratic terms. For each normal frequency, we obtain, from Eqs. (L.17–L.19),

$$\omega_1^2 = 0 \qquad x_1 = C_1\xi_1 \qquad x_2 = C_1\xi_1 \qquad x_3 = C_1\xi_1 \tag{L.20}$$

$$\omega_2^2 = k/m \qquad x_1 = C_2\xi_2 \qquad x_2 = 0 \qquad x_3 = -C_2\xi_2 \tag{L.21}$$

$$\omega_3^2 = 3k/m \qquad x_1 = -\tfrac{1}{2}C_3\xi_3 \qquad x_2 = C_3\xi_3 \qquad x_3 = -\tfrac{1}{2}C_3\xi_3, \tag{L.22}$$

where the C_i are constants for each frequency. For any set of linear equations, the complete solution is the sum obtained from solutions at each characteristic frequency; thus,

$$x_1 = C_1\xi_1 + C_2\xi_2 - \tfrac{1}{2}C_3\xi_3 \tag{L.23}$$

$$x_2 = C_1\xi_1 + C_3\xi_3 \tag{L.24}$$

$$x_3 = C_1\xi_1 - C_2\xi_2 - \tfrac{1}{2}C_3\xi_3. \tag{L.25}$$

Substituting Eqs. (L.23–L.25) into Eqs. (L.1) and (L.2), we obtain

$$T = \tfrac{1}{2}\left(3mC_1^2\dot{\xi}_1^2 + 2mC_2^2\dot{\xi}_2^2 + \tfrac{3}{2}mC_3^2\dot{\xi}_3^2\right) \tag{L.26}$$

$$V = \tfrac{1}{2}\left(2kC_2^2\xi_2^2 + \tfrac{9}{2}kC_3^2\xi_3^2\right). \tag{L.27}$$

Therefore, as expected, the normal coordinates, ξ_1, ξ_2, and ξ_3, are linearly related to the original coordinates, x_1, x_2, and x_3. More importantly, these normal coordinates lead to pure quadratic terms for both the kinetic and potential energies, as shown by Eqs. (L.26) and (L.27). This result confirms our supposition that the vibration of a polyatomic molecule can indeed be modeled as a set of independent harmonic oscillators.

APPENDIX M

Tabulation of Debye Function

$$D(x_D) = \frac{3}{x_D^3} \int_0^{x_D} \frac{x^3}{e^x - 1}\, dx$$

x_D	0.0	0.1	0.2	0.3	0.4	0.5	0.6	0.7	0.8	0.9	1.0
0.0	1.0000	0.9630	0.9270	0.8920	0.8580	0.8250	0.7929	0.7619	0.7318	0.7026	0.6744
1.0	0.6744	0.6471	0.6208	0.5954	0.5708	0.5471	0.5243	0.5023	0.4811	0.4607	0.4411
2.0	0.4411	0.4223	0.4042	0.3868	0.3701	0.3541	0.3388	0.3241	0.3100	0.2965	0.2836
3.0	0.2836	0.2712	0.2594	0.2481	0.2373	0.2269	0.2170	0.2076	0.1986	0.1900	0.1817
4.0	0.1817	0.1739	0.1664	0.1592	0.1524	0.1459	0.1397	0.1338	0.1281	0.1227	0.1176
5.0	0.1176	0.1127	0.1080	0.1036	0.0993	0.0952	0.0914	0.0877	0.0842	0.0808	0.0776
6.0	0.0776	0.0745	0.0716	0.0688	0.0662	0.0636	0.0612	0.0589	0.0566	0.0545	0.0525
7.0	0.0525	0.0506	0.0487	0.0470	0.0453	0.0437	0.0421	0.0406	0.0392	0.0379	0.0366
8.0	0.0366	0.0353	0.0341	0.0330	0.0319	0.0308	0.0298	0.0289	0.0279	0.0271	0.0262
9.0	0.0262	0.0254	0.0246	0.0238	0.0231	0.0224	0.0217	0.0211	0.0205	0.0199	0.0193
10.0	0.0193	0.0187	0.0182	0.0177	0.0172	0.0167	0.0163	0.0158	0.0154	0.0150	0.0146
11.0	0.0146	0.0142	0.0138	0.0135	0.0131	0.0128	0.0125	0.0121	0.0118	0.0115	0.0113
12.0	0.0113	0.0110	0.0107	0.0105	0.0102	0.0100	0.0097	0.0095	0.0093	0.0091	0.0089
13.0	0.0089	0.0087	0.0085	0.0083	0.0081	0.0079	0.0077	0.0076	0.0074	0.0073	0.0071
14.0	0.0071	0.0070	0.0068	0.0067	0.0065	0.0064	0.0063	0.0061	0.0060	0.0059	0.0058
15.0	0.0058	0.0057	0.0056	0.0054	0.0053	0.0052	0.0051	0.0050	0.0049	0.0048	0.0047

APPENDIX N

Maxwell–Boltzmann Energy Distribution

In Chapter 15, we found that the Maxwell–Boltzmann distribution for any single Cartesian velocity component, V_i, can be expressed as

$$f(V_i) = \left(\frac{m}{2\pi kT}\right)^{1/2} \exp\left(-\frac{mV_i^2}{2kT}\right). \tag{N.1}$$

Hence, Eq. (N.1) can be interpreted as a standard Gaussian distribution of the form

$$G(z) = \frac{1}{\sqrt{2\pi}\sigma} e^{-z^2/2},$$

for which the Gaussian variable is $z = (V_i - \mu)/\sigma$, where $\mu = 0$ is the mean and

$$\sigma^2 = \frac{kT}{m}$$

is the variance. In computational statistics, we are often concerned with the sum of the squares of independent standard Gaussian variables. Given Eq. (N.1), this sum for the three Cartesian velocity components can be expressed as

$$\frac{m}{kT}\left(V_x^2 + V_y^2 + V_z^2\right) = \frac{2\varepsilon}{kT}, \tag{N.2}$$

where ε is the kinetic energy of the particle.

According to statistical science, the sum of the squares of independent standard Gaussian variables is itself a random statistical variable, whose probability density function (PDF) follows the so-called chi-square distribution, which for three degrees of freedom becomes

$$f(\chi^2) = \frac{\chi e^{-\chi^2/2}}{\sqrt{2\pi}}. \tag{N.3}$$

Therefore, the derived quantity represented by Eq. (N.2) must conform to Eq. (N.3); as a result, for $\chi^2 = 2\varepsilon/kT$, we have

$$f\left(\frac{2\varepsilon}{kT}\right) = \frac{1}{\sqrt{2\pi}}\left(\frac{2\varepsilon}{kT}\right)^{1/2} \exp\left(-\frac{\varepsilon}{kT}\right), \tag{N.4}$$

which should represent the Maxwell–Boltzmann energy distribution. We can confirm this supposition by recognizing that

$$f\left(\frac{\varepsilon}{kT}\right) d\left(\frac{\varepsilon}{kT}\right) = f\left(\frac{2\varepsilon}{kT}\right) d\left(\frac{2\varepsilon}{kT}\right),$$

and thus

$$f\left(\frac{\varepsilon}{kT}\right) = 2 f\left(\frac{2\varepsilon}{kT}\right). \tag{N.5}$$

Combining Eqs. (N.4) and (N.5), we obtain finally

$$f\left(\frac{\varepsilon}{kT}\right) = \frac{2}{\sqrt{\pi}} \left(\frac{\varepsilon}{kT}\right)^{1/2} \exp\left(-\frac{\varepsilon}{kT}\right),$$

which indeed duplicates the expected PDF for the Maxwell–Boltzmann energy distribution, as confirmed at constant temperature by Eq. (15.25).

APPENDIX O

Force Constants for the Lennard–Jones Potential

$$\phi(r) = 4\varepsilon\left\{\left(\frac{\sigma}{r}\right)^{12} - \left(\frac{\sigma}{r}\right)^{6}\right\}$$

Experimental transport data			Experimental virial coefficient data		
Species	$\frac{\varepsilon}{k}$ (K)	σ (Å)	Species	$\frac{\varepsilon}{k}$ (K)	σ (Å)
Ne	35.7	2.79	Ne	35.8	2.75
Ar	124	3.42	Ar	119	3.41
Kr	190	3.61	Kr	173	3.59
Xe	229	4.06	Xe	225	4.07
H_2	38.0	2.92	H_2	36.7	2.96
N_2	91.5	3.68	N_2	95.1	3.70
O_2	113	3.43	O_2	118	3.58
CO	110	3.59	CO	100	3.76
CO_2	190	4.00	CO_2	188	4.47
NO	119	3.47	NO	131	3.17
N_2O	220	3.88	N_2O	193	4.54
CH_4	137	3.82	CH_4	148	3.81
Air*	97.0	3.62	Air*	101	3.67

*Based on the gravimetric composition of air (75.5% N_2, 23.1% O_2, 1.3% Ar, 0.1% CO_2)

APPENDIX P

Collision Integrals for Calculating Transport Properties from the Lennard–Jones Potential

T^*	$\Omega^{(1,1)*}$	$\Omega^{(2,2)*}$
0.60	1.877	2.065
0.80	1.612	1.780
1.00	1.439	1.587
1.20	1.320	1.452
1.40	1.233	1.353
1.60	1.167	1.279
1.80	1.116	1.221
2.00	1.075	1.175
2.20	1.041	1.138
2.40	1.012	1.107
2.60	0.9878	1.081
2.80	0.9672	1.058
3.00	0.9490	1.039
3.20	0.9328	1.022
3.60	0.9058	0.9932
4.00	0.8836	0.9700
5.00	0.8422	0.9269
6.00	0.8124	0.8963
8.00	0.7712	0.8538
10.00	0.7424	0.8242
20.00	0.6640	0.7432
40.00	0.5960	0.6718
50.00	0.5756	0.6504

APPENDIX Q

Reduced Second Virial Coefficient from the Lennard–Jones Potential

$$B(T) = \frac{2\pi}{3} N_A \sigma^3 B^*(T^*)$$

T^*	$B^*(T^*)$	T^*	$B^*(T^*)$
0.3	−27.881	2.6	−0.26613
0.4	−13.799	2.8	−0.18451
0.5	−8.7202	3.0	−0.11523
0.6	−6.1980	3.2	−0.05579
0.7	−4.7100	3.4	−0.00428
0.8	−3.7342	3.6	0.04072
0.9	−3.0471	3.8	0.08033
1.0	−2.5381	4.0	0.11542
1.1	−2.1464	4.2	0.14668
1.2	−1.8359	4.4	0.17469
1.3	−1.5841	4.6	0.19990
1.4	−1.3758	4.8	0.22268
1.5	−1.2009	5.0	0.24334
1.6	−1.0519	6.0	0.32290
1.7	−0.92362	7.0	0.37609
1.8	−0.81203	8.0	0.41343
1.9	−0.71415	9.0	0.44060
2.0	−0.62763	10.0	0.46088
2.2	−0.48171	20.0	0.52537
2.4	−0.36358	30.0	0.52693

APPENDIX R

References and Acknowledgments

R.1 References

1. Baierlein, R., *Thermal Physics*, Cambridge University Press, Cambridge, UK (1999).
2. Barrow, G. M., *Molecular Spectroscopy*, McGraw-Hill, New York (1962).
3. Bernath, P. F., *Spectra of Atoms and Molecules*, Oxford University Press, New York (1995).
4. Callen, H. B., *Thermodynamics*, Wiley, New York (1985).
5. Caretto, L. S., "Course Notes on Statistical Thermodynamics," University of California, Berkeley, CA (1968).
6. Carey, V. P., *Statistical Thermodynamics and Microscale Thermophysics*, Cambridge University Press, Cambridge, UK (1999).
7. Chandler, D., *Introduction to Modern Statistical Mechanics*, Oxford University Press, New York (1987).
8. Chase, W. W., Jr., Davies, C. A., Davies, J. R., Jr., Fulrip, D. J., McDonald, R. A., and Syverud, A. N., *J. Phys. Chem. Reference Data* **14**, Supplement 1 (1985)
9. Davidson, N., *Statistical Mechanics*, McGraw-Hill, New York (1962).
10. Davis, J. C., *Advanced Physical Chemistry*, Wiley, New York (1965).
11. DeGroot, M. H., *Probability and Statistics*, Addison-Wesley, New York (1975).
12. Eckbreth, A. C., *Laser Diagnostics for Combustion Temperature and Species*, Gordon and Breach, Amsterdam (1996).
13. Garrod, C., *Statistical Mechanics and Thermodynamics*, Oxford University Press, New York (1995).
14. Glasstone, S., Laidler, K. J., and Eyring, H., *The Theory of Rate Processes*, McGraw-Hill, New York (1941).
15. Goodisman, J., *Statistical Mechanics for Chemists*, Wiley, New York (1997).
16. Gopal, E. S. R., *Statistical Mechanics and Properties of Matter*, Wiley, New York (1974).
17. Hamming, R. W., *The Art of Probability for Scientists and Engineers*, Addison-Wesley, New York (1991).
18. Hecht, C. E., *Statistical Thermodynamics and Kinetic Theory*, Dover, Mineola, NY (1990).
19. Herzberg, G., *Atomic Spectra and Atomic Structure*, Dover, New York (1944).

20. Herzberg, G., *Molecular Spectra and Molecular Structure: Spectra of Diatomic Molecules*, Krieger, Malabar, FL (1989).
21. Herzberg, G., *Molecular Spectra and Molecular Structure: Electronic Spectra and Electronic Structure of Polyatomic Molecules*, Krieger, Malabar, FL (1991).
22. Hildebrand, F. B., *Advanced Calculus for Applications*, Prentice-Hall, Englewood Cliffs, NJ (1962).
23. Hill, T. L., *Introduction to Statistical Thermodynamics*, Addison-Wesley, Reading, MA (1960).
24. Hirschfelder, J. O., Curtiss, C. F., and Bird, R. B., *Molecular Theory of Gases and Liquids*, Wiley, New York (1967).
25. Huber, K. P., and Herzberg, G., *Constants of Diatomic Molecules*, Van Nostrand Reinhold, New York (1979).
26. Incropera, F. P., *Introduction to Molecular Structure and Thermodynamics*, Wiley, New York (1974).
27. Jeans, S. J., *An Introduction to the Kinetic Theory of Gases*, Cambridge University Press, Cambridge, UK (1952).
28. Kittel, C., and Kroemer, H., *Thermal Physics*, Freeman, New York (1980).
29. Laurendeau, N. M., and Goldsmith, J. E. M., "Comparison of Hydroxyl Concentration Profiles using Five Laser-Induced Fluorescence Methods in a Lean Subatmospheric-Pressure H_2/O_2/Ar Flame," *Combust. Sci. Tech*. **63**, 139–152 (1989).
30. Lay, J. E., *Statistical Mechanics and Thermodynamics of Matter*, Harper and Row, New York (1990).
31. Lewis, G. N., and Randall, M., *Thermodynamics*, McGraw-Hill, New York (1961).
32. Li, X., and Tankin, R. S., "Droplet Size Distribution: A Derivation of a Nukiyama-Tanasawa Type Distribution Function," *Combust. Sci. Tech*. **56**, 65–76 (1987).
33. Lucht, R. P., Peterson, R. C., and Laurendeau, N. M., "Fundamentals of Absorption Spectroscopy for Selected Diatomic Flame Radicals," Report PURDU-CL-78-06, School of Mechanical Engineering, Purdue University, West Lafayette, IN (1978).
34. Measures, R. M., *Laser Remote Sensing*, Wiley, New York (1984).
35. McQuarrie, D. A., *Quantum Chemistry*, University Science Books, Mill Valley, CA (1983).
36. McQuarrie, D. A., *Statistical Mechanics*, Harper and Row, New York (1976).
37. Mulcahy, M. F. R., *Gas Kinetics*, Wiley, New York (1973).
38. Parratt, L. G., *Probability and Experimental Errors in Science*, Wiley, New York (1961).
39. Pratt, G. L., *Gas Kinetics*, Wiley, New York (1960).
40. Present, R. D., *Kinetic Theory of Gases*, McGraw-Hill, New York (1958).
41. Reif, F., *Fundamentals of Statistical and Thermal Physics*, McGraw-Hill, New York (1965).
42. Rosser, W. G. Y., *An Introduction to Statistical Physics*, Wiley, New York (1982).
43. Schroeder, D. V., *Thermal Physics*, Addison Wesley Longman, San Francisco (2000).
44. Sonnessa, A. J., *Introduction to Molecular Spectroscopy*, Reinhold, New York (1966).
45. Sonntag, R. E., and Van Wylen, G. J., *Fundamentals of Statistical Thermodynamics*, Wiley, New York (1966).
46. Tien, C. L., and Lienhard, J. H., *Statistical Thermodynamics*, Hemisphere, Washington, DC (1979).

47. Walpole, R. E., and Myers, R. H., *Probability and Statistics for Engineers and Scientists*, MacMillan, New York (1989).
48. Wannier, G. H., *Statistical Physics*, Dover, New York (1987).

R.2 Source Acknowledgments

I acknowledge herewith those primary sources that have influenced the writing of this textbook. Specifically, credit is given for unique concepts or approaches informing each chapter or appendix. If appropriate, I also identify those sources whose general tenor strongly guided major portions of the book. In general, most of the references in Appendix R.1 were helpful either directly or indirectly in developing example problems or constructing the eight problem sets. Of particular significance in this regard are the textbooks written by Reif (1965), Sonntag and Van Wylen (1966), McQuarrie (1976), Incropera (1974), Kittel and Kroemer (1980), Rosser (1982), and McQuarrie (1983).

In Chapter 1, the notion that statistical thermodynamics constitutes a bridge between quantum mechanics and classical thermodynamics is due to Incropera (1974). Chapter 2 is patterned after a similar chapter in Sonntag and Van Wylen (1966), with some contributions from DeGroot (1975) and Hamming (1991). The derivations of the Poisson and Gaussian distributions from the binomial distribution mostly follow those put together by Parrat (1961) or Walpole and Myers (1989).

The development of the Maxwell–Boltzmann method in Chapter 3 resembles somewhat that found in Davidson (1962). The introduction to the basic postulates and their link to the ensemble method have profited from Hill (1960). The evolution of the most probable macrostate follows Caretto (1968). The derivation of equilibrium particle distributions for Bose–Einstein, Fermi–Dirac, and corrected Maxwell–Boltzmann statistics in Chapters 3 and 4 owes much to Davidson (1962). In Chapter 4, the approach to thermodynamic properties in the dilute limit encapsulates similar derivations offered by Davidson (1962), Caretto (1968), and Incropera (1974).

The historical survey of quantum mechanics in Chapter 5 follows that provided by Caretto (1968). The ensuing introduction to quantum mechanics has been strongly influenced by Caretto (1968), Incropera (1974), and McQuarrie (1983). Solutions to the steady-state Schrödinger wave equation for each energy mode in Chapters 5 and 6 are patterned after similar developments in Incropera (1974) and McQuarrie (1983). The discussions in Chapter 6 concerning electronic energies, spectroscopic term symbols, and selection rules rely on Herzberg (1944) for atoms and on Herzberg (1989) and Bernath (1995) for diatomic molecules. Finally, the spectroscopy of diatomic molecules in Chapter 7 follows comparable developments in Sonnessa (1966), McQuarrie (1983), and Bernath (1995).

The connection between particle and assembly properties in Chapter 8 has profited from a similar approach presented by Incropera (1974). The introduction to the phase integral has been influenced by Hill (1960) while the development of the equipartition principle follows Caretto (1968). Although the derivations of ideal gas properties in Chapter 9 are relatively standard, the sequence here is mostly based on similar developments provided by Sonntag and Van Wylen (1966), Incropera (1974), and McQuarrie (1976). The extension to ideal gas mixtures in Chapter 10 follows Sonntag and Van Wylen (1966) and

Incropera (1974). Various equilibrium constants are explored in more detail by McQuarrie (1976).

The introduction to concentration and temperature measurements in Chapter 11 owes much to Measures (1984). The ensuing discussions concerning absorption and fluorescence spectroscopy rely mainly on Lucht *et al.* (1978) and on Laurendeau and Goldsmith (1989), respectively. Further information on radiative processes and general diagnostic methods is available in Eckbreth (1996). The links to classical thermodynamics and to the Boltzmann definition of entropy in Chapter 12 largely follow similar developments provided by Rosser (1982). The shift to information theory is based on useful discussions found in both Gopal (1974) and Rosser (1982). The application of information theory to spray size distributions is taken from Li and Tankin (1987).

Chapter 13 has profited from similar elaborations in Sonntag and Van Wylen (1966), with additional insights coming from McQuarrie (1976). The critical evaluation of Debye theory and the discussion of metallic crystals near absolute zero owe much to Gopal (1974). The presentation of standing electromagnetic waves in Chapter 14 follows the development provided by McQuarrie (1976). However, the thermodynamics of blackbody radiation, beginning with the Planck distribution law, is based primarily on Sonntag and Van Wylen (1966) and on Incropera (1974).

The formulation of elementary kinetic theory in Chapter 15 has been influenced mainly by Present (1958) and Caretto (1968), with additional insights from Jeans (1952) and Hecht (1990). In Chapter 16, the extension to transport processes is based largely on Hirschfelder *et al.* (1967), with some contributions from McQuarrie (1976). The applications to chemical kinetics in Chapter 17 are drawn largely from Pratt (1960), Mulcahy (1973), and Glasstone *et al.* (1941).

Developments beginning with the canonical and grand canonical ensembles in Chapter 18 are based primarily on Hill (1960). However, the ensuing shift to equilibrium properties follows closely derivations provided by Sonntag and Van Wylen (1966), as do the extensions to fluctuations and the dilute limit. Applications to real gases in Chapter 19 mostly utilize Sonntag and Van Wylen (1966), with additional insights from McQuarrie (1976) and Hecht (1990). The evaluation of real gas properties owes much to Caretto (1968). Finally, the advanced topics summarized in Chapter 20 are mostly found in McQuarrie (1976) and Garrod (1995), with additional contributions from Hill (1960), Wannier (1987), Hecht (1990), Goodisman (1997), and Carey (1999). The title for Chapter 20 is borrowed from Incropera (1974).

Turning now to the appendices, the physical constants in Appendix A are selected from Bernath (1995). The Gaussian and Gamma–Riemann integrals of Appendix B,

$$\int_0^\infty x^n e^{-a x^2} dx \qquad \int_0^\infty x^p (e^x - 1)^{-1} dx,$$

are derived, discussed, or tabulated at different levels by Rosser (1982), Baierlein (1999), and Schroeder (2000). The method of Lagrange multipliers in Appendix D.1 is developed more fully by Hildebrand (1962). The more accurate version of Stirling's formula in Appendix D.2 is nicely derived by Hecht (1990). The Euler–Maclaurin summation formula in Appendix D.3 is verified by example in Sonntag and Van Wylen (1966).

The summary of classical thermodynamics in Appendix F is mostly based on Callen (1985), with further contributions from Caretto (1968) and Lewis and Randall (1961).

Appendices G and H on classical mechanics and operator theory, respectively, follow closely similar developments provided by Caretto (1968). Appendix I on spherical coordinates is generated from Hildebrand (1962) while the normal mode analysis of Appendix L is taken from Hill (1960). Appendix M borrows from Lay (1990), while Appendix N summarizes a written suggestion from a former student, Mr. David Foster. Finally, Appendices O, P, and Q are all from Hirshfelder *et al.* (1967).

R.3 Figure Acknowledgments

Ten figures in this textbook are either replicated from or based on materials previously published in other volumes. I thank the publishers of the indicated sources for permission to reproduce each figure. The full citations are found in Appendix R.1.

Figure Number	Figure Source
Figure 6.4	Figure 6-9 of McQuarrie (1983)
Figure 6.5	Figure 6-12 of McQuarrie (1983)
Figure 6.8	Figure 28 of Herzberg (1944)
Figure 6.10	Figure 195 of Herzberg (1989)
Figure 7.4	Figure 7.3 of Barrow (1962)
Figure 7.7	Figure 10-14 of Davis (1965)
Figure 13.3	Figure 7.3 of Sonntag and Van Wylen (1966)
Figure 13.5	Figure 5.15 of Sonntag and Van Wylen (1966)
Figure 13.8	Figure 9.2 of Gopal (1974)
Figure 19.3	Figure 3.6 of Hirschfelder, Curtiss, and Bird (1967)

Index